UNIVERSITY OF SOUTHAMPTON

Faculty of Engineering, Science and Mathematics
School of Geography

A WIRELESS MUTLI-SENSOR SUBGLACIAL PROBE FOR INVESTIGATING THE DEFORMING GLACIER BED

Kathryn Clare Rose

Thesis submitted for the Degree of Doctor of Philosophy

February 2008

UNIVERSITY OF SOUTHAMPTON

ABSTRACT

FACULTY OF ENGINEERING, SCIENCE AND MATHEMATICS
SCHOOL OF GEOGRAPHY

Doctor of Philosophy

A WIRELESS MUTLI-SENSOR SUBGLACIAL PROBE FOR INVESTIGATING THE DEFORMING GLACIER BED

by Kathryn Clare Rose

The mechanisms that control glacier dynamics and fast ice stream flow are still poorly understood, largely due to the inaccessibility of the subglacial environment. One of the ways to improve on current investigations is to broaden the methods used to monitor the subglacial environment. An autonomous multi-sensor wireless probe was developed for use within an Environmental Sensor Network at Briksdalsbreen, Norway. Probes were deployed at the base of boreholes, measuring temperature, pressure, resistance (a proxy for conductivity), case strain, and tilt, six times a day. The probes used radio communications to transfer data to a base station at the glacier surface. The data was then sent to a reference station, which uploaded it onto the internet on a daily basis.

In excess of a year's worth of data was obtained from several probes, deployed between 2004-2006. Readings of case strain and tilt indicated when the probes had become incorporated into the deforming bed. A reduction in sensor activity was displayed as the glacier changed from a summer to a winter regime. In the following spring, the sensors showed an increase in activity, particularly in water pressure. An Emergent Spring Event was recorded in February, followed by the actual Spring Event. This marked a transition to summer conditions within the glacier's hydrological system. Sliding was the dominant mechanism of basal motion during this time. In the summer, the probes began to rotate as the dominant form of basal motion transferred from sliding to till deformation. The movement of the probes was in keeping with the Taylor (1923) mechanism of clast rotation.

Sedimentological analyses under the scanning electron microscope presented a relatively simple model for grain erosion within the deforming bed. Erosion occurs within a continuum whereby processes of both fracture and abrasion combine, generating intermediate grain forms. The style of deformation experienced is controlled by the nature of the bedrock and the overall strain imposed on the till. At Briksdalsbreen there was good evidence for erosion, but little evidence for the production of a significant silt component.

This investigation demonstrates the potential for the use of ESNs within glacial environments. The probes provide a successful means by which the properties of and processes operating within the subglacial environment can be assessed over broad temporal and spatial scales. For the first time, activity was recorded within the subglacial environment much earlier than previously expected (January) and the spring event within unconnected regions of the bed was monitored and characterised. The records produced highlighted the complexity of hydro-mechanical interactions and the need for further study to constrain these processes. The probes also provided the first natural records of *in situ* clast rotation from within the deforming bed. This movement may have implications for models of clast rotation, the identification and classification of sediments, and models of grain interactions on the micro-scale.

TABLE OF CONTENTS

ABSTRACT i
CHAPTER HEADINGS ii
LIST OF FIGURES ix
LIST OF TABLES xv
LIST OF EQUATIONS xvii
DECLARATION xviii
ACKNOWLEDGEMENTS xix

CHAPTER 1
INTRODUCTION

1.1 RESEARCH BACKGROUND 1
1.2 THESIS AIMS AND OBJECTIVES 3
1.3 THESIS STRUCTURE 5

CHAPTER 2
THEORETICAL BACKGROUND

2.1 INTRODUCTION 6
2.2 THE DEFORMING BED 6
2.3 A BASIC RHEOLOGY 9
2.3.1 Stress 10
2.3.2 Strain 12
2.3.3 Yield strength 13
2.3.4 Till viscosity 14
2.3.5 Flow law for till 15
2.3.5.1 Newtonian viscous material 15
2.3.5.2 Perfectly plastic material 16
2.4 IMPORTANCE AND IMPLICATIONS 16
2.5 MONITORING TECHNIQUES 17
2.5.1 Traditional instruments 20
2.5.2 Instrument development 25
2.6 THEORETICAL FOUNDATION 25
2.6.1 Subglacial drainage morphology 26
2.6.2 Connected, unconnected and alternating 26
2.6.3 Seasonal drainage characteristics 28
2.6.4 Subglacial drainage morphologies 29
2.6.5 Hydrological parameters 35
2.6.6 Hydro-mechanical interactions 36
2.7 EXPERIMENTATION WITH TRADITIONAL INSTRUMENTS 37
2.7.1 Antarctica 38
2.7.2 Alaska 40
2.7.3 Trapridge Glacier, Canada 42
2.7.4 Haut Glacier d'Arolla, Switzerland 45
2.7.5 Svalbard 48
2.7.6 Summary 51
2.8 METHODOLOGICAL CONSTRAINTS 53
2.8.1 Criteria for a new instrument 57
2.8.2 MEMs and ESNs 58
2.8.3 Foundation for the thesis 60
2.9 SUMMARY 61

CHAPTER 3
FIELD SITE DESCRIPTION: BRIKSDALSBREEN

3.1 INTRODUCTION 62
3.2 BRIKSDALSBREEN, NORWAY 62
3.2.1 Frontal variations 68
3.2.2 Rationale 72
3.3 SUMMARY 72

CHAPTER 4
METHODS AND TECHNIQUES

4.1 INTRODUCTION 73
4.2 ENVIRONMENTAL SENSOR NETWORK 75
4.2.1 Sensor nodes 75
4.2.1.1 Probe design 76
4.2.1.2 Probe architecture 77
4.2.1.3 Micro-sensors 80
4.2.1.4 Probe calibration: tilt sensor interpretation 82
4.2.1.5 Probe calibration: resistance 84
4.2.1.6 Probe data collection and transfer 84
4.2.1.7 Probe communications 86
4.2.1.8 Power 87
4.2.2 Base station 88
4.2.2.1 Base station computing system 89
4.2.2.2 Communications 91
4.2.2.3 Base station GPS 92
4.2.2.4 Weather station 93
4.2.2.5 Power supply 93
4.2.3 Reference station 94
4.2.3.1 Reference station GPS 95
4.2.3.2 Café weather station 96
4.2.4 Sensor network server 96
4.2.5 System overview 98
4.3 FIELD WORK TECHNIQUES 98
4.3.1 Field survey 98
4.3.2 Glacier study sites 99
4.3.3 Ground penetrating radar surveys 101
4.3.3.1 GPR equipment and set up 101
4.3.3.2 Common mid point survey 103
4.3.3.3 Grid survey 103
4.3.4 Hot water drilling 106
4.3.5 Borehole observations 109
4.3.6 Sediment sampling 113
4.3.7 Probe deployment and the ESN 115
4.4 NORWEGIAN WEATHER DATA: EKLIMA 117
4.5 SEDIMENT ANALYSIS 118
4.5.1 Foreland sampling 118
4.5.2 Grain size analysis 119
4.5.2.1 Dry sieving 119
4.5.2.2 Laser granulometer 120
4.5.2.3 GRADISTAT v.5.0 121
4.5.3 SEM analysis 122
4.5.3.1 Sample preparation 122
4.5.3.2 Analysis of quartz grains 124
4.5.3.3 Quartz identification 124
4.5.3.4 Surface texture analysis 127

4.6 SUMMARY 130

CHAPTER 5
FIELD SURVEYS: GPS, GPR AND DRILLING RECORD

5.1 INTRODUCTION 131
5.2 GPS 131
5.3 GPR 140
5.3.1 Data processing 140
5.4 GPR INTERPRETATION 149
5.4.1 General features 150
5.4.2 Glacier depth 151
5.5 BOREHOLE INSTRUMENTATION 156
5.5.1 Drilling record 157
5.5.2 Instrument record 158
5.6 SUMMARY 163

CHAPTER 6
WINTER PROBE RECORD

6.1 INTRODUCTION 164
6.2 CONCEPTUAL IDEAS 164
6.3 2004/5 170
6.3.1 Probe 4 170
6.3.2 Probe 5 173
6.3.3 Probe 7 173
6.3.4 Probe 8 174
6.4 INTERPRETATION: 2004/5 175
6.4.1 Commencement 175
6.4.2 Triggers 179
6.4.3 Borehole closure 182
6.4.4 Incorporation into the deforming bed 183
6.4.5 Subglacial processes 186
6.4.5.1 Stage 1 186
6.4.5.2 Stage 2 192
6.4.5.3 Stage 3 193
6.4.6 Probe failure 196
6.5 PROBE 4 196
6.5.1 Commencement 196
6.5.2 Triggers 197
6.5.3 Borehole closure 199
6.5.4 Englacial processes 199
6.5.4.1 Stage 1 199
6.5.4.2 Stage 2 201
6.5.4.3 Stage 3 201
6.5.5 Comparisons 202
6.5.6 Synopsis: 2004/5 204
6.6 2005/6 204
6.6.1 Probe 10 207
6.6.2 Probe 12 207
6.6.3 Probe 15 208
6.6.4 Probe 16 208
6.7 INTERPRETATION: 2005/6 209
6.7.1 Commencement 209

6.7.2 Triggers 211
6.7.3 Borehole closure 213
6.7.4 Incorporation into the deforming bed 214
6.7.5 Subglacial Processes 217
6.7.6 Activity in Probe 15 221
6.7.7 Synopsis: 2005/6 223
6.7.8 Probe failure 224
6.8 HYDROLOGICAL PROCESSES 224
6.8.1 Connected versus unconnected 224
6.8.2 Evidence of a transition from winter to summer regimes 228
6.9 SUMMARY 232

CHAPTER 7
SPRING PROBE RECORD

7.1 INTRODUCTION 235
7.2 2004/5 235
7.2.1 Probe 4 237
7.2.2 Probe 8 238
7.3 INTERPRETATION: EVENT 1 239
7.3.1 Triggers 241
7.3.2 Subglacial processes 243
7.3.3 Englacial processes 244
7.4 INTERPRETATION: EVENT 2 245
7.4.1 Triggers 245
7.4.2 Triggers: Probe 4 247
7.4.3 Subglacial processes 247
7.4.4 Englacial processes 249
7.4.5 Probe failure 250
7.5 2005/6 250
7.5.1 Probe 10 253
7.5.2 Probe 12 253
7.5.3 Probe 15 255
7.6 INTERPRETATION: EVENT 1 256
7.6.1 Triggers 257
7.6.2 Subglacial processes 259
7.7 INTERPRETATION: EVENT 2 262
7.7.1 Triggers 262
7.7.1.1 Event 2a 262
7.7.1.2 Event 2b 263
7.7.1.3 Event 2c 264
7.7.2 Subglacial processes 264
7.7.2.1 Event 2a 264
7.7.2.2 Event 2b 266
7.7.2.3 Event 2c 267
7.7.2.4 Case strain and tilt: Event 2 269
7.8 THE SPRING EVENT 269
7.8.1 Timing 271
7.8.2 Characteristics 275
7.8.2.1 Probe 8 (2004/5) 276
7.8.2.2 Probes 10, 12 and 15 (2005/6) 277
7.8.3 Synthesis 280
7.9 HYDROLOGICAL PROCESSES 281
7.9.1 Drainage connectivity 281
7.9.1.1 Connected 281
7.9.1.2 Unconnected 282

7.9.1.3 Conceptual model *283*
7.9.2 Drainage morphology 286
7.10 MECHANICAL PROCESSES 291
7.10.1 Basal motion 291
7.10.1.1 Probe 10 ..... *292*
7.10.1.2 Probe 15 ..... *296*
7.10.2 Basal mechanics: theory 297
7.10.2.1 Scenario A *300*
7.10.2.2 Scenario B *300*
7.10.2.3 Scenario C *301*
7.10.3 Interpretation: basal mechanics 302
7.10.3.1 Probe 10 ..... *302*
7.10.3.2 Probe 15 ..... *303*
7.11 SYNTHESIS 305
7.12 SUMMARY 306

CHAPTER 8
SUMMER PROBE RECORD

8.1 INTRODUCTION 310
8.2 2004/5 312
8.2.1 Probe 8 312
8.3 INTERPRETATION: 2004/5 313
8.3.1 Correlations with external weather conditions 314
8.3.2 Subglacial processes 315
8.3.3 Drainage morphology 317
8.3.4 Probe movement 317
8.3.5 Basal motion 318
8.4 2005/6 320
8.4.1 Probe 10 323
8.4.2 Probe 12 323
8.4.3 Probe 15 322
8.5 INTERPRETATION: 2005/6 324
8.5.1 Correlations with external weather conditions 324
8.5.2 Subglacial processes 326
8.5.3 Drainage morphology 327
8.5.4 Probe movement 328
8.5.5 Basal motion 328
8.5.6 Probe 15: days 150-207 332
8.6 PROBE FAILURE 335
8.7 THEORETICAL BACKGROUND TO DEFORMATION 336
8.8 SUMMARY 339

CHAPTER 9
SEDIMENTOLOGY

9.1 INTRODUCTION 341
9.2 GRAIN SIZE ANALYSIS 342
9.2.1 Proglacial samples 342
9.2.2 Subglacial samples 345
9.3 INTERPRETATION 348
9.3.1 Texture 349
9.3.2 Grain size distribution 350
9.4 SEM ANALYSIS 352

9.4.1 Subglacial samples 354
9.5 INTERPRETATION: GRAIN PROVENANCE 356
9.5.1 Grain shape and surface texture 356
9.5.2 Grain formation 357
9.5.3 Summary 358
9.6 INTERPRETATION: SUBGLACIAL GRAIN EROSION 358
9.6.1 Grain shape and surface textures 360
9.6.2 Erosional history 363
9.6.2.1 Comparison with Ice Stream B 368
9.6.2.2 Comparison with the probes 369
9.7 SUMMARY 369

CHAPTER 10
CONCLUSIONS

10.1 INTRODUCTION 371
10.2 THEORETICAL BACKGROUND 371
10.3 KEY RESEARCH FINDINGS 373
10.3.1 Winter 373
10.3.2 Spring 375
10.3.3 Summer 376
10.3.4 Sedimentology 377
10.3.5 ESN project overview 378
10.3.6 Summary of key findings 379
10.4 FUTURE RESEARCH 380
10.4.1 Instrument design 380
10.4.2 Glaciological research 382
10.5 SUMMARY 383

APPENDIX A.....385
Hart, J.K., Martinez, K., Ong, R., Riddoch, A., Rose, K.C., Padhy, P. (2006). A wireless multi-sensor subglacial probe: design and preliminary results. *Journal of Glaciology*, 52(178): 389-397.

APPENDIX B.....394
Rose, K.C. and Hart, J.K. (2008). Subglacial comminution in the deforming bed: inferences from SEM analysis. *Sedimentary Geology*, 203(1-2): 87-97.

REFERENCES.....405

LIST OF FIGURES

Figure 2.1: Schematic diagram to show the movement of strain markers within the till at Breiðamerkurjökull, Iceland (adapted from Boulton and Hindmarsh, 1987)..8

Figure 2.2: Schematic diagram to show the relationship between the parameters associated with till rheology and flow. 10

Figure 2.3: Schematic diagram to show stress relations in the context of a glacial system. 11

Figure 2.4: Schematic graph showing the relationship between stress and strain..... 12

Figure 2.5: Schematic diagram showing the various methods available to glaciologists, based on Hart and Rose (2001)..... 18

Figure 2.6: Schematic diagrams of the most commonly used traditional instruments.... 22

Figure 2.7: Conceptual model to show the locations of connected, unconnected and alternating regions of the bed within a hypothetical drainage system. 27

Figure 2.8: Conceptual model to highlight the differences between winter and summer drainage morphologies. 28

Figure 2.9: Subglacial flow pathways for discrete and distributed drainage systems over hard and deformable beds (adapted from Benn and Evans, 1996).. 31

Figure 3.1: The location of Briksdalsbreen, part of the Jostedalsbreen ice cap, Norway. 63

Figure 3.2: Picture of Briksdalsbreen flowing down from the ice cap above (August, 2006). Note: all photographs are by the author, unless otherwise stated..... 64

Figure 3.3: Pictures of Briksdalsbreen (2004) (Photo a: K. Martinez). 65

Figure 3.4: Example features of the glacier foreland (Photos: J.K. Hart)..... 66

Figure 3.5: Example pictures from the glacier margin..... 67

Figure 3.6: View of Briksdalsbreen from the top of the Oldedalen valley, where the camp site and other tourist facilities are located..... 69

Figure 3.7: Photographic time series, displaying the advance and retreat of Briksdalsbreen (Photos: a-c, S. Winkler; d, NVE). 70

Figure 3.8: Example of one of many tree branches found within the glacier foreland (Scale: ~50 cm).. 71

Figure 4.1: Flow chart to show how the methods and techniques employed in this investigation inter-relate. 74

Figure 4.2: Schematic diagram showing the components of the ESN established at Briksdalsbreen. 75

Figure 4.3: Photographs showing the two halves of the probe and the internal electronics. (Photo: K. Martinez). 77

Figure 4.4: Schematic diagrams to show: a) the four main module components that comprised the probes electronics; and b) a simplified version of the probes' architecture (adapted from Hart *et al.*, 2006). 78

Figure 4.5: Pictures highlighting the modular design of the probe's hardware (Photos: K. Martinez). 79

Figure 4.6: Schematic drawing to show the location of the micro-sensors and hardware within the probe casing. 82

Figure 4.7: Conceptual diagram to show the orientation of the axes associated with the tilt sensors for: a) x-axis; b) y-axis; and c) z-axis..... 83

Figure 4.8: Probe resistance calibration curve. 84

Figure 4.9: Schematic diagram and photograph of the base station in 2005..... 88

Figure 4.10 Pelican box containing the hardware for the GPS, the weather station and the ESN computing system. 89

Figure 4.11: To show: a) a schematic diagram of the base station and its role in relation to the other sensing components (adapted from Hart *et al.*, 2006); and b) the base station architecture (Martinez *et al.*, 2004b)..... 90
Figure 4.12: Melkevoll Campsite Office, housed the reference station. (Photo: Melkevoll Campsite website: http://www.melkevoll.no/en/bild29.htm)..... 95
Figure 4.13: The GPS system (Photos: K.Martinez)..... 96
Figure 4.14: The probe data plotter web page (http://leo.ecs.soton.ac.uk/glacsweb/plotter.php)..... 97
Figure 4.15: Mobile hand held Topcon Legacy GPS unit (Photos: K.Martinez)..... 99
Figure 4.16: Schematic diagrams of the glacier study site grids created at Briksdalsbreen in: a) 2004; and b) 2005; and c) photograph of the ice auger..... 100
Figure 4.17: Schematic diagram to show the set up of the GPR. The antennae were accompanied by detachable handles..... 101
Figure 4.18: Photographs to show: a) the 50 MHz GPR antennae with transmitter and receiver attached; and b) the laptop, console, fibre optic cable and pulse sample button. (Photos: M.Westoby)..... 102
Figure 4.19: Schematic diagram to show the set up of the GPR antennae for the CMP survey..... 103
Figure 4.20: The GPR sledge (Photo c: M.Westoby)..... 105
Figure 4.21: Overview of the hot water drilling system..... 106
Figure 4.22: Photographs of the drill set up..... 107
Figure 4.23: Photographs to show a) the drill stem in use; and b) the drill tip, which is attached to the base of the drill stem..... 108
Figure 4.24: Photographs to show: a) the high pressure hose passing down the borehole during drilling; b) a completed borehole that drained; and c) the drill stem at the start of drilling. (Photos: a) D.Vaughn-Hirsh; b) S.Stafford; and c) K.Martinez)..... 110
Figure 4.25: Photographs of the BoreCam, showing: a and b) the 2005 CCTV type colour camera with LEDs set into a surround around the lens; c) the 2004 monochrome infra-red camera (between Jane Hart's feet), with wire reel and video camera; and d) viewing footage from the BoreCam in 2005. (Photos: K.Martinez)..... 112
Figure 4.26: Sediment sampling, showing: a) the percussion hammer attached to a wire reel, the anvil is at the base and the sediment sampler is attached below; b) the small and large sediment samplers; c) using the percussion hammer to insert the sampler at the glacier bed; and d) the resulting sediment sample as it is extracted from the sampler at the surface and bagged. (Photo b: A.Vowles. Photos c, d: E.Guizzo)..... 114
Figure 4.27: Photographs depicting the deployment of the probes (Photo a: E.Guizzo. Photos b, c: K.Martinez)..... 116
Figure 4.28: Map to show the location of the eKlima weather stations in relation to Briksdalsbreen, which is marked on the map above as Briksdal (adapted from MapQuest: http://www.mapquest.com/maps/latlong.adp)..... 118
Figure 4.29: Dry sieving, showing: a) example test sieves with different mesh sizes; and b) the test sieve shaker with a stack of 11 test sieves, a collection tray at the base, and a lid to clamp the stack in place..... 120
Figure 4.30: The GRADISTAT v.5.0 Excel spread sheet used for the analysis of multiple sediment sample data (Blott and Pye, 2001)..... 122
Figure 4.31: Schematic diagrams of the processes involved in SEM analysis..... 123
Figure 4.32: The images produced during SEM x-ray elemental mapping analysis..... 126
Figure 4.33: An example photograph of a quartz grain..... 126
Figure 4.34: Quartz grains, showing examples of the mechanical and chemical surface textures identified during analysis..... 129

Figure 5.1: GPS survey of Briksdalsbreen, including the foreland, lake and *in situ* sample sites on the glacier surface 133
Figure 5.2: GPS survey of the foreland, Briksdalsbreen. 134
Figure 5.3: Schematic diagram to show the retreat of the glacier from the lake (1996-2006). 135
Figure 5.4: Comparison of field site locations on the glacier from 2004-2005 136
Figure 5.5: Location of the boreholes in 2004. 137
Figure 5.6: Location of the boreholes and the base station in 2005. 138
Figure 5.7: Schematic drawings to show the GPR transects and borehole locations for: a) 2004; and b) 2005. 139
Figure 5.8: Flow diagram to show the stages of image processing employed to enhance the raw data image and determine the depth of the glacier along the radar transects. 141
Figure 5.9: GPR data files, displaying transect line X (2004): a) the raw data image prior to processing; and b) the data image corrected for surface air interference (Stage 1) and topography (Stage 2, Figure 5.8). 142
Figure 5.10: Graph series of transect W through each stage of processing. 143
Figure 5.11: Method of measuring the location of the glacier bed, measured in time (ns) on the left axis and distance (m) on the right axis.. 145
Figure 5.12: 2004 depth measurements (in meters) for the glacier bed based on: a) borehole data points; and b) GPR survey depths. 147
Figure 5.13: 2005 depth measurements (in meters) for the glacier bed based on a) borehole data points; and b) GPR survey depths. 148
Figure 5.14: Briksdalsbreen, November 2006. (Person for scale). 151
Figure 5.15: Graphs to show the correlation between 2004 glacier borehole depths and: a) the % difference between GPR and borehole depths; and b) radar velocity. 153
Figure 5.16: Graphs to show the correlation between 2005 borehole depths and: a) the % difference between GPR and borehole depths; and b) radar velocity 154
Figure 5.17: Schematic diagrams to show the location of the boreholes and instruments deployed in 2004/5 in relation to the GPR transects.. 159
Figure 5.18: Schematic diagrams to show the location of boreholes and instruments deployed in 2005/6 in relation to the GPR transects. 160

Figure 6.1: Conceptual model demonstrating the variety of probe locations after deployment and in response to the movement of the glacier and closure of the boreholes over time 167
Figure 6.2: Comparison of the winter sensor records, showing probe temperature, water pressure, case strain, resistance and average weekly probe temperature for: a) Probe 4; b) Probe 5; c) Probe 7; and d) Probe 8.. 171
Figure 6.3: Comparison of winter tilt sensor records for: a) Probe 4; b) Probe 5; c) Probe 7; and d) Probe 8 172
Figure 6.4: Conceptual diagram displaying the rate of borehole movement over the initial position of probe deployment, with respect to rates of ice motion versus till deformation. 178
Figure 6.5: Comparison of winter sensor records, showing: a) external weather conditions; b) Probe 5; c) Probe 7; and d) Probe 8 (2004/5). 180
Figure 6.6: Probe 5 winter sensor record for tilt, case strain and average weekly case strain. 184
Figure 6.7: Winter water pressure records for Probes 5, 7 and 8. 188
Figure 6.8: Winter tilt sensor and water pressure records for Probe 7. 188
Figure 6.9: Water pressure and resistance sensor records for: a) Probe 5; b) Probe 7; and c) Probe 8. Note: the dashed line highlights a change in the resistance sensor trends. 189

Figure 6.10: Winter sensor record for Probe 4, showing: a) external weather conditions; b) probe temperature, water pressure, case strain and resistance; and c) tilt (2004/5). 198
Figure 6.11: Comparison of winter sensor records, showing probe temperature, water pressure, resistance, case strain and average weekly probe temperature for: a) Probe 10; b) Probe 12; c) Probe 15; and d) Probe 16 (2005/6). 205
Figure 6.12: Comparison of winter tilt sensor records for: a) Probe 10; b) Probe 12; c) Probe 15; and d) Probe 16 (2005/6) 206
Figure 6.13: Comparison of the winter sensor records for: a) external weather conditions; b) Probe 10; c) Probe 12; d) Probe 15; and e) Probe 16 (2005/6). 212
Figure 6.14: Comparison of tilt sensor and case strain records for: a) Probe 10; b) Probe 15; and c) Probe 16 (2005/6) 215
Figure 6.15: Winter sensor record highlighting variations in average weekly probe temperature and water pressure: a) Probe 12; b) Probe 16. 220
Figure 6.16: Winter sensor record for Probe 15, showing: probe temperature, water pressure, resistance, and case strain on the secondary y-axis. 222
Figure 6.17: Average external weather conditions for temperature (max. and min.) and precipitation at Briksdalsbreen, Norway (2004-6) 231

Figure 7.1: Comparison of the spring sensor records, showing probe temperature, water pressure, resistance, case strain and average weekly probe temperature for: a) Probe 4; and b) Probe 8 (2004/5) 236
Figure 7.2: Comparison of the spring tilt sensor records for: a) Probe 4; and b) Probe 8 (2004/5). 237
Figure 7.3: Comparison of spring sensor records according to Events 1 and 2 (days 20-42 and 43-120, respectively) for: a) Probe 4; and b) the Probe 8 (2004/5).. 240
Figure 7.4: Spring record for: external weather conditions and Probe 8 water pressure (2004/5). 241
Figure 7.5: Comparison of spring sensor records, showing probe temperature, water pressure, resistance, case strain and average weekly probe temperature for: a) Probe 10; b) Probe 12; and c) Probe 15 (2005/6). 251
Figure 7.6: Comparison of spring tilt sensor records for: a) Probe 10; b) Probe 12; and c) Probe 15 (2005/6). 252
Figure 7.7: Spring sensor record highlighting fluctuations in case strain for: a) Probe 10; and b) Probe 15 (2005/6). 254
Figure 7.8: Comparison of spring water pressure records, displaying the timing of Events 1 and 2 (days 355-51 and 52-120, respectively), for Probes 10, 12 and 15 (2005/6) 257
Figure 7.9: Comparison of spring external weather conditions and Probe 15 sensor readings for water pressure and resistance (2005/6) 258
Figure 7.10: Monthly average temperature (max. and min.) and precipitation data for four glaciers that have recorded spring events: a) Briksdalsbreen, Norway; b) Haut Glacier d'Arolla, Switzerland; c) Trapridge Glacier, Canada; and d) Bench Glacier, Alaska. 273
Figure 7.11: Comparison of spring water pressure records for: a) Probe 8 (2004/5); and b) Probes 10, 12 and 15 (2005/6) 276
Figure 7.12: Conceptual model to demonstrate the different characteristics between the spring event in connected and unconnected regions of the bed 284
Figure 7.13: Schematic diagram to show the location of probes and their associated 'connectivity' within the subglacial drainage system for 2004/5 287
Figure 7. 14: Schematic diagram to show the location of probes and their associated 'connectivity' within the subglacial drainage system for 2005/6 288
Figure 7.15: Spring sensor records showing case strain and tilt for: a) Probe 10; and b) Probe 15 (2005/6) 293

Figure 7.16: Spring sensor readings showing critical yield strength and basal shear stress for: a) Probe 10; and b) Probe 15 (2005/6).....294
Figure 7.17: Spring sensor records showing water pressure and case strain for: a) Probe 10; and b) Probe 15 (2005/6).....295
Figure 7.18: Conceptual diagram for a glacier underlain by unlithified sediments, showing the relationship between parameters associated with the degree of coupling at the ice-bed interface.....299

Figure 8.1: Conceptual diagram to show the orientation of the axes associated with the tilt sensors for: a) x-axis; b) y-axis; and c) z-axis.....312
Figure 8.2: Summer sensor records for Probe 8 (2004/5), showing: a) probe temperature, water pressure, resistance and average weekly probe temperature; and b) tilt. 313
Figure 8.3: Summer sensor record for Probe 8, comparing external weather conditions with probe temperature, water pressure and resistance. 314
Figure 8.4: Summer record for Probe 8 showing: a) water pressure (Pw) in relation to overburden pressure (Pi), highlighting the most likely period of basal motion via enhanced sliding; and b) the critical yield strength (τ^*) of the till in relation to the basal shear stress (τ_b), showing the most likely period of till deformation when $\tau^* < \tau_b$. 319
Figure 8.5: Summer sensor records showing probe temperature, water pressure, resistance, case strain and average weekly probe temperatures for: a) Probe 10; b) Probe 12; and c) Probe 15 (2005/6). 321
Figure 8.6: Summer tilt sensor records for: a) Probe 10; b) Probe 12; and c) Probe 15 (2005/6). 322
Figure 8.7: Comparison of summer sensor records for: a) external weather conditions; b) Probe 10; c) Probe 12; and d) Probe 15 (2005/6).....325
Figure 8.8: Comparison between tilt and case strain sensor records for: a) Probe 10; and b) Probe 15. 329
Figure 8.9: Summer records for basal shear stress (τ_b) and sediment yield strength (τ^*), highlighting the most likely periods of till deformation (when $\tau^* < \tau_b$) for: a) Probe 10; b) Probe 12; and c) Probe 15.....331
Figure 8.10: Summer water pressure (P_w) records in relation to overburden pressure (P_i) for Probes 10, 12 and 15.....332
Figure 8.11: Total summer sensor record for Probe 15 (days 121-207). 333
Figure 8.12: Conceptual diagram depicting mechanisms of: a) Jeffery; b) Taylor; and c) March rotation (adapted from Carr and Rose 2003, p.1421).....337

Figure 9.1: Grain size cumulative frequency for proglacial samples from 2004 and 2006. 344
Figure 9.2: Ternary diagram to show the texture of proglacial sediment samples from 2004 and 2006 (Gradistat v5, Blott and Pye, 2001).....345
Figure 9.3: Grain size cumulative frequency for *in situ* subglacial sediment samples (2004-6) for: a) all samples; and b) average yearly sample values.....347
Figure 9.4: Ternary diagram to show the texture of *in situ* subglacial sediment samples (2004-6) (Gradistat v5, Blott and Pye, 2001). 348
Figure 9.5: Ternary diagram to show the texture of both proglacial (red) and *in situ* subglacial (black) sediment samples (Gradistat v5, Blott and Pye, 2001)..349
Figure 9.6: Grain size cummulative frequency curves comparing proglacial and *in situ* subglacial samples (2004-6) 351
Figure 9.7: Results of SEM analysis averaged for all the subglacial samples (2004-6), showing: a) grain shape, genetic shape and erosional form; and b) morphological, mechanical and chemical textures.....355

Figure 9.8: Grain size (< -2φ fraction) from two different basal tills: Ice Stream B, after Tulaczyk *et al.* (1998); and Breidamerkurjøkull, after Boulton *et al.* (1974). 359
Figure 9.9: Photographs of grain surface textures according to SEM analysis..... 361
Figure 9.10: Erosional continuum (Rose and Hart, 2008), after: a) Iverson *et al.* (1996); and b) Hart (2006b). 365
Figure 9.11: Photographs of grain surface textures..... 366
Figure 9.12: Pie charts to show the relative occurrence of the different erosional forms for subglacial samples (2004-6). 367
Figure 9.13: Grain size (<-2φ) from different deformation tills: Ice Stream B, after Tulaczyk *et al.* (1998); Breidamerkurjøkull, after Boulton *et al.* (1974); and subglacial samples from Briksdalsbreen, averaged between 2004-6. 369

LIST OF TABLES

Table 2.1: Traditional instruments and their role in subglacial investigations. 24
Table 2.2: Different drainage characteristics associated with winter and summer subglacial drainage regimes 29
Table 2.3: Summary of the subglacial *in situ* studies carried out on a variety of glaciers globally in accordance with the investigations discussed 52
Table 2.4: Details of the glacier types and locations discussed. 53

Table 3.1: Annual front variations for Briksdalsbreen, Norway (1956-2007) 71

Table 4.1: Glaciological and ECS design requirements for the components of the ESN (adapted from Martinez *et al.* 2004a). 76
Table 4.2: Specifications for the probe casing and other non-sensor components. 77
Table 4.3: Probe micro-sensor specifications. 81
Table 4.4: Operational protocol for data collection and communication for the probes, the base station and the reference station.. 85
Table 4.5: Details of the eKlima* weather stations, their location and correlation with the Briksdalsbreen base station weather readings. 117
Table 4.6: Tally sheet for surface texture analysis of quartz grains under the SEM based on work by Helland and Holmes (1997) and Mahaney *et al.* (1996). 128

Table 5.1: A record of glacier depth in both time (ns) and equivalent distance (m) based on GPR transect readings. 146
Table 5.2: Glacier depth readings in meters measured by the drill stem, the BoreCam and the GPR. 149
Table 5.3: Borehole drilling record for 2004/5 and 2005/6. 157
Table 5.4: Instrument record for 2004/5 and 2005/6. 158
Table 5.5: Record of sustained probe communications over time. 161
Table 5.6: Gant chart to show the duration of probe communications from 2004-2006. Only those probes which lasted longer than 10 days are displayed 161
Table 5.7: Record of probe sensor function following deployment. 162

Table 6.1: Predicted sensor trends associated with Scenarios A, B and C, outlined in Figure 6.1 168
Table 6.2: Location of the probes within the subglacial drainage system, according to the winter sensor trends in water pressure. 225
Table 6.3: Details of probe location and the time taken to change between time stages. 232

Table 7.1: Data displaying the correlation between decreases in resistance and temperature and precipitation peaks prior to the spring 258
Table 7.2: Summary of key findings relating to the characteristics of spring events from: Haut Glacier d'Arolla: Hubbard *et al.* (1995); Mair *et al.* (2001); Trapridge Glacier: Kavanaugh and Clarke (2001); and Bench Glacier: Harper *et al.* (2005). 270
Table 7.3: Comparison of the parameters associated with spring events from records at Briksdalsbreen, Haut Glacier d'Arolla, Trapridge Glacier, and Bench Glacier. 271

Table 7.4: Comparison of key environmental conditions at each study glacier. 272
Table 7.5: Similarities and differences in the characteristics of the spring events recorded by Probes 8 (2004/5), 10, 12 and 15 (2005/6) at Briksdalsbreen, Norway. 281
Table 7.6: The relationship between water pressure and the mechanical properties of till 298
Table 7.7: The dominant characteristics associated with the spring event, based on the analysis of subglacial hydro-mechanical interactions derived from probe sensor readings. 306

Table 8.1: Variations in the timing (in days) of the dominant mechanism of basal motion (sliding or deformation) according to readings of water pressure, critical yield strength and basal shear stress, and probe rotation. 319
Table 8.2: Variations in the timing (in days) of the dominant mechanism of basal motion (sliding or deformation) according to readings of water pressure, critical yield strength and basal shear stress, and probe rotation. 329

Table 9.1: Summary of the sediment samples collected from the proglacial environment at Briksdalsbreen (2004-6) and their average grain size 343
Table 9.2: Summary of *in situ* subglacial sediment samples 346
Table 9.3: Summary of the *in situ* subglacial samples collected from Briksdalsbreen (2004-6). 346
Table 9.4: Summary of SEM analysis for non-glacial (2004) and subglacial (2004-6) samples. 353

EQUATIONS

EQUATION 1: Ice overburden pressure.....11

EQUATION 2: Basal shear stress.....11

EQUATION 3: Mohr-Coulomb yield criterion.....13

EQUATION 4: Yield strength calculation based on ploughmeter readings.....13

EQUATION 5: Till viscosity.....14

EQUATION 6: Flow law for till.....15

EQUATION 7: Hydraulic conductivity.....30

EQUATION 8: Effective pressure.....35

EQUATION 9: SEM x-ray elemental mapping.....125

EQUATION 10: GPR pulse travel time.....155

EQUATION 11: Glen's flow law.....183

ACKNOWLEDGEMENTS

This is to thank all my friends and colleagues, without whom I would not have been able to finish this thesis. I am particularly indebted to my supervisor Professor Jane Hart, who has shown me unfailing guidance and encouragement. You have always been generous with your time and have enabled me to follow my interests freely. I have learnt so much. Thanks are also due to Dr. Kirk Martinez, who led the ECS side of this research. I have really enjoyed learning about your area of expertise and you have always taken the time to answer my questions. Your support and entertainment in the field, particularly on rescue missions, has been invaluable. Thank you both for allowing me to be part of such a great project.

I thank the University of Southampton, Geography Graduate School for financial support through the John Lewis Partnership Studentship, and for enabling me to attend numerous conferences, field trips and training courses. Without the support of the School I would not have been able to develop such an active academic life, with particular thanks to: Steve Darby, Mary Edwards, Maggie Harris, Pete Langdon and David Sear. I would also like to thank the QRA Executive Committee for welcoming me as Post-Graduate Representative and showing me support and encouragement both in that role and as a PhD student. Thanks to Bob Smith and colleagues in the Cartographic Unit for help with thesis production and Dr. Charles Kerr, Dr. Jim Wright, Kay and Jon for computing support. I am also grateful to Dr. Stefan Winkler (Universität Würzburg) for supplying photos of Briksdalsbreen. Thanks to Dr. Richard Pearce (NOC) for assistance with the SEM and Dr. Adrian Palmer (Royal Holloway, University of London) for guidance with the laser granulometer. My work in the field could not have been completed without the hard work and help of members of ECS and numerous undergraduate students, with particular thanks to: Hannah Brown Paritosh Padhy, Celine Ragault, Alistair Riddoch, Sarita Ward and Gang Zou. Thanks also to Inge and Gro Melkevol for their hospitality and help with logistics.

My postgraduate life at Southampton has been enriched by my fellow postgraduates and friends, whose support and entertainment has helped me to produce this work. Thanks to: Al, Cam, Dotti, Edith, Ellie, Elly, Emily F., Emily H., Greg, Jeff, Joey, Jules, Lee, Lulu and Team Britain, Mark, Matt A., Matt and Pam, Nick O., Roby, Simon, and the QRA PGs – you know who you are! Sorry to anyone I have missed, I thank you too. I am also indebted to Neil. I could not have done this without your continued support and unfailing belief in me. Finally, none of this would have been possible without my parents. You have always believed in me, encouraged me and supported me in every aspect of my life, and in all the choices that I have made that have brought me to produce this thesis. Thank you for everything.

Chapter 1

Introduction

1.1 Research Background

One of the core themes of research in contemporary glaciology has been determining the factors which control glacier motion. The work of numerous researchers has suggested that basal processes play a significant role in controlling glacier flow (e.g. Alley *et al.*, 1986; Blankenship *et al.*, 1986; Boulton and Jones, 1979; Iverson *et al.*, 1995; Nye, 1952; Weertman, 1964). The ability to monitor subglacial conditions has continued to challenge glaciologists, not least due to the inaccessibility of this zone. Investigations, traditionally carried out at the base of glaciers underlain by bedrock, suggested that glacier motion was controlled by sliding (e.g. Weertman, 1964). However, with ongoing research, there was a growing realisation that many glaciers rested on unlithified sediments, known as till, rather than bedrock alone.

Boulton and co-workers carried out the first *in situ* investigations of till beneath Breiðamerkurjökull, Iceland (Boulton, 1979; Boulton and Jones, 1979; Boulton *et al.*, 1974). Their work revealed a saturated layer of sediment, typically weaker than glacier ice, which could deform and contribute to 88-90% of glacier motion (Boulton, 1979; Boulton and Hindmarsh, 1987). Observation and analysis of a similar saturated layer of sediments beneath Ice Stream B (Alley *et al.*, 1986; Blankenship *et al.*, 1986; Engelhardt *et al.*, 1990) added further support to these findings. This resulted in a paradigm shift in research (Boulton, 1986; Murray, 1997), focusing investigations on the physical properties of these sediments and the mechanism of glacier flow through till deformation.

A viscous model of till rheology was presented by Boulton and Hindmarsh (1987) based on the movement of strain markers within the till at Breiðamerkurjökull. A flow law was developed based on these findings, predicting a steady strain rate with the application of shear stress (Boulton and Hindmarsh, 1987). This was later supported by Clarke (1987) and the work of Alley (1989) from Ice Stream B. In contrast, Kamb (1991) favoured a plastic rheology for till, whereby flow does not occur until the yield strength of the material is exceeded by the applied shear stress. In an attempt to resolve these disparities, Hindmarsh (1997) suggested that both of these processes are in operation, but on different scales within the deforming bed. Despite this, neither flow law provides an ideal fit to the range of observations from the field (Quaternary and contemporary). In response to this, models of glacier flow, which depend on such parameterisation, continue to show discrepancies. Consequently, field and laboratory studies to constrain basal processes further, continue.

In the last 30 years, the study of basal processes *in situ* has developed rapidly with the application of hot water drilling and borehole instrumentation. Numerous wired instruments have been developed to assess the physical and mechanical properties and processes operating at the base of glacier boreholes (e.g. Blake *et al.*, 1992, 1994; Fischer and Clarke, 1994). These investigations have provided a wealth of information concerning the properties and processes operating within the subglacial environment (e.g. Fischer and Clarke, 2001; Hooke LeB. *et al.*, 1992; Hubbard *et al.*, 1995; Humphrey *et al.*, 1993; Porter and Murray, 2001). In addition, this information is often combined with velocity readings, to determine the relationship between basal processes and temporal and spatial variations in glacier motion (e.g. Mair *et al.*, 2003). In particular, this research has highlighted the interactions between the mechanical and hydrological processes operating in the till (e.g. Fischer and Clarke, 2001). Basal water pressures are thought to be linked to the mechanical properties of till, affecting till rheology and flow (e.g. Clarke, 1987).

These instruments have greatly advanced our understanding of the properties of the deforming bed, basal processes, and their effect on the forward motion of glaciers. However, conflicting evidence with regards to the flow law of till and concern over change in global climatic conditions indicates that there is still further information to

be gained from the study of basal processes. There are two avenues of research, in particular, that may be of benefit. Firstly, the relationship between the physical conditions under which, and mechanical processes by which, till flows and contributes to glacier motion requires further constraint. This can be achieved with an improved understanding of hydro-mechanical and sedimentological interactions within the till. The former is of particular importance, whereby potential increases in melt water inputs, associated with changing climatic conditions, may act to increase glacier velocities and rates of retreat (Zwally *et al.*, 2002). Secondly, the traditional instruments currently in use are constrained by the borehole itself, and by the wires that tether them to data loggers at the glacier surface. Thus, inferences on till properties and till deformation are often made from monitoring conditions at the ice-bed interface, rather than from within the till. In light of this, the development of a new instrument that can behave independently within the subglacial environment and monitor basal processes more realistically, would greatly improve the quality and quantity of data obtained and our ability to achieve the first objective. In addition, such an instrument may reveal a wide array of new information concerning basal processes.

The general aim of this thesis is to deploy a new wireless instrument within the subglacial environment in order to determine what information can be gleaned about the deforming glacier bed. In particular, this will relate to subglacial hydrology, hydro-mechanical processes and the activity of grain interactions within the till.

1.2 Aims and Objectives

The primary aim of this thesis is:

> *"To investigate the deforming glacier bed with the use of an autonomous, wireless, multi-sensor subglacial probe."*

The main focus for this thesis was to examine what basal conditions and processes could be observed within the subglacial environment, and particularly the deforming

bed, with the use of a new autonomous, wireless, multi-sensor subglacial probe. In order to achieve this, a series of objectives were established as follows:

1. To work in conjunction with the School of Electronics and Computer Science at the University of Southampton, to develop a new multi-sensor instrument for monitoring the physical properties of the subglacial environment and deforming bed of a modern glacier.
2. To establish an environmental sensor network in a glacial environment, from within which the probe would communicate data.
3. To examine the information generated by the probes and, in light of this, determine the processes operating within the subglacial environment over time and space.
4. To assess the movement of the probes within the deforming bed in relation to the predicted activity of clasts.
5. To perform a series of studies to compare the sedimentology of the exposed foreland with the subglacial environment; and determine the erosional history of grains within the deforming bed on the micro-scale, to compliment data regarding the activity of larger scale clast (i.e. probe) movement.

The deforming bed is a complex system and trying to analyse the probe records with respect to all aspects of that system is unfeasible. As a result, analysis of the probe records (objective 3) will specifically focus on subglacial hydrological interactions with the deforming bed. The location of the probes with respect to the subglacial drainage morphology will be assessed. The changes in probe activity between seasons will be related to the hydrological system and the triggers that cause the changes in sensor readings will be determined. The hydro-mechanical properties of the deforming bed will also be examined, but to a lesser extent.

1.3 Thesis Structure

Chapters 1 and 2 introduce the foundation for this thesis. Chapter 2 expands on the theoretical basis for this study summarised in Chapter 1. The importance of the deforming bed is discussed and a review of published literature concerning the *in situ* investigation of the deforming bed, and associated basal processes, is presented. Chapter 3 outlines the field site at which this research was carried out, providing background to the glacier studied. The field, laboratory and analytical techniques employed in order to conduct the research, and achieve the objectives outlined above, are discussed in Chapter 4. Selected details from Chapter 4 are also included in Appendix A, as a publication on 'Instruments and Methods' derived from this project. Chapter 5 presents an overview of the field site in more detail. The different study areas investigated over two field seasons are portrayed with respect to global positioning system and ground penetrating radar surveys. A summary of borehole drilling and probe deployment is also provided as an introduction to the probe data sets that are discussed in Chapters 6, 7, and 8.

Chapter 6 examines the winter probe records, assessing the location and activity of the probes on deployment and in the months that follow. Chapter 7 focuses on the spring probe records, detailing the change and increase in activity within the subglacial environment after the winter. Chapter 8 assesses the summer probe records, with particular reference to the movement of the probes within the deforming bed during this time. Chapter 9 discusses the sedimentological investigations performed, examining samples collected from the glacier foreland and from boreholes via *in situ* sampling. Details from Chapter 9 are also included in Appendix B as a publication derived from this thesis. Finally, Chapter 10 presents a summary of the research carried out and proposes possible avenues for future research.

Chapter 2

Theoretical Background

2.1 Introduction

This section will provide a theoretical basis for the work undertaken in this thesis. The nature of the subglacial environment and the deforming bed are explained. The importance of the deforming bed hypothesis within glaciological research is highlighted, demonstrating the relevance of this work. The methods used to investigate the subglacial environment *in situ* are presented. Current understanding of the deforming bed is detailed with respect to contemporary field investigations. The various limitations of current methodologies and models are discussed and various techniques, aimed at minimising or eliminating these limitations, are proposed. In light of this, the instrument and techniques that are adopted in this investigation, as a more accurate means of investigating the subglacial bed *in situ*, are explained.

2.2 The Deforming Bed

The nature of the subglacial environment is still an area that is poorly understood within glaciology, largely due to the inaccessibility of this zone. Logically, as the area of greatest contact, the interaction between basal ice and the underlying geology must be fundamentally linked to glacier flow. To begin to understand this interaction knowledge of the processes occurring within the subglacial zone is required. Some of the first investigations of the glacier bed were confined to natural cavities beneath

the ice of rock-bed glaciers (e.g. Carol, 1947; Haefeli, 1951). Experimentation revealed that glaciers slid over bedrock on a thin film of water (Nye, 1952; Weertman, 1972). These limited observations of basal conditions, in conjunction with laboratory experiments, were used to underpin theories of glacier movement over bedrock (i.e. sliding), and from this, to determine glacier flow laws (Kamb and LaChapelle, 1964).

Although these theories appeared robust, assumptions were made, and it was obvious that field investigations were significantly lacking. Experimentation was generally limited to temperate bedrock valley glaciers, because they were more readily accessible. As a result, basal observations and flow laws assumed that all glaciers moved via sliding over lithified bedrock geologies. This was problematic in light of the extensive exposures of unlithified Quaternary and Tertiary sediments found to overly bedrock in areas of known former glaciation or glacier retreat. These deposits suggested that an unlithified layer of sediments might be present beneath some modern and palaeo glaciers. Ongoing investigations in the 1970s (e.g. Boulton, 1979; Boulton and Dent, 1974; Boulton and Jones, 1979; Boulton and Paul, 1976) provided critical evidence about the characteristics of these sediments and introduced fundamental questions as to the provenance of this material. Were these sediments located exclusively at the periphery of ice margins? What was the nature of their interaction with the ice? And how might this affect glacier flow? It became increasingly evident that these sediments and their potential presence beneath glaciers required further study. These questions drove pioneering experimentation at the glacier bed. Investigations were carried out with the aim of improving the theoretical analyses underpinning the flow laws of the time, and with the desire to monitor the subglacial environment more accurately.

Perhaps the most notable *in situ* study of basal conditions was performed by Boulton and co-workers at Breiðamerkurjökull, an outlet of the Vatnajökull ice cap, Iceland (e.g. Boulton, 1979; Boulton and Hindmarsh, 1987; Boulton and Jones, 1979). The team excavated the bed of a subglacial tunnel located at the glacier terminus, which was known to rest on a layer of unlithified sediment. Instruments were placed within the underlying sediment to determine the conditions at the ice-bed interface. Measurements of pore-water pressure, strain rate and density, revealed a crude

stratification within the underlying sediment: a low density, underconsolidated A horizon, with high strain rates; and a higher density, overconsolidated B horizon with small strain rates (Figure 2.1). These results provided unequivocal evidence that, not only was it possible for a sedimentary layer to be present beneath an ice mass, but also, that this sediment may actively deform in response to the movement of ice above it. In fact, the proportion of forward motion accounted for by deformation was between 50-80% of the total surface motion recorded during that period. This highlighted the significance of unconsolidated sediments within the subglacial environment in relation to the dynamics of glacier flow.

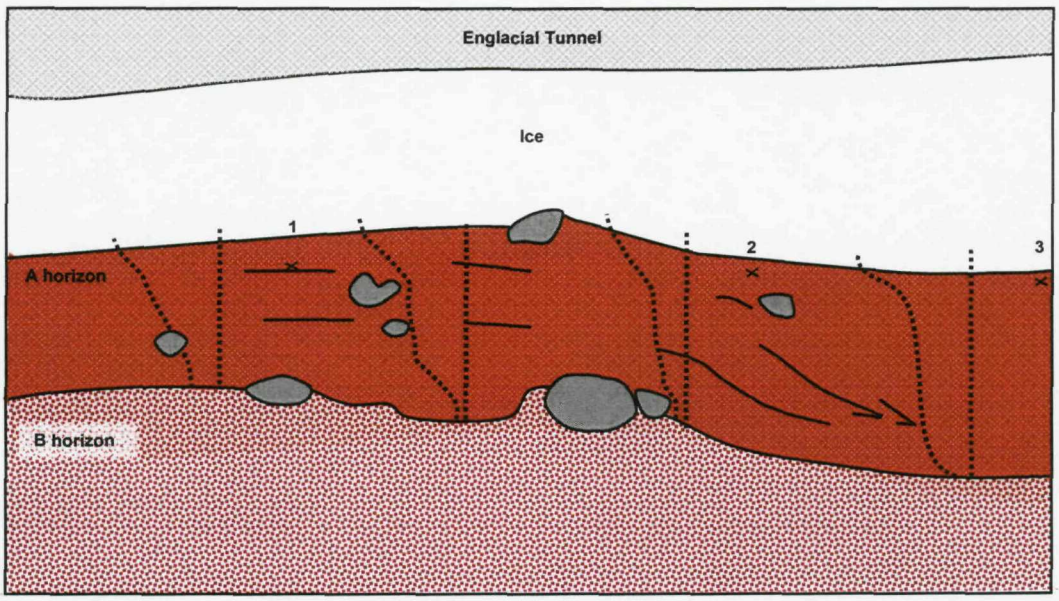


Figure 2.1: Schematic diagram to show the movement of strain markers within the till at Breiðamerkurjökull, Iceland. The dashed lines represent the location of strain markers before and after the 136 hour experiment. The crosses at 1, 2 and 3 represent the location of pore-pressure transducers (adapted from Boulton and Hindmarsh, 1987).

Further evidence to support these findings came from Antarctica, where different geophysical techniques were employed. In order to better understand conditions beneath large ice sheets, Blankenship *et al.* (1986) performed a series of seismic surveys of the bed of Ice Stream B, West Antarctica. The presence of two strong basal reflectors revealed a layer, averaging 5 m in depth, beneath the ice. The velocity of p and s waves indicated that this was a layer of weak saturated sediment,

with some internal stratification. In support of this, Engelhardt *et al.* (1990) probed the ice-bed interface directly beneath Ice Stream B and extracted samples of unlithified sediment. This provided direct evidence of subglacial sediments, in one location at least.

Working under the same project, Alley *et al.* (1986) went on to suggest that this layer of sediment was deforming and, similar to Boulton and Hindmarsh (1987), that it was acting as the primary contributor to flow at Ice Stream B. This conclusion was based on three principles: firstly, that the porosity of the layer was equivalent to that measured by Boulton *et al.* (1974) for dilatent till; secondly, the applied basal shear stress was more than twice that of the till strength, allowing the till to deform; and thirdly, the amount of water needed to account for total ice velocity via basal sliding was not generated by the ice stream. The latter point is particularly relevant, suggesting that other mechanisms (i.e. till deformation) must be contributing to ice velocity.

These innovative investigations provided key information about basal boundary conditions. The presence of a weak, saturated, dilatent and underconsolidated layer of sediment beneath the ice was clearly revealed. The results presented conclusively broke the assumption that 'all glaciers overlie hard bedrock'. This emphasised the importance of the properties of underlying bedrock to glacier dynamics. In particular, the ability of this layer to deform, and thus actively contribute to glacier velocities, was of great significance. In light of this, Boulton (1986) suggested that a 'paradigm shift' in glaciological research was required to focus future investigations on the deforming bed.

2.3 A Basic Rheology

The deforming bed model was generated to create a flow law for till. This section will give a brief description of the criteria that are used to assess the rheology of till, in order to generate such flows laws. The most comprehensive initial model was produced by the work of Boulton and co-workers (Boulton, 1979; Boulton and Hindmarsh, 1987; Boulton and Jones, 1979). Boulton and Hindmarsh (1987)

generated a flow law to fit the values of strain rate measured from seven data points at the terminus of Breiðamerkurjökull. The equations produced implied a slightly non-linear relationship between the applied shear stress and the strain rate of till. The application of stress caused the till to respond as a viscous or Bingham fluid, with a linear or mildly non-linear strain rate. This resulted in a strong relationship with subglacial pore-water pressures (or effective pressures). Criteria relating to the components of till rheology and flow are discussed in this section (Figure 2.2).

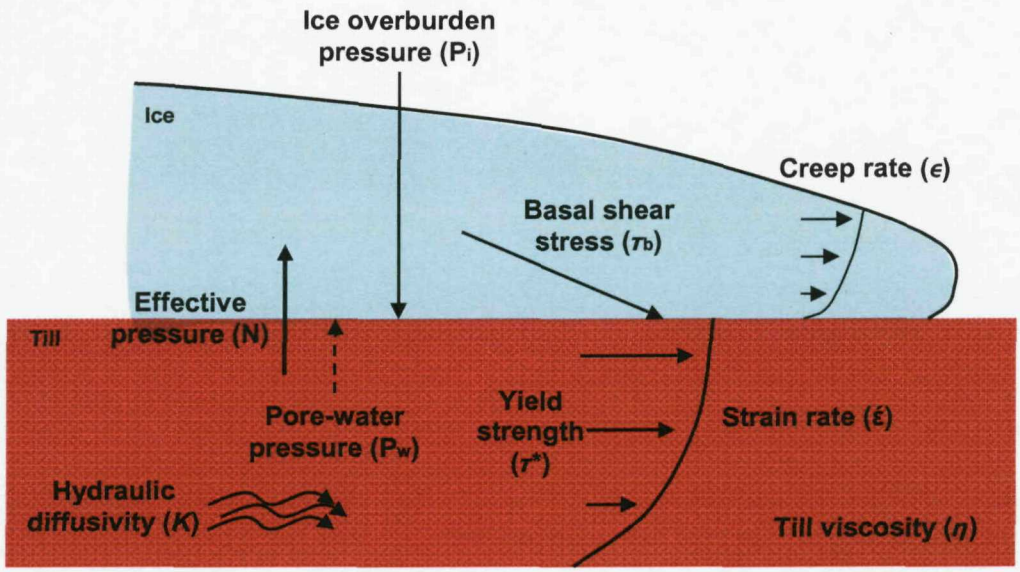


Figure 2.2: Schematic diagram to show the relationship between the criteria associated with till rheology and flow.

2.3.1 Stress

Stress represents the amount by which external forces push or pull a material. Stress can take on a number of forms depending on the material and the environment in which the stress is applied. Two examples are normal stress and shear stress (Figure 2.3). In the context of till deformation, the stress applied tends to be referred to as shear stress, where the forces applied cause a change in the shape of the material, without a significant change in volume. When a change occurs the material is said to have 'failed'. The failure of a material under stress can occur via brittle or ductile

deformation (Benn and Evans, 1996). The amount of stress that needs to be applied in order for failure to occur can vary according to the type of material that is being subjected to that stress. The key difference is that normal stress is applied perpendicular to the material, whereas shear stress has an angle or slope component (Figure 2.3).

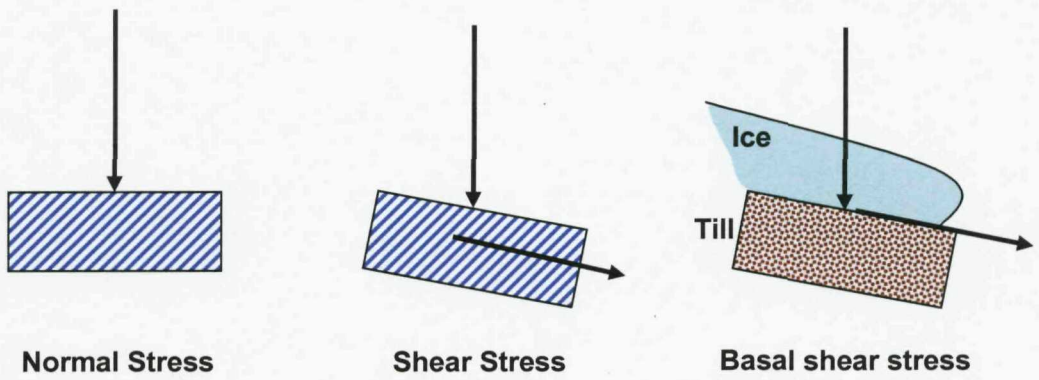


Figure 2.3: Schematic diagram to show stress relations in the context of a glacial system.

The normal stress in a glacial environment, or ice overburden pressure (P_i; Figure 2.2), can be calculated as:

$$P_i = \rho_i g h \tag{1}$$

where: ρ_i is the density of ice (900 kg m^{-3}), g is the gravitational constant (9.81 ms^{-1}), and h_i is the depth of ice. Basal shear stress is important to the deformation of till because it accounts for the force generated by the weight of the ice above as well as that generated by the surface slope of the ice (Figure 2.2). Basal shear stress (τ_b) includes a slope component and can be calculated with the equation:

$$\tau_b = \rho_i g h_i \sin\theta \tag{2}$$

where: ρ_i is the density of ice (900 kgm^{-3}), g is the gravitational constant (9.81 ms^{-1}), h_i is the depth of ice, and θ is the angle of the surface slope (Figure 2.3).

2.3.2 Strain

Strain is measured as the geometrical change in a given material as a result of an applied stress. Strain is commonly discussed in terms of strain rate ($\dot{\varepsilon}$) - a measure of the amount of strain (change in size or shape) over a unit time (Paterson, 1994). Strain is a complex parameter because the response of a material to a given stress can vary greatly. On one occasion a material may show an elastic response, returning to its original form once the applied stress is removed. However, a second application of the same stress may cause the material to change permanently. The reaction of a material can vary according to its strain history or the 'residual strength' of that material (Clarke, 1987). Alternatively, the strain energy resulting from a stress may be stored until a critical level of stress is reached. At this critical shear stress the strain energy will be released and failure will occur. The variety of possible responses can be demonstrated by a graph of shear stress and strain rate (Figure 2.4). This highlights three common relationships between these two factors.

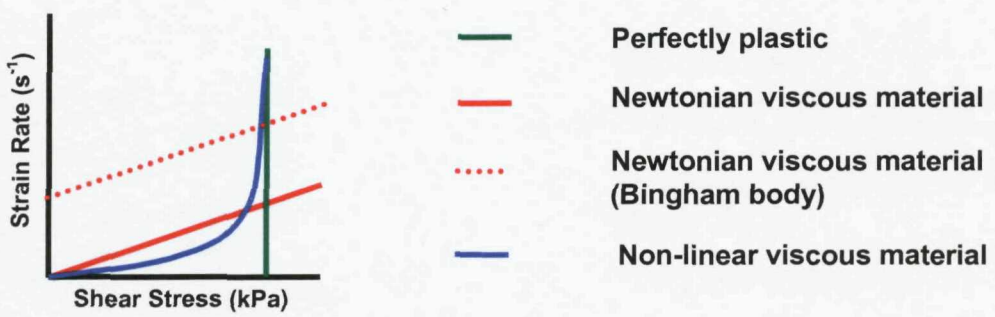


Figure 2.4: Schematic graph showing the relationship between stress and strain

In a perfectly plastic relationship the material remains rigid until the amount of shear stress equals or exceeds the material's yield strength. This dictates that the strength of that material is not dependent on the strain rate (Tulaczyk *et al.*, 2000). For a Newtonian viscous material strain rate is linearly proportional to the amount of shear stress applied. A Bingham body represents a Newtonian viscous material with a yield strength. In a non-linear viscous material, such as ice, the strain rate is non-linear. Unfortunately, the deformation of till is highly complicated because the constituents of till vary spatially, both at one glacier and between glaciers. The

physical properties of that material may also vary temporally, according to fluctuations in water content, for example. As a result of the heterogeneity of till, applying a single flow law to its response to shear stress is problematic.

2.3.3 Yield strength

Under the assumption that till behaves as a perfectly plastic, or Coulomb-plastic material, the yield strength (or critical shear strength) of till is important. It defines the point of failure at which deformation occurs, when the shear stress applied has exceeded the yield strength of till. The yield strength represents the minimum stress that is required to exceed the resisting forces holding the material together (Paterson, 1994). The Mohr-Coulomb yield criterion is traditionally used to approximate the yield strength of a granular material (Figure 2.2). It is represented by the following equation:

$$\tau^* = C + N \tan \phi \qquad (3)$$

where: τ^* is the yield strength (kPa), C is the cohesion value for till (0 kPa), N is effective pressure (kPa), and ø is the internal angle of friction for sediment grains within the till. Hooke *et al.* (1997) calculated a value of ø = 25.5°. However, this will vary according to the sedimentary composition of the till under analysis. In the field, the ploughmeter is used to determine sediment yield strength (k) according to the equation:

$$k = \frac{L}{4ac(2+\pi)} \qquad (4)$$

where: L is the force applied on the ploughmeter, a represents the ploughmeter radius and c is the length of the ploughmeter inserted into the till (Fischer and Clark, 1994; Porter *et al.*, 1997). This calculation is based on an ideal plastic solid model for till behaviour.

Equation (3) defines that the yield strength will be dependent on the material's cohesion and internal frictional strength across potential shear planes. The latter is

dependent on the presence of pore-water or local effective pressure (Paterson, 1994, p.161). Equation (3) is considered to be a reasonable assumption, but it is a simplification, and thus complicated by the omission of potentially important parameters. The inclusion of a term for porosity, for example, would be beneficial, as porosity influences the material's cohesion by defining inter-particle distance. An increase in porosity would reduce the yield strength of a till, irrespective of external change (Clarke, 1987). Clarke (1987) tried to take into account such possible variations in his analysis of till rheology by adapting the Coulomb equation. In contrast, Tulaczyk *et al.* (2000) employed the Hvorslev criterion for heavily overconsolidated (low porosity) till.

The term for cohesion (C) is also problematic (Equation [3]). It acts as a constant, whilst the material's friction is dependent on effective pressure (or the presence of pore-water). In reality, this may not be strictly true, particularly in clay-rich soils, where electrostatic forces dominate (Paterson, 1994). However, the presence of pore-water offsets some of the overlying weight, which is why effective pressure (Equation [8]) and not normal stress must be used in the equation. Unfortunately, data concerning porosity, cohesion and other such parameters are limited, and for simplicity and a scarcity of appealing alternatives the Mohr-Coulomb equation has continued to be used preferentially.

2.3.4 Till viscosity

The viscosity of till (η) can also be derived from strain rate and basal shear stress according to the following equation:

$$\eta = \frac{\tau_b}{2\dot{\varepsilon}_{xz}} \tag{5}$$

where: τ_b is basal shear stress and $\dot{\varepsilon}_{xz}$ is down glacier strain rate (Figure 2.2). This calculation is based on a viscous model of till behaviour, which assumes that till viscosity alone supplies the resistance to glacier motion (Porter and Murray, 2001).

2.3.5 Flow law for till

2.3.5.1 Newtonian viscous material

Boulton and Hindmarsh (1987), and then others, derived an equation for the steady state shear deformation of water saturated till:

$$\dot{\varepsilon} = B(\tau_b - \tau^*)^a N^{-b} \qquad \text{when: } \tau \geq \tau^* \qquad (6)$$

$$\dot{\varepsilon} = 0 \qquad \text{when: } \tau \leq \tau^*$$

where: έ is strain rate, τ_b is shear stress, τ^* is yield strength, N is effective pressure, and *a* and *b* are empirical constants. The equation assumes that till behaves as a Newtonian viscous material, which is one of the simplest stress/strain relationships to define. Boulton and Hindmarsh (1987) determined a variety of values for *a* and *b* based on the measured values of strain rate. They considered two models: one with a yield stress, where a=1 and b=2; and one without, where a=1 and b=1 (Figure 2.4). Alley (1989) applied the same principles to the analysis of till data from Ice Stream B. Alley (1989) included a yield strength and found values of a=1 and b=2. Paterson (1994) questioned the value of including yield strength in this equation because the simplest model allocates till the same yield strength as that of a Bingham body producing, a=1 and b=0. Boulton and Hindmarsh's (1987) model also suggests that there is an important relationship between strain and pore-water pressure. The latter is accounted for by the Mohr-Coulomb yield criterion (Equation [3]). Clarke (1987) also proposed a relationship of this kind but did not test this model on any data.

2.3.5.2 Perfectly plastic material

Kamb (1991) took a slightly different approach and based his analysis of till flow on principles of soil mechanics, likening till to a clay-rich soil. This work predicts that till will deform as a perfectly plastic material. This relationship produces values as high as a=100. In addition, perfectly plastic materials show an increase in shear stress with depth. Under these conditions deformation should be observed at depth, concentrated in a narrow shear band, contrary to the observations of Boulton and Hindmarsh (1987) (Figure 2.2). Kamb's (1991) experiments highlight the

discrepancies between laboratory tests based on soil mechanics and the findings of *in situ* investigations. The argument of till rheology seems to have split between a viscous or plastic mode of deformation. However, to date, there has been insufficient evidence to fully support either hypothesis; and although Hindmarsh (1997) tried to reconcile between the two, direct evidence is still lacking. Consequently, the rheology of till still remains poorly constrained.

2.4 Importance and Implications

In the last twenty five years Boulton's (1986) prediction of a paradigm shift in research has been realised, with a vast body of research focussing on the deforming bed. Sustained interest in the deforming bed has been possible due to the numerous critical implications that its presence has on the fields of glaciology and glacial sedimentology. The contribution of deformation to net glacier velocities affects current understanding of glacier dynamics and ice sheet stability (e.g. Alley *et al.*, 1986; Blankenship *et al.*, 1986; Boulton *et al.*, 2001; Engelhardt *et al.*, 1990; Haeberli *et al.*, 1999; Truffer *et al.*, 2001). The rheology of the deforming bed and the mechanism(s) by which the till deforms (flow laws) will impact the modelling of both palaeo and modern ice masses (e.g. Alley, 1989; Arnold and Sharp, 2002; Boulton and Clark, 1990; Boulton *et al.*, 1985; Clark, 1992, 1997; Hulbe and Payne, 2001; Jenson *et al.*, 1996; Payne, 1999; Payne and Baldwin, 1999; Payne *et al..*, 2006 Vieli *et al.*, 2006). The presence of a deforming bed of unlithified sediments beneath some ice masses also presents new scope for the reinterpretation and classification of glacigenic sedimentary sequences (e.g. Alley, 1991; Clayton *et al.*, 1985, 1989; Hart and Boulton 1991a, b; Piotrowski *et al.*, 2001); and models of landform generation and sediment erosion, transport and deposition (e.g. Benn, 1994; Boulton, 1979, 1996; Boulton and Clark, 1990; Boulton and Hindmarsh, 1987; Boyce and Eyles, 1991; Clark, 1993, 1999; Clark *et al.*, 2004; Eklund and Hart, 1996; Evans *et al.*, 2005, 2006; Hart, 1995).

The introduction of the deforming bed hypothesis to these areas of research has created and fuelled much debate within glaciological research (Clarke, 2005). The above list demonstrates the broad range of research themes that are affected. This in

itself can highlight the importance of this paradigm shift. It is evident that the deforming bed has numerous implications both on the small-scale (e.g. sedimentology) and the large-scale (e.g. ice sheet stability). Perhaps, the effect of deformation on glacier dynamics is of greatest importance to current research. Predicted changes in ice cover and ice sheet stability as a result of variations in climate have critical global implications (e.g. Zwally *et al.*, 2002). Consequently, there is great need to understand how, and to what extent, the deforming bed affects the glacier system. Research undertaken to help redress areas of weakness in our understanding of the deforming bed and associated flow laws is critical.

2.5 Monitoring Techniques

Glaciers have been monitored and studied for several centuries (Clarke, 1987b). The introduction of tax records for land ownership produced some of the first accurate records of variations in glacier activity over time (Grove, 1988). In areas such as Norway, a glacier encroaching on, or retreating from, farm land would have a significant impact on the livelihood of farmers (e.g. Nesje and Kvamme, 1991). In the last century the way in which glaciers are monitored and investigated has improved and diversified significantly (e.g. Hubbard and Glasser, 2005). Methodologies to assess all aspects of glaciology now range from *in situ* observations and analysis of glacial sediments, to laboratory experiments, modelling, and the use of remotely sensed data (Zwally, 1987; Hart and Rose, 2001).

The techniques used in this field are motivated and directed by new discoveries and research trends. Acknowledgement of the deforming bed and its potential contribution to glacier velocity was no exception to this. The late 1980s and 1990s saw a huge increase in work relating to the subglacial environment and the deforming bed (e.g. Alley *et al.*, 1986; Hooke *et al.*, 1997). Hart and Rose (2001) provide a useful discussion on, and summary of, the advantages and disadvantages of the techniques used to monitor bed deformation. Figure 2.5 provides an overview of the methodologies highlighted in their paper. In general, the techniques employed are designed to measure the mechanics of sediment deformation and the physical properties of that deformed sediment (Hart and Rose, 2001).

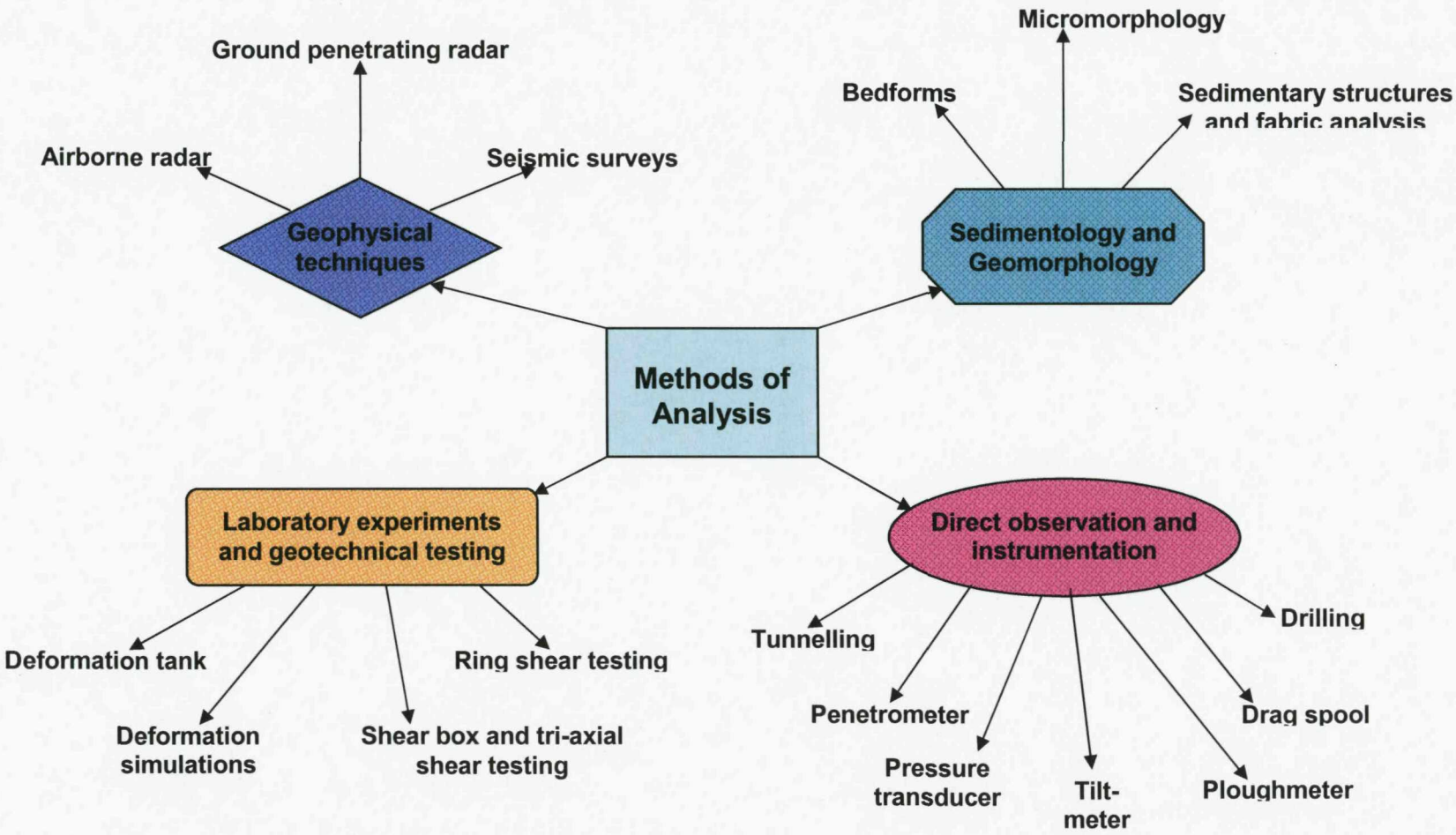


Figure 2.5: Schematic diagram showing the various methods available to glaciologists, based on Hart and Rose (2001).

Palaeo studies of bed deformation have been dominated by the analysis of sedimentary sequences (e.g. Pawley *et al.*, 2004) and landscape geomorphology (e.g. Clark *et al.*, 2004; Hart, 1999). Models determining how till undergoes deformation have been generated based on the properties and nature of landforms and sedimentary sequences (e.g. Lee, 2001). This has been carried out on a variety of scales, but increasingly the techniques of micromorphology (e.g. Roberts and Hart, 2005) and analysis under the scanning electron microscope (e.g. Strand *et al.*, 2003), have been implemented to determine the characteristics of the sediment grains themselves; and whether or not a group of features can be used to identify and classify processes of deformation (e.g. Hooyer and Iverson, 2000; Tulaczyk *et al.*, 1998). Laboratory experiments and geotechnical testing have been used to determine the behaviour, rheology, and mechanical response of till to shear stresses (e.g. Iverson *et al.*, 1997). This has been beneficial where the logistical difficulties associated with accessing the subglacial environment have prevented *in situ* data collection.

Ongoing technological developments (Zwally, 1987) have led to a rapid rise in the use of geophysical techniques to monitor and investigate glacial environments. Three techniques have been used preferentially within glaciology: seismic testing, airborne radar, and ground penetrating radar (GPR). In areas such as Antarctica, the use of seismic and airborne radar surveys (e.g. radio echo sounding) have greatly enhanced the number and quality of investigations into the basal zone of ice streams (e.g. Siegert *et al.*, 2004; Smith, 1997). Repeat surveys have become more feasible and the aerial extent of ice that can be monitored has risen greatly. Outside of Antarctica, the use of GPR to survey the internal and subglacial nature of glaciers has also become more widespread (e.g. Woodward *et al.*, 2003).

Finally, direct observation (e.g. Carol, 1947) and experimental monitoring (e.g. Boulton and Hindmarsh, 1987; Engelhardt *et al.*, 1978) of the subglacial environment has been possible via tunnels and through the use of specialised instrumentation. Methodologies of this kind allow for the collection of contemporaneous data from the specific area of interest – in this case the basal zone. These techniques are becoming increasingly important because it is the ability to directly monitor (with the minimal amount of disturbance) a chosen environment of

study *in situ* that affords the best opportunity to assess that environment in its most natural state. *In situ* data collection should ultimately drive the type of investigations, geophysical surveys, laboratory experiments and modelling carried out. It should also confirm or nullify current theories proposed by such methodologies. *In situ* monitoring is paramount and yet it is perhaps the most difficult to achieve in a glacial environment.

2.5.1 Traditional instruments

The ability to achieve high quality *in situ* observations of the deforming bed is largely constrained by the instruments available. This realisation has driven the design and production of instruments to monitor the subglacial environment *in situ* with the least amount of disturbance from its natural state. This section will briefly outline the origin and use of the instruments traditionally employed in *in situ* investigations of the basal zone.

The ability to access glacier beds via tunnels provides the opportunity for direct monitoring of the subglacial environment with the use of instruments placed directly at the ice-bed interface. The wealth of data produced from a subglacial tunnel at Breiðamerkurjökull by Boulton and Hindmarsh (1987) immediately launched further investigations into the layer of till beneath the ice. A subglacial tunnel at Engabreen, Norway, has been used by numerous scientists to investigation basal motion and subglacial processes (e.g. Iverson *et al.*, 2007; Lappegard *et al.*, 2006). Tunnels have even been excavated for investigations beneath glaciers in Antarctica (e.g Fitzsimons *et al.*, 2000). However, tunnels restrict experiments to the glacier margin, making them potentially unrepresentative of the glacier as a whole, and are often subject to problems of thermal interference. The hazards involved in monitoring the subglacial environment in this way were also evident from the experiences of Boulton and co-workers, who experienced tunnel collapse during their investigation.

As a result, in the last twenty years, there has been a huge increase in the number of instruments designed to monitor basal conditions by accessing the bed from the glacier surface. This has been driven by the use of hot water drilling (e.g. Hubbard and Glasser, 2005, pp.115-124). It is a fast and efficient means of producing

boreholes that access the ice-bed interface (Hubbard *et al.*, 1995). This technique has allowed instruments to progress from rudimentary designs used in subglacial tunnels (e.g. Boulton and Hindmarsh, 1987; Echelmeyer and Zhongxiang, 1987); to a series of traditional instruments that can access the glacier bed from the surface via these boreholes (Hubbard and Glasser, 2005, pp.124-147). This improved access to the glacier bed has driven a large increase in the number and efficacy of *in situ* subglacial studies.

In situ instrumentation is designed to be deployed at the ice-bed interface via boreholes, in order to assess the mechanical and hydrological properties of the deforming layer. The use of boreholes allows access to the glacier bed without the need for tunnelling which, which can be both difficult and dangerous. The design and application of subglacial instrumentation was largely pioneered by the work of Garry Clarke and co-workers (Blake and Clarke, 1992; Blake *et al.*, 1992, 1994; Fischer and Clarke, 1994, 1997a,b; Kavanaugh and Clarke, 2001; Stone and Clarke, 1996; Stone *et al.*, 1993). Traditionally some of the main instruments employed have included drag-spools, tilt meters, ploughmeters and pressure transducers (Figure 2.6). They measure sliding, strain, force and pressure, respectively. These four instruments are used widely in investigations of the glacier bed. A brief synopsis of each is given below.

The drag-spool is designed to measure sliding at the glacier bed (e.g. Engelhardt *et al.*, 1990) and one of the first versions was simply an anchor with a string connected to a reel and a chart recorder (Boulton and Hindmarsh, 1987). However, ongoing modifications have resulted in a more accurate model (Blake *et al.*, 1994). This consists of an anchor that is driven into the underlying till using a percussion hammer (Blake *et al.*, 1992). The anchor is connected by a string to a spool and a potentiometer that are encased and held within the borehole (Figure 2.6a). As the ice moves over its bed the string connected to the stationary anchor pays out, rotating a spool and changing the resistance of the potentiometer. The string payout is considered to be roughly equal to the displacement between the ice and the bed. This represents the amount (rate) of sliding at the glacier base (Porter and Murray, 2001).

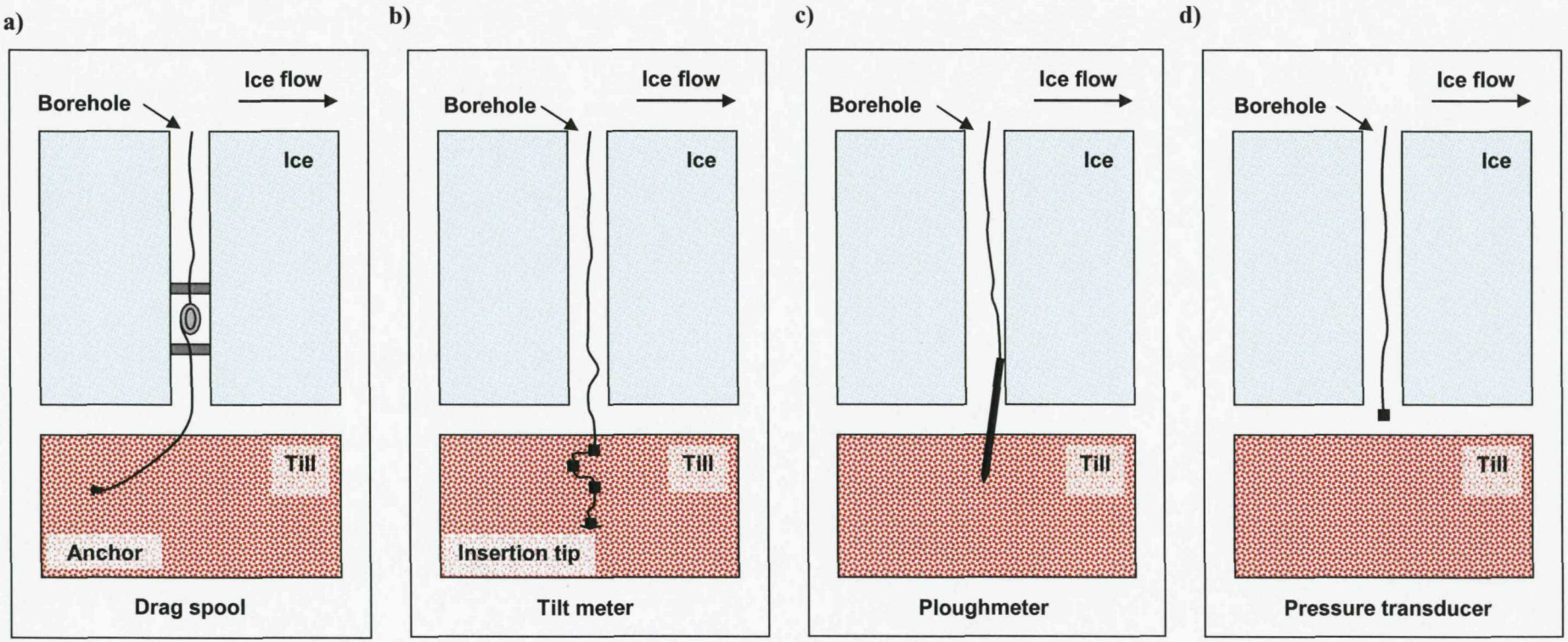


Figure 2.6: Schematic diagrams of the most commonly used traditional instruments, showing: a) the drag-spool (Blake *et al.*, 1994); b) a tilt meter (Blake *et al.*, 1992); c) a ploughmeter (Fishcer and Clarke, 1994); and d) a pressure transducer (Hodge, 1976).

Tilt sensors are designed to measure deformation (or strain rate) within subglacial till (Blake *et al.*, 1992; Figure 2.6b). Tilt cells (in this example three) are linked at different lengths in a chain and inserted into the underlying sediment with a percussion hammer. The cells are tethered to the surface, where they are connected to a data logger (e.g. Porter and Murray, 2001). The cells are high precision sensors, which can measure angular movement within the subglacial sediment. This was a considerable advance from the wooden stakes used by Boulton and Hindmarsh (1987) (Figure 2.1)

The initial idea for the ploughmeter resulted from an accident during drilling at Columbia glacier, Alaska (Humphrey *et al.*, 1993; section 2.7.2). The ploughmeter consists of four strain gauges, paired and encased in a stiff metal rod (Fischer and Clarke, 1994). The lower half is inserted into basal sediments (again using a percussion hammer), whilst the upper section remains in the borehole (Figure 2.6c). The forces acting on the base of the ploughmeter and the directions in which they are applied, are measured as it is dragged through the underlying sediment (Fischer and Clarke, 1994). Iverson *et al.* (1994) also developed an instrument called the dragometer. This was similar to the ploughmeter and measured sediment strength. Pressure transducers are used to measure basal water pressure (Hodge, 1976). They are placed at the bottom of boreholes just above the glacier bed (Figure 2.6d).

These instruments are connected to, and they communicate with, the glacier surface via a wire tether. Excess wire is normally left towards the base of the boreholes. This is done to account for the forward motion of the glacier, ice creep and closure of the boreholes which could sever the wire, or if the wire became stuck, could pull the instrument from the till. Data are generally received and stored at the surface by a Cambell CR-10 data logger (e.g. Murray and Porter, 2001). Readings are generally taken every 2 minutes but this can be adjusted according to season (e.g. 40 minutes in winter, 2 minutes in summer; Murray and Porter, 2001). Data are downloaded from the data logger at the end of the field season, or they can be left and collected at another time, provided that batteries and instrument survival are not limiting.

As previously mentioned, each instrument generates information concerning the mechanical and hydrological properties of the subglacial environment. The drag-

spool measures the rate of sliding, so that the relative contribution of sliding (verses deformation) to glacier motion can be calculated. The tilt sensors are crucial as they provide good evidence of deformation within subglacial sediments. They can be used to calculate strain rate within the till, as well as the type and depth of sediment movement. Ploughmeters are used to determine the yield strength and viscosity (i.e. sediment strength) of till (Equation [4], section 2.3.3 and Equation [5], section 2.3.4, respectively). This is a valuable means of interpreting the rheology of the till in accordance with a given model of sediment flow. Finally, pressure sensors, record patterns in basal water flow (Hodge, 1976). These trends can be assessed, in order to determine any associations between glacier hydrology and the mechanical properties of basal sediments, and potentially glacier flow (e.g. Murray and Porter, 2001). These are only four examples of instruments used *in situ* at the glacier bed, but numerous others have been developed to monitor a range of properties (Table 2.1).

Table 2.1: Traditional instruments and their role in subglacial investigations.

Instrument	Designed to measure?	Example Reference
Drag-spool	Sliding	Fischer and Clarke, 1997
Tilt meter	Strain rate	Truffer *et al.*, 2000
Ploughmeter	Strain	Murray and Clarke, 1995
Pressure transducer	Basal water pressure	Murray and Clarke, 1995
Geophone	Seismic activity	Kavanaugh and Clarke, 2001
Sediment sampler	Subglacial sediment	Humphrey *et al.*, 1993
Thermistors	Thermal regime	Murray and Porter, 2001
Penetrometer	Depth of till	Murray and Porter, 2001
Vertical strain sensor	Deformation in ice	Porter and Murray, 2001
Load bolt sensor	Strain	Kavanaugh and Clarke, 2001
Dragometer	Till strength	Iverson *et al.* 1994
Conductivity meter	Water conductivity	Stone *et al.*, 1993
Turbidity meter	Water turbidity/sediment content	Kavanaugh and Clarke, 2001

The instruments detailed in Table 2.1 have made a significant impact on research into the subglacial environment. In combination with boreholes, they have greatly advanced our ability to directly sample and monitor the glacier bed *in situ*. This has meant, for the first time, that changes at the glacier bed could be readily monitored over time periods of months (instead of days or hours) with minimal bed disturbance. Instruments can be left unattended and located away from the marginal zones of glaciers. The ability to locate these instruments over a wider aerial extent also recognises the high spatial variability in conditions at the glacier bed. Without direct

observations of this kind, understanding within this field of research would be limited to simply theoretical analyses based on laboratory experiments and modelling (e.g. Clarke, 1987; Kamb, 1991; Iverson *et al.*, 1998). Consequently, these instruments have been used to obtain crucial information about conditions and processes at the ice-bed interface (e.g. Mair *et al.*, 2003).

2.5.2 Instrument development

The development of new instruments began to slow as these traditional instruments began to produce successful results in numerous investigations. However, Harrison *et al.* (2004) and Truffer and Harrison (2006), have been working to create a new instrument. They deployed a wireless probe within the deforming bed at Black Rapids Glacier, Alaska. It contained two micro-sensors – a pressure transducer and tilt meter (Harrison *et al.*, 2004). The probe communicated with a receiver placed a few meters above the ice-bed interface via radio waves. Records of almost a year were achieved by some probes, but (after the first 5 days) data were only recorded once a day (Harrison *et al.*, 2004; Truffer and Harrison, 2006). The ability to monitor more than one property in any given location is an improvement on traditional instruments. However, many transmissions were lost and the data that were collected were relayed to a logger at the glacier surface (Harrison *et al.*, 2004; Truffer and Harrison, 2006). This presents the same issues of manual data collection and wire breakage, as the traditional instruments. In addition, the probe was shaped as a long rod (61 cm; Harrison *et al.*, 2004), preventing it from behaving naturally within the deforming bed, in comparison to a clast, for example. The probe represents a recent development in borehole instrumentation. However, a greater frequency of data sampling and the inclusion of more micro-sensors would add to this instrument's capabilities.

2.6 Theoretical Foundation

This section will provide a foundation to the glaciological principles and concepts that are to be discussed in the following section (2.7), concerning the information that has been generated about the subglacial environment through the use of

traditional instruments (Table 2.1). This will focus on a basic outline of subglacial hydrological processes in relation to the deforming bed.

2.6.1 Subglacial drainage morphology

One of the core themes that persist in section 2.7 is the relationship between the glacier and changes in subglacial hydrology. Boreholes are classified according to their location above the hydrological drainage system and are referred to as either connected, unconnected or alternating (e.g. Murray and Clarke, 1995). This demonstrates that the subglacial drainage system varies spatially. The research of Gordon *et al.* (1998), Kavanaugh and Clarke (2001) and Mair *et al.* (2003) reveals that there are temporal changes in subglacial drainage. They report seasonal transitions in the morphology of the drainage system, which act to influence glacier dynamics. Through the use of dye tracer experiments, Nienow *et al.* (1998) demonstrate more fully how glacier motion can change in response to the evolution of the subglacial drainage system. This section will review the basics of seasonal drainage characteristics and subglacial drainage morphologies.

2.6.2 Connected, unconnected and alternating

The trends displayed by water pressure readings can provide an indication as to the nature and spatial distribution of the subglacial drainage system. Boreholes (and the subglacial environment) are classified as either connected, unconnected or alternating, according to instrument response. Traditionally, in connected regions, pressure transducers reveal elevated and highly fluctuating water pressures. In unconnected regions pressures are low and fluctuations minimal, as the dominant flow pathways occur through the underlying sediments (Murray and Clarke, 1995). Regions of the bed that show both connected and unconnected signals of water pressure have been termed as alternating. This is thought to occur when water pressures are sufficient to cause an expansion of the connected drainage system. The system encompasses a nearby, previously unconnected area, so that it becomes temporarily connected (Murray and Clarke, 1995). Figure 2.7 displays a conceptual model highlighting these classifications.

In the connected system melt water inputs and outputs are recorded, predominantly as diurnal fluctuations. This is because well developed subglacial drainage systems tend to have a significant source of melt water derived directly from surface inputs, via moulins, for example. As a result, there tends to be a correlation between external weather conditions (e.g. diurnal melt cycles) and trends in water pressure within connected drainage pathways (e.g. Fountain and Walder, 1998; Mair *et al.*, 2001, 2003). Mechanical interactions between the bed and the hydrological system should also be evident (e.g. Murray and Clarke, 1995). In contrast, the unconnected system will register minimal water pressures, with only minor fluctuations from independent sources at the ice-bed interface. Unconnected regions are thought to remain relatively inactive and thus, traditionally boreholes that appear to be unconnected tend not to be instrumented. The alternating regions of the bed will show a combination of both trends.

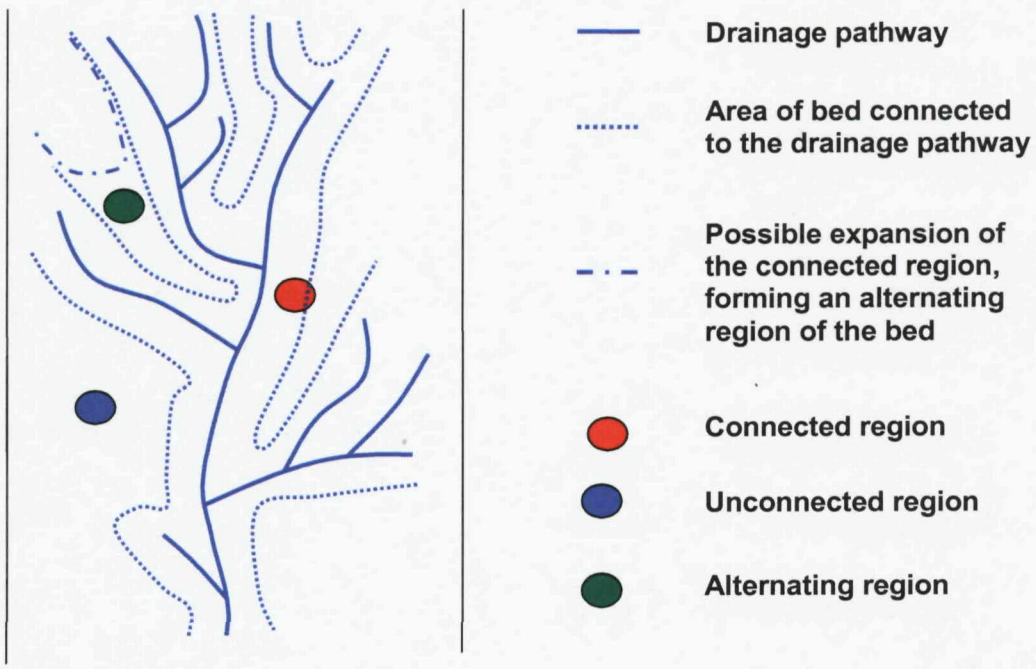


Figure 2.7: Conceptual model to show the locations of connected, unconnected and alternating regions of the bed within a hypothetical drainage system.

2.6.3 Seasonal drainage characteristics

In order to recognise the seasonal transition between a winter and a summer drainage regime, one first needs to recognise the characteristics of each. Research suggests that, traditionally, during the winter the glacial hydrological system shuts down. Declining external temperatures cause subglacial drainage routes (depending on size) to become reduced in size, or to close completely (Willis *et al.*, 1990). Melt water inputs decrease; both through a reduction in surface melt generated by thermal heating, and as rainfall is replaced by snowfall and the glacier becomes covered by a winter snow pack (ablation and accumulation zones). As melt water inputs and temperatures decrease frictional melting is reduced, until it becomes insufficient to maintain channel diameters (Benn and Evans, 1996). Channels then close as ice creep dominates. The winter drainage system produces a characteristic pressure record that shows continuously high pressures with little fluctuation (e.g. Kavanaugh and Clarke, 2001). This reflects a constricted drainage system with a low drainage capacity, in the absence of external inputs (Figure 2.8; Table 2.2).

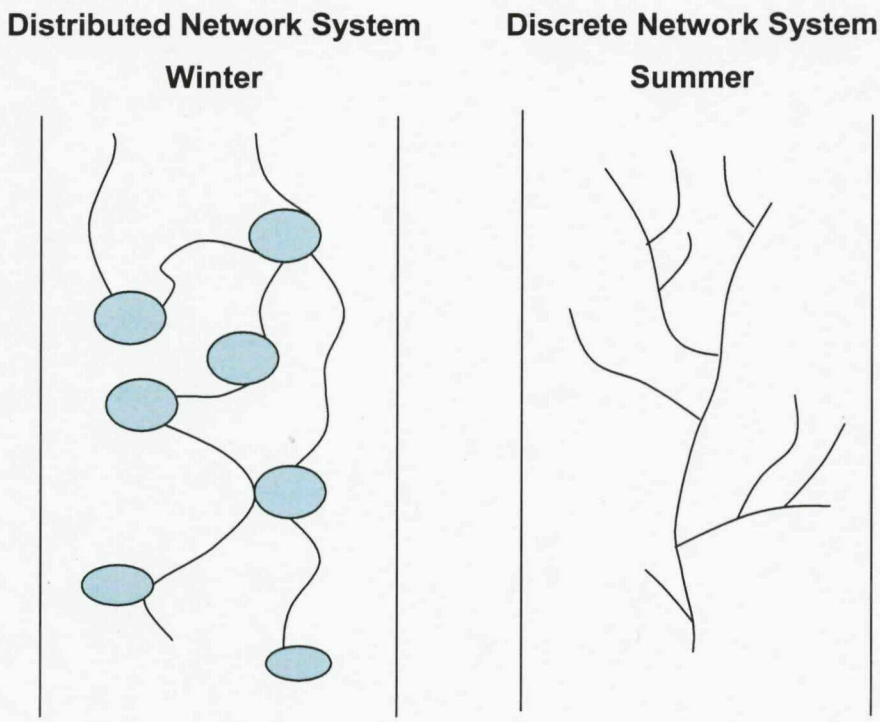


Figure 2.8: Conceptual model to highlight the differences between winter and summer drainage morphologies.

Table 2.2: Different drainage characteristics associated with winter and summer subglacial drainage regimes.

Winter	Summer
Poorly developed	Well developed
Hydraulically inefficient	Hydraulically efficient
Low capacity	High capacity
Continuous, non-fluctuating, high water pressures	Fluctuating water pressures

In contrast, summer drainage regimes reflect the opposite (Table 2.2). Daily variations in melt water generation, associated with incoming solar radiation, provide a continuous influx of melt water into the subglacial drainage system, which is augmented by rainfall events. This results in fluctuations, often diurnal in nature, within the water pressure record. Drainage routes become well connected and enlarged as external temperatures and the quantity of melt water inputs increase (e.g. Nienow *et al.*, 1998). High discharge, in combination with external temperatures, increases frictional melting and prevents channel closure by creep. The development of the subglacial drainage system is reflected by generally reduced but highly variable water pressures (Table 2.2). Even as the drainage capacity of the system increases fluctuations are common and large precipitation and melt events can result in pressure peaks in excess of winter values.

2.6.4 Subglacial drainage morphologies

The subglacial drainage system is referred to as heterogeneous due to its temporal and spatial variability. Drainage morphologies result from a combination of factors including: subglacial water discharge; basal thermal regime; geology (e.g. permeability); meteorological inputs; and basin (slope, roughness) and glacier (slope, depth, density) topography (Benn and Evans, 1996; Sharp *et al.*, 1993). Numerous studies involving dye tracing (e.g. Nienow *et al.*, 1998; Sharp *et al.*, 1993; Willis *et al.*, 1990) theoretical analyses (e.g. Walder and Fowler, 1994) and more recently drainage models (e.g. Clarke, 1996; Flowers and Clarke, 2000; Gordon *et al.*, 2001) have been employed to characterise subglacial drainage morphologies.

Two specific types of drainage system have been proposed: discrete and distributed (Figure 2.8). As the name suggests, drainage within discrete systems is carried out by a few well defined channels that allow rapid and efficient water transport (Benn and Evans, 1996). The dendritic channel network is the only discrete system proposed (Figure 2.9a). In a distributed system, drainage takes place over a much greater proportion of the bed (Figure 2.8) and a number of different flow morphologies can result from this (Figure 2.9b-h). The spatial extent of the distributed network results in an inefficient system that is poorly connected, forcing melt water to follow tortuous flow paths that are more difficult to predict (Benn and Evans, 1996).

Traditionally, water drainage within sediments occurs via three modes of pore-water flow: bulk movement, Darcian flow and pipe flow (Figure 2.9b,c,d). Pore-water flow is considered to be negligible within bedrock (with the exception of limestone), but potentially significant within sediments. The application of shear stress to subglacial sediments generates bulk movement water flows (Clarke, 1987); whilst hydraulic gradients cause water movement relative to mineral grains in the form of Darcian flow (Murray and Dowdeswell, 1992). The ability for water to flow through subglacial sediments by these mechanisms is described as the hydraulic conductivity (or diffusivity; Figure 2.2) (e.g. Boulton and Jones, 1979; Clarke, 1987; Fischer *et al.*, 1998; Freeze and Cherry, 1979; Murray and Porter, 2001; Paterson, 1994), which is calculated according to the equation:

$$K = \frac{\rho g \kappa}{\eta} \tag{7}$$

where: K is the hydraulic conductivity (ms^{-1}), ρ is the pressure of fluid in the pores, g is acceleration due to gravity (ms^{-1}), κ is the hydraulic permeability (m^2), and η is the viscosity of the fluid in pores (PaS at 0°C) (Paterson, 1994, p.160). According to this equation, hydraulic conductivity is dependent on the permeability (or porosity) and strain rate of subglacial sediments. Rates of conductivity will increase if sediments become dilated (i.e. porosity increases) (Clarke, 1987; Murray and Dowdeswell, 1992). Thus, unless sediments are coarse grained and highly sorted (e.g. previously fluvial), or pressure gradients are very high, Darcian flow is

characterised by low drainage rates (Boulton and Jones, 1979; Murray and Dowdeswell, 1992).

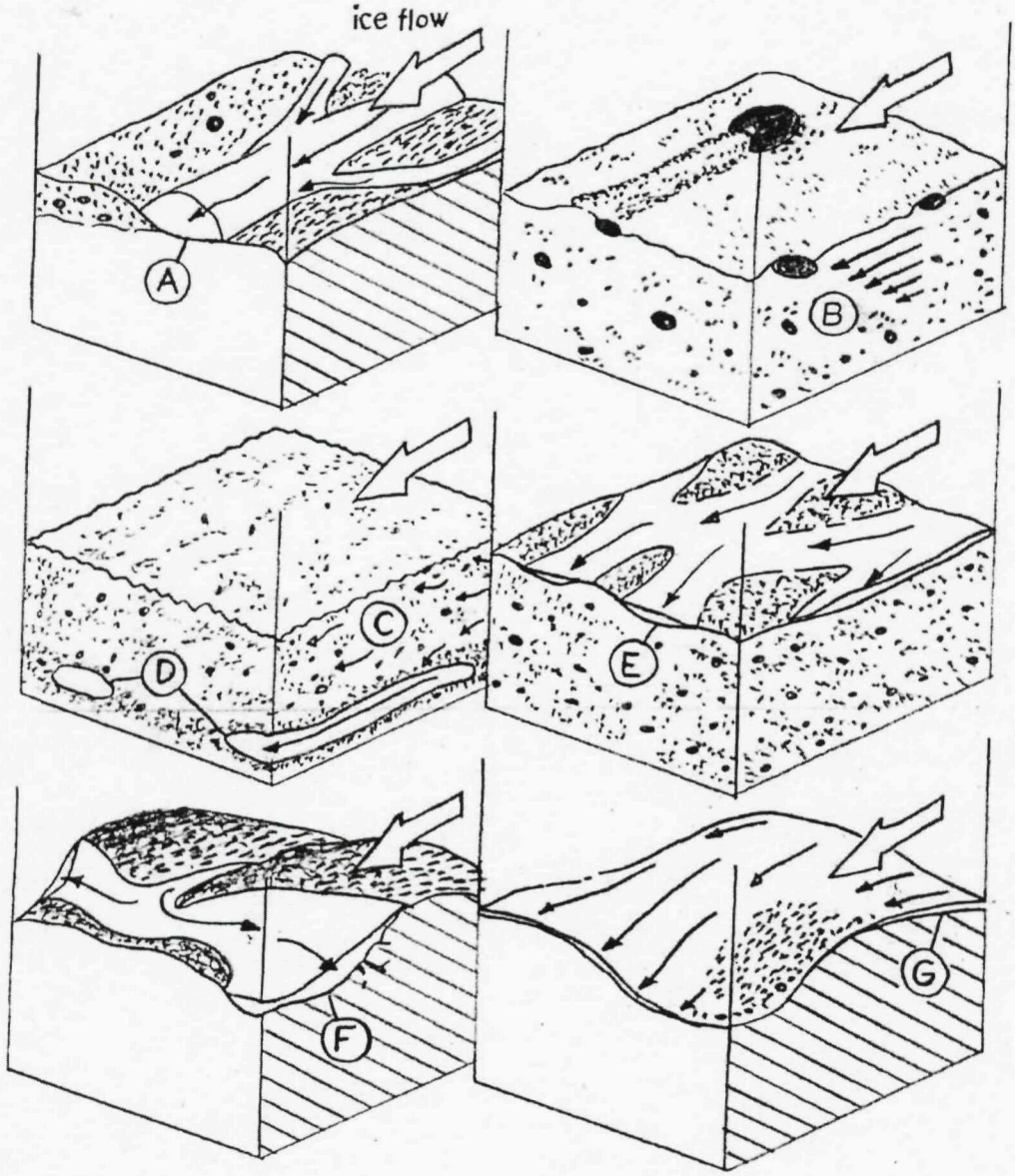


Figure 2.9: Subglacial flow pathways for discrete and distributed drainage systems over hard and deformable beds (adapted from Benn and Evans, 1996), showing: a) dendritic channel network; b) bulk water movement through subglacial sediments; c) Darcian flow of water through pore spaces in subglacial sediments; d) pipe flow, favoured through soluble (e.g. limestone) or unconsolidated subglacial sediments; e) braided canal network; f) linked cavity system; g, h) thin films or sheets of water. Note: the discrete system is characterised by (a), whereas the others (b-h) represent distributed drainage systems.

The low drainage capacity associated with pore-water flows can only be sustained whilst water influx into the subglacial hydrological system does not exceed the capacity of the subglacial sediments to drain that flow through the bed (Benn and Evans, 1996). In general, meltwater must escape by localised drainage at the glacier sole, because it is thought that subglacial drainage via Darcian flow is never sufficient to evacuate all the water (Walder and Fowler, 1994). Despite this, pore-water flows are important through their association with more efficient channelised flows at the ice-bed interface (e.g. Boulton and Hindmarsh, 1987; Hubbard *et al.*, 1995). It has become increasingly accepted that where water influxes exceed pore-water capacity the subglacial drainage system will convert to a more efficient drainage morphology (e.g. Nienow *et al.*, 1998; Willis *et al.*, 1990). Boulton and Hindmarsh (1987) propose that if pipe flow within sediments fails it is most likely to be substituted by drainage in the form of a dendritic channel network. However, wide spread in-field support for this is lacking. Consequently, one of the challenges of research into subglacial hydrology is to determine changes in the morphology of the subglacial drainage system and when and how these changes will occur.

Dendritic channel networks are discrete networks that can readily accommodate high water influxes (Figure 2.9a). Single peak arrival times in dye tracing experiments reflect an efficient centralised drainage system, without storage, providing evidence for dendritic drainage (e.g. Nienow, *et al.*, 1996, 1998; Willis *et al.*, 1990). This network consists of discrete channels that drain large areas of the glacier bed. These may be R-channels, which are cut into the overlying ice (Röthlisberger, 1972); or N-channels (Nye, 1973), which are cut into the bed.

R-channels tend to have lower pressures than the surrounding ice and are kept open against processes of ice creep through frictional heating by melt water (Röthlisberger, 1972). At times of high discharge channels become enlarged, but contract during periods of low water pressure. Low in-channel pressure allows larger R-channels to preferentially capture water from smaller ones at high pressures. Channel capture produces a characteristic dendritic (or arborescent) morphology (Benn and Evans, 1996; Figure 2.9a) where large low pressure channels are associated with high discharge. As a result, water flow tends to be centralised and fed by tributaries, except at the glacier snout where flow may be diverted from the

centre to the margin (Willis *et al.*, 1990). The effect of bed topography is very important within the subglacial environment where subglacial hydraulic potentials may be sufficient to allow channels to flow uphill and/or across slopes. In particular, descending flow can produce steeply arched channels (Benn and Evans, 1996). N-channels produce more consistent flows, in areas with steep gradients or uneven topography, where hydraulic gradient exerts a strong control. Channels tend to consistently follow the same flow paths and form single channel or braided networks (Benn and Evans, 1996). Tunnel valleys tend to form branching morphologies and are associated with the drainage of subglacial aquifers (Boulton and Hindmarsh, 1987).

The concept of braided canal networks (Figure 2.9e) was introduced by Clark and Walder (1994) and Walder and Fowler (1994), specifically for drainage over deformable beds. They argue that the formation of a channelised network from a thin film at the ice-bed interface is unstable. They propose that the formation of shallow, wide, ice-roofed canals cut into the till would create a more stable but less efficient drainage network (Walder and Fowler, 1994). The canals will form distributed, non-arborescent drainage networks where effective pressures and surface slopes are low (N = 1 bar; slope = 10^{-3}; e.g. ice sheets) and till is relatively clay rich (Clark and Walder, 1994). Conversely, they propose that R-channels will form where surface slopes and effective pressures are high (10^{-1}, e.g. valley glaciers; N>1 bar) and till is relatively clay poor. Their theory states that raised water pressures result in increases in discharge within the distributed canal network. In contrast, as water pressure decreases within R-channels discharge increases (Clark and Walder, 1994). The relationship between water pressures and discharge is steady state. Evidence within the geologic record is presented in support of this proposal. However, Walder and Fowler (1994, p.13),

> "emphasise that actual data on the geometry of the basal drainage system is practically nil".

That is to say, they have no direct in-field evidence for their proposed drainage system configuration. Consequently, this model should be considered with caution.

The morphology of linked cavity systems (Lilboutry, 1979; Figure 2.9f) creates tortuous flow routes resulting from poor drainage connections (orifices) and subglacial water storage (cavities) over bedrock surfaces. This is demonstrated in dye tracer experiments where the drainage morphology is characterised by multiple peaks as water drains inefficiently from the glacier bed (e.g. Willis *et al.*, 1990). Similar to R-channels, the size of cavities will increase and decrease in accordance with melt water inputs and effective pressure (Kamb, 1987). However, opposite to R-channels, when pressures are low, increases in water pressure result in increases in discharge capacity (i.e. at low pressures cavities will not 'capture' other cavities), preventing the formation of a dendritic network (Kamb, 1987). This stable system fails at high pressures when frictional ice-melting becomes the dominant process as discharge increases. Cavities then begin to enlarge through the same mechanism of channel capture experienced by R-channels. As fewer large cavities begin to dominate, the drainage system starts to reflect a more hydraulically efficient channelised network. This acts as a mechanism for subglacial drainage evolution or switching from inefficient braided to efficient conduit systems (e.g. Kamb *et al.*, 1985; Willis *et al.*, 1990).

Although some research has suggested that linked cavities can exist on deformable beds (Kamb, 1987; Walder and Fowler, 1994), this has not yet been widely documented or observed. However, it is important to recognise that where drainage is on a rigid bed the water discharge and pressure characteristics produced vary from those associated with deformable beds (Röthlisberger, 1972; Walder, 1986). As a result, investigations into the evolution of drainage networks beneath glaciers with deformable beds are important (e.g. Hubbard and Nienow, 1997; Nienow *et al.*, 1996; Sharp *et al.*, 1993; Willis *et al.*, 1990). However, a full classification that could act to categorise these differences has yet to be achieved, probably because the nature of drainage evolution over deformable beds is so complex.

Thin films and sheets of water occur at the ice-bed interface and are differentiated only by their thickness (Figure 2.9g, h). Water films generally relate to theories of glacier sliding and there is common agreement that a thin (mm) film of water will be produced at the bed of glaciers as a result of pressure melting. This film acts as a lubricant to sliding (Kamb and LaChappelle, 1964), but does not have the transport

capacity for large-scale drainage of the subglacial environment. Larger scale sheets of water (cm to m thick) have also been proposed (e.g. Shoemaker, 1992). However, continued research would suggest that sheets thicker than only a few millimetres could not be sustained under the ice, but would become unstable and form channels (Walder and Fowler, 1994).

The drainage configurations presented here provide a variety of mechanisms by which melt water can be evacuated from the glacier bed. The conditions of formation for each are subject to a variety of factors. Topography of both the ice surface and the glacier bed, for example, affects the hydraulic gradient of channels, and determines their flow path and thus morphology (e.g. braided vs. dendritic channel networks, Walder and Fowler, 1994). The geology of underlying sediments affects the flow of water through the till (e.g. pipe flow in limestone), which can affect the drainage capacity (i.e. porosity) and morphology of channels (e.g. dependence of braided networks on clay content). In addition, any variations in the physical nature of the glacial environment will be added to by temporal and spatial variability in meteorological inputs, which show even less short-term predictability. It is for these reasons that determining the spatial form and temporal changes of drainage over a deforming bed is challenging.

2.6.5 Hydrological parameters

Effective pressure (N) relates to the actual pressure that is in effect given the pore-water pressure, which will act to offset some of the applied ice overburden pressure. It is calculated according to the equation:

$$N = P_i - P_w \tag{8}$$

where: P_i is the ice overburden pressure (Equation [1]) and P_w is the measured pore-water pressure. Measured water pressures are often referred to in terms of effective pressure. However, in order to make comparisons between water pressures from different investigations, water pressures are often discussed as a percent of overburden. Overburden pressure (also known as flotation pressure) equates to the equivalent water pressure to the weight of the overlying ice. It represents the water

pressure threshold beyond which the ice would float. This has implications for mechanisms of glacier decoupling and sliding and is calculated as a percent of the glacier's measured overburden pressure (Equation [1]).

2.6.6 Hydro-mechanical interactions

The sections above have highlighted the spatial variability and heterogeneity that can characterise subglacial drainage systems. The nature of drainage morphology may vary and the flow pathways may be either connected or unconnected with surface inputs of melt water. In the same way the nature (or rheology) of the deforming bed may also show great spatial and temporal heterogeneity. Investigations have revealed that the deforming bed is characterised by a patchwork of strong and weak zones of till, which may move and vary in accordance with changes in external physical conditions. These changes tend to be initiated by variations in water pressure, suggesting that the relationship between the hydrological system and the deforming bed is complex and very important to mechanisms of basal motion (both sliding and deformation).

A theory of stick-slip motion has been developed to explain the relationship between sliding and deformation with respect to strong and weak areas of the deforming bed. Fischer and Clarke (1997) generated an elastic block model, incorporating aspects of basal ice mechanics (such as, ice rheology, basal stress and strain rates), to simplify glacier behaviour. Fischer *et al.* (1999) build on this idea, by incorporating data from ploughmeters into a model of 'sticky spots' to more fully incorporate mechanical processes within their hypothesis. The concept of sticky spots was perhaps first introduced by Alley (1993), as an area of the bed that can support relatively high basal shear stresses, in comparison to surrounding areas that are well lubricated and support a lower shear stress. Fischer *et al.* (1999) provide their own definition:

> "Sticky spots are localized regions of the bed where basal shear stress is concentrated and which balance some or all of the applied driving stress"
>
> (Fischer *et al.*, 1999, p.352).

In these regions, ice is strongly coupled to the underlying bed due to poor lubrication, whilst surrounding areas allow sliding to continue. In terms of mechanical properties, low water pressures generate a zone of increased basal drag or friction, with raised bed shear strength (Fischer *et al.*, 1999). Enhanced coupling between the glacier and subglacial sediment makes deformation more likely in these areas. These ideas are supported by Fischer *et al.*'s (1999) modelled results of ice flow over a bed with variable resistance to flow. The figures produced suggest that ice slows around a sticky spot and is diverted (continues to slide) around to areas of higher pressure, allowing ice flow to converge and accelerate again once behind the sticky spot (Fischer *et al.*, 1999). In time, strain builds up in the ice above the sticky spot. It is only when water pressures begin to rise above a threshold value that shear-strain rates decrease and the ice may lift and become decoupled from its bed (Fischer and Clarke, 1997). If the ice becomes decoupled the strain is suddenly released and drag is reduced limiting deformation, but increasing sliding in a previously 'sticky' region (Fischer *et al.*, 1999). This model highlights that the hydrological and mechanical properties of the subglacial environment are not uniform. Instead, the deforming bed presents a 3D mosaic of changing conditions in both time and space that makes monitoring and modelling this environment so complicated.

2.7 Experimentation with Traditional Instruments

The extensive use of traditional instruments in the last twenty years has provided a good foundation to our understanding of the properties (rheology) of the deforming bed and the basal processes that act to affect this layer both spatially and temporally. It is impossible to review the entire body of literature involving traditional instruments. As a result, this section will focus on the findings from five regions: Antarctica, Alaska, Canada, Switzerland, and Svalbard. This section will review the main findings derived from these studies to outline the basis for our current understanding of the deforming bed, its coupling to ice, and its role in the subglacial environment. The work undertaken in these regions is comprehensive, but this is by no means an exhaustive review. The theoretical foundations for many of the concepts discussed have been outlined in the previous section.

2.7.1 Antarctica

Antarctica is a continent synonymous with glaciation; notable for the rapid flow and instability of its ice sheets (Harrison *et al.*, 1993). Investigations into the contemporary and palaeo nature of the Antarctic continent are extensive and ongoing. Since the 1980s, many investigations concerning the subglacial zone in Antarctica have gathered data remotely, through the use of techniques such as seismic surveys (e.g. Smith, 1997) and radio-echo sounding (RES) (e.g. Gades *et al.*, 2000; Siegert *et al.*, 2004). Accessing the basal zone is most problematic in Antarctica, due to the depth of ice (>1 km), logistics and the physical environment. As a result, very little work involving traditional instruments has actually been carried out there. However, Antarctica is notable for inclusion due to the pioneering results that have been obtained by the few experiments that have been achieved.

Initially, a series of seismic surveys in the 1980s excited research into the nature of the subglacial environment of Antarctic ice sheets, particularly at Ice Stream B. Analysis of seismic reflections revealed landmark data, suggesting that a saturated and porous material was underlying the ice stream (Blankenship *et al.*, 1986). Calculations projected that the strength of this layer was insufficient to support the basal shear stress generated from the ice sheet above. Thus, it was likely that the layer was deforming under this force, and that ice stream motion was dominated by this process (Blankenship *et al.*, 1986). Subsequent papers by this group expanded on, the data sets retrieved, their analysis, and the evidence given for their conclusions (Alley *et al.*, 1987; Blankenship *et al.*, 1987; Rooney *et al.*, 1987). Alley *et al.* (1986) defend their hypothesis with three lines of evidence: till porosity, basal force balance, and water balance. This work outlined inferences about the rheology of till; and the implications of till and till deformation to ice sheet flow (Alley *et al.*, 1987). It came at a time when Boulton and Hindmarsh (1987) were publishing their work on subglacial sediment deformation from Breiðamerkurjökull.

In 1988 and 1989, Engelhardt *et al.* (1990) managed to drill to the base of Ice Stream B, in order to test the hypotheses set forward from the seismic surveys. Experiments investigated basal temperature profiles and water pressures and the sedimentology of the till. High basal water pressures were recorded, which would allow basal sliding to occur but could also promote the action of deformation, by lowering sediment

strength through water saturation (Engelhardt *et al.*, 1990). A high till porosity (~0.4) was recorded, indicating that the till had indeed experienced active shear deformation causing the till to dilate (Engelhardt *et al.*, 1990). In addition, calculations to determine the amount of melt water generated by the ice stream were insufficient to account for total glacier motion (Alley *et al.*, 1986). The occurrence of till deformation could account for this discrepancy in velocities.

The abundance of fossils originating from a variety of time frames found within sediment samples supported the process of deformation within the till (Engelhardt *et al.*, 1990). Tulaczyk *et al.* (1998) also analysed sediment samples from beneath Ice Stream B. They inferred the physical conditions of subglacial till formation and erosion, based on the textural and compositional characteristics of the sediment. They concluded that the deformation of weak fine-grained till did not result in significant comminution between grains. This could account for the preservation of the numerous fossils found by Engelhardt *et al.* (1990).

The insertion of instruments into the bed of ice streams is highly difficult, due to the depth of ice. However, Englehart and Kamb (1998) were able to insert a tethered stake (similar to the drag-spool) into the bed of Ice Stream B in order to monitor subglacial sliding. The relative proportion of sliding and deformation was calculated from the readings of obtained. Values varied from 75-100% sliding and 17-31% deformation. Overall sliding was deemed to represent an average of 83% of total motion, making it the dominant form of movement. This differed slightly from the inferences made by Alley *et al.* (1986) and Engelhardt *et al.* (1990). However, deformation was simply calculated as the difference between total ice motion and the motion recorded as sliding. In addition, only one stake was used in a single borehole.

These investigations produced pioneering data from the environment beneath Antarctic ice streams, with implications for glacier flow mechanisms. Despite the discovery of the deforming bed beneath Ice Stream B, the majority of subsequent investigations have concentrated on near surface motion (e.g. Harrison *et al.*, 1993), models of basal shear stress variations (e.g. Alley, 1993) and the subglacial hydrological system (e.g. Alley 1989; Engelhardt and Kamb, 1997). However, these

investigations have been used to make inferences about the subglacial environment. Experiments monitoring basal water pressures, for example, aimed to assess the role of the subglacial hydrological system at controlling basal sliding and bed deformation. This provided inferences about the stability of flow of these fast moving ice sheets (Engelhardt and Kamb, 1997). Thus, although relatively little *in situ* experimentation has been achieved in Antarctica, the data produced from this region have helped to drive investigations in other areas of the globe, where accessing the basal zone can be achieved more readily.

2.7.2 Alaska

In Alaska, investigations to examine the *in situ* strength of subglacial tills began in the late 80s and early 90s. The work of Humphrey *et al.* (1993) at Columbia Glacier, Alaska (a fast moving tidewater glacier) is of particular interest. During hot water drilling the tip of the drill stem became stuck and was dragged through the basal zone for five days before it could be extracted. The drill had been bent and subsequent examination of striations and the curve of the stem were used to infer the nature and strength of the subglacial sediment. The character and density of striations pointed towards a layer of till (up to 65 cm in depth) experiencing a constant rate of shear with depth (Humphrey *et al.*, 1993).

Measurement of the stem curve suggested that it had become suddenly lodged onto an obstacle at the bedrock-till interface. It was only when the stem had bent 18 cm that the obstacle was overcome and the drill was dragged down glacier through the underlying till (Humphrey *et al.*, 1993). Analysis of the forces required to curve the drill stem allowed models of both viscous and plastic till behaviour to be employed, in order to determine sediment strength. In the plastic model yield strength and effective viscosity were both less than that of basal shear stress. This implies that till was actively deforming beneath the ice and thus, contributing to glacier flow (Humphrey *et al.*, 1993). Humphrey *et al.* (1993) offer the simplest logical model to fit the results of their unique 'experiment'. However, they also demonstrate that, within reason, the data can be manipulated to fit a preferred theory. Despite this, the trapped drill stem has influenced the development of the ploughmeter (Fischer and

Clarke, 1994), which is currently used to determine the mechanical properties of the glacier bed.

Investigations examining subglacial sediment at Black Rapids Glacier, Alaska are also of interest, particularly due to the thickness of the till layer in this location. Black Rapids is a surge type glacier, underlain by up to 7 m of unconsolidated sediment. Experiments by Truffer *et al.* (2000) used borehole instrumentation and GPS to determine the relative contribution of basal motion to glacier velocity. Readings of surface motion and ice deformation indicated that 50-70% of glacier velocity occurred in the basal zone. However, readings from subglacial tilt sensors revealed minimal deformation within the top 2 m of till. In light of this, Truffer *et al.* (2000) propose that basal motion must occur at depths greater than 2 m, through either sediment movement along discrete shear planes, or via sliding of the entire till body across the underlying bedrock.

To confirm this, measurements of basal water pressure and pore-water pressure were also collected. Truffer *et al.* (2000) assumed that pressure fluctuations reflected variation in till pore-water pressures. They assumed that the upper layers of till will become stronger in the summer as effective pressures increase in response to the reduction in overall water pressures in a well developed summer hydrological drainage system. However, pore-water diffusivity changes with depth. As a result, effective pressures will be lower in the underlying till layers, producing weaker sediments in this zone (Truffer *et al.*, 2000).

If the shear load applied to the till is greater than the maximum effective pressure previously experienced by the till, then it is likely to fail. The zone of least maximum effective pressure was calculated to be at a depth of approximately 3.5 m (Truffer *et al.*, 2000). This line of weakness represents a shear zone and the depth at which the till is most likely to fail. The shear zone provides a mechanism by which till at depth can contribute to glacier flow. The tilt sensor readings are explained as the till moving as a discrete layer, without any significant internal deformation (Truffer *et al.*, 2000). The idea that the whole till body can slide over the bedrock is also supported by Cuffey and Alley (1996). The strength of till is also dependent on

sediment texture and investigations of glacial sedimentology support the scenario proposed (e.g. Hiemstra and van der Meer, 1997).

The till at Black Rapids is coarse and clast rich, which creates a texture that increases till strength and makes deformation less probable (Truffer *et al.*, 2000). Truffer *et al.* (2000) propose that the action of till sliding over bedrock, in addition to processes of plucking, results in sufficient erosion to generate the 7 m layer of till recorded. Indeed, Truffer *et al.* (2000) suggest that large-scale mobilisation of till in this way, could trigger the surges observed at Black Rapids. Further evidence for this is not discussed, but their work does highlight the importance of good constraints on till (and ice) rheology, when determining glacier flow mechanisms.

2.7.3 Trapridge Glacier, Canada

Extensive work was carried out by the University of British Columbia from 1989-1995 at Trapridge Glacier, Yukon Territory, Canada. Trapridge is a warm-based surge-type glacier underlain by unconsolidated sediments, up to 10 m deep (Fischer and Clarke, 1997). Processes of basal sliding and basal deformation may contribute to glacier movement and, in turn, both of these are influenced by subglacial hydrological system (Kavanaugh and Clarke, 2001). The main aim of the work carried out at Trapridge Glacier was to determine the nature of the subglacial hydrology, the mechanical properties of the glacier bed and the interactions between the two. Thus, in order to understand the controls on basal sliding and deformation, and the mechanisms that cause them to vary both spatially and temporally, the glacier was heavily instrumented over six years. In this time, measurements of water pressure, conductivity, turbidity, strain, and sliding rate were collected.

The nature of the subglacial hydrological system at Trapridge Glacier was found to be highly heterogeneous. Water pressure records revealed 'connected', 'unconnected', and 'alternating' regions of the glacier bed, which fluctuate from 'connected' to 'unconnected' (Murray and Clarke, 1995). Diurnal variations in water pressure in the connected regions were strongly out of phase (180°) with the disconnected regions. This anticorrelation suggests that the connected system was forcing water pressure in disconnected regions. Sporadic fluctuations in alternating

regions are explained as the result of large rises in water pressure occurring at nearby connected sites. These intermittent and large water pressures cause hydraulic jacking of the bed, and the subsequent temporary spatial expansion of connected areas into regions that were previously unconnected (Murray and Clark, 1995). The water pressure at which these switching events (from connected to unconnected, and vice versa) occurred did not have a given threshold value. Thus, the hydrological system was considered to be stochastic in nature (Murray and Clark, 1995).

The expansion of connected regions during high pressure events has further implications. Hydraulic uplift of the ice will initiate a transfer of ice overburden pressure from connected to unconnected regions. This results in a shift of mechanical support beneath the ice and a change in sediment porosity (Murray and Clarke, 1995). Consequently, the extension of a connected region initiates mechanical decoupling at the ice bed interface through the uplift of ice and the transfer of load. These responses (porosity and decoupling) are enhanced exponentially when the water pressure in the connected system increases from an already high steady pressure (Murray and Clarke, 1995). Thus, it becomes evident that the mechanical nature of the subglacial sediment, and the magnitude of changes it experiences, is coupled to variations in the hydrological system.

To further explore how these processes control the division between mechanisms of sliding and deformation at the ice bed interface, Fischer and Clarke (1997) describe comparisons between sliding rates and water pressures observed during the 1992 field season. Similarly, Fischer *et al.* (1999) discuss those same pressure trends in conjunction with data from ploughmeters, deployed in the same year. The ploughmeter (Fischer and Clarke, 1994) can be used to gather data concerning changes in the mechanical properties of the bed, to compliment those measurements of sliding variability collected by the drag-spool (Blake *et al.*, 1994). The ploughmeter showed variation in sediment strength according to changes in basal water pressure. Diurnal variations in sliding rates and ploughmeter responses correlated well with those of water pressure. The rates of sliding were greatest during rising, as opposed to peak, water pressure values; and whilst one ploughmeter was in phase with water pressure rises, another was exactly 180° out of phase. This

trend was explained according to Fischer and Clarke's (1997) and Fischer *et al.*'s (1999) elastic block model of stick-slip motion (section 2.6.6).

Data from the ploughmeters also suggest that as water pressures rose and the ice became decoupled, there was a transfer of load from the sticky spot onto surrounding regions. The redistribution of shear stress during a slip event accounted for the 180° out of phase trend observed in the second ploughmeter. High forces were experienced during periods of low pressure as a result of enhanced basal drag but forces were released during decoupling (high water pressure). This trend is similar to Murray and Clarke's (1995) explanation for 'alternating' water pressure signals and the associated load transfer with hydraulic jacking. Once the build-up of strain has been discharged, the elastic block model (Fischer and Clarke, 1997) indicates that any further increases in water pressure will have little affect on sliding rates. This accounts for peak sliding velocities during rising and not peak, water pressures. Again, the pressure threshold at which these events occur varied, demonstrating the individual nature of each slip event and the stochastic conditions under which they are produced (Fischer and Clarke, 1997).

The inclusion of ploughmeter data established the idea that there is a reorganisation of shear stress to surrounding areas during a high pressure event (Fischer *et al.*, 1999). If the expansion of connected regions of the glacier bed during periods of elevated pressure is taken into account (Murray and Clarke, 1995); it would be logical to assume that a similar reorganisation of the mechanical properties of the glacier bed also occurs at the same time. Kavanaugh and Clarke (2001) identify such phases of hydrological and mechanical reorganisation in response to a "spring event".

Spring is a critical time as the subglacial water system only has a low capacity as it has not yet fully established its summer drainage morphology. Thus, a large input of early season melt water can easily exceed current subglacial drainage capabilities. This may provoke hydrological and mechanical instability within the subglacial environment, namely a spring event (Kavanaugh and Clarke, 2001). At Trapridge, pressure transducers in connected boreholes showed two distinct modes during the spring: non-fluctuating and fluctuating (a diurnal signal).

The initial non-fluctuating mode is indicative of a winter hydrological system, where pressures are high and steady due to the poorly connected nature of the system and the lack of mobilised water (Kavanaugh and Clarke, 2001). The second mode, however, seems to occur in response to spring events. Phases of elevated air temperatures and high night time minimum temperatures generate an excess of melt water. This can force the hydrological system to expand and switch to a connected system in order to accommodate this anomalous input. Kavanaugh and Clarke (2001) recorded raised subglacial water pressures during a spring event, accompanied by an increase in strain within the till. The response of the ploughmeters suggested that high water pressures caused the ice to decouple from a previously sticky spot at the glacier bed (Kavanaugh and Clarke, 2001). Basal stresses were transferred to peripheral regions (rising ploughmeter readings) and increased lubrication of the bed precipitated rapid glacier movement in this area. These spring events demonstrate the ability of the glacier system to efficiently resolve both mechanical and hydrological instabilities at its bed, through a series of feedback mechanisms.

Fischer and Clarke (2001) summarise much of the work highlighted here. They emphasise the spatial and temporal heterogeneity evident in the data collected at Trapridge Glacier. The work yielded by Clarke and co-workers has provided both empirical and conceptual frameworks to explain the processes of mechanical and hydrological coupling at the ice-bed interface. The concept of sticky spots producing stick-slip motion beneath the ice emphasises the spatial and temporal variability of subglacial conditions (Fischer and Clarke, 1997; Fischer *et al.*, 1999). Processes of sliding and deformation are not continuous, but respond to an increase (deformation) or a decrease (sliding) in ice-bed coupling, resulting from changes in the hydrological and mechanical properties of the subglacial environment (Fischer and Clarke, 2001).

2.7.4 Haut Glacier d'Arolla, Switzerland

A comprehensive body of literature has been derived from investigations at the Haut Glacier d'Arolla, a temperate valley glacier in Switzerland. This has involved joint contributions since 1989 from a variety of Research Institutes and Universities

globally (e.g. Hubbard *et al.*, 1995). The majority of early literature examines patterns of water circulation and water quality within the hydrological system; and some of the trends identified can be related to the findings of others (e.g. Murray and Clarke, 1995; Trapridge Glacier).

Hubbard *et al.* (1995), identified diurnal pressure patterns in the late melt season comparable with the 'fluctuating' mode recorded in boreholes dissecting a connected subglacial channel system at Trapridge Glacier (Kavanaugh and Clarke, 2001). The diurnal pressure signal was located above a well established subglacial channel or variable pressure axis (VPA). Hubbard *et al.* (1995) noted that this signal decreased with distance away from the VPA. This implies that the channel occupied a relatively limited zone, encompassed by a more widespread, less hydraulically efficient, distributed drainage system (Hubbard *et al.*, 1995). This hydraulic gradient was also related to spatial variations in subglacial sediment texture derived from turbidity and conductivity readings. High pressures during the day forced water along a pressure gradient from the VPA into the distributed system. In contrast, low night time pressures reverse the gradient and allowed water to re-enter the channel bringing with it sediment fines. This causes eluviation of the sediment closest to the subglacial channel and has implications for, sediment texture, porosity and permeability, and glacier bed erosion (Hubbard *et al.*, 1995). Again, this process decreased with distance away from the VPA.

Gordon *et al.* (1998) explore seasonal changes in the drainage system, referring to fluctuations of 'water level' in substitution of the term 'basal water pressure'. Boreholes showed poorly coordinated fluctuations in water level with weak diurnal signals, even when 'connected' to the drainage system. In this instance, variations appeared to be the result of forcing from supraglacial and englacial sources, as opposed to basal regimes (Gordon *et al.*, 1998). The chaotic and minimal water level fluctuations observed by Gordon *et al.* (1998) may reflect a sticky spot, where the drainage system is poorly developed and the glacier is strongly coupled to the bed. It is unfortunate that measurements of sediment strength or deformation do not accompany their results. Such readings would clarify this point and enable comparisons with the findings of Fischer and Clarke (1997) and Fischer *et al.* (1999).

Gordon *et al.* (1998) also recorded a dramatic change in the characteristics of water level trends, following a high volume melt event. New, pronounced, diurnal fluctuations implied that the drainage system had become reorganised into a more hydraulically efficient, connected drainage system. This is similar to the drainage redistributions predicted during spring events by Kavanaugh and Clarke (2001). In addition, anticorrelated fluctuations (offset by 180°) were observed between some boreholes. This kind of relationship was highlighted by Murray and Clarke (1995) and implies that some regions of the bed had become connected to a well-developed drainage system, whilst others remained unconnected (anticorrelated).

In more recent literature research focused on the interactions between subglacial hydrology and the deformation of subglacial sediments. Mair *et al.* (2003) recognised the need to combine hydrological parameters with measurements of surface ice flow and basal mechanics, in order to understand more fully the way these processes interact in both time and space. In addition to pressure transducers, ploughmeters and tilt meters were also deployed to measure sediment strength and strain rates (deformation), respectively. The use of flow markers to monitor surface motion highlighted the onset of speed-up events, as well as spatial variations in glacier flow that are often linked to spring events (e.g. Kavanaugh and Clarke, 2001).

Mair *et al.* (2003) report two distinct trends in glacier motion based on observations of three spring events recorded in 1998 and 1999. The first trend observed in instrument readings was the initial spring event of each season. Increased water input into an inefficient drainage system resulted in high pressures and reduced strain rates (Mair *et al.*, 2003). Surface velocities indicated that ice motion was trending towards a primary subglacial channel, the VPA (Hubbard *et al.*, 1995; Gordon *et al.*, 1998). The reduction in strain rates (deformation) but coincident increase in velocity suggested that the ice decoupled from its bed. High water pressures resulted in enhanced sliding and a reduction in deformation, supporting the idea of a stick-slip mechanism of movement in this area (Fischer and Clarke, 1997; Mair *et al.*, 2003).

The second trend was associated with a subsequent spring event, recorded in 1998. Areas of both raised and steady water pressures were observed. High pressure zones indicated decoupling of the ice from its bed, whilst those with lower pressures were

coincident with increases in strain rate recorded by tilt sensors. Enhanced deformation in these areas of low pressure suggests strong ice-bed coupling. This may be explained by decoupling elsewhere, resulting in the transfer of mechanical support from those zones of high pressure to surrounding regions. This would lead to enhanced basal shear stress within peripheral regions of the VPA, increasing coupling and deformation rates. Elevated strain rates were restricted to the top ~8 cm of subglacial sediment, marking this as the active zone of deformation. Observation of this second 1998 spring event is of particular value. It demonstrates the variable nature of flow events in response to similar hydrological triggers. This event was initiated by melt, as was the 1999 event; whereas the first 1998 event resulted from rainstorms (Mair *et al.*, 2003). This may have occurred if the hydrological changes induced by the first spring event of the season had a lasting effect. Erosion and channel formation created by the first event may have left a more efficient drainage system, so that the next episode of high melt saw reduced high pressure events, confined to a smaller area of the bed (Mair *et al.*, 2003)

2.7.5 Svalbard

Murray, Porter and co workers, for example, have carried out a range of investigations at Bakaninbreen, Spitsbergen, Svalbard. Again, traditional instruments were used to investigate the rheology of till and its relationship with subglacial hydrology. Bakaninbreen is a surge-type glacier resting on a bed of unconsolidated sediments (~0.5 m deep). It was experiencing a prolonged surge phase during the time of experimentation: 1995-1996 (Porter and Murray, 2001). The work of Porter *et al.* (1997) focused around a surge front and measurements were concentrated up and down glacier of this feature. Ploughmeters were used to determine sediment yield strength, which ranged from 16.6-87.5 kPa. Comparisons between sediment yield strength and calculated values of basal shear stress (according to the equation by Kamb and Echelmeyer, 1986) were then used to identify areas of basal sediment that were likely to be deforming.

Up-glacier (but not down glacier) shear stress exceeded the yield strength of sediments implying that they are likely to be deforming in this location (Porter *et al.*, 1997). Similar to Fischer and Clarke (1994), Porter *et al.* (1997) suggest that the

saw-tooth pattern of force readings indicated that the ploughmeter was being dragged through a coarse-grained bed material. Elevated force readings up glacier also suggested that sliding was enhanced in this area, a theory supported by drag spool measurements. In contrast, only gradual increases in force were recorded down ice. Porter *et al.*, (1997) suggest that this steady response was the result of the surge front moving down ice, gradually increasing sliding velocities and changing till properties. Murray and Porter (2001) and Porter and Murray (2001) incorporated measurements of basal hydrology into their interpretation of till response. Deformation and pore-water pressures were measured with tilt sensors (strain rate) and pressure transducers (inserted into the till), respectively. Water pressures were generally high both up and down glacier implying that the glacier bed was poorly drained (Murray and Porter, 2001). There were more rapid fluctuations and a greater range of pressures observed down glacier, but the absence of a diurnal signal within the results indicated that surface water did not reach the bed (Murray and Porter, 2001). In addition, comparisons between water pressure and pore-water pressure revealed interesting results. Although large-scale peaks and troughs were shared between data sets, pore-water pressure revealed greater fine-scale fluctuations (Porter and Murray, 2001).

In terms of till properties, similar to the force measurements of Porter *et al.*, (1997), strain rates were an order of magnitude greater up glacier than down glacier. This supports the idea that the greatest amount of deformation was occurring in the till up glacier of the surge front (Porter *et al.*, 1997). Those tilt cells closest to the ice bed interface also recorded more elevated strain rates than those located deeper in the till. This indicated that the surface layers (0.1-0.2m) were more active and ready to deform, than those at depth (Porter and Murray, 2001). Despite this, the proportion of glacier motion attributed to deformation was very low. Porter and Murray (2001) found evidence that less than 10% of glacier motion originated in the till. They also tried to calculate the viscosity of till (Equation [5]) based on measurements of strain rate and basal shear stress. However, the anomalous nature of their results indicated that other mechanisms were actively resisting basal shear stress; and that till viscosity, whilst contributing to this, did not solely control the rate of flow (Porter and Murray, 2001).

Measurements of water pressure and pore-water pressure were also used to investigate the hydrological properties of the till. Till diffusivity is a measure of the rate at which water, and thus pressure, is transferred throughout the sediment and to other regions of the bed (Porter and Murray, 2001). There is a lag between the peaks and troughs recorded in water pressure (boreholes) and those recorded in pore-water pressure (till) at Bakaninbreen. This would suggest that water pressure, acting in response to changes in the hydrological system, forces variations in pore-water pressure within the till (Porter and Murray, 2001). However, pressure values are likely to be localised, recording only spatially constricted variations (Porter and Murray, 2001).

Murray and Porter (2001) examine the patterns of force (ploughmeter records) reported by Porter *et al.* (1997), in relation to patterns of water pressure described by Porter and Murray (2001). Their analysis suggests a poor correlation between these two factors, in opposition to the assumption that basal mechanics respond to fluctuations in basal hydrology. On the few occasions when a strong correlation does exist, high water pressure is associated with strong forcing, in opposition to trends found elsewhere (e.g. Fischer *et al.*, 1999). As a result, Murray and Porter (2001) conclude that the forcing recorded at Bakaninbreen is more likely to be the result of changes in till granulometry or variations in the degree of ice-bed coupling.

The data described above demonstrate complicated associations between basal hydrology and bed mechanics. However, the trends determined from Bakaninbreen may also be influenced by the polythermal nature of the ice. The till was also shown to exhibit cryogenic properties up glacier. A warm till layer (~0.2m) overlies a frozen permafrost layer, which dominates the till down glacier (Murray and Porter, 2001). Yield strength increases down glacier where the bed is cold, whilst sliding and deformation rates are reduced. In light of these findings, Murray and Porter (2001) conclude that the surge mechanism at Bakaninbreen is thermally regulated. This emphasises that other factors, or localised anomalies, such as thermal regulation, can act to influence subglacial interactions. Thus, the explanations given in the literature concerning the mechanisms of the glacier bed have the potential to be site specific.

2.7.6 Summary

This section has highlighted a wide range of glacial investigations (Table 2.3) that have been carried out on a variety of glaciers globally (Table 2.4), with extensive use of traditional instruments (Table 2.1). These techniques, in combination with hot water drilling, have accelerated data collection and greatly enhanced our understanding of the glacier bed. Early experimentation was used to make inferences about the sedimentology and strength of till *in situ*, suggesting the depth at which till is active. Following this, greater attention was given to the importance of basal motion contributions to surface velocities. The relative contributions of sliding and deformation have been calculated more accurately through the use of combined measurements of ice deformation and surface motion.

As more information was gathered about the properties of subglacial till, and models of till rheology were developed; the incorporation of subglacial hydrology and its interaction with the subglacial bed has become prevalent within investigations. This has yielded numerous important proposals concerning: the 'connected' and 'disconnected' nature of hydrological systems; the ability of water pressure to decouple the ice from its bed; the transfer of load from one region of the bed to another; the existence of sticky spots and their relation to models of stick-slip movement; the effect of seasonal reorganisation of the subglacial hydrological system during spring events; and associated periods of enhanced glacier motion.

The investigations reviewed in this section have shown continued progression in our understanding of the mechanisms that control the deforming bed, the properties of the deforming bed, and the factors that cause these characteristics to vary both spatially and temporarily. However, uncertainties about the deforming bed continue. An agreed rheology for till has not yet been achieved. This has hindered the production of flow laws for till which are crucial to assessing the stability of ice masses and modelling ice sheet behaviour. In addition, great variability is found between glaciers. The relationship between water pressure and till strength found by Murray and Porter (2001), for example, contrasted with that found by Fischer *et al.* (1999), suggesting that there is still much to be learnt about the hydro-mechanical processes operating between the deforming bed and the ice above. The variety of factors that influence the nature of the subglacial environment and the inherent

variability of the factors themselves (e.g. melt events) emphasises that the deforming bed is a very complex system that still requires greater understanding. This investigation aims to consider many of the aspects of subglacial hydrology and till mechanics summarised here.

Table 2.3: Summary of the subglacial *in situ* studies carried out on a variety of glaciers globally in accordance with the investigations discussed within this chapter.

Study	Location	Time Scale	Area	Reference
Hydrology and rheology	Trapridge, Canada	July1990-95	20,000 m^2	Kavanaugh and Clark, 2001
Conductivity and turbidity	Trapridge, Canada	1989 – 1991 JD 188-220		Stone *et al.*, 1993
Sliding	Trapridge, Canada	1990-1992		Blake *et al.*, 1994
Rheology – ploughmeter (effective viscosity)	Trapridge, Canada	1991		Fischer and Clarke, 1994
Hydrology and rheology	Trapridge, Canada	1992 (1989-1995)	70 boreholes	Murray and Clarke, 1995
Conductivity and turbidity	Trapridge, Canada	1990		Stone and Clarke, 1996
Sliding (stick-slip)	Trapridge, Canada	1992		Fischer and Clarke, 1997
Strain and hydrology	Trapridge, Canada	July 1992	~10 m study site diameter	Fischer *et al.*, 1999
Hydro-mechanical coupling	Trapridge, Canada	Review		Fischer and Clarke, 2001
Water pressure, subglacial drainage	Arolla, Switzerland	1993 (from 1989)	6.33 km^2 glacier	Hubbard *et al.*, 1995
Subglacial drainage, pressure, turbidity, conductivity	Arolla, Switzerland	July – August 1993	250 x 50 m 24 boreholes	Gordon *et al.*, 1998
Spring events, hydrology, velocity	Arolla, Switzerland	1998-1999		Mair *et al.*, 2003
Sediment strength, water pressure, turbidity	Columbia Glacier, Alaska		1,100 km^2 5 boreholes ~5 m apart	Humphrey *et al.*, 1993
Surface motion, sliding, pressure, ice and sediment deformation	Black Rapids Glacier, Alaska	1997 > 1 year of data		Truffer *et al.*, 2000
Sediment strength	Variegated Glacier, Alaska	~1981-82 (surge 82-3)		Richards, 1988
Deformation and pressure	Black Rapids Glacier, Alaska	2002		Harrison *et al.*, 2004
Deformation, surge, properties of till	Bakaninbreen, Svalbard	1994-95 to 2000		Porter *et al.*, 1997
Rheology, hydrology, deformation,	Bakaninbreen, Svalbard	1995-2000		Porter and Murray, 2001
Basal conditions	Bakaninbreen	1994-2000		Murray and Porter, 2001

Table 2.4: Details of the glacier types and locations discussed in this chapter.

Name	Location	Type	Authors
Columbia Glacier	Alaska	Fast moving, tidewater	Humphrey *et al.*, 1993
Black Rapids Glacier	Central Alaska Range	Surge-type (1936/37)	Truffer *et al.*, 2000
Variegated Glacier	Alaska	Surge-type (1982/83)	Kamb *et al.*, 1985; Richards, 1988
Trapridge Glacier	Yukon Territory, Canada	Surge-type	e.g. Fischer and Clarke, 1997
Haut Glacier d'Arolla	Switzerland	Valley glacier	e.g. Hubbard *et al.*, 1995
Bakaninbreen	Spitsbergen, Svalbard	Surge-type (1985-86; 1995-96)	e.g. Porter *et al.*, 1997

2.8 Methodological Constraints

The previous section has highlighted areas of uncertainty within current research into the deforming bed. The ability to generate robust hypotheses and models is closely linked to the quality and quantity of data that can be gathered from the environment of study. In this area of glaciology, it is increasingly obvious that the limitations associated with models of the deforming bed and ice-bed interactions may be the result of constraints on instrument design.

The difficulties associated with accessing the glacier bed and designing instruments that can monitor the subglacial environment is a challenging aspect of glaciological research. New designs for instrumentation were rapidly produced in the 1990s in accordance with the paradigm shift in research (e.g. Blake *et al.*, 1992, 1994; Fischer and Clarke, 1994). In the context of research, the development of these instruments is still within their infancy (Hart and Rose, 2001). They allowed the glacier bed to be accessed directly from the surface, and enabled instruments to be emplaced directly within the till. Experimentation of this kind provided the benefits of direct observation to establish temporal changes. However, a number of limitations are associated with these techniques. It is now evident that the restricted capabilities and the delicate nature of these instruments combine to hinder the accuracy, duration and breadth of data collected from the subglacial environment.

Tunnelling at the glacier bed is not only difficult, but also very dangerous (e.g. the experiences of Boulton and co-workers; Boulton and Hindmarsh, 1987). The use of hot water drilling is an efficient and much more effective means of accessing the glacier bed. However, boreholes may trigger a change in state at the ice-bed interface as hot water, under high pressure, is used to melt the ice. The process of drilling can disturb and excavate subglacial sediments to a scale of several decimetres (Blake *et al.*, 1992) and lead to thermal interference at the ice-bed interface. This general disruption and warming of the bed may influence results, so that a period of adjustment must be accounted for following initial instrument insertion (Murray and Porter, 2001). The curvature of boreholes, as an artefact of the drilling process, also presents deployment uncertainties that can be overcome, in part, by borehole inclinometer measurements (Blake and Clarke, 1992; Harbor *et al.*, 1997).

Common to each traditional instrument is that they are tethered with a cable that connects to a data logger at the glacier surface. It is generally acknowledged within environmental process research that the act of monitoring can, in itself, disturb the environment in question. The instrument wires, for example, can interfere with the behaviour of the instrument at the bed by constricting movement (Blake *et al.*, 1992). In addition, if the wire is damaged in the borehole this could disrupt or cause instrument failure, resulting in the loss of some or all of the data. However, allowing slack to be left in the boreholes can help to offset this difficulty (Blake *et al.*, 1992). The fragility of the instruments is also of importance. The process of emplacing the instruments at the glacier bed, as well as the adverse conditions at the ice-bed interface, ensures a high probability of mechanical instrument failure (Mair *et al.*, 2003; Stone and Clarke, 1996). This limits the amount (temporal extent) of meaningful data that can be collected and often results in reduced spatial coverage of these instruments. Fischer and Clarke (2001), for example, note that their instruments were constricted to an area of approximately 10 m^2.

The time over which data are collected also tends to be limited to the summer months. This is often because data have to be retrieved manually from the loggers at the glacier surface. Systems are often not robust enough to winter on the ice surface, preventing seasonal monitoring of glaciers (Fischer and Clarke, 2001). A notable

exception to this is the work of Murray, Porter and co-workers, who produced an approximately 4 year record of subglacial conditions at Bakaninbreen from an array of boreholes. However, the fact that data have to be retrieved manually means that there is no way of monitoring the system. A fault may occur, for example, the day after the system has been left, resulting in a significant loss of data. This cannot be determined without visiting the site again in person, which can be costly and inefficient.

There is also a variety of limitations specific to each instrument. The drag spool is very delicate and the spool can easily be unravelled prior to insertion at the glacier bed (Blake *et al.*, 1994). As the string is only paid out and not let back in, any string release would create a delay period following insertion (Murray and Porter, 2001). In this time the ice must slide sufficiently for the string to become taught again, enabling any further string pay out to be registered by the potentiometer. This represents a loss of data that may be problematic when the duration of monitoring is limited to the provision of string within the casing and the survival of the instrument at the glacier bed. The maximum survival time of an instrument for Blake *et al.* (1994) was three to five weeks. During instrument insertion it is also difficult to determine how deep the anchor has been inserted into the till and if it is sufficiently stuck fast. Consequently, the string pay out provides an upper limit for the amount of sliding (Fischer and Clarke, 2001). The anchor may plough through the sediment and the drag spool is unable to differentiate between sliding and ploughing (deformation). In an extreme case, where total glacier motion occurs via deformation of subglacial sediments, this movement would all be recorded as sliding by the drag-spool (Murray and Porter, 2001). Despite this the drag-spool is still the most effective way of measuring glacier sliding *in situ*.

Tilt sensors share some of the same problems. Difficulties may arise when trying to insert the cells into the till and maintain water tight instrument integrity. The depth of insertion may be difficult to assess and the cells may fall over if the cable in the borehole is slack during deployment (Blake *et al.*, 1992). In addition, movement associated with the wire tether and thermoelastic deformation in the initial stages of experimentation, may create noise within the data record (Bonaccorso *et al.*, 1999). The scale at which deformation within the till can be measured by the tilt cells is also

relatively limited. The cells only measure deformation at a scale comparable to large clasts, which may be problematic considering the heterogeneous nature of subglacial sediments (Blake *et al.*, 1992). The ploughmeter is a relatively robust instrument. The dominant uncertainties lie in relating variations in force to activity within the deforming bed. The deformation of material around the ploughmeter as it is dragged though the till can affect calculations of till properties (Fischer and Clarke, 1994, 1997b). The movement of the ploughmeter through underlying sediments can also cause pressure melting on the ice wall of the borehole. This can create additional movement via regelation, which would affect the results recorded (Fischer and Clarke, 1994).

Pressure transducers are designed to measure changes in water pressure (Hodge, 1976). They operate under the assumption that any trends recorded are the result of variations in the subglacial hydrological system (Gordon *et al.*, 2001). However, it is well documented that a change in water pressure can occur as the subglacial hydrological system adjusts to the input of fresh water from the drill and the release of ice pressure in this area. In temperate glaciers, it is also common for boreholes to remain open past drilling (Gordon *et al.*, 2001). As a result, trends in water pressure may be disturbed by supra or englacial water joining subglacial channels via open boreholes (Fountain and Walder, 1998; Stone and Clarke, 1996). Consequently, readings should be interpreted with consideration of the depth of ice and the length of the water column in the borehole above the sensor (Mair *et al.*, 2003).

These factors, in combination with uncertainties about basal conditions, hinder our ability to interpret the data sets generated by these instruments with confidence. Reliable field experiments are crucial in order to develop glacial theory on the subglacial environment and verify models and lab experiments of till rheology. It is easy to criticise failings in current instrumentation, but it is well known that they have produced a large range of data concerning the subglacial environment. However, further instrument development is crucial to continue improving the quality, quantity and reliability of data obtained *in situ* from the subglacial environment. As such, it would seem logical to consider the development of, and approaches to, subglacial instruments further, in light of the limitations that investigations to date have highlighted.

2.8.1 Criteria for a new instrument

Instruments should be designed to mimic their natural environment as closely as possible by causing minimal interference within that environment. Borehole drilling, despite the above mentioned limitations, is still the most efficient means by which the glacier bed can be accessed. It is also less invasive than tunnelling and is not restricted to glacier margins. As a result, an instrument designed to be emplaced at the ice-bed interface via boreholes would still be of benefit. However, it should not require wires to tether it and allow it to communicate data with the surface. The ability to do this wire-free would enable the instrument to behave more naturally within the subglacial environment and allow it to become readily incorporated into the till. The excavation of subglacial sediments beneath the borehole by the drilling process (Blake *et al.*, 1992) would aid in this process. It would also need to be robust enough to withstand crushing conditions at the ice-bed interface to prevent numerous instrument failures.

Ideally, the instrument would measure a variety of parameters relating to those traditionally collected, namely: water pressure, sediment strength, and strain rates. The inclusion of conductivity and/or turbidity meters would also be of benefit for comparison with pressure readings (e.g. Gordon *et al.*, 1998). In their work, Murray *et al.* (2000) measured the temperature profile of a borehole, but not the underlying till. The inclusion of a temperature sensor within the instrument could provide added information about conditions within the deforming bed. This might be particularly useful when monitoring the subglacial conditions of polythermal glaciers (e.g. Murray and Porter, 2001). The combination of sensors within one instrument would allow comparison of parameters in the same location, as opposed to linked observations between boreholes. However, the ability to measure basal velocities (i.e. sliding and/or deformation) in combination with deformation would perhaps be more complicated. It would require an instrument positioning system of some kind, relating instrument movement to net glacier surface velocities.

The ability to collect, store and communicate data over large time spans, namely a year or more, would be necessary to build a complete picture of annual changes in glacier activity. The ability to monitor the system remotely would also present a great advantage. This would allow any failures to be assessed immediately and

allow data interpretation to occur on a continuous basis. It could also reduce the need for costly return visits to field sites. This would require a complex system for retrieving instrument data, and maintaining a system within a potentially remote hostile environment. Monitoring capabilities over a large spatial area would be advantageous, requiring the instrument to be easy to transport and relatively cheap, to allow for the production of numerous replicas. Traditional instruments have been used on alpine and coastal glaciers, as well as on ice sheets in Antarctica. As a result, the new instrument should also be easy to deploy, widely available and applicable for use under a variety of ice masses.

At the outset, the above discussion has highlighted a very demanding set of requirements for an instrument, given the inaccessible, hazardous and heterogeneous nature of the subglacial environment. It requires a completely new approach to methodological design within glaciology, but it is the primary aim of this research to develop a new instrument that is capable of investigating the deforming glacier bed. In order to meet as many of the above requirements as possible, this project has collaborated with the department of Electronics and Computer Science (ECS) at the University of Southampton. New and innovative technology within the field of Micro Electro-Mechanical systems (MEMs) can been used to develop an instrument designed to fulfil the above criteria where possible; whilst the application of an Environment Sensor Network (ESN) can enable long term wireless communications and data transfer.

2.8.2 MEMs and ESNs

Environmental monitoring is a long-standing procedure and the basis of experimentation in many research fields, including glaciology. At its simplest monitoring can consist of measuring barometric pressure with a paper plotter. However, with recent advances in technology environmental monitoring projects have begun to evolve rapidly. The 21st century has seen an enormous growth in the miniaturisation of technology (Gharavi and Kumar, 2003). MEM devices only centimetres (or less) in size are becoming more widespread, and in recent years environmental monitoring projects have begun to incorporate MEMs within an ESN.

In an environmental setting, microsensor devices for light, temperature and pressure, for example, may be put to good use (Gharavi and Kumar, 2003).

MEMs have been developed in conjunction with both processing and communication technology. Sensors are becoming smaller whilst still maintaining or increasing processing power (Gharawi and Kumar, 2003), and minimising power use (Chong and Kumar, 2003). Developments in global positioning systems (GPS), short range radio, and optical communications enable sensors to be located geographically and allow fluent transfer of data. It is almost at the stage where the programming required to operate these sensors cannot keep up with the rate of advance in hardware technology (Gharawi and Kumar, 2003).

ESNs work using one or many sensors (nodes) that are deployed within the environment of interest. A mode of communication is established between the nodes and a central server. In some cases inter-node (*ad hoc*) communication and intelligent decision making may also occur (Chong and Kumar, 2003). Data from nodes can then be uploaded onto the central server where data integration, analysis and sharing can take place. ESNs may have a single function, such as a seismic network (e.g. Lorincz *et al.*, 2004), or a generic function, such as habitat monitoring (e.g. Szewczyk *et al.*, 2004). Akyildiz *et al.* (2002), Chong and Kumar (2003), and Hart and Martinez (2006) provide further details on the history and development of ESNs.

Alongside technological developments, an in-depth understanding of the environment in question is essential for the network and sensor nodes to be constructed, deployed and fully operational in accordance with the research requirements for that given environment. Consequently, a close relationship needs to be developed between computer scientists, communications experts, electrical engineers and environmental scientists in order for a sensor network to operate to its full potential. A series of projects where ESNs have been developed in this way have been reported globally. These include Berkeley's modelling of bird populations at Great Duck Island (Szewczyk *et al.*, 2004); the NASA/JPL project on biological flourishes and hydrology in Antarctica (Delin *et al.*, 2003 and 2004, respectively); the CORIE project to study the Columbia river estuary (Steere *et al.*, 2000); the

FLOODNET project to provide flood warning within the UK (De Roure, 2005); and the SECOAS project to monitor coastal erosion (http://envisense.org/secoas.htm).

2.8.3 Foundation for the thesis

The potential of this kind of system for monitoring a subglacial environment is immediately evident. The ESN allows nodes to monitor, record, and transmit data from a series of sensors *in situ*. The technology used is relatively cheap allowing for the production of numerous nodes that can be dispersed over large spatial areas. Processing capabilities ensure that nodes are 'smart' and can adapt to changes in their environment (e.g. short term losses in communication). Programming ensures that power losses are minimal and a power supply can be sustained for a year or more. Nodes are networked so that they can be controlled remotely and data can be uploaded onto servers, such as the Internet, for the end user. Communication developments can provide remote, wireless sensing and ensure good data transfer. In collaboration with ECS, the nodes can be designed with the most recent MEM devices, according to the needs of the glaciologist. The use of miniaturisation technology can allow a combination of micro-sensors within one instrument, and this will ensure that the instrument is small enough for deployment via boreholes. The shape of the instrument can also be designed to represent small a subglacial clast. This would cause the least disturbance to the subglacial environment and allow the instrument to become incorporated into the deforming bed and result in more 'natural' monitoring. Specifications of this kind will allow some of the limitations recorded by Harrison *et al.* (2004) and Truffer and Harrison (2006) to be overcome. These instrument and networking capabilities provide the potential to greatly improve the techniques used to monitor the subglacial environment.

The discussions raised in this chapter have highlighted the two main themes to this research project. The first is the development of a new instrument for monitoring the subglacial environment, and the second is the analysis of data from that instrument to make new conclusions about the processes operating in the deforming bed. The development of this instrument encompasses a new methodological approach within glaciology – the use of an ESN. As a result, this research is as much about determining whether or not an ESN can be established and if the new instrument

works; as it is about the information that can be gathered from that instrument. In accordance with the research aims (section 1.2, Chapter 1), this project intends to create a new sensor node that will be established as a sensor node within an ESN in a glacial environment. The data obtained will be interpreted to assess the processes operating in the subglacial environment, and the movement of the instrument in comparison to clasts and the sedimentology of the deforming bed.

2.9 Summary

This chapter has introduced the deforming bed and put forward arguments for its importance to glaciological research. The theoretical basis to research into the deforming bed has been outlined in terms of till rheology and subglacial hydrological processes. The instruments designed to monitor the subglacial environment *in situ* and our knowledge resulting from these experiments has been discussed. Shortcomings within data sets are largely the result of limitations within current subglacial instrumentation and a series of improvements for an 'ideal' instrument have been suggested. The use of ESNs as an alternative approach to monitoring environmental processes has been demonstrated. Technological advances now allow the production of MEMs that can monitor a range of environmental parameters. It is the aim of this research to both design and test the feasibility of using a new instrument or sensor node within an ESN at the ice-bed interface. The quality and quantity of data retrieved by an ESN should then contribute to closing the gaps in research outlined in section 2.7.6.

Chapter 3

Field Site Description: Briksdalsbreen

3.1 Introduction

This investigation is concerned with examining the deforming glacier bed *in situ*. This was to be achieved by placing a new wireless instrument within the subglacial environment via boreholes; whilst establishing an ESN that would support wireless communications between the instrument and the end user. These specifications provided a series of constraints on the selection of a contemporary glacier for this study. The primary requirement was that the glacier chosen was underlain by a layer of unlithified sediments, which were able to deform. The next requirement was appropriate field conditions in which to perform *in situ* borehole investigations and establish an ESN. Preliminary field surveys by Hart in 2000 and 2001 indicated that these requirements could all be met at Briksdalsbreen in Norway.

3.2 Briksdalsbreen, Norway

Briksdalsbreen is a temperature valley glacier located within the inner fjord region of south western Norway (61°40'N, 6 °57'E; Elvehøy, 2001; Figure 3.1). It is a west facing outlet glacier of the Jostedalsbreen ice cap which, at 487 km^2, is the largest remaining ice mass on the European continent (Winkler and Nesje, 1999). Briksdalsbreen is roughly 11.94 km^2 in size and ranges in altitude from 350-1915 m a.s.l. (Nesje, 2005). The majority of the glacier is accommodated on the plateau above, between 1500-1915 m (Elvehøy, 2001).

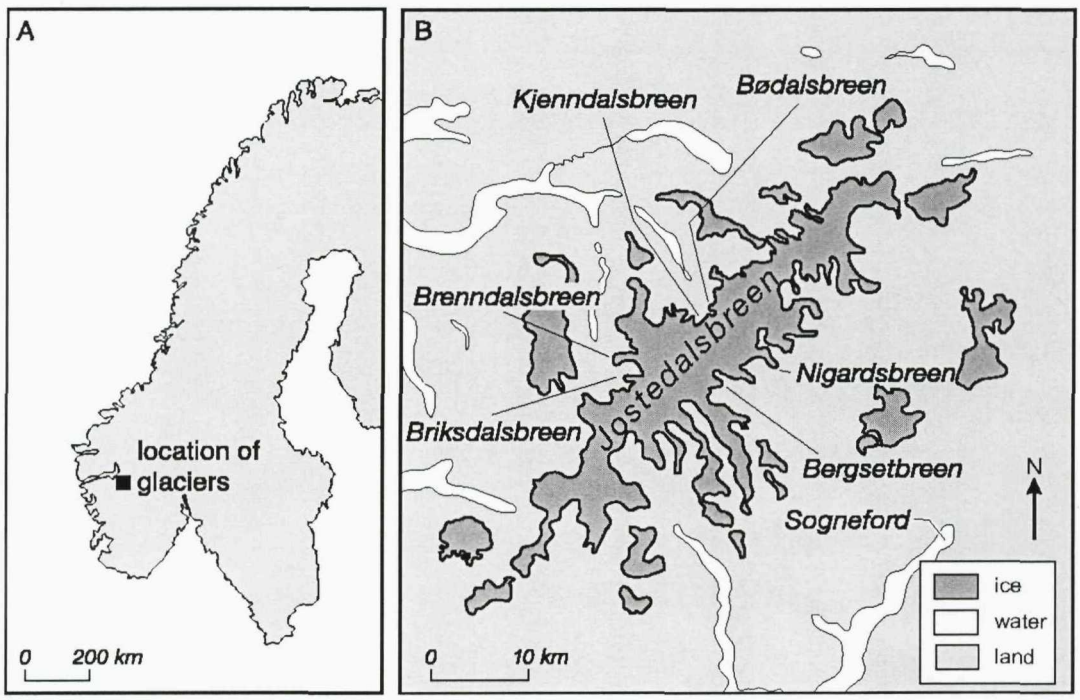


Figure 3.1: The location of Briksdalsbreen, part of the Jostedalsbreen ice cap, Norway.

The glacier is underlain by unlithified sediments over a Precambrian gneiss bedrock. Until recently (November, 2006), the glacier terminated in a proglacial lake, Briksdalsvatnet, which lies at 346 m a.s.l. (Figure 3.2). The lake was formed by erosion and over-deepening of the bedrock basin in this area (McManus and Duck, 1988). The proglacial area is dominated by steep valley sides that are partially covered by talus and glacial diamicton (Figure 3.2 and 3.3). The lateral parts of the foreland are relatively steep, but the central proglacial zone is almost horizontal (Winkler and Nesje, 1999). The foreland is occupied by numerous flutes and push moraines (Figure 3.4; Hart, 2006b), which provide an almost annual record of glacier retreat. Till is visible beneath the ice in cavities and is extruded at the margins of the glacier (Figure 3.5).

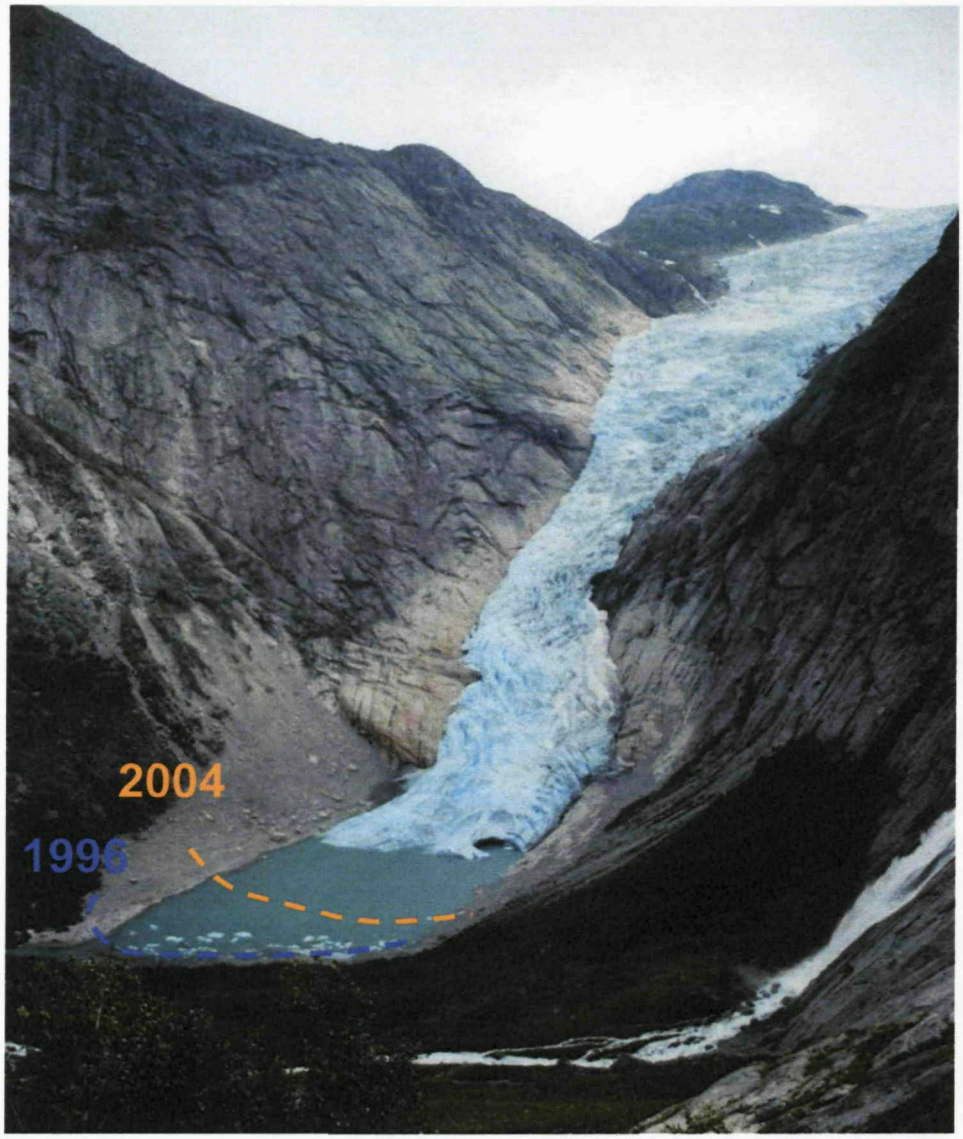


Figure 3.2: Picture of Briksdalsbreen flowing down from the ice cap above (August, 2006). The glacier terminates in Briksdalsvatnet and the foreland can be seen on the left hand side. A rough guide as to the extent of the glacier in 1996 and 2004 is marked by the dashed lines. The vertical distance from the lake to the top of the picture is roughly 1500 m. Note: all photographs are by the author, unless otherwise stated.

a)



b)



Figure 3.3: Pictures of Briksdalsbreen (2004): a) from ground level; and b) from above with a view onto the Jostedalsbreen ice cap. During the LIA the glacier moved down valley following the path of what is now the proglacial river, past the edge of the picture. (Photo a: K. Martinez).

a)



b)



Figure 3.4: Example features of the glacier foreland, showing: a) a flute emerging from beneath the glacier; and b) a push moraine marking the maximum extent of the summer advance (2004) (Photos: J.K. Hart).

a)



b)



Figure 3.5: Example pictures from the glacier margin, showing: a) till being extruded from beneath the ice; and b) till revealed in a cavity beneath the ice. This provided good evidence that the glacier was underlain by unlithified sediments.

3.2.1 Frontal variations

The outlet glaciers of the Jostedalsbreen ice cap experience relatively frequent fluctuations in glacier mass balance in response to short term climatic perturbations, namely the North Atlantic Oscillation (NAO) (Jones *et al.*, 1997; Nesje and Kvamme, 1991; Nesje *et al.*, 2000; Oerlemans, 2000). The NAO affects both glaciers in southern Norway and those in the Alps. In Norway, a positive phase of the NAO produces above normal winter snow accumulation, resulting in a positive net mass balance and *vice versa* (Nesje, *et al.*, 1995). The Alps are affected in the opposite way. In Norway, the effect of the NAO becomes evident through a combination of enhanced winter precipitation and reduced summer temperatures. These variations show close association with decadal scale frontal fluctuations in Norwegian glaciers (Nesje, 2005). Briksdalsbreen is thought to have a response time of approximately 3 years and has undergone significant and rapid fluctuations in frontal extent in the last 20 years (Nesje, 2005).

The most recent maximum glacial extent occurred during the Little Ice Age (LIA) in 1750 (Nesje *et al.*, 1991). At that time the glacier extended down the tributary valley almost reaching the Oldedalen valley itself (Figure 3.6). In combination with all the valley glaciers of the Jostedalsbreen ice cap, Briksdalsbreen underwent a phase of retreat (with three small readvances) between the LIA maximum (1750) and 1955 (Winkler, 1996). Briksdalsbreen reached its minimum extent in 1955, retreating out of the proglacial lake which had formed and back up onto the bedrock at the base of the ice fall. Since 1955, Briksdalsbreen readvanced 464 m (Nesje *et al.*, 1995; Figure 3.7; Table 3.1). In comparison with the other glaciers, Briksdalsbreen progressed the furthest and the fastest, advancing most rapidly between 1988 and 1996 (Nesje *et al.*, 1995; NVE; Figure 3.7a and b; Table 3.1). The glacier moved 305 m during this time, down from the ice fall and across the proglacial lake. This activity has been associated with a positive phase of the NAO (Nesje and Dahl, 2003).

At the height of its readvance (1996), Briksdalsbreen had completely overridden the Lake Briksdalsvatnet (Figure 3.7b); and literally bulldozed the birch forest that had become established on the glacier foreland since the glacier's retreat in the 1950s.

Numerous branches and tree trunks are still evident in the foreland today (2007), bent and aligned with the dominant glacier flow direction (Figure 3.8). Briksdalsbreen was the first glacier in the region to cease advancing and remained relatively stable between 1997 and 2001. A relatively slow average retreat rate of 7.2 m a^{-1} was recorded during this time. In 2002, Briksdalsbreen began to retreat more rapidly, withdrawing by 379 m from 2002-2006 (Figure 3.7c and d; Table 3.1). In 2006, this retreat was marked by a catastrophic calving event. This saw the glacier loose a further 133 m of ice from 2006-2007, causing it to retreat back onto the bedrock at the base of the ice fall (Figure 3.7d). Briksdalsbreen has retreated by a total of 556 m since 1996, past the previous minimal point of retreat in 1955.

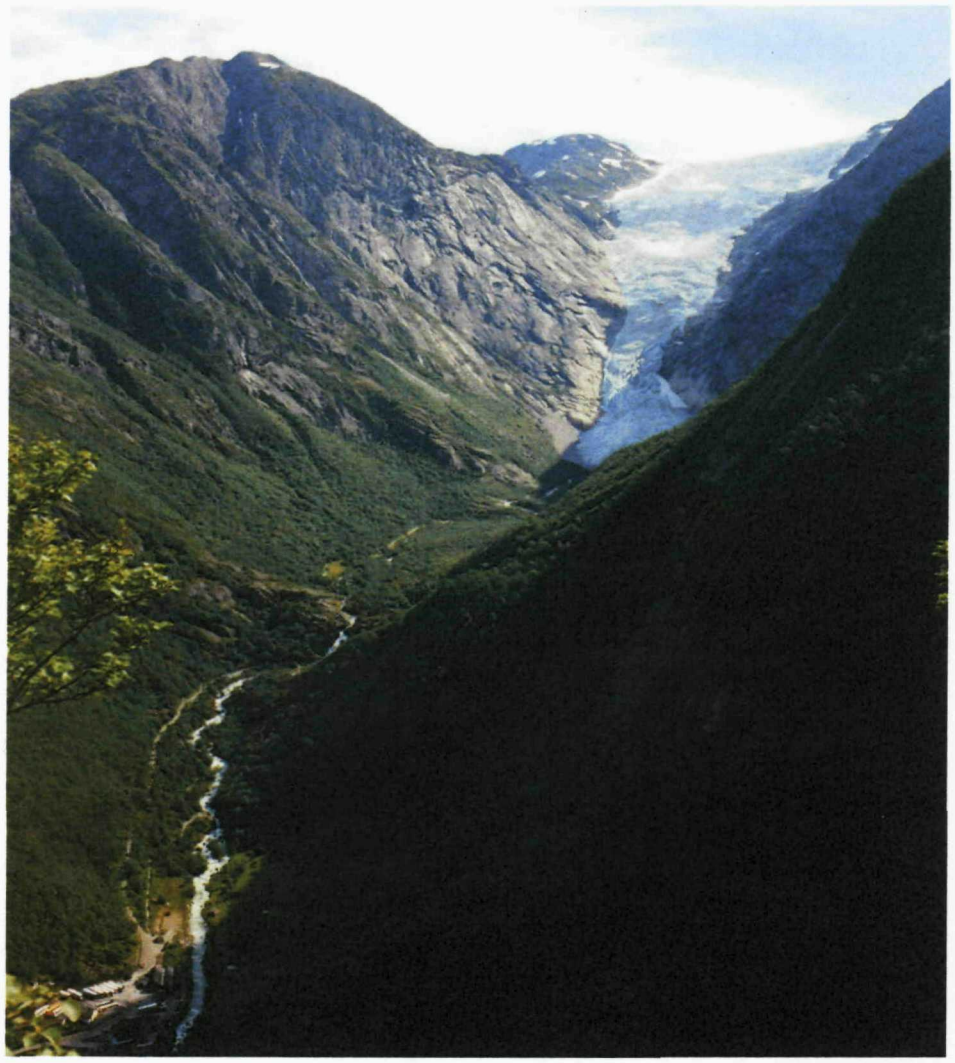


Figure 3.6: View of Briksdalsbreen from the top of the Oldedalen valley, where the camp site and other tourist facilities are located. These buildings are just visible in the lower left hand corner of the picture and mark the maximum extent of the glacier in the LIA. It is a 45 minute walk from this location to the glacier foreland

a)



b)



c)



d)



Figure 3.7: Photographic time series, displaying the advance and retreat of Briksdalsbreen for: a) 1989; b) 1996; c) 2002 and d) 2007. (Photos: a-c, S. Winkler; d, NVE).

Table 3.1: Annual front variations for Briksdalsbreen, Norway (1956-2007). The glacier advanced 464 m between 1956 and 1996, but retreated 423 m between 1996 and 2006. The variations between NVE and Glacsweb readings are the result of measuring the retreat of the glacier from different locations. Note: Glacsweb is the Southampton field team (Martinez *et al.*, 2004b); NVE is the Norwegian Water Resources and Energy Administration team.

Year	NVE Distance (m)	Year	NVE Distance (m)	Glacsweb Distance (m)
1956-1987	+159*	1997	-2	-2
1988	+29	1998	-3	-3
1989	+1	1999	-2	-2
1990	+24	2000	-38	-31
1991	+8	2001	+1	-2
1992	+28	2002	-16	-42
1993	+60	2003	-48	-34
1994	+61	2004	-120	-68
1995	+50	2005	-50	-55
1996	+44	2006	-145	-67
1988-1996	+211	2007	-	-133*

*values from Nesje *et al.*, 1995



Figure 3.8: Example of one of many tree branches found within the glacier foreland (Scale: ~50 cm). The branch marks the remains of a birch tree overridden by Briksdalsbreen in the height of its advance (1996) and aligned is with the glacier flow direction.

3.2.2 Rationale

Briksdalsbreen was chosen as the field site for this investigation for a number of reasons, both scientific and logistical. The foreland at Briksdalsbreen was comprised of glacial diamicton, which was also seen within basal cavities and extruded from beneath the glacier margin (Figure 3.5). This suggested that Briksdalsbreen was underlain by a bed of unlithified sediments. In addition, the glacier foreland was characterised by push moraines and flutes, which could also been seem emerging from the glacier margin (Figure 3.4). The presence of flutes, in particular, indicated that these unlithified sediments were deforming beneath the ice, so that the glacier foreland reflected an exposed subglacial surface. Thus, Briksdalsbreen satisfied the criteria for a glacier underlain by a deforming bed.

A second dominant control on this investigation was the production and deployment of a new instrument, set within a wireless sensor network. In order for this to be achieved the glacier needed to be suitable for borehole drilling. Briksdalsbreen is a notably 'clean' glacier, free of supraglacial debris (Figure 3.3). In addition, the surface topography of the glacier was relatively smooth, with only a small zone of crevassing through the middle, which could be traversed on foot. These conditions provided an ideal environment for drilling. The field site also had to be accessible and with good communications. This would be necessary to accommodate the requirements of the ECS team members, during the preliminary stages of set up and design. Fortunately, a campsite was located at the top of the Oldedalen valley (Figure 3.6). This provided cabins to shelter the delicate electrical equipment, a ready power supply, GSM (global system for mobile) telephone coverage, and a local ISDN (integrated services digital network) telephone connection (i.e. the internet). These factors made Briksdalsbreen an ideal site for the research project.

3.3 Summary

This chapter has introduced the study site, Briksdalsbreen. A brief summary of the glacier's history and the rationale for choosing this glacier for research has been outlined.

Chapter 4

Methods and Techniques

4.1 Introduction

A variety of methodologies were employed at Briksdalsbreen during the summer field seasons of 2004 and 2005, in order to address the aims of this investigation (section 1.2, Chapter 1). This involved field based work, laboratory work, and office based data processing. This investigation was also a group project, involving contributions from members of the ECS department at Southampton. Contributions included a range of computer based work, software programming and hardware construction, which will not be discussed in detail here. Figure 4.1 aims to simplify the various components of the investigation and how these methodologies inter-relate in terms of: the sequence of techniques carried out, where the methods were carried out, how they relate to the other aspects of the project and any subsequent processes of data analysis. A paper detailing the set up of this investigation and initial results is already in publication (Hart *et al.*, 2006) and is reproduced in Appendix A.

This research was based on the use of an ESN. This system provided the foundation from which sensor nodes could monitor long term changes in the nature of the subglacial environment. The ESN not only allowed the *in situ* instruments to relay their information to the end user, it also provided the means by which GPS (global positioning system) measurements could be taken. The development of the ESN is discussed first, followed by a detailed account of the field work. A series of field techniques were carried out systematically each year to enable to the sensor nodes to be deployed within a fully functional ESN at the end of the field season. The

laboratory analyses that followed, based on the samples collected in the field, are outlined at the end.

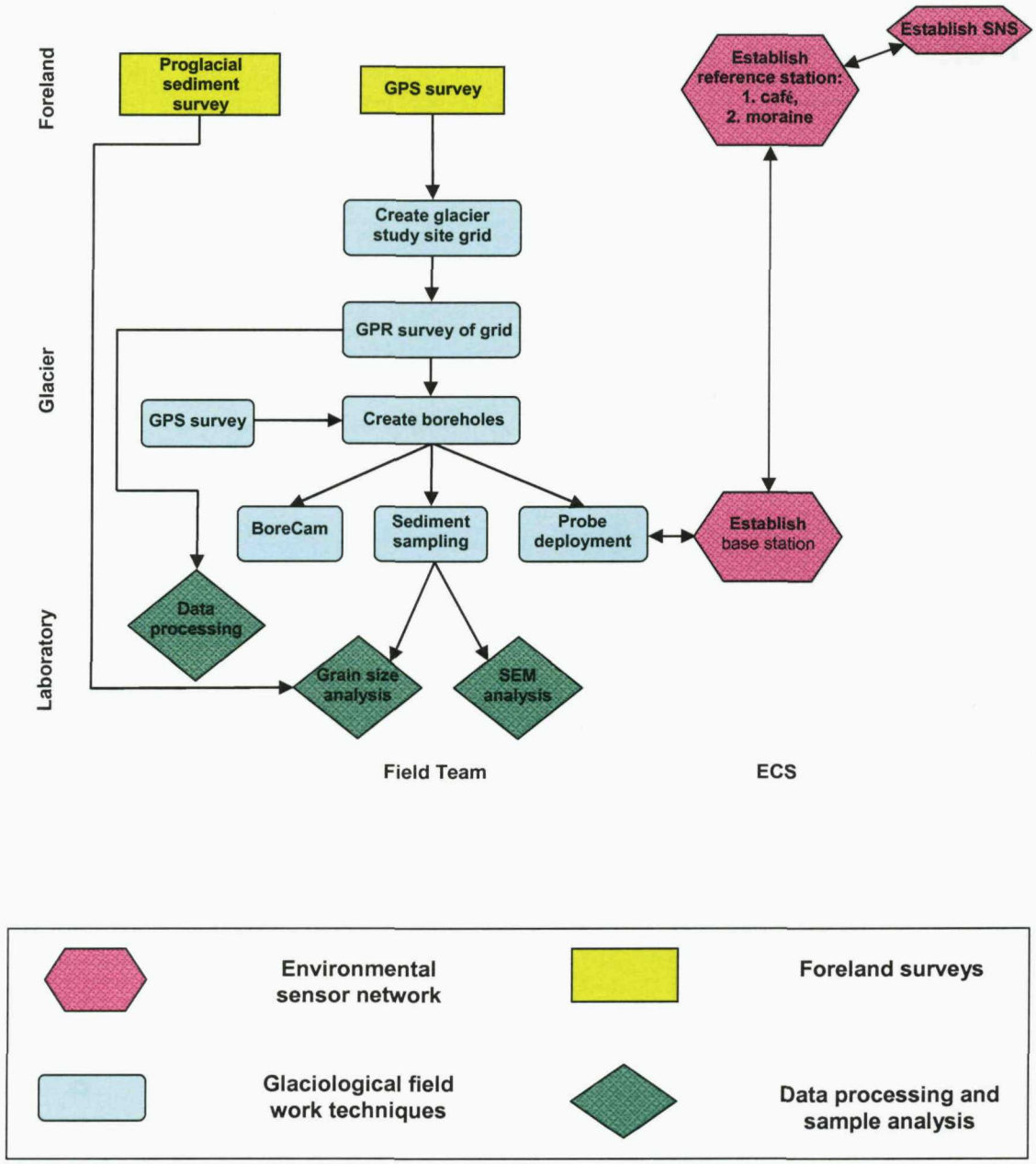


Figure 4.1: Flow chart to show how the methods and techniques employed in this investigation inter-relate.

4.2 Environmental Sensor Network

The principle of an ESN is to establish a network of sensor nodes to independently monitor environmental conditions, and then actively communicate those findings, to an end user via a sensor network server (SNS). In this section, each component of the ESN employed will be discussed in turn, from the glacier based to the computer based components. An overview of the ESN developed at Briksdalsbreen is displayed in Figure 4.2.

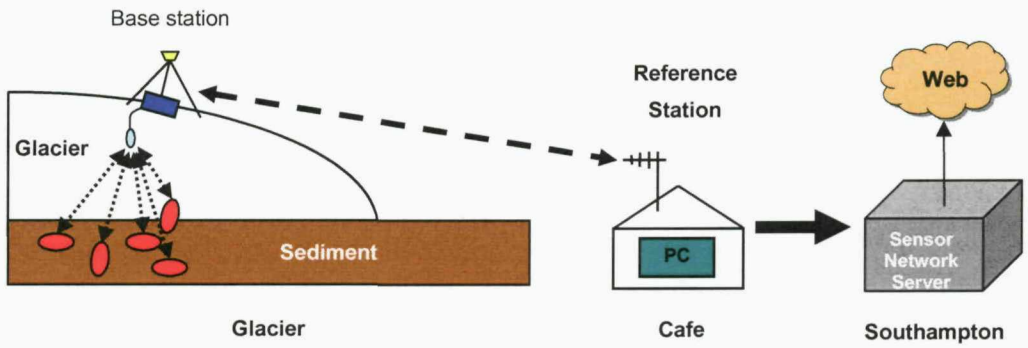


Figure 4.2: Schematic diagram showing the components of the ESN established at Briksdalsbreen.

4.2.1 Sensor nodes

The key component of the ESN was the sensor nodes that were used to monitor the environment in question. The sensor nodes were designed so that the environmental criteria under observation were those required to answer the aims of the investigation. The nodes also needed to be cost-efficient to produce to make their use within such investigations feasible. It was also important to recognise what could be achieved in a sensor node in terms of current hardware and software capabilities. The glaciological and sensor network based requirements of the sensor nodes are outlined in Table 4.1 (see also section 2.8.1, Chapter 2). The sensor nodes designed for Briksdalsbreen were termed probes and were non-recoverable once deployed.

Table 4.1: Glaciological and ECS design requirements for the components of the ESN (adapted from Martinez *et al.* 2004a).

ESN Component	Requirement	Rational
Sensor Nodes	Low power	To ensure long term operation
	Automated	To remain maintenance free
	Mechanically robust	To withstand subglacial conditions
	Wireless	To maintain low environmental disturbance
	Resemble a clast	To monitor the motion of subglacial clasts
	Non-intrusive	To maintain low environmental disturbance
	Micro-sensors	To monitor several physical and mechanical properties in node location
	Technically robust	To withstand errors and failures for long term operation
	Low cost	To produce numerous units to achieve the required spatial coverage
Communications	High power	To ensure communications through ice
	Low data rate	To minimise data losses
	Back up channels	To minimise data losses
	Error detection and correction	To minimise data losses
	Wireless capabilities	To achieve low environmental disturbance and remote data collection
	Long range	To ensure communications between base station and reference station (Figure 4.2)
Computing	Micro-controllers	To control sensor node functions
	Low power systems	To enable long term monitoring capabilities
	Routing and message passing	To ensure data transfer
	Server	To create and interface for remote data collection

4.2.1.1 Probe design

The probes consisted of a hollow polyester capsule, intended to represent a small clast that might be found within the subglacial environment (Figure 4.3; Table 4.1). The capsule was designed in the programme CAD (computer aided design) and produced from a solid rod of polyester (plastic) in a CNC (computer numerical control) milling machine. The size of the probe casing was designed so that it would be able to accommodate the antenna, electronic hardware and power supply required for the probe to function fully (Table 4.2). The sensor node was housed within the capsule and the two halves were joined using an epoxy resin sealant. The capsule could not be filled with a potting compound, which might increase its ability to withstand the forces acting on it beneath the ice, because this interfered with the

internal electronics. As a result, the capsule remained filled with air, rendering the sealant between the two capsule halves as the weakest point. Despite this, testing at the National Oceanography Centre, Southampton, revealed that the probe could withstand a pressure equivalent of 100 m of water without failure. This was deemed sufficient for survival within a subglacial environment.

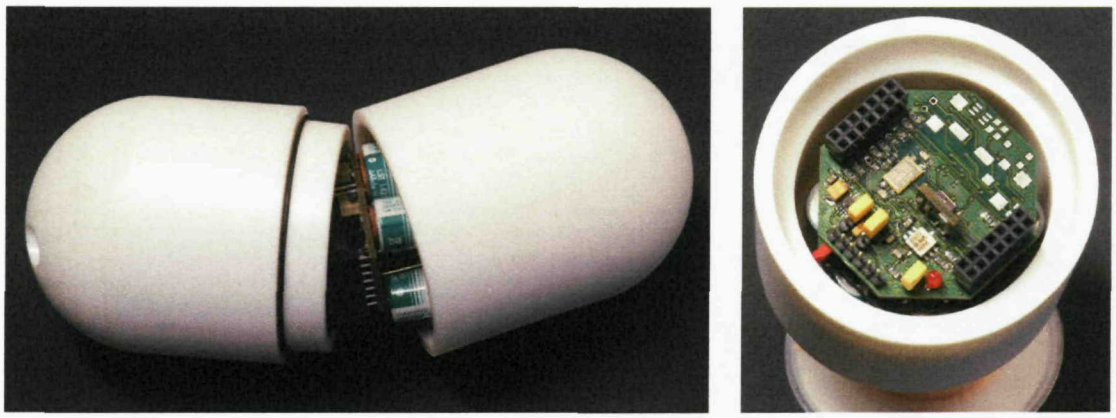


Figure 4.3: Photographs showing the two halves of the probe and the internal electronics. 2005 probe, 16 cm in length (Photo: K. Martinez).

Table 4.2: Specifications for the probe casing and other non-sensor components.

	2004	**2005**
External diameter	6.8 cm	6.2 cm
Length	14.8 cm	16 cm; ratio 2.9:1
Power supply	6 half AA cells - 3.6V Lithium Thionyl Chloride batteries.	
Radio transceiver	Quarter wavelength 'stubby' helical antennas	
Data store	Compact flash card (FlashRom), 64 kB capacity	

4.2.1.2 Probe architecture

The probes comprised of 4 basic modules: processing, sensing, transceiver and power (Figure 4.4). The processing module consisted of a PIC (peripheral interface controller) 8-bit micro controller (PIC16F876) with both analogue and digital (I^2C; inter-integrated communication protocol) components. The sensing module comprised a range of both analogue and digital micro-sensors to monitor the physical and mechanical conditions within the subglacial environment (Table 4.1). The transceiver and power modules are self explanatory (Table 4.2). Additional

components included the real time clock (RTC) and the compact flash storage centre (Figure 4.4b; Table 4.2).

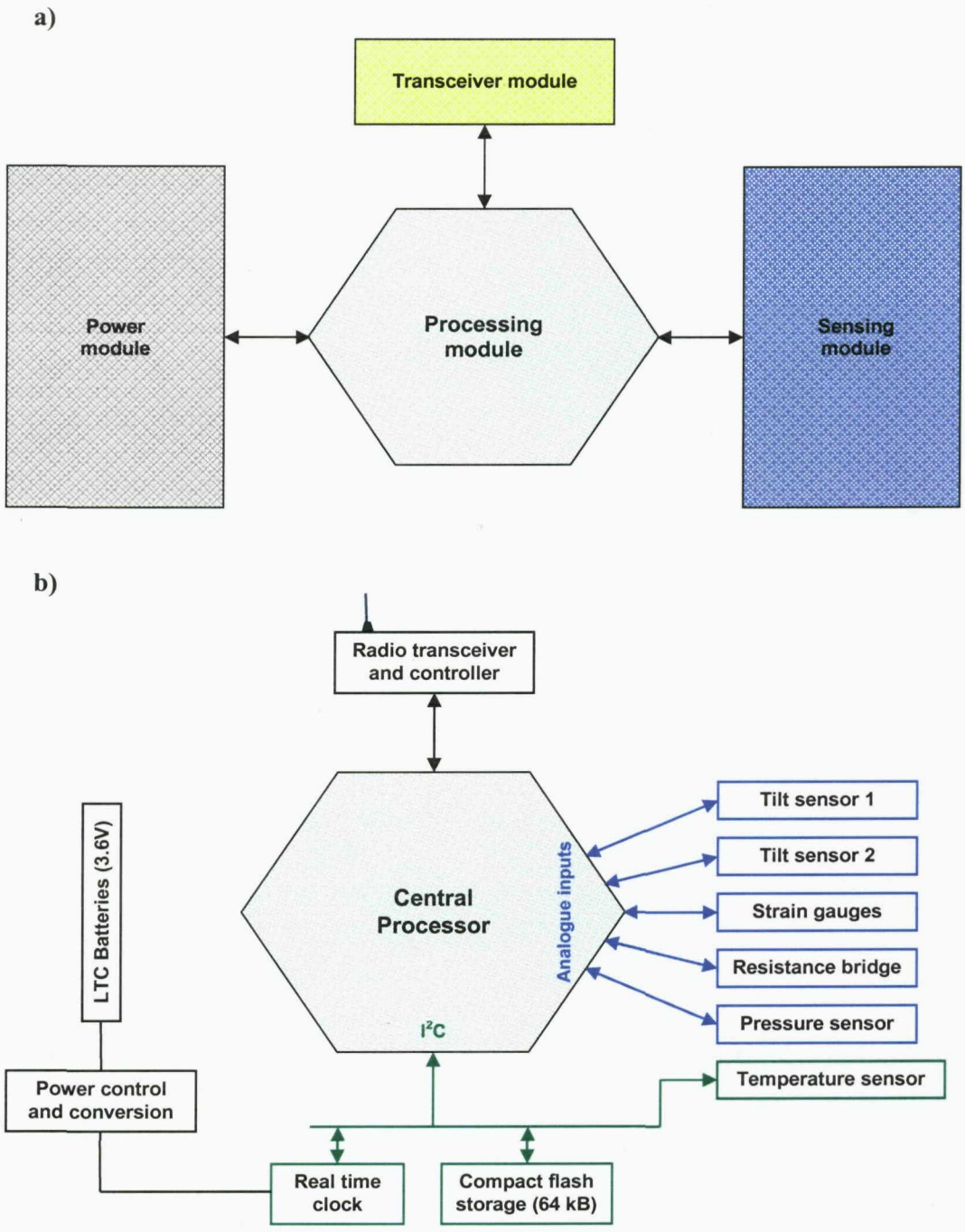


Figure 4.4: Schematic diagrams to show: a) the four main module components that comprised the probes electronics; and b) a simplified version of the probes' architecture (adapted from Hart *et al.*, 2006).

The physical expression of these modules was in the form of three custom-made octagonal PCBs (printed circuit boards): transceiver, digital and analogue (Figure 4.5a). The ability to stack the PCBs resulted in a cylindrical modular design, which enabled the most efficient use of space within the probe capsule (Figure 4.3 and 4.5b,c). The antenna was located on the surface of the transceiver module, fitting into one end of the probe case (Figure 4.5). The power supply, consisting of six lithium batteries, was connected beneath the three PCB modules (Figure 4.5b,c; Table 4.2).

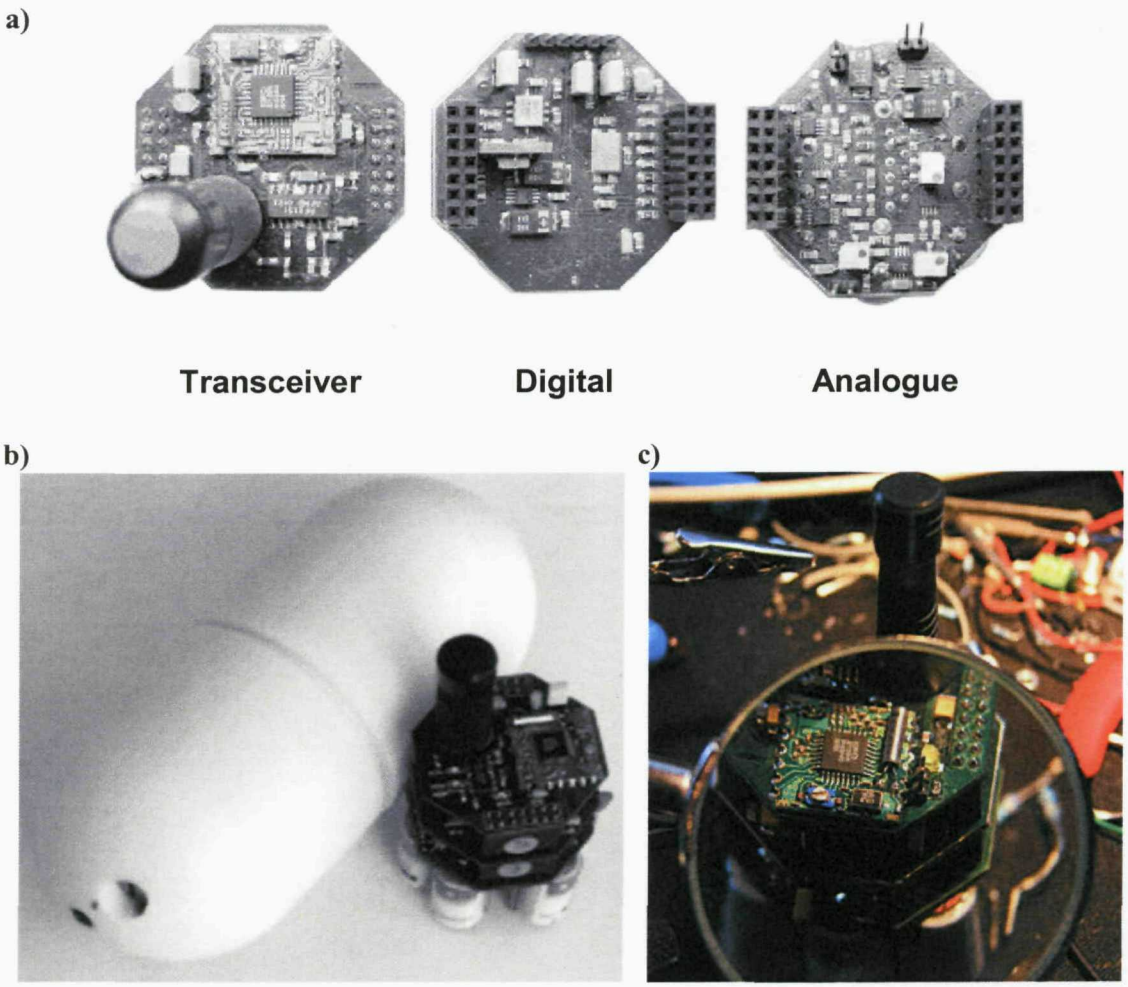


Figure 4.5: Pictures highlighting the modular design of the probe's hardware showing: a) the 3 octagonal PCBs used; b) the probe and the connected modules prior to insertion into the probe; and c) a close up of the connected modules. Note: one bolt, used for the resistance bridge, is visible in photo b, the pressure membrane, the black circle, is located to the left of the bolt. (Photos: K. Martinez).

The transceiver module was responsible for communications and was powered by the analogue module. The digital module (I^2C) supported the digital components, namely the PIC micro-controller, temperature sensor, RTC and the 64 kB FlashROM (Figure 4.4b). The analogue module maintained the micro-sensors that required differential inputs, namely the tilt sensor, strain gauge, resistance bridge and pressure transducer (Figure 4.4b). The connectors for the micro-sensors were located under the analogue module with the battery power supply. The use of connectors allowed the boards to communicate with each other and each board could self regulate and decouple its own power supply (Martinez *et al.*, 2006). This system required the use of more connectors, but it was better for detecting, isolating and correcting faults on individual modules. The PIC micro-controller managed the module functions by interpreting commands, configuring the RTC, and collecting and storing data.

The PIC micro-controller functioned through the use of custom-made software, known as 'firmware'. The probe used two types of firmware: programme space and user space (Martinez *et al.*, 2006). The programme space ensured that the PIC micro-controller was configured correctly and performed its tasks when powered up. This software could not be reprogrammed once uploaded. The user space supported all the programmes that the probe was to perform, as a series of commands. It was a highly flexible system that could be reprogrammed from the UK and then executed the next time the probe was powered up. This allowed programmes to be added, removed or reshuffled within the automated sequence of commands (Martinez *et al.*, 2006).

4.2.1.3 Micro-sensors

The micro-sensors incorporated into each probe are outlined in Figure 4.4b, and their specifications are detailed in Table 4.3. The array of micro-sensors employed was chosen to fulfil the requirements for study outlined in Table 4.1 and section 2.8.1 (Chapter 2). The micro-sensors were discussed in terms of probe architecture in section 4.2.1.2 and their locations are displayed in Figure 4.6.

Table 4.3: Probe micro-sensor specifications.

Sensor	Property	Traditional Instrument	Rationale	Technical Specifications	Resolution (step size)	Range
Temperature sensor	Temperature	-	To determine the thermal conditions in the deforming bed, further to the work of Murray and Porter (2001)	ADT7301ARMZ	0.03°C	-15°C to +15°C
Pressure transducer	Water pressure	Pressure transducer	To monitor hydrological changes	Honeywell 24PCGFM6G	0.5 psi	0-250 psi 0-1724 kPa
Strain gauges	Case strain	Ploughmeter	To monitor changes in the mechanical properties of the deforming bed (e.g. sediment strength)	Strain gauge	0.1%	0-1023% micro strain
Resistance bridge	Resistance	Conductivity meter / turbidity meter	Only a general correlation to traditional instruments, used to determine the relative 'wetness' of the till, to provide inferences on mechanical properties (section 4.2.1.5)	Resistance bridge	0.1%	0-10 M Ohm (2004) 0-20 M Ohm (2005)
Tilt sensor 1	Tilt: x axis and y axis	Tilt meter	To monitor sediment deformation the movement of subglacial clasts	Dual axis 180° MEM sensor accelerometer	1%	-90° to +90°
Tilt sensor 2	Tilt: z axis	Tilt meter	To monitor sediment deformation the movement of subglacial clasts	Dual axis 180° MEM sensor accelerometer	1%	-90° to +90°

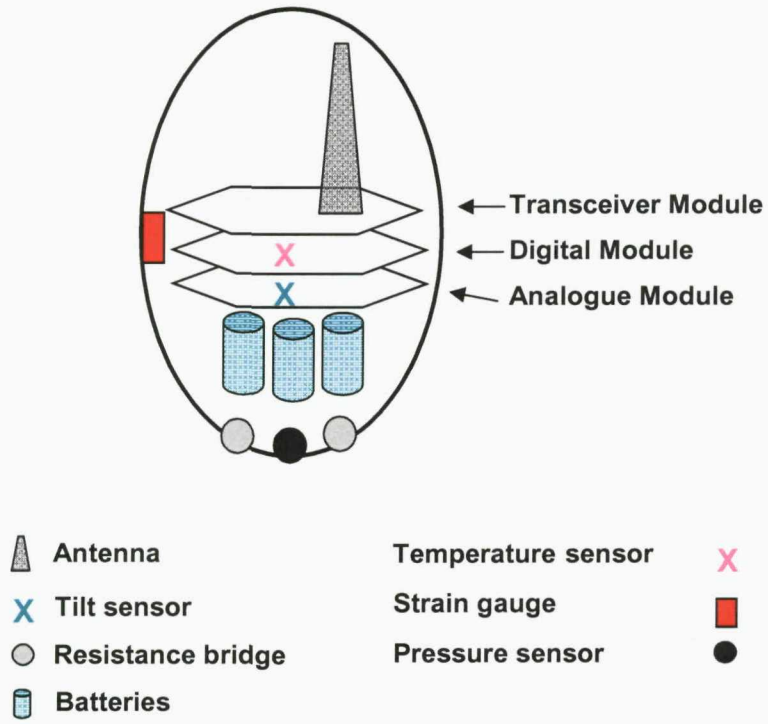


Figure 4.6: Schematic drawing to show the location of the micro-sensors and hardware within the probe casing. The locations of the resistance bridge and pressure transducer are also displayed in Figure 4.5b. Note: three batteries are displayed but six are used in total.

Temperature and tilt were measured inside the probe and located on the digital and analogue modules, respectively. The strain gauge was attached to the inside of the probe case, measuring the degree to which the probe case was compressed, either from above (a-axis) or from the side (b-axis). Resistance was measured across two bolts, which were exposed at the base of the probe, on either side of the pressure membrane (Figure 4.5b and 4.6).

4.2.1.4 Probe calibration: tilt sensor interpretation

The tilt sensors employed measured tilt along three axes: x, y and z. Figure 4.7 displays these axes and the angle of movement associated with probe tilt along each axis. The axes (and thus tilt measurements) are relative to the probe. A change in x, for example, is equivalent to a change in the orientation of the long axis. Despite this, the general orientation of the probes at an instant in time can be determined relatively easily, taking into account the orientation of the axes. However, the trends

in movement along these axes over time are more complex and not immediately obvious from the raw data.

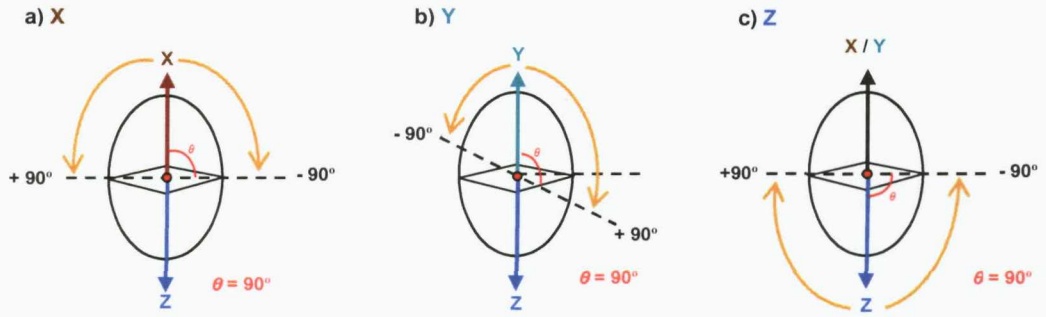


Figure 4.7: Conceptual diagram to show the orientation of the axes associated with the tilt sensors for: a) x-axis; b) y-axis; and c) z-axis.

To gain a better understanding of how the tilt records relate to actual probe movement, experiments changing the orientation of the probes under controlled conditions were carried out in the laboratory. These tests revealed that when the probes are moving in three dimensions over time, one degree of change on one axis does not necessarily equate to one degree on another axis. This means that variations in tilt cannot always be considered as absolute. This is particularly true for variations in the z-axis. The z-axis measures 90° consistently, until tilt along the x-axis exceeds 90°. Readings on the z-axis then begin to change, accounting for any measurements of tilt on the x-axis greater than 90°. As a result, movement along the z-axis was only considered when the angle of tilt in the x-axis exceeded or remained at 90°. This axis could perhaps be conceptualised as x_2. The tests also showed that when the x and y (or z and y) axes changed in combination with each other, showing either an increase or decrease in tilt *in the same direction,* the probe was rotating. If tilt along these axes moved in opposite directions rotation did not occur, the probe was simply changing orientation. This information was used in order to determine how and when the probes were moving. In particular, this meant that the rotation of the probes could be identified.

4.2.1.5 Probe calibration: resistance

A small laboratory experiment was carried out to test the function of the probe resistance bridge. The probe was placed in a container of a known volume of dry till obtained from Briksdalsbreen. The resistance bridge was submerged in the till and a reading was taken. Aliquots of distilled water were then added progressively to the till in increments of 0.5% of the total volume of till present. Resistance values were noted after each new addition and the results are displayed in Figure 4.8. There was an overall decline in resistance as the percent of water present increased. In dry till readings of 25 M Ohm were obtained, but when the till contained 10% or more of water, values of less than 4 M Ohm were displayed. In excess of 33% water the change in resistance recorded was very small, showing a range of only 0.3 M Ohm. Generally, high resistance readings were associated with 'dry' conditions, whilst low values were associated with 'wet' conditions.

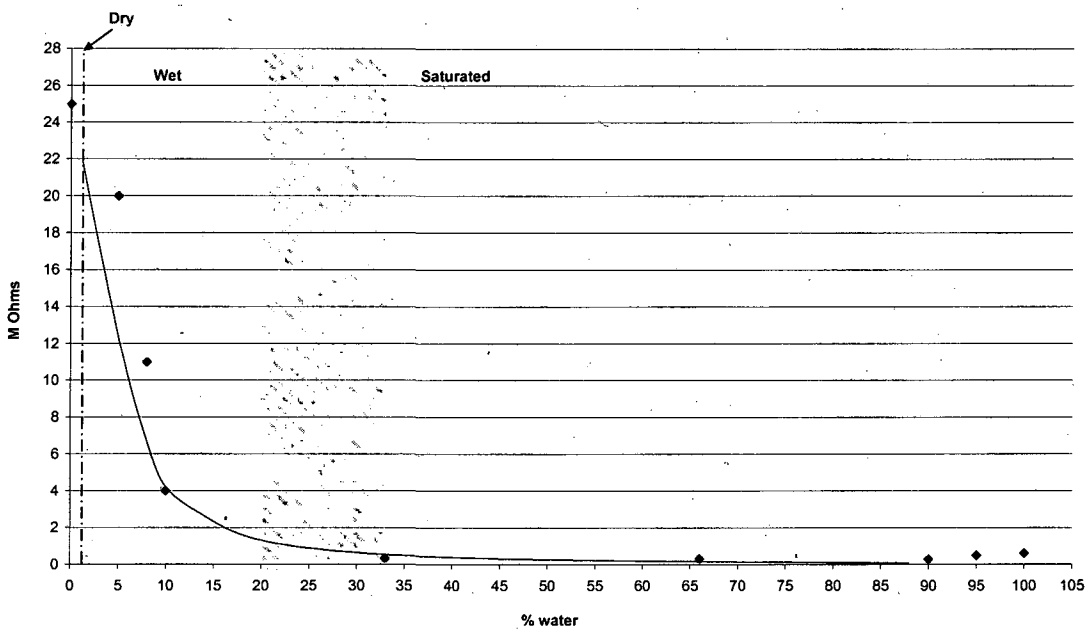


Figure 4.8: Probe resistance calibration curve. Note: the diagonal shaded area marks the transition to saturation which occurs at a water content of between 20-33% water.

4.2.1.6 Probe data collection and transfer

The probes collected data from the micro-sensors 6 times daily (every 4 hours) according to a given protocol (Table 4.4). The probes woke up in accordance with

the RTC for a maximum of 15 seconds to record sensor readings. The data were then collated into a 'packet' that was time-stamped and stored in the compact flash card until they were due to be transferred. The probe packets consisted of a string of data ordered as: probe ID, month, day, temperature, pressure, strain, resistance and x, y, and z tilt. The data, typically 5-20 bytes, were stored in a ring-buffer system that could preserve data for 682 days, or almost 2 years (Hart *et al.*, 2006; Martinez *et al.*, 2006). Any data that could not be transferred, due to temporary communications failure, remained stored. Old data would only be overwritten if the compact flash card reached maximum capacity.

Table 4.4: Operational protocol for data collection and communication for the probes, the base station and the reference station. Data were collected in the log periods and transferred during the communications period. In the transfer period data were uploaded onto the SNS. The time schedule was determined by the RTCs, based on GPS time (UTC).

Time (UTC^)	Probe	Base Station	Reference Station
00.00	Data log		
03.00		GPS log	GPS log
04.00	Data log		
08.00	Data log		
12.00*	Data log / Comms	Comms.	Comms.
16.00	Data log		
19.00			Transfer
20.00	Data log		

** system wide window; ^co-ordinated universal time (UTC)*

The transfer of data packets was achieved by establishing a 'master-slave' communications protocol between the probes and the base station computer (Figure 4.2). This meant that the probes were only one link away from the base station, generating an infrastructure system that also rendered the probes as essentially passive. This system contrasted with the ad-hoc networks that are normally associated with ESNs, but ensured that collisions in data transfer did not occur. The probe transceivers were enabled once a day for data transfer, during the communications period (Table 4.4). In this time, the base station also powered up and requested all undelivered data packets from the probes, in accordance with its fixed software command set. This was similar to the probe user space. In the event of a temporary communications failure, this allowed any old data stored by the

probes to be transferred. The base station transferred the data in packets using a protocol with error detection capabilities. This meant that the base station could check the integrity of the data packets on receipt and report any errors. The protocol also allowed up to 3 retries in the event of initial transfer or communication error.

The base station contacted each probe in turn, transferred their data, updated their RTCs using GPS time (UTC), checked their battery voltage and then put them back to sleep. If required, the base station could also reset probe data logging. The probes normally remained powered up for no longer than 3 minutes. The probe RTC was reset to prevent clock drift, which might otherwise amount to 2 s day^{-1} and result in some nodes becoming 'lost' (Martinez *et al.*, 2004b). The probe volt readings were collated by the base station into a general log file that was generated to check the system. The communications period described above was also used as a system wide window (Table 4.4). At this time the ESN components (probes, base station and reference station) would become idle for a short period after they had completed all their tasks, enabling remote access to the system from the UK (section 4.2.3).

4.2.1.7 Probe communications

Radio communications through ice were highly complicated. It was essential that the correct radio frequency was chosen to ensure robust communications, and thus data transfer, between systems, particularly the probes and the base station. The ability of radio waves to propagate through ice is dependent of the relative permittivity of the ice and the dielectric loss factor (Hart *et al.*, 2006). The dielectric constant of ice at 0°C is approximately 3.17 (Glen and Paren, 1975). It was predicted that with a dielectric constant of 3.17, at a frequency of 1.8 GHz, radio wave losses would only amount to roughly -25 dB (Martinez *et al.*, 2006). Evans and Smith (1969) have determined that the absorption of radio over 100 m of ice at -1°C (100-1000 MHz) is less than 10 dB. Dowdeswell and Evans (2004) also argue that at frequencies of 800 MHz absorption is negligible.

It was based on these calculations that in 2003 the first prototype probe was designed to transmit at a frequency of 868 MHz. However, the pilot project demonstrated that in practice the true losses in glacier ice were much greater than predicted. It is likely that the transmission of radio waves was hindered due to the inherent variability of

the environment (both spatial and temporal); and the variety of media (i.e. air, water and sediment) that the radio wave might have to pass through to reach the appropriate transceiver. As a result, in 2004, the probe communication frequency was reduced to 433 MHz, greatly increasing the success of data transfer (Hart *et al.*, 2006). The associated wavelength was thought to be sufficient to exceed the size of any water bodies or sediment packets in the glacier that might impede the signal (Padhy *et al.*, 2005). The addition of wired transceivers, lowered down boreholes from the base station also improved communication success by decreasing transmission distance (section 4.2.2.2).

The probes were equipped with a Xemics 433 MHz transceiver combined with a 10 mW radio frequency power amplifier. This boosted the signal to over 100 mW giving a communications range of over 100 m through ice (Martinez *et al.*, 2006). Omnidirectional antennas maintain signal strength in all directions of orientation. However, quarter wavelength "stubby" helical antennas were chosen because they were more robust in the presence of PCBs and metal. The probes were also able to move freely within the subglacial environment so that data could be transferred at some point. Intermittent transmissions had been predicted given both the antenna used and due to changes in local environmental conditions. This meant that the ability of the probes to store data locally until transferred was a highly important back up to the system. However, in practice the antennae seemed to work very well and in 2005 a slightly longer helical antenna was tested. This improved the signal strength to such a degree that the 2005 probe cases were modified (Table 4.2) to accommodate the extra antenna length (Martinez *et al.*, 2006).

4.2.1.8 Power

The probe power supply ensured that the sensor nodes remained functional once deployed and irretrievable. Data logging and transmission were designed to be intermittent to reduce the amount of time that the probes were powered up. Six half AA sized Lithium Thionyl Chloride batteries were used (3.6 V), supplying 5 Ah. These batteries supported a high energy density and low temperature characteristics that enabled them to function fully at low temperatures. The approximate daily power consumption for the probes was 5.8 mW h, suggesting that, with the given power supply, the probes could last for approximately 10 years. The power supply to

the probes was in constant check as volt readings were sent to the base station in each data packet.

4.2.2 Base station

A base station was established on the ice surface to support a variety of functions (Figure 4.1), including communications, the GPS, a weather station, and the ESN computing system (Figure 4.9). The base station was supported by a relatively flexible metal pyramid frame, with a hollow steel rod that fed through the centre of the pyramid. The metal frame was chosen so that it was strong enough to provide sufficient support and withstand conditions on the glacier; but flexible enough so that it could adapt to any changes in surface ice topography. The metal also melted into the glacier surface, helping to stabilise the whole structure. As a further precaution, the base station was also tethered to an anchor placed 15 m down a borehole.

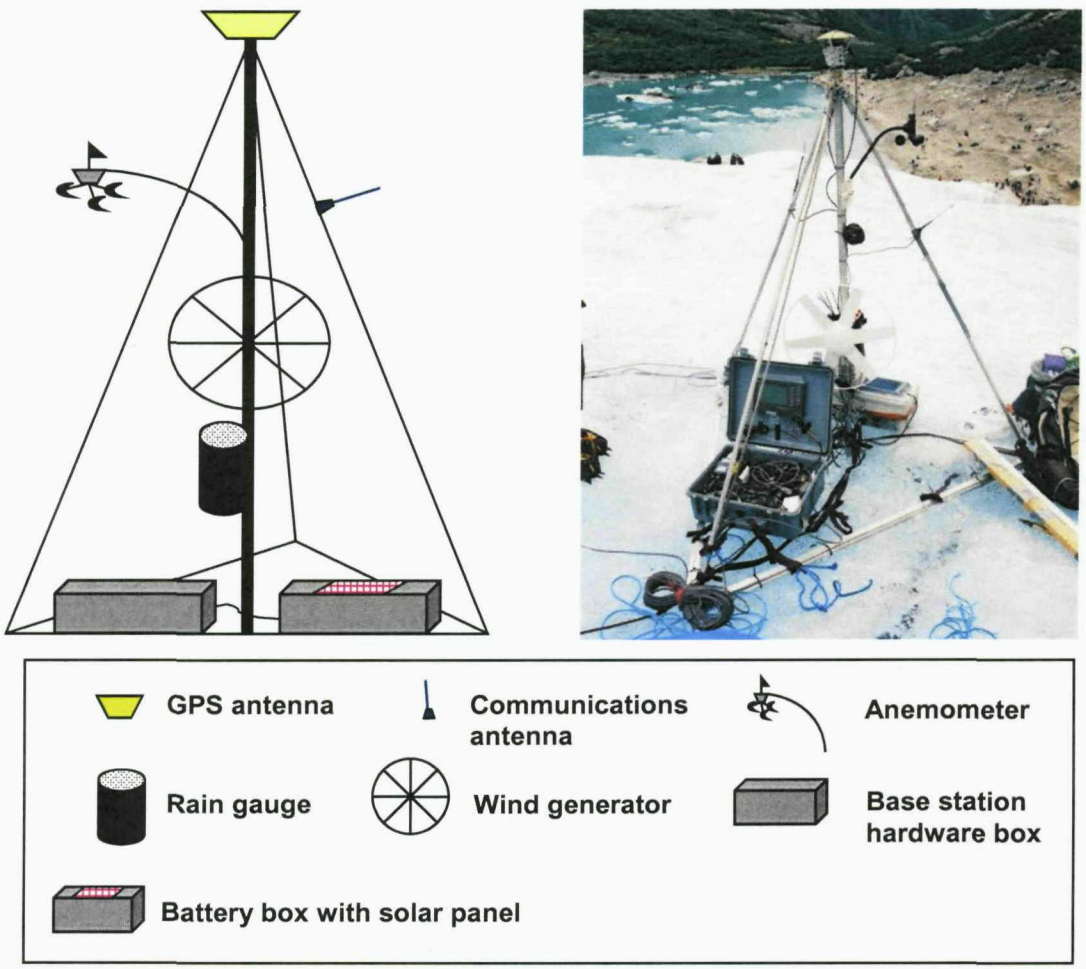


Figure 4.9: Schematic diagram and photograph of the base station in 2005.

The GPS antenna was mounted on the top of the central steel support. The rain gauge and wind generator (60 W, Rutland 503) were attached below the GPS but at a height that prevented them from becoming covered in snow in the winter (Figure 4.9). A YAGGI type antenna and anemometer (with a wind vane) were fixed to the legs of the pyramid. The ESN, GPS and weather station console (hardware) systems were located within a water tight and shock resistant 'Pelican case' (Figure 4.10). The Pelican case and a second sealed box containing the battery supply were placed on the ice, within the base of the pyramid (Figure 4.9). The boxes were tethered to the central support and the sides of the pyramid and filled with sachets of silica gel to absorb any water leaks and reduce humidity.

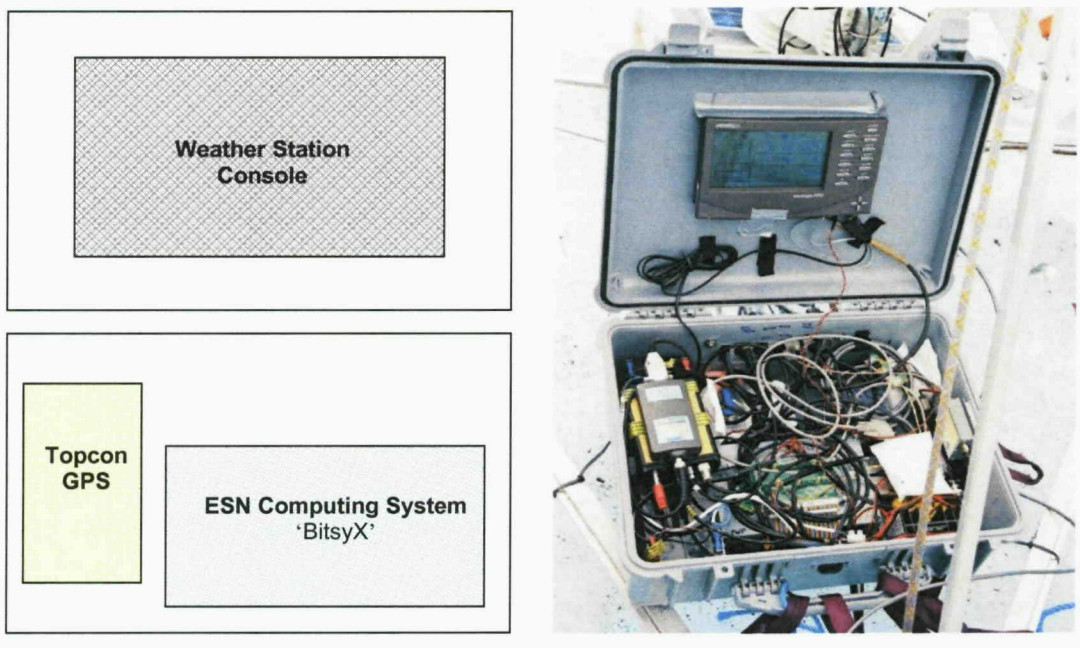


Figure 4.10: Pelican box containing the hardware for the GPS, the weather station and the ESN computing system.

4.2.2.1 Base station computing system

The most important component of this set up was the ESN computing system (Figure 4.10), which was referred to as the base station. The base station was responsible for controlling the probes and all the other systems, and storing and transferring the data obtained by each to the reference station (Figure 4.2). Figure 4.11 presents the role

of the base station in relation to the other components of the system and a technical drawing of the base station's architecture.

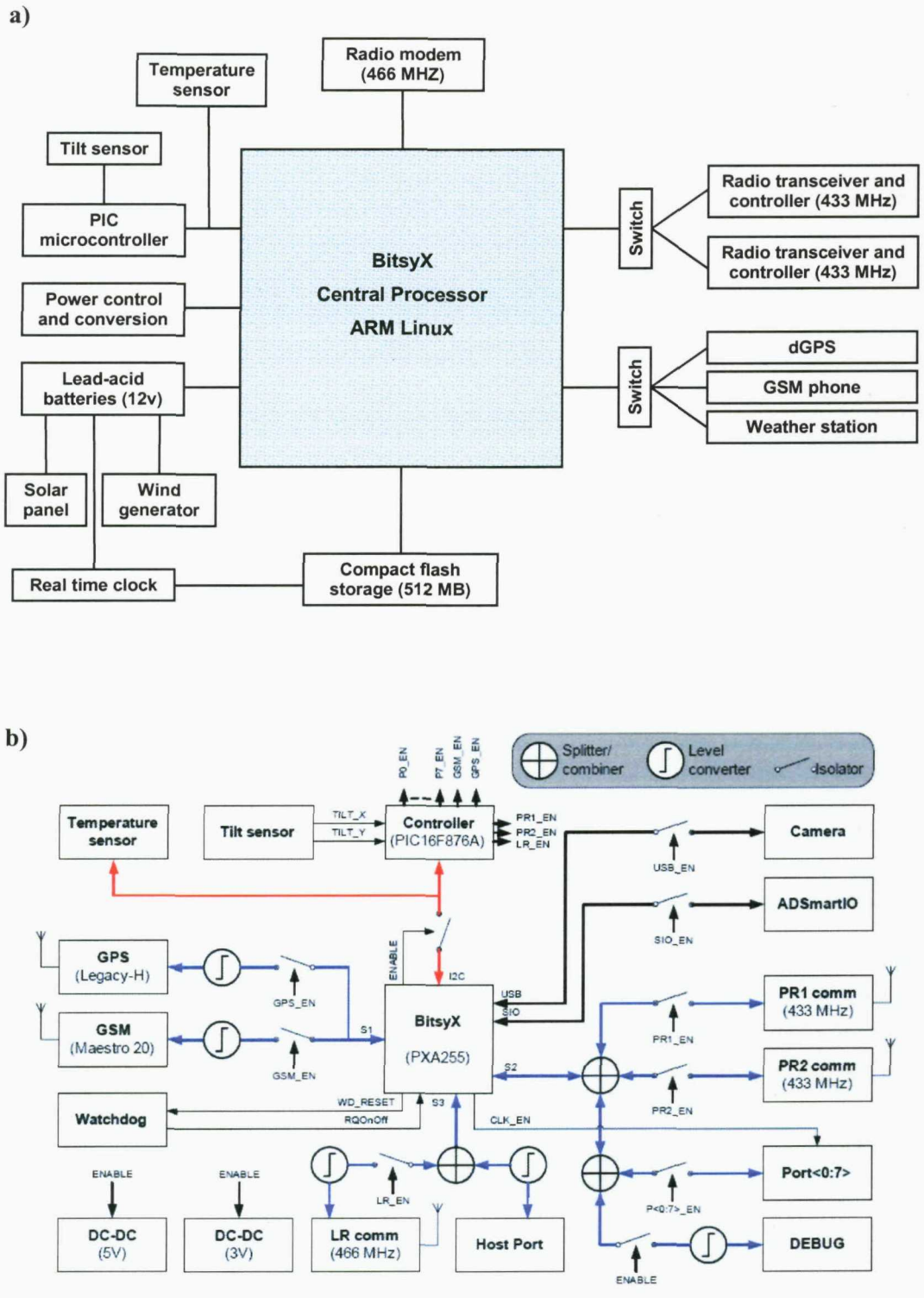


Figure 4.11: To show: a) a schematic diagram of the base station and its role in relation to the other sensing components (adapted from Hart *et al.*, 2006); and b) the base station architecture (Martinez *et al.*, 2004b).

The base station consisted of a low power StrongARM board (microprocessor) or BitsyX. It was controlled by a PIC (PIC16F877) running Linux software, which enabled remote access for diagnostics and maintenance. To conserve battery power, a 'switcher' controlled each component allowing them to be powered off when not in use. The data compiled by the base station were stored on a compact flash card. A more detailed technical description of the base station is given by Martinez *et al.* (2004a, b) and Padhy *et al.* (2005).

The operation of the other systems was orchestrated and co-ordinated by the base station (ESN) computing system. It also acted as a communications relay, storing and transferring the data obtained to the reference station. In order for this to be achieved successfully a protocol was initiated within the base station to standardise these functions (Table 4.4). The base station RTC was configured to power up the system from standby once a day, generating an operational window of 5 minutes. In this time, the base station recorded the weather station measurements and communicated with the probes (section 4.2.1.4). The tasks performed were established on a custom made version of 'cron', which is a UNIX-based scheduler. This essentially provided the base station with a schedule of tasks, enabling it to run separate jobs without clashes in communications or data transfer. It also allowed the base station to log communication retries, behaviour change and failures. Once a week, the base station remained powered up for a further 10 minutes, in order to record its location with the dGPS. Once all the sensor packages had been compiled, the base station transferred the data to the reference station, before it powered down. The ability of the base station to function correctly was highly important, as the key component for data collection and transfer.

4.2.2.2 Communications

The base station required both short and long range communication capabilities in order to exchange information with the probes, and then transfer data to the reference station, respectively. In order to aid short range communications a series of wired radio transceivers were connected to the base station (Figure 4.11). The greatest losses through ice were found to occur in the top 10 m of ice (Martinez *et al.*, 2004b). As a result, the transceivers (housed within probe cases) were lowered 20-30 m down boreholes to reduce the communication distance between the base station

and the probes. Loops of spare wire were left in the boreholes to accommodate ice movement over time and prevent the wire from breaking. The transceivers used a radio frequency of 433 MHz (in agreement with the probes, section 4.2.1.5), supported by a 100 mW power amp, to boost the signal. Any information obtained from the probes was transferred directly back to the base station via their serial cables (RS-232). The base station also had the potential to accommodate other sensors if required, such as the traditional wired instruments described in section 2.5.1, Chapter 2.

Long range communications were essential to relay the data collected by the base station to the reference station. The reference station was located 2.5 km away, without out a clear line of sight due to the rock crest of the valley. However, the additional height of the glacier in the valley meant that communications were achieved with a 466 MHz (500 mW) high powered radio modem (Figure 4.11). An omnidirectional YAGGI type antenna was used to maintain signal strength with any changes in the orientation of the base station (Figure 4.9). This system provided a 9600 baud rate (9.6 kbit s^{-1}data transfer rate), which was sufficient for the quantity of data transferred, and resulted in a reasonable transmission time and a low bit error rate (Martinez *et al.*, 2004a). In addition, because the glacier had GSM telephone coverage, a GSM modem was incorporated into the system (Figure 4.11). This was used as an additional back up so that, in the event of a failure in the long range radio communications, the data collected could also be sent back to a server in the UK via a text message (SMS). This system was tested and SMS were received. However, the success of the long range data transfer meant that this service was only initiated once during the study period.

4.2.2.3 Base station GPS

The base station was equipped with a Topcon GPS (Legacy). Differential GPS capabilities were achieved through communication with the reference station. The base station calculated its location by communicating with the reference station, which was in a 'known' location and also supported a GPS unit. The base station used the correction factor from the reference station to determine its own location more precisely. This dGPS system could provide measurements to within 5 mm and any data not retrieved were stored on a compact flash card linked to the GPS unit.

The number of available satellites at Briksdalsbreen was highly variable due to the limited sky coverage, resulting from the high and steep valley walls in the study area. Normally 4-6 satellites were visible, accounting for only half of those available. The location of the base station was determined once a week, providing a sufficient record of glacier velocity. It was also possible to vary the GPS data collection window to accommodate the shift in satellite visibility throughout the year.

4.2.2.4 Weather station

The base station weather station (VP2™ Cabled) collected data on temperature, humidity, solar radiation (sun hours), UV, pressure, wind speed, wind direction, and rainfall at hourly interval. The data generated by the weather station were stored by the base station and transferred to the reference station on a daily basis. The weather station was employed to provide a record of *in situ* conditions on the glacier, which could be related to sensor activity and glacier velocities. In the event of communication or power failures, weather data were also available from other nearby stations governed by the Norwegian Meteorological Institute (eKlima). The data used from this external source is discussed in full in section 4.4.

4.2.2.5 Power supply

The base station and its supporting components were powered by a 12 V (96 Ah/1152 W h) lead-acid gel battery. The longest operating window was of 15 minutes, once a week during the dGPS readings, resulting in a maximum power consumption of 5 W h each day (Padhy *et al.*, 2005). The battery was kept fully charged (12-13 V) with the use of a wind generator (60 W, Rutland 503) and a solar panel (15 W), which was attached to the top of the battery box (Figure 4.9). The solar panel could produce up to 15 W h per day in the summer, potentially providing up to 100 extra days of energy, for the base station (Padhy *et al.*, 2005). However, the wind generator was introduced in 2005 after the battery ran flat during the winter of 2004. Subsequently, the battery remained fully charged throughout the year.

The battery box and the central pole also provided a valuable mechanism by which the base station could be weighed down and stabilised on the ice surface. The wind generator also helped to lower the base station's centre of gravity, whilst remaining

above average snow depths in the winter, allowing it to function continuously. As a further precaution, the base station was also equipped with a tilt sensor. This acted as a guide to the movement and stability of the base station on the glacier surface. In order to keep a constant watch on the systems power supply and status, the base station generated a log file, to help prevent data loss and system failure. The log file contained readings of the probe and base station volt measurements, a log of all the probe communications (e.g. details on any retries or probe data packet errors), and the base station tilt sensor records.

4.2.3 Reference station

The reference station represented the central link in the ESN (Figure 4.1). It was responsible for communicating with the base station and ensuring that the data obtained were uploaded onto the SNS (Figure 4.2). The reference station was based in the Melkevoll Campsite Office, termed the 'café', located at the head of the Oldedalen valley, 2.5 km from the glacier (Figure 4.12). It comprised a mains powered mini-ITX PC (EPIA-PC, 500 MHz). This is a low power consumption motherboard (or PCB), running Linux (RedHat 9) software. The system was linked with the internet via an ISDN dial-up connection (Martinez *et al.*, 2004b). Long range communications via a radio modem (466 MHz/500 mW) allowed the reference station to receive data from the base station on a daily basis. A PPP (point-to-point) protocol was employed, to simplify the software it required. This system also allowed multiple retries to be performed at any time in the case of initial communication failure. All the collected and any previously unsent data were then uploaded onto the SNS via the ISDN dial-up connection (Table 4.4). The data were also archived onto the hard disk to ensure that, in the event of a communications failure with the SNS, all the data could be stored and then resent when the system was functioning again.

The reference station also acted as a gateway for system maintenance and reprogramming. A temporary communications window at 1200 h UTC was used to connect to the base station and probes via the reference station PC (Table 4.4). A secure shell protocol (ssh) tunnel was employed to access the reference station from Southampton and then a telnet session was created to reach the base station. In this

window, the base station was commanded to remain awake so that changes to the software or system configuration could be made. This system was important as it enabled complete remote reconfiguration of every component without disrupting the system's operation.



Figure 4.12: Melkevoll Campsite Office, housed the reference station. (Photo: Melkevoll Campsite website: http://www.melkevoll.no/en/bild29.htm).

4.2.3.1 Reference station GPS

In 2004, the reference station was also equipped with a Topcon GPS (Legacy) system. It acted as the position reference point, enabling dGPS capabilities for the base station, to reduce spatial errors (Figure 4.13a). Communications between the two GPS systems enabled the base station to record its location on a weekly basis. Unfortunately, in 2004 the success rate of these readings was low. As a result, in 2005, the GPS system was relocated to the glacier foreland, forming 'reference station 2' (Figure 4.13b; Figure 5.2, Chapter 5). The system was placed on the 1996/7 moraine bordering the birch forest, greatly improving the reliability of readings. The GPS antenna was mounted on a boulder of known location, whilst the accompanying components were housed in a Pelican case. The system was powered by two small sealed lead-acid type rechargeable batteries (12 V/7 Ah). They remained charged with the use of another wind generator (60 W, Rutland 503) and

solar panel (15 W). Communications were achieved via another radio modem (466 MHz, 500 mW).

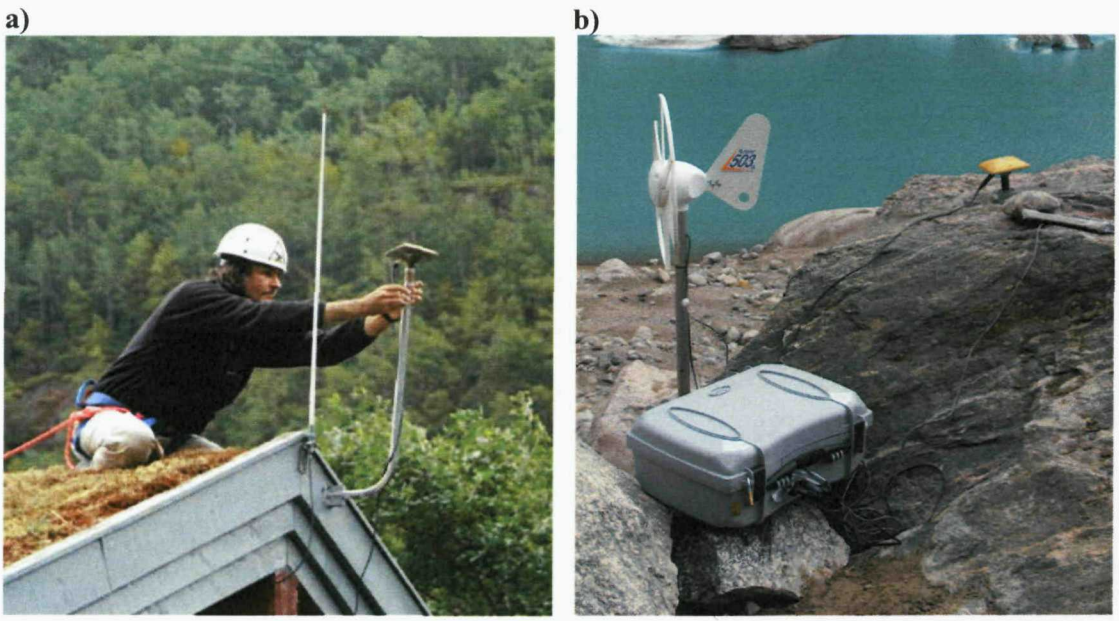


Figure 4.13: The GPS system for: a) the reference station in the café; and b) reference station 2 located on the 1996-7 moraine in the glacier foreland. The reference stations were positioned in 'known' location and enabled dGPS capabilities. (Photos: K.Martinez).

4.2.3.2 Café weather station

In 2005 an additional weather station (VP2™ Cabled) was established at the café. This generated another source of weather data from the head of the Oldedalen valley, below Briksdalsbreen. The weather station was connected with the reference station, so that data could be uploaded onto the SNS on a daily basis.

4.2.4 Sensor network server

The final component of the ESN comprised the SNS (Figure 4.1). This was established in Southampton and was essentially a Linux based data repository linked to the internet. The SNS received files from the reference station on a daily basis in accordance with the ESN system protocol (Table 4.4). It could also receive the back up SMS files directly from the base station. The information was accessed from the SNS by an end user in the form of a text file via a custom made web page. Another

web page was also designed to plot the data in graph format (Figure 4.14). The required readings and time span could be chosen by the user from a series of drop down menus, which then plotted the information automatically. This presented a fast and efficient way in which the data could be observed and compared by users. The SNS also has the potential to collate all the information generated as a database for glaciologists and for compilation into wider scale data sets.

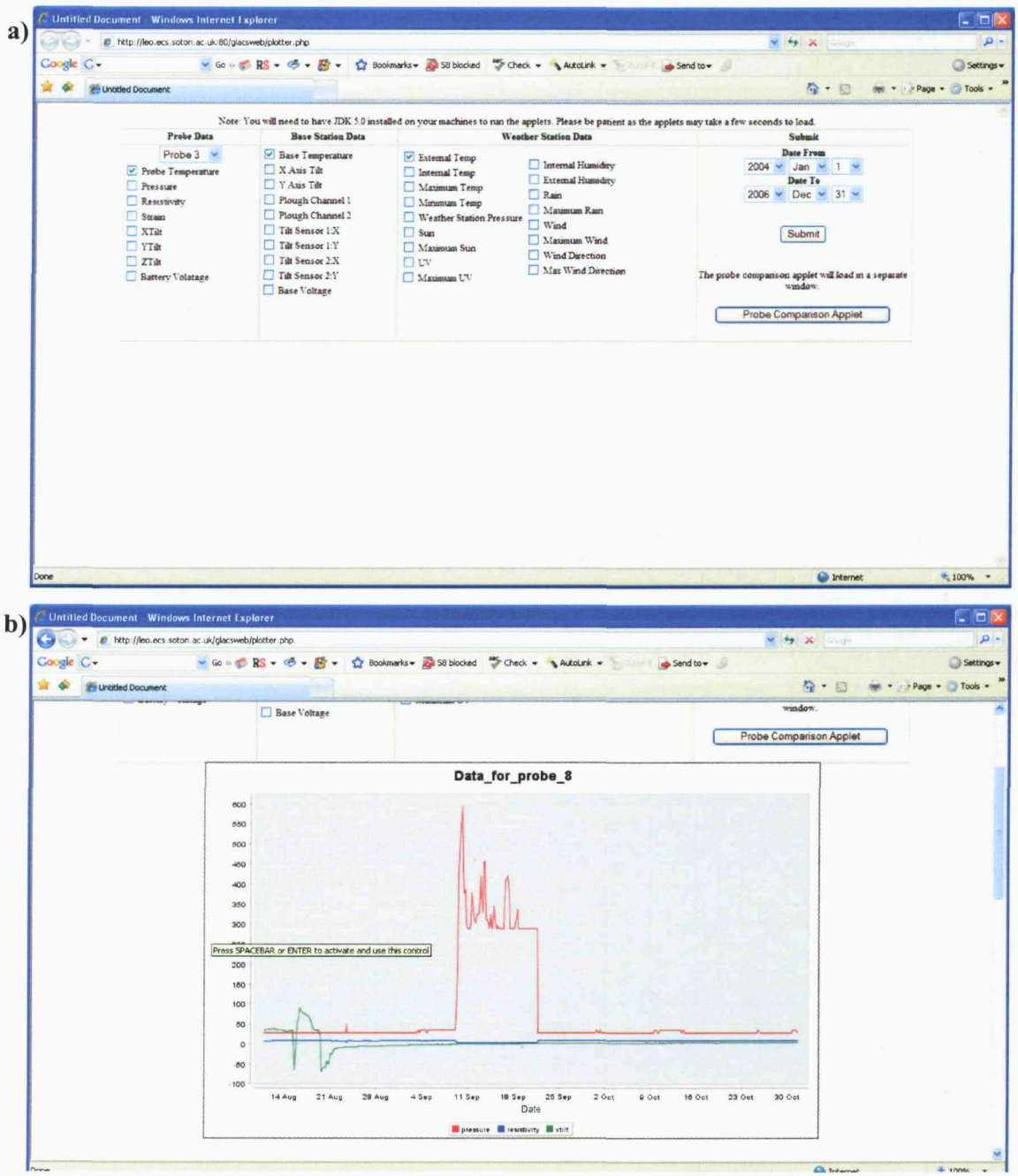


Figure 4.14: The probe data plotter web page, showing: a) the drop down menus and tick boxes used to select the readings and time span of data required; and b) a data plot produced at the bottom of the webpage (http://leo.ecs.soton.ac.uk/glacsweb/plotter.php).

4.2.5 System overview

The ESN employed at Briksdalsbreen comprised four main components: the sensor nodes, the base station, the reference station and the SNS (Figure 4.2). The probes collected, stored and transferred data from the subglacial environment on a daily basis. The base station controlled the systems operating on the glacier, co-ordinating the collection of surface information (i.e. weather and GPS readings) and probe data. The base station and the SNS were linked to the reference station which acted as a gateway, enabling remote control of the system. The data generated from the glacier were sent by the base station to the reference station, which uploaded the information onto the SNS. The reference station was also equipped with GPS capabilities. The SNS acted as the interface between the end user and the data gathered in the field. The use of linked systems meant that any or all the components could experience errors or failure at any time, disrupting the network. This weakness was counteracted with the use of built in data stores at each data collection and transfer point. The system was also designed so that all components could be modified or reprogrammed remotely, as required, to ensure the successful function of the ESN. The components of the ESN were developed and maintained by the ECS team members. However, assistance was given in the field to establish the base station and reference station, and their various components.

4.3 Field Work Techniques

A number of field work techniques were carried out systematically each year at Briksdalsbreen, in order to gather information about the study area and to help establish the ESN successfully (Figure 4.1). The techniques used are described in this section.

4.3.1 Field survey

A GPS survey was conducted at Briksdalsbreen including both the foreland and the glacier study sites (Figure 4.1). This was done to map the location of the field study sites, equipment and to monitor any changes in glacier advance or retreat between years. The GSP system used consisted of a hand held unit (on which to collect and

store data points), a GPS antenna (mounted on a graphite pole with leveller), and a rucksack, containing the power supply and communications equipment (Figure 4.15). In the glacier foreland, moraines, flutes, the lake edge and the ice margin (where accessible) were surveyed. Points were taken along the crest of each moraine ridge. On the glacier surface the location of the boreholes were recorded each year, in combination with other points of interest (e.g. the base station). The field maps produced from these surveys are presented in Chapter 5.

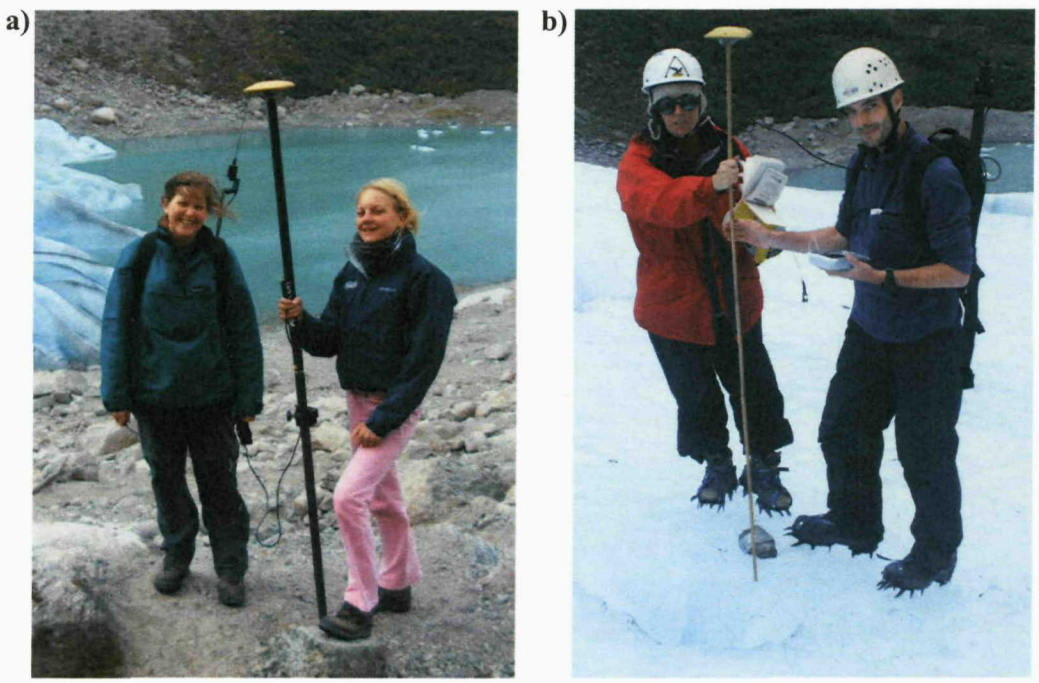


Figure 4.15: Mobile hand held Topcon Legacy GPS unit for surveying: a) the glacier foreland; and b) the ice surface. (Photos: K.Martinez).

4.3.2 Glacier study sites

An on-ice study site was established on the glacier each year (Figure 4.1). The sites were chosen away from the glacier terminus and towards the central flow line, in regions that were crevasse free and, where possible, with moderate relief. The survey sites were established as 30 x 30 m grids. An ice auger was used to create holes up to 2 m in depth, in which bamboo canes were placed to mark out the grid layout (Figure 4.16). The grids were used as the foundation from which all subsequent on-ice investigations were carried out.

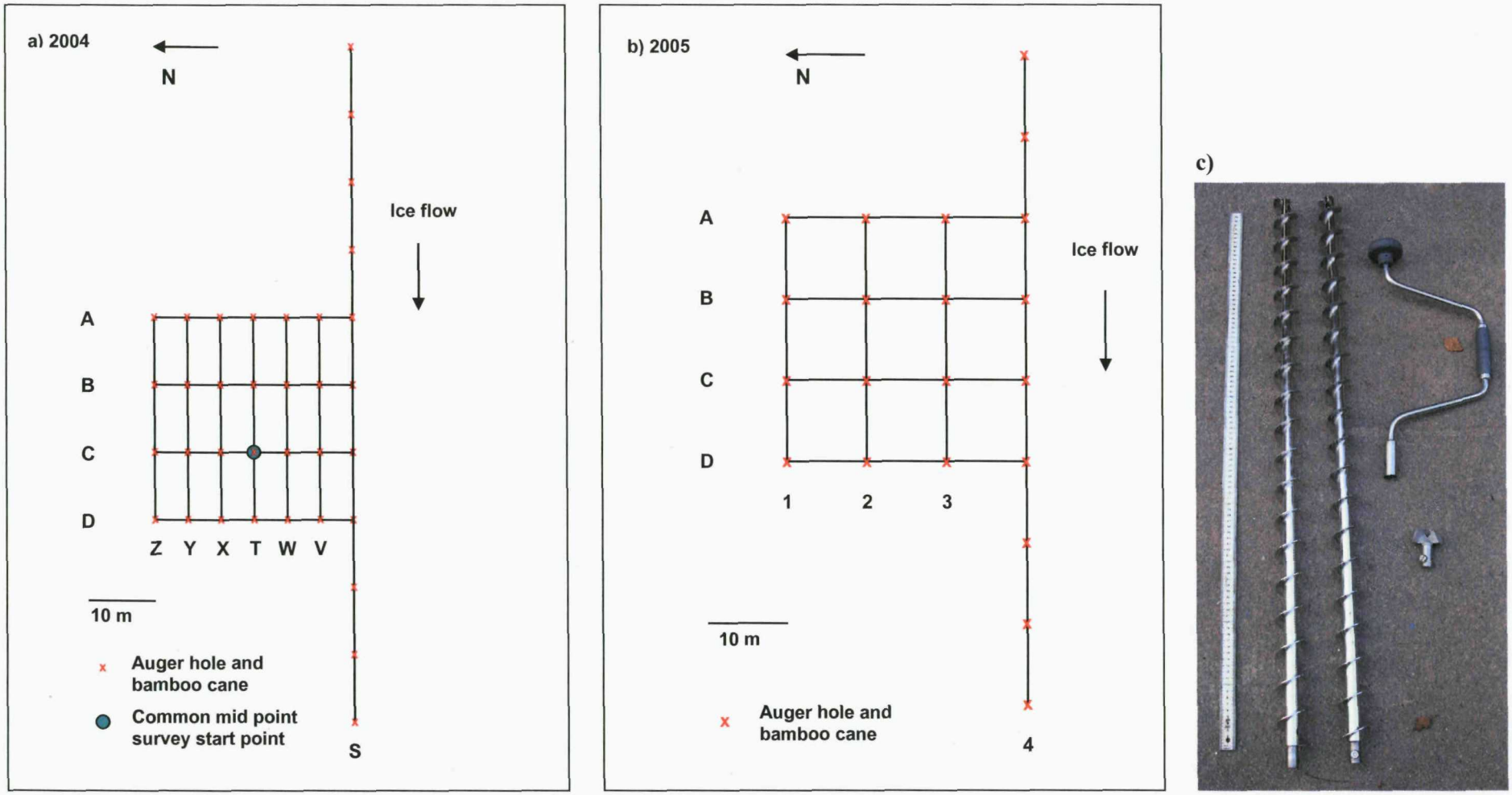


Figure 4.16: Schematic diagrams of the glacier study site grids created at Briksdalsbreen in: a) 2004; and b) 2005; and c) photograph of the ice auger.

4.3.3 Ground penetrating radar surveys

A ground penetrating radar (GPR) survey was carried out each year following the establishment of the study grids (Figure 4.1). GPR was used to provide an estimate of the glacier depth, survey the topography of the glacier bed and determine any features of interest both at the bed and within the ice column. The GPR surveys were carried out to provide supporting field information, rather than contribute large data sets of in depth analysis. The GPR survey was performed along the length of each grid transect (Figure 4.16). The extended transects 'S' and '4' were used to generate a long profile of the glacier bed.

4.3.3.1 GPR equipment and set up

A pulse EKKO 100 GPR was used at Briksdalsbreen. It consisted of two antennae, a 1000 V transmitter, a receiver, a console, a laptop and a power supply (Figure 4.17). The transmitter and receiver were each attached to an antenna (Figure 4.18). The transmitter emitted the radar pulse into the ice via the antenna. The pulse return reflections were then recorded by the receiver antenna. The size of the antennae varied according to the pulse frequency required. At Briksdalsbreen 50 MHz antennae, with a 2 m spacing and a 0.5 m sampling interval, were used for the grid transect surveys (Figure 4.18a). Fibre optic cables connected the transmitter (input) and receiver (input and output) to the system console, which was linked to the system laptop and a power supply (Figure 4.17). A separate power source was used to ensure that the survey was completed without the laptop battery expiring.

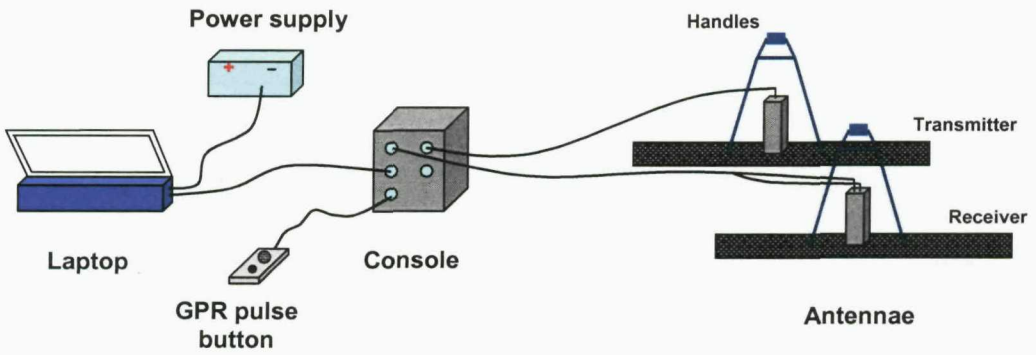


Figure 4.17: Schematic diagram to show the set up of the GPR. The antennae were accompanied by detachable handles.

a)



b)

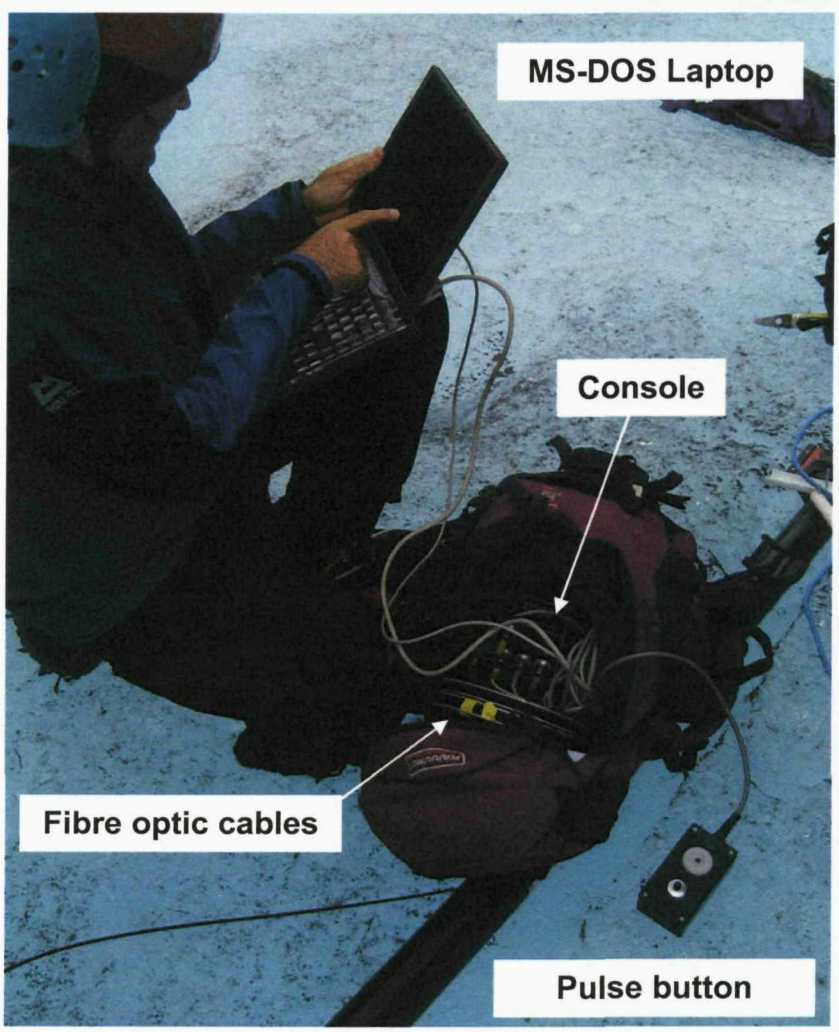


Figure 4.18: Photographs to show: a) the 50 MHz GPR antennae with transmitter and receiver attached; and b) the laptop, console, fibre optic cable and pulse sample button. Note: the power supply was placed in the base of the rucksack (Photos: M.Westoby).

4.3.3.2 Common mid point survey

The velocity of the radar can change or become attenuated as it passes through different materials, similar to the absorption of radio waves discussed in section 4.2.1.5. In order to determine the velocity of the radar pulse through the ice at Briksdalsbreen, a common mid point (CMP) survey was performed in 2004 near the centre of the study grid (Figure 4.16a). Handles were attached to the 50 MHz antennae and they were placed 50 cm apart, equidistant on either side of the centre point (Figure 4.19). The distance was noted with a tape measure placed along the grid transect C (Figure 4.16a). A pulse was taken and the antennae were then moved a further 25 cm each away from the centre point, increasing the distance between the two by a total of 50 cm. This process was repeated for the length of the transect. The survey determined that the radar velocity through ice at Briksdalsbreen was 0.16 m ns^{-1} (Hart *et al.*, 2006). This information was required for the subsequent analysis of GPR data in the REFLEXW (v. 3.0) software package (section 5.3, Chapter 5).

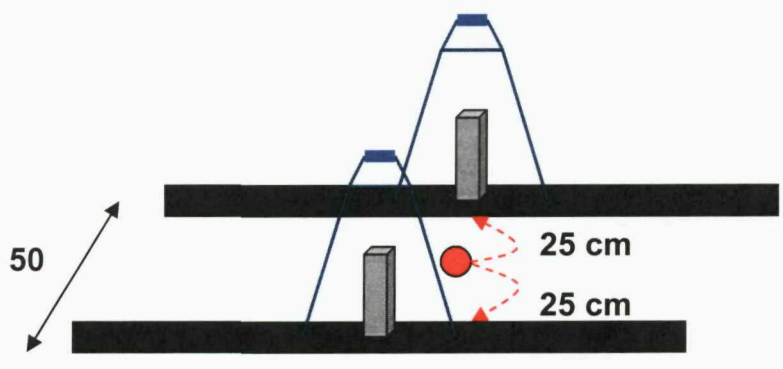


Figure 4.19: Schematic diagram to show the set up of the GPR antennae for the CMP survey. The transmitter and receiver were connected to the rest of the system as shown in Figure 4.15.

4.3.3.3 Grid survey

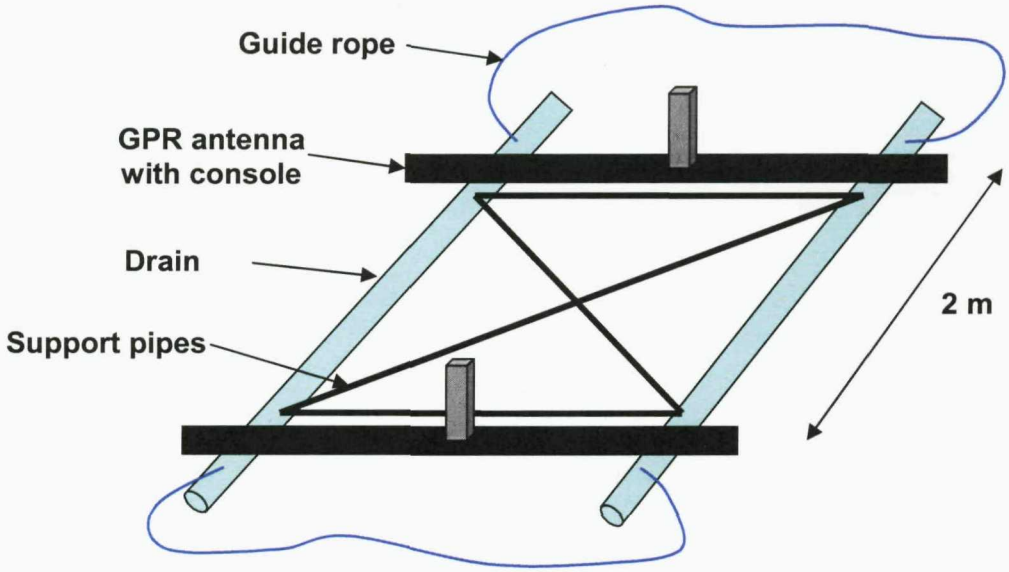
The study grids were surveyed with the 50 MHz antennae. This frequency provided a good compromise between signal resolution and attainable survey depth (i.e. the size of the radar foot print). To facilitate the surveying of the study grids, a 'sledge' was designed, to separate the antennae at the required fixed distance and assist their

movement over the glacier surface (Figure 4.20). The sledge consisted of two drain pipes held in parallel alignment by cross piping. Plastic was used wherever possible, as metal might interfere with the radar. The antennae were placed exactly 2 m apart in custom made slots cut out of the piping. This allowed the antennae to lie flush with the ice surface. The antennae were fastened with gaffa tape and the whole structure was guided using rope attached at both ends.

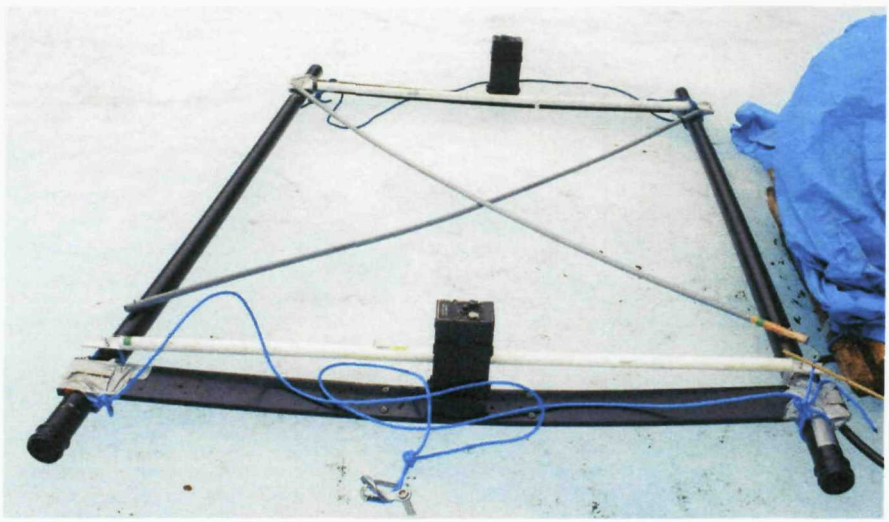
Three people were used to take the GPR transects: one to take pulse readings and control the system with the laptop and two to ensure that the sledge was stable and in the correct location along the transect. In order to systematically take readings along the transect, the console, power supply and fibre optic cables connecting to the transmitter and receiver were placed within a rucksack (Figure 4.20c). The laptop was held in-hand in order to run the system. The sledge was drawn along each transect, marked out by a tape measure, and a pulse was taken at a sampling interval of 0.5 m. The transmitter and receiver were mounted on the antennae facing in the same direction and the transmitter was always moved first along the transects. The transects were surveyed east to west in the longitudinal direction and from north to south in the latitudinal direction (Figure 4.16).

The data were stored for analysis using the REFLEXW (v. 3.0) software programme. An initial review of the raw data was performed in the field in order to determine if there were any unusual characteristics at the glacier bed or within the ice column. The information was used in subsequent investigations to avoid irregularities, which might interfere with, or damage, instrumentation.

a)



b)



c)



Figure 4.20: The GPR sledge: a) schematic diagram; b) photograph of the GPR sledge with antenna; and c) the whole system in operation. (Photo c: M.Westoby).

4.3.4 Hot water drilling

The information provided by the GPR survey acted as a foundation for the *in situ* borehole investigations that followed each year. The hot water drill was transferred to the glacier surface via helicopter. This was used to create the boreholes, via which the subglacial environment was accessed and then instrumented (Figure 4.1). The hot water drilling system comprised four basic components: a water source, a drill, a high pressure hose and a drill stem (Figure 4.21 and 4.19).

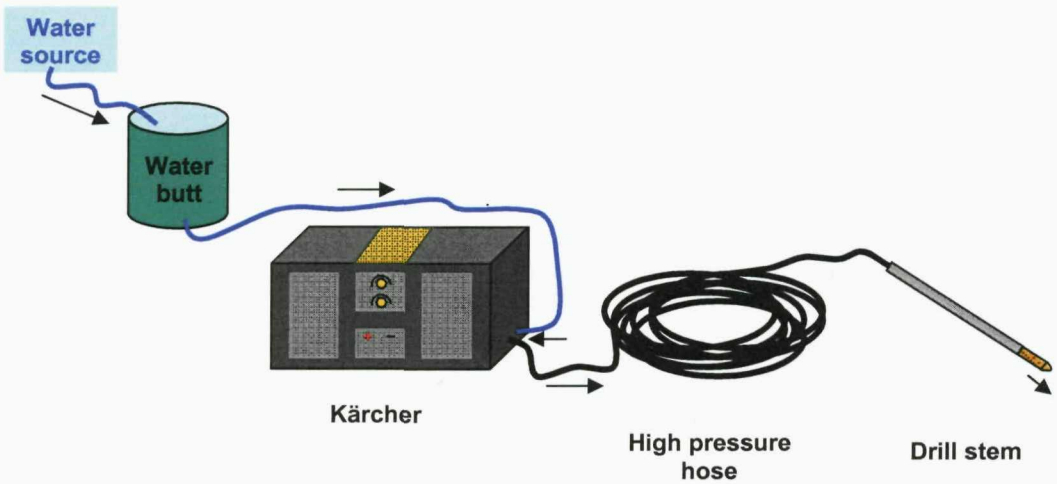
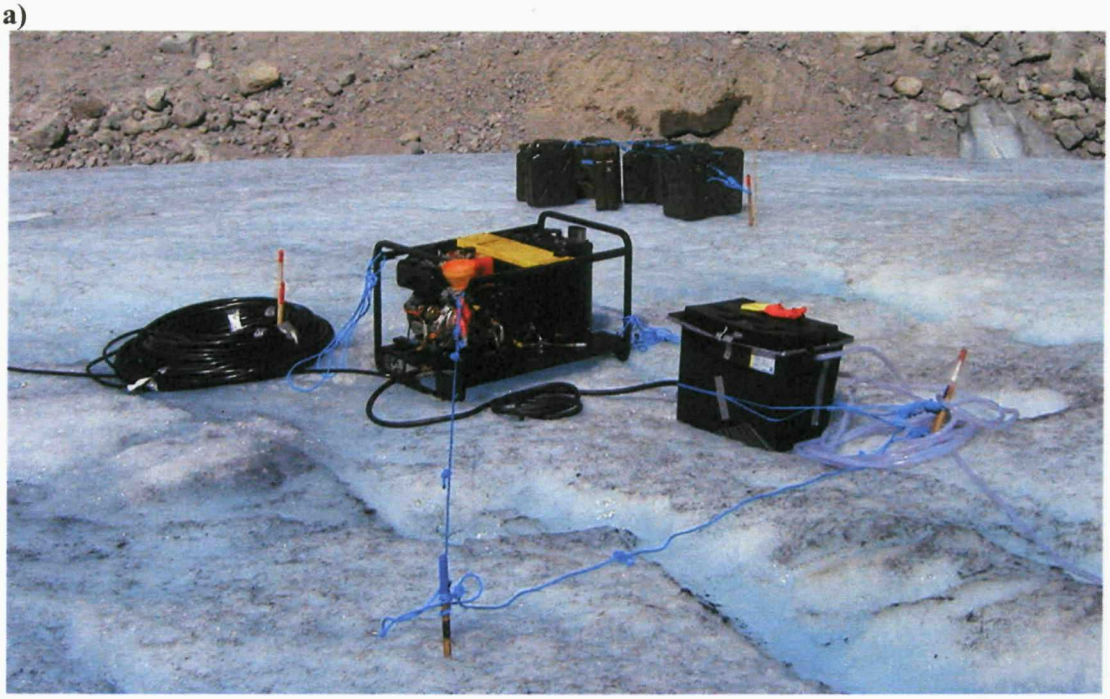


Figure 4.21: Overview of the hot water drilling system.

The hot water drill was a Kärcher HDS 1000DE car wash (Figure 4.22b). The Kärcher consisted of a diesel powered engine designed to heat (0-150 °C) and then release water at high pressure (0-300 psi). In order to create the boreholes, a high pressure hose and drill stem were attached to the Kärcher. The drill stem was a rigid hollow steel pole (similar to scaffolding), 2 m in length and capped by a drill tip (Figure 4.23). The drill stem was attached to a high pressure pipe of required length, which was connected to the Kärcher (Figure 4.22a and 4.21a).

a)



b)

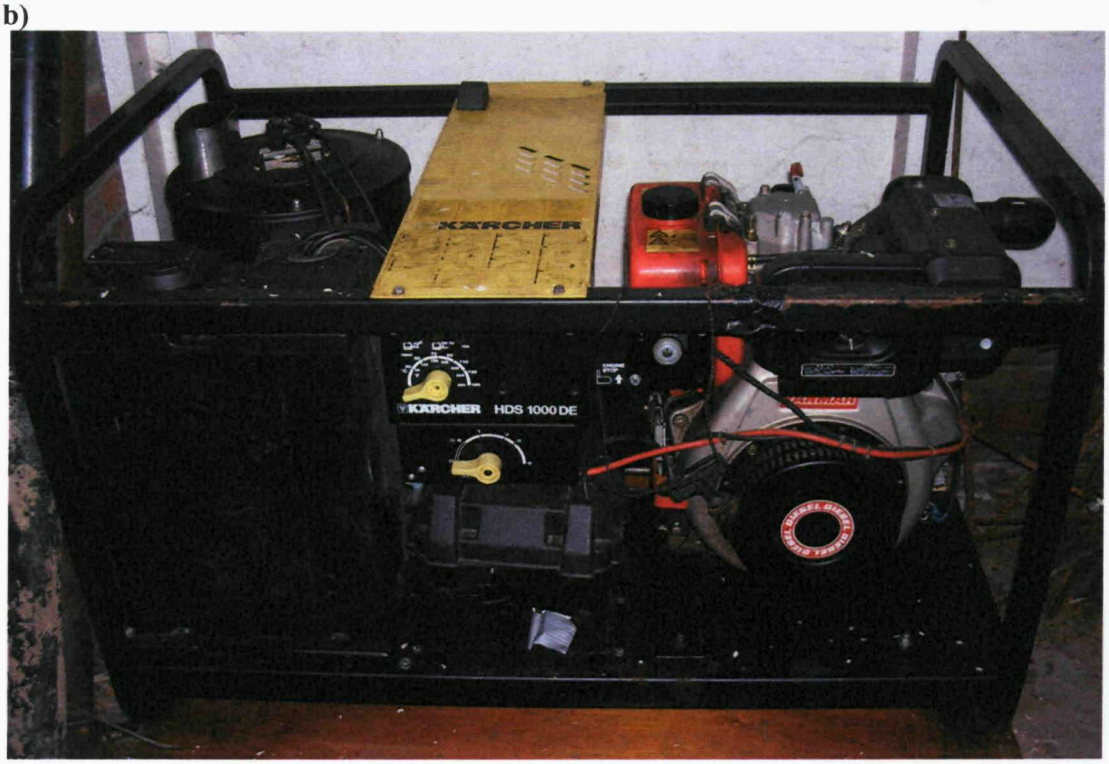


Figure 4.22: Photographs of: a) the drill set up, showing (from left to right) the high pressure hose, the Kärcher (with jerry cans behind), the water butt, and the hose feeding the butt from the supra-glacial water source; and b) the Kärcher, showing the fuel tank in the front left with the water heater behind, the battery and temperature controls in the centre, and the engine on the right.

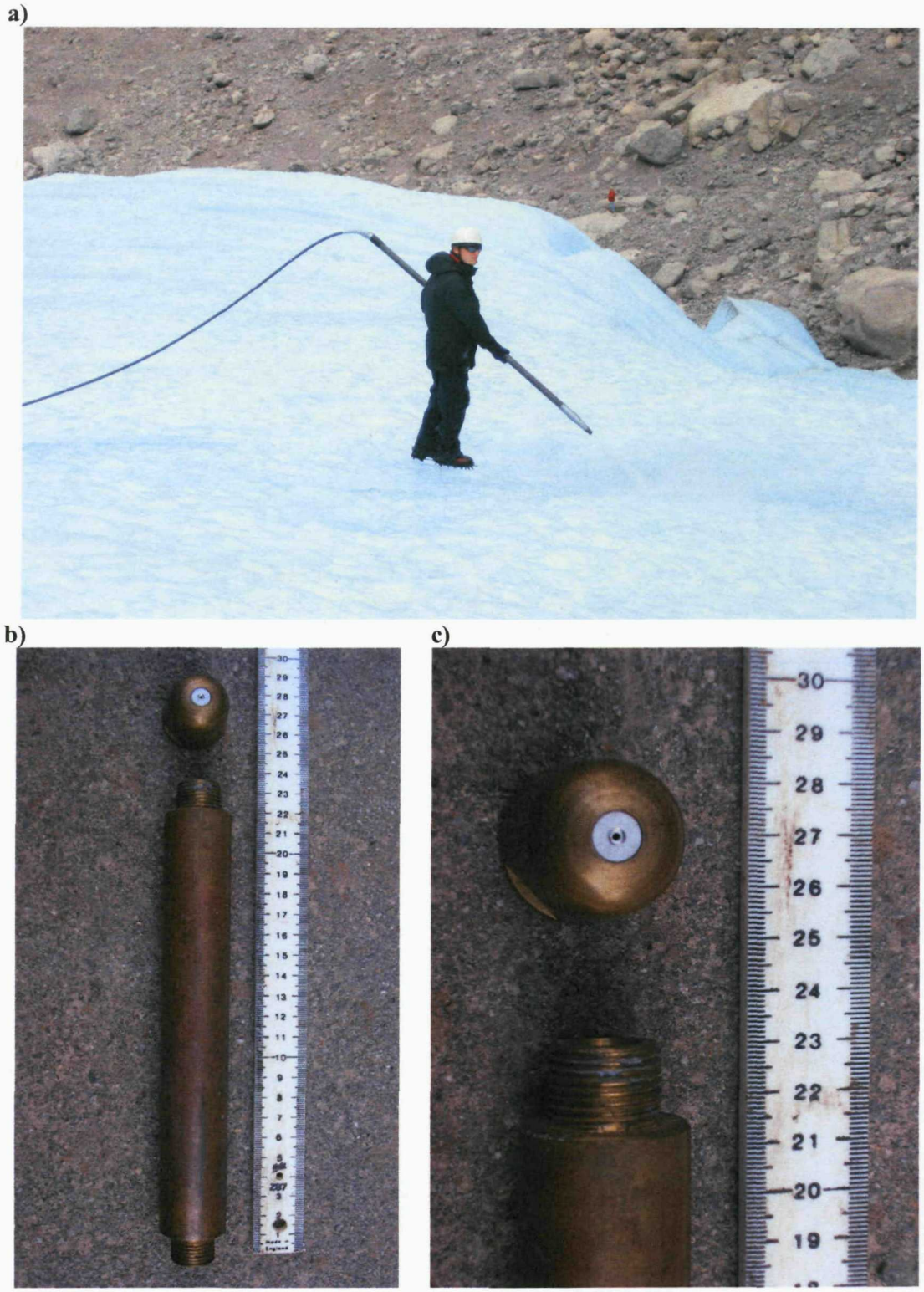


Figure 4.23: Photographs to show a) the drill stem in use; and b) the drill tip, which is attached to the base of the drill stem. The aperture for the drill tip can be changed as required. This focuses the hot, pressurised water, which melts the ice and create a borehole.

The drill stem helped the borehole to remain straight on drilling, whilst the single outlet drill tip focused the pressurised water (Figure 4.23b,c). The pressurised hose was measured and marked at 10 m intervals from the drill tip to the end, totalling 115 m in length. This was done in order to measure the length of the boreholes and thus, the depth of the glacier. This also provided a depth measurement for any events that occurred on drilling, such as borehole draining or the release of air or sediment from an englacial pocket.

A continuous and bubble free water source was fed into the drill from a water butt located up ice (gravitational flow). Filters (200 μm, and 280 μm) were also attached to both the inlet and outlet pipes from the water butt to remove any particulates, which could damage the drill's internal structure. The area under investigation at Briksdalsbreen was free from snow, which is normally melted as the primary source of water for the drill. As a result, the water supply to the butt was sourced from supra-glacial channels and cavities via additional piping (Figures 4.19 and 4.20a). In these circumstances, even though Briksdalsbreen was a very 'clean' glacier with little surface debris, the use of filters was essential. Once a continuous water supply had been established and the water butt was at capacity, drilling commenced (Figure 4.24a,c). As the ice melted under the hot water the hose was fed into the borehole until the glacier bed was reached. It was hoped that the drill would excavate a small indentation within the till (Blake *et al.*, 1992), that would encourage the probes to become incorporated into the deforming bed.

4.3.5 Borehole observations

A borehole record was maintained throughout drilling, noting the positions and depths of the boreholes, and any events that occurred during drilling. Boreholes were typically 10-20 cm in diameter at the surface (Figure 4.24a, b). The number of boreholes drilled each year and their depth varied according to the needs of the investigation. The majority of the boreholes were drilled to the glacier bed, but some were drilled to different depths within the ice column to accommodate englacial probes and the wired transceivers (section 4.2.2.2). The position of the boreholes was allocated in relation to the established survey grid and based on the results of the GPR survey. The boreholes were labelled from 1-16 in 2004, and from A-M in 2005.

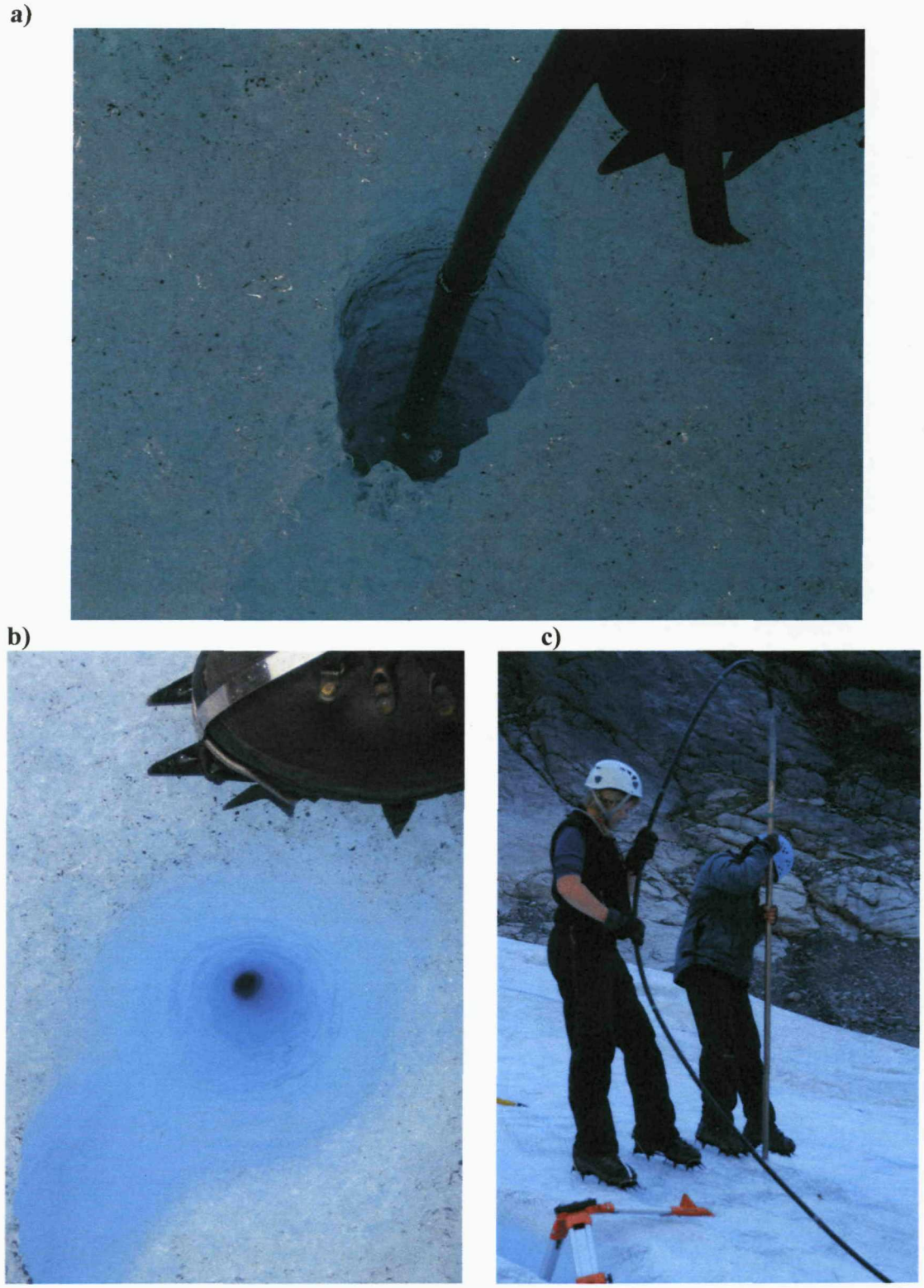


Figure 4.24: Photographs to show: a) the high pressure hose passing down the borehole during drilling; b) a completed borehole that drained; and c) the drill stem at the start of drilling. (Photos: a) D.Vaughn-Hirsh; b) S.Stafford; and c) K.Martinez).

A custom made CCD video camera, termed the BoreCam, was used to investigate as many boreholes as possible (Figure 4.1). However, not every borehole was inspected each year. In 2004 the BoreCam consisted of a monochrome, infra-red (900 nm) camera (Figure 4.25c). In 2005, a similar colour camera was used instead, illuminated by white LEDs (Figure 4.25a, b). The BoreCam was sealed within waterproof casing, linked to the surface via a cable. The cable measured 120 m and was labelled at 1 m and 5 m intervals to provide a second measurement of borehole depth and to allow the depth of any englacial features to be noted. The cable was attached to a reel that allowed the camera to be readily fed into the borehole. The video footage produced was viewed at the glacier surface with a hand held digital video camera, providing instant information on the subglacial environment (Figure 4.25d). The video footage revealed conditions at the glacier bed, confirming the presence of till and/or bedrock, and flowing water, which might indicate a subglacial channel. The BoreCam was also used to verify the location of the probes once deployed.



Figure 4.25: Photographs of the BoreCam, showing: a and b) the 2005 CCTV type colour camera with LEDs set into a surround around the lens; c) the 2004 monochrome infra-red camera (between Jane Hart's feet), with wire reel and video camera; and d) viewing footage from the BoreCam in 2005. (Photos: K.Martinez).

4.3.6 Sediment sampling

In situ sediment sampling was attempted in every borehole that connected with the glacier bed (Figure 4.1). This was carried out with the use of a sediment sampler, which consists of a sample chamber attached to a percussion hammer. The percussion hammer (Blake *et al.*, 1992; Figure 4.26a) was used to insert the sediment sampler (Figure 4.26b) into the underlying till. It consisted of a steel rod body (2 m in length) with a striker and anvil at the base. The striker was 40 cm in length and weighed approximately 2 kg. It behaved like a sheath and was able to move along the steel rod, pulled by the attached wire cables. A lip at the top of the steel rod, and the anvil at the base, prevented the sheath from coming off. The sediment sampler was attached below the hammer's anvil. The instrument was lowered to the bed of the borehole using a reel (Figure 4.26a, c). The striker was then raised and dropped onto the anvil numerous times, gradually hammering the sampler into the till (Figure 4.26c). Once the sediment sampler was fully inserted, the whole instrument was pulled back to the surface (Figure 4.26d).

The sampler comprised a chamber with a moveable sheath (Figure 4.26b). When hammered into the subglacial sediment the sheath was forced upwards. This exposed a window to the hollow interior of the chamber, into which the sediment was forced. Two sizes of sampler were used: a 'large' sampler with a sediment collection volume of 106.8 cm^3 and a window size of 22.8 cm^2; and a 'small' sampler with a sediment collection volume of 125.7 cm^3 and a window size of 12.0 cm^2 (Figure 4.26b). The different samplers were tested each year and the one that obtained the most sediment was used preferentially. Once at the surface, the sediment was extracted and sealed in a labelled sample bag for analysis later (Figure 4.26d). Although the sediment sampler was used in the majority of boreholes, sediment samples were not always retrieved, even if till had been viewed with the BoreCam (section 4.3.5).



Figure 4.26: Sediment sampling, showing: a) the percussion hammer attached to a wire reel, the anvil is at the base and the sediment sampler is attached below; b) the small and large sediment samplers; c) using the percussion hammer to insert the sampler at the glacier bed; and d) the resulting sediment sample as it is extracted from the sampler at the surface and bagged. (Photo b: A.Vowles. Photos c, d: E.Guizzo).

4.3.7 Probe deployment and the ESN

The final task at the study sites was the deployment of the probes (Figure 4.1). The construction of the probes was completed by the ECS team members at the Melkevoll camp site (e.g. final software and hardware checks and sealing). Once sealed, the probes were fully operational and began to collect sensor readings. The probes were preferentially deployed in boreholes that were known to contain till. This was done to increase the chances of probe incorporation into the deforming bed. A number of probes were also placed in boreholes that did not connect with the glacier bed to monitor conditions with the ice column (englacial probes). If the boreholes remained full of water the probe was simply dropped into the water column, allowing it to fall slowly to the base of the borehole. If the borehole had drained, a length of fishing wire was attached to the probes with electrical tape (Figure 4.27). The fishing wire was strong enough to hold each probe, but flexible enough that it could be removed with a sharp tug once the probe had reached the glacier bed. Once in place at the ice-bed interface the BoreCam was often used to check the location of the probes. The probes were left *in situ* to become incorporated into the subglacial environment and potentially the deforming bed.

Over the course of the field season, the base and reference station components of the ESN had been established. The ECS team members had ensured that the software and hardware components of these systems were operational. The communications systems were also tested. The base station structure was already established on the ice but assistance was provided to locate the station, enable the systems and ensure they were functional. The same was true for the reference station(s). The systems were established so that the probes could commence communications and data transfer with the base station immediately (sections 4.2.1.4 and 4.2.2.1). Normally, data collection began whilst the team was still in the field. This meant that any errors in the base station and reference station set up could be rectified prior to the end of the field season. The deployment of the probes was the final stage in establishing the ESN at Briksdalsbreen. At the end of the field season the ESN was in operation (Figure 4.2). The probes were within the subglacial environment, the base station was established on the ice, and the reference station(s) were functioning.

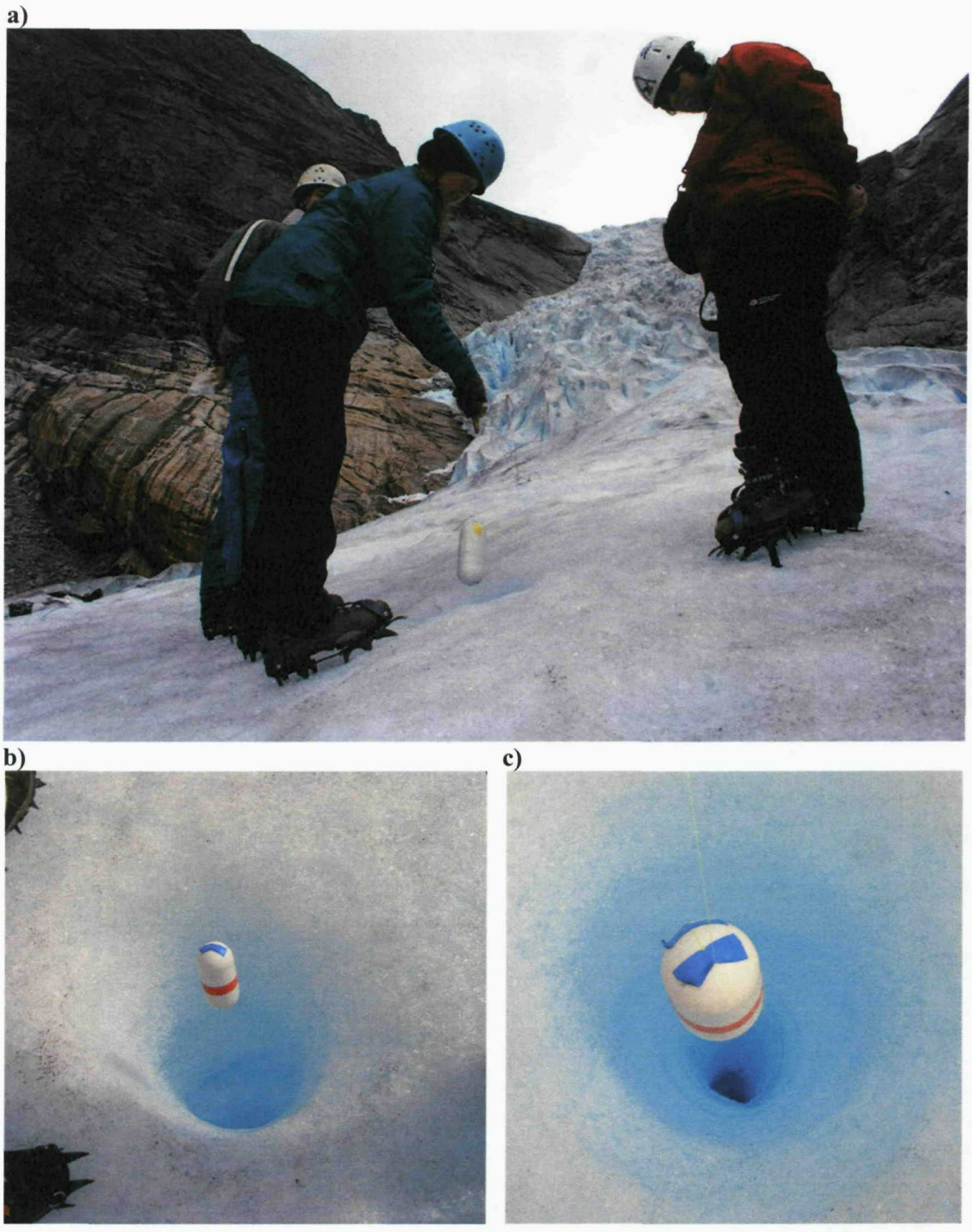


Figure 4.27: Photographs depicting the deployment of the probes. Fishing wire was attached to the probes with electrical tape. The probes were lowered to the glacier bed before the wire was pulled free. (Photo a: E.Guizzo. Photos b, c: K.Martinez).

4.4 Norwegian Weather Data: eKlima

A weather station was established on the base station to record *in situ* weather conditions from the glacier (Figure 4.9, section 4.2.2.4). Unfortunately, the weather station suffered frequent mechanical problems. As a result, data were obtained from the Norwegian meteorological office (eKlima) to fill in the data gaps. A series of weather stations, located in proximity to Briksdalsbreen, were identified and temperature records were obtained from each (Figure 4.28). The data were then plotted against that from the Briksdalsbreen weather station and a regression line was fitted (Table 4.5). The eKlima weather station with the strongest correlation to the base station data were used as the primary data source (i.e. the Stryn station). The equivalent temperatures for Briksdalsbreen were calculated using the coefficient equation from the primary eKlima station. If data were missing from both the weather station and the primary station, the secondary eKlima station was employed to complete the few remaining data gaps.

Daily precipitation data were obtained from an eKlima rain gauge located near Briksdalsbreen, in the Oldedalen valley (Figure 4.28; Table 4.5). The data from this rain gauge were considered to provide a good representation of precipitation on the glacier. As a result, the data were not modified. The final weather data set used for this investigation consisted of a combination of the *in situ* base station weather data and extrapolated data from neighbouring eKlima weather stations. The data set comprised daily precipitation values and temperature readings every four hours, in accordance with the number and timing of daily probe readings.

Table 4.5: Details of the eKlima* weather stations, their location and correlation with the Briksdalsbreen base station weather readings.

Location	Station Number	Latitude	Longitude	R^2 2004/5	R^2 2005/6
Base station weather station	-	61.40	6.57	-	-
Stryn	58900	61.9157	6.5592	0.8022	0.8088
Sogndal	55700	61.1500	7.1333	0.6699	-
Sognefjellhytta	55290	61.5852	7.9982	-	0.8126
Briksdal rain gauge	58480	61.6945	6.8097	-	-

*http://shimmer.oslo.dnmi.no/portal/page?_pageid=35,96278,35_96303&_dad=portal&_schema=PORTAL



Figure 4.28: Map to show the location of the eKlima weather stations in relation to Briksdalsbreen, which is marked on the map above as Briksdal (adapted from MapQuest: http://www.mapquest.com/maps/latlong.adp).

4.5 Sediment Analysis

A series of sedimentological analyses were performed at Briksdalsbreen. This included both investigations in the glacier foreland, as well as laboratory work on the sediment samples retained from the study sites each year (Figure 4.1). The methods used are described in this section.

4.5.1 Foreland sampling

Two 10 x 10 m areas were chosen at random in the glacier foreland; one in a glacier proximal location, and one in a distal location. Similar to the glacier study sites (section 4.3.2), each area was divided into a grid of nine sample points, each 5 m

apart. The texture of the material at each sample point was noted as either 'till', 'coarse till' (contained large clasts), or 'boulder'. Bulk sediment samples were collected for further analysis from all grid points, except those allocated as 'boulders'. This included a sediment sample from a flute. In November 2006, the glacier had retreated so much that the area in which the *in situ* sediment samples had been collected was exposed. As a result, a bulk sample was also taken from this area.

4.5.2 Grain size analysis

The sediment samples collected *in situ* from the subglacial environment (section 4.3.6) and from the glacier foreland (section 4.5.1) underwent grain size analysis in the laboratory. This involved a combination of first dry sieving and then laser granulometry.

4.5.2.1 Dry sieving

The process of dry sieving divided sediment samples into different grain size fractions by weight. The samples were separated by a series of Endecotts laboratory test sieves with different mesh sizes (Figure 4.29a). The sieve sizes used decreased in half phi increments, ranging from an equivalent of 64000-2000 μm. The sieves were stacked from smallest to largest mesh size (bottom to top) and a collection tray was placed at the base to collect those particles less than 2000 μm in size. The sieve stack was placed on an Endecotts EFL 2000 test sieve shaker. The sediment sample under analysis was weighed and then fed into the topmost sieve (64000 μm), which was then sealed with a lid. The whole stack was held in place by a second lid, which clamped the sieves in place and stopped them rotating with the movement of the shaker (Figure 4.29b). The shaker was turned on for 10 minutes, during which time the sediment sample separated out into the different test sieves according to grain size. The test sieves were then removed one by one and the sediment fraction inside each was removed, weighed, and bagged. The sediment that remained in the basal tray was removed, weighed and classed as the less than 2000 μm fraction.

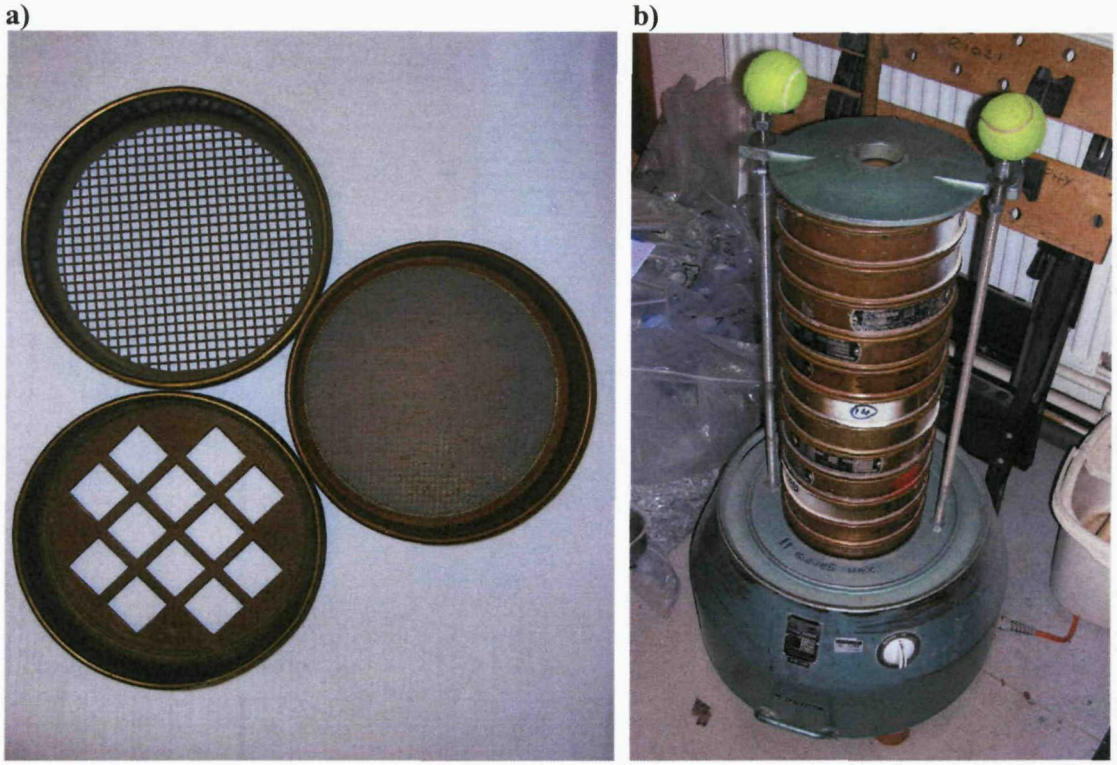


Figure 4.29: Dry sieving, showing: a) example test sieves with different mesh sizes; and b) the test sieve shaker with a stack of 11 test sieves, a collection tray at the base, and a lid to clamp the stack in place.

4.5.2.2 Laser granulometer

The less than 2000 μm fraction of the sediment samples underwent further analysis with a Malvern Mastersizer 2000 laser granulometer, with a Hydro 2000 MU sampling unit. This was used to determine the grain size distribution of the fine fraction of the sediment samples by volume. The samples were pre-prepared for use in the laser granulometer. If the sample was large enough the sediment was sub-sampled using a quartering technique. Two sub-samples of 0.4 g (sample A) and 0.5 g (sample B) were placed in glass pots three quarters full of 0.5% sodium hexameta-phosphate. If the sample was small, which occasionally occurred with the *in situ* subglacial samples, the whole sample was mixed with the sodium hexameta-phosphate. The samples were then agitated gently for 5 minutes with ultra sound in a Kerry tank.

The laser granulometer programme was configured for manual use. The pump speed was set at 2700 and the required obscuration level was between 10-20%. Prior to

analysis, the rotator blade was cleaned in a beaker of deionised water (and on occasion with an ultra sound pulse for 10 seconds) and background interference was measured. A fresh beaker of deionised water (~700 ml) was used to analyse each sample. The samples were added to the beaker when prompted by the machine and the results were recorded automatically. Three runs were completed for each sample and an average of the readings was recorded. The sample results were saved in an Excel spread sheet, as a percent of the total volume. The grain size distribution fractions were measured in quarter phi unit increments, equivalent to a range of 1692-1.261 μm.

4.5.2.3 GRADISTAT v.5.0

The samples were analysed using the GRADISTAT v.5.0 programme (Blott and Pye, 2001). The sample results were input into this Excel based programme. This included the associated grain size fraction, the sample identity, initial weight and the percent of sediment in each grain size fraction, as a proportion of the total sample weight (Figure 4.30). This was calculated from a combination of both dry sieving (64000-2000 μm) and laser granulometer results (1692-1.261 μm). The amalgamation of results in this way, despite the use of different techniques, has become standard, with minimal associated errors in this context (Blott and Pye, 2006). Once the data were inputted into the spread sheet the sample statistics were calculated for use, as required. The programme produced various spread sheets of data including: sample statistics, ternary diagrams, and grain size distribution graphs. The sample statistics included a variety of methods for calculating the sample mean, sorting, skewness and kurtosis. The Folk and Ward (1957) method was used in preference.

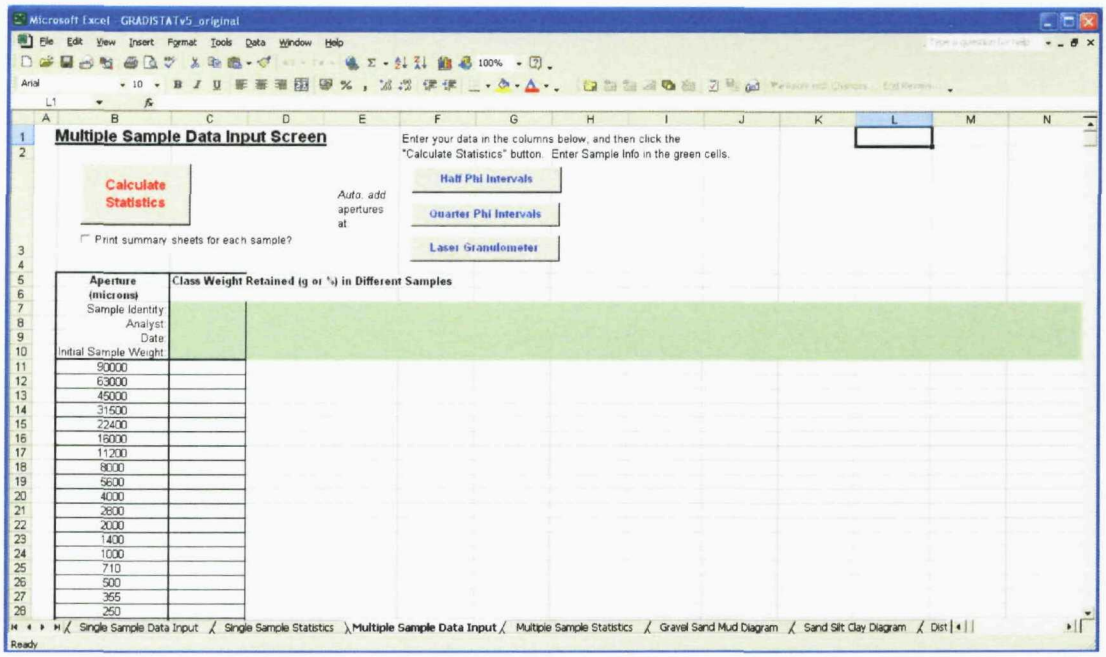


Figure 4.30: The GRADISTAT v.5.0 Excel spread sheet used for the analysis of multiple sediment sample data (Blott and Pye, 2001).

4.5.3 SEM analysis

The *in situ* subglacial samples collected in 2004, 2005 and 2006 were analysed with the scanning electron microscope (SEM). The sample preparation and subsequent grain analysis under the SEM is discussed in this section. An overview of the process, which was systematically repeated for all the samples, is depicted in Figure 4.31a.

4.5.3.1 Sample preparation

A variety of techniques were available for the preparation of grains for analysis under the SEM (e.g. Helland and Holmes, 1997; Mahaney *et al.*, 1996; Strand *et al.*, 2003). The less than 2000 μm fraction of the subglacial samples were prepared in accordance with Figure 4.31b. The samples were sub-sampled into quarters and grains mounted onto a carbon coated SEM pin stub (12 mm stub face diameter, 6 mm length). Excess and loose grains were removed from the edge of the stub with tweezers and a gentle tap, respectively. The stub was then labelled underneath with the sample name and a black line was marked on the side of the stub.

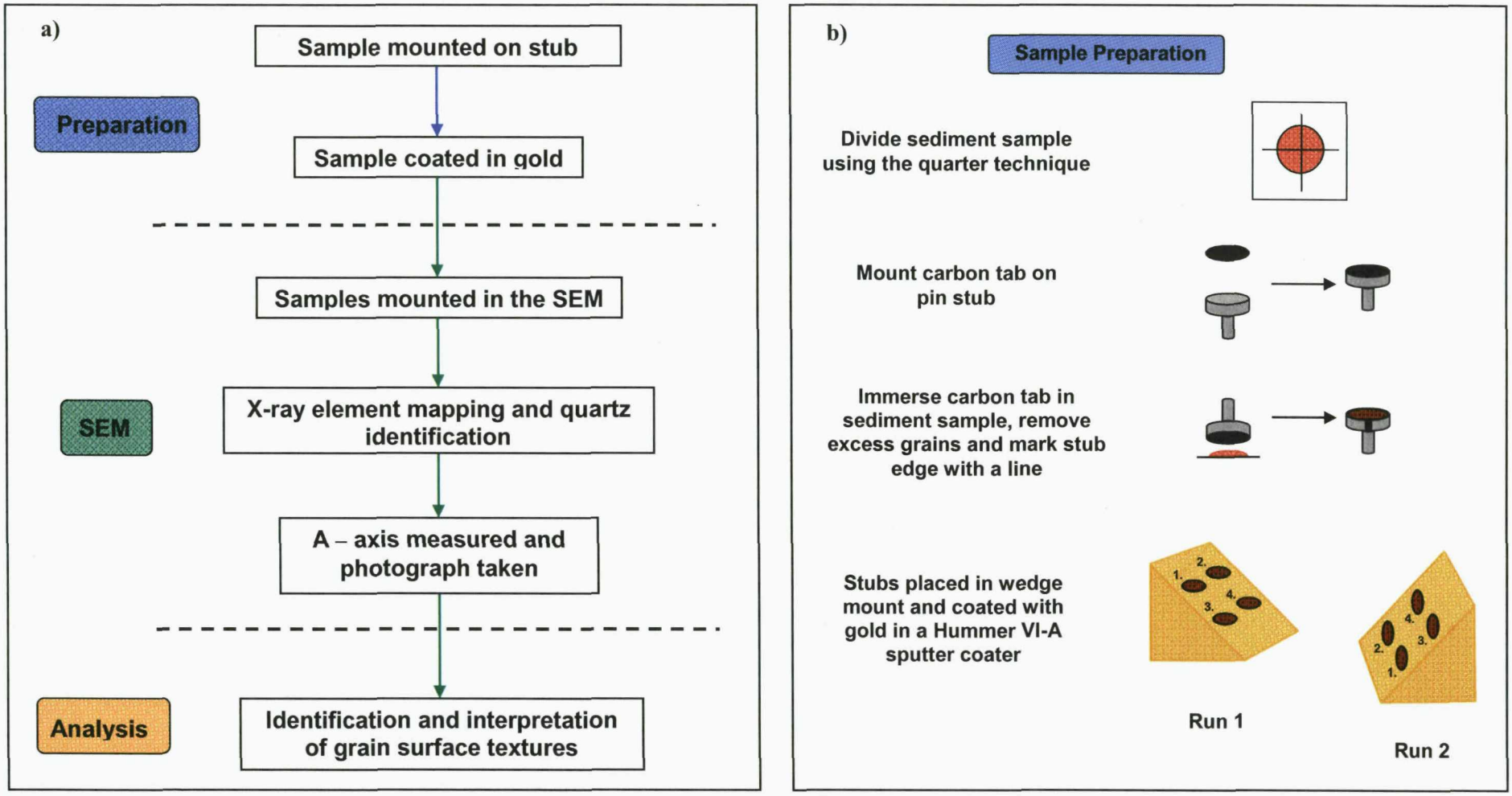


Figure 4.31: Schematic diagrams of the processes involved in SEM analysis, showing: a) an overview of the stages of SEM analysis: preparation, observation and interpretation; and b) the stages of sample preparation.

Once the pin stubs were prepared they were placed in a wedge mount (up to four at any one time) for coating. The grains were coated with gold (~20 μm thick) using a Hummer VI-A Sputter Coater. This prevented the samples from becoming charged in the SEM and the gold is thought to provide better resolution images (Krinsley and Doornkamp, 1973). The specimens were placed in a vacuum chamber from which the air was extracted down to a pressure of roughly 20 millitorr. Once this was achieved, pressure was then increased to 60 millitor, and a current of roughly 10 mA was induced, coating the samples with gold. This was sustained for 4 minutes before the current was stopped and atmospheric pressure was returned to the chamber. This process was repeated again for the same four specimens but, on the second run, the wedge mount was orientated 90° in the opposite direction, in an attempt to coat the specimens evenly (Figure 4.31b).

4.5.3.2 Analysis of quartz grains

> "Quartz is one of the most common rock-forming minerals. It is one of the main constituents of granites, sandstone and many metamorphic rocks: its composition is nearly pure SiO_2."
>
> MacKenzie and Adams (2000, p.48).

The analysis of quartz grains under the SEM has now become a standard procedure. It has led to the creation of consistent classification schemes, enabling comparison between numerous studies of this kind. Quartz is analysed, not only because it is a very common mineral, but also because it is very resistant to diagenesis. When many other minerals have been altered or degenerated quartz tends to persist, even after two or three episodes of reworking (MacKenzie and Adams, 2000). Consequently, it is readily available for sampling and analysis within a wide range of deposits.

4.5.3.3 Quartz identification

The identification and separation of quartz grains can be carried out by a variety of techniques (e.g. Krinsley and Doornkamp, 1973; Helland and Holmes, 1997). However, a new method of x-ray elemental mapping was adopted in this study (Hart,

2006b; Rose and Hart, 2008; Figure 4.31a). This enabled the quartz grains to be identified without the grain separation, washing, and carbon coating that is generally required for other preparation techniques (e.g. Helland and Holmes, 1997). In addition, the quartz grains did not have to be individually mounted onto the stubs. Consequently, this technique provided a faster and more efficient means of identifying and analysing quartz grains with an SEM.

The samples were analysed under a LEO1450VP SEM (Carl Zeiss, Jena, Germany). The line marked on the side of the pin stubs (Figure 4.31b) was used to align the specimens with a numbered line engraved on the SEM stage. The stage was loaded into the SEM chamber and the system was started in accordance with standard operating procedures. The stage position of the stubs was saved as a co-ordinate, to allow the specimens to be reoriented to the same position if ever viewed again (Figure 4.32a). The SEM was then connected to a UNIX Workstation, whereby the quartz grains within the samples were identified using x-ray elemental mapping at x150 scale. The x-ray identified the various quantities of elements within sample grains and processed those readings using an IMIX image processing package (Princeton Gamma-Tech, Princeton, HJ, USA) (Hart, 2006b; Rose and Hart, 2008). Quartz dominantly consists of silicon dioxide (MacKenzie and Adams, 2000). Accordingly, peaks for silicon were identified, whilst other trace elements, namely aluminium, were removed from the signal with the use of the following programme specific formula:

$$\text{“Si K”} - (\text{“Al K”}*2) \qquad (9)$$

where Si is silicon, K is potassium and Al is aluminium. This allowed those grains with a high Si content (i.e. the quartz grains) to be identified. The processing package produced an image that represented those areas with the greatest Si content as bright white amongst darker areas (Figure 4.32b). Once the element map was obtained the sample was inspected under normal view in the SEM (Figure 4.32a). The x-ray analysis image was used as a map, from which the locations of quartz grains were identified under normal view (Figure 4.32a). In this way, quartz grains were found and chosen within samples quickly and efficiently. The grains were magnified to a suitable size, photographed as an image file, and then their a-axis was

measured using a digital measuring tool (Figure 4.33). Twenty five grains were imaged per sample. This was considered to be a representative sample size in accordance with standard techniques (Krinsley and Doornkamp, 1973; Mahaney *et al.*, 1996).

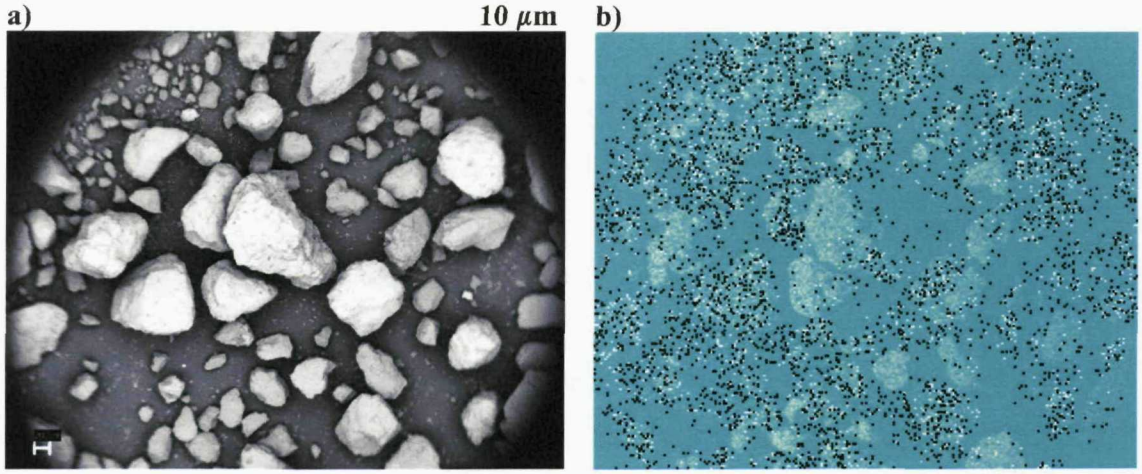


Figure 4.32: The images produced during SEM x-ray elemental mapping analysis showing: a) sediment grains mounted on a pin stub; and b) the same image after x-ray elemental mapping. The image is artificially coloured showing the quartz grains in white.



Figure 4.33: An example photograph of a quartz grain. Note the scale bar in the bottom left hand corner (10 μm).

4.5.3.4 Surface texture analysis

The grain images were collected in order to review the surface texture of each grain (Figure 4.31a). A series of surface features have been associated with quartz grains and categorised into morphological, mechanical and chemical textures. The presence or absence of these features was recorded for each grain with the use of a tally table (Table 4.6). The table used was adapted from a list of standard features for SEM quartz grain surface texture identification (Helland and Holmes, 1997; Mahaney *et al.*, 1996; Strand *et al.*, 2003 and references therein). A standard classification system for quartz grains enables comparison with other studies from glacial environments, aiding the interpretation of glacial sedimentary histories.

The classification of grains was achieved through close inspection of the literature. Features were compared with those previously identified and labelled in order to maintain consistent classification (e.g. Krinsley and Doornkamp, 1973; Strand *et al.*, 2003). A number of example grains and surface features are presented in Figure 4.34. In addition to the standard list of surface textures, three other distinct categories were added to the tally table (Table 4.6) in accordance with more recent work by Hart (2006b) and Rose and Hart (2008). The categories of 'angular outline' and 'rounded outline' were omitted from the morphological texture category. Instead, a more comprehensive classification for shape (ranging from 'very angular' to 'very rounded') was included, based on Powers' (1953) standard images of particle roundness. This allowed an RA value - the percent of 'angular' and 'very angular' grains - to be calculated (Benn and Ballantyne, 1993).

A new category recording the 'genetic shape' of particles was also included (Table 4.6). This concept was derived from work by Hart (2006b), who used this category to relate the shape of a quartz grain with its erosional history. Five terms were developed and used: ellipse, hand axe, diamond, triangular and rectangular. These classifications take into account a more 'three dimensional' image of grains. This can compliment descriptions of shape, which tend to give greater generalisation of grain form.

Table 4.6: Tally sheet for surface texture analysis of quartz grains under the SEM based on work by Helland and Holmes (1997) and Mahaney *et al.* (1996).

Grain Number	1	2	3	4	5
Morphological Textures					
Low relief					
Medium Relief					
High Relief					
Mechanical Textures					
Large conchoidal fractures					
Small conchoidal fractures					
Arcuate steps					
Linear steps					
Crescentic gouges					
Imbricated blocks					
Breakage blocks					
Fracture plates					
Sub-parallel linear fractures					
Curved grooves					
Straight grooves					
Mechanical percussion cracks					
V-shaped cracks					
Meandering ridges					
Edge abrasion					
Deep troughs					
Chemical Textures					
Preweathered surfaces					
Weathered surfaces					
Small precipitation features					
Large precipitation features					
Adhering particles					
New growth					
Pits					
Cracks					
Low relief joints (scales)					
High relief joints (blocks)					
Shape					
Very angular					
Angular					
Sub angular					
Sub rounded					
Rounded					
Very rounded					
Genetic shape					
Ellipse					
Hand Axe					
Diamond					
Triangular					
Rectangular					
Erosional Form					
Abraded					
New impacts - medium relief					
New impacts - low relief					
Conchoidal					
Jagged					
% Face jointed					

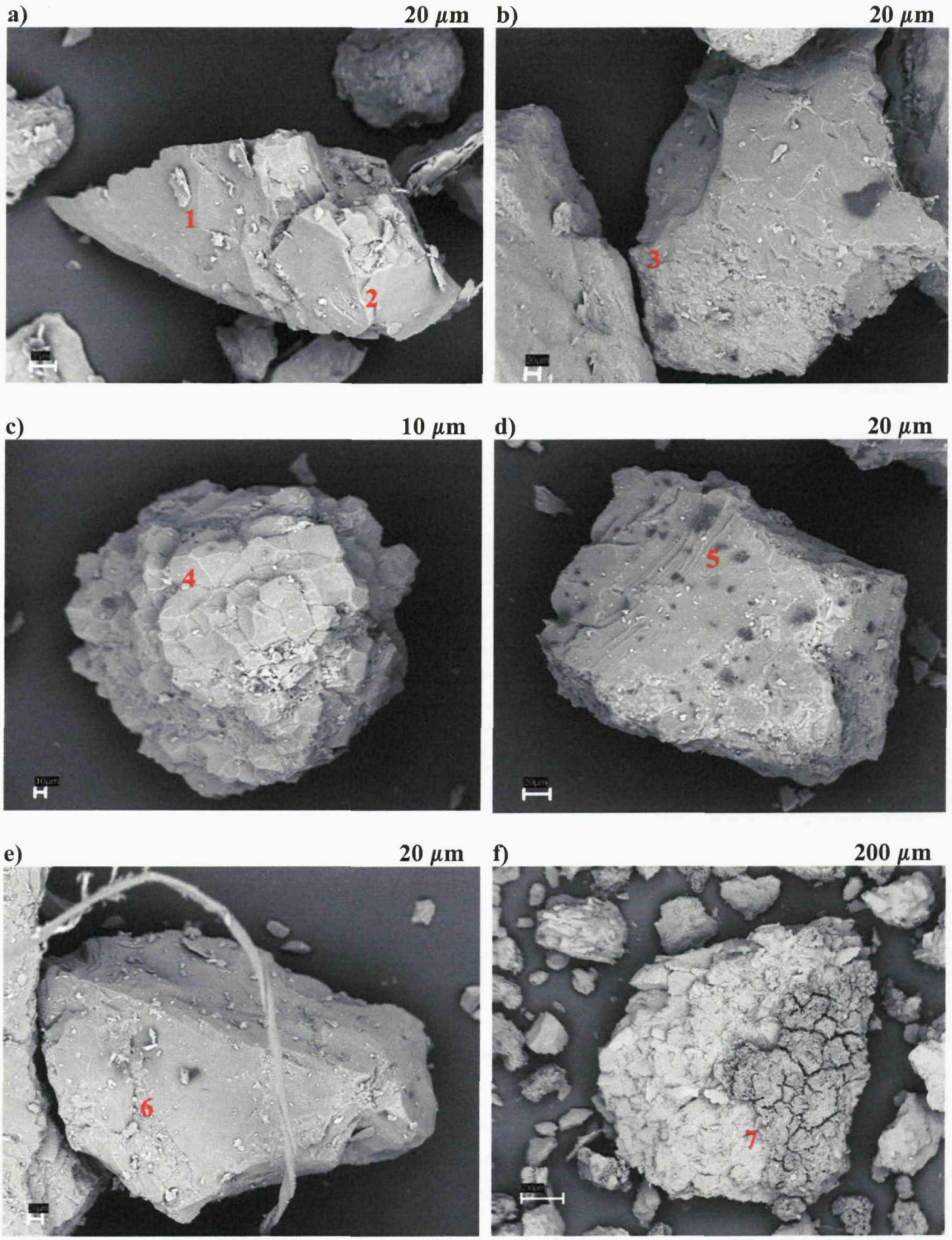


Figure 4.34: Quartz grains, showing examples of the mechanical and chemical surface textures identified during analysis: a) comparison of arcuate (1) and crescentic gouges (2); b) imbricated blocks (3); c) breakage blocks (4); d) sub-parallel linear fractures (5); e) preweathered surface low relief joints (6); f) preweathered surface high relief joints (7).

The analysis of grain surface textures only provides a classification according to grain form and morphology (Krinsley and Doornkamp, 1973). As a result, the final category of 'erosional form' was developed in an attempt to combine genetic grain shape with all the features of surface texture in one category (Table 4.6). The erosional form of grains was assessed on a combination of grain form and surface textures. Hart (2006b) developed this idea in her discussion of grain 'style'. This approach aimed to provide a means of analysing grains in a way that allows their erosional history (amount and style) to be inferred according to a given category. This enabled grain histories to be compared more readily (e.g. Hart, 2006b; Rose and Hart, 2008).

4.6 Summary

This chapter has described the variety of techniques employed at Briksdalsbreen (Figure 4.1). The methods used were in good agreement with standard field work procedures associated with *in situ* glacier investigations, many of which were highlighted in Chapter 2. In each field season, the ESN was established and probes were deployed at the ice-bed interface in accordance with the primary aim: to investigate the deforming glacier bed with the use of an autonomous wireless multi-sensor subglacial probe (section 1.2, Chapter 1). The dGPS survey provided a record of the field site and the location of the areas investigated. The GPR survey generated information on the characteristics of the glacier itself so that the probes could be placed in the best possible position. The BoreCam was used to investigate the boreholes, the glacier bed, and the location of the probes on deployment. Subglacial sediments were sampled and analysed from both the foreland and via boreholes to determine the nature of the till that comprised the deforming bed under investigation. These techniques all provided supporting information to enable the successful establishment of the ESN and to aid in the interpretation of the data anticipated from the probes.

Chapter 5

Field Surveys: GPS, GPR and Drilling Record

5.1 Introduction

A detailed survey of the field site was required in order to provide a better understanding of the setting in which the investigation was to be carried out. A GPS survey was carried out on the ice and in the foreland at Briksdalsbreen and a GPR survey was carried out on the glacier surface each year. The GPS survey provided an overview of the glacier bed before a series of boreholes were created, in which the probes were deployed. This chapter will discuss the details of the GPS and GPR surveys and provide an overview of the borehole drilling and probe deployment records.

5.2 GPS

In the last few decades, the use of GPS has become a standard surveying technique. Improvements in technology mean that surveys can be carried out by an individual and survey points can be located, precise to within centimetres. At Briksdalsbreen surveys of the glacier foreland, ice margin, and lake edge were carried out in 2004 and 2005, as described in section 4.3 (Chapter 4). The surveys enabled the retreat of the glacier and the extent of the lake to be mapped. On the glacier surface, the location of the grid transects and boreholes were surveyed each year to record the location of the investigations carried out. The location of the boreholes, in particular, provided a starting point for the probes' positions following deployment. These surveys also allowed the exact location of the glacier transect grids and boreholes to

be revisited following the glacier's retreat. A variety of maps detailing these results are displayed below in Figures 5.1-5.7.

Figure 5.1 displays all the survey points collected for the field site as a whole. The location of the boreholes can be seen in relation to the changing glacier margin, the foreland and the lake. In the figures that follow these data points have been smoothed and joined. Figure 5.2 displays the foreland, highlighting the almost annual sequence of preserved moraine ridges, the river outlet, and the retreat of the glacier margin (2004–2005). The south side of the lake was not survey extensively because this was a restricted area. A schematic diagram showing the retreat of the glacier from the lake is presented in Figure 5.3. Figure 5.4 compares the location of the 2004 and 2005 study grids and boreholes (sections 4.3.2 and 4.3.4, Chapter 4). These are also displayed individually in Figures 5.5 and 5.6. The transect lines presented are largely extrapolated from borehole point positions, rather than reflecting a precise record of the transect locations. As a result, schematic diagrams of the transects and boreholes are also presented in Figure 5.7. GPS failures meant that not all the data points for the GPR transects were obtained.

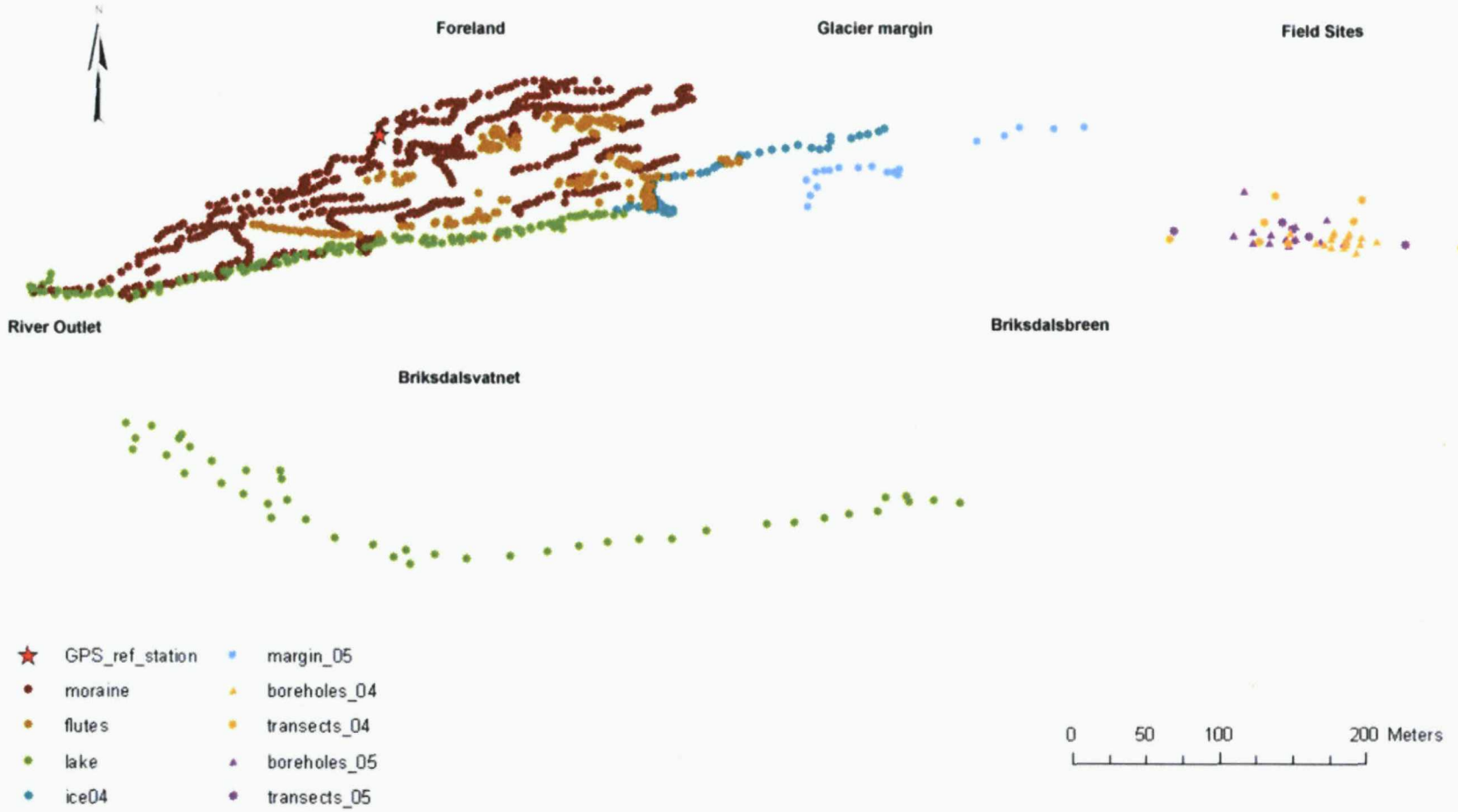


Figure 5.1: GPS survey of Briksdalsbreen, including the foreland, lake and *in situ* sample sites on the glacier surface.

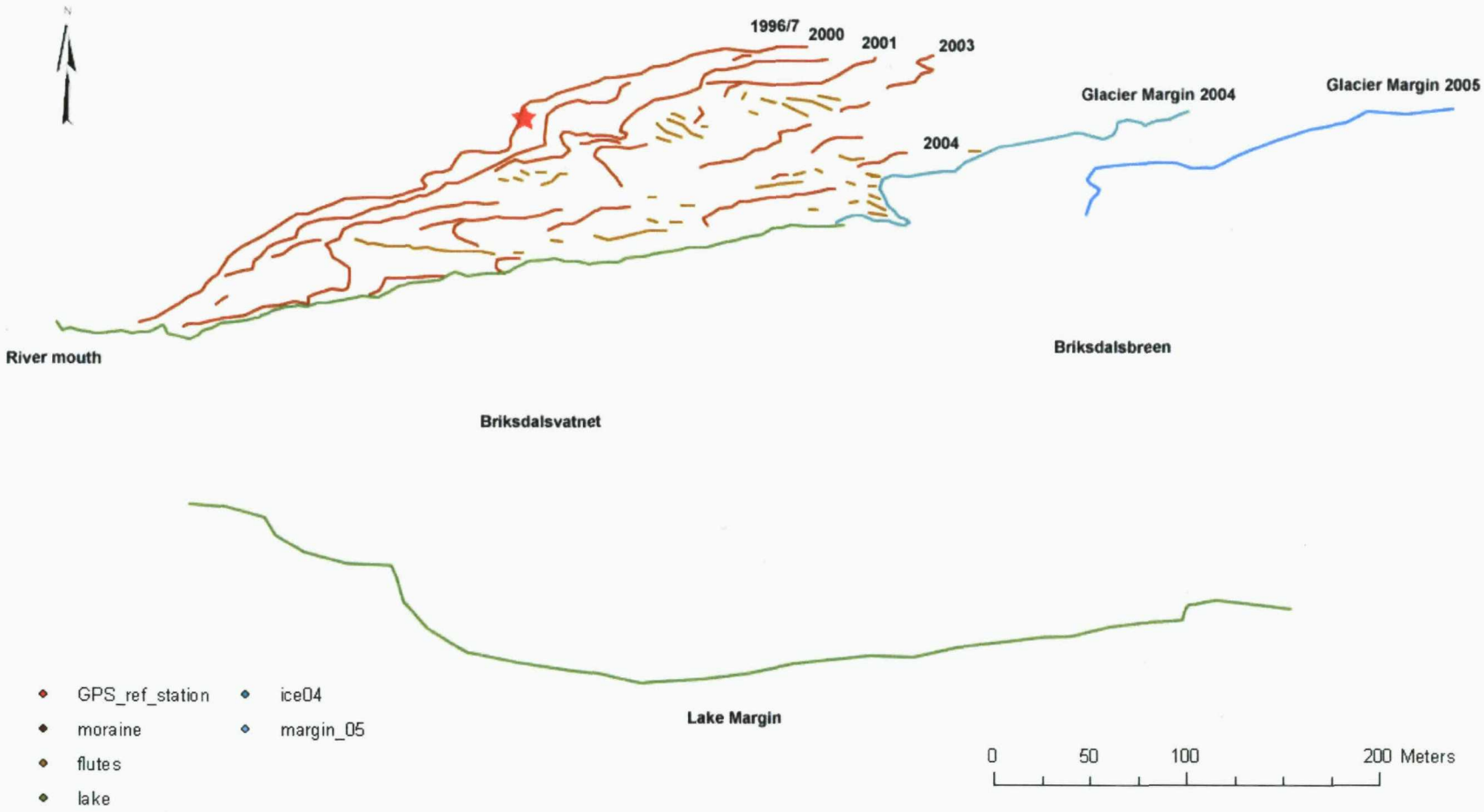


Figure 5.2: GPS survey of the foreland, Briksdalsbreen.

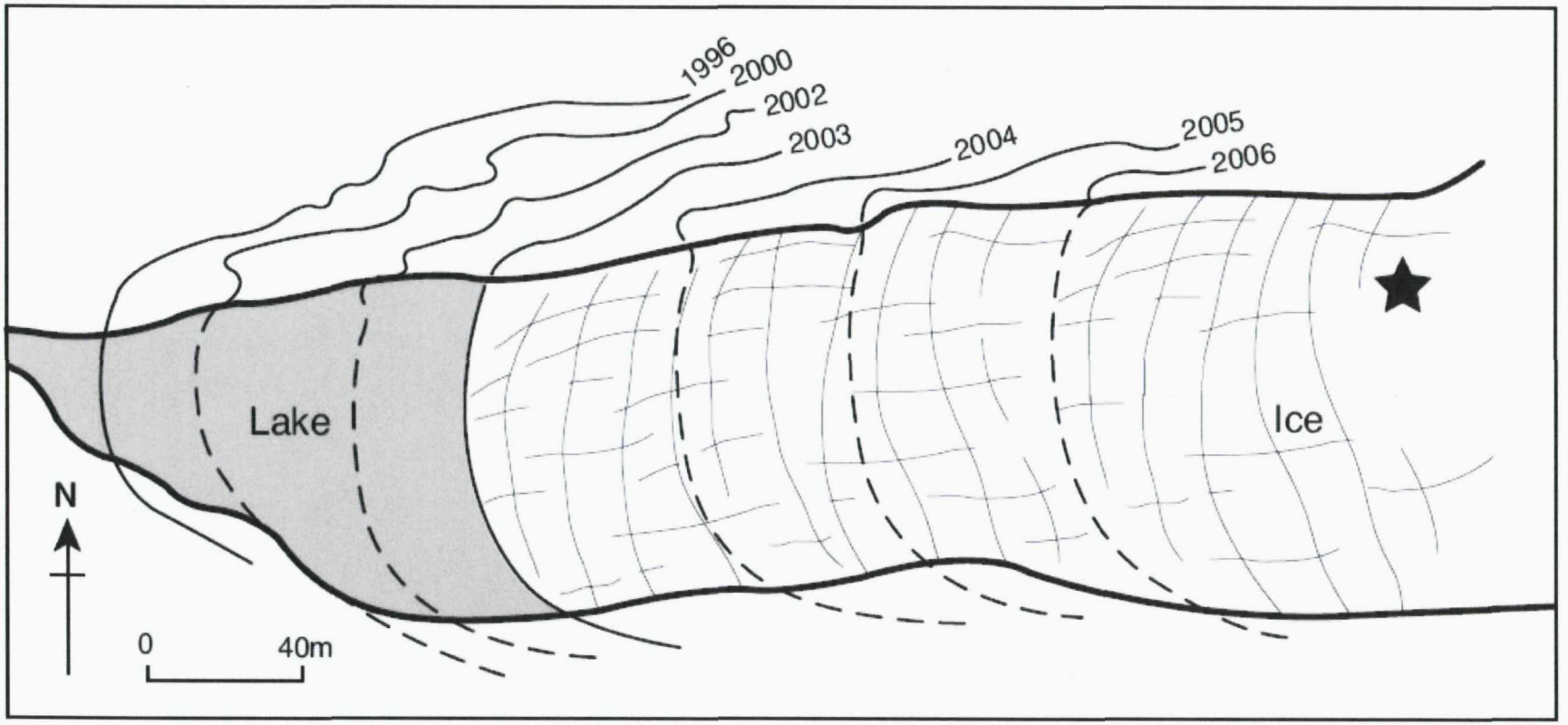


Figure 5.3: Schematic diagram to show the retreat of the glacier from the lake (1996-2006). Note: the star marks the location of the borehole and transect sites.

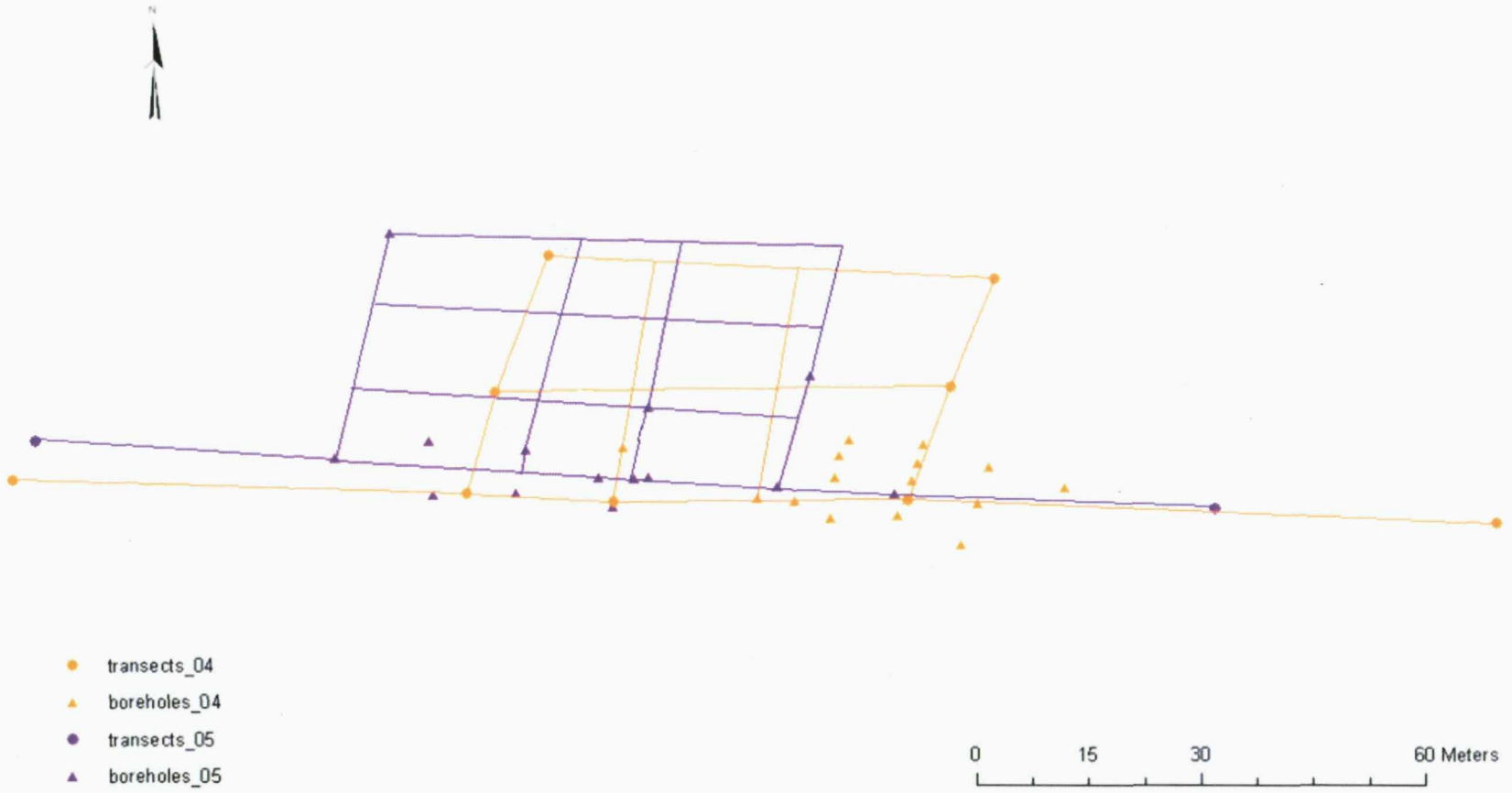


Figure 5.4: Comparison of field site locations on the glacier from 2004-2005. Note: due to the limited number of GPS transect points, the transects marked are largely extrapolated from borehole point data.

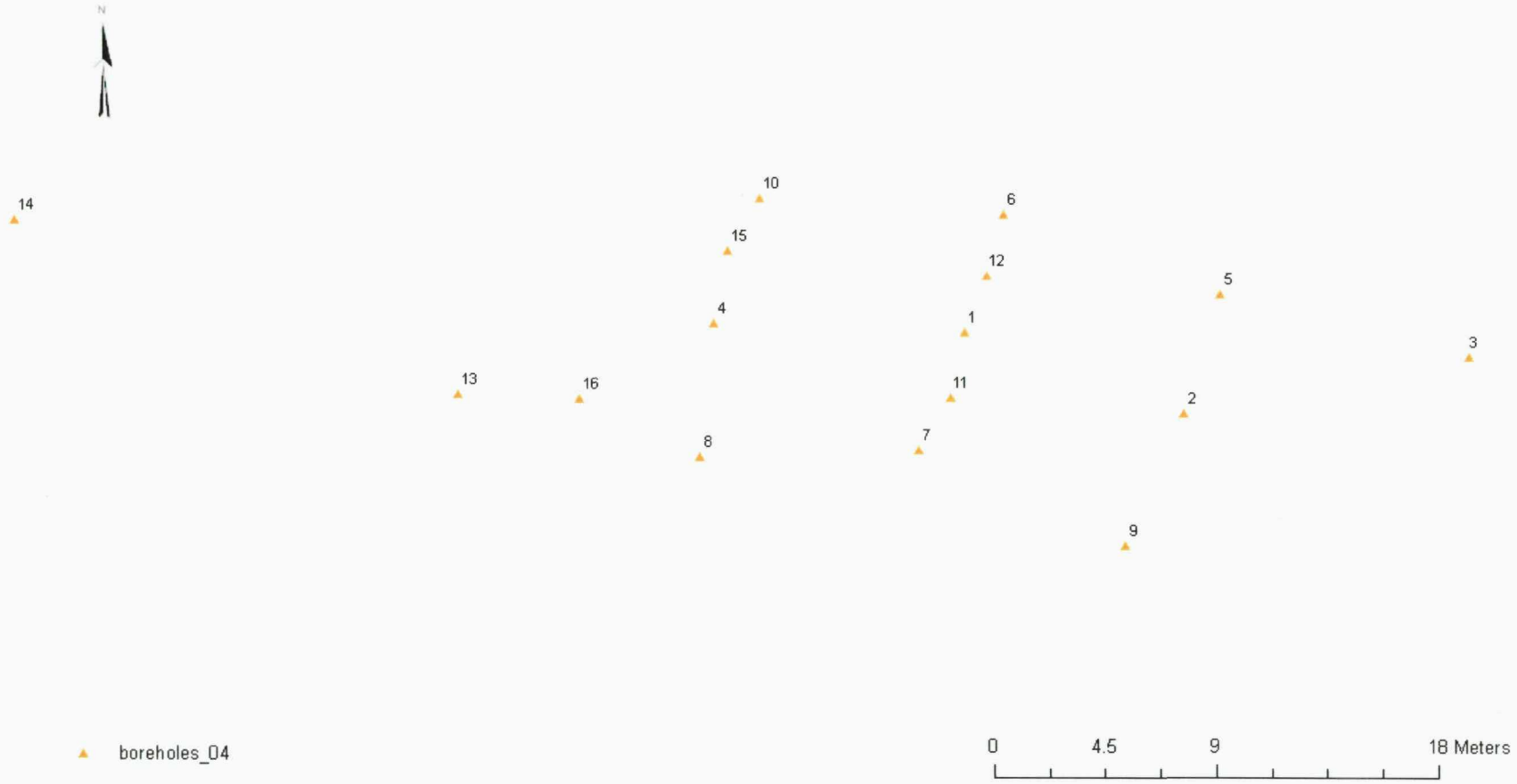


Figure 5.5: Location of the boreholes in 2004.

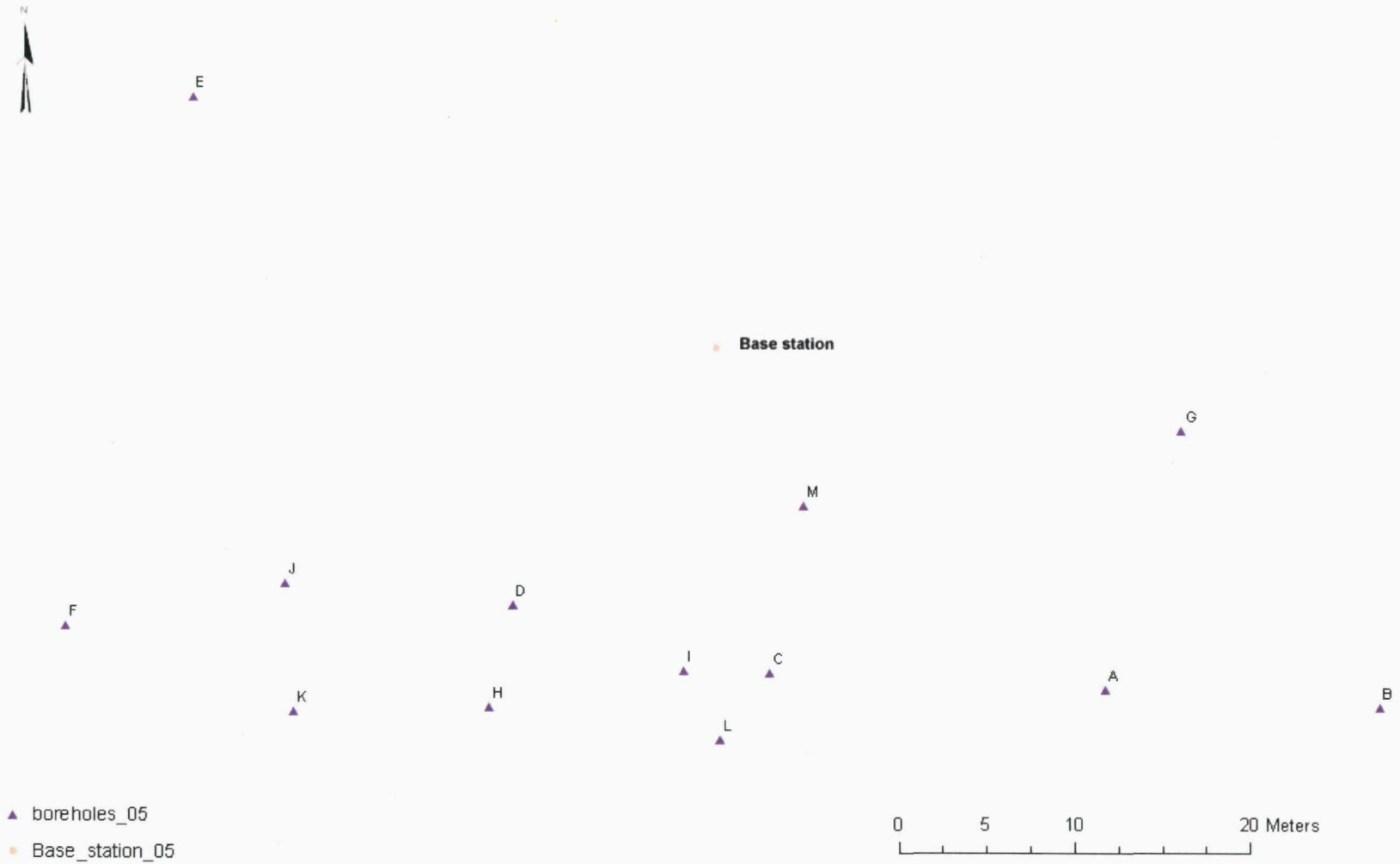


Figure 5.6: Location of the boreholes and the base station in 2005.

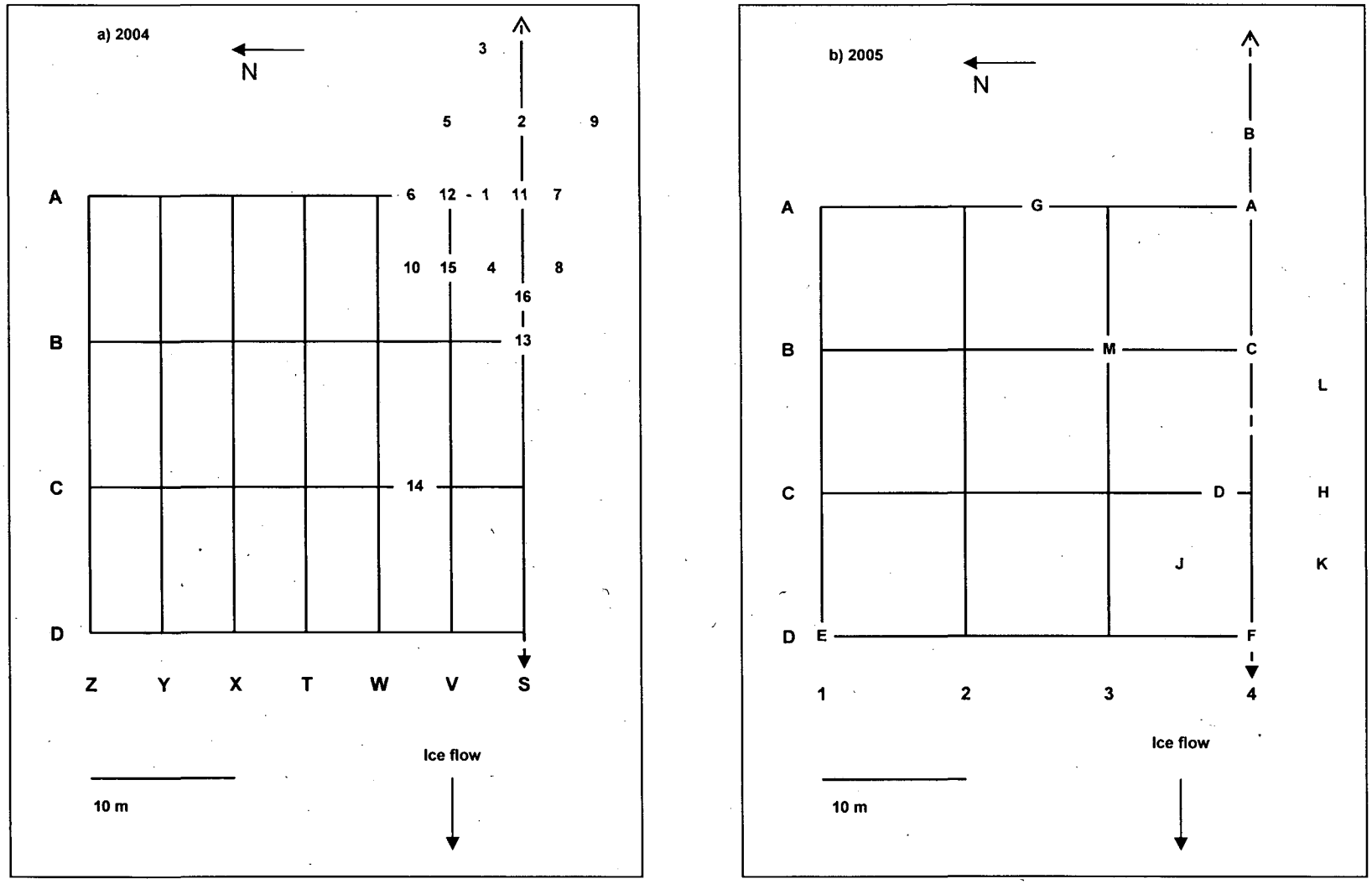


Figure 5.7: Schematic drawings to show the GPR transects and borehole locations for: a) 2004; and b) 2005.

5.3 GPR

A GPR survey of the glacier surface area under investigation was carried out each year (Figure 5.7), as described in section 4.3.3 (Chapter 4). This was done in order to locate and survey the glacier bed. This would allow the boreholes to be positioned away from irregularities within the ice column and at the glacier bed, ensuring that the probes were placed in areas that were most likely to support their survival. GPR surveys can provide a variety of information concerning the nature of the glacier bed and the ice column (e.g. Woodward and Burke, 2007). However, only determining the location of the glacier bed will be discussed here.

5.3.1 Data processing

The raw data generated by the GPR often provided a good indication as to the location of the glacier bed. However, in order to refine the records and improve those that were less clear, the data were processed in five stages (Figure 5.8). Figure 5.9a displays an example of a raw data image where the glacier bed is readily visible. The top layer of the data, which is distinctly different from the rest, represents the movement of the radar pulse through the air before entering the ice. In order for the data to be interpreted correctly, this is removed (stage 1) and the image is corrected to take into account the surface topography of the glacier (stage 2; Figure 5.9b). The data were then processed further (Figure 5.10). A 'subtract mean' or 'dewow' filter was applied in stage 3 to remove some of the variation in the data (Figure 5.10b). The strength of the radar signal decreases with depth, as more of the signal is lost through reflection and diffraction. Thus, in stage 4, to enhance the basal signal and clarify the location of the glacier bed, 'gain' was applied to the data (Figure 5.10c). Only a gain of 5 db was used because the depth of the glacier was under 100 m. Further irregularities were removed from the data to enhance the bed signal in stage 5 (Figure 5.8), using either a Kirchoff migration filter (Figure 5.10d), or a diffraction stack filter (Figure 5.10e). A filter parameter of only 3 was applied due to the clearly defined glacier bed shown in many of the transects. The filter that produced the best image was used preferentially.

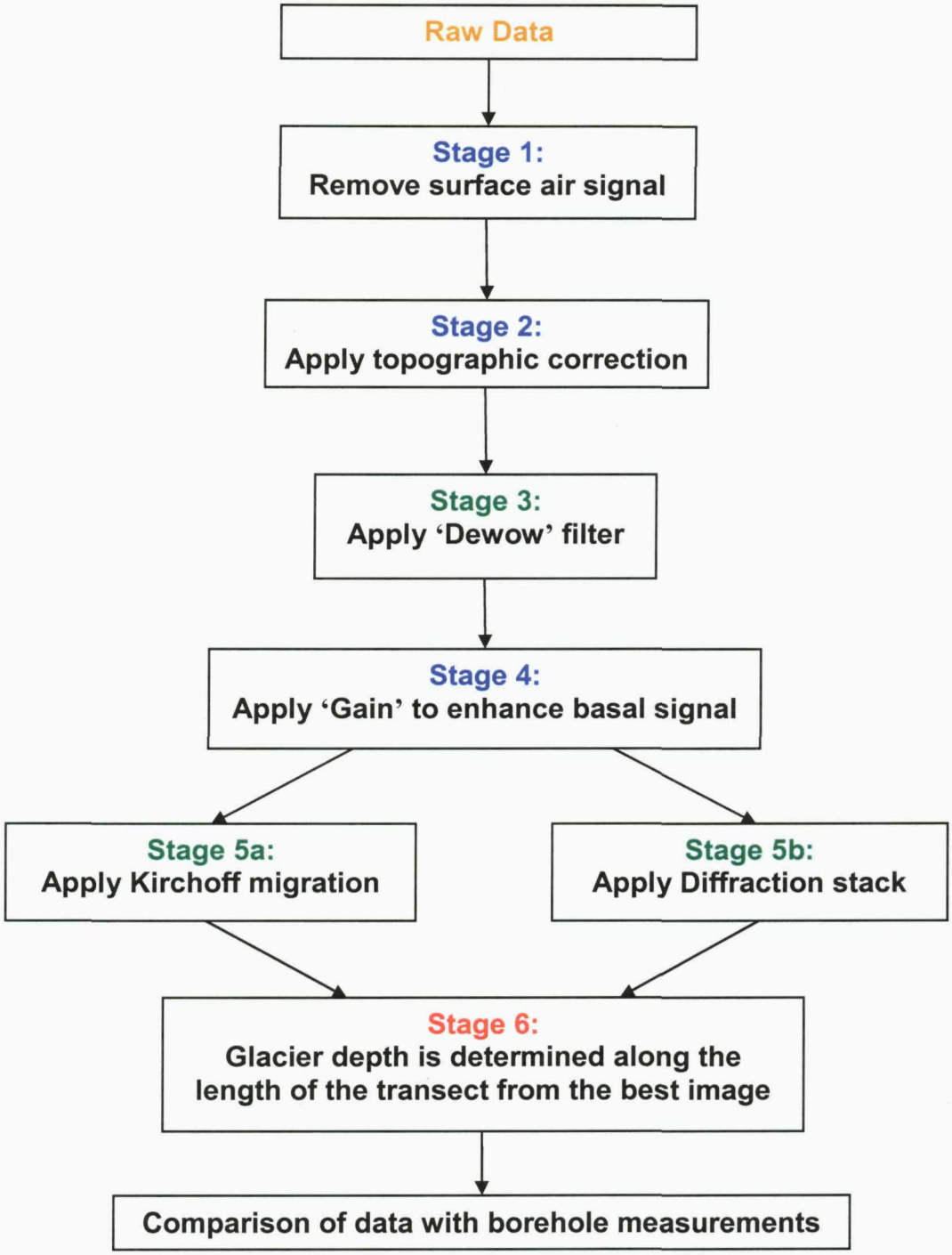


Figure 5.8: Flow diagram to show the stages of image processing employed to enhance the raw data image and determine the depth of the glacier along the radar transects.

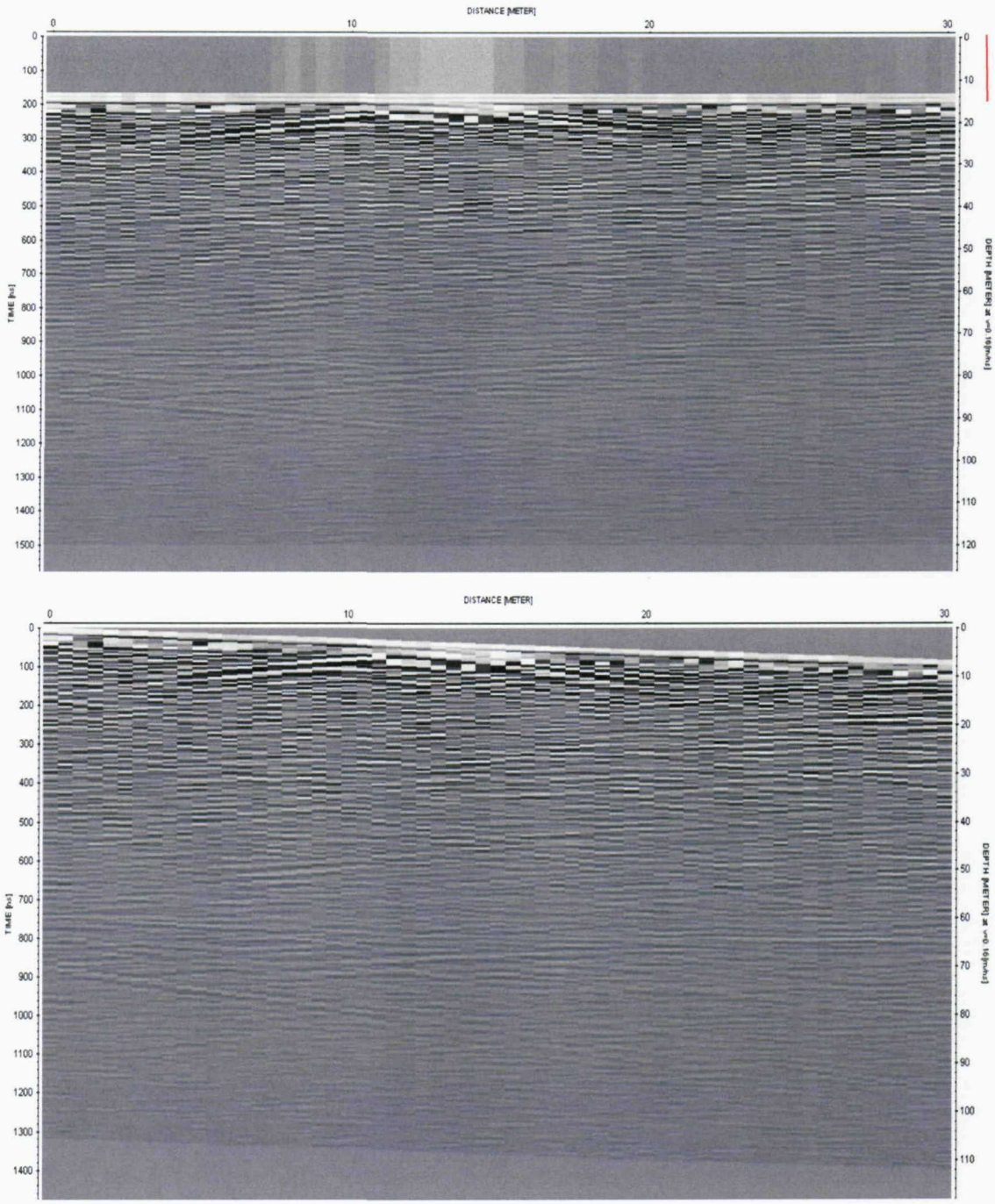


Figure 5.9: GPR data files, displaying transect line X (2004): a) the raw data image prior to processing; and b) the data image corrected for surface air interference (Stage 1) and topography (Stage 2, Figure 5.8). Note: the red line marks the extent of surface air interference.

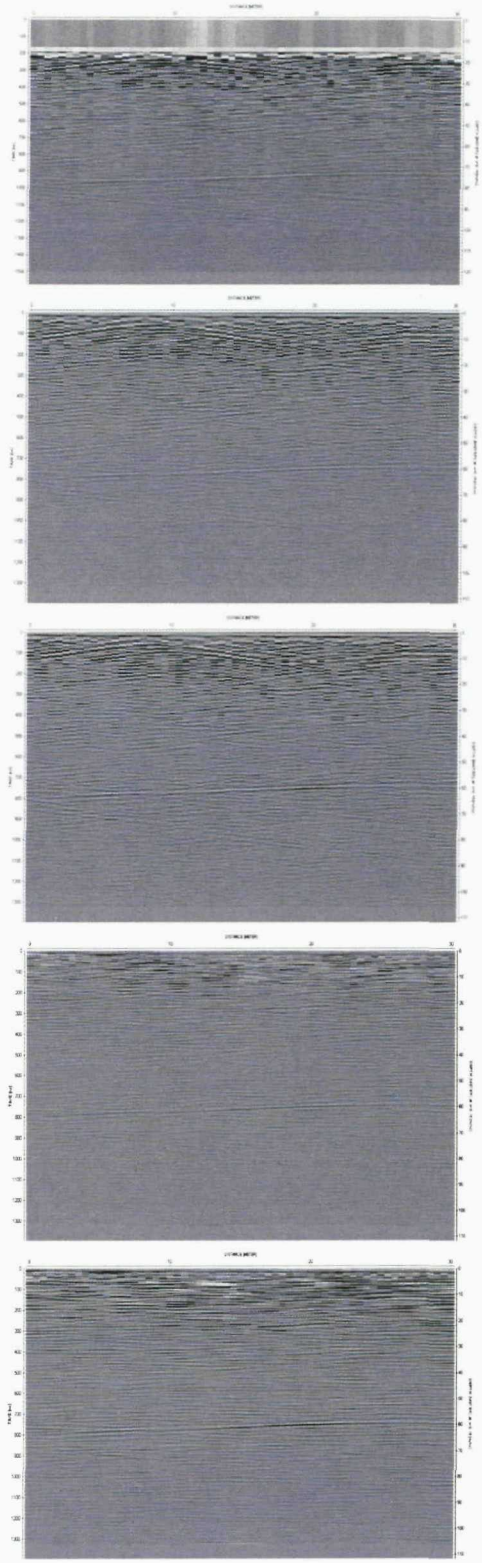


Figure 5.10: Graph series of transect W through each stage of processing, showing: a) initial raw data image; b) Stage 3, dewow filter; c) Stage 4, gain; d) Stage 5, Kirchoff migration; and e) Stage 6, diffraction stack. Note: the strength of the line representing the glacier bed improves through each stage of processing.

These stages were carried out in order to improve the clarity of the radar image so that the location of the glacier bed could be identified more readily. The best images produced were chosen in stage 6 (Figure 5.8) and the depth of the glacier bed was noted at 10 m intervals along the longitudinal (or vertical) transect lines. Readings were also taken where transects intersected with boreholes. Only the longitudinal transect lines were used because they intersected the greatest number of boreholes and surveys performed in different directions cannot be readily compared. The glacier depth was recorded manually as both the pulse travel time (ns) and the equivalent depth in meters (Figure 5.11; Table 5.1). The depth in meters was determined under the assumption that the travel time of the pulse through ice was 0.16 ns, based on the CMP survey (section 4.3.3.2, Chapter 4).

The boreholes also enabled measurements of glacier depth to be taken. Depths were measured with the length of the drill hose and the BoreCam (section 4.3.5, Chapter 4). These measurements provided spot checks of glacier depth that could be compared with the data obtained from the GPR surveys (Figures 5.12 and 5.13; Table 5.2).

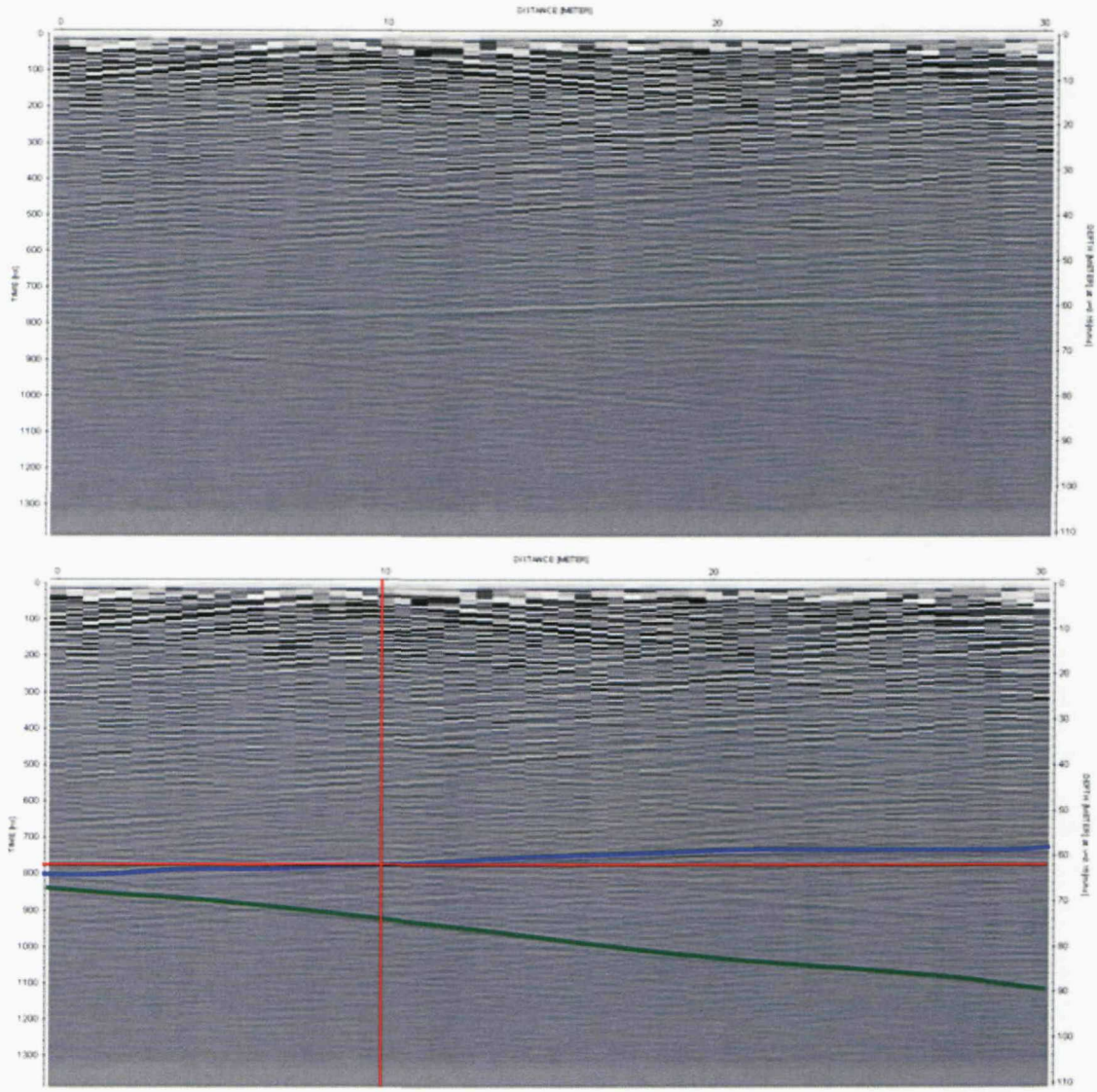


Figure 5.11: Method of measuring the location of the glacier bed, measured in time (ns) on the left axis and distance (m) on the right axis, showing: a) the final processed image (transect W); and b) the annotated image, showing the glacier bed (blue), the bedrock beneath (green), and the line intersects used to read off the depth measurements (red). In this example, at 10 m along the transect, glacier depth is equivalent to 775 ns or 62 m ($v = 0.16$ ns).

Table 5.1: A record of glacier depth in both time (ns) and equivalent distance (m) based on GPR transect readings.

Year	Transect	Glacier Depth (ns)					Glacier Depth (m)				
		-10	**0**	**10**	**20**	**30**	**-10**	**0**	**10**	**20**	**30**
2004	**Z**	-	725	725	725	750	-	58	58	58	60
	Y	-	900	875	820	800	-	72	70	66	64
	X	-	875	850	775	725	-	70	68	62	58
	T	-	820	75	750	750	-	66	62	60	60
	W	-	800	775	740	725	-	64	62	59	58
	V	-	820	785	775	710	-	66	63	62	57
	S	900	840	860	900	860	70	67	69	72	69
2005	**1**	-	500	485	500	500	-	40	39	40	40
	2	-	540	540	510	500	-	43	43	41	40
	3	-	590	550	525	510	-	47	44	42	41
	4	675	625	600	560	600	54	50	48	45	48

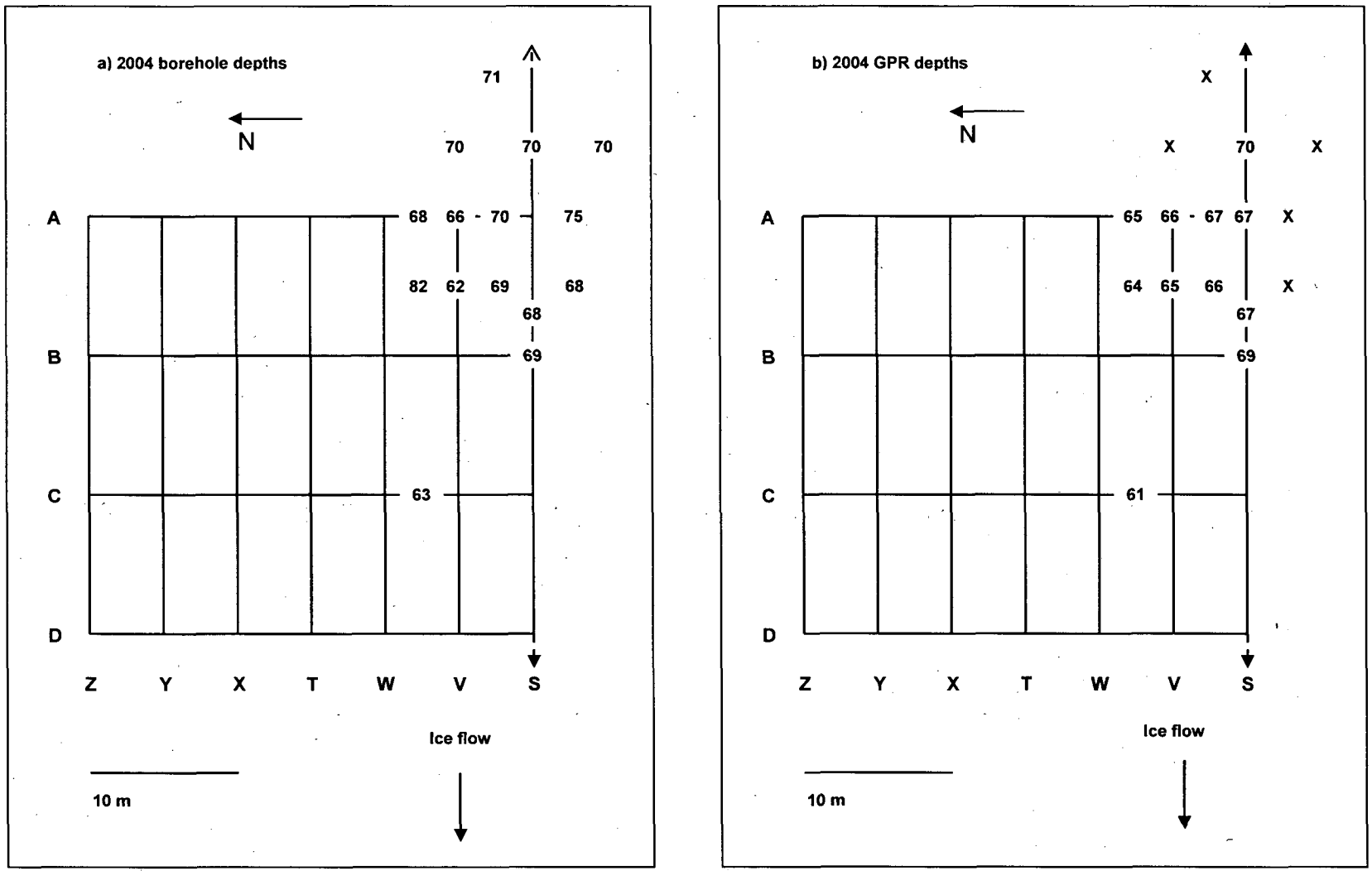


Figure 5.12: 2004 depth measurements (in meters) for the glacier bed based on: a) borehole data points; and b) GPR survey depths.

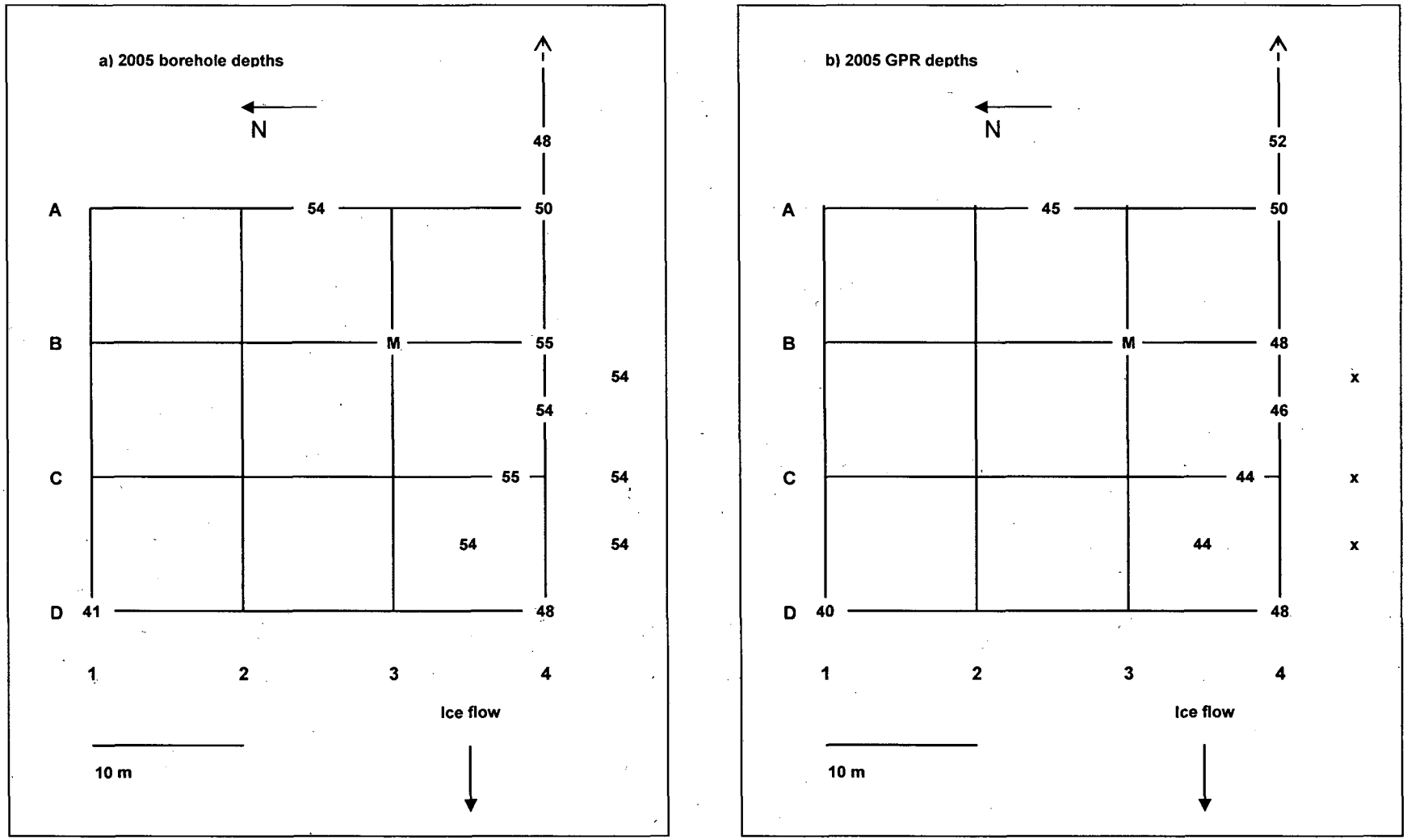


Figure 5.13: 2005 depth measurements (in meters) for the glacier bed based on: a) borehole data points; and b) GPR survey depths.

Table 5.2: Glacier depth readings in meters measured by the drill stem, the BoreCam and the GPR.

Year	Borehole	Drilling Depth (m)	Camera Depth (m)	GPR Depth (ns)	GPR Depth (m)
2004	1	74	-	830	66.5
	2	72	-	870	69.5
	3	69	70	-	-
	4	72.5	70	826.3	66.3
	5	72	-	-	-
	6	70	68	810	65
	7	77	74	-	-
	8	69	68	-	-
	9	65	-	-	-
	10	85* (72)	-	795	63.8
	11	30	-	840	67
	12	66	66	820	66
	13	69	70	860	69
	14	62	65	757.5	60.5
	15	70	66	802.5	64.5
	16	70	67	840	67
Average		70	68	823	60
2005	A	50	-	625	50
	B	48	-	650	52
	C	55	53.5	600	48
	D	55	-	551.3	44.3
	E	41	41	500	40
	F	50.5	49.5	600	48
	G	50	-	565	45
	H	54	-	-	-
	I	54	53	570	45.5
	J	54	52	548.8	44
	K	54	-	-	-
	L	54	-	-	-
	M	35	-	-	-
Average		52	50	579	46

*It is likely that 85 m is an anomalous value. A reading of 72 m is more in keeping with depths in this area of the bed.

5.4 GPR Interpretation

The GPR transects were carried out over the study grids, which had been assigned to borehole drilling and instrumentation. The GPR records generated an overview of the topography of the glacier bed and the depth of the ice column, highlighting any unusual features. This information could be used in conjunction with *in situ* data

collection and sensor readings. The results of the surveys will be discussed briefly, to highlight key findings concerning basal topography and glacier depth.

5.4.1 General features

Overall, the clearest images of the glacier bed were recorded in 2004, although readings varied both between transects and years (2004-5). The initial raw data file often showed a good image of the glacier bed (e.g. Figure 5.9a). Several of the transect lines from 2004 also showed a steeply sloping line running up ice to down ice beneath the glacier bed. This line can be seen meeting with the bed reflector in Figures 5.9 and 5.11.

Briksdalsbreen flows from an ice fall to a steeply sided valley bottom overlain by unlithified sediments. As a result, this line was considered to represent the bedrock underlying the glacier's deforming bed. The detection of the bedrock was considered to be quite unusual for a supra-glacial GPR survey and a potential artefact of processing. However, following the retreat of the glacier in 2007 the location of the bedrock as it passes beneath the till was identified, confirming this hypothesis (Figure 5.14). The depth of the glacier, or a low free-water content in the ice during 2004 may have enabled the bedrock to be imaged.

The survey records from 2005 did not show the same reflector strength as those in 2004, despite a reduction in glacier depth. It is likely that this was the result of an increase in the water content of the ice column, as the rate of glacier retreat began to increase into 2006. The influence of changing glacier water content shall not be discussed in detail here, but work presenting these findings is under preparation by Hart and co-workers. The reduction in reflector strength during 2005 was offset by image processing, which allowed the bed of the glacier to be successfully identified. In general, the GPR transects did not reveal any unusual subglacial topographic features or anomalies. Again, this was in good agreement with proglacial observations following glacier retreat (2007), which revealed a generally smooth subglacial surface (Figure 5.14).



Figure 5.14: Briksdalsbreen, November 2006. This picture shows the bedrock feeding down from the back wall of the ice fall, overlain by unconsolidated sediments and the proglacial lake. The region in the forefront of the picture reflects an exposed subglacial surface, which is relatively free of irregularities, in keeping with the GPR survey records. (Person for scale).

5.4.2 Glacier depth

The GPR readings placed the bed of the glacier at a depth of between 61-70 m in 2004 and 40-52 m in 2005 (Table 5.1). This indicates a loss of between 18-21 m in glacier depth from 2004-5, in this area (Figure 5.4). This is comparable with the change in drilling depths between years. The transects showed an overall decrease in glacier depth with distance down ice, with the exception of transect Z (2004). This trend reflects the movement of the glacier over the ice fall. Up ice, the glacier thickens, as it is constrained by the bedrock (Figures 3.2 and 3.3, Chapter 3); but as it passes from the ice fall and into the proglacial lake it is able to spread out and thin, resulting in a decrease in depth down ice.

The GPR, drill hose and BoreCam depth measurements for the boreholes are displayed in Table 5.2. The omitted GPR readings reflect those boreholes that either

did not reach the glacier bed (i.e. hole 11, 2004, and hole M, 2005), or were located in positions that could not be extrapolated from neighbouring transect lines. The drill hose measurements are used in preference to the Borecam, because a reading was obtained for each borehole. The BoreCam depths were generally less than those recorded by the drill hose by 1-4 m in 2004, and 1-2 m in 2005. The GPR values recorded prior to the creation of the boreholes also consistently under represented the borehole depths obtained, with the exception of boreholes 12, 13 and A (Table 5.2). Generally, the readings were anywhere between 0-11 m less than the borehole records. The borehole measurements were recorded on drilling or shortly afterwards with the BoreCam. Thus, the migration of the boreholes due to other processes, such as ice deformation (Harper *et al.*, 1998), could not account for the degree of difference in depths recorded. Instead, it was more probable that the boreholes provided an overestimation of glacier depth.

Briksdalsbreen was a relatively thin glacier, never measuring more than 85 m (2004 onwards). Willis (pers. comm.) has investigated the accuracy of manual drilling by using a magnetic oriented borehole inclinometer (Blake and Clarke, 1992b; Harbor *et al.*, 1997) and has suggested that for boreholes less than 100 m, the base can deviate from the top by up to 9m (average 2.6 m, s.d.= 2.5 m). In light of this, borehole inclinometry, which is used to correct for the curvature of boreholes away from vertical, was not performed at Briksdalsbreen. However, although Briksdalsbreen was not overly deep, the profile of the boreholes may have still drifted away from vertical, increasing the recorded glacier depth. In addition, there were several occasions when, even though the borehole had drained, suggesting it had connected with the glacier bed, the drill stem could still be lowered continually into the borehole, presumably into a cavity or drainage channel. This occurred whilst drilling borehole 10 (2004), which, in comparison to the surrounding borehole depths, displayed an anomalously high reading of 82 m (Table 5.2). Given the depths of the other boreholes in this region, a value of around 72 m is much more probable (Figure 5.12a). This trend implies that borehole depths may deviate from vertical more as the depth of the glacier increases. In light of this, the borehole depth measurements (2004-5) have been plotted against, the percent difference recorded between the GPR and borehole depth readings (Figures 5.15a and 5.16a).

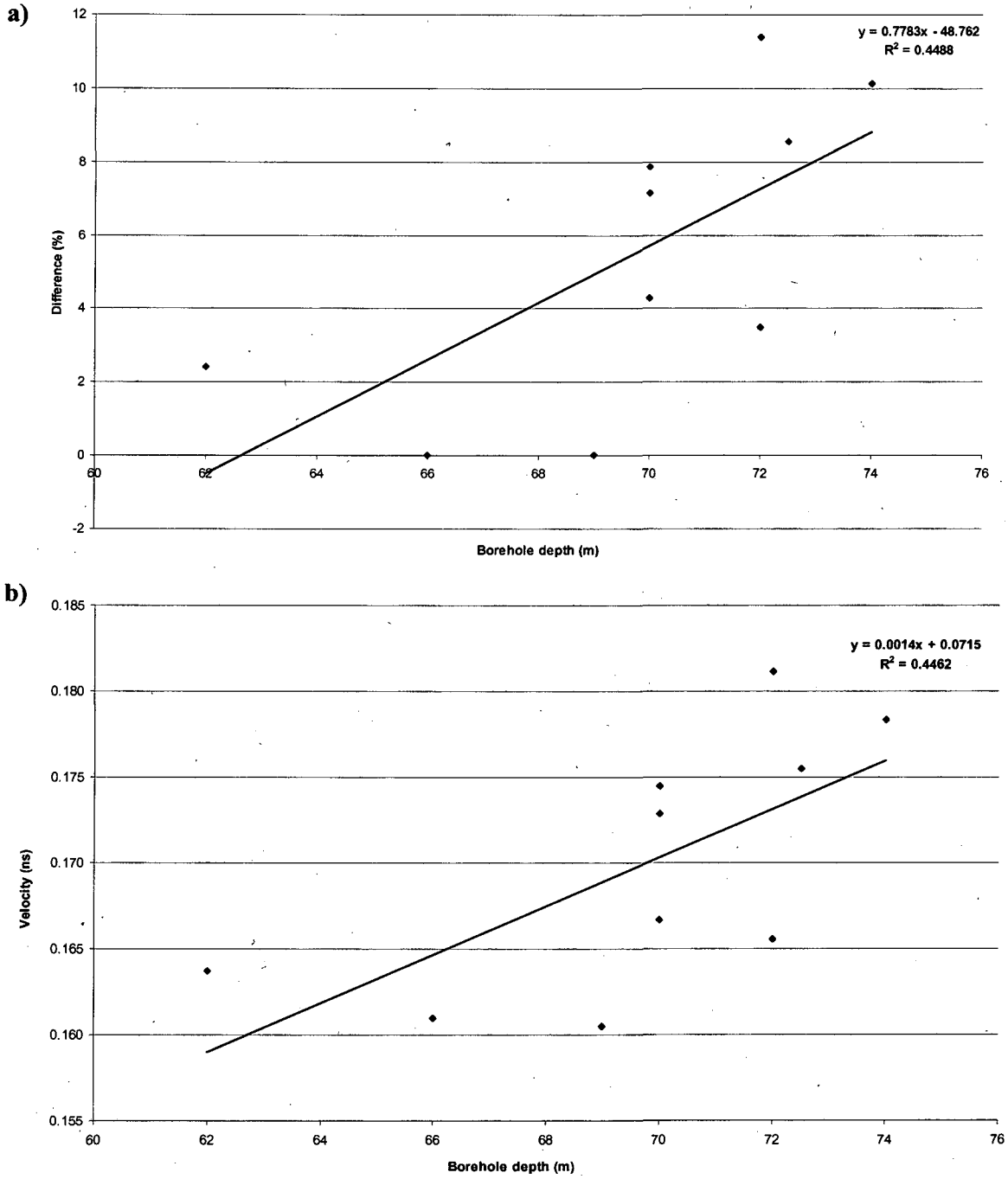


Figure 5.15: Graphs to show the correlation between 2004 glacier borehole depths and: a) the % difference between GPR and borehole depths; and b) radar velocity.

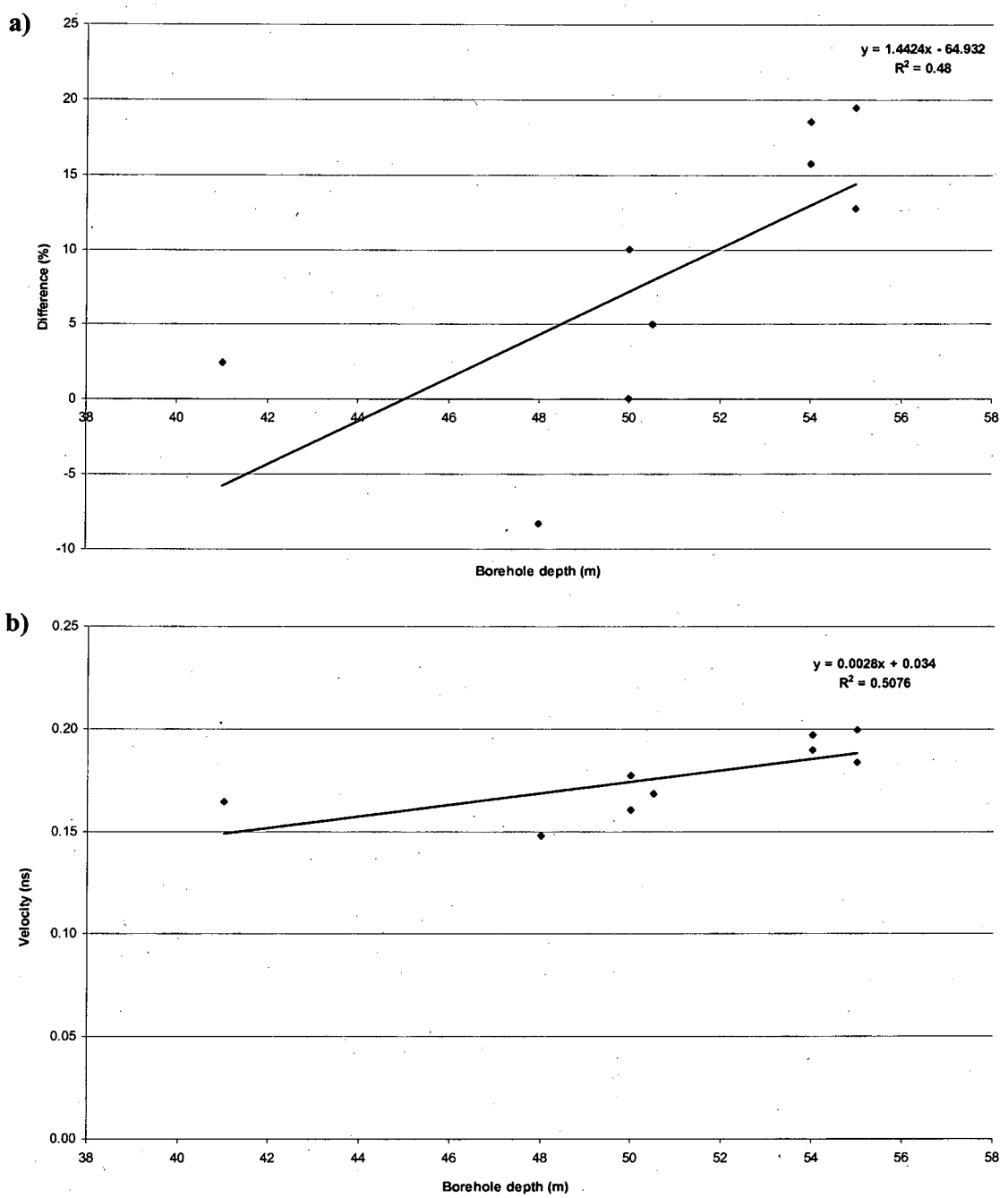


Figure 5.16: Graphs to show the correlation between 2005 borehole depths and: a) the % difference between GPR and borehole depths; and b) radar velocity.

An alternative explanation for the discrepancy between GPR and borehole depth measurements may be associated with the assumed radar velocity in ice. The velocity was determined to be 0.16 ns, based on a CMP survey performed in 2004 (section 4.3.3, Chapter 4). GPR glacier depths recorded as a distance in meters will vary according to this calculated velocity, whereas the pulse travel time remains the same. Unfortunately, the velocity can change between years and potentially even

between days. Variations in the properties and structure of the ice column, the depth of the glacier, and even variations in the subglacial environment (e.g. drainage morphology) may have caused a velocity change between 2004-2005. On a daily basis, variations may occur with changes in glacier water content.

Given this potential variability, the velocity of the radar (v) was calculated for the known borehole depths and their associated GPR travel times (Table 5.2), based on the equation:

$$v = \frac{2\,d}{n} \qquad \textbf{(10)}$$

where d is the glacier depth and n is the travel time recorded by the GPR. The values of velocity calculated are compared with borehole depths in Figures 5.15b and 5.16b

In graphs *a*, an R^2 value of 1 would indicate that the degree of discrepancy between borehole and GPR depth readings increases with borehole depth. This would support the idea that the curvature, and thus length, of the boreholes increases with drilling depth. The correlations produced by Figures 5.15a and 5.16a suggest that there is some relationship between the depth of the boreholes and the percentage of discrepancy ($R^2 = 0.45$ and 0.48, 2004 and 2005, respectively). This signifies that there is a slight tendency for the amount of deviation to increase with borehole depth, which implies that the boreholes may show greater curvature with glacier depth.

In graphs *b*, an R^2 value of 0 would suggest that there was no relationship between velocity and depth, indicating that the velocity of the radar remained constant (e.g. at 0.16 ns) with changing depths. Figures 5.15b and 5.16b suggest that there is some relationship between the depth of the glacier and radar velocity ($R^2 = 0.45$ and 0.51, 2004 and 2005, respectively). Velocity appears to increase slightly with depth. The strength of these correlations also appears to increase between 2004 and 2005. Average return radar velocities for 2004 and 2005 were 0.170 m ns^{-1} and 0.176 m ns^{-1}, respectively. The slight increase in velocity recorded in 2005 suggests that there was a greater air content and a decrease in water content in comparison to 2004.

The R^2 values recorded approximate 0.5. This implies that whilst some of the discrepancies observed may be attributed to the given parameter; it is likely that the variations recorded can only be fully accounted for by a combination of both variations in borehole length and changes in radar velocity. Although these sources of error have only been touched upon briefly, they should be of serious consideration to any future data analysis and GPR surveys performed. The use of both borehole inclinometry and the continual reassessment of radar velocity are crucial to help counteract these errors.

5.5 Borehole Instrumentation

The deployment of instruments in each field season was guided by the nature of the boreholes. Instruments were preferably placed in boreholes where till had been observed with the BoreCam, or sampled directly. The probes were also deployed in boreholes that did not appear to connect directly with a channel, in order to reduce the possibility that they could be swept away beneath the ice. Boreholes that did not connect with the glacier bed were also drilled. This was done in order to place some probes within the ice column, for comparison with those located within the subglacial environment. A number of wired transceivers were also suspended within boreholes (section 4.2.2.2, Chapter 4). The drilling records and details of probe deployment and operational success are presented below in Figures 5.17-5.18 and Tables 5.3-5.6.

5.5.1 Drilling record

Table 5.3: Borehole drilling record for 2004/5 and 2005/6.

Year	Borehole	Borehole depth (m)	Camera depth (m)	Drained?	Drainage connectivity ¤	Till? *	Till sample?
2004	1	74	-	N	UC	Y	Y
	2	72	-	Y	C	N	N
	3	69	70	N	UC	N	N
	4	72.5	70	N	UC	Y	Y
	5	72	-	Y	C	Yc	N
	6	70	68	Y	C	Yc	Y
	7	77	74	Y	C	Y	N
	8	69	68	Y	C	Yc	N
	9	65	-	N	UC	Y	N
	10	72	-	N	UC	N	N
	11	30	-	N	UC	N	N
	12	66	66	Y	C	Y	Y
	13	69	70	Y	C	Y	N
	14	62	65	Y	C	Y	N
	15	70	66	Y	C	Y	N
	16	70	67	N	UC	Yc	N
2005	A	50	-	Y	C	Y	Y
	B	48	-	Y	C	-	-
	C	55	53.5	Y	C	Y	Y
	D	55	-	Y	C	Y	Y
	E	41	41	Y	C	Y	Y
	F	50.5	49.5	N	UC	Y	Y
	G	50	-	Y	C	Y	Y
	H	54	-	Y	C	Y	Y
	I	54	53	Y	C	Y	Y
	J	54	52	Y	C	Y	Y
	K	54	-	N	UC	Y	Y
	L	54	-	Y	C	Y	Y
	M	35	-	N	UC	-	-

¤**C** – connected
¤**UC** – unconnected
***Yv** – till was visible with the BoreCam
***Yc** – till and a clast was visible with the BoreCam

5.5.2 Instrument record

Table 5.4: Instrument record for 2004/5 and 2005/6.

Year	Instrument	Borehole	Borehole depth (m)	Initial instrument depth (m)	Instrument in till or ice	Start date (Julian Day)	End date (Julian Day)	No. of days operational
2004	**1**	10	82	82	Till	223	223	0
	2	4	70	70	Till	219	219	0
	3	8	64	64	Till	219	227	9
	4	2	72	72	Ice	227	144*	283
	5	16	64	64	Till	227	340	114
	6	7	74	74	Till	223	223	0
	7	1	74	74	Till	223	293	71
	8	13	70	17	Till	227	236*	375
	Transceiver 1	4	72.5	20	Ice	219	-	-
	Transceiver 2	7	77	20	Ice	223	-	-
2005	**10**	C2	55	38	Till	213	221*	374
	11	F	50	59	Till	216	216	0
	12	J	54	41	Till	215	221*	372
	13	D	55	55	Till	217	217	0
	14	H	54	54	Till	215	217	3
	15	I	54	54	Till	215	207*	358
	16	L	54	35	Till	215	321	107
	Transceiver	M	35	30	Ice	215	-	-

* day in the following year

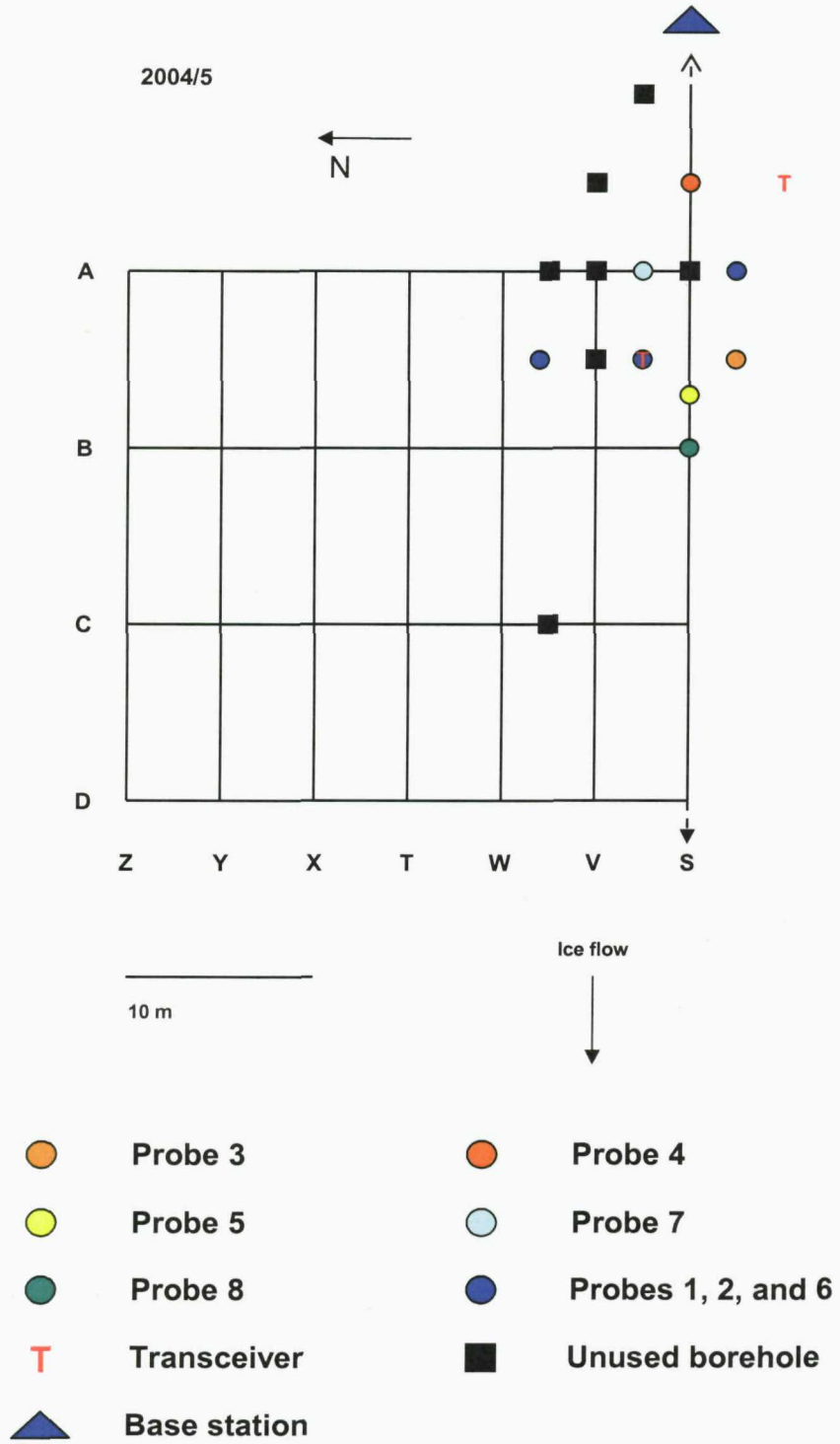


Figure 5.17: Schematic diagrams to show the location of the boreholes and instruments deployed in 2004/5 in relation to the GPR transects. Note: the location of the base station is approximate.

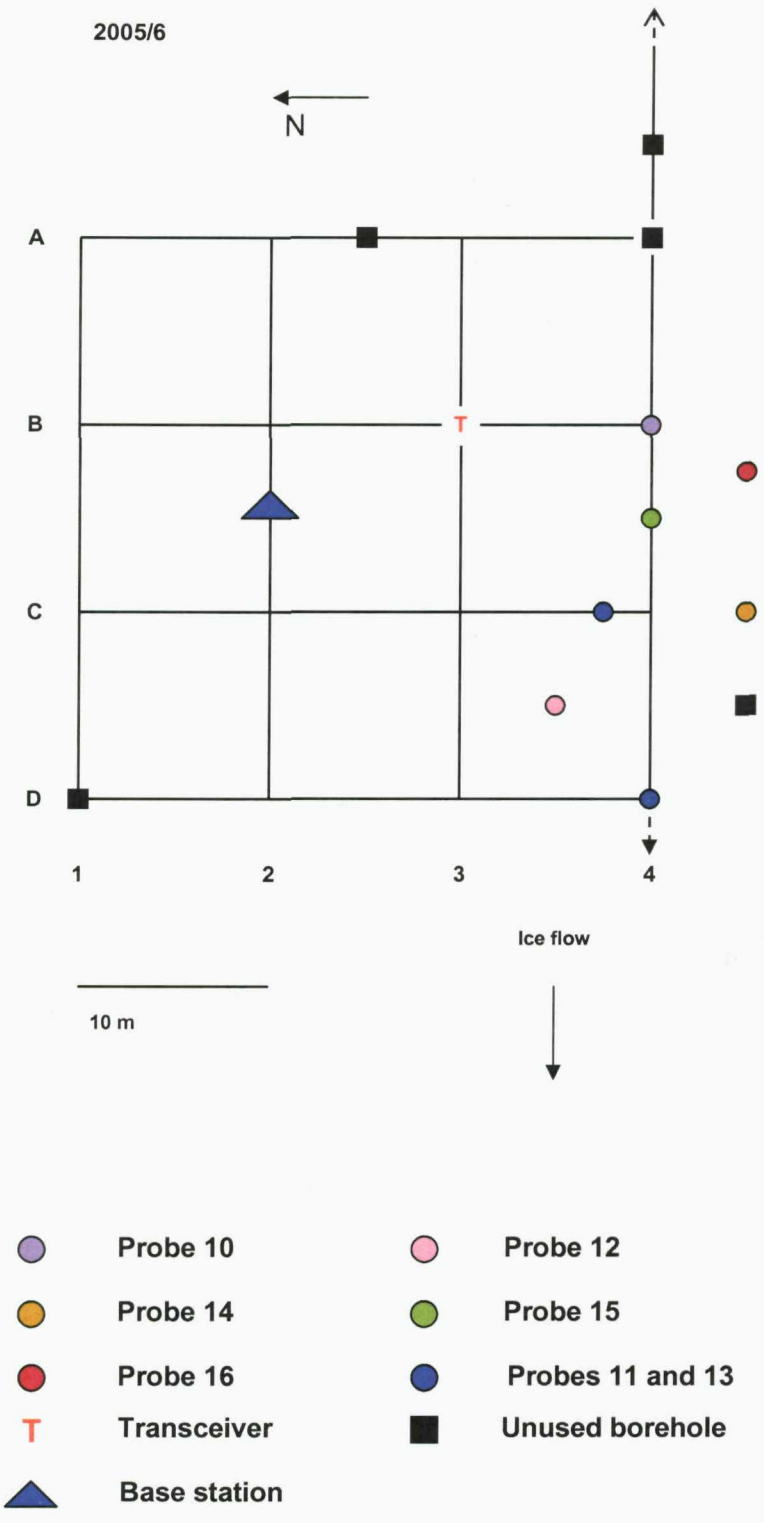


Figure 5.18: Schematic diagrams to show the location of boreholes and instruments deployed in 2005/6 in relation to the GPR transects. Note: the location of the base station is approximate.

Table 5.5: Record of sustained probe communications over time.

	2004/5	**2005/6**
No. of probes deployed	8	7
% which communicated	63	71
% operational for ≥ 1 week	63	57
% operational for ≥ 1 month	50	57
% operational for 6 ≥ months	25	43
% operational for ≥ 1 year	13	29

Table 5.6: Gant chart to show the duration of probe communications from 2004-2006. Only those probes which lasted longer than 10 days are displayed.

Year	2004					2005												2006							
Month	A	S	O	N	D	J	F	M	A	M	J	J	A	S	O	N	D	J	F	M	A	M	J	J	A
Probe 3																									
Probe 4																									
Probe 5																									
Probe 7																									
Probe 8																									
Probe 10																									
Probe 12																									
Probe 15																									
Probe 16																									

Table 5.7: Record of probe sensor function following deployment.

Year	Probe	Temperature	Pressure	Case strain	Resistance	Tilt	% sensors operational
2004	**3**	Y	Y	Y	Y	Y	100
	4	Y	Y	Y	Y	Y	100
	5	Y	Y	Y	Y	Y	100
	7	Y	Y	N	Y	Y	80
	8	Y	Y	N	Y	Y	80
Average							92
2005	**10**	Y	Y	Y	Y	Y	100
	12	Y	Y	N	N	Y	60
	14	Y	Y	Y	Y	Y	100
	15	Y	Y	Y	Y	Y	100
	16	Y	Y	Y	Y	Y	100
Average							92

The success of the probe sensors and communications increased between years with continued improvements to probe design and ongoing calibration (Tables 5.5 and 5.6). One probe remained operational for over a year in 2004/5, whereas 2 (almost 3) probes achieved this in 2005/6. In total 6 probes sustained communications for over six months (Table 5.6). The function of the micro-sensors within the probes was also monitored (Table 5.7). Only 4 sensors failed in the 10 probes deployed and on-going testing and calibration should ensure that such failures are prevented in future years. To date, the excellent success rate of probe communications and sensors has resulted in a series of large data sets. The data encompasses deployment in the winter to the remobilisation of the glacier in the following spring and summer. In light of this success, the activity of the probes has been divided into winter, spring and summer seasons, the details of which are discussed in Chapters 6, 7 and 8, respectively. To note in these chapters: only those probes which lasted longer than 10 days are discussed; Probe 4 was placed in an englacial borehole and so was not overlain by any ice, as such water pressure is displayed as meters water equivalent; all other pressure records are presented as a percent of overburden pressure; the 2004/5 resistance is calibrated within a range of 0-10 M Ohm, whereas the 2005/6 probes have a range of 0-20 M Ohm (see Figure 4.8 and Table 4.3, section 4.2.1.5, Chapter 4).

5.6 Summary

This chapter has presented the setting for the *in situ* instrumentation that was carried out at Briksdalsbreen from 2004-5. The series of maps produced from the GPS survey provide a comprehensive overview of the field areas investigated and the changing nature of the glacier and its foreland. The mapping of the boreholes also enabled comparison between the locations of the instrumented areas between years and following glacier retreat. The use of the GPR provided an overview of the subglacial environment, allowing any potential irregularities in subglacial topography and internal ice structure to be identified. This enabled the boreholes to be located in the best possible position for instrumentation. The glacier depth recorded by the boreholes was consistently greater than that shown by the radar signal, reflecting the deviation of the boreholes from vertical during drilling and variations in pulse travel time. In general, the depth of the glacier decreased down ice and there were few irregularities at the glacier bed. A number of boreholes were drilled successfully each year and 8 and 7 probes were deployed in 2004 and 2005, respectively. The success of the instruments varied but was generally high. The details of the probe records are discussed according to seasonal trends in Chapters 6, 7 and 8.

Chapter 6

Winter Probe Record

6.1 Introduction

This chapter will discuss the winter probe records, comprising the period from deployment (various dates in August) to the end of either the probe record, or December. The winter is thought to mark a period of quiescence in the glacier system. Glacier velocities decrease and only minimal activity is sustained within the subglacial environment. This section will focus on the characteristics of the probe records following deployment, in order to differentiate between the initial stages of probe incorporation into the till and the sensor patterns that are indicative of 'normal' conditions within the subglacial environment. Analysis of the probe records will be carried out to derive features diagnostic of probe incorporation into the till, the closure of boreholes and sensor activity within the subglacial environment during the winter.

6.2 Conceptual Ideas

The aspect of greatest concern following deployment, if the probes are to become incorporated into the deforming bed, is ensuring that they have settled at the ice-bed interface. The probes may become positioned in a number of locations, both following their release and in the weeks and months that ensue. Long-term changes are of particular importance when determining if the probes have become incorporated into the deforming bed.

Figure 6.1 presents a conceptual model for the various scenarios that may arise following probe deployment and how this may affect the location of a probe within the subglacial environment over time. Time stage 1 reflects the location of a probe on deployment. Scenario A represents a probe that has become stuck within the bottom of the borehole and is unable to reach the ice-bed interface. In time stage 2, the probe has remained within the borehole column but moved away from the area of the bed over which it was deployed. At time stage 3, ice creep has begun to close the borehole and the probe becomes incorporated into the ice column. In scenario B, the probe rests flat on its side at the ice-bed interface. It is likely that hot water drilling will excavate a small indentation within the till (Blake *et al.*, 2001) to facilitate probe incorporation into the deforming bed. At time stage 2, the glacier has moved past the initial area of deployment and has overridden the probe, sealing it within the deforming bed. The borehole has begun to close shut by time stage 3, while the probe remains incorporated into the till and is now located much further away from the borehole, as the glacier above continues to move forward. Scenario C is perhaps the most likely situation to occur on deployment. The probe becomes positioned upright at the ice-bed interface, partly within the till and partly within the borehole. In time stage 2, the glacier has moved forward and the borehole has begun to close. The probe may be dragged through the till, still partially trapped within the borehole. Under these conditions, two outcomes may arise with further time within the subglacial environment. In the first, time stage 3i, the probe moves further into the till and out of the borehole as the overlying ice overrides the glacier bed. However, in time stage 3ii, the probe becomes trapped or sealed within the borehole column. As a result, the probe will continue to be dragged through the deforming bed, in a style similar to that associated with ploughmeters (section 2.4.1, Chapter 2).

The movement of the ice and the closure of the borehole will subject the probes to different subglacial processes over time. Glacier motion and the topography of the ice and bed, will affect the incorporation of the probe into the ice-bed interface. The glacier will continue to move throughout the period of deployment and into the winter months, through a combination of ice creep, sliding and sediment deformation (Boulton, 1996). At Briksdalsbreen, measurements of surface velocity and till deformation suggest that 36% of total glacier motion occurs within the deforming

bed. This signifies that the overlying ice will move more rapidly than a probe set within the deforming bed.

The probes are likely to see a great deal of sensor activity during and following deployment, as they travel down the borehole and position themselves at the ice-bed interface (time stage 1). On deployment, the boreholes are still fully open at the surface of the glacier, where they may receive surface inputs of melt water and precipitation (time stage 1). These inputs may be recorded within probe sensor readings. Accordingly, as the borehole moves further away from the probe, and begins to close through ice deformation, the signal of surface inputs and changing weather locations may be removed from the records (time stages 2-3). The location of the probe within the highly heterogeneous subglacial system will also affect the sensor records produced. It is important that these different influences on the probes are identified and characterised, so that the probe sensor records may be interpreted sensibly. Table 6.1 provides a summary of the different sensor activity that is predicted for each scenario and time stage. This will provide a bench mark against which to assess the probe records.

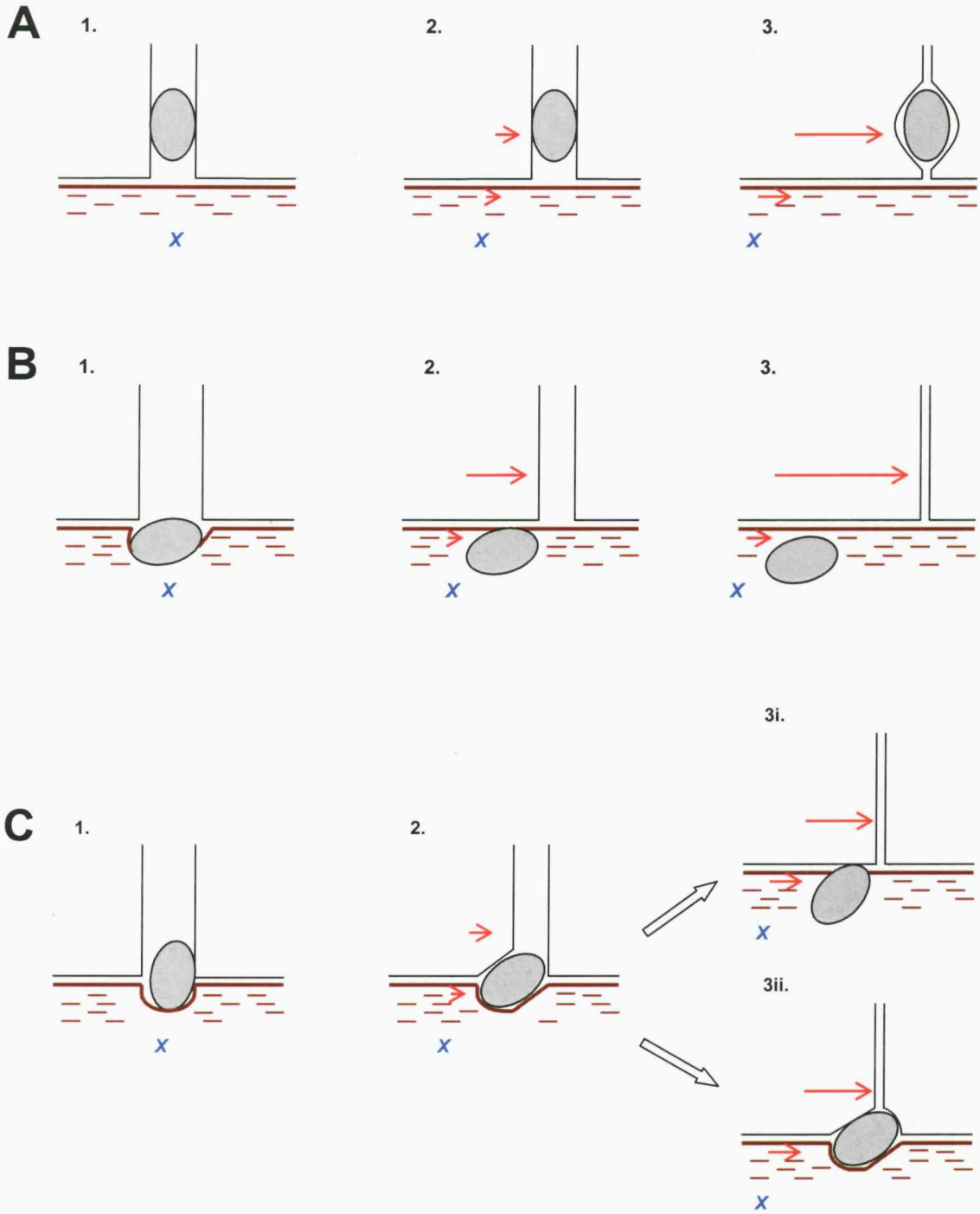


Figure 6.1: Conceptual model demonstrating the variety of probe locations after deployment and in response to the movement of the glacier and closure of the boreholes over time. Note: the red arrows denote the relative movement of the ice and the till; *x* marks the location of the probe on deployment.

Table 6.1: Predicted sensor activity associated with Scenarios A, B and C, outlined in Figure 6.1.

Sensor		Probe temperature	Water pressure	Resistance	Case strain	Tilt
Scenario	**Time stage**					
A	**1**	Close to 0°C in line with subglacial conditions.	Fluctuating pressures, reflecting external weather conditions.	Variations correlate with changes in water pressure.	Minimal strain experienced as probe rests in borehole.	High activity during the initial stages of deployment.
	2	"	Fluctuating pressures, less indication of weather conditions.	"	Case strain increases in one direction as the borehole closes.	Variations in tilt decrease as the borehole closes.
	3	Temperatures may decrease if the probe becomes frozen within the borehole.	Pressures may cease fluctuating if the probe becomes sealed within the ice with no indication of external weather conditions.	Variations in resistance change as the probe becomes sealed within the borehole.	"	Very slow changes in tilt, in accordance with ice creep if the probe is sealed within the borehole.
B	**1**	Close to 0°C in line with subglacial conditions.	Fluctuating pressures, reflecting external weather conditions.	Variations correlate with changes in water pressure.	Minimal strain recorded as probe rests at the ice-bed interface.	High activity during the initial stages of deployment.
	2	"	Pressure fluctuations may change as probe is incorporated into the bed, less indication of external weather conditions.	Activity may vary as the probe becomes fully incorporated in to the bed, less indication of external weather conditions.	Strain increases and shows oscillations as the probe is over-ridden by the ice and interacts with the till.	Tilt shows gradual changes as the probe is incorporated into the deforming bed.
	3	"	Pressure will reflect activity within the deforming bed, no signal of external weather conditions.	Fluctuations may change as the borehole closes, no signal of external weather conditions.	Strain continues to show oscillations as the probe moves within the deforming bed.	Oscillations and an increase in activity, if the till undergoes deformation.

Table 6.1: continued...

Sensor		Probe temperature	Water pressure	Resistance	Case strain	Tilt
Scenario	**Time stage**					
C	**1**	Close to 0°C in line with subglacial conditions.	Fluctuating pressures, reflecting external weather conditions.	Variations correlate to changes in water pressure.	Minimal strain recorded as probe rests at the ice-bed interface.	High activity during the initial stages of deployment.
	2	"	Pressure fluctuations may change as probe is incorporated, less indication of external weather conditions.	Activity varies as the probe is incorporated into the deforming bed, less indication of external weather conditions.	Strain increases and shows oscillations as the probe moves into the till and is constricted by the borehole.	Activity decreases, tilt shows gradual changes as the borehole closes and constricts the probe.
	3i	"	Pressure will reflect trends within the deforming bed, no signal of external weather conditions.	Trends in resistance change as the probe is fully incorporated into the deforming bed, no signal of external weather conditions.	Strain increases and shows oscillations as the probe is overridden by the ice and interacts with the till.	Oscillations and an increase in activity if the till undergoes deformation.
	3ii	"	Pressure will reflect trends within the deforming bed, no signal of external weather conditions. Trends may be affected as the probe is dragged through the deforming bed.	Trends vary as the borehole closes and the probe is dragged through the deforming bed.	Case strain increases in one direction as the probe is dragged through the till and trapped in the borehole.	Gradual change in tilt in one direction, as the probe is dragged through the till.

6.3 2004/5

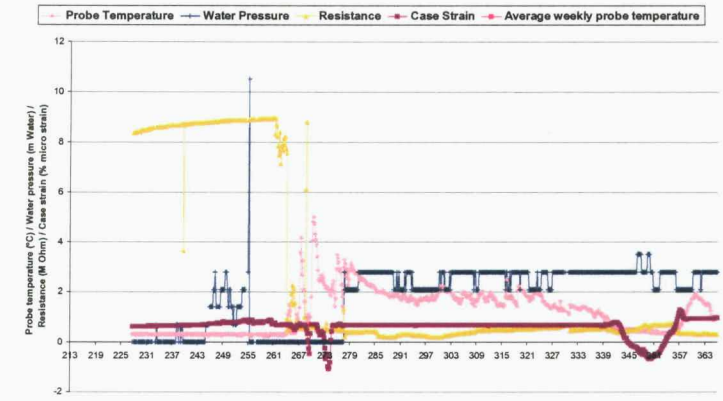
In 2004, Probes 4, 5, 7 and 8 maintained communications following deployment. The relative location of the probe boreholes and the details of deployment are summarised in Figure 5.17 and Tables 5.3 and 5.4, respectively, (section 5.5, Chapter 5). The winter (August-December) data records for these probes are summarised in Figures 6.2 and 6.3. The records for each probe are outlined before they are discussed.

6.3.1 Probe 4

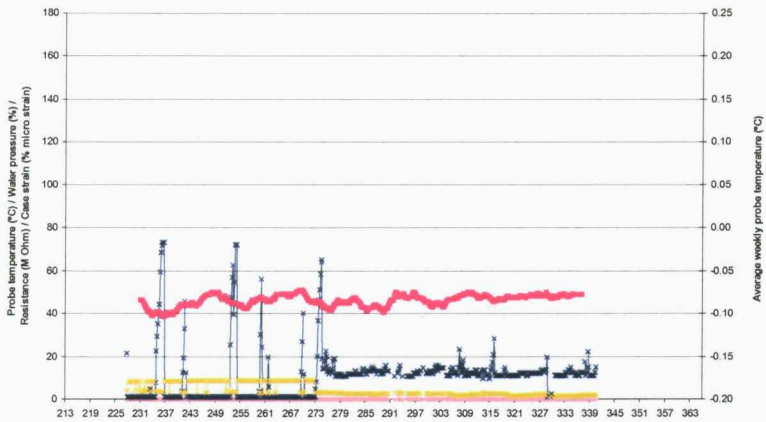
The winter record for Probe 4 showed a large variety of fluctuations (Figures 6.2a and 6.3a). Probe temperature remained at 0.3°C between days 227-263, before values began to fluctuate (Figure 6.2a). Temperatures began to increase rapidly and a peak value of 5°C was reached on day 270. Following day 270, average temperatures began to fall, whilst continuing to oscillate. Probe temperatures reduced to 3.1°C by day 279, and from this point showed a steadier decline, with less fluctuation (days 279-341). Constant temperatures (0.4-0.5°C) were maintained between days 342-356. This was followed by an increase in temperatures, peaking at 1.9°C on day 360, before slowly falling to 1°C on day 365. Initial water pressures were low, showing small-scale fluctuations between days 227-255. Pressure peaked at 10.5 m on day 255, before values decreased to 0 m, where they remained until day 277. Pressure then rose to 2.8 m and recorded small-scale oscillations for the rest of the record.

The resistance record was relatively stable between days 227-261, showing a gradual increase in values from 8.3-8.9 M Ohm. Resistance then began to fall and fluctuate, reaching 0.4 M Ohm on day 264. Values then remained below 1.0 M Ohm, showing minor oscillations for the rest of the record. Case strain increased gradually between days 227-255. Readings then began to oscillate and two peaks in strain were recorded (days 268-275), before values became relatively constant (days 277-339). An increase in strain occurred before the direction of strain changed and increased between days 341-350. Values then increased in the opposite direction, returning to previous levels by day 358 for the rest of the winter record.

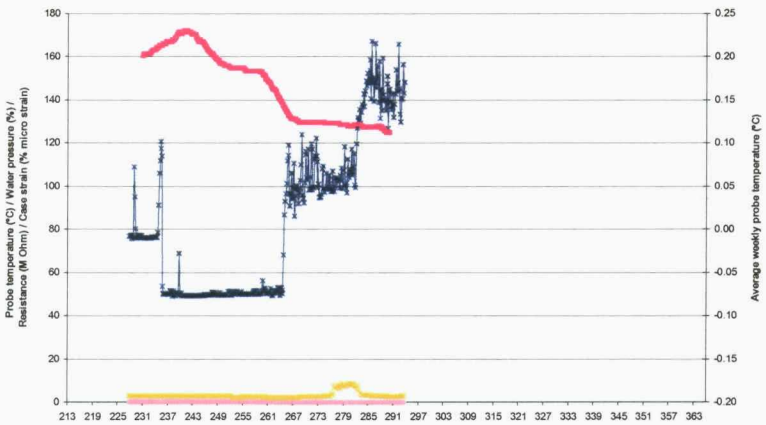
a)



b)



c)



d)

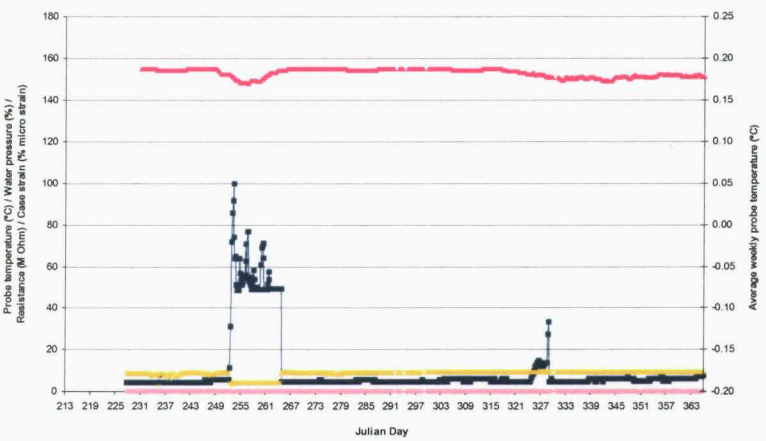


Figure 6.2: Comparison of the winter sensor records, showing probe temperature, water pressure, case strain, resistance and average weekly probe temperature for: a) Probe 4; b) Probe 5; c) Probe 7; and d) Probe 8. Note: a change in y-axis scale for Probe 4.

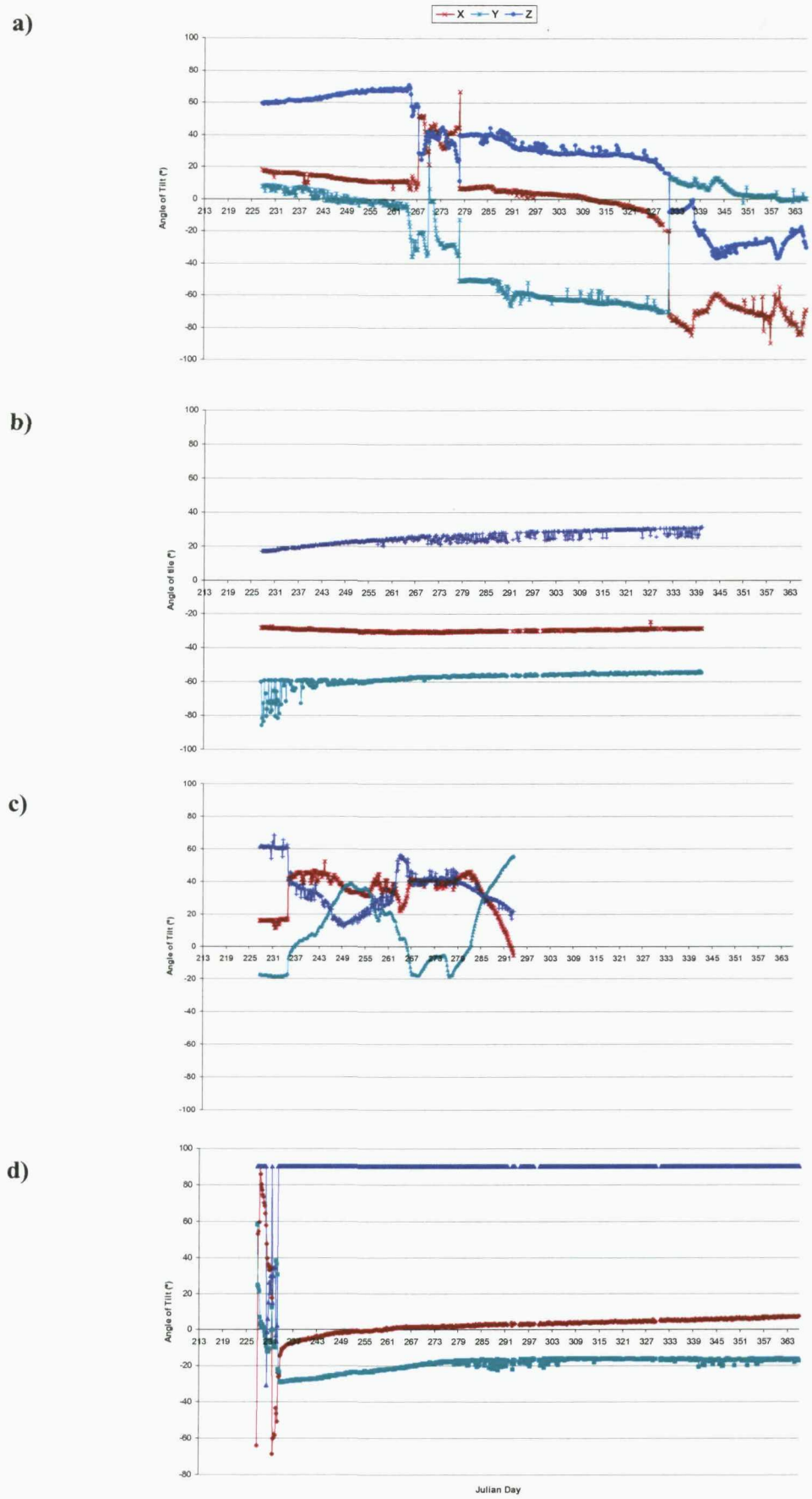


Figure 6.3: Comparison of winter tilt sensor records for: a) Probe 4; b) Probe 5; c) Probe 7; and d) Probe 8.

The record for probe tilt displayed general phases of stability followed by periods of increased oscillation that broadly correlated between each axis (Figure 6.3a). There was relatively little probe movement between days 227-263, before tilt began to oscillate more vigorously along all three axes. This was sustained until day 277 when tilt suddenly stabilised along all three axes. Gradual change in tilt, accompanied by small-scale oscillations, was sustained between days 277-331. On day 331, tilt showed a sudden shift along all three axes. This was followed by an increase in the variety and amplitude of oscillations, to the end of the winter period.

6.3.2 Probe 5

Figures 6.2b and 6.3b display the record for Probe 5 (days 227-341). Probe temperatures ranged between 0°C and -0.13°C for the duration of the record, with average values oscillating throughout (Figure 6.2b). Initial activity in water pressure was characterised by a series of sudden, rapid, pressure peaks, rising from minimal and stable basal flows (1.2%). Pressure peaks normally lasted 1-2 days and ranged between 73.1-19.9%. This pattern changed on day 275, as base flows increased to 11.2%. Pressure values remained relatively constant but showed a greater frequency of small-scale oscillations for the remainder of the record.

The start of the resistance record was characterised by oscillations ranging between 8.1-0.1 M Ohm. These ceased on day 275 and readings fell to 2.9 M Ohm. Resistance continued to show small-scale fluctuations and a gradual decline in average values for the rest of the record. Case strain showed rapid short lived oscillations around an average base level. The tilt record (Figure 6.3b) showed an initial phase of rapid, high frequency oscillations, particularly along the y-axis (days 227-244). Activity decreased from day 245, and slow and steady changes in tilt continued for the rest of the record. However, an increase in small-scale oscillations along the z-axis was evident from day 270.

6.3.3 Probe 7

Probe 7 lasted between days 227-293 (Figures 6.2c and 6.3c). Probe temperatures ranged between 0.06-0.25°C throughout this period. Average probe temperature displayed an increase in values to 0.23°C by day 241. This was followed by a two

stage 'terraced' decline in average temperatures from day 242. Initial values of water pressure recorded by Probe 7 were high, with a sustained base level of 76.2%. This was punctuated by two pressure peaks on days 228 and 235 (108.8% and 121.0%, respectively). On day 235, base flows decreased to 49.5%, showing only two pressure rises (68.8% and 56.2%). Pressures then increased from day 264 to 119.0% (day 265) and began to show high frequency oscillations. Following this, pressures remained elevated, fluctuating around an average of 103.3% and remaining above 86.2%. A final change in water pressure was recorded on day 282. Values increase above 127.1% and fluctuating around an average of 143.2%.
Resistance was relatively constant at the start of the record, varying between 3.0-2.8 M Ohm. Values rose abruptly on day 276 (~8 M Ohm) and began to fluctuate (days 277-282), before falling abruptly on day 282. During the rest of the record, resistance showed only small-scale fluctuations between 2.4-3.4 M Ohm. The tilt sensors (Figure 6.3c) showed little fluctuation at the start of the record (days 227-234). However, from day 235, the record began to show significant and rapid fluctuations along all three axes, lasting for the rest of the record.

6.3.4 Probe 8

The sensor records for Probe 8 are shown in Figures 6.2d and 6.3d. Probe temperature showed minor oscillations ranging between 0.13-0.19°C (Figure 6.2d). Average weekly probe temperatures were generally constant, between days 227-231. Values showed a brief decline between days 249-256, reaching 0.17°C, before returning to previous levels. Average temperatures showed a more persistent decline, with greater fluctuations from day 317. This decline plateaued from day 327, showing oscillations between 0.17-0.18°C. At the start of the record water pressure maintained a base level of 4.5% (days 227-252). A small, short lived (< 8 hours) peak in water pressure (8.0%) was recorded on day 235. Pressure suddenly increased on day 252, reaching 100.0% by day 253. Values then began to oscillate (up to 77.0%) from a new base level of 48.9%. On day 264, water pressure fell abruptly, returning to initial base levels and displaying only minor fluctuations (days 264-324). This pattern was interrupted by an increase in pressure up to 33.6% (days 324-328). Following this, small-scale oscillations at base level continued for the remainder of the winter.

Resistance showed some variation at the start of the record with minor oscillations between 6.5-8.9 M Ohm. There was an abrupt drop to 2.9 M Ohm on day 235 (< 8 hours), followed by a second prolonged decrease to 4.1 M Ohm (days 252-264). Values increased again on day 264 and minor oscillations continued for the rest of the year. Significant activity was displayed in the tilt record between days 227-232 (Figure 6.3d). This pattern changed abruptly on day 233 and was replaced, for the remainder of the record, by a gradual change in tilt along all three axes, punctuated by small-scale oscillations.

6.4 Interpretation: 2004/5

The sections below will discuss the activity recorded by the probes in a series of stages. The records will be considered with respect to the conceptual ideas outlined above, looking for evidence of probe locations following deployment; influences from external weather conditions; borehole closure; probe incorporation into the till; the physical processes operating in the subglacial environment during the winter; and probe failure. Probes 5, 7 and 8 were deployed within boreholes that connected with the glacier bed and will be considered first in this section. Probe 4 was placed within a closed borehole that did not reach the glacier bed. This was done deliberately in an attempt to produce an englacial probe that would monitor conditions within the ice column. As such, it will be considered separately in section 6.5.

6.4.1 Commencement

The activity of the probes on deployment and immediately after release is best represented by the tilt records (Figure 6.3; see also section 4.2.1.4, Chapter 4 for details on tilt sensor interpretation). Probe 5 displayed frequent oscillations between days 227-244, particularly along the y-axis (Figure 6.3b). This activity demonstrates that the probe was still adjusting to its surrounding environment and shifting position, which correlates well with predicted readings in Table 6.1, time stage 1. The rate of change along the axes infers that it was not yet incorporated into the deforming bed. Instead, this movement implies that the probe was oscillating at the base of the borehole, at the ice-bed interface. This was confirmed by the BoreCam, which showed Probe 5 propped up against a clast at the base of a borehole shortly

after deployment. This revealed that there was a definite space or indentation at the base of the borehole, in which the probe could become positioned. The video footage, in combination with the tilt record, indicated that Probe 5 was in scenario C1 (Figure 6.1; Table 6.1). The rate of change in tilt decreased on day 245, becoming slow and steady, interspersed with small-scale oscillations. This stabilisation implied a fast transition from scenario C1 to C2 (Figure 6.1; Table 6.1).

Probe 8 showed a similar record of tilt activity (Figure 6.3d). Significant movement was recorded at the start of the record (days 227-232), agreeing with time stage 1 (Table 6.1). The BoreCam revealed that Probe 8 was initially lodged within the borehole at a depth of 17 m from the surface. However, the activity in tilt implies a period of intense movement as the probe fell to the ice-bed interface in the days that followed. At this point, the tilt readings suggested that Probe 8 was orientated upright within the base of the borehole. Concurrent probe temperatures also suggest that it was in the subglacial environment. These patterns indicate that Probe 8 had moved from scenario A1 on deployment, to scenario C1 at the ice-bed interface between days 227-233 (Figure 6.1). The sudden drop in the rate of movement on day 233 signified that the probe had finally settled at the ice-bed interface, transitioning to scenario C2 (time stage 2, Table 6.1).

The record for Probe 7 also began on day 227, but the orientation of the probe remained relatively stable between days 227-234 (Figure 6.3c). The probe was in an upright position, showing only minor fluctuations, which is consistent with scenario C1. It was only from day 235 that the readings of tilt began to fluctuate significantly. This pattern differed to that displayed by Probes 5 and 8 and was contrary to the activity predicted for a probe within the subglacial environment following deployment (Table 6.1). The absence of significant activity during the first few days may be explained by the probe's location. The BoreCam revealed that it was lodged upright against two clasts, which may have helped to stabilise its position. The sudden oscillations in tilt from day 235 coincided with a change in the pressure record, which may have initiated the change in tilt (Figures 6.2c and 6.3c). The step change in pressure may have caused the probe to move, or resulted in sudden motion at the glacier bed, which had the same effect. Whatever the cause, the probe obviously became destabilised from this point and was located in an area of the

glacier bed where it was able to change orientation relatively rapidly. These oscillations may have been in response to the high pressure flows recorded in this area of the bed.

The change in tilt recorded by Probe 7 suggested that it was lying almost flat at the glacier bed (Figure 4.7, section 4.2.1.4). This indicates that it had transitioned from scenario C1 to C2 (or possibly even B2, given the angle of repose), moving to time stage 2 within the first 9 days (Figure 6.1; Table 6.1). The reduction in tilt activity recorded by Probes 5 and 8 reflected a transition to time stage 2. In contrast, the activity in tilt recorded by Probe 7 was sustained. This would suggest that the activity in tilt predicted in Table 6.1, which assumed that the probe would be relatively constrained at the ice-bed interface, was incorrect. However, continued oscillations might be achieved if the probe could move freely within a cavity, or if Probe 7 was oscillating in response to the high pressure flows in this area of the bed.

This activity shows that the tilt records can be used to reconstruct probe movement from deployment and then into a period of adjustment as the probes 'settle' at the ice-bed interface. Once the location of a probe has stabilised, it is more likely that it will start to become incorporated into the deforming bed. The records for Probes 5 and 8 appeared to stabilise very quickly. This may reflect the movement of the ice over the probes in those locations, allowing them to become rapidly incorporated. The time sequence displayed by Figure 6.1 emphasises that the movement of the ice over the glacier bed occurs faster than the rate of bed deformation (section 6.2).

Rates of ice movement can be used to determine how quickly the borehole will move away from the initial location of deployment via sliding (Figure 6.4). Surface velocities during the time of deployment (August) averaged 0.08 m day^{-1}. This suggests that it would take 30 hours for the complete diameter of the borehole (~0.1 m) to move past the initial location of probe deployment (position *x*); taking into account the proportion of motion via deformation (36%). This is only a rough estimate of borehole displacement, as the movement of the ice is faster at the surface than at the base of the glacier, causing attenuation of the borehole (Harper *et al.*, 1998, 2002). The value of 30 hours reflects the minimal amount of time required if

surface velocities were equal to basal velocities. Thus, in reality it is likely that this process took slightly longer.

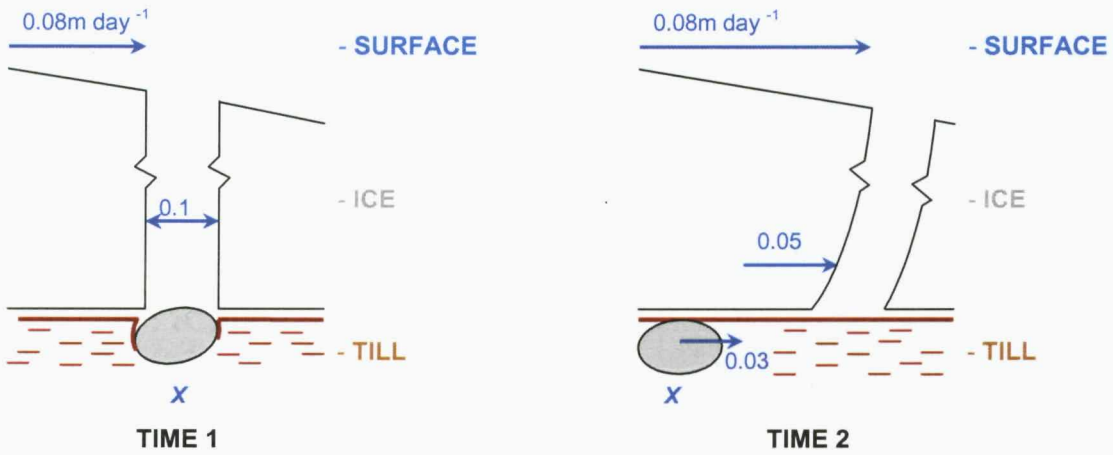


Figure 6.4: Conceptual diagram displaying the rate of borehole movement over the initial position of probe deployment, with respect to rates of sliding versus till deformation. Note: differential deformation rates within the ice column may cause the borehole to become attenuated.

The tilt records for Probes 5 and 8 stabilised after 19 and 7 days, respectively, whilst the Probe 7 record remained active. This implies that in reality the movement of the boreholes at the bed was less rapid, or that despite the movement of the boreholes, the probes took longer to become fully constrained within the subglacial environment. This would certainly apply to Probe 7. The differences in timing also indicate spatial variability within the subglacial environment. The time in which the probes settle is likely to vary according to local sedimentology, bed topography, and water movement across the glacier bed, as well as local variations in glacier velocities (e.g. stick-slip motion resulting from the occurrence of sticky spots; Fischer *et al.*, 1999). The small cavities that allowed Probes 5 and 7 to rest on their sides may have been maintained, despite glacier movement. This may be why it took longer for the Probe 5 tilt record to stabilise, and why the Probe 7 record remained active throughout. The rate of glacier motion suggests that the probes had transitioned into time stage 2 (Figure 6.1); but that Probe 7 remained relatively unconstrained within the borehole, in contrast to the predictions of Table 6.1.

6.4.2 Triggers

External weather conditions for 2004 are displayed in Figure 6.5, in combination with the sensor records for Probes 5, 7 and 8. Temperature and precipitation signals can provide an explanation for the magnitude and oscillations in water pressure within the subglacial environment. This is because both factors, in a positive relationship, act to influence the amount of surface melt water generated and passed through the glacier system. This effect dominates in summer and autumn when melt water production is at its highest, resulting from both augmented external temperatures and precipitation and rainfall derived melt water.

The effect of elevated melt water generation should also be particularly obvious following instrument deployment (time stages 1-2). This is because open boreholes will provide a direct pathway for surface melt water inputs into the glacier system, in addition to any contributions from englacial or subglacial flows. Figure 6.1 and Table 6.1 predict that variations in external weather conditions will be reflected within sensor readings, particularly water pressure and resistance. However, this signal is likely to weaken or be removed by time stage 3, as the boreholes close and move away from the location of the probes, which are becoming further incorporated within the deforming bed (Figures 6.1 and 6.4). This section will examine the sensor patterns at the start of the probe records in order to identify any such relationship.

The probes showed some correlation to weather events, namely precipitation, at the start of the records (Figure 6.5). However, this was very sporadic and generally disappeared as the winter progressed. Probe 5 pressure peaks lagged precipitation events, normally by 2 days, and often occurred in combination with periods of elevated temperature (Figure 6.5b). The best correlations were recorded at the start of the record when some pressure peaks occurred in unison with precipitation events (e.g. day 241). However, the response in water pressure was relatively independent of the size of precipitation events, which might suggest that the association was simply random. At the end of the record, small-scale pressure oscillations occurred in combination with, and independent from, precipitation events. For example, pressure did not increase following 53.6 mm of precipitation on day 319. This suggests that, from this point, there was no immediate response in pressure fluctuations to surface events.

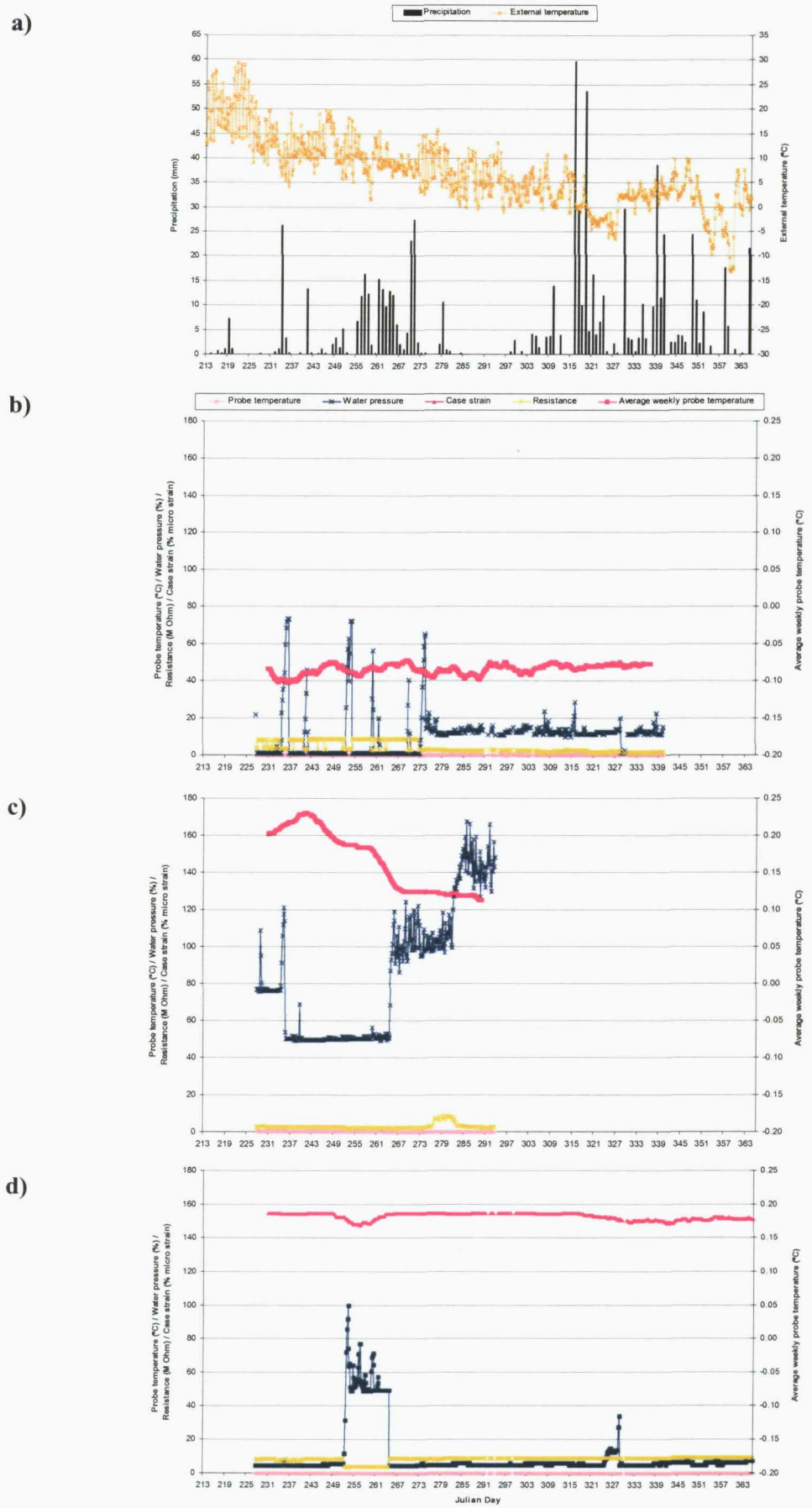


Figure 6.5: Comparison of winter sensor records, showing: a) external weather conditions; b) Probe 5; c) Probe 7; and d) Probe 8 (2004/5).

Probe 7 showed a similar relationship (Figure 6.5c). The second pressure peak of the record followed a precipitation event on day 235. However, after this, peaks showed only a poor association with weather fluctuations. Oscillations in water pressure often occurred both, in conjunction with and without precipitation events. In addition, major changes in pressure appeared to be independent of the size and timing of precipitation events. A pressure peak of 121.0% on day 235, for example, followed a precipitation event of 26.2 mm on day 234. However, another pressure peak of 68.8% occurred on the same day as a precipitation event of 0.3 mm (day 239). This pattern is difficult to assess. It may suggest that the two were not directly related or it may simply reflect the changing capacity of the subglacial drainage system or till porosity through time. Strong links to variations in external temperatures were also not evident.

Probe 8 displayed some correlation between pressure peaks and weather conditions between days 252-264 (Figure 6.5d). However, the lack of response in pressure to similar weather conditions prior to and following these pressure peaks makes it unclear whether the record was displaying a true association or coincidence. In addition, the second Probe 8 pressure event (days 324-328) occurred during a period of diminished average daily temperatures, suggesting that water pressure was responding to different processes at this time (Figure 6.5d). These correlations present an ambiguous relationship between water pressure and external weather conditions.

There is perhaps a broad correlation between prolonged heavy rainfall and increases in water pressure. However, the lack of immediate direct correlations is unexpected, particularly with respect to the precipitation events. Following deployment, the addition of surface water (melt and precipitation) via boreholes should have a direct effect on the probe pressure readings. This should be particularly evident in time stage 1, immediately following deployment, when the boreholes remained fully open directly above the probes (Figure 6.1; Table 6.1). The lack of response may suggest that the boreholes had closed, but this seems unlikely so soon after deployment. Field observations in the days following deployment also verified that this had not occurred. This anomaly might be explained if melt water was constrained to well-defined streams and moulins at the glacier surface, rather than being diverted directly

down the boreholes. This may account for variability in surface flows into the boreholes, resulting in the sporadic correlations noted within the records. The lack of direct correlations could also reflect subglacial storage processes, which may be responsible for the broad association with long term weather conditions (Figure 6.5). The absence of strong correlations also accounts for the lack of high frequency (i.e. diurnal) oscillations in the pressure records. An absence of diurnal oscillations during the summer has also been recorded elsewhere by Fudge *et al.* (2005).

In time stage 2, Figure 6.1 and Table 6.1 indicate that the influence of external weather conditions on water pressures will decrease as the borehole moves away from the probe deployment position x. Figure 6.4 outlined that this movement could be achieved in 30 hours. This would suggest that the poor response of the probes to external weather conditions was the result of the rapid incorporation of the probes within the subglacial environment. It would appear that the probe pressure peaks were dominantly influenced by melt water inputs from subglacial and englacial flow pathways or stores, rather than borehole inputs.

6.4.3 Borehole closure

The section above outlined that the transition of the probes between time stages 1 and 2 occurred quickly (Figure 6.1; Table 6.1). In time stage 3, the location of the probes should reflect more natural conditions at the glacier bed as direct surface inputs from the boreholes are removed and they start to close. The time at which the boreholes close is unknown and may vary significantly between boreholes. This has been particularly evident from field observations. Table 6.1 suggests that variations in the sensor records may provide a rough indication as to when the boreholes close.

The internal motion of ice has been investigated and modelled by a number of researchers. This is generally done in relation to glacier velocities, by monitoring englacial tilt and through repeat borehole inclinometry (e.g. Harper *et al.*, 1998, 2002; Paterson, 1977; Weertman, 1983; Willis *et al.*, 2003). Ice deforms under an applied stress and results from the dislocation of crystals along a basal plane (Weertman, 1983). The way in which boreholes close can occur isotropically or anisotropically (i.e. evenly or unevenly), depending on the direction and application

of stresses (Schwerzmann *et al.*, 2006). In addition, crystal dislocations can also pile up, which conversely strengthens the material subject to deformation and reduces creep rates (Paterson, 1994, p.81). These factors can lead to temporal and spatial variability in deformation within the ice column, leading to inconsistencies in the time of closure between boreholes.

In order to determine if the boreholes were likely to have closed by the end of the winter, the creep rate (or strain rate) of ice (ε) was calculated according to the equation:

$$\varepsilon = A\tau^n \tag{11}$$

where: A is a flow parameter (6.8 x 10^{-15} $s^{-1}(kPa)^{-3}$ at 0°C), τ is the basal shear stress (Equation 1, section), *n* is a constant (3), and ε is s^{-1} (Paterson, 1994, p.91). The rate of ice deformation was calculated as $6.01x10^{-9}$ s^{-1}. This value of strain indicates that it would take 192 days for the ice to deform by 0.1 m (the approximate diameter of the borehole). This value is only an estimate, as the strain rate of the ice will be subject to variations in: basal shear stress; the direction of applied stress, variations within the physical properties of the ice column itself (such as temperature); and the occurrence of dislocation stacking (Paterson, 1994; Schwerzmann *et al.*, 2006; Weertman, 1983). In addition, deformation at the surface of the borehole will occur at a faster rate than at the base (Harper *et al.*, 1998, 2002). The speed of closure will also change as the borehole is stretched and thinned (in diameter) as a result of deformation. Allowing for some inaccuracy, this figure suggests that the boreholes would not close until early in the next year (roughly, February, 2005). This is in rough agreement with the findings Hooke *et al.* (1987), who noted that their boreholes had closed in June, 10 months after creation. The closure of boreholes is calculated to occur so slowly that it seems unlikely that this process would affect winter sensor readings (Table 6.1). As a result, this process will not be considered.

6.4.4 Incorporation into the deforming bed

Once at the ice-bed interface it is important that the probes become fully incorporated into the deforming bed. In the absence of a GPS like system, the

identification of markers within the probe records, which suggest that they are fully incorporated and interacting with the till is vital. The probes are designed to represent small clasts, which should aid their incorporation into the till. Readings of case strain and tilt can identify the movement of the probes from the space at the ice-bed interface into the till (Table 6.1). Variations of case strain indicate interactions with the till sedimentology (Fischer and Clarke, 1997), whilst tilt sensors display probe movement into the bed (Figure 6.1).

In 2004, only the Probe 5 case strain sensor remained fully operational (Figure 6.6). The start of the record showed little change in average case strain, despite frequent oscillations in tilt. This reflects the probe's location at the ice-bed interface, without the application of significant stress (scenario C1; Figure 6.1). Strain oscillations began to increase from day 235, but remained fairly consistent, only showing a small range of values. It was from day 284 that values showed larger-scale oscillations. At this time, the tilt record also began to display an increase in oscillations along the z-axis and continued rotation along all axes (Figure 6.6).

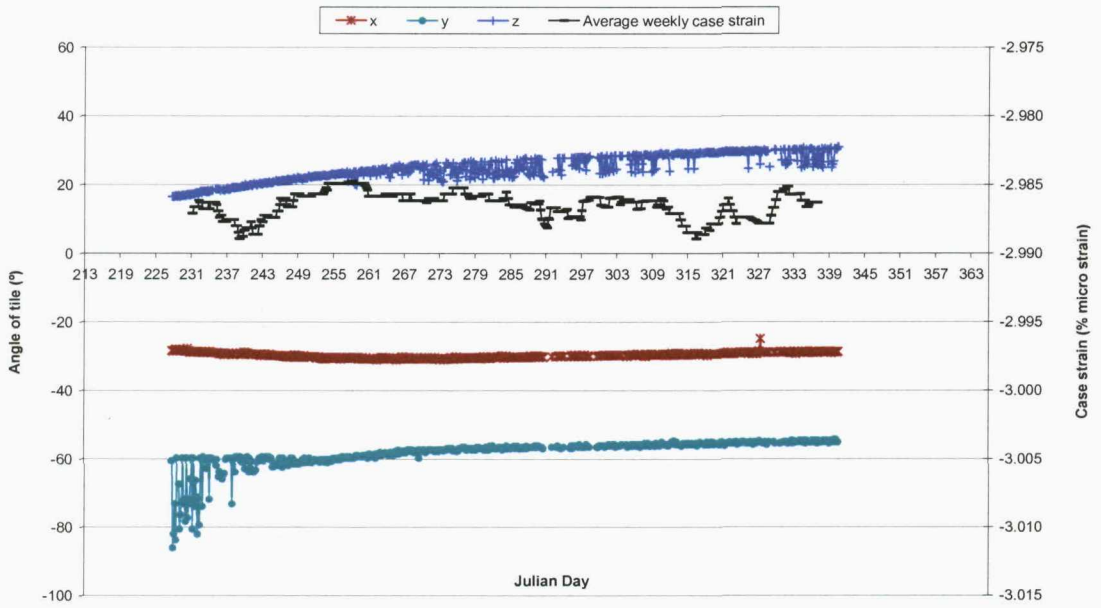


Figure 6.6: Probe 5 winter sensor record for tilt, case strain and average weekly case strain.

It is likely that this reflects the time required for the probe to become fully incorporated into the bed and start functioning as a normal clast in response to

deformation of the surrounding sediments. This represents a more lengthy transition between time stages 2 and 3, scenario C (Figure 6.1). The activity in tilt from day 285 would suggest that the probe was rotating very slowly. This movement, in combination with an increase in activity in the case strain record, implies that the probe was becoming incorporated into the deforming bed and interacting with the till. It also suggests that, from this point, Probe 5 had transitioned to scenario C3i because rotation is unlikely to occur within the borehole.

Figure 6.6 demonstrates that the variations in case strain were not large-scale. However, this minor change in activity could be sufficient enough to reflect incorporation into the deforming bed. The scale of variations may be dependent on the local sedimentology of the till around Probe 5 (e.g. Fischer and Clarke, 1997b; Porter and Murray, 2001). The record also only provides a minimum time from which the probe had begun to move into the deforming bed. The probe may have been incorporated prior to this but gradual movement of the probe and factors of till sedimentology may not immediately reflect this change. This time delay may also reflect relatively constricted movement of the probe if it was still positioned close to the clast, as seen on deployment. Another record from 2004/5 would be useful to constrain this relationship further.

Probe 7 was also located in scenario C2 (Figure 6.1), but did not have a functioning strain sensor (Figure 6.2c). Despite this, the rate of movement shown in the tilt record (Figure 6.3c) suggests that either the probe had become incorporated very quickly or that it was still oscillating in a cavity at the ice-bed interface. The former would suggest a transition to scenario C3 within the first 9 days, which is very rapid. However, this could be achieved given the rate of surface velocities at this time (section 6.4.1); and the probe's rapid transition of the probe to time stage 2, where it was lying almost flat with the deforming bed. Probe 7 also showed a brief period of net rotation between days 247-263, suggesting that it was incorporated in the till. This occurred 21 days after deployment, which is more in keeping with the time taken to transition to time stage 3, as recorded by other probes (see section 6.7.4). This rotation would place Probe 7 in scenario C3i (Figure 6.1; Table 6.1). Unfortunately, in the absence of a case strain record this hypothesis cannot be substantiated any further.

The case strain sensor for Probe 8 was also dysfunctional (Figure 6.2d) so its location cannot be determined with a high degree of certainty. However, an increase in tilt oscillations along the y-axis (day 281) might indicate that the probe had become incorporated into the till (Figure 6.3d) and moved to scenario C3 (Figure 6.1). This change correlated with a transition in the activity of the resistance sensor (section 6.4.3), which may suggest that the probe was surrounded by a different material. It also seems more likely that Probe 8 moved into scenario C3i (Figure 6.1). Although the case strain sensor did not function, the gradual change in tilt and the rotation indicated by the variations along the y-axis, would suggest that the probe was located within the till and not trapped in the borehole (Table 6.1). In addition, the rate of change in tilt was perhaps too rapid to coincide with changes in probe orientation resulting from ice deformation. The rotation of the probes indicates that deformation was occurring during the autumn. However, more robust confirmation of the probes' locations is likely to come from the sensor records during the spring and summer, when the glacier is more active.

6.4.5 Subglacial processes

The discussions above have established the majority of the sensor activity displayed by the probes on release into the subglacial environment and throughout the winter record. The patterns observed have confirmed the location of the probes within the subglacial environment. The relationships between the probes and external weather conditions (section 6.4.2), borehole closure (section 6.4.3) and incorporation into the deforming bed (section 6.4.4) have also been established. This section will highlight the subglacial processes operating during the winter record in terms of three stages, dictated by variations in the sensor records. This is simply as a means of structuring and simplifying the discussion.

6.4.5.1 Stage 1

At the start of the winter all three probes showed consistent low magnitude water pressures that were punctuated by pressure peaks. This reflects pulses in water pressure through a system that is characterised by steady base pressure. Probe 8 showed similar base pressure to Probe 5, but the nature of the first Probe 8 pressure rise differed from the short lived, rapid response peaks recorded by Probes 5 and 7

(Figure 6.7). Although the peak occurred equally as quickly, it was prolonged and punctuated by further pressure peaks. This signifies a different pattern of water pressure in this area of the bed.

The base level water pressures recorded by Probe 7 varied from those of Probe 5 and 8. Probe 7 recorded highly elevated basal water pressures 76.2%, dropping to 49.5%, with peaks above overburden (Figure 6.7). This implies a greater volume of water in this area of the bed. Murray and Clarke (1995) have recorded similar pressure in unconnected regions experiencing a strong hydraulic gradient with neighbouring connected regions of the bed. The shift in base levels to 49.5% (day 235) was also interesting. The tilt record (Figure 6.8) showed a sudden change in probe orientation and an increase in activity on the same day. It seems likely that this movement resulted from this sudden step change in water pressure.

Despite these differences, there was some correlation between the timing of probe pressure peaks, even though the style and duration of those peaks often differed. Probes 5 and 7 recorded pressure peaks on day 235, for example, whilst Probes 5 and 8 share peaks between days 252-264 (Figure 6.7). The Probe 8 pressure peak also decreased as Probe 7 recorded another increase in pressure, suggesting that the probes were not directly linked to each other at the bed. This demonstrates a general, large-scale correlation in activity in water pressure occurring at the glacier bed, accompanied by localised variations.

Figure 6.9 highlights the relationship between water pressure and resistance during the winter records. Resistance is associated with water pressure as a measure of the relative wetness of the surrounding environment. High resistance values indicate dry conditions, whereas low values indicate wet conditions. Water pressure continues to fluctuate in response to changing water inputs. However, the relationship between water pressure and resistance seems to vary with time. Probe 5 showed numerous fluctuations in resistance both independent from, and in association with, peaks in water pressure (Figure 6.9a). Fluctuations between days 227-272 were frequent and sudden, in keeping with the style of pressure peaks. The record then showed a drop in resistance on day 272 indicating wet conditions (possible till saturation, Figure 4.8). This may have been in response to the increase in base level water pressure.

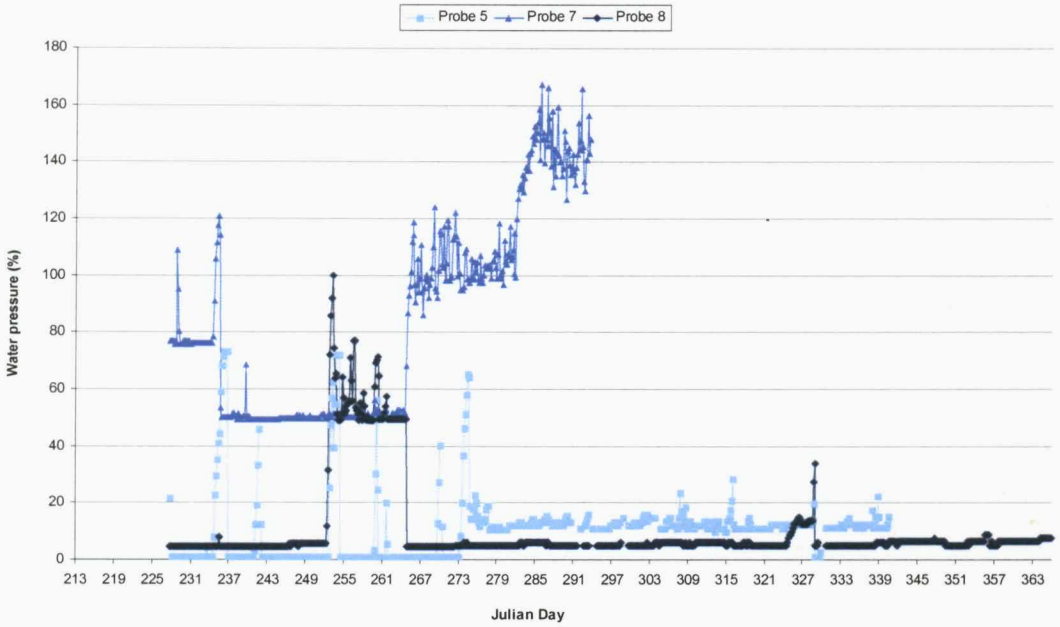


Figure 6.7: Winter water pressure records for Probes 5, 7 and 8.

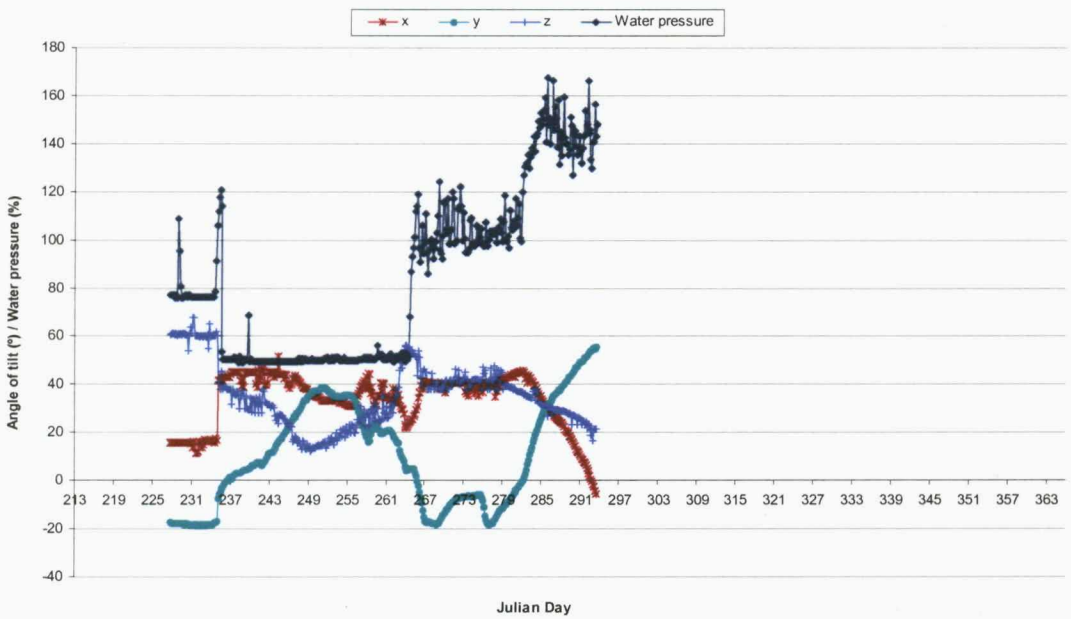


Figure 6.8: Winter tilt sensor and water pressure records for Probe 7.

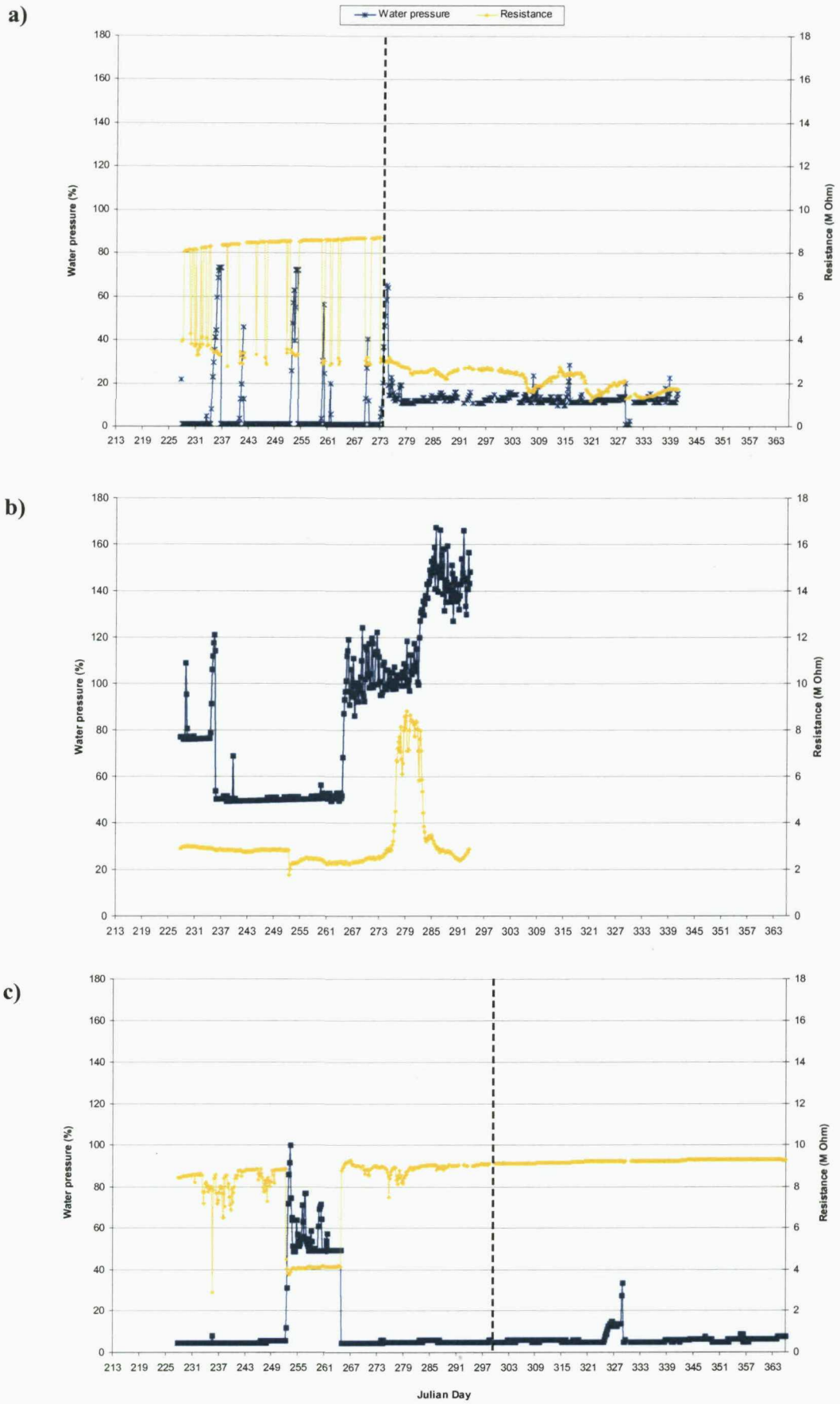


Figure 6.9: Water pressure and resistance sensor records for: a) Probe 5; b) Probe 7; and c) Probe 8. Note: the dashed line highlights a change in the resistance sensor readings.

The pattern of oscillations that followed differed from that displayed prior to day 272. Resistance no longer showed the sudden and rapid troughs in values (days 272-341). Readings began to show small-scale oscillations accompanied by an overall decline in values throughout the rest of the record. The correlation between water pressure and resistance fluctuations diminished. These variations are in good keeping with those predicted for water pressure and resistance in Table 6.1, scenario C3. The change in the relationship between water pressure and resistance may reflect the effect of probe incorporation, borehole movement or simply changing conditions at the glacier bed. It is unclear, based on these readings alone, whether or not these changes reflect a transition to stage C3i or C3ii.

Probe 8 resistance showed a similar pattern to that of Probe 5 (Figure 6.9c). The record displayed frequent oscillations and a close agreement with the pressure record between days 227-300. Values decreased in accordance with the increase in water pressure, reflecting wet conditions at the glacier bed (days 231 and 252-264). Fluctuations also occurred independently from water pressure signals. This suggests that the sensor was responding to small-scale changes in water content that were not detected by the pressure sensor. The fluctuations in Probe 8 resistance began to decrease from day 281, and by day 300 resistance had begun to show a gradual increase in values (with only minor oscillations) that continued throughout the winter. Resistance readings did not show any indication of the pressure rise recorded between days 324-328. This change in response to water pressure is in keeping with scenario C3 (Table 6.1).

The resistance record for Probe 7 was more complicated (Figure 6.9b). The start of the record showed only minor fluctuations and values were low, in keeping with the high magnitude of pressure recorded (days 227-264). A sudden decrease in resistance occurred on day 252, corresponding with pressure peaks in both Probes 5 and 8 (Figure 6.9a, c). However, this variation was not accompanied by a peak in the Probe 7 pressure record. This implies that the resistance, rather than the pressure, sensor was responding to changes from nearby areas of the bed. This response occurred after the probe showed signs of rotation, suggesting that the subsequent variations in resistance may be associated with the probe's location in the deforming bed (scenario C3i). The activity observed demonstrates that the relationship between

water pressure and resistance changes over time. This may be the result of the borehole moving away from the probe, the probe becoming incorporated into the till, or even changing external weather conditions towards the winter months. It is likely that a combination of all three factors contribute to this effect.

The probe temperature records can provide supporting evidence as to the location of the probes. A relationship was evident between probe temperature and fluctuations in water pressure. Temperature patterns differ between the probes and are generally best represented by a running weekly average (Figure 6.2). Probe 8 showed the least variation (Figure 6.2d). At the start of the record values were consistent with those within the subglacial environment (~0°C), indicating that the probe was no longer lodged in the borehole. This was supported by the activity in the tilt record (section 6.4.1; Figure 6.3d). Average probe temperatures fell in response to the pressure rise on day 252, reflecting an increase in the amount of melt water within that area of the bed. Readings returned to previous values, as water pressure fell. The Probe 5 record was more variable, showing a number of slowly undulating peaks and troughs in average probe temperature, during the initial stages of the winter record (Figure 6.2b). The greatest minima in temperature corresponded with the highest pressure peaks (days 236 and 253), whilst more elevated readings roughly correlated with periods of base flow. This reflects the relationship between probe temperature and water pressure, whereby an increase in the amount of melt water within the subglacial environment results in a reduction in probe temperature.

The record for Probe 7 differed slightly (Figure 6.2c). Average probe temperatures were in keeping with those of Probe 8, but values began to increase from the start of the record. This may simply indicate a prolonged period of adjustment following deployment as the probe moved from an upright position to flush with the glacier bed. Average temperatures only began to fall from day 242 when pressures were less elevated and activity increased in the tilt record (Figure 6.8). The change in temperature may reflect the probe becoming incorporated into the deforming bed as probe rotation began shortly afterwards (day 247-263). It may also be a precursor to the increase in water pressure that followed (day 264).

Also of note is that the average probe temperatures recorded by Probe 5 were much lower than those recorded by Probes 7 and 8, with values sustained below 0°C. These values were maintained throughout Probe 5's record suggesting that it was located in a 'cold' region of the bed (scenario C3i; Figure 6.1). The activity in water pressure, resistance, case strain and tilt, excludes the idea that the probe had become frozen within the borehole or at the ice-bed interface (i.e. scenario C3ii; Figure 6.1). These reduced temperatures may reflect the proximity of the probe to melt water inputs. Water may be colder with a shorter residence time at the glacier bed. Alternatively, it may indicate larger-scale spatial variations in the warmth of the subglacial environment or the deforming bed that are not obvious from external conditions or the accompanying probe measurements.

6.4.5.2 Stage 2

The probes recorded a period of relatively consistent sensor activity at the start of the winter record. However, Probes 5 and 7 experienced a shift change within the sensor records, varying the readings displayed. Probe 5 displayed a shift in water pressure on day 274 (Figure 6.2b). Prior to this the probe's pressure record was characterised by a series of sudden, rapid, pressure peaks deviating from minimal and stable basal flows (1.2%). A final peak in pressure occurred on day 274, followed by a permanent change in pressure oscillations from day 275. This was accompanied by a corresponding change in resistance and marked a change in the sensor readings, which continued to the end of the probe record (day 340). During this phase, water pressure showed more numerous and continuous fluctuations. However, the magnitude of pressure rises was much less, never exceeding 28.5%, in comparison to the 73.1% recorded during stage 1. In addition, base flows increased to 11.2%, but showed less consistency.

Probe 7 experienced the same transition (Figure 6.2c). A different pattern of water pressure was evident from day 265, following a large pressure rise on day 264. Pressure values increased to above overburden (119%, day 265) and began to show continual oscillations. Similar to the start of the record, water pressure also showed a two step increase in average flows. Values oscillated around 103.3% (days 265-281), before increasing to an average of 143.2% (days 282-293). This change marked an increase in the magnitude and frequency of Probe 7 pressure oscillations.

Probe 8 did not show such a step change. Base flows generally remained consistent during this period and oscillations in resistance decreased from day 281.

This step change poses several questions. Initial analysis might question: is it the result of changing external weather conditions; does it reflect the closure of the boreholes; does it mark the timing of the probes becoming fully incorporated into the deforming bed; or perhaps it is the effect of abrupt basal motion? The previous sections have done much to answer these questions. It would appear that changes in external weather conditions do not have a significant affect on sensor activity (section 6.4.2) and rates of ice deformation suggest that the boreholes had not yet closed (section 6.4.3).

The incorporation of the probes into the deforming bed was outlined in section 6.4.4 and demonstrates that Probe 5 began to integrate into the bed at an early stage (day 245). Probe 7 also showed signs of incorporation from day 247. The step changes appear to occur too late in the record to reflect a transition between time stages 2 and 3 (Figure 6.1; Table 6.1). In contrast, Probe 8 did not show any response, even though the timing of the pressure shifts corresponded with its incorporation into the till (day 281). This was marked by a small-scale change in the probe's resistance record (sections 6.4.4 and 6.4.5.1). It is most likely that the change in sensor readings is the result of variations in the activity of water pressures within the subglacial environment, or abrupt glacier motion. The change in Probe 7 tilt associated with the shift in water pressure, for example, supports this idea (Figure 6.8). Alternatively, this change may reflect a larger scale, long term variation in the processes operating or the morphology of the drainage system, as the winter months progress.

6.4.5.3 Stage 3

The discussion above and section 6.4.4 suggest that Probes 5 and 8 had begun to transition into time stage 3, where the probes are fully incorporated into the subglacial environment. As a result, it is assumed that the sensor activity discussed in stage 3, reflects conditions within the till (Figure 6.1; Table 6.1). The greatest variations following the step change were observable within the water pressure records. Probe 5 experienced an increase in base pressure to 11.0%, but a reduction

in the magnitude of pressure oscillations. Pressure and resistance values remained relatively constant, showing only small-scale oscillations from base pressure for the remainder of the record. The tilt record did not change at this point, suggesting these variations were not the result of a change in the probe's location. This indicates that these sensor patterns simply reflect an alteration in the amount of water flowing through this area of the bed. This is in keeping with winter patterns of subglacial activity found by other researchers (e.g. Mair *et al.*, 2002a). However, the minimal water pressures displayed were in opposition to the elevated but consistent winter pressures recorded by others (e.g. Fudge *et al.*, 2005). This must be the result of the location of the probes with respect to the subglacial drainage system in this area of the bed.

The pressure record for Probe 7 was more complex. Water pressure showed a marked increase in both magnitude and variability, reflecting an increase in the amount of water in this area of the subglacial environment. The change in tilt that accompanies the shift in pressure supports this idea (Figure 6.8). The rise in resistance between days 276-283 also poses questions about the Probe 7 record (Figure 6.2b). This change indicates dry conditions, even though water pressures were fluctuating around overburden pressure. It also occurs just prior to a third shift in water pressures to above 121.1% (day 282). Explanations for this pattern are not forthcoming. Probe temperature remained above 0°C and tilt activity suggested that the probe was not frozen, which could also account for a rise in resistance. Similarly, daily external temperatures were still above 2°C, with average values of 4-10°C. Water pressure did not decrease, ruling out the idea of a relative increase in 'dryness'. In addition, pressure and resistance values of a similar magnitude have been recorded by probes elsewhere and are within the stated capabilities of the sensors (Table 4.3, Chapter 4). Therefore, sensor error or damage seems unlikely.

The rise in resistance, just prior to the step change in water pressure, does suggest that the two might be linked. The sudden influx of water may actually reflect a decrease in water conductivity (increase in resistance) in conjunction with a large influx of water to this area of the bed (Gordon *et al.*, 1998). The relatively short lived nature of this resistance rise suggests that the system recovered from this period of 'dilution'. The resistance sensor was thought to measure the relative wetness of

the environment, but the turbidity of the water may also affect these readings. The fact that this had not occurred before suggests that there may be a threshold value of pressure when this occurs. Further calibration work would clarify this issue (section 4.2.1.5, Chapter 4).

In comparison to Probes 5 and 7, Probe 8 only recorded minimal activity following its deployment, showing just two pressure rises. The initial rise has been discussed, but the second pressure rise lasted between days 324-328 and was of a slightly different nature (Figure 6.3d). The low, mildly oscillating water pressures recorded by Probe 8 are indicative of the winter months, when activity (water flow) in the subglacial environment is reduced (e.g. Willis *et al.*, 2003). Probe 8 was responding to continuous base flows through the till. Thus, the second rise in pressure appears to be highly unusual at this time of year (days 324-328). The resistance record did not respond to the pressure rise. This may be associated with changing conditions, as the probe became further incorporated into the till and the distance from the borehole increased in a transition between time stage 2 and 3i (Figure 6.1).

Probe temperatures, following the step changes in water pressure, showed only slight variations. Probe 5 continued to show small-scale fluctuations in average values until day 271 (Figure 6.2b). Then oscillations in temperature diminished and were replaced by a gradual, small-scale, increase in values for the rest of the winter. Probe 7 had continued to show a consistent gradual decline in average temperatures since day 268, after the pressure change. However, the rate of decline slowed towards the end of the record (Figure 6.2c). Probe 8 also showed a decrease in average temperatures from day 317, accompanied by small-scale oscillations (Figure 6.2d). The increase in values recorded by Probe 5 would suggest that there was a net loss of fresh melt water from the till. In contrast, the decrease in temperature experienced by Probe 7 was in keeping with the continued, elevated, water pressures recorded. The change experienced by Probe 8 was slightly more unusual. This occurred just before the rise in water pressure between days 324-328. The continued decline and oscillations in values indicates a gradual increase in water moving through this area of the bed, commencing from the second pressure rise.

6.4.6 Probe failure

Probes 5 and 7 ceased data transfer on day 340 and 293, respectively (Figure 6.2 and 6.3). The sensor readings provided little indication as to why this occurred. Probe 5 showed no signs of deviating from the readings sustained from day 275. This would suggest that the probe either experienced sudden and catastrophic damage, or it simply lost communication links with the base station. Given the consistency of the sensor readings the latter scenario seems more probable. In comparison, Probe 7 showed high levels of tilt and water pressure activity (Figures 6.2c and 6.3c). Pressure was extremely elevated, reaching maximum values of 167.3% (958 kPa). This was not in excess of those recorded elsewhere (e.g. Probe 15, 2005/6) and was insufficient to damage the integrity of the probe case. However, the abrupt nature of the pressure shifts might have caused the membrane in the pressure sensor to burst (Kavanaugh and Clarke, 2000), causing the whole probe to stop functioning. In addition to this, tilt showed rapid changes towards the end of the record. This might indicate that the case was crushed or the probe had moved out of communication distance with the base station. Given the magnitude of water pressure at this time, this probe may have even been driven into a different location, either to the glacier bed, or perhaps even up and out of the borehole.

6.5 Probe 4

The Probe 4 sensor record is displayed in Figure 6.10 in combination with weather data for this period. Probe 4 was placed within a closed borehole that was drilled to a depth of 72 m. The location of Probe 4 differed from that in scenario A (Figure 6.1; Table 6.1) because the borehole did not connect with the glacier bed. This englacial probe would enable comparison with probes located at the ice-bed interface. Details of deployment and location are displayed in Figure 5.17 and Tables 5.3 and 5.4 (section 5.5, Chapter 5).

6.5.1 Commencement

The tilt record and BoreCam were used to determine the movement and location of the probe following deployment. Probe 4 was lodged upright at the base of the hole

and its depth was confirmed by the length of the camera cable. The tilt record (Figure 6.10c) showed relatively little movement immediately following deployment (days 228-263), which might be expected in an englacial borehole. The gradual change in the angle of tilt along all three axes implies that the probe was moving slowly. Its location may have adjusted to inputs of melt water, or the changing dimensions of the borehole, resulting from ice deformation (Harper *et al.*, 1998).

6.5.2 Triggers

Water pressure readings show some correlation with external weather conditions (Figure 6.10a, b). This occurred during periods of relatively elevated external temperatures. Towards the end of the winter record, minima in external temperatures also appeared to correspond, intermittently, with minor reductions in water pressure. There does not seem to be any such relationship between water pressure and precipitation events. This was demonstrated when pressure decreased on day 255, and remained low during a period of almost daily precipitation events (days 255-274), which often exceeded 10 mm.

The poor correlation with external weather conditions is unexpected given that the probe cannot move away from the borehole opening. This is problematic for the interpretation of the water pressure peaks and their driving force. Pressure changes, although relatively minor, must be the result of melt water inputs. Comparison with the precipitation record suggests that direct inputs from the surface of the borehole are not common. Consequently, the pressure fluctuations, which do show a weak correlation with external temperatures, must be the result of inputs from englacial drainage pathways and/or limited flows from the surface. The pressure record shows only small-scale fluctuations, indicating that these inputs were small and sporadic in nature.

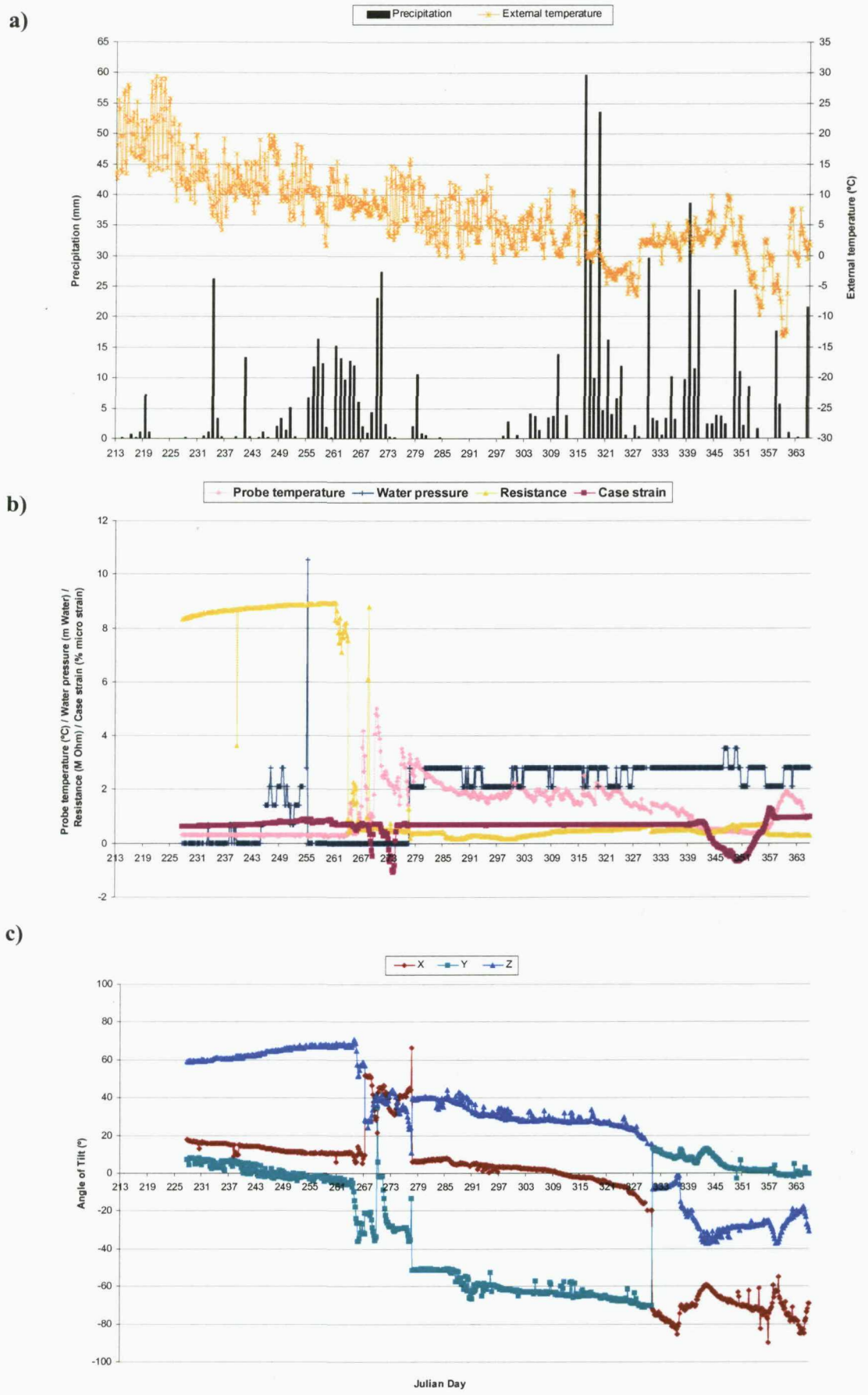


Figure 6.10: Winter sensor record for Probe 4, showing: a) external weather conditions; b) probe temperature, water pressure, case strain and resistance; and c) tilt (2004/5).

6.5.3 Borehole closure

There appears to be little evidence of borehole closure within the Probe 4 record during the winter (Figure 6.10). However, given the calculated creep rate of ice (section 6.4.3) the borehole would remain open above the probe during the winter. As a result, any changes in sensor readings would not be the result of borehole closure. The records for water pressure and resistance do not show the same activity as those displayed by the subglacial probes (Figure 6.2). Case strain showed a slight increase towards the end of the winter (days 340-361), but then returned to previous levels. This indicates that the probe was simply experiencing a short term change in conditions within the borehole and was not actually becoming encased through ice deformation.

6.5.4 Englacial processes

The processes recorded by the Probe 4 winter sensor redings are discussed below. The activity within the borehole is not related to the conceptual model outlined in Figure 6.1 and Table 6.1 (section 7.2), because the base of the borehole did not connect with the subglacial environment. As such, it will be subject to different mechanisms. The sensor readings will be examined within three time stages to facilitate discussion.

6.5.4.1 Stage 1

On deployment, Probe 4 showed relatively little activity (Figure 6.10b). Minor fluctuations in water pressure, resistance and case strain indicate that there were some active processes operating within the borehole (days 227-269). The fluctuations in water pressure dictate that the borehole was receiving inputs of melt water. These ceased on day 255, following a short lived pressure peak. Resistance remained elevated during this time indicating 'dry' conditions within the borehole. Readings did not respond to the fluctuations in water pressure. The gradual increase in case strain at the start of the record suggests that the probe was being squeezed, presumably via ice deformation (Figure 6.10b).

These gradual, small-scale changes in sensor readings were interrupted on day 262 by a significant period of sensor activity that lasted until day 277. During this

period, water pressure remained low and constant, but resistance began to fluctuate and then fell abruptly (day 264). Probe temperature showed large-scale oscillations (day 264), with values increasing to 5°C (day 270). At the same time case strain began to fluctuate, with significant elevations in strain peaking on days 269 and 273. These variations coincided with a period of sudden activity in the tilt record (days 264-277; Figure 6.10c), which ended abruptly on day 277. At this point, large-scale fluctuations in probe temperature, resistance, and case strain ceased.

The tilt record suggests that there was a sudden event within the borehole (Figure 6.10c). The increases in case strain (days 269 and 273-274) indicate that ice movement had caused the borehole to change in dimension, applying pressure to the probe case. The drop in water pressure to 0 m and the increase in probe temperature to 5°C would suggest that this movement caused the borehole to drain. Probe temperature, in particular, suggests that the probe was interacting directly with air. It seems highly unlikely that such elevated and rapidly fluctuating temperatures could be achieved within a water column. However, the only way for water to be removed from this system is via the development of an englacial drainage pathway at the base of the borehole. The activity in strain and tilt may reflect exactly that (Figure 6.10b,c).

In contradiction to the scenario described above resistance decreased on day 264, indicating an influx of water into the system, when pressures were low. Water inputs could cause the probe to oscillate in the base of the borehole, as demonstrated by the variety of tilt activity. An influx of water within a confined englacial borehole might also result in the increase in case strain recorded. However, the lack of response in water pressure and the activity in probe temperature is in contradiction with the resistance record. The sensors are all located in the same position on the probe, making it hard to account for this variation. The change in the resistance reading may reflect the sensor adjusting to conditions in the borehole. The sensor may have experienced some error prior to day 261 and the drop in resistance, reflecting wet conditions within the borehole (days 227-260), was therefore delayed. Alternatively, the processes recorded by the resistance sensor may be more subtle than originally conceived. The variety of probe temperatures recorded was also highly unusual. No other probe recorded temperatures as high at 5°C, or as many fluctuations. The

change in probe temperature and sensor activity followed a period of extended rainfall activity, when average weekly external temperatures ranged between 5-10°C (Figure 6.10a). This would suggest that the probe was responding directly to external air temperatures.

6.5.4.2 Stage 2

The sensor readings that followed stage 1 were much more moderated, producing relatively constant conditions and subdued activity (Figure 6.10). Water pressure rose to 2 m on day 277, and showed only minor fluctuations between 2.1-3.5 m for the remainder of the winter. This implies that a small body of water remained within the borehole. Subsequent changes in pressure are likely to be the result of small changes in probe location, borehole dimensions and englacial inputs. The low, gently oscillating readings in resistance, which had been established from day 278, support the idea that the probe was located in water. Probe temperatures had already begun to decrease and show fewer fluctuations at this point and coinciding with an influx of water.

Tilt and case strain readings both saw an abrupt change on day 277 (Figure 6.10b, c). The return of case strain to normal conditions indicates that any changes in the dimensions of the borehole were insufficient to permanently apply pressure to the probe, and/or the probe shifted into a different position releasing the applied pressure. This also led to a stabilisation of activity in the tilt record (days 277-330). The record showed the probe slowly tilting forward throughout this period. This may reflect deformation of the borehole in response to glacier movement (Harper *et al.*, 1998).

6.5.4.3 Stage 3

Stage 2 was interrupted by another abrupt phase of activity towards the end of the winter. The tilt record displayed a 'jump' in readings on day 331 (Figure 6.10c). The amplitude of tilt fluctuations then increased, showing a faster rate of change. This was accompanied by a sudden small-scale fluctuation in the resistance record and increase in probe temperature. The main period of activity recorded by the other sensors occurred between days 340-361 (Figure 6.10b). During this time, water

pressure recorded two small peaks (days 347 and 349), indicating two small inputs of water into the borehole that were drained away rapidly. Again, the increase in resistance, although small, conflicts with the increase in water pressure. This might occur if the rise in pressure was the result of the borehole water freezing, but as the probe temperature remained above 0°C this cannot have been the case. The increase in case strain from day 337 suggests that the movement of the probe resulted in an increase in the applied strain. Deformation of the borehole may also have contributed to this applied strain. The decline in probe temperature at this time is associated with the increase in water pressure, even though it was only small.

The record for Probe 4 stabilised by day 361 and resumed readings similar to those recorded prior to day 330. This pattern suggests that the previous event was the result of a short term variation in englacial activity, rather than a long term change in the processes operating within the ice. The subsequent lull in activity marked the end of the winter record for Probe 4. The patterns observed demonstrate that activity, even if only very small, keeps occurring within the glacier body during the winter. The tilt record, in particular, showed considerable variations, reflecting the freedom of the probe to oscillate and adjust to changes in the dimensions of the borehole. This is something that will be unique to englacial probe records and again shows that movement within the ice column was still active during the winter.

6.5.5 Comparisons

It is important to recognise the differences between Probe 4 and those probes placed within boreholes that connected with the ice-bed interface. Obtaining a record from an 'englacial probe' can enable better identification of any future probes which are deployed to the ice-bed interface, but remain stuck within the borehole. The Probe 4 sensor readings showed a number of differences from those recorded by Probes 5, 7 and 8. Probe 4 temperature readings were in excess of those recorded by Probes 5, 7 and 8. Probe 4 temperature values reached as high as 5°C and recorded much greater and more frequent oscillations, which continued throughout the winter. Average readings remained above 0.3°C throughout. This was not observed for the other probes, where temperatures did not exceed 0.2°C.

The activity recorded by case strain was also in excess of that recorded by Probe 5. Probe 4 displayed not only fluctuations in case strain, but also significant changes in the magnitude and direction of applied case strain. The Probe 5 record differed from this, only displaying gradual fluctuations in average weekly strain values. This is logical as the application of stress at the ice-bed interface will be accommodated in part by the till and by the water present within the bed. In addition, the probe can move within the till in response to shear strains. In contrast, within the ice, the probe will be compressed more readily within an enclosed environment, where it is more difficult to adjust position.

The Probe 4 oscillations in water pressure and resistance were quite similar to those recorded by the other probes. However, the pressure magnitudes recorded by Probe 4 were much lower. Triggers to the pressure events showed only a weak correlation with precipitation events, although the relationship with external temperatures was somewhat stronger. The effect of surface melt water inputs down the borehole appeared to be minimal, in agreement with the other probe records. The relationship between resistance and water pressure appeared to be the same for all the probes (i.e. generally a drop in resistance was accompanied by an increase in water pressure). However, comparisons between these sensors are very difficult. Activity can be highly variable, simply according to probe location and temporal variations in melt water inputs. In light of this, water pressure and resistance cannot be used alone to characterise probe location.

Finally, the movement of Probe 4 within the ice column varied significantly from that of the other probes. The tilt record showed periods of relative stability, followed by sudden periods of rapid fluctuation throughout the winter record (Figure 6.10c). The oscillations recorded along each axis were also of a greater magnitude. This reflects its position, lodged within the borehole, and provides a good example of how such patterns can help to determine the location of probes. In contrast, the probes within the subglacial environment showed more continuous and complex variations in tilt, often rotating. These variations reflect the different probe locations.

6.5.6 Synopsis: 2004/5

In 2004 the subglacial probes were characterised by a three phase winter record. In the first phase, variations were dominated by infrequent pressure peaks that fluctuated from stable base flows. Similar small-scale fluctuations were recorded in the resistance record. Little activity was recorded by the other sensors. This phase ended with a sudden step change (phase 2), marking a change in sensor activity. In the third phase, Probes 5 and 8 showed only minor variations in sensor readings around stable base values. Probe 7 saw a marked increase in both the magnitude of pressure and the frequency of oscillations. The pressure peaks recorded by Probe 7 were of a greater magnitude than those recorded by Probes 5 and 8, exceeding overburden pressure. This suggested that Probe 7 was linked to a drainage route, whilst Probes 5 and 8 were only influenced by sporadic pressure pulses associated with basal flows in the subglacial environment. The tilt record, in combination with case strain, gave a clear indication, throughout the winter record, of the changes in probe location within the subglacial environment.

In the englacial borehole, Probe 4 recorded continual activity in all sensors during the winter record. The most significant variations were recorded after deployment. This was followed by more stable small-scale oscillations, around base sensor values, before a final 'sensor event' occurred at the end of the record. Again, stable conditions were resumed after this short term period of activity. This indicates that small-scale changes in englacial conditions continued during the winter.

6.6 2005/6

The probe records for 2005/6 began at the start of August (days 213-217), with deployment slightly earlier than in 2004/5. Four probes were still operational after the first week: Probes 10, 12, 15 and 16. The details of probe deployment are summarised in Tables 5.3 and 5.4 and the relative probe positions are displayed in Figure 5.18 (section 5.5, Chapter 5). All four probes were placed within boreholes that connected with the ice-bed interface. No englacial probes were operational during this year. The probe sensor records during the winter are outlined below and an overview of sensor activity is displayed in Figures 6.11 and 6.12.

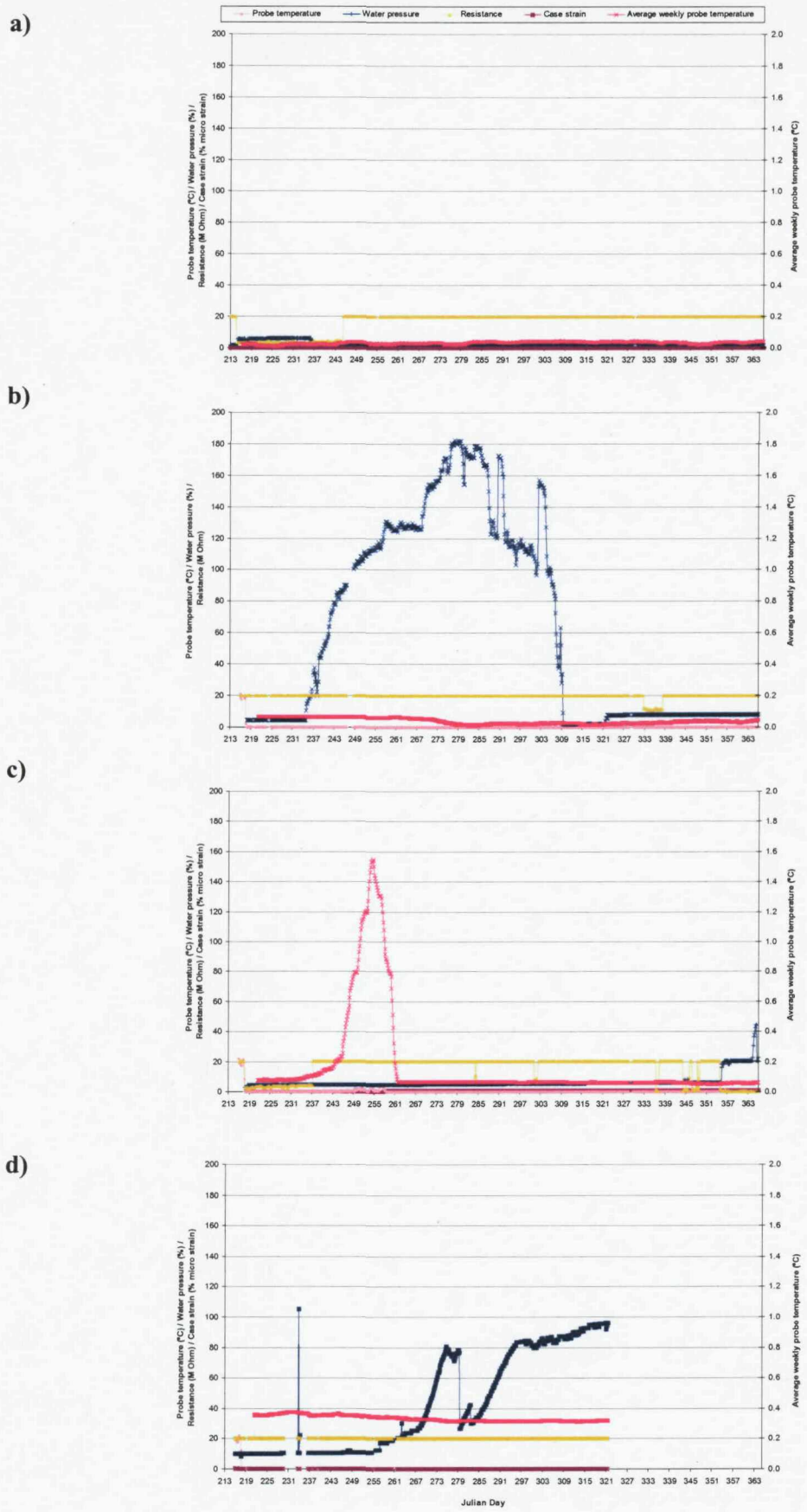


Figure 6.11: Comparison of winter sensor records, showing probe temperature, water pressure, resistance, case strain and average weekly probe temperature for: a) Probe 10; b) Probe 12; c) Probe 15; and d) Probe 16 (2005/6).

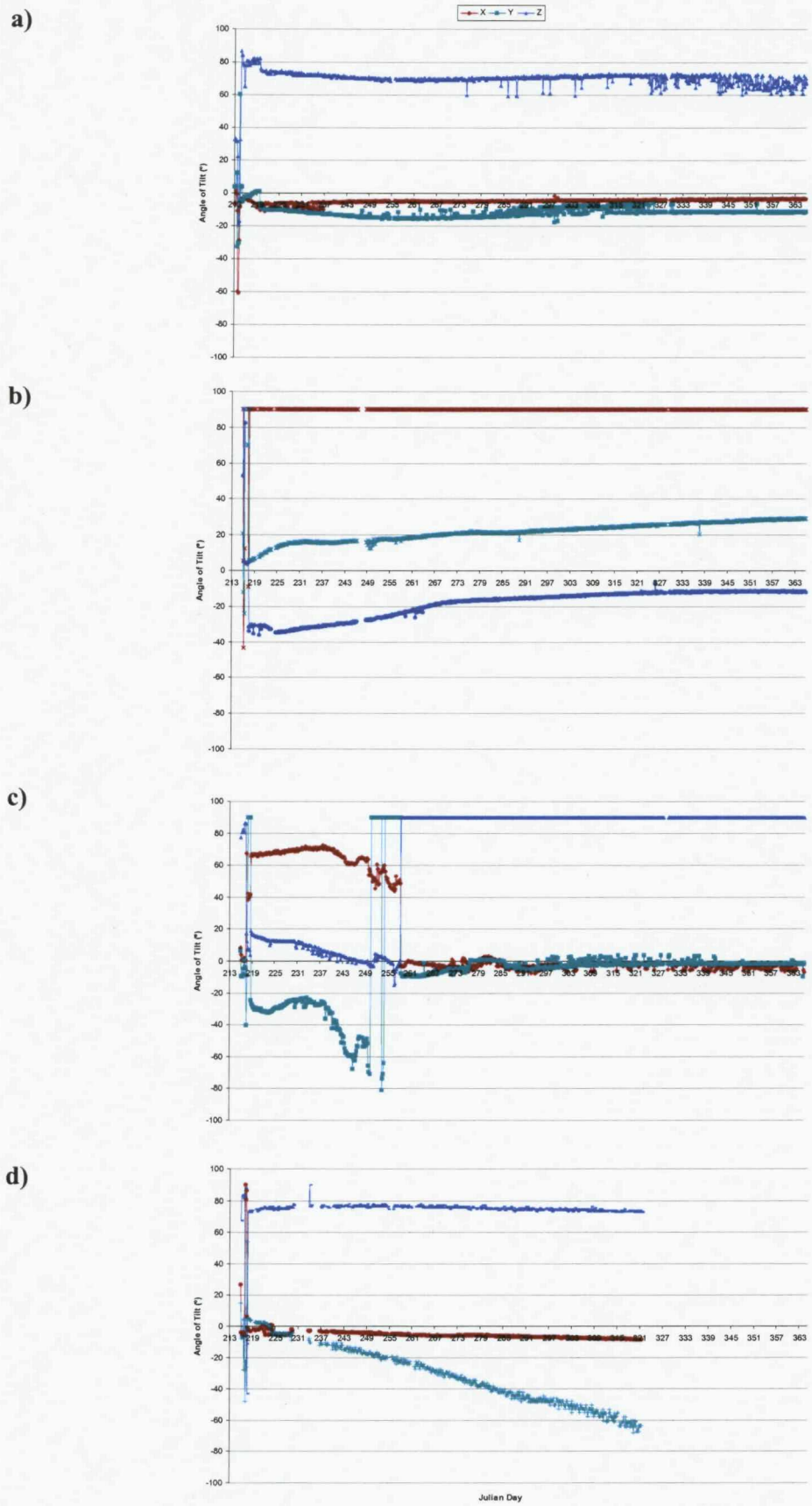


Figure 6.12: Comparison of winter tilt sensor records for: a) Probe 10; b) Probe 12; c) Probe 15; and d) Probe 16 (2005/6).

6.6.1 Probe 10

Figures 6.11a and 6.12a display the sensor record for Probe 10. There were minor fluctuations in both absolute and average weekly probe temperatures throughout the winter record. Water pressure maintained base levels flows between 1.4-2.0%. The only activity in water pressure occurred at the start of the winter record when pressures increased to 5.8% (days 215-236). This period was accompanied by a few small-scale oscillations until base flows were resumed on day 236. Resistance showed greater variation, decreasing from 20.2 M Ohm to 3.1 M Ohm on day 214. Values remained low, showing small-scale oscillations until day 245, when resistance abruptly rose again, back to values of 20.2 M Ohm for the rest of the winter record.

Case strain remained relatively constant between days 213-245, with small-scale oscillations. An increase in oscillations began from day 246 and an overall increase in strain was recorded for the rest of the winter. The tilt record (Figure 6.12a) showed significant activity between days 213-220. This was then replaced by a gradual change along all three axes, accompanied by small-scale oscillations.

6.6.2 Probe 12

The record for Probe 12 showed considerable activity during the winter (Figures 6.11b and 6.12b). Probe temperatures fluctuated between 0-0.1°C, with average values remaining constant at 0.1°C (days 221-251). Average probe temperatures declined rapidly from day 251, reaching minimum values on day 281. Values began to fluctuate from this point, gradually increasing through the rest of the winter. The water pressure record showed the greatest variation. Pressure remained at base levels (4.3%) until day 235 when values suddenly increased, reaching above overburden pressure on day 250. Pressure continued to increase, showing greater oscillations and reaching a maximum of 182.5% on day 277. Readings then decreased, whilst still fluctuating, returning to new minimum base values (1.4%) by day 309. This was sustained until day 322, when base flows increased slightly to 7.7%. Values continued to increase gradually for the remainder of the winter reaching 8.1% (day 365). Resistance was generally constant at 20.2 M Ohm. A change was only recorded between days 332-338, when values fell to 12.4 M Ohm. Small-scale

fluctuations followed until day 338, when values returned to 20.2 M Ohm for the rest of the record. A period of rapid change in tilt (Figure 6.12b) occurred between days 218-223. This was followed by a more gradual and consistent trend of movement, displaying only sporadic oscillations, for the remainder of the record.

6.6.3 Probe 15

The winter record for Probe 15 is displayed in Figures 6.11c and 6.12c. Probe temperature was highly variable between days 217-257. Values began to increase rapidly from day 237, showing many large-scale oscillations. Fluctuations increased in amplitude towards day 257, with temperatures ranging between 0.1-4.3°C. This activity was reflected by a sharp increase in average probe temperatures. Values decreased suddenly from day 257, reaching 0.1°C (days 258-288). Small-scale oscillations and a gradual decline in temperatures were reinstated from day 289. Water pressure showed relatively little activity, remaining at base values of 4.3-6.0% (days 218-344). It was only towards the end of the record that pressures began to rise, reaching 20.1% on day 356, with a peak of 44.4% on day 365.

The record for resistance also showed variation, falling from 20.2-2.4 M Ohm (day 217). Resistance continued to show small-scale oscillations before increasing abruptly back to 20.2 M Ohm on day 237. This was maintained until day 284, when oscillations began again (days 284; 301-2; 336-7; 344-5; and 347-9). The frequency, amplitude and duration of these oscillations increased towards the end of the record. Resistance finally fell to 0.3 M Ohm between days 355-365. Case strain showed numerous small-scale oscillations at the start of the record (days 217-257), before increasing on day 258. Small-scale oscillations were recorded between days 255-319, followed by larger-scale changes (days 320-365). The tilt record (Figure 6.12c) showed significant activity between days 215-258, particularly during the first three days. Activity suddenly changed on day 259, becoming more stable, but still showing numerous small-scale fluctuations, particularly along the x and y axes.

6.6.4 Probe 16

Probe 16 showed some activity during the winter record (Figures 6.11d and 6.12d). Probe temperatures ranged between 0.4-0.3°C. Average values showed minor

oscillations and a slight increase towards the start of the record, before declining from day 245. Initial water pressures were low (10.1-10.9%) between days 217-254. However, a large and rapid peak above overburden was recorded on day 233 (105.6%). Pressures increased and began to fluctuate from day 255. Values remained elevated (>82.6%), and began to show small-scale oscillations and a gradual increase from day 298. Resistance remained constant at 20.2 M Ohm throughout the entire record. Case strain displayed constant readings between days 218-242. Values then began to increase and oscillate. Tilt recorded significant activity between days 217-223 (Figure 6.12d). This decreased between days 224-232 and then showed consistent change for the rest of the record.

6.7 Interpretation: 2005/6

This section will follow the same structure as that of section 6.4. The probes will be discussed in terms of their activity following deployment; influences from external weather conditions; probe incorporation into the till; the physical processes operating during the winter in the subglacial environment; and probe failure. Borehole closure is not discussed as rates of ice deformation dictate that the boreholes are likely to remain open during the winter. The conceptual model outlined in section 6.2 (Figure 6.1; Table 6.1) will provide the basis for the interpretations presented here.

6.7.1 Commencement

The probe tilt records (Figure 6.12) indicate the movement of the probes following deployment (Figure 6.1). Probes 10, 12 and 16 were all characterised by an initial period of significant activity followed by a reduction in tilt rates. Probe 10 showed particular activity during the first two days, until day 220, when the rate of change in the angle of tilt slowed abruptly. The initial activity recorded by Probes 12 and 16 (Figure 6.12b, d) actually reflected probe movement prior to deployment. However, after deployment, a period of relatively rapid change occurred (days 218-223 and 218-224, Probes 12 and 16, respectively), before more gradual and consistent movement was initiated.

The phases of heightened activity between days 213-220, 218-223 and 218-224 (Probes 10, 12 and 16, respectively) reflect the movement of the probes at the ice-bed interface. The angle of tilt recorded on the x-axis by Probes 10 and 16 signifies that they were positioned upright within the boreholes. This corresponds to scenario C1 (Figure 6.1; Table 6.1). In contrast, Probe 12 was located almost flat within the borehole, which is representative of scenario B1 (Figure 6.1; Table 6.1). In this first week, the probes rapidly shifted into stable positions within the subglacial environment. The sudden decrease in the activity on days 220, 223 and 224, (Probes 10, 12, and 16, respectively), suggests that the probes had become incorporated into the subglacial environment. This marked a transition into scenario C2 and, in the case of Probe 12, scenario B2 (Figure 6.1; Table 6.1). This corresponded well with rates of glacier motion (Figure 6.4), suggesting that the time taken for the probes to stabilise was within reason.

Probe 15 showed a different record of activity (Figures 6.11c and 6.12c) that reflected the circumstances of its deployment. When Probe 15 was lowered into its borehole it came loose about 5 m below the surface. On release, it fell and became lodged on a small englacial crevasse or ledge that had split from the side of the borehole. Thus, until day 258, the activity recorded in probe tilt reflects the movement of the probe on this ledge. This period is discussed more fully in section 6.7.7. The sudden shift in tilt on day 258 reflects the movement of the probe off the ledge and into the borehole, marking the start of Probe 15's subglacial record. Similar to the other probes, once within the borehole, the tilt record suggested that Probe 15 quickly settled at the ice-bed interface. This was displayed by the sudden decrease in tilt activity, accompanied by small-scale oscillations. The tilt record indicates that Probe 15 was sat upright at the base of the borehole, placing it in scenario C1 (Figure 6.1). The record displayed a variety of relatively small changes (days 258-286), which were replaced by more gradual changes in tilt, accompanied by small-scale oscillations. In accordance with the patterns outlined in Table 6.1, this change suggests a transition to scenario C2 (Figure 6.1; Table 6.1).

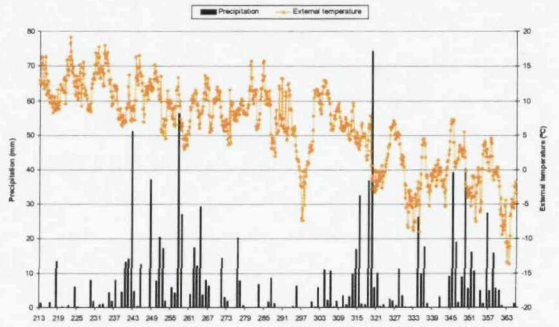
6.7.2 Triggers

Figure 6.13 displays the external weather conditions for winter 2005 in combination with the probe records. Table 6.1 proposes that there will be a strong correlation between water pressure and resistance, and external weather conditions during time stage 1. This association will weaken as the borehole moves away from the location of deployment and the borehole closes (Figures 6.1 and 6.4). The association between external weather conditions and probe sensor readings varied. Probe 10 showed only the most infrequent correlations with external temperatures and none with precipitation (Figure 6.13b). Activity in water pressure and resistance was only recorded between days 213-245. During this time, there was sporadic correlation between increases in temperature and reductions in water pressure. This pattern is out of phase with predicted relationships between water pressure and external temperatures.

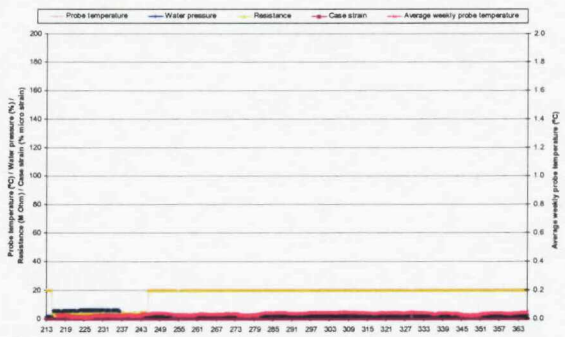
Probe 12 displayed the strongest association between external temperatures and water pressure between days 284-309 (Figure 6.13c). In this time, maxima and minima in pressure lagged peaks and troughs in external temperatures by approximately 16 hours. However, this was still only a coarse agreement with temperatures, as not every peak and trough coincided. This pattern ceased when pressures returned to base flows (1.9%). Although, a period of reduced temperatures, below 0°C (days 319-323), coincided with an increase in base flows of water pressure (7.7%). The relationship between water pressure and external weather conditions was transient and a correlation prior to and following this period was not recorded. Resistance did not show any fluctuations throughout this time.

Water pressure and resistance showed relatively little activity in the Probe 15 record (Figure 6.13d). Variations were mainly confined to the start and end of the record (days 217-237 and 336-365). In contrast to the other probes, resistance, rather than pressure showed some out of phase correlation with external temperatures (days 217-237). Diurnal peaks and troughs in temperature were accompanied by minima and peaks in resistance, respectively. There was also some correlation between the size of the precipitation events and the amount by which resistance decreased. Again, this relationship was sporadic in nature ceasing on day 237.

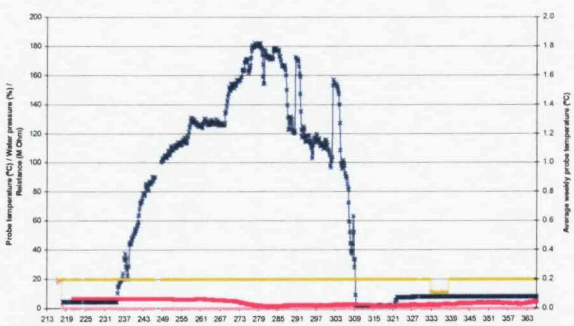
a)



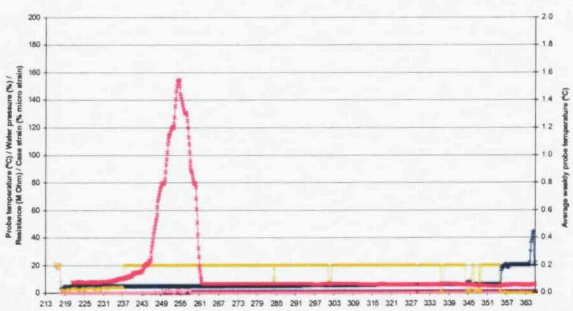
b)



c)



d)



e)

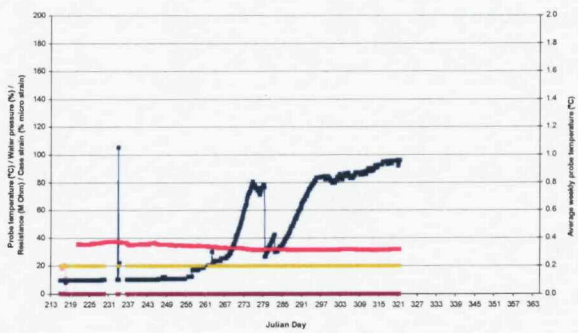


Figure 6.13: Comparison of the winter sensor records for: a) external weather conditions; b) Probe 10; c) Probe 12; d) Probe 15; and e) Probe 16 (2005/6).

Probe 15 water pressure did not show any association with either precipitation or external temperature. Probe 16 did not show any activity in water pressure prior to day 255, and none at all in resistance. As water pressure began to fluctuate, minimum pressure values showed some association with reductions in temperature, but none with precipitation events. However, as temperatures fell to -7.4°C on day 297 pressures remained elevated and stable.

The transient relationship between water pressure (or resistance) and external weather conditions was similar to that shown by the 2004/5 probes. The strangest relationship was shown by Probe 12, which only displayed a correlation at the end of a prolonged large-scale pressure peak. Probe 15's out of phase relationship between resistance and temperature was also unusual. It seems likely that this activity was the result of localised drainage characteristics or changing drainage morphologies. The poor correlation with precipitation events also suggests that inputs directly via boreholes were uncommon and/or that any events did not result in a significant effect at the glacier bed. Section 6.7.1 described the fast transition of the probes between time stages 1 and 2 (Figure 6.1). The rapid transition to time stage 2 could account for the intermittent and unusual correlations between external weather conditions and the sensor records (Table 6.1).

6.7.3 Borehole closure

In section 6.4.3 the creep rate of ice at Briksdalsbreen was calculated (Equation [11]). This suggested that the boreholes were unlikely to close before the next year. This implies that any change in sensor readings, particularly in the relationship between water pressure and resistance, did not reflect closure of the boreholes. Table 6.1 also specifies that closure of the boreholes should weaken the correlation with external weather conditions. Although the interactions recorded by the probes with external weather conditions were intermittent, they were not constrained to the start of the winter record (time stages 1 and 2). In fact, it was at the end of the Probe 15 winter record that resistance showed growing association with changes in the weather. This gives support to the idea that the boreholes were still open and

highlights inter-annual variations in probe responses. For a more detailed discussion refer to section 6.8.

6.7.4 Incorporation into the deforming bed

The incorporation of the probes into the deforming bed is a key aspect of this investigation. The records for case strain and tilt were analysed to identify the timing of this incorporation, in accordance with the trends predicted in Table 6.1. As the probes become more fully integrated into the deforming bed a transition between time stages 2 and 3 should be evident (Figure 6.1). Probes 10, 15 and 16 displayed full records for case strain (Figure 6.14).

Probe 10 case strain remained at zero at the start of the record, showing only minor fluctuations despite significant changes in the tilt record (Figure 6.14a). Readings of case strain only began to change in combination with the tilt record from day 236. After this, case strain fluctuations were accompanied by an increase in the rate of change and oscillations in the tilt record. The calculated rate of ice deformation (section 6.4.3) was insufficient to trap the probe within the ice and then drag it through the till at this time. In addition, probe temperatures remained above 0°C suggesting that the probe had not frozen into the borehole. Although Probe 10 remained relatively upright, the variations in case strain, in combination with active (albeit slow) rotation showed by the tilt sensors, suggest that the probe was interacting with clasts within the deforming bed. The record for case stain also recorded a change in the direction of the applied strain. This would not be expected if the probe was being actively dragged through the till in one direction (Table 6.1). Thus, it is more likely that this reflects the probe's continued incorporation into the deforming bed and a transition to scenario C3i (Figure 6.1).

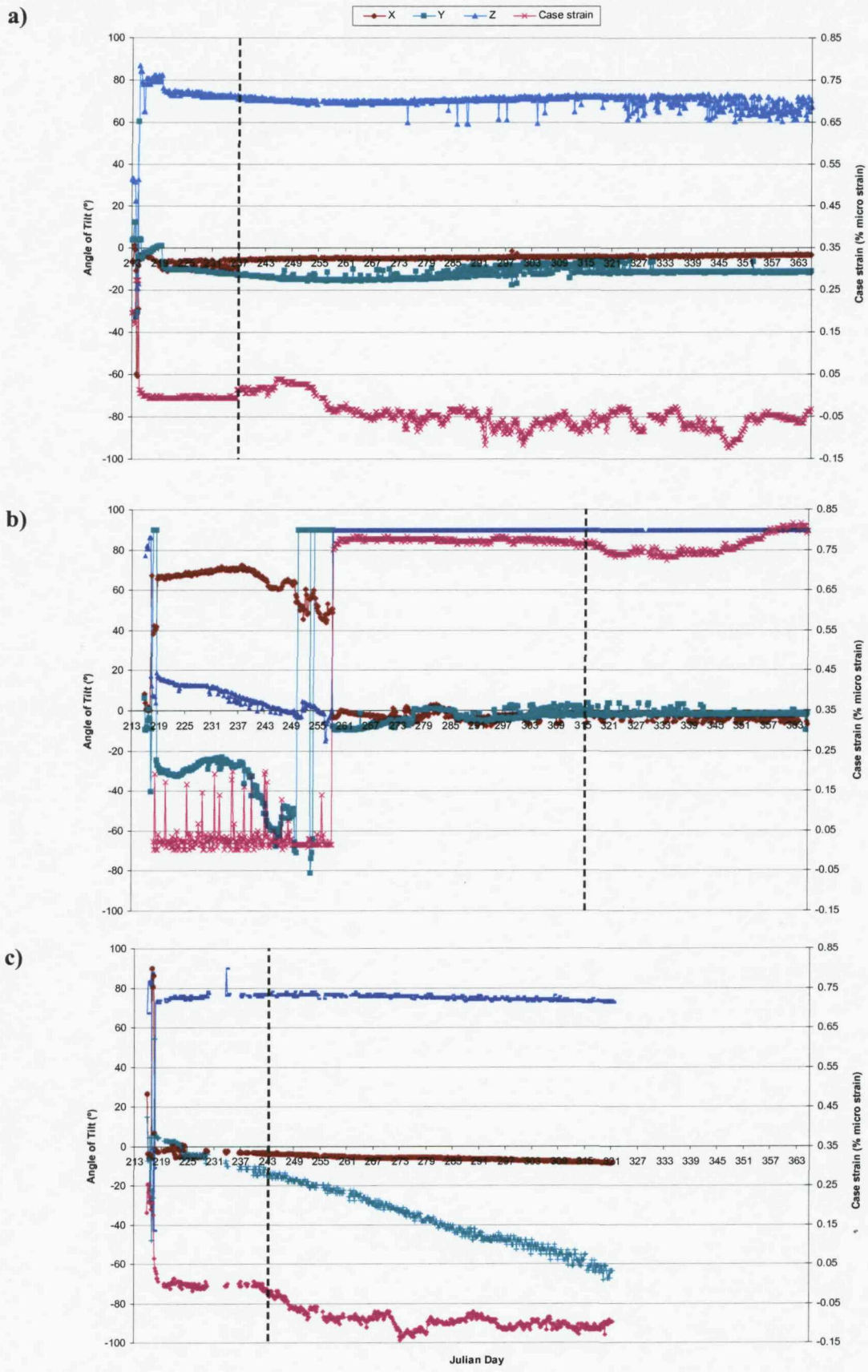


Figure 6.14: Comparison of tilt sensor and case strain records for: a) Probe 10; b) Probe 15; and c) Probe 16 (2005/6). Note: the dashed line marks a minimum time for probe incorporation into the deforming bed.

Probe 15 recorded a slightly different pattern of activity. The direction of strain varied as the axis about which there was the greatest rotation changed (Figure 6.14b). This might appear to be an obvious correlation. However, similar to Probe 10, values of case strain had previously remained constant between days 260-312, despite periods of significant tilt activity. It was only from day 313 that the two sensor readings began to show some correlation. The same lines of evidence discussed for Probe 10 can also be applied to Probe 15. The continued change in the direction of case strain, in particular, reflects the movement of the probe within the deforming bed in scenario C3i (Figure 6.1). The correlation between case strain and tilt occurred somewhat later than the time at which the probe settled at the bed. However, the activity identified here is likely to reflect when the probe started to move or interact within the till more naturally, as opposed to when it was first incorporated (Table 6.1).

Probe 16 displayed similar readings to Probe 15 (Figure 6.14c). The probe case remained unstrained despite significant activity in tilt following deployment. Only from day 242, did case strain start to increase and begin to show fluctuations, as the rate of change in the angle of tilt began to increase along the y-axis. Case strain varied in the same direction, suggesting that the probe was being dragged through the till in scenario C3ii (Figure 6.1; Table 6.1). However, the tilt readings indicate that the probe was slowly rotating (section 4.2.1.4; Figure 4.7). It seems less feasible for such rotation to occur if the probe was lodged within the borehole in scenario C3ii (Figure 6.1). In addition, probe temperature did not suggest the probe was frozen and ice deformation was insufficient to trap the probe. Thus, it is more likely that Probe 16 was located in scenario C3i (Figure 6.1; Table 6.1). The winter readings are somewhat limited because the probes are entering the subglacial environment during a time of decreasing glacial activity. Consequently, greater indication of the probes' whereabouts is likely to be reflected in the spring and summer sensor readings.

The Probe 12 case strain sensor did not work. However, the orientation of the probe could be determined from the tilt record (Figure 6.12b). A change in tilt activity was recorded from day 269, showing that Probe 12 was lying almost completely flat.

This signifies that the probe was completely separated from the borehole and had become fully incorporated into the deforming bed beneath (scenario B3; Figure 6.1; Table 6.1). The activity of the probes demonstrated that the overall transition between time stages 1 and 3 occurred quite rapidly. Thus, although the boreholes were not closed, the probes still showed a change in sensor readings. This is feasible due to the relatively rapid movement of the borehole away from the initial locations of probe deployment (Figure 6.4).

The amount and variability of changes in case strain differed between the probes. This is expected in line with spatial variations in the composition of the deforming bed. In fact, Fischer and Clarke (2001), noted differences in the texture of subglacial sediments only 10 m apart (based on ploughmeter readings). Variations in sediment texture may also explain why Probe 5 showed lower magnitude changes in case strain (section 6.4.4). This variation may also relate to the year of deployment and model of probe used (Table 4.3, Chapter 4). Probes 10, 15 and 16 all showed similar sensor patterns, in comparison to Probe 5. Another record from 2004/5, in combination with one from scenario A would be useful to further these comparisons.

6.7.5 Subglacial processes

The probes recorded relatively minimal activity during the winter record (Figures 6.11 and 6.12). The majority of sensor activity relating to the location of the probes and their interaction with external conditions have been discussed above. However, there are a number of patterns in sensor activity that require further discussion. Probes 10 and 15, in particular, recorded relatively little activity during the winter. The probes displayed short-lived fluctuations followed by generally consistent base pressures. This activity suggests that these regions of the bed were responding to only minimal subglacial flows. Small-scale melt water inputs, varying the amount of basal flow, resulted in the intermittent small-scale oscillations observed. This might also explain why there was such a weak correlation with external weather conditions.

In contrast, Probe 12 showed the greatest activity in, and magnitude of, water pressure. Readings began to increase from day 235, exceeding overburden pressure on day 250, and reaching a maximum of 182.5% on day 277 (Figure 6.11b).

Pressures in excess of overburden reflect a considerable magnitude of water passing through the till in this area of the bed. Water pressures were sustained, indicating that Probe 12 was located in a flow pathway supplied by continuous and significant melt water inputs. The decrease in water pressure from day 277 reflects diminishing melt water followed by a period of stability for the rest of the winter.

The pressure record for Probe 16 reflected a combination of stable and fluctuating readings (Figure 6.11d). Pressures were above base values following deployment (10.1-10.9%), indicating consistent water flows through this area of the bed. The sensor readings began to show greater activity from day 243 and water pressure increased from day 255. Pressure continued to increase and fluctuate from this point, reaching maximum values of 96.2%. This change in activity reflects an increase in the quantity of melt water inputs, which may have resulted from a change in water drainage elsewhere at the bed. Water pressure appeared to stabilise from day 295, showing only minor oscillations and a steady overall increase in values. This implies that the change in water inputs resulted from a permanent change in flow pathways and/or water inputs to the area around Probe 16.

Resistance is strongly associated with water pressure, as an indicator of the wetness of the surrounding environment. At the start of the winter variations in Probe 10 resistance corresponded well with the pressure record, decreasing on day 214 as water pressure rose (Figure 6.11a). Resistance then increased (dry conditions) on day 245, following the fall in pressure back to base flows on day 236. The lag in the resistance record suggests that it was more sensitive to the amount of water within the till than water pressure. The record of resistance for Probe 12 showed minimal activity (Figure 6.11b), omitting any corresponding change in resistance during the period of elevated water pressure (days 235-309). This was unexpected, given the significant increase in pressure. In addition, resistance decreased during a period of continuous, low water pressures. Probe temperatures remained above 0°C, suggesting that the surrounding environment was not frozen. This implies that the sensor was responding to different processes or that it was broken, because that fluctuation was the only change in resistance recorded throughout the entire probe record.

Activity in the Probe 15 resistance record was still evident subsequent to day 258. The activity of water flow within the till is highlighted by three short lived decreases in resistance (days 284, 301 and 336). These changes were not accompanied by any variation in water pressure. Again, this indicates that the resistance record was more sensitive to changes in the water content of the till than the pressure sensor. It also suggests that small-scale variations were still occurring within the subglacial environment during the winter. The Probe 16 resistance sensor did not show any variation throughout the entire record. Again, this was unusual, particularly as pressures exceeded overburden. This may suggest that the sensor was responding to different variations in the properties of the till, or that it was broken, as no fluctuations were recorded throughout the whole record.

A variety of patterns were displayed in probe temperature. To increase the clarity of readings, the average weekly values for Probes 12 and 16 have been reproduced in Figure 6.15. Reductions in probe temperature have been associated with influxes of fresh melt water into the subglacial environment. In accordance with this relationship, Probe 10 recorded continual small-scale oscillations but an overall increase in temperature as water pressure fell to base values on day 236 (Figure 6.11a).

Probe 12 displayed an unusual pattern, recording a significant lag between average weekly probe temperature and water pressure (Figure 6.15a). Values only began to decline once water pressure had exceeded overburden. Readings decreased rapidly reaching minimum values shortly after water pressure peaked. The drop in temperature reflects the amount of fresh melt water passing through the till at this time. Probe temperatures then began to increase as water pressure fell. The continued increase in probe temperature may reflect a reduction in melt water inputs into the deforming bed through the winter.

The temperature record for Probe 15 remained constant from day 258, in line with the low stable water pressures recorded. Average probe temperatures only began to show a slight decrease towards the end of the winter period. This is supported by the short lived fluctuations in resistance, which suggest that there was a slight increase in

the water content of the till in this area of the bed, towards the end of the winter record.

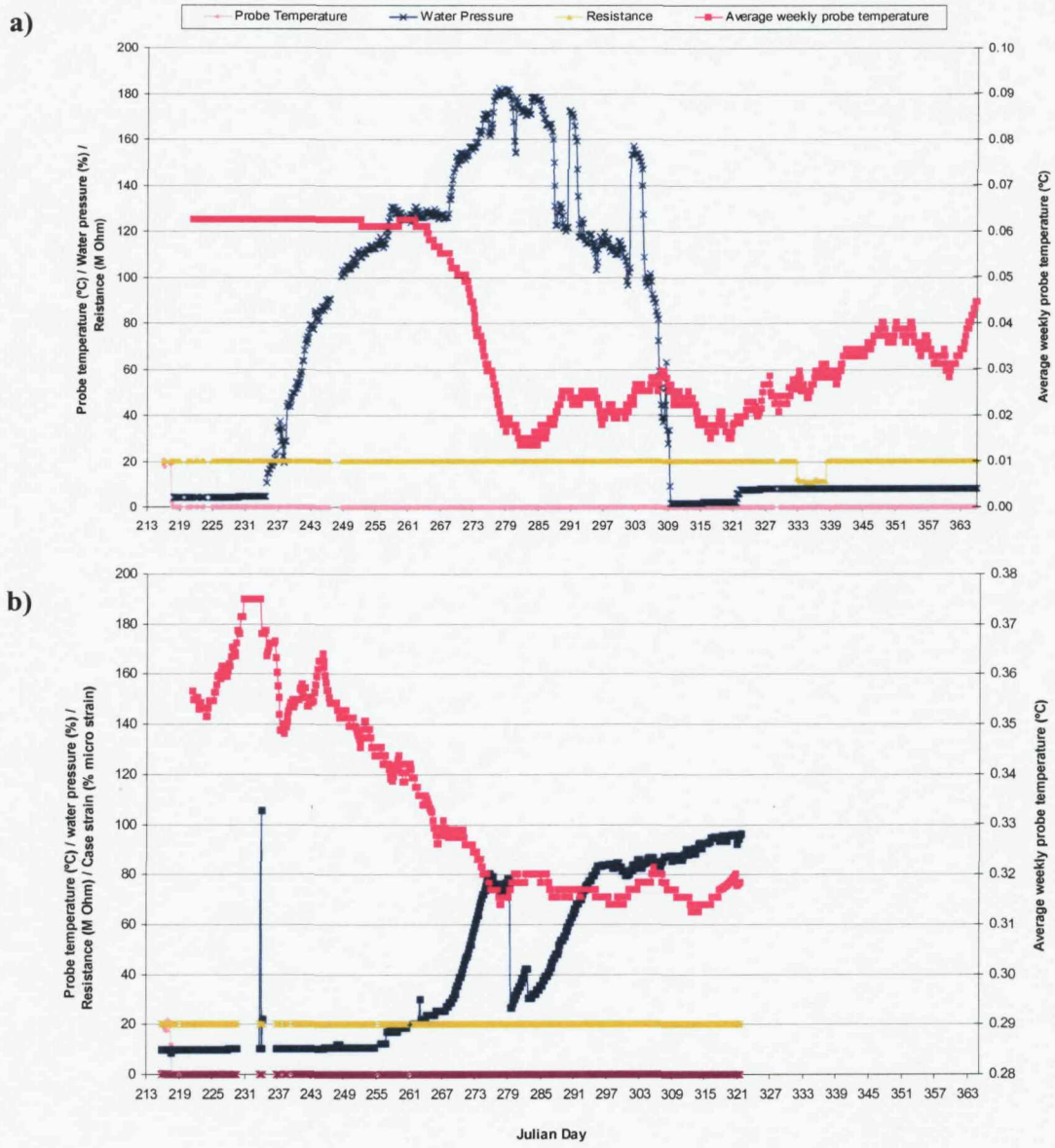


Figure 6.15: Winter sensor record highlighting variations in average weekly probe temperature and water pressure: a) Probe 12; b) Probe 16. Note: different scales on the secondary y-axes.

Similar to Probe 12, Probe 16 showed a sudden change in probe temperature (Figure 6.15b). Values at the start of the record remained elevated and displayed high amplitude oscillations, whilst water pressures remained relatively low (12.3%). Average temperatures began to fall from day 253, just prior to the increase in water

pressure on day 255. This implies that probe temperature, as well as resistance is more sensitive to variations in till water content than water pressure. This also makes the lag in temperature recorded by Probe 12 more unusual.

In general, the activity recorded by the probes during the final stages of the winter record is in good agreement with the trends outlined in Table 6.1. A weather signal was no longer evident and trends of case strain and tilt would suggest that the probes were interacting with the till. Variations in water pressure, resistance and probe temperature were responsive to each other and reflect conditions within the till (time stage 3; Figure 6.1). It is also of note that, unlike the 2004/5 probes, these did not display a step change in sensor readings during the winter record. Instead, in general, Probes 10 and 12 showed more consistent, minimal activity, whilst Probes 15 and 16 displayed an increase in activity towards the end of the winter record.

6.7.6 Activity in Probe 15

This section will discuss the activity of Probe 15 following deployment and at the end of the record (Figure 6.16). Probe 15 began recording conditions on an englacial ledge, within a borehole that had drained (days 217-258). During this time, water pressure remained low and constant. Resistance remained low, displaying small-scale fluctuations. These readings indicated that the probe was sat in a puddle. The high frequency oscillations recorded by case strain indicate that the probe was subjected to significant changes in force within the englacial cavity. The nature of these oscillations might suggest that the probe was responding to continuous small-scale movements of the ice, applying pressure to the probe case. The variation in case strain during this period, in comparison to when the probe was within the subglacial environment, can be used to distinguish the location of probes with the glacier.

On day 237, resistance increased abruptly, reflecting dry conditions. This might occur if ice deformation, for example, caused the ice to crack or a hole to open in the cavity, releasing the water. It was at this time (day 237) that probe temperature began to increase rapidly and show many large-scale oscillations (Figure 6.16). The increase in probe temperature above 4°C supports the idea that melt water had been

evacuated from the englacial cavity. The probe was responding directly to fluctuations in external air temperatures. The high thermal capacity of water means that the probe would not be able to respond as quickly to changes in external temperatures if it was submerged.



Figure 6.16: Winter sensor record for Probe 15, showing: probe temperature, water pressure, resistance, and case strain on the secondary y-axis.

Probe temperatures decreased suddenly from day 257, reaching 0.1°C on day 258. This decline corresponded with a sudden change in case strain that occurred on the same day (Figure 6.16). The rapid response of both sensors indicates a significant change in the probe's surrounding environment, namely that the probe had become dislodged from the englacial ledge and fallen to the base of the borehole. This hypothesis is supported by the tilt record (Figure 6.12c). The probe showed continual variation in tilt prior to day 258. The rate of change in the angle of tilt increased just prior to day 258, when a sudden switching in tilt activity occurred. The tilt record following this showed less activity, and changed over a smaller range of angles. This is in line with trends in tilt that have been displayed by the probes located at the glacier bed (Figure 6.1; Table 6.1).

The activity in probe temperature and tilt during this initial period strongly resembles that of Probe 4 (2004/5). This supports the idea that the probe was in the ice and not at the ice-bed interface. The range, and oscillations, in temperature recorded only occur in the ice and correspond to the probes interaction with the air. The activity in tilt was also a good match to that displayed by Probe 4. In turn, the changes that ensued were much more in keeping with the sensor patterns recorded by probes that were successfully incorporated into the subglacial environment (Figure 6.1; Table 6.1).

The winter record for Probe 15 was also slightly unusual in that the sensor readings began to show greater activity towards the end of the winter (Figure 6.16). Following a period of quiescence (days 261-343), resistance displayed a greater frequency of oscillations and case strain began to increase in the opposite direction. Probe temperature also showed a gradual decline in values. These changes suggest an increase in the activity, or processes operating, within the subglacial environment. This was highlighted by the sudden increase in water pressure from base levels on day 355. The sudden change in water pressure indicated a fresh influx of melt water into this area of the bed. This was unexpected at the end of the winter when melt water inputs are thought to be minimal. The significance of this activity is considered in greater detail in section 6.8.

6.7.7 Synopsis: 2005/6

A greater variety of sensor patterns were evident within the 2005/6 probe records, even though they did not record a significant step change. Probes 10 and 12 were characterised by initial activity, followed by a period of quiescence for the rest of the winter record. Probe 15, once within the subglacial environment, showed little activity until the end of the winter record. Probe 16 saw an change in sensor readings from stable records following deployment, to an increase in activity towards the end of the winter. The variety of activity reflects the diversity of probe locations across the glacier bed and the spatial variability within the subglacial drainage system. Similar to 2004, the probe tilt records showed a transition from high activity on deployment, to more continuous change in the angle of tilt, marking a transition in the location of the probes within the subglacial environment.

6.7.8 Probe failure

Probe 16 was the only probe to fail during the winter. The cause for this was not obvious from the record. Readings of water pressure and case strain were not in excess of values recorded by other probes, suggesting that the probe case did not leak, and was not crushed. In addition, the probe case and sealant have been extensively tested and are known to withstand the maximum forces likely to occur beneath the ice. Consequently, rather than sensor failure, the most likely explanation is that Probe 16 moved into a position where it could no longer communicate with the base station.

6.8 Hydrological Processes

The 2004/5 and 2005/6 probe sensor records have been discussed in relation to subglacial processes in sections 6.4.5 and 6.7.5, respectively. These sections have highlighted the information that can be determined about the conditions within the subglacial environment during the winter record. The probes were subject to an initial period of adjustment, both in their location, and in their response to changes in the subglacial environment, during the first stages of deployment. However, the time for the probes to become at least partially incorporated into the deforming bed and separated from the overlying borehole occurred quite rapidly. As a result, the activity in water pressure and other sensor readings can provide a tentative indication as to the location of the probes with respect to the subglacial drainage system at the end of the summer. This section will give further consideration to the relationship between the probes and the subglacial hydrological regime. It will assess the location of the probes within either connected or unconnected drainage routes and determine if a transition in the subglacial drainage morphology from a summer to a winter regime can be identified.

6.8.1 Connected versus unconnected

The characteristics of the pressure records (Figures 6.2 and 6.11) were examined to determine whether or not they corresponded with the pressure records of connected or unconnected drainage regions (Murray and Clarke, 1995). The winter records

revealed by the probes in both years did not show any diurnal or highly fluctuating water pressures. As a result, the probes are thought to be associated with unconnected drainage areas. Despite this, the probes often recorded significant magnitudes of water pressure. In light of this, further classification has been added to the terminology outlined by Murray and Clarke (1995). The unconnected regions have been termed 'inactive' if they show only minimal variations in pressure and 'active' when significant water pressures are recorded.

The low, mildly oscillating water pressures recorded by Probes 5 and 8 at the end of the records were indicative of unconnected regions and a winter regime, when activity in the subglacial environment was reduced (Figure 6.2b, d). In these unconnected regions water pressures remained low, as opposed to high, which is normally associated with winter regimes (e.g. Fudge *et al.*, 2005). The difference in the style of the pressure pulse experienced by Probe 8 reflects a change in the type of drainage network, or source of melt water inputs, in this area of the bed. The probes were responding to continuous base flows through the till (low pressure), as opposed to highly pressurised water passing through constricted winter drainage pathways (Benn and Evans, 1996; Fountain and Walder, 1998). Probes 5 and 8 also recorded very low base flows (1.2% and 4.5%, respectively) and sporadic pressure pulses (Figure 6.2b, d). This activity was of a relatively low magnitude and frequency, again implying that Probes 5 and 8 were located in inactive unconnected regions (Table 6.2).

Table 6.2: Location of the probes within the subglacial drainage system, according to the winter sensor readings in water pressure.

Probe	Location?	Activity?
5	Unconnected	Inactive
7	(Un)connected	Active
8	Unconnected	Inactive
10	Unconnected	Inactive
12	Unconnected	Active
15	Unconnected	Inactive
16	Unconnected	Active

Probe 7 showed a slightly different pattern, recording elevated base flows and high frequency and magnitude pressure fluctuations (Figure 6.2c). These oscillations

reflect great variability in the amount of water passing through the subglacial environment. It suggests that the probe was located within a highly pressurised area of the bed, indicating that if the probe was connected to the subglacial drainage system. However, the pressure peaks recorded did not correlate with weather fluctuations (melt water inputs), and thus, did not display the diurnal fluctuations that are normally associated with connected regions during the summer months (Murray and Clarke, 1995). The magnitude of pressure recorded also seemed to be too much in excess of overburden to reflect a connected drainage route, which should be highly efficient and at high capacity during the summer (e.g. Willis *et al.*, 1990).

Consequently, Probe 7 was located in an active but unconnected area of the bed (Table 6.2). The high pressures experienced by the probe, particularly in the second half of the record (Figure 6.2c) were comparable to the 'superfloatation' pressures recorded by Murray and Clarke (1995), who found that pressures in unconnected regions were often consistently in excess of overburden. This can reflect a strong pressure gradient between connected and unconnected regions of the bed (Murray and Clarke, 1995). In unconnected regions flow is presumable constrained to inefficient pathways within the till. The variability in the pressure readings might be achieved if this area was fed by stored sources of water; or if the water inputs to the system were far enough up ice, and/or received sufficient input from other water sources (e.g. englacial or from the open borehole), to remove any diurnal signal.

The magnitude of water pressure recorded by Probe 7 was also unusual as it occurred in October, when melt water inputs should decline with external temperatures (Figure 6.5a). This pressure pattern may simply represent the high capacity of water flow at the ice-bed interface, which indicates greater activity in the unconnected regions than previously assumed. Alternatively, the increase in pressure magnitude in October may reflect a decrease in the efficiency of the connected drainage system towards the winter months, resulting in less efficient water transfer. In contrast, the work of Fudge *et al.* (2005) at Bench Glacier in Alaska, might suggest that Probe 7 was in a connected region (Table 6.2). They observed an absence of diurnal fluctuations in connection regions as early as day 191, before diurnal melt water inputs had ceased at the glacier surface. Unfortunately, it is not possible to determine which scenario is correct based on the given data.

The sensor activity recorded by Probes 10 and 15 indicate that they were located in an unconnected region of the bed. Water pressures were low and consistent, with intermittent small-scale oscillations, resulting from variations in the amount of basal flow. The basal flows recorded are likely to reflect the throughflow and sheet flow that is sustained throughout the year at the base of temperate ice masses (Fountain and Walder, 1998). The absence of oscillations suggests that the probes were located in inactive unconnected regions that were not in receipt of significant melt water inputs (Table 6.2). It is likely that Probes 10 and 15 were recording base flow through the till via bulk movement or Darcian flow (Benn and Evans, 1996).

Probe 12 also appeared to be in an unconnected region of the bed due to the lack of diurnal fluctuations and the low, relatively consistent, base flows recorded. However, Probe 12 did show a prolonged and highly elevated pressure peak, implying that this region was active (Table 6.2). The source of melt water for this pressure peak appears to be temporary and may have resulted from spatial variations in the location of drainage pathways. This would coincide with the intermittent correlations with external weather conditions. This loss of activity from day 277 suggests that either the source of melt water had been removed, or the drainage pathway had closed or moved to a different area of the bed.

Probe 16 showed a similar pattern of fluctuations in water pressure, after an initial period of quiescence. This suggests that it was near to a flow pathway or pressurised area of the bed. The sudden activity in pressure may reflect a redirection, or new source, of melt water to this area of the bed. However, the lack of diurnal oscillations and more frequent fluctuations in pressure would suggest that the probe was not directly linked to a connected drainage system. Instead, Probe 16 was located in an active unconnected region (Table 6.2).

In the winter, the probes were new to the subglacial environment and the hydrological system was in a state of change from a summer to winter regime. As a result, the activity in water pressure discussed above provides a preliminary idea as to the location of the probes in relation to the subglacial drainage system. The locations of the probes are likely to become more evident in the spring, as the summer drainage system becomes re-established, whereas the general trend of

minimal activity recorded is in keeping with subglacial conditions during the winter months. The location of drainage networks can vary between years but the trends observed in the spring are likely to become sustained into the summer, for that year. As a result, the sensor activity summarised in Table 6.2 may only reflect conditions during the winter record.

6.8.2 Evidence of a transition from winter to summer regimes

The winter probe records did not show any direct or lasting correlations to weather events. However, it may still be possible to identify larger scale changes in the subglacial drainage system, marking a transition between summer/autumn and winter regimes. A change in the hydrological regime of the glacier will result from long term variations in the external weather conditions, namely a decline in temperature and an increase in snowfall (i.e. stored precipitation). Gradual changes in the activity of the sensor records would provide an indication of this transition.

Probes 5 and 7 showed a step change in sensor readings during the winter records (days 275 and 264, respectively). For Probe 5 this resulted in low, mildly oscillating water pressures, characteristic of a winter regime. However, this change appeared to occur too suddenly to be attributable to variations in external weather conditions and the overall regime of the glacier. The omission of an indicator for this transition may be attributable to Probe 5's location, in an unconnected region of the bed. The final step increase in water pressure recorded by Probe 7 (day 282), may reflect a transition towards a winter regime, if it reflected the constriction of drainage pathways in neighbouring connected regions of the bed (section 6.8.1). This would account for the increase in pressures even further above overburden. However, the timing of this event does appear to be quite early and again it occurs suddenly.

Probe 8 was located in an inactive unconnected region of the bed. As such, a record of the transition from summer to winter drainage regimes was not expected. However, the second pressure rise towards the end of the winter record (days 324-328) is of note, particularly as it did not correlate with an increase in external temperatures. Average values of probe temperature actually began to decline from day 317 prior to the pressure rise, indicating an increase in the water content of the

deforming bed. However, the Probe 8 pressure and resistance record remained inactive. As a result, this decline might suggest cooling conditions within the subglacial environment in accordance with reduced external air temperatures in the winter months. It was only on day 319, when temperatures suddenly fell, reaching below -5°C on day 325, that water pressure began to rise.

Prior to the decline in temperatures the subglacial drainage system was obviously able to accommodate the melt water inputs generated in the preceding days. However, the rise in pressure as temperatures decreased suggests that drainage pathways elsewhere at the bed were becoming constricted. As the drainage capacity decreased in connected regions, water flows were diverted into the once unconnected area of the bed around Probe 8. Probe temperature continued to decline during this time and remained reduced (compared to summer values) for the remainder of the winter. This probably reflects a combination of excess melt water and cooling external temperatures. So, although Probe 8 did not show an obvious transition, the pressure response implies a change in the nature of the subglacial drainage system in the connected regions of the bed.

The stable conditions recorded by Probes 10 and 15 were characteristic of minimal subglacial activity in the winter. For Probe 10 these stable conditions occurred very suddenly, after an initial period of small-scale oscillation. This is not indicative of a gradual transition in external conditions and the processes operating within the subglacial environment. For Probe 15, the conditions recorded on reaching the subglacial environment appeared to be immediately indicative of a winter regime as they remained constant throughout the winter record. The timing of this activity is too early in the season (early to mid September) to reflect the glacier's transition to a winter regime. Thus, although this change in conditions must occur, the records for Probes 10 and 15 only reflect the location of the probes in an inactive and unconnected region of the bed, rather than a long term transition in glacier conditions. It is likely that the connected regions of the bed were still showing summer trends in activity at this time. Given that the dominant change in the winter is the closure and constriction of drainage pathways, a signal for this change may only be evident in those areas that encompass, or are directly connected to, drainage pathways. In which case, a signal for the transition in Probes 10 and 15 would not be expected.

Probe 12 was located in an active unconnected region of the bed. After initial activity (days 235-309) the remainder of the record marks a period of stability during the winter when large volumes of melt water were no longer produced and subglacial activity was at a minimum. The remaining base flows (day 309) indicate that this area of the bed had 'shut down' for the winter. In fact, the slight increase in base flows on day 322 may reflect the exact timing of this change in this area of the bed. This elevation in pressure may indicate that drainage routes across the bed had become constricted, decreasing in capacity, as a result of reduced external temperatures, and thus, melt water production. This occurred in mid November, which is feasible, in terms of external temperatures, for such a change to occur.

The Probe 16 record is similar to that of Probe 12. A change in the connectivity of, or inputs to, that area of the bed resulted in fluctuations and an increase in water pressure. Following initial fluctuations, water pressure showed sustained and mildly oscillating high pressures (day 295), indicative of water pressure in a winter drainage regime (Fudge *et al.*, 2005). This change reflects the stabilisation of the drainage route in this area of the bed, and a possible shift towards winter conditions. Although, day 295 may appear to be relatively early it is still a feasible time for a transition to a winter regime.

The transition to a winter regime is not expected to be uniform across the glacier due to the heterogeneous nature of drainage networks. The range of dates from Probes 7, 12 and 16 suggests that a change in conditions had begun to occur from early to mid October (days 282, 322, and 295, respectively). Variability in this timing would be expected both between years and depending on the location of the probes at the glacier bed. However, these dates appear to be in good agreement with the weather record for Briksdalsbreen at this time of year (Figure 6.17). In October, average temperatures for Briksdalsbreen fall below 15°C (max.) and below 0°C (min.) and continue to decrease from this point. October also recorded particularly low values of precipitation. This would aid in the constriction of drainage pathways, as a scarcity of precipitation would further reduce the amount of melt water generated. A reduction in melt water inputs decreases the action of frictional melting and the ability of channels to sustain their summer drainage capacities.

The continued decline in temperatures into November and December implies that a greater proportion of precipitation events will occur as snow. Thus, precipitation will be stored, decreasing melt water contributions further. In combination with a reduction in external temperatures, this will aid the transition to a winter regime and cause the glacier system to shut down. The timing of these changes in external weather conditions confirms that the step change in readings recorded by Probe 5 was too early to relate to a change in the drainage regime.

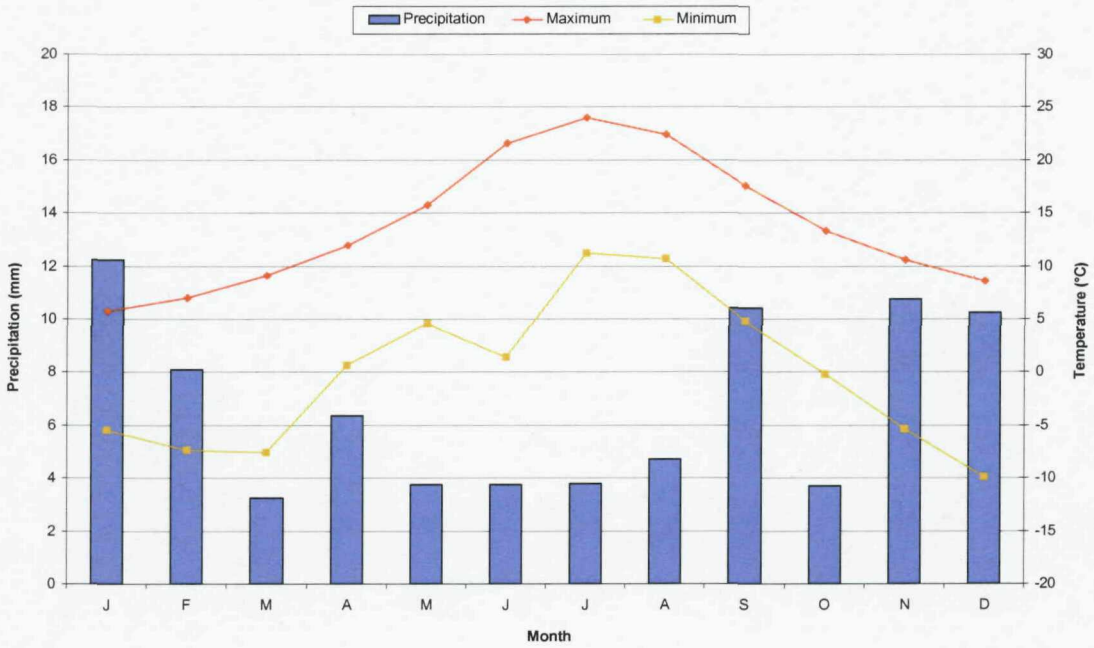


Figure 6.17: Average external weather conditions for temperature (max. and min.) and precipitation at Briksdalsbreen, Norway (2004-6)

Figure 6.17 shows that there is a good agreement between the timing of the sensor variations and the transition to winter conditions. However, the nature of the events recorded by Probes 7, 12 and 16, still appear to occur quite suddenly. The gradual transition in conditions that one might expect within the subglacial environment does not appear to be recorded. Instead, the most likely evidence of this transition appears to be marked by sudden changes in the sensor records. This would suggest that only when a critical level of 'change' in external conditions is reached, or sustained for a given amount of time, do the probes record a sudden change in conditions within the subglacial environment. An exact correlation appears to be lacking. However, an

example of such a critical level might include the reduction of average external daily temperatures below 10°C for a sustained period of time. This occurred on day 264, in 2004 and on day 271, in 2005. The changes in the probe readings occurred around two weeks after this change had occurred.

6.9 Summary

The winter sensor records have generated a range of information about the initial stages of probe deployment, detailing probe incorporation into the deforming bed and winter conditions within the subglacial environment. A record for winter englacial conditions was also obtained from Probe 4.

It was important that the sensor readings could be used to identify and characterise the location of the probes at the glacier bed and their subsequent incorporation into the deforming bed. The conceptual theory outlined in section 6.2 provided a foundation from which sensor readings could be analysed, whilst Figure 6.1 and Table 6.1 presented a framework from which the probe positions and processes could be classified. The majority of probes became positioned in scenario C and saw a rapid transition to time stage 2, where they became incorporated into the subglacial environment (1-19 days). It took longer for the probes to reach time stage 3 and become fully integrated into the deforming bed (21-57 days). A summary of these findings is displayed in Table 6.3.

Table 6.3: Details of probe location and the time taken to change between time stages, derived from the conceptual ideas displayed in Figure 6.1 and Table 6.1.

Probe	**5**	**7**	**8**	**10**	**12**	**15**	**16**
Scenario at Time Stage 1	C	C	C	C	B	C	C
Time to Achieve Time Stage 2 (days)	19	9	7	9	7	1	7
Time to Achieve Time Stage 3 (days)	57	21	55	24	52	56	25

The probe sensor readings were also used to describe the processes operating in the subglacial environment during the winter. In general, the probe records showed that there was continued (both small and large-scale) activity within the subglacial

environment throughout the winter period. The key sensor findings are summarised below.

- The incorporation of the probes into the subglacial environment (time stage 1; Figure 6.1) was marked by a decline in probe temperature to around 0°C and a reduction in probe tilt rates (Figure 6.12).
- There were only sporadic correlations between water pressure and resistance fluctuations and external weather conditions (Figure 6.5 and 6.13). This suggested that the probes were not receiving direct melt water inputs, either from well connected subglacial drainage routes, or from surface inputs via the boreholes (sections 6.4.2 and 6.7.2).
- Autumn surface velocities indicated that the boreholes would move away from the initial location of probe deployment within 30 hours. This marked a rapid transition to time stage 2 (Figure 6.1; Table 6.3) and might account for the lack of correlation with weather conditions (section 6.4.1; Figure 6.4).
- Values of case strain showed more frequent and high magnitude oscillations when the probes became incorporated into the deforming bed (time stage 3; Figure 6.1). This was accompanied by a signal of probe rotation in the tilt record (Figure 6.6 and 6.14). In combination, these readings indicated that the probes were interacting with the till (sections 6.4.4 and 6.7.4). Rotation would not be achieved if the probes remained in a borehole (Figure 6.1).
- Generally, the probes did not display any diurnal or highly fluctuating water pressures indicating that they were located in unconnected drainage areas (Figure 6.2 and 6.11). However, the high magnitude pressure recorded by some probes suggested that they were in *active* unconnected regions (section 6.8; Table 6.2).
- The minimal activity displayed by the probes at the end of the winter record (Figures 6.2 and 6.11) was characteristic of winter subglacial drainage conditions (Willis *et al.*, 1990; section 2.6.3).

The Probe 4 sensor readings provided a record for the englacial environment and allowed comparison with subglacial probe records. A number of differences and some similarities were noted between the two environments, based on sensor readings. These are summarised below.

- Probe 4 recorded temperatures in excess of 1°C, demonstrating that it was not located within the subglacial environment but within the borehole column (e.g. Probe 4, Figure 6.10b; Probe 15, Figure 6.16).
- There was little correlation between water pressure and resistance readings and external weather conditions (Figure 6.10), suggesting that Probe 4 was also not affected by direct surface inputs via the borehole.
- The magnitude and direction of applied case strain fluctuated greatly in conjunction with changes in the tilt record. This suggested that the probe was responding to variations in the dimensions of the borehole (Figure 6.10).
- The magnitude of case strain was greater than that recorded by probes within the subglacial environment.
- The tilt record showed much greater variation than that displayed by probes within the subglacial environment (Figure 6.10).

To summarise, the winter sensor records showed the incorporation of the probes into the deforming bed and the processes operating in the subglacial environment during the winter. Comparison of probe records also highlighted the differences between englacial and subglacial conditions.

Chapter 7

Spring Probe Record

7.1 Introduction

This section will examine the sensor records for the spring, representing the period between days 1-120 (January-April, inclusive). The spring is an important period because it marks a phase of transition between winter and summer regimes in the glacier's dynamics. If the winter regime marks a period of quiescence, one of the best indicators of 'spring' within the glacial system is the start of, or an increase in, the variability of sensor readings. This section will discuss the changes within the subglacial environment throughout the spring, as the glacier transitioned towards a summer regime. In consideration of the readings displayed the description and interpretation of the subglacial probe records is divided into two separate phases, Event 1 and Event 2. Analysis of the sensor records will explore the processes operating within the subglacial environment in order to: monitor the mechanisms operating during the spring; characterise the nature of the subglacial drainage system; assess the location of the probes with respect to that system; and determine the triggers for the changes observed.

7.2 2004/5

Probes 4 and 8 were operational in the spring of 2005. Probe 4 was still emplaced within the englacial borehole, whilst Probe 8 remained within the deforming bed. The relative location of Probes 4 and 8 is displayed in Figure 5.17 (section 5.5,

Chapter 5). The spring sensor records are displayed in Figures 7.1 and 7.2. The spring record was deemed to last between days 1-120. However, the Probe 4 record ceased only 24 days later (day 144). As a result, for completeness, the whole of the remaining Probe 4 record is considered within the spring period, so that the graphs displayed run from day 1-144.

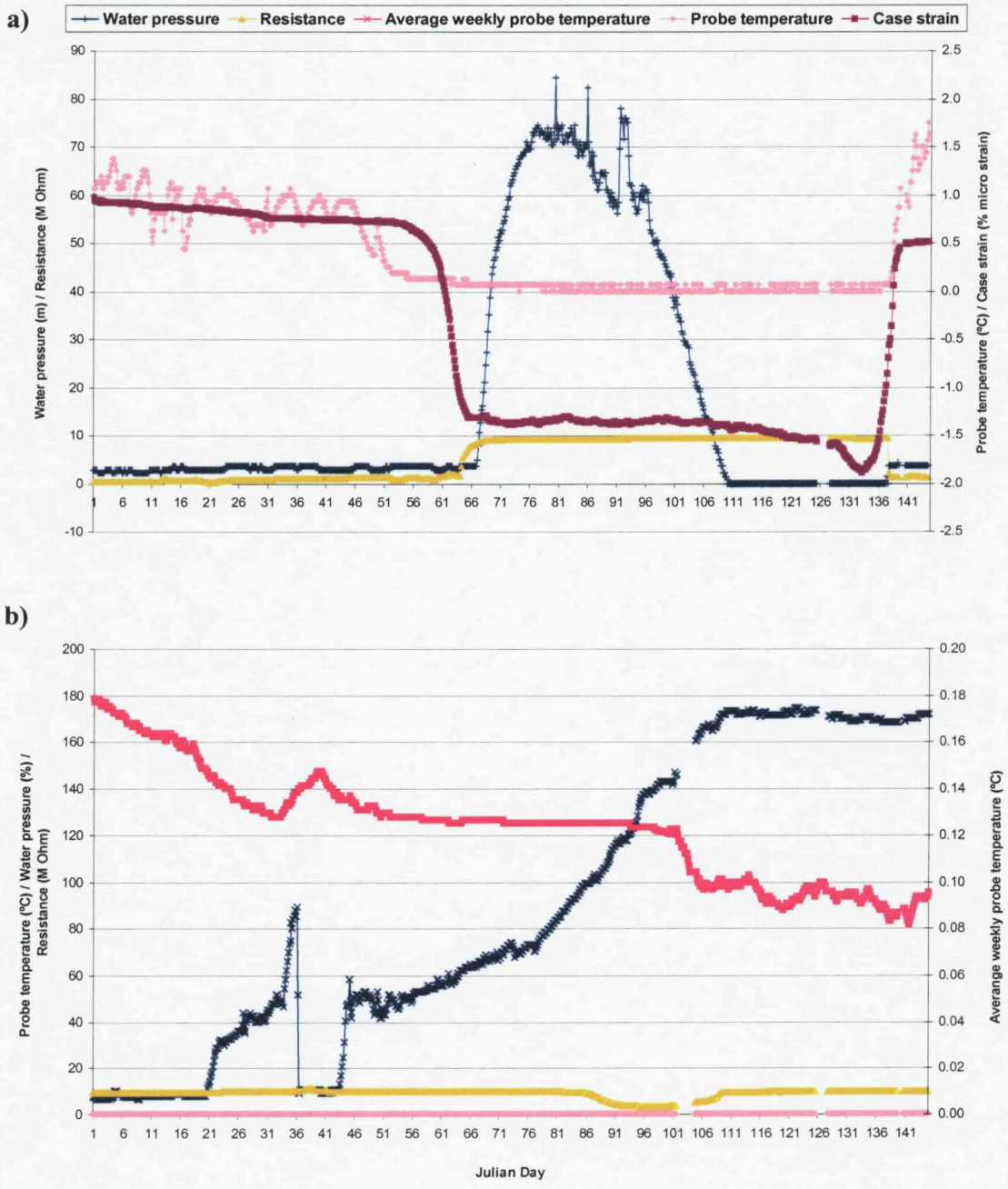


Figure 7.1: Comparison of the spring sensor records, showing probe temperature, water pressure, resistance, case strain and average weekly probe temperature for: a) Probe 4; and b) Probe 8 (2004/5). Note: the difference in axes scales and sensor units between the probes.

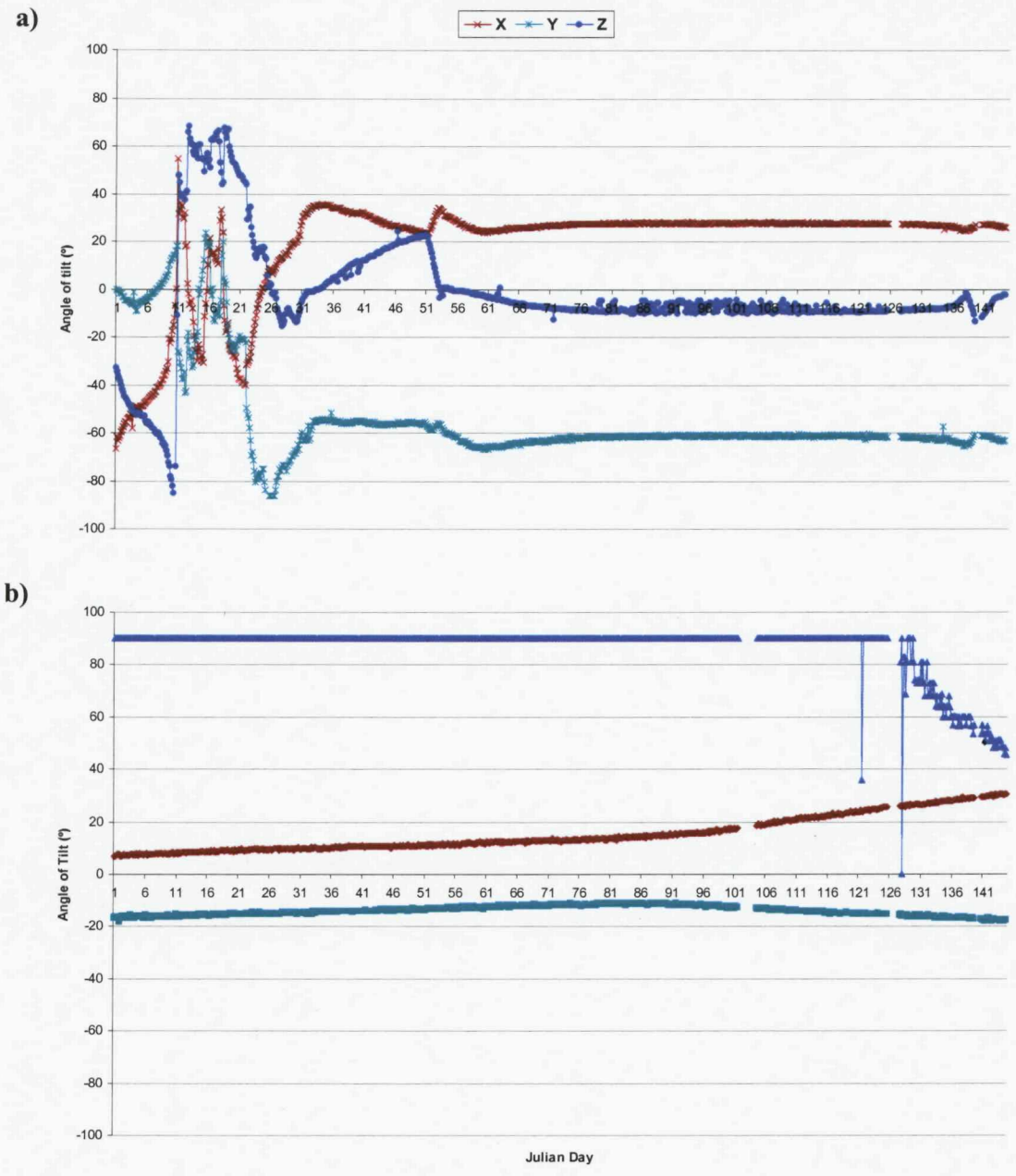


Figure 7.2: Comparison of the spring tilt sensor records for: a) Probe 4; and b) Probe 8 (2004/5).

7.2.1 Probe 4

The spring record for Probe 4 (days 1-144) is displayed in Figures 7.1a and 7.2a. Probe temperature showed numerous fluctuations at the start of the record (Figure 7.1a) and a gradual decline to 0.1°C (day 55). Temperature fluctuated greatly in a series of peaks and troughs that, in some instances, weakly reflected diurnal variations (e.g. days 4-8). Where this was the case, peak temperatures occurred at

night with minima during the day. Probe temperature remained low (0-0.1°C) between days 55 and 137, but increased rapidly to 1.8°C at the end of the data set.

Water pressure showed relatively little activity at the start of the record, remaining low and relatively constant (1-3 m). Pressure increased suddenly and rapidly from day 67, achieving 71 m by day 75. Pressure peaked on day 77 and then began to oscillate (without a diurnal signal), recording pressure peaks greater than 75 m on days, 80, 85 and 91. The falling limb of the pressure peak was rapid, reaching 0 m by day 110. Pressure remained at 0 m for 28 days (days 110-137) before rising back to original values of 4 m (day 345) for the rest of the record. Small-scale fluctuations in resistance were recorded from the start of the spring (days 1-63). Resistance began to increase from day 64, rising from 1.5 M Ohm to 9.0 M Ohm on day 69. Values remained constant between days 70-137, before resistance rapidly fell back to 1.0 M Ohm (day 137). Minor fluctuations continued to the end of the record.

Case strain showed a series of variations throughout the spring. Strain values rose and gradually increased between days 1-54, before the rate of change increased rapidly (days 55-65). This slowed between days 65-125, then displayed a final increase in the rate of change (days 127-133), before a greater change in strain was recorded in the opposite direction (days 133-139). Case strain became relatively constant from day 140 to the end of the record.

The start of the Probe 4 tilt record was marked by a period of considerable variation along all three axes (Figure 7.2a). The angle of tilt along the axes changed gradually until day 11 when rapid, highly oscillating, variations began (days 11-17). These fluctuations were followed by more consistent changes in tilt, punctuated by two sudden 'shift' events, on days 51 and 138. In between these shifts, tilt was relatively stable.

7.2.2 Probe 8

The spring sensor records for Probe 8 are displayed in Figure 7.1b and 7.2b. The variations in probe temperature are best displayed by the average weekly values, which had begun to fall from the start of the record. The rate of decline increased

from day 18, reaching values of 0.13°C on day 31. Average temperatures then increased rapidly, from day 35, to 0.15°C (day 39). Temperatures began to decrease from day 40 and the rate of decline was fastest between days 40-49. The rate then slowed and temperatures decreased gradually, until day 101 when values dropped abruptly. Average probe temperatures showed more frequent oscillations from day 106, but continued to show an overall decline to the end of the spring.

Water pressure showed the greatest variation of all the sensors (Figure 7.1b). At the start of the spring fluctuations in water pressure were low with base levels between 6.4-9.0%. Water pressures began to show significant variations from day 20, when pressures rose to 89.3% (day 36). On day 36, water pressure fell abruptly, with values close to winter base levels (9.1%). Low and constant water pressure was maintained for 8 days, until values rose suddenly on day 43, to 58.3%. Water pressure increased gradually accompanied by some oscillations between days 43-77. Pressure then increased again abruptly, rising to 173.4% between days 77-110. Water pressure then remained elevated above 171.4 %, showing minor oscillations for the rest of the spring record (days 110-120). No diurnal variations in pressure were evident throughout the spring period.

The Probe 8 resistance record remained relatively constant at 9.3 M Ohm. Values showed a slight increase to 10.9 M Ohm between days 36-39, and a more prolonged decline in values to 2.9 M Ohm between days 86-109. Values then returned to 9.4 M Ohm for the remainder of the spring. The rate of change along the tilt axes increased throughout the spring, although there were few fluctuations (Figure 7.2b). Tilt on the x and y axes increased in the same direction between days 1-96. Tilt on the y-axis then changed direction (day 97), as angles continued to increase for the rest of the spring. Tilt remained constant in the z direction (days 1-120).

7.3 Interpretation: Event 1

The sensor record for Probe 8 will be discussed in terms of the two separate events, which became apparent within the sensor readings during the spring: Event 1 and Event 2. These phases are outlined in Figure 7.3. Event 1 encompasses the period

between days 20-42, whilst Event 2 comprises days 43-120. Similarly, Probe 4 recorded an initial period of minimal activity, followed by a second phase of heightened activity (Figure 7.3). Probe 8 will be discussed first to determine the processes operating within the till. The activity recorded by Probe 4, within the ice column, will then be considered with respect to the activity within the subglacial environment.

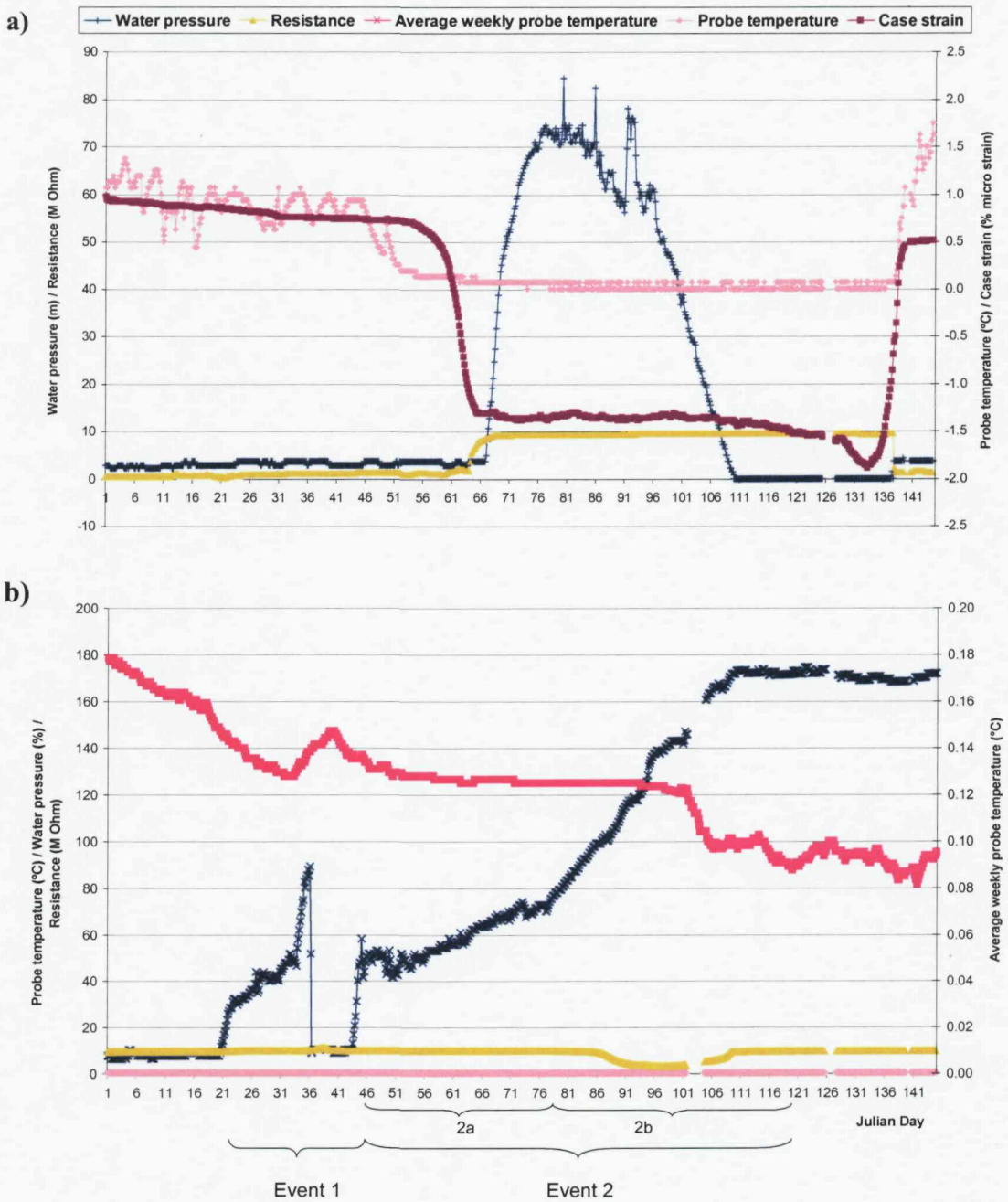


Figure 7.3: Comparison of spring sensor records according to Events 1 and 2 (days 20-42 and 43-120, respectively) for: a) Probe 4; and b) the Probe 8 (2004/5). Note: the subdivision of Event 2 into Events 2a and b (days 43-76 and 77-120, respectively).

7.3.1 Triggers

The oscillations in water pressure and resistance recorded by Probe 8 during the spring must result from a fresh influx of melt water into the subglacial hydrological system after the winter. As such, the oscillations in these sensor readings are considered with respect to external weather conditions, in order to identify conditions that would generate melt water inputs into the subglacial environment (Figure 7.4). The nature of the external weather conditions at the end of December was very conducive to melt water production. Numerous precipitation events were recorded (days 1-19) and temperatures were elevated reaching up to 8.6°C. Thus, it was unusual that a corresponding rise in water pressure was not recorded until day 20 (Figure 7.4).

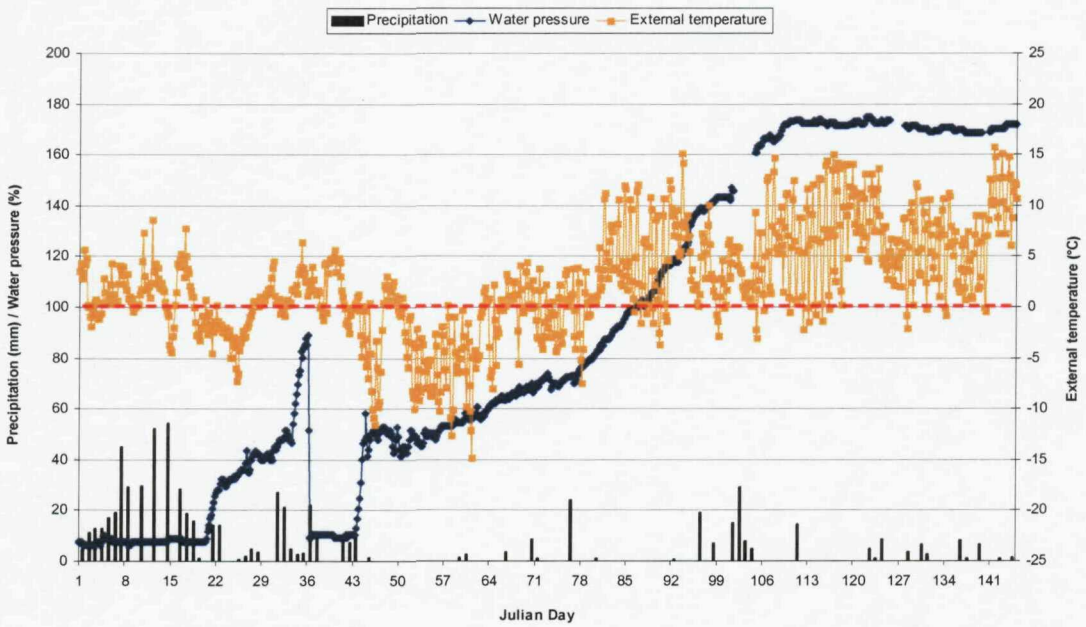


Figure 7.4: Spring record for: external weather conditions and Probe 8 water pressure (2004/5).

During the spring, lags in pressure response, greater than a few hours to a day, have not been reported. However, it is unlikely that melt water was not produced between days 1-19. Consistently elevated temperatures would generate melt and allow the snow pack, which is present at this time of year, to become isothermal (0°C). Once isothermal, melt water can move freely within the pack, enabling it to access the glacier bed (Harper *et al.*, 2005). In addition, the fact that temperatures were

elevated during the night would prevent refreezing and allow continued surface melt. Precipitation events would also add to and aid melt water production. The lack of response in water pressure suggests that: the melt water was being kept in storage at the bed, in the snow pack, or within crevasses; or that the melt water input did not exceed the drainage capacity of the winter drainage system; or that Probe 8 was located in an unconnected region of the bed, as suggested by the winter sensor readings (Chapter 6).

The small pressure rises (<4%) recorded during this time (days 1-19) suggest that melt water was reaching the glacier bed rather than being held in storage (Figure 7.4). The small-scale of these fluctuations might suggest that the drainage capacity of the bed was not exceeded by the melt water input(s). However, the degree of temperature elevation, in combination with the amount of precipitation recorded, would suggest that there was a large input of melt water into the subglacial environment over this time. As a result, it would be unusual for the capacity of a poorly developed winter drainage system not to be exceeded. However, if Probe 8 was located in an unconnected region of the bed; the small pressure fluctuations may reflect the probe's response to much larger changes in water pressure, occurring in nearby connected regions of the bed. This may have occurred if the capacity of the connected system was exceeded causing excess flows to be transferred to unconnected regions of the bed. This is highly probable given the time of year, as the capacity of the winter drainage system would be constrained (Willis *et al.*, 1990). This marks the start of increased flows through the subglacial environment and highlights the complexity of the relationship between external conditions and the glacier system.

In light of these conclusions, the sudden rise in pressure on day 20, marking the start of Event 1 was not directly associated with the weather conditions of days 1-17. Instead, it was triggered in response to a sudden lowering of external temperatures from day 18 (Figure 7.4). This caused the toe of the glacier to become frozen to its bed, and/or subglacial winter drainage routes to become narrowed or frozen shut. Flow pathways can become constricted when reduced ambient temperatures exceed the ability of low winter water volumes to maintain conduits through frictional melting (Benn and Evans, 1996; Fountain and Walder, 1998). This would be

particularly effective following a period of high melt water, which would have begun to develop and expand flow pathways in the connected regions of the bed. Subglacial cooling could reduce the capacity of connected drainage routes and potentially block water outflow into the lake. Base flows would then build up at the ice-bed interface, producing a pressure rise within the till from day 20. This idea is supported by previous evidence within the probe record (section 6.8.2, Chapter 6). The lack of significant fluctuations in the tilt record suggests that the probe was constrained within the deforming bed. This prevented significant oscillation in response to changes in water pressure. In the winter record, the period between days 316-319 was characterised by significant precipitation and warm temperatures (>10°C). However, a response in pressure only occurred following a sudden temperature drop (days 324-328). Again, this implies that a response in pressure was only seen when drainage pathways elsewhere at the bed were closed or reduced in capacity.

The stable conditions recorded by Probe 4 during Event 1, might be expected from a probe located within the ice at the end of the winter (Figure 7.3a). The glacier was still covered in snow and ice velocities are presumed to be low at this point. Positioned within a relatively enclosed environment it would take longer for the englacial probe to respond to changes in external conditions.

7.3.2 Subglacial processes

Probe 8 recorded a decline in average probe temperatures from day 2, shortly after small-scale fluctuations in water pressure had begun. This implies that melt water had begun to enter the till and cause cooling (Figure 7.3b), indicating activity within the subglacial environment was becoming re-established. The pattern of small pressure rises recorded by Probe 8 (days 1-19) indicates that free melt water was gradually beginning to mobilise within this region, prior to the pressure peak. The relationship between probe temperature and water pressure is highlighted by the rapid fall in average probe temperature that compliments the rise in pressure during Event 1 (Figure 7.3b). Temperatures reached a minimum in unison with the final pressure peak, confirming the presence of cold melt water within the till.

The sudden drop in pressure on day 36 signifies the expansion of connected drainage pathways. Elevated temperatures enabled drainage pathways within the till to expand (Fountain and Walder, 1998), and allowed melt water to drain freely from the bed (Figure 7.4). A sudden increase in probe temperature occurred as pressures fell, reflecting warmer conditions within the till as the build up of melt water was removed. This activity was also accompanied by a slight increase in resistance (days 36-40), reflecting relatively drier conditions (Figure 7.3b). The sudden purge of water as drainage pathways opened could cause the till to become relatively 'dry'. Resistance could also increase as the sudden loss of water flow decreased the conductivity of this area of the bed (Gordon *et al.*, 2001).

The Probe 8 tilt record showed only a gradual change during Event 1 (Figure 7.2b). The angle of tilt along the x and y axes continued to increase gradually, showing a slight change in orientation within the till. This low rate of activity is in keeping with the minimal sensor activity that had been evident during the winter and the start of the spring. The response of the other sensors during this time demonstrates that there is considerable activity within the till much earlier in the year than perhaps previously thought.

7.3.3 Englacial processes

The Probe 4 sensors recorded little activity at the start of the year (Figure 7.3a). The absence of activity between days 1-44 indicates that the englacial environment was still relatively dormant. This suggests that rates of ice deformation, and thus glacier velocities, were low during this time. Despite this, the decrease in probe temperature does suggest an increase in englacial melt water was causing a decrease in temperature. This might occur if water was entering the borehole from the snow pack, which had become isothermal, as indicated by external weather conditions (Figure 7.4). The small-scale fluctuations in water pressure during this time may reflect such surface inputs. Correspondingly, resistance remained low, indicating the presence of melt water within the englacial cavity. The gradual change in case strain between days 1-44 also indicates slowly changing conditions within the ice column.

In contrast, the tilt record showed continuous activity throughout the start of the spring (Figure 7.2a). These oscillations appear to be highly unusual, given the lack of other sensor activity. Significant changes in the ice column would not be expected so early in the year, as glacier velocities and the rate of ice deformation should be at their lowest. The fluctuations in probe temperature and water pressure, in combination with the tilt record, might suggest that the probe was responding to changes in external conditions. However, why this might cause the position of the probe to fluctuate is uncertain. Numerous precipitation events were recorded during this time and temperatures were elevated. Thus, the fluctuations of the probe orientation might be associated with melt water inputs.

7.4 Interpretation: Event 2

Event 2 occurred between days 43-120 when the Probe 8 sensor record was characterised by greater activity in water pressure. This event has been subdivided further into Event 2a (days 43-76) and Event 2b (days 77-120) (Figure 7.3b). These phases mark a change in the rate and nature of water pressure accumulation during the spring. The Probe 4 record also showed greater sensor activity later in the spring (days 45-144).

7.4.1 Triggers

The trigger for the initial Probe 8 pressure rise recorded in Event 2 was unclear. A decline in external temperatures may have contributed to the rise, in a similar fashion to Event 1 (Figure 7.4). However, temperatures were not overly low during this period (-2.5°C to 1.3°C). The rise in pressure was also too sudden and of a magnitude too great (58.3%) to be the result of a -2.5°C drop in temperature one day prior to the event. Instead, this pressure rise could be the result of a long term change within the small-scale variations in external temperature. The winter months were characterised by either increasing or decreasing temperature trends that oscillated with a frequency of days. Towards the summer months, temperature fluctuations increased in frequency, varying over hours, and moving closer to a diurnal signature of temperature variation that is characteristic of the summer months. This change becomes evident in the temperature record from day 43 (Figure

7.4). Temperatures also began to rise from day 64, fluctuating above and below 0°C. In addition, there was a large increase in average daily temperatures from day 79, with values dominantly remaining above 0°C (Figure 7.4).

The increase in the number of sun hours and the enhanced frequency of temperature oscillations could generate sufficient melt water to drive Event 2. These factors will both increase melt at the glacier surface and may cause the snow pack to become isothermal more frequently. This process would also become more effective from day 79, when average daily temperatures increased above 0°C (Figure 7.4). This may have resulted in the accelerated pressure rise that marks the start of Event 2b (day 77; Figure 7.3b). As average external temperatures increased a more continuous supply of melt water to the glacier bed would allow the increase in water pressure recorded in Event 2b to be sustained.

An alternative trigger to Event 2a (day 43) is the sudden release of a water body. This could occur if a water-filled crevasse connected with the glacier bed, or flow behind the ice fall mobilised. As ambient temperatures and sun hours increase towards the summer, crevasses across the glacier are likely to become connected with the bed, particularly if the amount of melt water produced is rising. The linking of crevasses with the bed would suddenly release a large storage of melt water and/or provide another route for melt water to the glacier bed.

Similarly, as the number of sun hours increases, so too will the duration of light hitting the ice fall. The path of the sun at Briksdalsbreen tracks up the valley, moving from the glacier terminus to the accumulation zone (west to east). The increase in sun hours between January and February may be sufficient to lubricate the ice fall. The sudden rise in pressure could represent the ice fall 'opening up', initiating drainage pathways from the ice above down to the glacier terminus. Unfortunately, these hypotheses cannot be verified, so the trigger for Event 2a remains vague. However, high pressure events initiated by the evacuation of water from crevasses into the subglacial drainage system, have been recorded in the literature (e.g. Mair *et al.*, 2001; Harper *et al.*, 2005).

7.4.2 Triggers: Probe 4

The sensor activity recorded by Probe 4 generally began to increase from day 45 (Figure 7.3a). This correlated with the change in external weather conditions recorded from day 43. These sensor variations mark the start of enhanced glacier activity, which implies that the glacier has begun to transition from a dormant winter regime. The pressure rise recorded by Probe 4 (day 67) occurred as external temperatures had begun to rise above 0°C (day 64). Enclosed within the ice the source of melt water may have resulted from water movement through the snow pack, in response to an increase in ambient temperatures. Alternatively, a new englacial channel may have developed since probe deployment, when none were visible on the BoreCam.

7.4.3 Subglacial processes

Similar to Event 1, average weekly probe temperature fell as pressure rose during Event 2a, reflecting the influx of melt water into the till (Figure 7.3b). As pressure gradually increased, following the initial rapid peak on day 43, the rate of reduction in probe temperature diminished. Probe temperature became more constant, indicating an equilibrium with the amount of water in the till. This suggests that the rate of water transfer within the till had become well established, perhaps constant, and that there was only a gradual decrease in temperature as water pressure built up.

This pattern changed from day 101 when temperatures fell at a faster rate and began to show much greater variability (Figure 7.3b). This followed the start of Event 2b (day 77), when water pressure began to increase more rapidly and eventually exceeded overburden pressure (day 86). The sudden drop in probe temperature suggests that as more water, or a sudden input of water, entered the system, the equilibrium between water pressure and probe temperature was exceeded. The quantity of water within the till was obviously sufficient to cause a sudden and more rapid drop in temperature. The decline in resistance (days 86-109) as pressure exceeded overburden, indicated wet conditions within the till. Prior to this, resistance had remained constant, despite fluctuations in pressure. This change highlights the enhanced magnitude of water passing through the system at this time.

Probe 8 temperatures continued to oscillate and decline gradually as water pressures remained high.

Located in an unconnected region, Probe 8 showed a significant response in water pressure, as values increased sufficiently to exceed overburden in this area of the bed. This response may reflect the proximity of Probe 8 to a subglacial drainage route. This also signifies that drainage routes within the till around Probe 8 had developed sufficiently to allow this capacity of melt water to be transferred. The continued increase in pressure at this time suggests that the supply of water was increasing towards peak summer discharge values. The fact that water pressure was sustained following the pressure rise might indicate a combination of well developed drainage, as well as a plentiful source of melt water.

The lack of diurnal oscillations and general large-scale variations within this event confirms that Probe 8 was in an unconnected region. However, the magnitude of this event suggests that large quantities of water were following through this area of the bed. Water is captured by connected drainage routes as subglacial water flows from high pressures in the till to low pressures within a hydraulically efficient drainage pathway (Fountain and Walder, 1998). It is possible that water was being drawn from areas around Probe 8, past its location and to a nearby drainage route, creating a strong hydraulic gradient (Murray and Clarke, 1995), and resulting in the high pressure observed. This verifies this area as an *active* unconnected region of the bed.

The rate of change in the angle of tilt along the x and y axes increased further during Event 2 (Figure 7.2b). This suggests that activity within the subglacial environment was increasing, in keeping with the other sensor readings. Consistent variations signify that the probe was constrained within the till. The change in x and y tilt in opposite directions suggests that the probe was gradually moving orientation within the till. At the ice-bed interface, or within a borehole, it is more likely that the probe would show significant oscillations in response to such pressure variations.

7.4.4 Englacial processes

The period between days 45-144 recorded significant activity in the Probe 4 sensor readings. Probe temperature, case strain and resistance all showed sudden activity just prior to water pressure (Figure 7.3a). Water pressure increased suddenly on day 67 and elevated pressures were sustained until day 110. However, resistance showed an increase in values prior to the increase in water pressure. This would suggest that conditions within the borehole were dry, contradicting the rise in water pressure recorded. Probe temperature decreased rapidly (day 45) following a decline in external temperatures and a prolonged period of cooling (days 44-63) (Figure 7.3a). The reduction in probe temperature signifies the introduction of melt water reflects a period of external cooling and is in good agreement with the rise in water pressure that followed.

The sudden change in case strain suggests that the location of the probe had changed and/or that force was being applied from a different direction (Figure 7.3a). The latter implies that the borehole had changed shape through ice deformation. This indicates an increase in the rate of ice movement or deformation and activity within the glacier, which could imply an increase in glacier velocities, occurring as early as March. The rise in case strain might also occur in response to the increase in pressure, which may have caused the location of the probe to change, or affect the forces acting on it within a confined space. Probe temperature, case strain and water pressure all suggest that there was an influx of melt water into the borehole cavity. This water input may have been derived from the snow pack above or the opening of an englacial cavity.

As a result, the rise in resistance is an anomaly (Figure 7.3a). Elevated resistance may indicate that the probe had become frozen within the englacial environment but probe temperatures continued to fluctuate between 0-1°C. The rise in resistance can only be explained if the sensor was measuring the dilution of the mineral content of the water already present within the borehole. This would result in an increase in resistance (decrease in conductivity) as the ions in solution are diluted by the influx of melt water recorded by the pressure rise (Gordon *et al.*, 2001).

In terms of probe movement, there was a sudden shift in position on day 51 (Figure 7.2a). The direction of applied case strain changed rapidly (days 55-65), which may have been in response to the shift in probe location between days 51-53. There was only gradual change in tilt, with some small-scale oscillations, after day 53. This may well indicate that the probe had become lodged, in keeping with the increase in case strain. This would also explain the lack of motion in response to the rise in water pressure, in contrast to the rapid oscillations recorded at the start of the spring.

7.4.5 Probe failure

The Probe 4 record ceased on day 144, when probe temperature and case strain were increasing. Although, case strain had begun to plateau, another sudden shift in probe location at the end of the record (Figure 7.2b) may have been a precursor to another increase in case strain. These sudden movements may have caused the probe's seal to fail in response to crushing within the ice column. A water leak could damage the probe's circuitry and cause it to fail. Alternatively, the base station may simply have lost communication with the probe. It is difficult to determine from current records the precise cause for failure.

7.5 2005/6

Probes 10, 12 and 15 were still operational throughout the spring (days 1-120; Figures 7.5 and 7.6). Probes 10 and 12 showed similar activity, whilst Probe 15 recorded much more varied and large-scale fluctuations. Probe 15 was the first to show a variation in water pressure, which actually occurred on day 355, prior to the start of the spring (day 1). This oscillation is associated with the spring pressure fluctuations that followed, as indicated in Chapter 6. As a result, the spring sensor records are displayed from day 345 to encompass this.

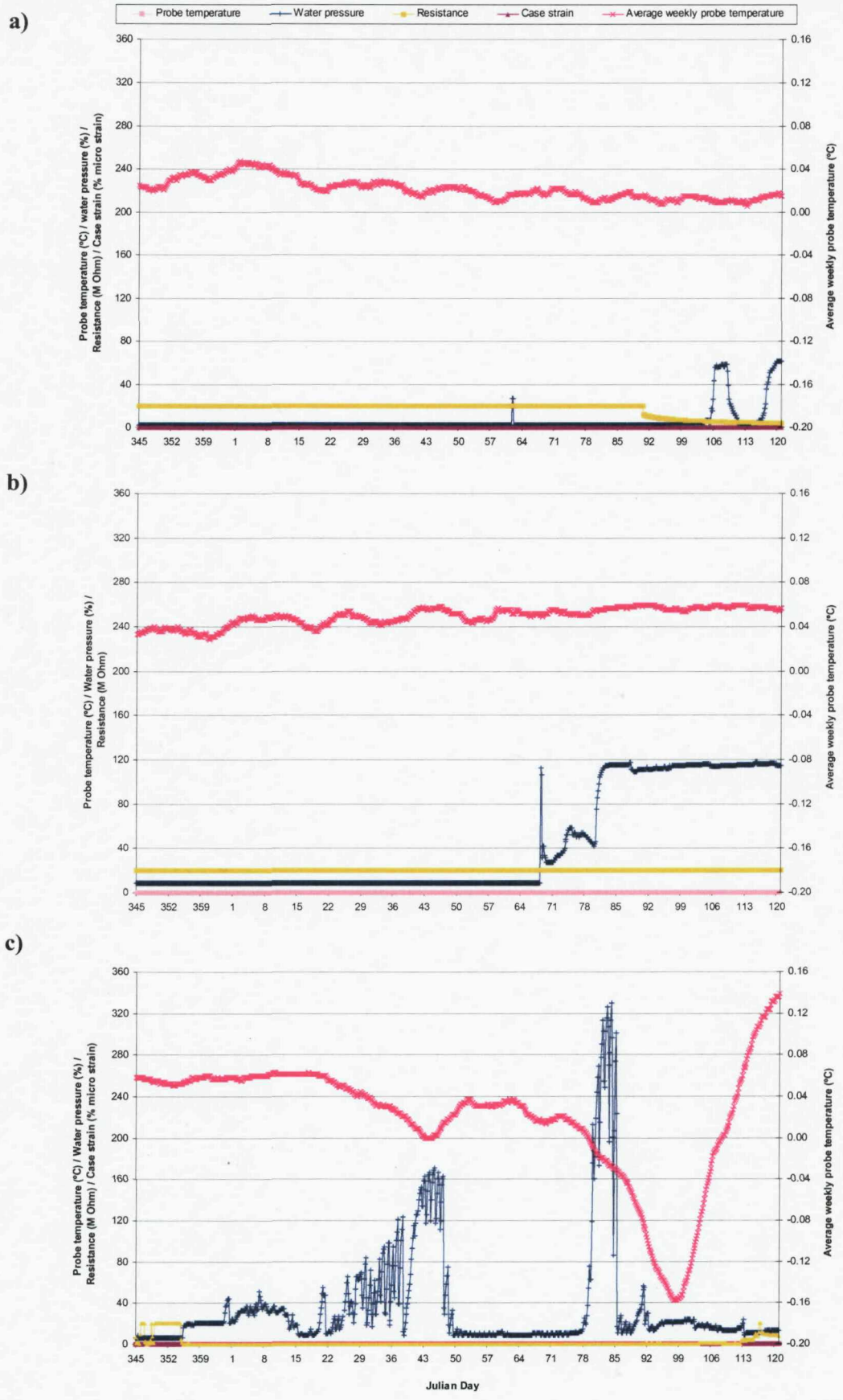


Figure 7.5: Comparison of spring sensor records, showing probe temperature, water pressure, resistance, case strain and average weekly probe temperature for: a) Probe 10; b) Probe 12; and c) Probe 15 (2005/6).

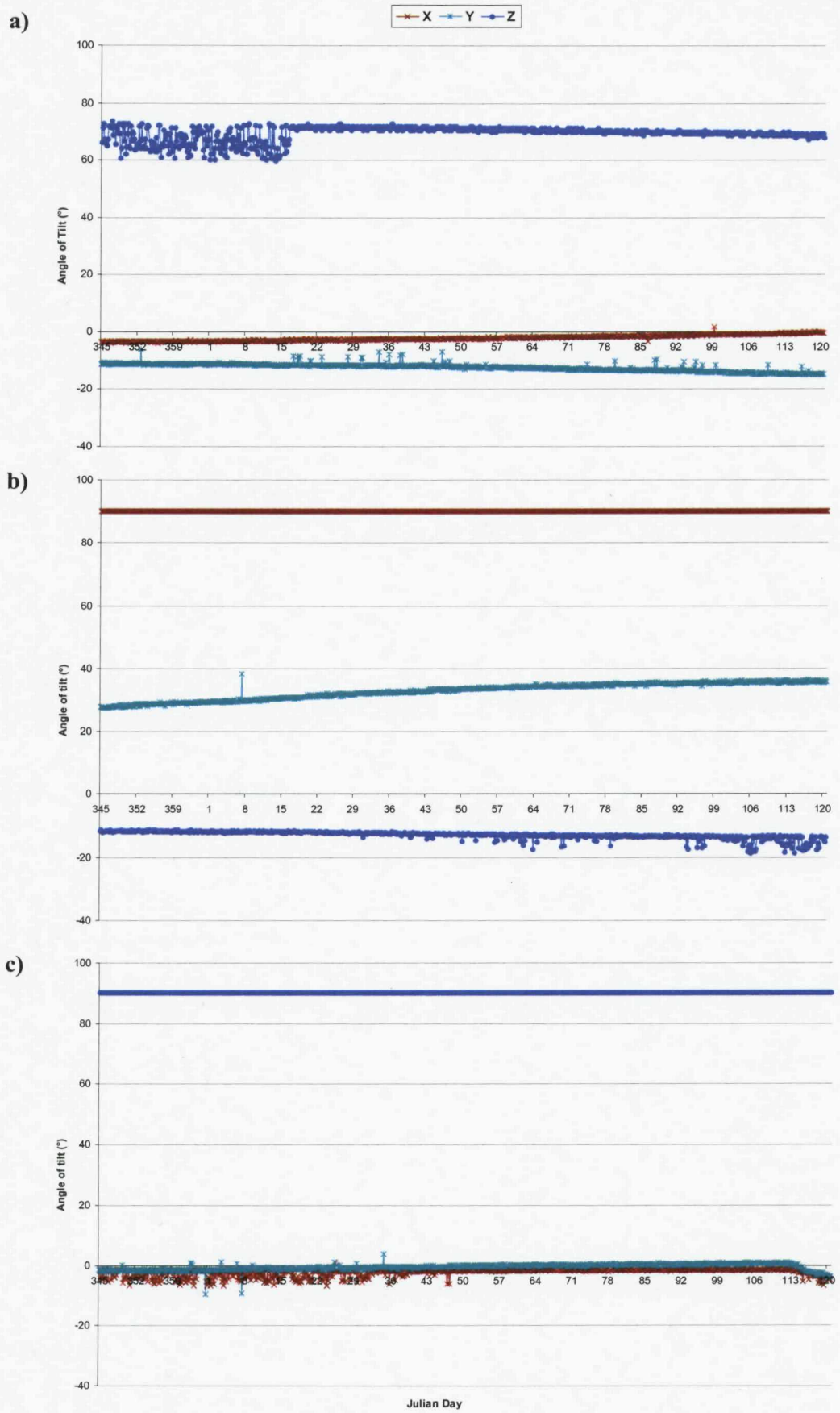


Figure 7.6: Comparison of spring tilt sensor records for: a) Probe 10; b) Probe 12; and c) Probe 15 (2005/6).

7.5.1 Probe 10

Probe 10 recorded relatively little sensor activity during the spring (Figures 7.5 and 7.6). The variations in probe temperature were best displayed by average weekly values, which showed continual fluctuation throughout the spring (Figure 7.5a). There was an overall decline in average temperatures from 0.05-0.01°C (days 1-120). Water pressure remained low at 2.0% (days 1-96), although there was a peak to 26.9% on day 61. Pressure increased slightly to 4.3% (days 97-105), followed by a sudden increase in pressure (day 105) to 58.3% (day 108). Values decreased to 2.2% between days 109-111. Water pressure rose again on day 115, reaching 61.6% by day 120. Resistance remained constant at 20.2 M Ohm between days 1-89. Values then fell abruptly from day 90, reaching values of 4.3 M Ohm by day 120. Case strain showed a variety of small-scale oscillations during the spring (Figure 7.7a).

There was some variation in the Probe 10 tilt record throughout the spring (Figure 7.6a). The angle of tilt on the x and y axes increased gradually in opposite directions. Tilt along the z-axis fluctuated at the start of spring, between days 1-16. Oscillations then decreased and showed a gradual change in tilt for the rest of the spring. The rate of change on the y-axis increased steadily throughout the spring from 0.02-0.05° day^{-1}. However, on the x-axis this rate decreased over the spring.

7.5.2 Probe 12

The spring record for Probe 12 is displayed in Figures 7.5 and 7.6. Average weekly probe temperatures fluctuated throughout spring (Figure 7.5b). Oscillations decreased in amplitude and values showed an overall increase from 0.04-0.06°C (days 1-120). Water pressure remained low (8.1-8.3%) between days 1-67. Values then rose suddenly, peaking at 112.0% (day 68). Pressure fell to 27.0% on day 69, before increasing again to 58.3% (day 75). Again, values fell, reaching 41.7% on day 80, before a final increase to 114.8% on day 82. Values then displayed minor fluctuations between 108.8-117.8%. Resistance remained constant throughout at 20.2 M Ohm.

There was steady change, but only relatively minor fluctuations, in the Probe 12 tilt record (Figure 7.6b). Tilt on the x-axis remained constant throughout the spring.

The z and y axes showed gradual change in tilt in opposite directions, accompanied by minor oscillations, particularly along the z-axis. At the end of spring, the rate of change in tilt decreased from 0.02-0.01° day^{-1} on the z-axis, and 0.07-0.03° day^{-1} on the y-axis.

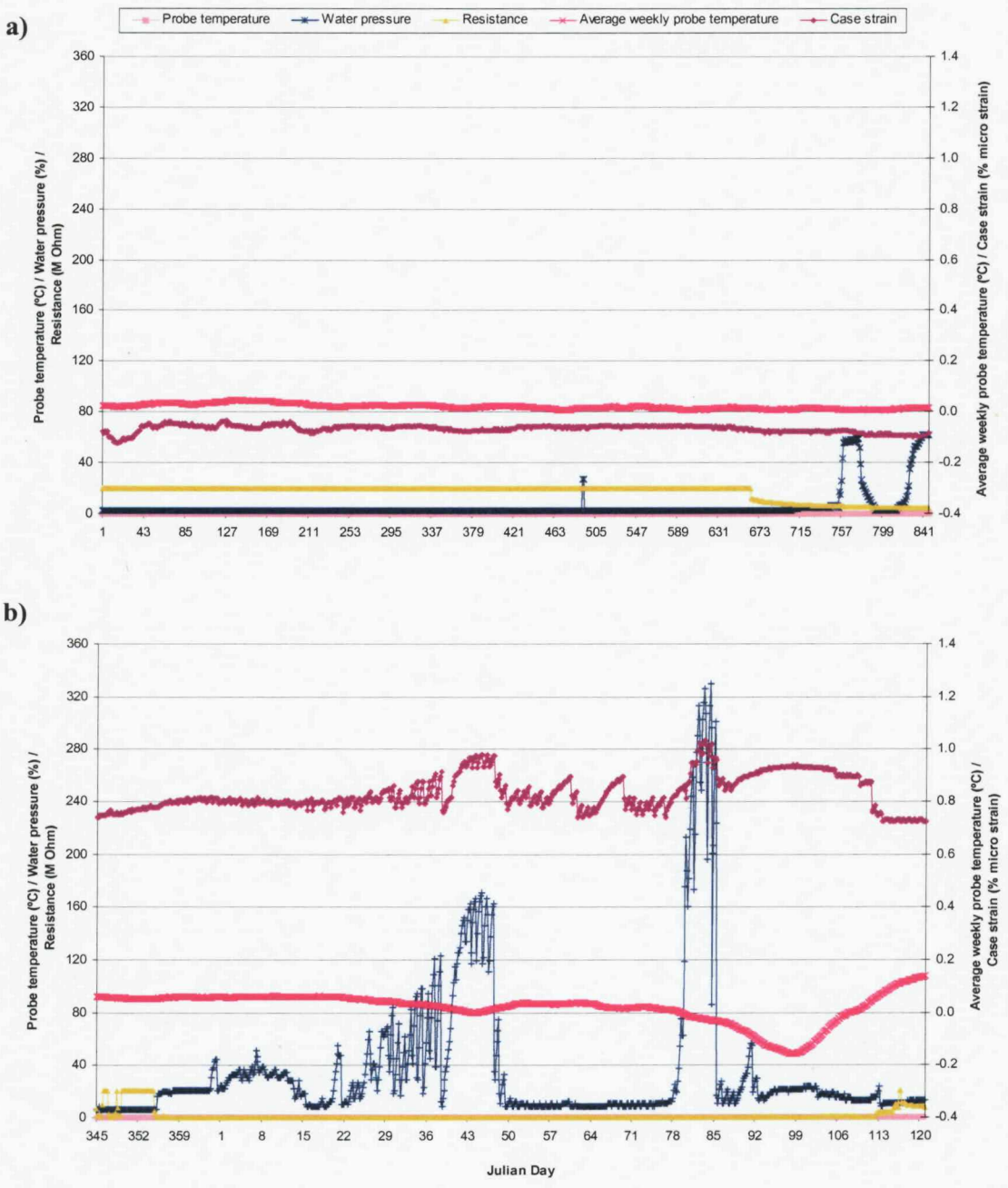


Figure 7.7: Spring sensor record highlighting fluctuations in case strain for: a) Probe 10; and b) Probe 15 (2005/6).

7.5.3 Probe 15

Probe 15 displayed the greatest sensor activity during the spring (Figures 7.5 and 7.6). Average weekly probe temperatures fluctuated between 0.05-0.06°C (Figure 7.5c). Values began to show a gradual decline between days 19-43, before increasing to 0.04°C on day 52, with gentle fluctuations. A second decline in average probe temperatures occurred on day 66. Values decreased to -0.2°C (day 97), before rising again from day 99. Average probe temperatures reached 0.1°C by day 120. Probe 15 was the first probe to show a response in water pressure on day 355. Pressure rose from base levels (6.0%) reaching 20.1 % on day 356. This was sustained (days 355-364), until a pressure peak (44.4 %) was recorded (days 364-365). Water pressure then began to show greater frequency fluctuations. Values increased gradually between days 365 to 7, reaching 50.6%, before falling back to base levels (days 7-15).

The next short lived peak in pressure occurred on day 21 (55.0%) and was closely followed by diurnal fluctuations in pressure (days 23-38). The diurnal fluctuations recorded peaks at 08.00 and minima at 16.00 hours. The fluctuations also increased in amplitude and magnitude during this time, with values exceeding overburden between days 37-38. Pressures returned to base levels on day 38 for a few hours, before increasing again suddenly. Values exceeded overburden on day 40 and recorded a peak pressure of 170.6% (day 45). Diurnal fluctuations above and below overburden pressure continued between days 42-46. On day 47 values fell rapidly below overburden, until day 50, when they returned to base values. Diurnal oscillations continued throughout this time (days 42-58), even when base level flows (8-10%) were re-established. This pattern ceased between days 59-66, but was reinstated from day 67.

Water pressure began to increase above base pressure values on day 77 and saw a sudden, rapid rise in values on day 78. Pressures exceeded overburden (day 79) and rose to 212.6% on day 80. Diurnal fluctuations continued as pressures rose further (days 80-85). Values reached a maximum of 329.9% on day 84. Pressure fell as quickly as it had risen, returning to base levels (10.4%) on day 85. The diurnal fluctuations continued until day 89 when a relatively small-scale (56.6%) pressure peak was recorded (days 89-91). This was followed by a series of small-scale

pressure fluctuations (days 92-120) and an overall decline in values towards the end of the spring. Resistance showed a series of fluctuations deviating from 20.2 M Ohm between days 345-349. Values then remained constant at 20.2 M Ohm until day 354, when readings again fell close to 0 M Ohm. These readings were sustained until day 103 when resistance began to fluctuate again. The amplitude of oscillations increased from day 112, with an overall increase in values to 9 M Ohm (day 120).

Probe 15 case strain increased gradually at the start of the spring (Figure 7.7b). Diurnal fluctuations were evident from day 1, but began to increase in amplitude from day 15, mimicking those in water pressure. Values decreased suddenly on day 38, before increasing again and continuing to fluctuate between days 38-47. Values decreased and recorded a series of 'saw tooth' fluctuations (days 48-77). Case strain increased again between days 78-85, as oscillations and diurnal fluctuations continued throughout this time. This pattern changed on day 85 when values fell, and then increased gradually (day 86), with much fewer oscillations. A gradual decrease in strain occurred from day 101, followed by a sudden step decline in values on day 111. Minimum values were achieved on day 113 and sustained for the remainder of the spring.

The Probe 15 tilt data presented relatively little activity for the majority of the spring (Figure 7.6c). Variations along the x and y axes appeared to be similar. Small-scale oscillations were recorded between days 1-47. The changes in tilt then stabilised until days 113 and 115, when tilt began to increase in the same direction along the x and y axes, respectively. The rate of change in tilt was 1-0.5° day^{-1} during this period (days 113/115-120). Tilt on the z-axis remained consistent throughout.

7.6 Interpretation: Event 1

The probes displayed two separate events during the spring period. As a result, similar to the 2004/5 probes, the sensor records are divided into Events 1 and 2. These events were determined according to the water pressure records for Probes 10, 12 and 15, as displayed in Figure 7.8. Event 1 comprised the period between days 355-51, whilst Event 2 encompasses days 52-120. Probes 10 and 12 did not show

any significant activity during Event 1 (Figure 7.5b, c; Figure 7.8). As a result, only the Probe 15 sensor record is discussed in detail within this first section.

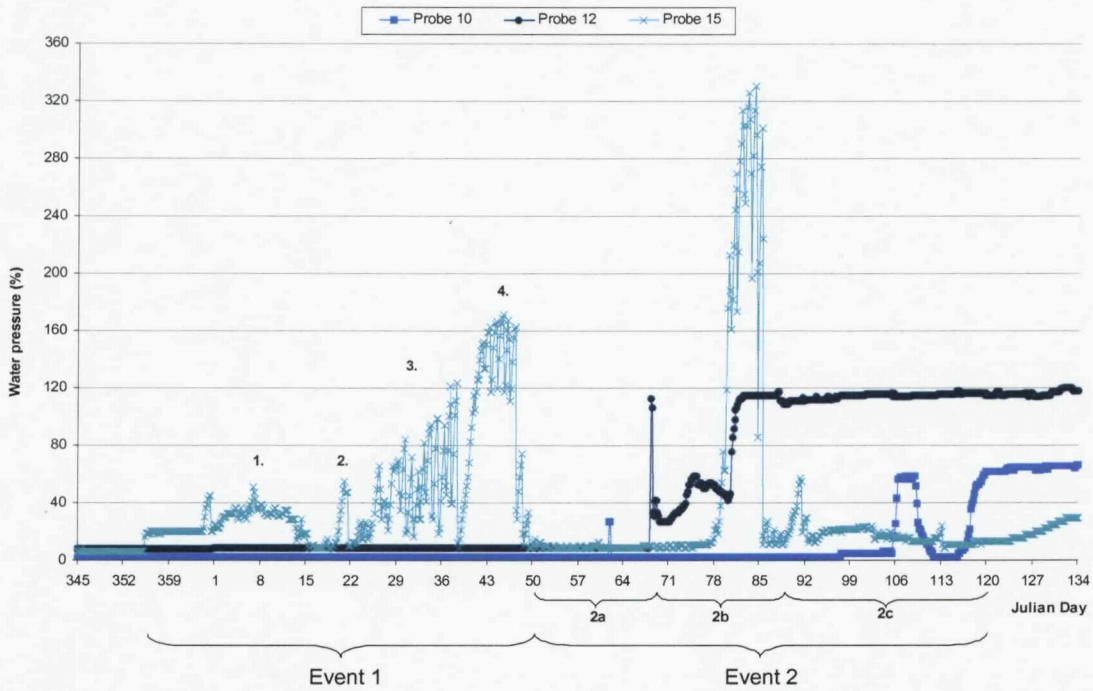


Figure 7.8: Comparison of spring water pressure records, displaying the timing of Events 1 and 2 (days 355-51 and 52-120, respectively), for Probes 10, 12 and 15 (2005/6). Note: the Probe 15 pressure peaks of Event 1 have been labelled 1-4 to aid identification; Event 2 has been subdivided into Events 2a, 2b and 2c (days 52-69, 70-88 and 89-120, respectively).

7.6.1 Triggers

On first inspection there appeared to be little correlation with water pressure and external weather conditions (Figure 7.9). This might be expected given that the winter record implied Probe 15 was located in an unconnected region of the bed. However, resistance began to fluctuate from day 345, between wet (0.4 M Ohm) and dry (20.2 M Ohm) conditions. Each peak corresponded with elevated temperatures and precipitation peaks in the weather record (Figure 7.9; Table 7.1). This implies that short pulses of water (lasting ~24 hours) were passing through the till. These pulses increased in duration until resistance dropped permanently on day 355.

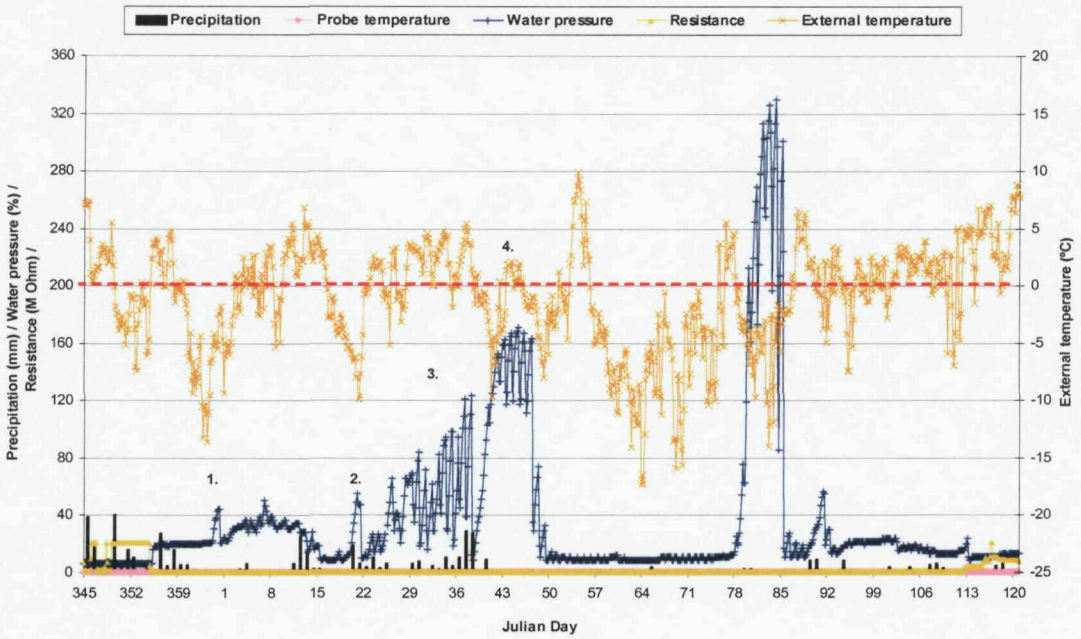


Figure 7.9: Comparison of spring external weather conditions and Probe 15 sensor readings for water pressure and resistance (2005/6). Note: the dashed red line marks 0°C; the Event 1 pressure peaks have been labelled 1-4 to ease identification.

Table 7.1: Data displaying the correlation between decreases in resistance and temperature and precipitation peaks prior to the spring. Day 355 represents the final fall in resistance, which remained low for the remainder of the spring record.

Drop in Resistance (Julian Day)	Temperature Peak (°C)	Precipitation (mm)
345	7.3	39.1
347	3.6	1.5
355	4.1	1.1

The fluctuations in resistance indicate a gradual build up of activity within the till at the end of the winter record, signifying a transition from stable winter to active spring conditions. A small rise in pressure (8.0%) from base flows (6.0%) was also recorded on day 345, corroborating this idea. This supports the idea that resistance is more sensitive to changes in water content within the subglacial environment than the pressure sensor. This activity suggests that free water had become available at the bed, resulting from temperature peaks and numerous precipitation events that occurred over this time. Precipitation may be a key factor at this time of year, not only adding water to the system but also, generating excess water through surface contact melt. This may be a critical process, which can account for the occurrence of

pressure oscillations in December and January, when temperatures were still oscillating above and below freezing.

The first small rise in water pressure (1) on day 355 was driven by a temperature peak (4.1°C) and a series of precipitation events (Figure 7.9; Table 7.1). These events generated sufficient melt water to cause a rise in pressure within the till. The reduction in temperature to -13.7°C (day 363) initiated the small pressure peak on day 364. This extreme drop in temperature would have caused a reduction in the capacity of drainage pathways and/or caused the glacier toe to become frozen, resulting in a build up of pressure within the till. This peak was short lived, as temperatures quickly began to rise again. Night time temperatures remained above 0°C from day 10, causing pressures to decrease to base levels. At this time of year, prolonged temperatures above 0°C would allow drainage pathways to redevelop (Fountain and Walder, 1998).

The next short lived pressure peak (2) on day 21 occurred in response to falling temperatures (-10°C) and a series of precipitation events (Figure 7.9). Again, pressures increased as drainage pathways became constricted and was relieved as temperatures rose again. Elevated and oscillating external temperatures (day 23), accompanied by daily precipitation events, resulted in the next pressure rise (3). This was characterised by a progressive increase in average daily pressures and diurnal oscillations (Figure 7.9). Pressure returned to base levels on day 38, but a large precipitation event (27.3 mm), followed by a decrease in temperatures (-1.6°C), caused pressure to rise again rapidly in the final peak (4). The diurnal oscillations that characterised the pressure fluctuations from day 23 signified, not only that melt water was generated on a daily basis at the glacier surface, but also that the melt water produced there was reaching the subglacial hydrological system. It was unusual to observe such activity so early in the year.

7.6.2 Subglacial processes

The response of water pressure to the changes in external weather conditions detailed above suggests that the till had become 'active'. The sensor readings display a gradual transformation of processes within the till. Activity increased from short

term drops in resistance and small rises in pressure (days 345-22), to diurnal oscillations and pressures exceeding overburden (days 23-51). The response in water pressure increased in accordance with precipitation events, elevated external temperatures, and presumably the development of drainage pathways in the till. The pressure peaks that resulted from reduced temperatures indicate that the system in place was still only marginal and highly dependent on melt water supply and ambient temperatures.

The diurnal signal recorded during Event 1 was also significant. It implied that Probe 15 was located in a region connected to the subglacial drainage system. This was in contrast to the winter sensor record that suggested the probe was in an unconnected region (section 6.8.1, Chapter 6). On closer inspection, the diurnal oscillations recorded showed peaks at 08.00 hours and minima at 16.00 hours. The 'normal' pattern of diurnal pressure signals associated with glacial environments is converse to this (Benn and Evans, 1996; Hodge, 1976). The discharge regime of glaciers characteristically record peak flows in the afternoon and low flows at night and in the mornings (Hodge, 1976; Paterson, 1994). This is in response to the cycle of surface melt water generation, which produces a peak in the afternoon in accordance with maximum exposure to solar radiation. The opposite is true for minimum flows. In their record for diurnal pressure variations at the Haut Glacier d'Arolla, Switzerland, Hubbard *et al.* (1995) found troughs between 11.00-12.00 and peaks between 16.00-17.00. However, this was observed in the summer, so a direct comparison may not be entirely applicable.

The inconsistency within the pressure record can be readily explained, by taking into account the observations of Murray and Clarke (1995). The probe pressure record was 180° out of phase with predicted diurnal patterns. This implies that Probe 15 was indeed unconnected from the subglacial drainage system, and that the pressure signal observed was actually the result of 'pressure forcing' from neighbouring connected regions of the bed (Murray and Clarke, 1995). High pressures within connected regions can cause the glacier to become decoupled from its bed through a process of hydraulic jacking. This allows the spatial extent of the connected region to expand in order to accommodate the increase in water inputs. This change relieves the pressure in unconnected regions causing pressure to drop while pressure

is still high in connected regions (Murray and Clarke, 1995). This process results in low pressures in unconnected regions (Probe 15) when there are high pressures in connected regions and vice versa, accounting for the out of phase pressure fluctuations recorded by Probe 15.

At Briksdalsbreen pressure records directly from connected regions of the bed were not observed. This means that F-R plots (Gordon *et al.*, 1998; Murray and Clarke, 1995), which would help to corroborate this theory, cannot be generated. However, based on the documented patterns in the discharge regimes of glaciers and borehole behaviour, the observations of Murray and Clarke (1995) provide a highly applicable explanation for the Probe 15 pressure pattern. Although Probe 15 was unconnected from the subglacial drainage system, the signal still shows that there was a diurnal cycle of melt water production at the glacier surface. This also demonstrates that in some areas of the bed at least, the subglacial drainage system was connected with the glacier surface, enabling it to receive these melt water inputs. Thus, the signal recorded by Probe 15 can be considered as a proxy for the pressure fluctuations occurring within the connected regions of the bed.

The forcing of water pressure into unconnected regions of the bed suggests that the drainage system was in its infancy, as would be expected at that time of year. In the summer, when the drainage system is fully developed this response is the result of high melt water inputs (Murray and Clarke, 1995). However, in the spring this pattern is more likely to be the result of an increased sensitivity to relatively low melt water inputs within a constricted, low capacity drainage system. Minor melt water inputs in the winter could readily exceed the capacity of the connected drainage system, accounting for the forced pressure responses, sometimes in excess of overburden, observed by Probe 15.

The resistance record in combination with water pressure is an important indicator of subglacial conditions (Figure 7.9). The pulses in resistance, prior to Event 1, indicate a gradual change in stable winter conditions, where there is minimal water content in the till. The drop in resistance (day 354) at the start of Event 1, signifies a sustained shift to spring conditions in this area of the bed. The increase in activity in water pressure correlates well with a simultaneous drop in resistance (day 354). These

conditions imply that water had begun to flow within the subglacial environment and at the ice-bed interface more freely, or at a greater volume, and that previously dormant flow pathways within the till were now being exploited (e.g. as Darcian flow; Benn and Evans, 1996). Activity in probe temperature also provides an indication of subglacial water transport at this time. Average weekly probe temperature began to decrease from day 19. Actual values dropped to 0°C (day 40-48) and remained constant during the final large-scale pressure peak (4) of Event 1 (Figure 7.9). This decline in temperatures confirms that a large amount of fresh melt water was being flushed through the till. Average probe temperature went on to increase slightly as pressures returned to base levels.

The record for case strain highlights changes in the mechanical properties of the subglacial environment (Figure 7.7b). The timing of changes in strain corresponded with pressure peaks, indicating that there was a relationship between the two. This suggests a response in the forces acting on the probe with variations in the physical properties (i.e. water content) of the till. This relationship is discussed in more detail in section 7.10. The Probe 15 tilt record showed relatively little activity during the spring (Figure 7.6c). However, frequent small-scale oscillations were observed on the x-axis between days 345-47. These minor oscillations suggest that the probe was responding to the sudden increase in activity within the till.

7.7 Interpretation: Event 2

Event 2 covers the period between days 52-120. This event was subdivided further into Events 2a, 2b and 2c, according to the nature of the sensor fluctuations. These events span days: 52-69; 70-88; and 89-120, respectively (Figure 7.8).

7.7.1 Triggers

7.7.1.1 Event 2a

Event 2a marked a period of relative quiescence for Probes 10, 12 and 15, where correlations with external weather conditions became less clear (Figure 7.8). Temperatures generally remained below 0°C, with the exception of a peak at 9.8°C

(day 54); and precipitation events were infrequent. As external temperatures remained below 0°C, Probe 15 water pressures continued to record small-scale diurnal fluctuations. This activity was only interrupted briefly between days 59-66, when external temperatures were oscillating around -10°C (days 59-64).

Probe 10 recorded a pressure peak of 26.9% (day 61); whilst Probe 12 displayed two, measuring 112% (day 68) and 27% (day 69) (Figure 7.5a, b and 7.8). These occurred just prior to periods of minimum temperature: -14.1°C on day 62 (Probe 10); and -13.6°C (day 68) and -15.9°C on day 69 (Probe 12). These minima in external temperature may have triggered these pressure pulses by reducing the capacity of drainage pathways within the till. The lack of response in Probes 10 and 12 prior to this, suggests that this area of the bed had not been affected by melt water inputs previously. This prolonged period of cooling may have resulted in different or more spatially extensive changes within the subglacial environment. The effects of these changes were also shown by Probe 15, as the diurnal pattern in water pressure ceased during this time.

7.7.1.2 Event 2b

Probe 10 did not show any sensor variations during Event 2b (days 70-81). However, the Probe 12 pressure record was characterised by a peak-trough-peak sequence (Figure 7.8). The first peak in this sequence (day 75) occurred as external temperatures were still as low as -10.5°C. Melt water generation at such temperatures is unlikely, suggesting that the pressure rise resulted from a reduction in the capacity of drainage pathways within the till. The brief rise in external temperatures above 0°C (days 76-78) corresponded with a reduction in Probe 12 pressure. These temperatures also appeared to trigger the following pressure rises recorded by Probes 12 and 15 (days 80 and 78, respectively). The sudden elevation in temperatures may have generated an influx of melt water following the extended period of cold conditions. As temperatures suddenly fell below 0°C the melt water generated will have been trapped in the subglacial system. This caused pressure to rise as drainage pathways became constricted, whilst trying to discharge the brief influx of water.

The significance of this melt water input is demonstrated by the magnitude of the pressure rises. Probe 12 water pressure exceeded overburden on day 81. Values reached 114.8% on day 82, shortly before temperatures reached a minimum of -14.1°C (day 83). Similarly, Probe 15 pressures greatly exceed overburden remaining above 160.5% and reaching peak values of 329.9% (day 84). This activity reflects the difference in the locations of the probes at the glacier bed. The lack of response by both Probes 10 and 12 prior to Event 2 suggests that they were located in regions that were less active and required a greater 'trigger', or critical point, to induce a rise in water pressure. Alternatively, this could be a symptom of the stochastic response of subglacial systems, highlighted by Murray and Clarke (1995).

7.7.1.3 Event 2c

Probe 10 showed the same peak-trough-peak sequence of pressure fluctuations during Event 2c (days 89-120), as displayed by Probe 12 in Event 2b. This occurred just after the more significant pressure rises of Probes 12 and 15. The trigger for the pressure rise also appeared to be slightly different as Probe 10 responded to an increase in external temperatures. The first rise (day 105) was triggered by several precipitation events (days 104-109) and melt water generated in response to elevated temperatures that exceeded 0°C at night (day 102). The pressure record also showed some correlation with precipitation events. As precipitation stopped and temperatures fell below 0°C (days 110-114), pressure also fell. However, when temperatures remained above 0°C and precipitation events were recorded (days 117-118), pressure began to rise again (day 119). This would suggest that precipitation had a significant effect on melt water generation. Probes 12 and 15 did not respond to these variations suggesting a change in the processes operating within theses areas of the bed.

7.7.2 Subglacial processes

7.7.2.1 Event 2a

The diurnal pressure fluctuations displayed by Probe 15 during Event 2a suggests that oscillations in external temperatures were still sufficient to generate a diurnal melt signal, albeit a small one (<2%; Figure 7.9). This may be because the drainage

system was still poorly developed and of a low capacity at this time. The small-scale of response also indicates that the drainage capacity within the connected regions was only exceeded to a small degree. It seems unusual that there was diurnal flux given that temperatures were below 0°C and so unlikely to generate melt. In light of this, an alternative explanation may be a freeze thaw cycle. A reduction in external temperatures overnight could cause the capacity of the subglacial drainage pathways to decrease, increasing water pressures. As temperatures warmed in the afternoon and drainage capacity increased, pressure decreased. The temperature peak on day 54 may have supplied the input of melt water during this period. This pattern was not considered to be linked to activity associated with the proglacial lake, because the distance between the study sites and the lake was too far to be associated with any pressure forcing (Ruth Mottram, pers. comm., based on work with pressure transducers at the margin of Breidamerkurjøkull, Iceland).

The very low temperatures recorded between days 60-75 may have interrupted this signal. A lack of fresh melt water, in combination with reduced temperatures, would help to close drainage pathways, possibly freeze the glacier to its bed, and reduce the quantity of free water within the connected system and the till. Average daily temperatures began to increase from day 65, and on day 67 temperatures rose close to 0°C (Figure 7.9). This relative increase in ambient temperatures may have been sufficient to reinstate the diurnal signal recorded by Probe 15 from day 67. Given that this signal had been recorded previously at temperatures below 0°C, this seems to be feasible. The resistance record for Probe 15 remained unchanged throughout this period suggesting that conditions within the till were still wet (Figure 7.5c). This is in keeping with the continued fluctuations in water pressure. Probe temperatures also remained relatively low throughout this period indicating that the presence of water within the till was sustained (Figure 7.5c).

Probes 10 and 12 recorded short lived pressure peaks during Event 2a. The lack of response in probe resistance to these peaks was unusual. The delay in the pressure records of Probes 10 and 12, compared with Probe 15, suggests that they were in less active unconnected regions of the bed. Variations in pressure fluctuations over small spatial scales have been noted within the subglacial environment (Porter and Murray, 2001). The change in sensor activity following these events indicates that they mark

the start of a change in conditions within these areas of the subglacial environment. Unfortunately, whether the peaks were the cause or result of the change is uncertain. The lack of response from Probes 10 and 12 prior to this suggests that they were not being forced by connected regions of the bed. As a result, these short lived peaks reflect different activity, which may be associated with the distance of these probes from connected regions of the bed. The probes may be relatively isolated and prior to this water was constrained to the areas that had remained relatively well connected during the winter.

The gradual change in average probe temperature throughout this period also reflects slowly changing conditions in the till around Probes 10 and 12. Probe 12 showed an overall increase in average temperature throughout the spring, but values began to stabilise from day 59, showing smaller scale oscillations. This suggests the environment was adjusting to changing conditions within the till. The increase, as opposed to decrease, in probe temperature may reflect the location of the probe in scenario B3 (Figure 6.1, Chapter 6). Since deployment, Probe 12 had been located in a more horizontal position than the other probes, which might affect its interaction with the till and temperature readings. A similar response was recorded by Probe 7, which was also located flush with the glacier bed (section 6.4, Chapter 6). Alternatively, this may just be a localised pattern specific to this area of the bed.

7.7.2.2 Event 2b

In Event 2b, Probe 12 was the first to show a pressure fluctuation (days 71-82), closely followed by Probe 15 (78-85). The continued response in water pressure recorded by Probe 12 suggests that this region of the bed had become active and that the amount of melt water reaching this unconnected area of the bed had increased. This might have been a change in the location or connectivity of subglacial drainage pathways, resulting from Event 2a. The magnitude of pressure recorded by Probe 12, although less than Probe 15, was still in excess of overburden. This suggests a strong hydraulic gradient had been established in this area. This may have been achieved via sheet flow at the ice-bed interface, or Darcian or pipe flow within the till. This also implies that Probe 12 was located relatively closer to a connected region than Probe 10, whose pressure record did not exceed overburden.

The second Probe 15 pressure rise (329.9%) occurred prior to that of Probe 12 (114.8%), and was of a much greater magnitude, with diurnal oscillations. The pressure peak indicates that there had been a significant melt water input into the connected region of the bed. This would help to develop drainage pathways in that area. Probe 15 was subject to forcing from a connected region, whereas Probe 12 was responding to localised increases in melt water flow. The diurnal oscillations and the magnitude of pressure highlight the differences in subglacial drainage between the probes. The fact that Probes 10 and 12 did not experience this pressure forcing implies that they were located further from a connected region than Probe 15.

The resistance record for Probes 10 and 12 did not change during Event 2b. This was expected for Probe 10, which did not show a significant response in water pressure. A change may have been expected in association with the fluctuations experienced by Probe 12. However, the overall lack of response in the spring suggested that Probe 12's resistance sensor had failed. Probe 10 temperatures continued to decline during this time suggesting that there was a slight increase in the water content of the local environment. Probe 12 also showed few oscillations in probe temperature reflecting pressure fluctuations. The rate of decline in Probe 15 temperature increased from day 74, in advance of the pressure rise on day 78.

7.7.2.3 Event 2c

As water pressures remained relatively stable for Probes 12 and 15 in Event 2c, Probe 10 displayed a peak-trough-peak sequence of pressure fluctuations (Figure 7.8). The timing of this event, and the reduction in pressure magnitude, may reflect the location of the Probe 10 with respect to the connected subglacial drainage system or a source of melt water. Hubbard *et al.* (1995) and Mair *et al.* (2001) have suggested that pressure responses migrate up glacier with the snow line. The timing of the pressure oscillation supports this, occurring later in the season in April when the snow pack will have begun to melt from the ablation zone (section 7.8). However, this record could also just reflect the potential for spatial heterogeneity over short distances within the subglacial environment (Porter and Murray, 2001). The pressure magnitude could also be lower as the hydraulic gradient between connected and unconnected regions of the bed decreases away from a connected drainage route (Murray and Clarke, 1995).

The Probe 10 resistance record decreased suddenly from day 90. This indicated a change in the water content of the till, suggesting that drainage routes had become more active (Figure 7.5a). As external temperatures increase and the snow pack melts the till will become more saturated as more free water becomes available, both in channels and as a film at the ice bed interface. The decrease in resistance indicates significant throughflow operating within the till in this location. This occurred prior to the rise in water pressure, demonstrating the sensitivity of the resistance sensor. The lack of response in the Probe 12 resistance record despite pressures in excess of overburden suggests that it was not functioning.

In Event 2c, Probe 10 showed sustained pressures following the fluctuation, Probe 12 recorded sustained pressures throughout, whilst Probe 15 displayed a decline in pressures and small-scale oscillations (Figure 7.8). The sustained pressures recorded by Probes 10 and 12 (from days 82 and 119, respectively), were indicative of continual flow through the till during the summer in established drainage pathways. The diurnal signal recorded by Probe 15 ceased gradually and, after a final pressure peak on day 92, values remained low and mildly oscillating. This change in pressure activity suggests that Probe 15 was no longer experiencing forcing from the connected regions of the bed. The low flows and minor oscillations indicate that the probe was once again unconnected and experiencing minimal pressure activity.

Probe 10 resistance remained low (wet conditions) throughout the rest of Event 2c, in keeping with the pressure fluctuations experienced (Figure 7.5a). The change in resistance recorded by Probe 15 reflects the change in water pressures and subglacial conditions following the pressure rise of Event 2c. This reflects a net loss of water from this area of the bed (Figure 7.8). The average weekly temperatures for Probe 10 continued to oscillate throughout Event 2c, but did show an overall decline in values in accordance with the influx of water pressure at this time (Figure 7.5a). Probe 12 continued to show small-scale oscillations in average temperature. However, the range of fluctuations had become more consistent, indicating that the probe had adjusted to the change in water pressure within this area of the bed. The average probe temperature recorded by Probe 15 continued to decline throughout Event 2c (Figure 7.5b). Readings reached minimum values on day 97, before temperatures rapidly began to increase again. This occurred when water pressures

had decreased back to base flows and ceased fluctuating. This signifies the net loss of melt water from this area of the bed, following the pressure rise in Event 2b.

7.7.2.4 Case strain and tilt: Event 2

Probe 10 case strain showed small-scale fluctuations throughout the spring, but little variation in other sensor readings in response to increases in water pressure during Events 2b and 2c (Figure 7.7a). These oscillations showed that the direction of applied strain continued to vary throughout this period, indicating that the probe was interacting with the till. The Probe 15 record for case strain was much more complex throughout the spring period (Figure 7.7b). Case strain increased steadily during the spring and was characterised by diurnal fluctuations that corresponded with those in water pressure. This suggests that water pressures were affecting the mechanical properties of the till, making this a highly active area of the bed. The significance of this activity in case strain is discussed in full in section 7.10.

The probe tilt record showed minimal activity for all the probes during Event 2, in keeping with the whole of the spring period (Figure 7.6). Similar to Event 1 the probes showed a gradual increase in the rate of change in tilt. However, small-scale oscillations suggested that the probes were experiencing minor changes in orientation in response to activity within the subglacial environment. Probe 15 was the first probe to show a significant increase in activity in tilt at the end of the spring record (Figure 7.6c). The rate of change along the x and y axes suddenly increased in the same direction from days 113 and 115, respectively. This change in activity reflects the variation in sensor readings recorded by water pressure, resistance and probe temperature after the pressure rise of Event 2b. The initiation of probe rotation suggests that new or different processes were now operating within the till.

7.8 The Spring Event

Subglacial activity within the spring is normally associated with what has been termed the 'spring event' (e.g. Harper *et al.*, 2005; Kavanaugh and Clarke, 2001; Mair *et al.*, 2001). The spring event is important because it has been linked to distinct changes in glacier activity, as sudden variations in water pressure are

imposed upon a winter glacier regime. Sudden pressure events can cause instability within the subglacial environment, triggering a multitude of changes in subglacial conditions and consequently glacier velocities. Three good examples where the spring event has been recorded comprehensively include: Haut Glacier d'Arolla, Switzerland (e.g. Hubbard *et al.*, 1995; Mair *et al.*, 2001); Trapridge Glacier, Yukon, Canada (Kavanaugh and Clarke, 2001); and Bench Glacier, Alaska (Harper *et al.*, 2005). These events are outlined in full in section 2.7 (Chapter 2) and summarised below (Table 7.2).

Table 7.2: Summary of key findings relating to the characteristics of spring events from: Haut Glacier d'Arolla: Hubbard *et al.* (1995); Mair *et al.* (2001); Trapridge Glacier: Kavanaugh and Clarke (2001); and Bench Glacier: Harper *et al.* (2005).

	Haut Glacier d'Arolla, Switzerland	**Trapridge Glacier, Canada**	**Bench Glacier, Alaska**
Timing	June	June-July	April-June
Trigger	Elevated temperatures, removal of the snow pack, high precipitation events.	Elevated daily and night temperatures, drainage of a water-filled crevasse.	Initiation of the melt season and a gradual build up/storage of water at the glacier bed.
Result	Rise in water pressures. Diurnal water fluxes. Water pressure exceeds overburden. Enhanced glacier movement.	Rise in water pressures. Diurnal water fluxes. Water pressure exceeds overburden. Enhanced glacier movement.	Drop in water pressures. Diurnal water fluxes. Water pressure exceeds overburden. Enhanced glacier movement and flood.

These investigations define the spring event through changes in water pressure. The relationship between water pressure and the subglacial environment has been associated with changes in drainage morphology and glacier velocity. However, the triggers to, and mechanisms involved in, this interaction require further understanding. Indeed, a generally accepted definition for the spring event has yet to be given. Despite this, a number of criteria are referred to in association with the event, namely: timing, snow pack, weather, diurnal oscillations, and overburden pressure (Table 7.3). In order to identify the spring event at Briksdalsbreen, the probe water pressure records will be reviewed with respect to observations within the literature (Table 7.2) and the criteria outlined in Table 7.3. The other probe sensor records will be analysed in combination with water pressure readings, to identify and then characterise the spring event at Briksdalsbreen. A classification for the spring event will also be derived for future use.

Table 7.3: Comparison of the criteria associated with spring events from records at Briksdalsbreen, Haut Glacier d'Arolla, Trapridge Glacier, and Bench Glacier.

Location / Probe	Timing of spring events	Snow pack removal	Weather conditions	In excess of overburden pressure	Diurnal oscillations
Probe 8	January-March	April	Correlated	Yes	No
Probe 10	March-April	April	Correlated	No	No
Probe 12	March	April	Correlated	Yes	No
Probe 15	December-March	April	Correlated	Yes	Yes
Haut Glacier d'Arolla, Switzerland	June-July	June/July	Correlated	Yes	Yes
Trapridge Glacier, Canada	June-July	-	Correlated	Yes	Yes
Bench Glacier, Alaska	April-June	July	Not correlated	Yes	Yes

7.8.1 Timing

The timing of the pressure events at Briksdalsbreen is significant as water pressure reacts to melt water inputs derived from external weather conditions. It is useful to determine if there are specific ambient conditions likely to trigger a spring event. This might provide a rough guide as to when to expect a spring event, or even as a means of classification. Weather conditions have been correlated with spring events elsewhere (Tables 7.2 and 7.3) so it is important to verify if similar conditions were involved at Briksdalsbreen.

The absolute timing of pressure variations at Briksdalsbreen appears to be much earlier than those highlighted in the case studies (Table 7.3). However, their timing, with respect to ambient temperatures and the removal of the snow pack, is more in keeping with the observations in the literature. This implies that the range of start dates for spring events is the result of the varied climatic locations of each glacier. Table 7.4 provides a summary of the key environmental factors associated with the location of each glacier and Figure 7.10 presents the annual temperature and precipitation data for each location.

Table 7.4: Comparison of key environmental conditions at each study glacier.

	Briksdalsbreen, Norway	**Haut Glacier d'Arolla, Switzerland**	**Trapridge Glacier, Canada**	**Bench Glacier, Alaska**
Location	61° 41'N 6° 51'E	45° 58'N 7° 32'E	61° 14'N 140° 20'W	61° 00-03'N 145° 42-37' W
Glacier type	Terrestrial Valley	Terrestrial Alpine, valley	Terrestrial Surge Type	Terrestrial Valley
Thermal regime	Warm based	Warm based	Warm based	Warm based
Surface features	Ice Falls Debris Free	Debris covered	Ice falls	-
Subglacial features	Till	Till	Till	Bedrock with till patches
Proglacial fluvial features	Lake, River	River	River	River
Summer months	J,J,A	J,A,S	J,J,A	J,J,A
Average maximum temperature (month, °C)	24 July	17 July	20 July	17 July
Average minimum temperature (month, °C)	-10 December	-7 January	-25 January	-8 January
Precipitation trends	Seasonal	Uniform	Seasonal arid	Seasonal
Average maximum precipitation (mm)	12 January	70 August	3 July	233 September
Altitude (m a.s.l.)	350-1900	2650-3500	2250-3000	940-1625
Removal of snow pack (month, °C)	April 12	June/July 12-17	June 19	July 17
Timing of spring event (month, °C)	December–April 6-12	June-July 12-17	June-July 19-20	April-June 7-16

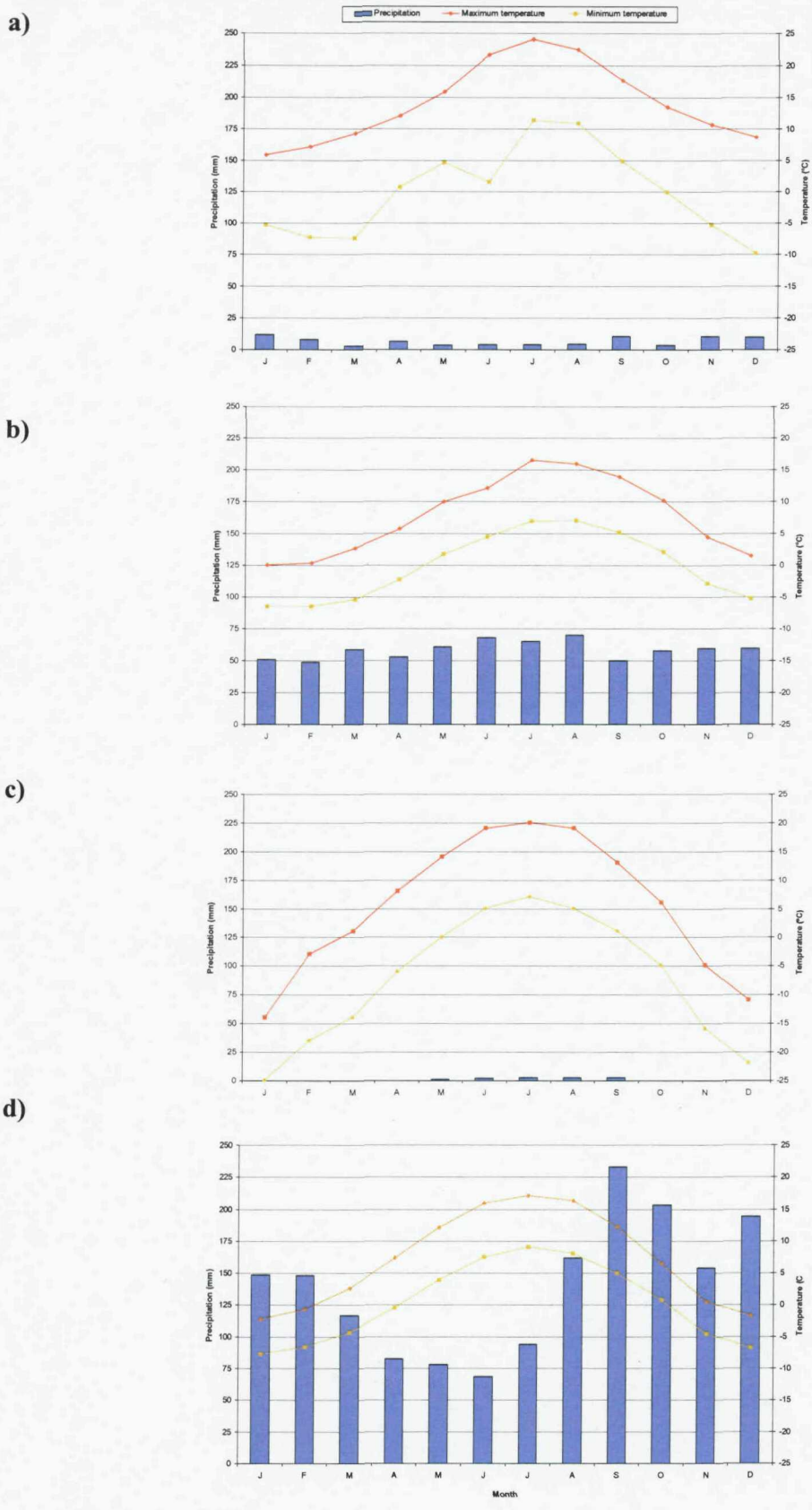


Figure 7.10: Monthly average temperature (max. and min.) and precipitation data for four glaciers that have recorded spring events: a) Briksdalsbreen, Norway (average 2004-6); b) Haut Glacier d'Arolla, Switzerland; c) Trapridge Glacier, Canada; and d) Bench Glacier, Alaska. Note: weather data for the comparison glacier is based on average annual values from 'long term' observations. Dates are not specified.

In terms of ambient temperature, spring events have been recorded when temperatures range anywhere between 7-20°C (Table 7.4). The spring pressure peaks recorded at Briksdalsbreen occur when average external temperatures range between 6-9°C, which is within the range of the other records (Table 7.4). Minimum winter temperatures occur in December at Briksdalsbreen, but in January for the other glaciers (Figure 7.10; Table 7.4). Peak summer temperatures occur in July, rather than August, and values are more elevated, reaching 24°C, versus <20°C elsewhere (Table 7.4). Thus, ambient temperatures began to increase earlier in the year at Briksdalsbreen, in comparison with the other glaciers (Figure 7.10; Table 7.4). This implies that spring activity could occur earlier in the calendar year, at Briksdalsbreen, in keeping with ambient temperatures. The other glaciers experience lower maximum summer temperatures, and minimum winter temperatures occur later, in January (Figure 7.10). In addition, the Haut Glacier d'Arolla and Trapridge Glacier are located at altitudes significantly greater than Briksdalsbreen, as is the terminus of Bench Glacier (Table 7.4). These factors will act to delay the required ambient spring temperatures and associated melt water generation until later in the calendar year.

Spring events have also been linked to the removal of the snow pack, occurring just prior to, or during, snow pack retreat (Tables 7.2 and 7.3). At Briksdalsbreen, the pressure events were also timed prior to the removal of the snow pack, in April. Average temperatures associated with snow pack removal at Briksdalsbreen (12°C) correspond with those recorded at the other glaciers (12-17°C; Table 7.4). The fact that the removal of the snow pack occurs earlier in the year is simply a result of the climatic conditions discussed above.

The relationship between specific pressure fluctuations and external weather conditions at Briksdalsbreen was complex. On the local and small (annual) scale the timing of the spring events generally coincided with external temperature variations (both elevated and reduced), high precipitation events and the removal of the snow pack. Where correlations with the weather were weak, it was difficult to suggest an alternative source for the pressure fluctuations. The proglacial lake or the ice fall, for example, may have an effect on the subglacial system. However, this has not been well documented in the literature and the locations of the probes were too far away

from the terminus to experience forcing from the lake (Ruth Mottram, pers. comm.). In addition, from 2004 to spring 2006 the glacier remained fully grounded at its margins. The most likely source of input is perhaps the drainage of water filled crevasses linking with the subglacial drainage system (e.g. Kavanaugh and Clarke, 2001). This is a probable explanation at Briksdalsbreen, given the zone of crevassing that divides the north and south sides of the glacier, and the ice fall up glacier of the study site.

In summary, the timings of recorded spring events were never identical and there is variation both between glaciers, and inter-annual variations at the same glacier (e.g. Mair *et al.*, 2003). This is likely to be the result of localised annual oscillations in temperature and precipitation trends. The spring pressure oscillations at Briksdalsbreen began when temperatures ranged between 6-9°C and the snow pack began to retreat. Lasting changes within the water pressure records appeared to occur later in the spring, in combination with the removal of the snow pack, and when average external temperatures had increase to 12°C or more (April). At Briksdalsbreen, the timing of the pressure peaks within the climatic record is in keeping with the occurrence of spring events within the literature. Thus, the pressure oscillations recorded during the spring have the potential to be spring events. The ambient weather conditions associated with these oscillations in pressure could be used as a means of identifying and characterising spring events in the future.

7.8.2 Characteristics

The greatest variability recorded by the probe sensors during the spring, similar to other investigations, was shown within the water pressure record (Figure 7.11). The nature of the pressure rises themselves can provide the strongest indication of whether or not a given fluctuation is part of the spring event (Tables 7.2 and 7.3). This introduces an important question about the sort of characteristics that are expected during the spring in unconnected regions of the bed. Diurnal signals, for example, which are generally associated with spring events, would not be expected within unconnected regions, unless in relation to pressure forcing (Murray and Clarke, 1995). Thus, the characteristics displayed must be compared with the other sensor activity in order to determine if they constitute part of the spring event.

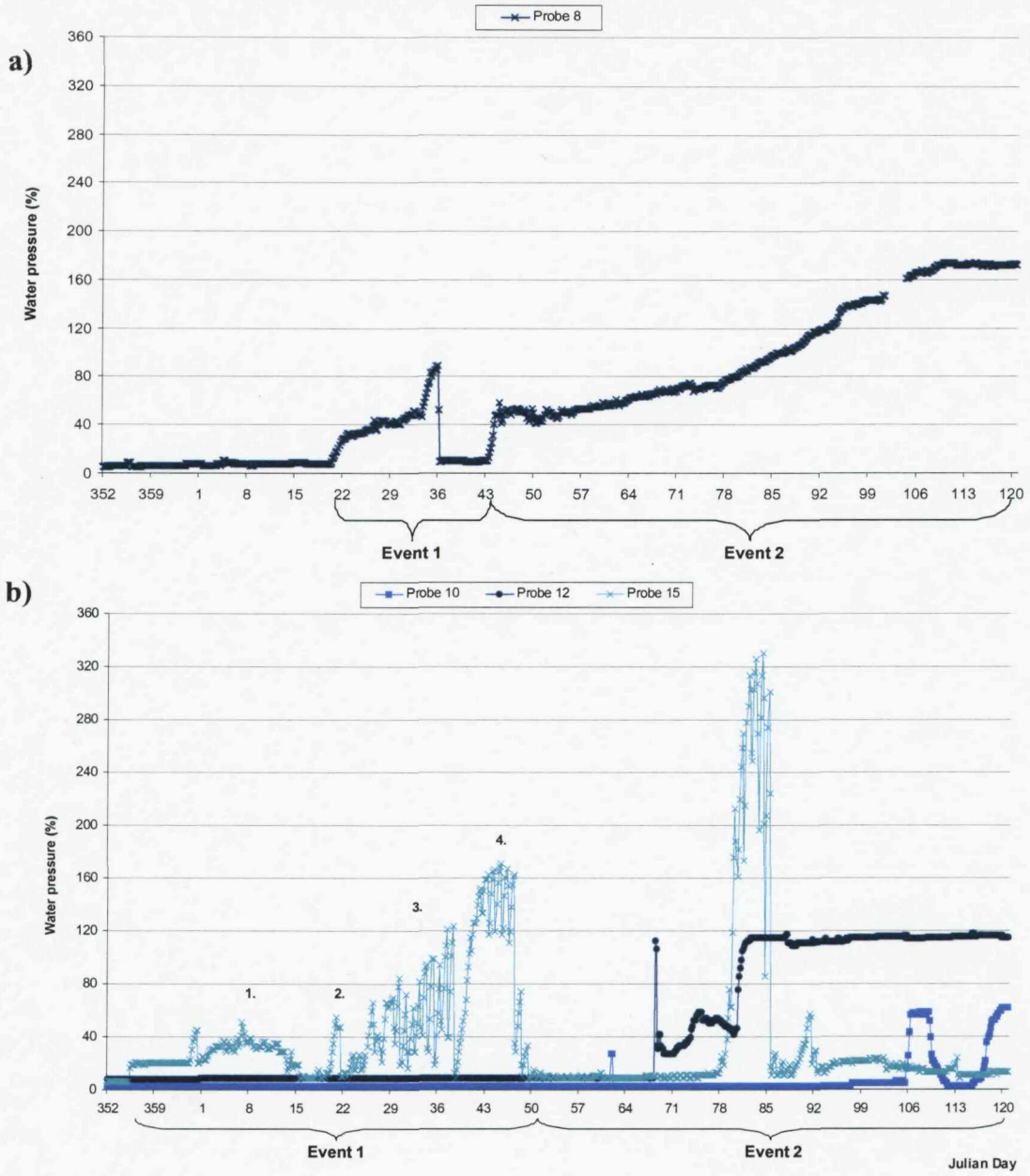


Figure 7.11: Comparison of spring water pressure records for: a) Probe 8 (2004/5); and b) Probes 10, 12 and 15 (2005/6).

7.8.2.1 Probe 8 (2004/5)

The Event 1 pressure rise (Figure 7.11a) was not considered to be part of the spring event because the majority of its characteristics differed from key factors associated with the spring event (Table 7.2). The trigger for the event was associated with external weather conditions. However, the build up of water pressure was relatively minor and did not exceed overburden pressure (Table 7.2). In addition, probe resistance did not change (fall), which would have been a strong indicator of a large

influx of melt water into the system. The timing of this event was also very early in the year. These factors suggest that, despite a reduction in probe temperature, and an increase in water pressure, the magnitude of the event was not in keeping with that of a spring event. The changes that occurred were not sufficient to result in large-scale subglacial instabilities, even though there were some similarities with the spring event. The activity recorded was perhaps more in keeping with the small-scale changes in pressure reported by Harper *et al.* (2005) just prior to their spring events. As a result, this phase has been categorised as the 'Emergent Spring Event'.

The nature of the Probe 8 pressure rise in Event 2, particularly from day 77 (Event 2b), was more in keeping with a spring event (Figure 7.11a). This was reflected by the magnitude of the event, as pressure exceeded overburden (Table 7.2). This may seem insufficient to classify Event 2 as a spring event. However, diurnal oscillations (Table 7.2) were not expected because Probe 8 was unconnected from the subglacial drainage system. In addition, data from the other sensors suggest that significant instabilities were produced within the till. Probe temperature decreased rapidly, particularly from day 101, and resistance fell (days 86-109) with the increase in water pressure above overburden (day 86). This suggests that Event 2 was the result of a significant influx of water into the till. This caused important changes in the physical properties (water content) and drainage conditions within this area of the bed. This was demonstrated by the sustained pressures that followed this event, implying that a strong hydraulic gradient, with a well developed connected drainage system, had become established. Thus, Probe 8 Event 2 is considered to represent what will be termed the 'Main Spring Event'.

7.8.2.2 Probes 10, 12 and 15 (2005/6)

Only Probe 15 recorded pressure fluctuations during Event 1 (Figure 7.11b). The first pressure rise was unusual as it began very early in the season, at the end of December, and was characterised by a variety of oscillations. This event was triggered by external weather conditions. Peaks 1 and 2 were of a relatively low magnitude. However, peaks 3 and 4 both displayed diurnal oscillations, and exceeded overburden pressure (Figure 7.11b). These characteristics are in keeping with those associated with spring events (Table 7.2). In further support of this, resistance and probe temperature began to decrease and case strain showed greater

variability, implying changes were occurring in the mechanical properties of the till (Table 7.2).

The pressure oscillations of Event 1 also showed characteristics not previously associated with spring events. The pressure fluctuations occurred very early in the year and progressed over a period of 1.5 months, much longer than the spring events recorded elsewhere (e.g. 4-9 days; Mair *et al.*, 2003). The build up of pressure in peaks 1 and 2 and the start of peak 3 was also gradual and generally of a relatively low magnitude. Initial pressure oscillations did not exceed 80% until day 33, and overburden pressure was only just exceeded at certain times of the day during the final two days of peak 3 (Figure 7.11b). The fluctuations, displayed prior to peak 4, are move suggestive of a gradual build up of activity within the till, rather than a sudden large-scale pressure rise that characterises the spring event. This suggests that peaks 1-3 are more representative of an emergent spring event. Over the course of a month these pressure fluctuations culminated in the sudden high magnitude pressure oscillations associated with peak 4.

The rapid rising and falling limbs of peak 4 were more in keeping with a sudden high magnitude water input into the subglacial environment, associated with spring events (Table 7.2). The duration over which peak 4 occurred (10 days) was also comparable with those recorded elsewhere (e.g. Haut Glacier d'Arolla; Mair *et al.*, 2003). These characteristics are indicative of a spring event. However, the timing of this peak was still very early in the year and pressures returned to base flows following this event. This suggests that there had not been a lasting change in the conditions within the subglacial environment. This was probably due to the external weather conditions at this time, which could not support a sustained increase in subglacial activity. In addition, Probe 15 was the only probe to show a response at this time of year suggesting that this event was highly localised. As such, it may not represent a glacier wide change in conditions. In light of these associated factors, despite the similarity of peak 4 with a spring event, it is considered to represent an emergent spring event.

Event 2 was characterised by a series of pressure variations recorded by Probes 10, 12 and 15 (Figure 7.11b). The timing and nature of these events were in keeping

with that of a spring event. Event 2a reflected a period of relative quiescence prior to the main pressure rise. Probe 15 recorded small-scale diurnal oscillations in pressure. Diurnal patterns are associated with spring events, but the magnitude of these variations was constrained by external weather conditions (reduced temperatures). The small pressure peaks experienced by Probes 10 and 12 implied that throughflow processes had become active within the unconnected regions of the bed.

It was not until Events 2b and 2c (Probes 12 and 15, and Probe 10, respectively) that there was sufficient melt water available and suitable external conditions to generate a spring event. The Probe 15 spring event was marked by a sudden increase in water pressure, which exceeded overburden and displayed diurnal oscillations (Table 7.2). The rate and degree of decline in probe temperature, the variations in case strain and low resistance values were all characteristic of a large influx of water into the subglacial environment that might be associated with a spring event. The magnitude and nature of variations shown by Probe 15 indicates that Event 2 was more significant than Event 1. The patterns recorded also resulted in lasting changes within the subglacial environment (Table 7.2). These changes were characterised by the small-scale fluctuations in water pressure that followed, and the change in the other sensor readings.

The fluctuations shown by Probes 10 and 12 were perhaps not immediately suggestive of a spring event (Figure 7.11b). However, these records represent new data concerning spring activity within active but unconnected regions of the bed. In Events 2b and 2c, Probes 12 and 10, respectively, were marked by a sudden increase and fluctuations in water pressure, which in the case of Probe 12, exceeded overburden. Probe temperatures continued to fluctuate and Probe 10 showed an increase in the activity of case strain and a drop in resistance, just prior to the pressure rise. These factors are in keeping with the sensor readings recorded by Probes 8 and 15 during the spring event.

The records differ in that diurnal oscillations were not recorded and Probe 10 pressures did not exceed overburden. The omission of these characteristics is thought to reflect probe location. As the drainage system in these areas of the bed

did not connect with surface inputs diurnal variations were not recorded. In the case of Probe 10 there was also insufficient melt water to cause water pressure to exceed overburden. However, the magnitude of pressure may also reflect the distance of Probe 10 from a connected region. The accompanying changes in other sensor readings also suggested that this event was of sufficient magnitude to result in lasting changes in subglacial conditions, characterising it as the main spring event.

Pressures in excess of overburden in the unconnected regions (Probes 8 and 12) imply that the drainage capacity of the till is not the limiting factor; rather the location of the probes is a more important constraint on the magnitude of water flow recorded within the subglacial environment. It is likely that this is a reflection on the hydraulic gradient between connected and unconnected regions of the bed (Murray and Clarke, 1995); and that pressures in excess of overburden signify a strong gradient and proximity to a connected drainage route. The nature of the Probe 8, 10 and 12 pressure fluctuations was similar, displaying a final pressure peak followed by sustained and relatively elevated pressures. This pattern appears to characterise the main spring event in unconnected regions of the bed.

7.8.3 Synthesis

The evidence discussed above has highlighted the spring events recorded in 2005 and 2006. The identification of these events has been based on the characteristics of the pressure peaks recorded in relation to those reported as spring events in the literature; and new supporting evidence from the other probe sensors. Consistent with the literature the pressure fluctuations occur suddenly at a time when minimal activity is expected at the glacier bed; occur just prior to the recession of the snow pack; exceed overburden pressure; and display diurnal oscillations. The main spring event also results in a change in the activity and processes operating within the subglacial environment. The sensor patterns observed have also demonstrated the variability of spring events, not only between glaciers, but also between years, and according to the spatial heterogeneity of the conditions at the glacier bed (Table 7.5). Overall, the recorded probe activity reflects characteristics that can be correlated with ambient environmental conditions and associated with those patterns recorded in the literature for the spring event.

Table 7.5: Similarities and differences in the characteristics of the spring events recorded by Probes 8 (2004/5), 10, 12 and 15 (2005/6) at Briksdalsbreen, Norway.

Similarities
• Variations occurred suddenly at a time of year when little activity was expected. • Pressure rises occurred just prior to or as the snow pack was removed. • Pressure readings exceeded overburden pressure. • Rises in pressure were accompanied by a drop in probe temperature. • Resistance fell as pressure increased.
Differences
• Probe 8 displayed one prolonged period of pressure increase. • A diurnal pressure signal was only recorded in Probe 15. • Probe 15 displayed a series of pressure peaks that were more dynamic in nature. • Pressures did not remain elevated following the spring event in Probe 15.

7.9 Hydrological Processes

The spring event has also been associated with a seasonal reorganisation of the subglacial drainage system. This event results in the transition from a winter to a summer drainage regime (e.g. Willis *et al.*, 1990). The changes that occur can produce periods of enhanced glacier motion, which some studies have suggested are faster than in the summer (Harper *et al.*, 2005). In light of this, the effect of the spring event on the subglacial hydrological regime is considered further in this section. The activity recorded by the probes is examined further to determine what information can be revealed about the distribution, morphology and general characteristics of the subglacial drainage system at Briksdalsbreen.

7.9.1 Drainage connectivity

The nature of the pressure variations involved in the spring event differed between the probes according to their location at the glacier bed. The response of the probes was largely dependent on whether they were in a connected or unconnected region of the bed. The characteristics of the spring event are discussed below in relation to probe connectivity with the subglacial hydrological regime.

7.9.1.1 Connected

The Probe 15 record was markedly different from that displayed by the other probes during the spring (Figure 7.11). Probe 15 was located within an unconnected region

of the bed. However, it differed from the other probes due to its spatial proximity with a connected region of the bed. The pressure record displayed 180° out of phase diurnal oscillations, indicating that it was experiencing forcing from a proximal connected region (section 7.6.2). This allowed Probe 15 to act as a proxy for pressure variations within the connected drainage region. The pressure peaks recorded by Probe 15 were 'flashy' in nature, in comparison with the other records. Pressures both rose and fell suddenly and rapidly, with diurnal variations increasing the short term variability of the records. In general, the magnitudes of the pressure peaks were much greater than the others recorded. Again, this reflects the location of the probe and the quantity of excess water that exceeded the capacity of the connected system at this time.

Overall, the diurnal signal, rapid pressure response and high magnitude pressure peaks recorded by Probe 15 reflect patterns within a connected region of the bed. The flashy response indicates a greater sensitivity to water inputs within the connected regions of the bed, as might be expected. The Probe 15 sensor readings changed after the spring event and a diurnal signal did not reappear in the pressure record, indicating that the probe was still located in an unconnected region.

7.9.1.2 Unconnected

Probes 8, 10 and 12 were also located in unconnected areas. However, the probes were positioned sufficiently far away from any connected drainage routes that they did not experience pressure forcing. As a result, the pressure responses displayed were more moderated, and although often sudden, they were more gradual in nature. The lack of diurnal oscillations also reduced the variability of these records. This response reflects the different processes occurring within the connected and unconnected regions of the bed. Following the spring event, pressure rises were also sustained and remained elevated. This emphasises the stability in the drainage of water through the till, and presents a slightly different shape to the spring event pressure curve.

Despite this, the magnitude of the pressure rises (often in excess of overburden) suggests that large quantities of water were present in these areas of the bed. This may reflect a strong hydraulic gradient between connected and unconnected regions

(e.g. Harper *et al.*, 2002), and implies that flow pathways within the till were developing and contributing to subglacial drainage. Thus, there is perhaps greater drainage within the till and unconnected regions of the subglacial environment than previously thought. The variety of pressure magnitudes experienced by Probes 8, 10 and 12, reflect further differences within the unconnected regions and the availability of water in each individual probe locality.

7.9.1.3 Conceptual model

The differences between connected and unconnected probe sensor readings are most readily described by Figure 7.12. In the first diagram (a), Probe 15 is represented by the red probe and is affected by the connected region of the bed; whilst Probes 8, 10 and 12 reflect the blue probe, located in unconnected regions, and solely affected by independent basal flows. The second diagram (b) outlines the form of the spring event at Briksdalsbreen in terms of the water pressure record. This conceptual model highlights the relative timing, and variations in the form, of pressure response between the emergent spring event (Event 1) and the main spring event (Event 2; Figure 7.12).

The emergent spring event marks the first pressure rise of the year, acting as a precursor to the main spring event. The timing of this event was highly unusual, recording activity as early as the end of December and the start of January. This event shows a broad spectrum of variations, some or many of which display the characteristics of a spring event. Pressure rises exceed previous basal variations and in some cases (i.e. Probe 15) display diurnal oscillations. However, pressures are generally moderated, rarely exceeding overburden, particularly in the unconnected regions. This event is characterised by the variety of dominantly small-scale oscillations and peaks in pressure that occur. The pressure variations are accompanied by similar small-scale changes in the other probe sensors that mark the start of changing conditions within the subglacial environment.

The variety of pressure oscillations recorded during the emergent spring event reflect the development of drainage conditions and processes at the ice-bed interface and within the till. The multitude of variations, coupled with the gradual increase in activity, both in the frequency and magnitude of pressure events, signifies the

transition in the physical properties and subglacial processes occurring in the spring. The response of the probes demonstrates that there is considerable activity within the till and unconnected regions much earlier in the year than perhaps previously thought. This is also a reflection on the relationship between the glacier and external weather conditions, suggesting that subglacial processes are sensitive to changes in the ambient environment. The fluctuations produced indicate a large response to potentially small-scale changes in melt water inputs of external conditions when the subglacial environment has been inactive for a prolonged period of time and the drainage system is highly constricted. However, the changes in subglacial processes recorded during the emergent spring event are often minor and are not sustained.

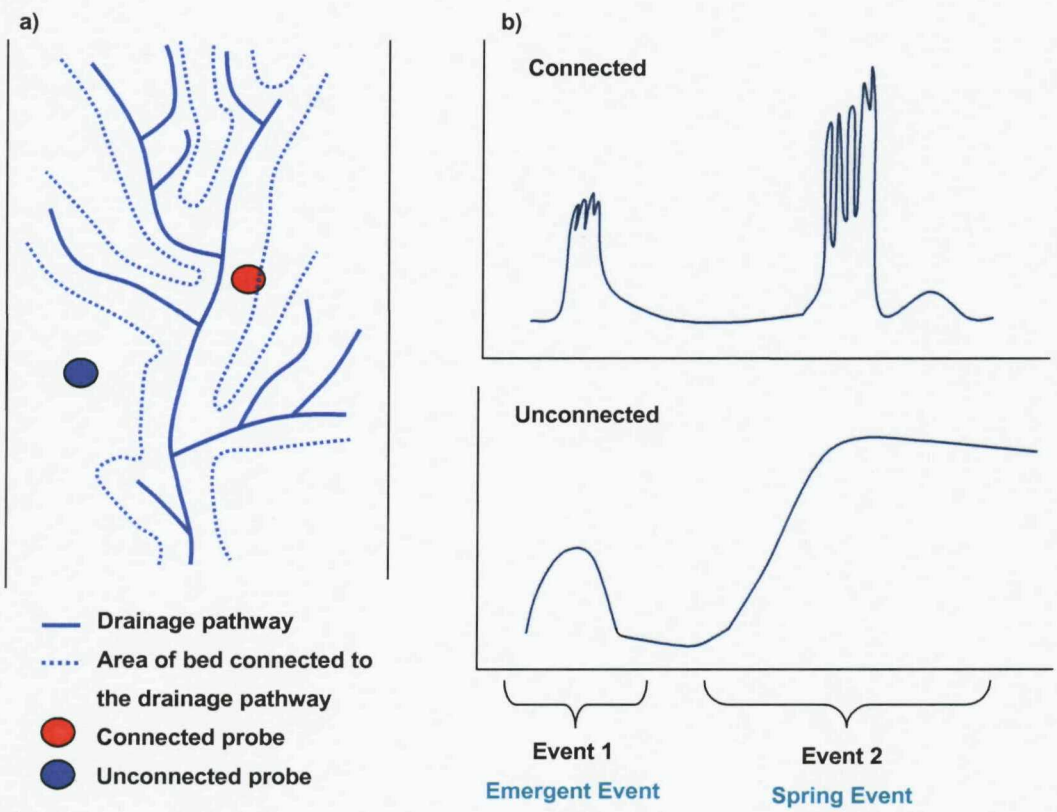


Figure 7.12: Conceptual model to demonstrate the different characteristics between the spring event in connected and unconnected regions of the bed, showing: a) the potential location of the probes in each scenario within a hypothetical drainage system; and b) the form of the spring event according to the water pressure records, which reflect probe location within the subglacial drainage system.

In the main spring event more extensive changes occur at the glacier bed (Figure 7.12). This is displayed by the magnitude of pressure fluctuations in Event 2 and the change in pressure activity following this event. The main spring event occurs later in the year because there needs to be sufficient and sustained melt water inputs and external conditions to result in lasting changes to the hydrological regime and the processes acting in the subglacial environment. The main spring event is recognised by its timing, its magnitude and oscillations, and the changes in sensor readings that ensue. The pressure variations of the emergent spring event are insufficient to cause these permanent changes. Later in the year temperatures have become more elevated, the number of sun hours has increased and the snow pack has begun to retreat. This provides more suitable conditions in which to generate large and sudden water inputs, which are followed by an overall increase in melt water generation. At Briksdalsbreen, this occurs at the end of March/start of April. The lasting change in conditions is demonstrated by the sustained water pressures in Probes 8, 10 and 12, and the sudden change in sensor readings recorded by Probe 15.

In summary, the spring event at Briksdalsbreen records a two stage transition through the spring. The initial emergent spring event acts as a warm up to the main spring event, which occurs later. This high magnitude pressure event drives a transition in the regime of the subglacial drainage system. The variety of pressure fluctuations recorded by the probes during the spring reflects the temporal variability inherent to water pressure within the subglacial environment. In addition, the differences between the connected and unconnected readings in sensor response display the spatial heterogeneity in drainage across the bed of the glacier. The probes have recorded the first long term record of water pressure from within the till. They have shown that activity occurs much earlier in the till than previously thought and that high pressure can occur in unconnected regions through independent flows. Additionally, the probes can improve comparisons between connected and unconnected regions of the bed, which can provide us with a better understanding of the distribution and morphology of drainage routes at the ice-bed interface.

7.9.2 Drainage morphology

The above discussion has highlighted that it is possible to determine the location of the probes in connected or unconnected regions of the bed. It is also possible to detect long term changes in sensor readings that reflect a change in the subglacial hydrological regime. However, the actual morphology of the connected system is harder to assess. Only Probe 15 reflected the conditions within the connected regions of the bed, and only through proxy. Figures 7.13 and 7.14 have been compiled to provide a rough outline of the spatial distribution of connected and unconnected regions of the glacier bed associated with the study areas during 2004/5 and 2005/6, respectively.

The spring is an important time in the subglacial environment as conditions evolve from a winter to summer regime (Willis, 1995; Willis *et al.*, 1990). The spring event is of particular significance because it acts as the driving mechanism for the seasonal change within this system. This event generates significant instability within the subglacial drainage system as a result of the large and sudden influx of melt-water into a poorly developed low capacity drainage system. This, in turn, affects the mechanical stability of the till and can instigate changes in glacier velocity (e.g. Hubbard *et al.*, 1995; Mair *et al.*, 2001, 2003). The spring event pressure rise has such a significant impact on the drainage system because it occurs as an anomaly at a time when seasonal temperatures should still be low, precipitation events are in the form of snow and the glacier is still snow-covered in the ablation zone.

The response in water pressure that follows these sudden melt water inputs reflects the nature (e.g. morphology and drainage capacity) of the subglacial hydrological system at that time. Consequently, the pressure fluctuations recorded by the probes can be used to track changes within the drainage system during the spring and any impact that they might have on the dynamics of the glacier as a whole. Probe 15 presented a proxy for the activity within the connected drainage system. However, once the spring event was complete Probe 15 no longer mimicked the connected regions of the bed so that changes in drainage morphology could no longer be assessed. Despite this, the fact that Probe 15 was no longer subject to pressure forcing did in itself reflect a key change in the nature of the drainage network.

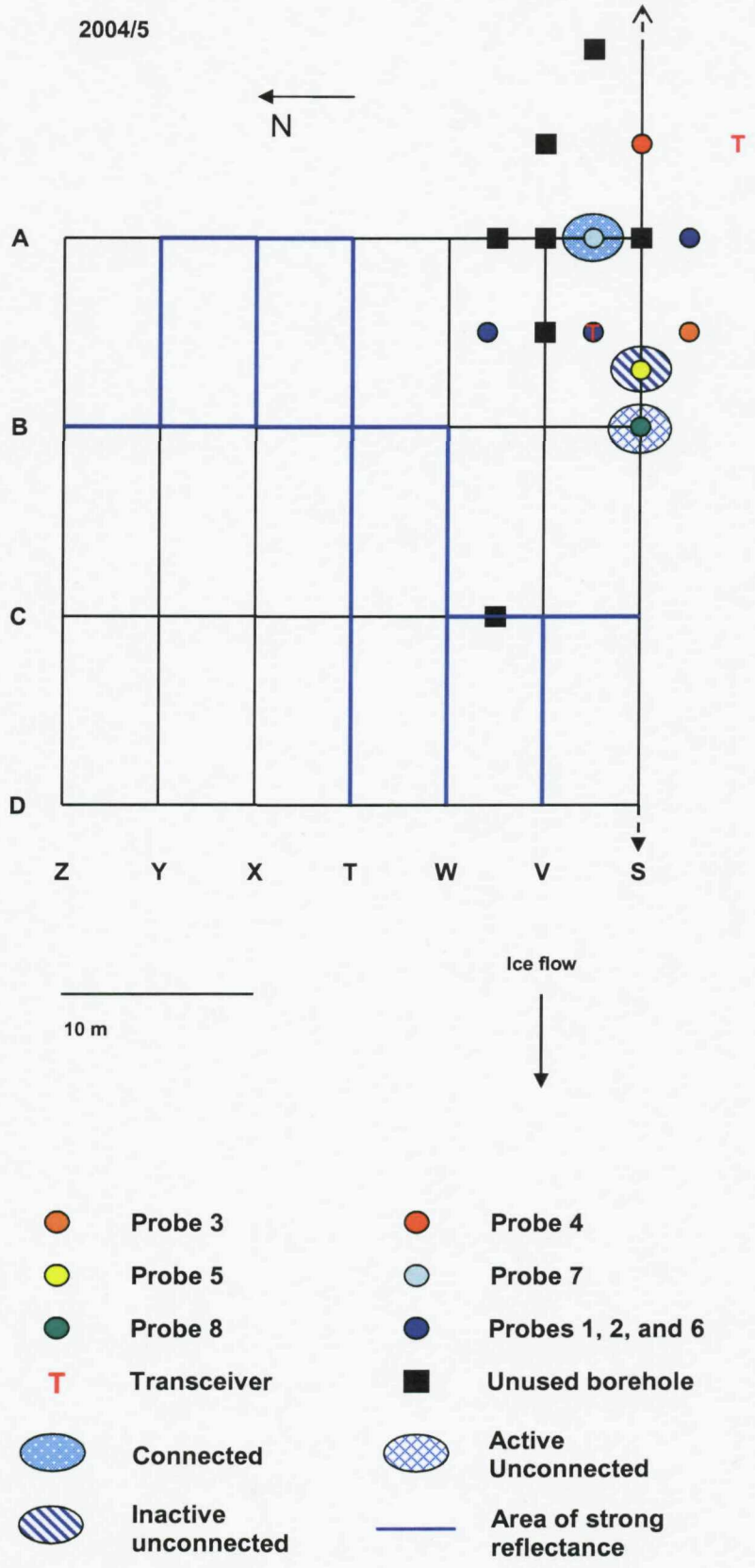


Figure 7.13: Schematic diagram to show the location of probes and their associated 'connectivity' within the subglacial drainage system for 2004/5. Note: the blue lines represent areas of high basal reflectance from the GPR surveys, which may indicate a concentration of water at the glacier bed.

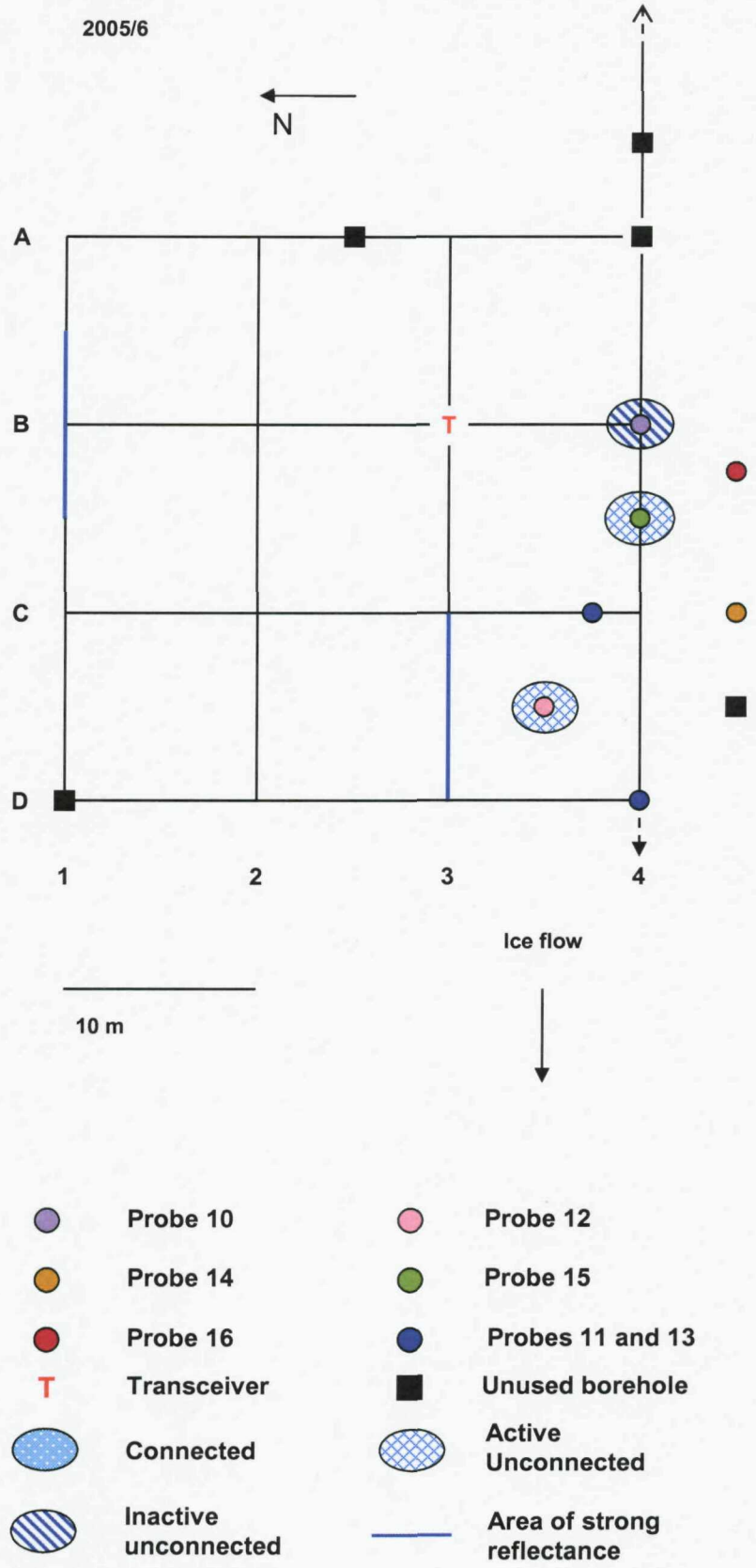


Figure 7. 14: Schematic diagram to show the location of probes and their associated 'connectivity' within the subglacial drainage system for 2005/6. Note: the blue lines represent areas of high basal reflectance from the GPR surveys, which may indicate a concentration of water at the glacier bed.

The pressure forcing experienced by Probe 15 was the result of sudden melt water inputs into an inefficient, poorly developed winter drainage system, which is normally characterised by a distributed network. Melt water inputs were in excess of the capacity of the connected subglacial drainage system. The increase in pressure accommodates a greater load at the glacier bed, decreasing pressure in unconnected regions. High pressures return when flows decrease in the connected region and load is transferred back onto unconnected areas of the bed, increasing water pressures. This ceased after Event 2 indicating that the drainage capacity of the connected region had changed. This suggested that the connected region had established a well developed, high capacity, drainage network that could accommodate the high flows associated with a summer regime. Studies elsewhere have suggested that this results in a discrete, arborescent drainage morphology beneath the ice (e.g. Willis, 1995).

Thus, the loss of diurnal fluctuations from Probe 15 indicates a transition from a winter to summer subglacial hydrological regime, namely a transition from a distributed to discrete drainage network. It is assumed that such morphologies are in place beneath Briksdalsbreen, based on investigations at other glaciers underlain by deformable beds (e.g. Nienow *et al.*, 1996, 1998; Sharp *et al.*, 1993; Willis *et al.*, 1990). In support of this, the Probe 8, 10 and 12 pressure readings were greatest during the main spring event as melt water was flushed through the system. The magnitude of the Probe 8 and 12 pressure rises, in particular, may reflect the development of the connected drainage system. These sustained high pressures may represent the development of a strong hydraulic gradient between the newly established high capacity drainage network and unconnected regions (Murray and Clarke, 1995).

Pressures did not increase further following the main spring event but declined. The net loss in pressure indicates that new water inputs were being transferred more quickly and directly into newly developed, and more efficient, connected regions of the bed. This is in keeping with a discrete drainage network. The probe records are able to identify this large-scale shift in drainage characteristics. However, they are unable to provide greater evidence of the precise morphology of that system at this time. This is an area that the probe data can add to given a wider spatial coverage of

the glacier bed. This would enable the maps outlined in Figures 7.13 and 7.14 to be expanded upon.

Discrete drainage networks tend to be associated with summer regimes, whilst distributed networks are more characteristic of winter systems. Although this assessment was traditionally applied to glaciers underlain by bedrock (Benn and Evans, 1996), continued work in this field would suggest that the same is true for glaciers underlain by deforming beds (e.g. Nienow *et al.*, 1996, 1998; Mair *et al.* 2002a; Willis, 1995). In general, flow through the till is likely to occur through Darcian flow and possibly pipe flow. Bulk movement of water may occur, but during the winter it is likely to be minimal in line with glacier motion. These characteristics were displayed by the low mildly undulating probe pressure records during the winter months.

Flow at the ice-bed interface of a glacier underlain by a deforming bed has generally been associated with R and N channel formation (discrete networks) and linked cavity systems (distributed networks), as outlined in section 2.6.4 (Chapter 2). Clarke and Walder (1994) suggest that, taking into account surface slopes, at a valley glacier such as Briksdalsbreen, R-channels are most likely to form in a discrete network, resulting in high discharge through low pressure channels. However, Clark and Walder (1994) and Walder and Fowler (1994) contributed a new hypothesis, suggesting that braided canal networks could form at the ice-bed interface. Unfortunately, this hypothesis has not yet been substantiated by field evidence. Summer and winter regimes can also be differentiated by the relative proportion of networks. A well established dendritic network in the summer is still likely to be fed by a good proportion of distributed networks across the glacier. Similarly, during the winter the drainage system will be dominated by distributed networks, however, some of the larger, well established channels from the summer may well remain active.

Field work has revealed a number of different transitions in subglacial drainage. Boulton and Hindmarsh (1987) predicted that pipe flow in deforming tills at Breidamerkurjokull would be replaced by a dendritic channel network. However, a linked cavity system also provides a good framework for the transition of conditions

from winter (distributed) to summer (discrete) systems. In this investigation, the lack of data from connected regions of the bed makes it difficult to determine the exact morphology of the drainage system at Briksdalsbreen. However, field observations, including a bathymetric survey of the lake (not presented in this thesis), indicate that there was a primary subglacial channel with its outlet on the south side of the glacier into the lake. This channel was in the same location during the 2004-6 field seasons and appeared to have the form of an R-channel, with a cave forming upward into the ice during each summer. It is likely that this channel was sustained, albeit at a reduced capacity, throughout the winter.

The combination of probe sensor records, GPR and borehole information has provided an indication of the distribution of the subglacial drainage system and the transition that it undergoes between the winter and summer, during the spring event. However, ultimately to obtain a good morphology and modelling of the subglacial drainage morphology a comprehensive dye tracer study is required (e.g. Bingham *et al.*, 2005; Nienow *et al.*, 1996, 1998; Sharp *et al.*, 1993; Willis *et al.*, 1990).

7.10 Mechanical Processes

A number or researchers have observed that basal mechanics interact with the hydrological system (e.g. Fischer *et al.*, 1999; Iverson *et al.*, 1994). As a result, the relationship between case strain and water pressure requires closer investigation. The following section will discuss the hydro-mechanical interactions observed at Briksdalsbreen in terms of basal motion and till mechanics.

7.10.1 Basal motion

The interactions between subglacial hydrology and the mechanical properties of till have been linked to glacier dynamics through the mechanisms of sliding and/or deformation (e.g. Fischer and Clarke, 1997; Iverson *et al.*, 2003). Probe case strain measures sediment strength, or the forces operating within the till. As a result, records of case strain in combination with water pressure can indicate mechanisms of basal motion (i.e. sliding or deformation). It is important to know when these processes are operating and the proportional contribution that each mechanism

makes to glacier movement. This will improve current understanding of the processes governing and initiating changes in subglacial motion, and their sensitivity to changes in physical conditions.

The likelihood that deformation and/or sliding will occur is controlled by how well the glacier is coupled to its bed. This relates to the amount of drag experienced in a given location at the ice-bed interface. Mechanisms of coupling and decoupling at the ice-bed interface have been associated with variations in water pressure and sediment strength (e.g. Alley, 1989b, 1993; Anderson *et al.*, 2004; Boulton *et al.*, 2001; Fischer and Clarke, 2001). Locally, increases in water pressure can promote sliding by causing decoupling between the ice and its bed, or can initiate enhanced bed deformation by weakening subglacial sediments (Fischer and Clarke, 2001). The records for water pressure, case strain and tilt will be examined for Probes 10 and 15 (the only probes with functioning strain gauges; Figure 7.15). The critical yield strength (Equation [3], section 2.3.3, Chapter 2) of sediments associated with these probes has also been calculated with respect to basal shear stresses (Equation [2], section 2.3.1, Chapter 2; Figure 7.16). Water pressure may indicate whether or not sliding is occurring, whilst the yield strength of sediments in combination with records of tilt and case strain can suggest if deformation is occurring. Figure 7.17 displays the records for water pressure and case strain.

7.10.1.1 Probe 10

Probe 10 showed relatively little activity during the spring (Figure 7.15a and 7.17a). Tilt on the x and y axes was relatively static between days 1-15, whilst frequent oscillations were recorded on the z-axis. This was followed by gradual but steady change in tilt along the x and y axes. Oscillations in case strain were also greatest between days 1-15, followed by gradual fluctuations. Although, the degree of strain recorded was minimal. This suggests that there was little activity within the till during the spring. The deformation of subglacial sediments is thought to cause clasts within the bed to rotate (Carr and Rose, 2003; Hart, 1994; van der Meer, 1997). The gradual change in tilt indicates that the probe was slowly moving orientation, rather than rotating during this time. Thus, without evidence of probe rotation, the process of deformation is thought to be unlikely. This is supported by calculated yield strengths (Figure 7.16a), which remained in excess of (i.e. able to withstand) the

applied basal shear stresses (e.g. Porter *et al.*, 1997). This implies that deformation was not occurring.

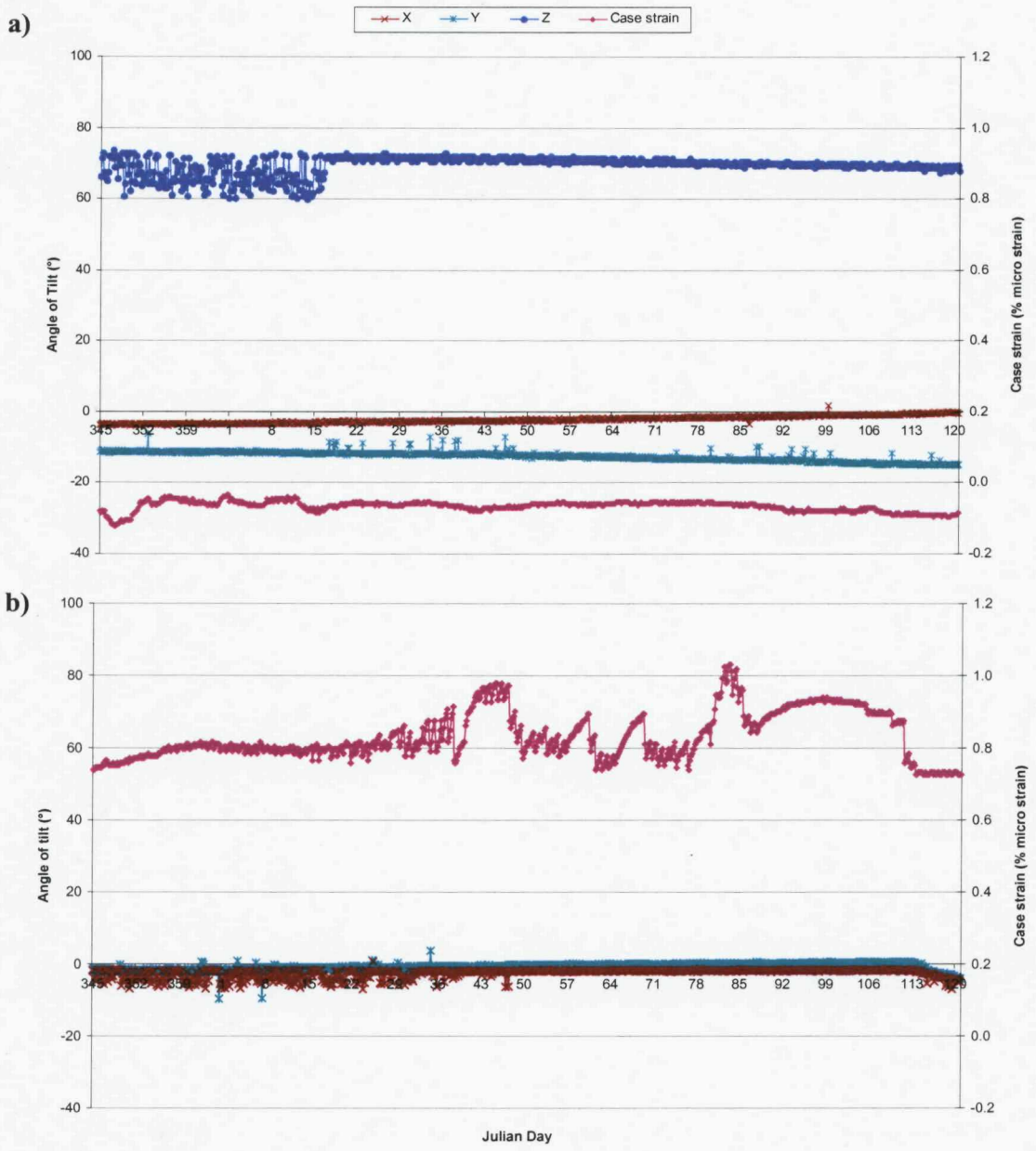


Figure 7.15: Spring sensor records showing case strain and tilt for: a) Probe 10; and b) Probe 15 (2005/6).

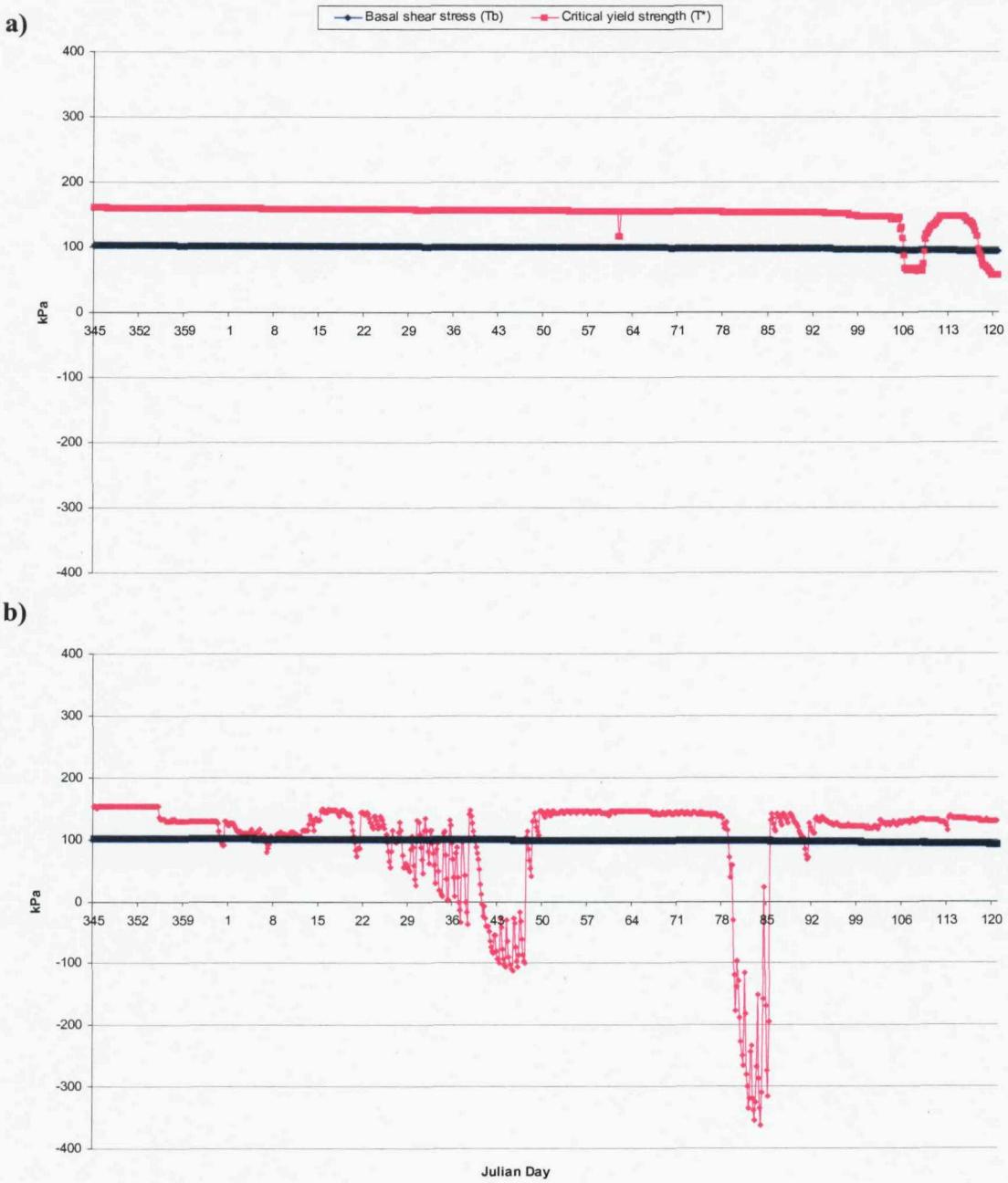


Figure 7.16: Spring sensor readings showing critical yield strength and basal shear stress for: a) Probe 10; and b) Probe 15 (2005/6).

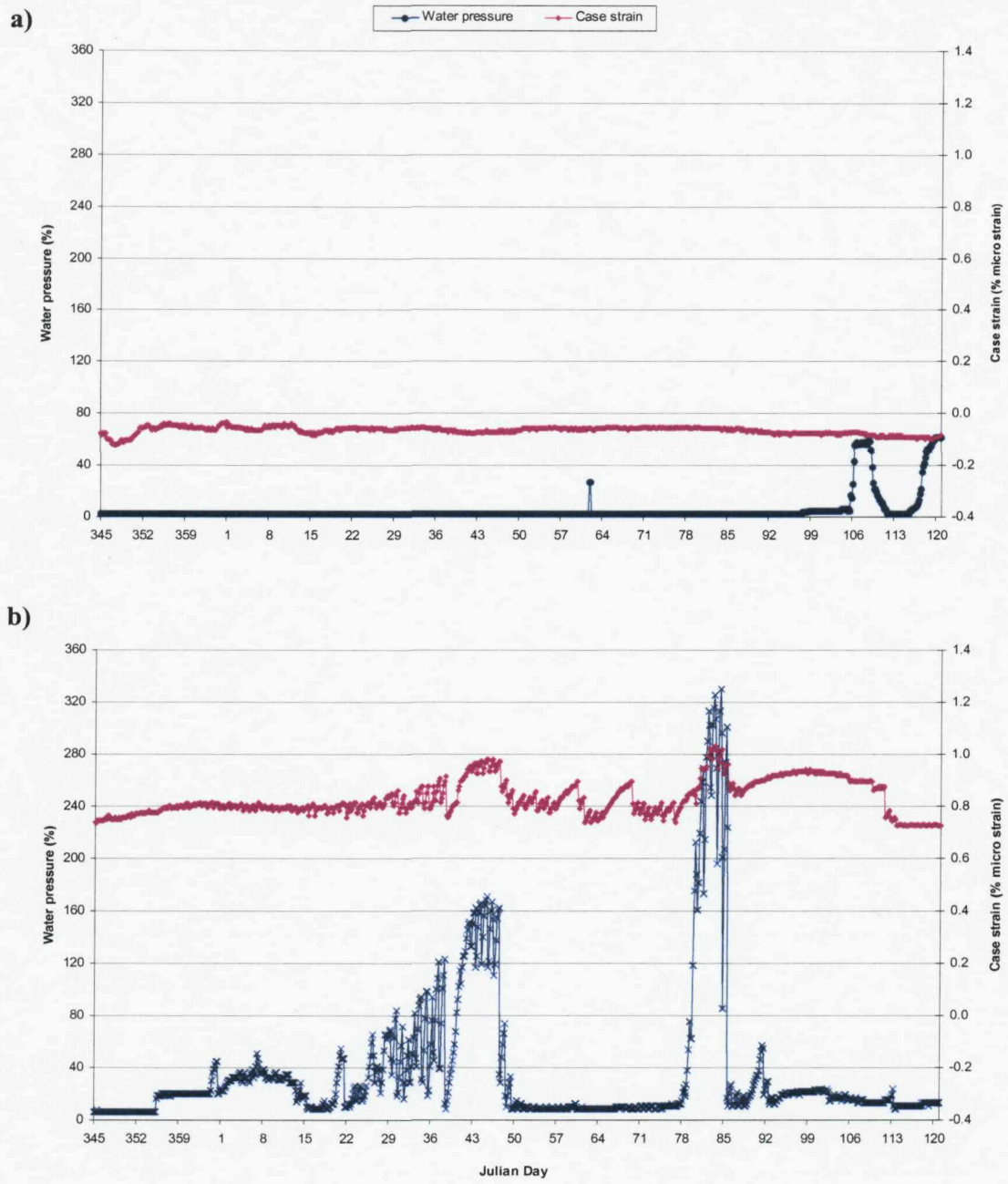


Figure 7.17: Spring sensor records showing water pressure and case strain for: a) Probe 10; and b) Probe 15 (2005/6).

The record for water pressure during this time also showed minimal activity (Figure 7.11b). Pressure only rose and fluctuated at the end of the spring and did not exceed overburden. This infers that pressures were insufficient to cause decoupling and enhanced sliding. These records suggest that rates of basal motion were low in this area of the bed. Despite this, activity within the till was clearly evident from the fluctuations in tilt and case strain (days 1-15, in particular). This indicates that the

probe was interacting with the till and reflects the effect of changing shear stresses on the deforming bed as glacier activity increased during the spring (Figure 7.15a). Base flows of water were also sustained throughout this time (Figure 7.11b). Thus, any motion that was achieved may have occurred through a combination of both deformation and sliding. However, even in combination, the magnitude of these variations does imply very low velocities and may suggest that Probe 10 was located in a sticky spot (Fischer *et al.*, 1999).

7.10.1.2 Probe 15

The Probe 15 record showed greater sensor activity during the spring (Figures 7.15b and 7.17b). Tilt changed gradually, accompanied by frequent fluctuations, between days 1-50. However, the case strain record showed numerous fluctuations, recording a much greater magnitude of strain than Probe 10 (Figure 7.15b). The fluctuations in tilt, particularly at the start of the spring, indicate that the probe was oscillating and changing orientation within the bed. The record for case strain indicates that the probe was interacting with the surrounding till and responding to significant changes in shear stress. These variations may be the result of deformation.

Sediment yield strength was calculated in order to clarify this relationship further (Figure 7.16b). The graph shows that yield strength was only exceeded by basal shear stresses during periods of elevated (~ >30%) water pressure. In the periods where pressures were raised, but below overburden, deformation may have occurred. However, the majority of the pressure peaks recorded during the spring were highly elevated, at 'superfloatation' (Murray and Clarke, 1995; Figure 7.11b). When pressures were in excess of overburden it is more probable that decoupling, and thus sliding, was in operation (section 7.8), even though at times calibrated basal shear stresses were in excess of yield strengths. The tilt record also suggests that, whilst the probe was oscillating at the ice bed interface, it was not rotating (Figure 7.15b), which also implies that deformation was not occurring. This supports the idea that sliding rather than deformation was the dominant form of basal motion during the spring. However, this account is still problematic because it does not provide a definitive explanation for the pattern of case strain recorded whilst sliding was thought to dominate. This issue is discussed further below in the sections that follow.

The dominance of sliding during the spring, particularly in relation to the spring event has been recorded elsewhere (e.g. Kavanaugh and Clarke, 2001). Other processes may also operate in response to such subglacial activity. During decoupling the glacier surface will experience uplift and may undergo a period of enhanced sliding as the film of water at the ice bed interface thickens and reduces friction at the bed (Kavanaugh and Clarke, 2001; Mair *et al.*, 2002b, 2003). The reduction of load from one area of the bed is also likely to be transferred to other surrounding areas of the bed (Murray and Clarke, 1995). Changes in glacier velocity, surface elevation, and load transfer are all processes that have been associated with spring activity in water pressure and sediment strength at the glacier bed (e.g. Mair *et al.*, 2003). It is reasonable to postulate that these changes also occurred during the spring event at Briksdalsbreen. However, this activity cannot be verified by direct measurement.

7.10.2 Basal mechanics: theory

The previous section assessed basal motion according to basal drag and sediment strength. However, any hydro-mechanical interactions also have implications for how deformation actually occurs, in terms of the changes in the physical properties of the till and the mechanical processes that it undergoes. Fluctuations in water pressure have been associated with variations in force, strain rate and yield strength; all of which govern deformation (Table 7.6). Traditionally, ploughmeter (force) and/or tilt meter (strain rate) readings have been used in combination with pressure transducers to determine these relationships (e.g. Fischer *et al.*, 1999; Iverson *et al.*, 1995). These instruments equate to probe case strain, tilt and water pressure, respectively.

A variety of results have been generated concerning the association between water pressure and sediment strength/deformation (force and/or strain rate) within the subglacial environment. Negligible, direct and inverse correlations between these two parameters have been observed (Table 7.6). A number of mechanical processes have been put forward to explain these correlations, and the resultant effect on basal motion. These hypotheses can be simplified into three scenarios. Figure 7.18 provides a simplified diagrammatic explanation of the interactions between water

pressure and the deforming bed, in terms of the degree of coupling at the ice-bed interface, sediment strength, strain rate, and the predicted amount of basal motion that may occur as a result.

Table 7.6: The relationship between water pressure and the mechanical properties of till.

	Breidamerkurjøkull, Iceland	**Trapridge, Canada**	**Bakaninbreen, Svalbard**	**Storglaciären, Sweden**
Instruments	Strain markers and pore-pressure transducers	Ploughmeter; pressure transducer	Ploughmeter; tilt sensor; pore-pressure transducer	Ploughmeter; tilt sensors; pressure transducer
Parameters	Strain rate; water pressure	Force; water pressure	Force; stain rate; water pressure	Force; Strain rate; water pressure
Trends	Increase in strain rate with an increase in pore-water pressure	#1: diurnal fluctuations, inverse correlation #2: diurnal fluctuations, direct correlation	Gradually increasing force: negligible and strong correlations	Strain rate decreased with high water pressures.
Correlation	Yes: direct	Yes: inverse	Yes: direct and No	Yes: inverse
Rheology	Viscous fluid	Viscous fluid or Coulomb plastic	Neither present a good fit	Coulomb plastic
Reference	Boulton and Hindmarsh, 1987	Fischer and Clarke, 1994; Fischer *et al.*, 1999	Porter *et al.*, 1997; Murray and Porter, 2001; Porter and Murray, 2001	Iverson *et al.*, 1995; Hooke *et al.*, 1997; Fischer *et al.*, 1998

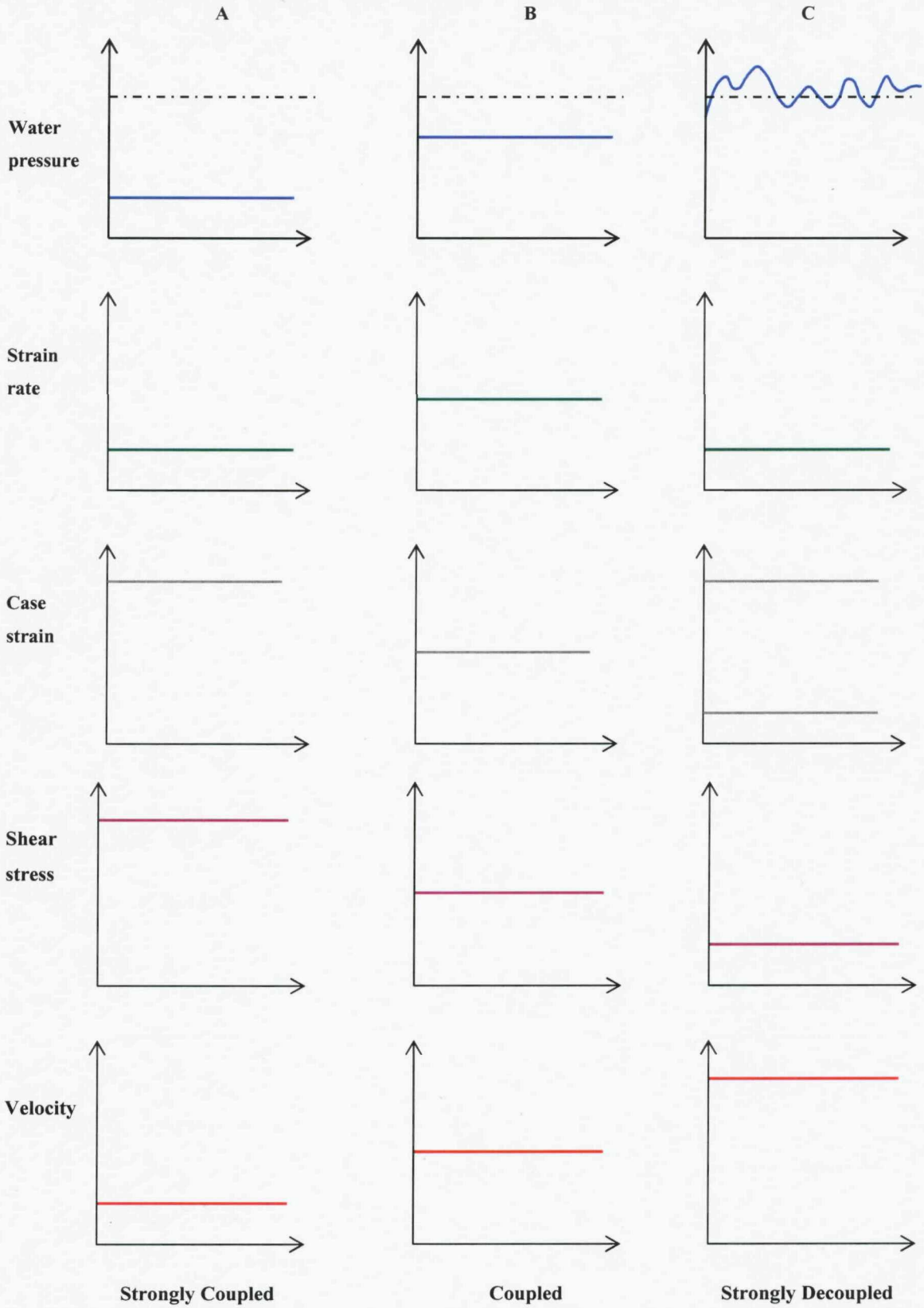


Figure 7.18: Conceptual diagram for a glacier underlain by unlithified sediments, showing the relationship between parameters associated with the degree of coupling at the ice-bed interface in scenarios: a) Strongly coupled, all mechanisms of basal motion may be equal; b) coupled, deformation may dominate basal motion; and c) decoupled, sliding dominates basal motion. Note: the dotted line represents overburden pressure.

7.10.2.1 Scenario A

The glacier is considered to be strongly coupled to its bed when water pressure is low and the applied shear stress is at its maximum (Figure 7.18a). Under these circumstances, when the till is relatively devoid of water and porosity is reduced, the till may become consolidated. Till strength increases as grains fit closely together, compacted by the weight of the overlying ice. This physical state is reflected by high case strains (with low water pressures) as the till supports the full application of shear stress from the ice above. The strength of the basal sediments is such that the yield strength of the till (τ^*) is not exceeded by the applied shear stress and strain rates remain low or negligible (Alley, 1989). As a result, deformation is predicted to be at a minimum, but forward motion at the bed may be achieved by sliding. At the bed of temperate glaciers in particular, pressure melting will generate some lubrication to enable this. However, sliding is likely to be minimal in keeping with water pressures. Strong coupling reflects significant basal drag at the ice-bed interface, resulting in low glacier velocities.

7.10.2.2 Scenario B

When water pressure within the till becomes active, but remains well below overburden, coupling between the ice and the bed is slightly reduced (Figure 7.18b). Elevated water pressures increase lubrication (reduce friction) at the bed. Under these conditions, the application of shear stress may result in the shearing of those subglacial sediments. As sediment strain rate increases with shear the till may undergo dilation (Alley, 1989). When this occurs the volume, and therefore the porosity, of the till increases as grains move over one another (Murray and Dowdeswell, 1992). This process has been associated with tills that are overconsolidated (Boulton *et al.*, 1974; Clarke, 1987). The forces acting on the till are partially alleviated as shear stress decreases (Figure 7.18b) and the presence of water between grains acts to support some of the weight of the overlying ice. This is the basis for the calculation of effective pressure (N; Equation [8], section 2.6.5, Chapter 2). An increase in the water content of the till will reduce the effective pressure acting on the till and decrease case strain (Iverson *et al.*, 1995).

This intermediate phase supports the most ideal conditions for subglacial sediment deformation (Figure 7.18b). An increase in water pressure (decrease in N) increases sediment volume and porosity, thereby reducing inter-granular friction, and causing the till to weaken (Iverson *et al.*, 1995). As the mechanical properties of the till change, the sediment yield strength (τ^*) is reduced below that of the applied shear stress (τ_b). When this occurs, when till deformation ensues, resulting in an increase in strain rate (probe tilt). Glacier flow by deformation may dominate under these conditions but movement via sliding may also still occur at the bed. This scenario highlights the importance of water pressure to mechanisms of basal motion. In the presence of water the shear stress required to cause deformation is less than that in scenario A. Water acts to weaken the till so that deformation and an increase in basal velocities occurs, rather than overconsolidation and a decrease in basal velocities.

7.10.2.3 Scenario C

Scenarios A and B reflect a positive correlation between hydrological and mechanical processes; whereby an increase in water pressure is accompanied by an increase in the strain rate of till as sediment strength decreases, and vice versa. However, a third scenario has also been observed (scenario C; Figure 7.18c). During periods of high (in excess of overburden) and/or fluctuating water pressure there is sufficient water flowing at the ice-bed interface to enable drainage development and decoupling. As the ice separates from the bed the applied shear stress is alleviated. Shear stress no longer exceeds the sediment yield strength, reducing strain rates (deformation). This produces a negative correlation between pressure and strain rate (e.g. Iverson *et al.*, 1995). Strain rates decrease with a reduction in the applied shear stress and an increase in water pressure.

Although strain rates are reduced, two outcomes relating to sediment strength (case strain) can occur under these conditions, producing both positive and negative correlations with water pressure (Fischer *et al.*, 1999). When strain rates fall below a threshold value dilation cannot be sustained and grain collapse leads to a drop in pore-water pressure and an increase in the density (or strength) of the till (Alley, 1989). This process is known as dilatancy hardening (Kavanaugh and Clarke, 2001) and results in an increase in case strain with water pressure, as sediment strength increases, despite a reduction in the applied shear stress.

In the second outcome a reduction in case strain is observed with an increase in water pressure. Fischer and Clarke (2001) explain this negative relationship as a process of elastic relaxation. As the ice decouples from its bed, the shear strain that has accumulated during periods of enhanced deformation (such as scenario B) is suddenly released. The till undergoes elastic relaxation, resulting in a decrease in sediment strength (case strain) with the removal of shear stress.

In accordance with this process, Iverson *et al.* (1995) suggest that negative tilt rates reflect an increase in till thickness, as sediments are squeezed into the cavity created at the ice bed interface during decoupling events. Unfortunately, Iverson *et al.* (1995) do not detail any ploughmeter readings. However, presumably an increase in thickness would result in an increase in till volume with water pressure, and a reduction in sediment strength (case strain). This relationship conforms with the second outcome reported above.

7.10.3 Interpretation: basal mechanics

In consideration of scenarios A, B and C, the records for probe water pressure and case strain are discussed below in order to provide further constraint on the timing and mechanisms of basal motion, particularly deformation (Figure 7.17).

7.10.3.1 Probe 10

Probe 10 showed relatively little correlation between case strain and water pressure (Figure 7.17a). The first half of the record resembles scenario A, where water pressure and deformation remain low under high shear stresses. However, a response in case strain would be expected with the increase in water pressure from day 97. This was not observed suggesting that there was actually no relationship between these two parameters. This does not fit well with any of the scenarios presented here. Negligible correlations were also found by Murray and Porter (2001) at Bakaninbreen (Table 7.6). This might suggest that water pressures were insufficient to affect the till, but the record for Probe 15 shows that this was not the case (Figure 7.17b). This variation between probes might reflect spatial differences at the glacier bed, which might result from variations in till granulometry or simply

the degree of ice-bed coupling. This might be the case if Probe 10 was located in a sticky spot.

7.10.3.2 Probe 15

The case strain record for Probe 15 showed an immediate correlation with water pressures and significant activity during the spring (Figure 7.17b). Case strain fluctuations increased throughout the spring and showed a diurnal signal that was directly in keeping with water pressure. This relationship is most obvious when pressures exceed overburden. Similar direct correlations have been observed by Murray and Porter (2001), and in one ploughmeter record by Fischer *et al.* (1999) (Table 7.6). Activity in the case strain record began very early in the season (day 346). The occurrence of this signal in December, in combination with fluctuations in resistance indicates that these sensors were already responding to changes in the water content of the till, prior to variations in water pressure (Figure 7.7b). Fluctuations in resistance reflect the presence of water flowing through the till at this time. The accompanying pattern in case strain suggests that these supposedly minor changes in water content were sufficient to initiate changes in the mechanical properties of the till. Although these changes in case strain (sediment strength) occurred prior to any significant variations in water pressure, the amplitude of fluctuations increased with the activity of water pressure. This occurred on day 1, following the first significant rise in water pressure and sustained drop in resistance (day 355).

The records of pressure and strain also became highly synchronous with the start of Event 1, demonstrating a strong relationship between the two. The correlation did not show any significant lag following day 23, similar to the findings of Murray and Porter, 2001. This implies that the strength of the subglacial sediment is dependent on water pressures and that, in turn, the motion at the glacier bed (either via deformation and/or sliding) is dependent on water pressure. An increase in sediment strength (case strain) with water pressure, although documented elsewhere (Table 7.6), is contrary to the more frequently reported inverse relationship between these two parameters (e.g. Hooke *et al.*, 1997). Under these conditions, periods of high or strongly fluctuating water pressure enable drainage development and decoupling. As the applied shear stress is removed till dilation cannot be sustained and grain collapse

results in dilatancy hardening (Alley, 1989; Kavanaugh and Clarke, 2001); and an increase in case strain (scenario C). This process occurs during decoupling, which suggests that sliding rather than deformation is occurring. The Probe 15 tilt record was also in support of this, showing minimal activity during the spring. This signifies little or no deformation (or clast rotation) in this area of the bed during this time, in keeping with scenario C. However, calculated yield strengths remained below basal shear stresses during periods of heightened water pressure (Figure 7.16b); when in scenario C, an increase in sediment strength (case strain) would be expected in order to reflect the process of dilatancy hardening.

Till strengthening through dilatancy hardening suggests that the till was previously in a state of shear and dilated. However, in the case of Probe 15, case strain remained high and constant throughout the winter, as water pressure remained low. Again little activity was recorded by the tilt sensors. These conditions are indicative of scenario A, whereby sediment strength is sufficiently high as to resist processes of deformation and dilation. The activity seen during the spring was simply an increase in case strain further to winter levels (i.e. in the same direction). The correlation with water pressure later in the spring would suggest conditions within the till have switched between scenarios A and C, without the requirement of a transitional phase of dilation, scenario B. It seems unlikely that this could be achieved within the till. Thus, a fitting explanation remains elusive and scenario C does not provide an ideal fit to the activity displayed by Probe 15. The direct relationship between water pressure and case strain is problematic and has challenged other researchers (e.g. Murray and Porter, 2001). The explanation may indeed be the result of spatial variations in coupling and till sedimentology, as suggested by Murray and Porter (2001).

The Probe 15 record also has implications for till rheology. The relationship between water pressure, force and deformation is linked to the critical yield strength of sediment. The analysis of basal motion in the previous section, for example, was based on the assumption that deformation will occur as basal shear stresses exceed sediment yield strength. This occurs if till behaves as a Coulomb-plastic material prior to failure. This dictates that water pressure and strain are strongly correlated in an inverse relationship, which was not seen at Briksdalsbreen. This might suggest

that the flow relations from Breidamerkurjøkull (Boulton and Hindmarsh, 1987) provide a more appropriate description of the till at Briksdalsbreen. However, more detailed results of the relationship between strain rates and effective pressure would be required to constrain this further; and allocate an appropriate model of flow to the deforming bed at Briksdalsbreen. Porter and Murray (2001) encountered the same difficulties at Bakaninbreen. This perhaps only goes to highlight the complexity of the system and the difficulties associated with current models of till rheology.

It should also be noted that the probe readings of case strain differ from those of the ploughmeter, which were used to generate the scenarios described above. The ploughmeter is dragged through the till, so that changes in force may result from variations in: the strength of the substrate; sliding rate; insertion depth; and till granulometrey or viscosity (Porter *et al.*, 1997; Fischer *et al.*, 1999). In contrast, the probes are not dragged through the till and the depth of their insertion should not vary rapidly. In order to understand the probe records more fully, and improve current interpretations, further probe calibration and testing is required. However, the above discussion has only aimed to highlight some of the complexities involved in assessing the hydro-mechanical relations associated with the deforming glacier bed. Developing a new model of hydro-mechanical interactions is beyond the scope of this thesis.

7.11 Synthesis

The previous two sections have discussed the nature of the subglacial hydrological regime and the mechanical processes associated with the spring event. The probe water pressure records provide an indication of the connectivity of the drainage system and the way in which it changes in response to the spring event. Unfortunately, the probe data can only be used to make inferences about the morphology of the connected drainage system. However, a transition in this system seems to occur. The mechanical processes associated with the spring suggest that periods of water pressure in excess of overburden result in decoupling, which may lead to enhanced sliding. Sliding, rather than deformation, appears to be the dominant mechanism of basal motion during the spring. These findings allow the

characteristics of the spring event to be constrained further for future comparison with other investigations (Table 7.7).

Table 7.7: The dominant characteristics associated with the spring event, based on the analysis of subglacial hydro-mechanical interactions derived from probe sensor readings.

Emergent Spring Event
Pressure rises in response to sudden relatively small-scale melt water inputs at a time of year when little or no activity is expected. Fluctuations share some or many of the characteristics of a spring event but do not result in a permanent increase in subglacial activity and change in the processes operating within the subglacial environment. Basal velocities are low and may result from a combination of sliding and deformation, but sliding generally dominates.
Main Spring Event
A sudden and rapid increase in water pressure that exceeds overburden, displays diurnal oscillations when associated with connected regions, and results in a permanent change in the activity and processes operating within the subglacial environment. This pressure rise results from a sudden high magnitude melt water input that occurs at a time of year when external temperatures are above 10°C and the snow pack has begun to retreat. It triggers a reorganisation of the morphology of the subglacial drainage system from a winter regime, where the drainage system is constricted (low capacity) and poorly developed, to a well connected summer drainage system, which can support higher water fluxes. The dominant mechanism of basal motion occurs via sliding and pressures in excess of overburden may result in decoupling and enhanced glacier velocities.

7.12 Summary

This chapter has discussed the findings of the spring sensor records, with particular focus on the spring event. In the spring, the probes are fully incorporated into the till so that a better idea of conditions in the subglacial environment can be obtained. The probe sensors displayed a sudden increase in activity during the spring, indicating that the subglacial environment had become active, after a period of quiescence during the winter. The dominant sensor activity recorded is summarised below.

- Water pressures suddenly increased and began to fluctuate (Figures 7.1b and 7.5). Pressures in excess of overburden were often recorded and Probe 15 displayed diurnal fluctuations (Figure 7.5c).
- The sensor records were divided into two events. Event 1 marked the first rise in water pressure and was followed by a return to previous conditions. Event 2 represented the second rise in water pressure and was followed by different sensor activity (Figures 7.3 and 7.8).

- Probe temperatures and resistance declined in accordance with increases in water pressure (e.g. Figures 7.1b and 7.5a,c).
- Variations in external temperature and ablation of the snow pack were associated with increases in water pressure (Figures 7.4 and 7.9).
- The lack of diurnal pressure oscillations and high frequency fluctuations indicated that the probes (apart from Probe 15) were located in unconnected regions of the subglacial hydrological system (Figures 7.1 and 7.5a,b). They did not respond to or receive direct inputs from surface derived melt water.
- The diurnal pressure fluctuations displayed by Probe 15 were out of phase with daily melt water production cycles (Figure 7.5c). This pattern was the result of pressure forcing from a neighbouring connected region of the bed (Murray and Clarke, 1995), signifying that Probe 15 was acting as a proxy for activity in connected drainage routes (section 7.6.2).

Variations in water pressure during the spring are often related to what has been termed the 'spring event' (section 7.8). The sensor activity recorded by the probes was assessed to determine if it corresponded with those characteristics traditionally associated with spring events (Tables 7.2 and 7.3). The spring event was identified in terms of the characteristics of the pressure fluctuations recorded, the timing of these events, and the changes in the subglacial hydrological system that followed (Table 7.7), as summarised below.

- The timing of Event 1 occurred very early in the year. The timing of Event 2 corresponded with the climatic conditions (e.g. max. and min. temperatures) usually associated with spring events (Figure 7.10; Table 7.4).
- Event 2 occurred during the retreat of the snow pack, corresponding with other spring events (Figure 7.10; Table 7.4).
- Event 1 was classified as the Emergent Spring Event. The pressure rises occurred prior to the retreat of the snow pack and were generally less than overburden pressure (section 7.8.2). This event did not result in a sustained change in subglacial processes but was also followed by a period of quiescence (Figure 7.11; Table 7.7).

- Event 2 was termed the Main Spring Event. The pressures rises occurred suddenly and were often in excess of overburden (Figure 7.11). The pressure fluctuations were followed by a change in sensor activity, indicating a permanent change in subglacial processes. These characteristics were more in keeping with spring events recorded elsewhere (Tables 7.2, 7.3 and 7.7).
- The form of the spring event (pressure fluctuations) differed between connected (Probe 15) and unconnected regions of the bed. These variations were described by a conceptual model of subglacial hydrology (Figure 7.12).
- The sudden, high magnitude pressure fluctuations of the spring events caused the subglacial hydrological system to develop. A transition from a winter to a summer drainage regime was evident in the change in sensor activity following the spring event (section 7.9.1; Figure 7.12; Table 7.7).

An attempt was made to relate the spring activity in water pressure to changes in the mechanical properties of the deforming bed and mechanisms of basal motion (section 7.10). This involved comparisons between water pressure, case strain, tilt and the critical yield strength of till for Probes 10 and 15. The main findings are summarised below.

- Probe 10 showed relatively little activity in water pressure, case strain and tilt during the spring (Figures 7.15a and 7.17a).
- Probe 15 recorded a direct relationship between fluctuations in case strain and water pressure, but showed little activity in tilt (Figures 7.15b and 7.17b).
- Probe 10 critical yield strength was in excess of basal shear stress, indicating that sliding was the dominant form of basal motion (Figure 7.16a).
- The critical yield strength calculated for Probe 15 was exceeded by basal shear stress during periods of high magnitude water pressure (Figure 7.16b). However, pressures in excess of overburden suggested that sliding was the dominant form of basal motion, causing the ice to become decoupled from its bed. The dominance of sliding rather than deformation was supported by the lack of probe rotation in the tilt record (Figure 7.15b).
- A direct correlation between water pressure and sediment strength (Probe 15) was also recorded at Bakanninbreen, Svalbard (Table 7.6). This was not in

keeping with the majority of investigations and is difficult to explain with current models for till rheology and basal mechanics (section 7.10.3).

Probe 4, located in the englacial environment, was also functional during the spring. The sensor activity displayed readings specific to the englacial environment.

- Tilt readings showed the greatest activity at the start of the spring, indicating that the probe was oscillating in the base of the borehole. This may have been in response to surface water inputs (Figures 7.1a and 7.2a).
- As the spring progressed, water pressures and case strain increased, as probe temperature decreased.
- The rise in case strain indicated that the probe was responding to changes in the dimensions of the borehole, triggered by enhanced ice deformation, as glacier velocities increased towards the summer.
- A gradual change in tilt with small oscillations suggested that the probe was now confined within the borehole.
- Probe 4 ceased communicating data at the end of the spring. Probe failure may have resulted from crushing or simply a loss of communication.

To summarise the spring, sensor activity (particularly in water pressure) began very early in the year and was correlated to changes in external weather conditions. The spring event was identified based on the characteristics of the pressure fluctuations recorded, the timing of these events, and the changes in the subglacial hydrological system that followed (Table 7.7). The fluctuations in water pressure were associated with a two stage spring event, an initial emergent spring event followed by the main spring event. The main spring event resulted in the development of the subglacial hydrological system and a change in the processes operating at the glacier bed. These records demonstrated that there was considerable activity within unconnected regions of the subglacial hydrological system. Sliding via decoupling, appeared to be the dominant mechanism of basal motion during the spring. However, the relationship between sediment strength (case strain) and water pressure was not fully constrained. Further study of hydro-mechanical interactions is required to resolve this issue.

Chapter 8

Summer Probe Record

8.1 Introduction

This chapter will discuss the activity of the probes during the summer record. This encompasses the period following the spring event, starting in May and running to the end of the probe records. The longest probe records finished at the start of August, equating to over a year of data collection. Five probes were still operational during this time, two from 2004/5 and three from 2005/6. After nine months within the subglacial environment the probes were fully incorporated into the deforming bed and able to monitor environmental conditions consistently. In the summer, melt water production is at its highest. As a result, the subglacial drainage system is also well developed and able to sustain highly variable high magnitude flows.

In the summer month, glacier velocities tend to increase with the amount of melt water inputs. The processes of sliding and till deformation are inter-related (hydro-mechanical coupling) and both can contribute to total basal velocities. Melt water inputs to the subglacial environment can lubricate the bed, reducing basal drag and enhancing glacier velocities via sliding. When water pressures exceed overburden the glacier may become decoupled from its bed, causing a further increase in velocity. If water pressures are low, basal drag is increased and the glacier becomes strongly coupled to its bed. This can lead to sediment deformation. The application of shear stresses causes those sediments to move via processes of ductile deformation, brittle shear, or as a discrete body along internal shear planes or over underlying bedrock (Benn and Evans, 1996). Deformation can occur when the

critical yield strength of the sediment is exceeded by the applied shear stress. In the subglacial environment, this tends to occur when the till becomes saturated. This reduces inter-granular friction and causes the till to weaken. The critical shear strength of sediments is related to their water content through the Mohr-Coulomb yield criterion (Equation [3]). Deformation is also associated with the movement of clasts within that till, in response to the overall shear of the sediment body.

Mechanisms of sliding and deformation can occur at the same time, but it is thought that normally one process dominates over the other. In light of this, this section will focus on identifying the subglacial processes operating during the summer period, when glacier activity is at its maximum. The sensor records will be examined to identify the mechanisms of basal motion, their temporal occurrence and spatial distribution.

This chapter is dominantly concerned with the movement of the probes within the deforming bed. Glacier velocities are at their greatest in the summer months and it is during this time that mechanisms of basal motion will contribute most effectively to net glacier velocities. The probes were designed so that they could behave naturally as clasts within the deforming bed. As such, the probe tilt sensor records were analysed more closely to determine the orientation and movement of the probes during the summer. The type of probe movement can indicate if the till is subject to deformation, and the temporal and spatial variations associated with that process. This information, in conjunction with water pressure readings, can provide an indication as to when processes of sliding and/or deformation are occurring, and in what relative proportions. The angle and direction of probe tilt along each axis was explained in section 4.2.1.4 (Chapter 4) and will be discussed in this section. Testing revealed that when tilt on the x and y (or z and y) axes changed in combination, showing either an increase or decrease in tilt *in the same direction,* the probe was rotating. If tilt along these axes moved in opposite directions rotation did not occur, the probe was simply changing orientation. Figure 4.7 is replicated as Figure 8.1 below to aid in the interpretation of probe tilt.

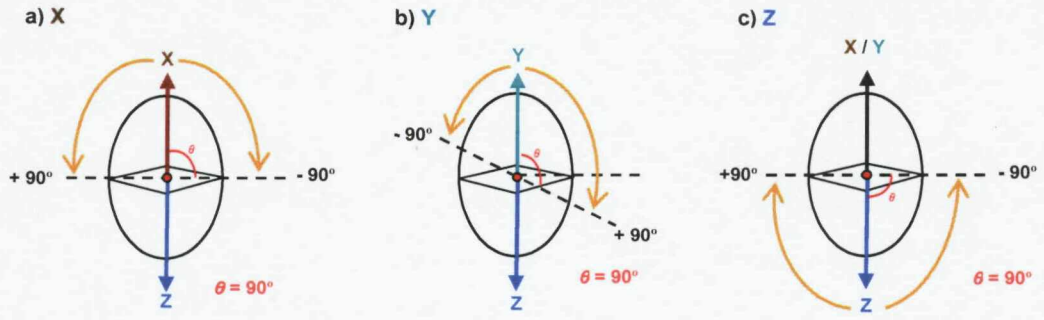


Figure 8.1: Conceptual diagram to show the orientation of the axes associated with the tilt sensors for: a) x-axis; b) y-axis; and c) z-axis.

8.2 2004/5

Probes 4 and 8 were still functioning during the summer period in 2005. The summer record for Probe 4 was very short, finishing on day 144. As a result, the end of this record was incorporated into the spring period and was discussed in Chapter 7. Only Probe 8 remained functional for the whole of the summer (Figure 8.2). In total, the probe record lasted for over a year (375 days). The relative position of Probe 8 is shown in Figure 5.17 (section 5.5, Chapter 5).

8.2.1 Probe 8

Probe 8 continued to show activity throughout the summer, until day 236 when the record ceased (Figure 8.2). Average weekly probe temperatures continued to oscillate throughout the summer (Figure 8.2a). Temperatures remained between 0.08-0.10°C until day 175, when values began to increase. Average values continued to oscillate but generally remained above 0.10°C from day 182, reaching 0.13°C by the end of the record. Water pressure was already high at the start of the summer record. Values were sustained above overburden pressure and characterised by small-scale fluctuations. Pressures oscillated between 139.5-146.1% (days 121-170), before showing a gradual decline. Pressures decreased from 143.9-120.5% between days 171-217. A second, more rapid phase of decline ensued between days 218-236. Pressures fell below overburden on day 224, reaching 20.1% before failure.

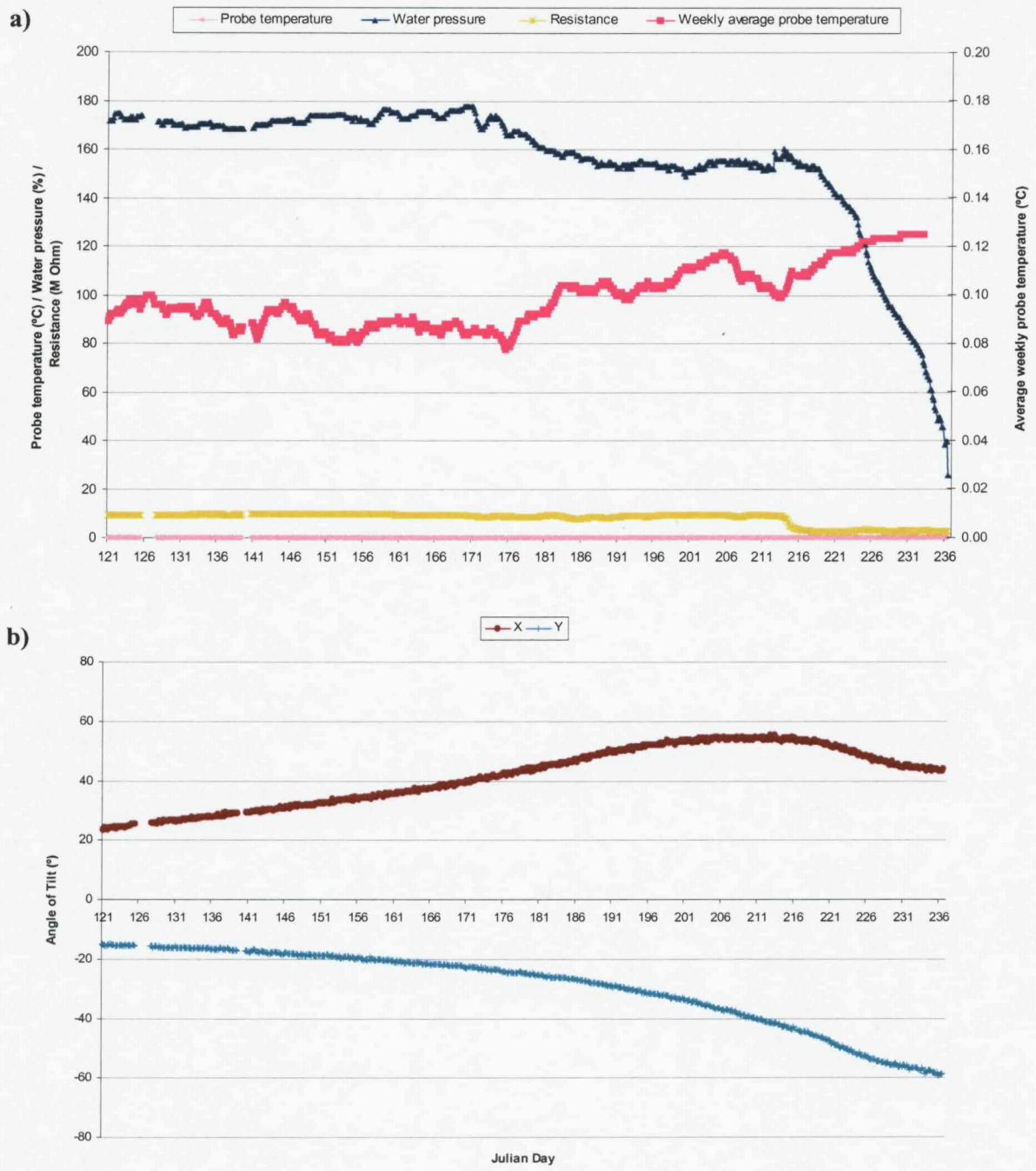


Figure 8.2: Summer sensor records for Probe 8 (2004/5), showing: a) probe temperature, water pressure, resistance and average weekly probe temperature; and b) tilt. Note: tilt on the z-axis is not displayed because the record did not show any change.

8.3 Interpretation: 2004/5

The subglacial activity recorded during the summer months was initiated during the spring event (Chapter 7). These processes were sustained by enhanced melt water inputs, generated by precipitation events and increases in external temperatures. The

summer has traditionally been associated as the period of greatest glacier activity. The Probe 8 record was examined in order to identify correlations with the changing weather conditions and subglacial processes, particularly with respect to mechanisms of basal motion.

8.3.1 Correlations with external weather conditions

Probe 8 did not show any correlations with small-scale external weather conditions during the summer (Figure 8.3). Water pressures remained elevated and any oscillations were not diurnal in nature and did not coincide with precipitation events. The lack of response was expected given the location of Probe 8 in an unconnected region of the bed (section 7.9.1, Chapter 7). Despite this, there were some long term variations in the magnitude of external temperatures that appeared to correspond with variations in the pressure record.

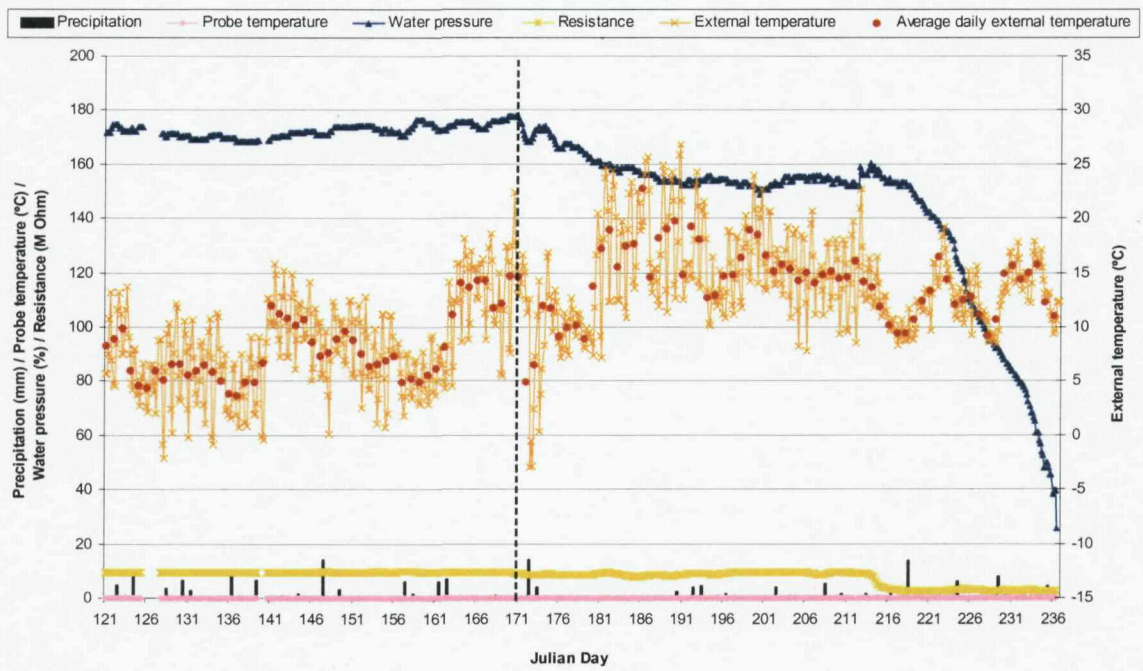


Figure 8.3: Summer sensor record for Probe 8, comparing external weather conditions with probe temperature, water pressure and resistance. Note: the dashed line marks the start of a decline in water pressure as external temperatures increased above 20°C.

At the start of the summer external temperatures were still fluctuating below 0°C, even though average daily values generally fell between 5-10°C (Figure 8.3). Temperatures peaked at 22.4°C on day 170, and it was after this that water pressures began to decline (day 171). As external temperatures increased above 25°C, (with average daily values between 10-20°C) water pressure continued to decrease. The rate of this decline increased from day 218. Pressures fell as elevated external temperatures enhanced the drainage capacity of connected regions of the bed. This resulted in a reduction in the amount of melt water transferred to the area around Probe 8, which was not directly within a connected region of the bed. The subsequent increase in the rate of decline (day 218) may simply reflect an accelerated effect from the expansion of drainage routes in response to the prolonged period of average daily temperatures above 15°C (days 180-212; Figure 8.3).

8.3.2 Subglacial processes

Probe 8 was located in an unconnected region of the bed. This was demonstrated by the absence of diurnal pressure oscillations, which continued into the summer months (Figure 8.2a). However, the sustained water pressures, above overburden, signify that large quantities of melt water were passing through this area. These pressures may reflect the dominance of sheet flows or a strong hydraulic gradient with a well developed neighbouring connected region. This would enable such pressures to be sustained for this length of time. Again, the lack of diurnal oscillations would suggest that the source of melt water was not directly derived from surface inputs.

The subsequent decrease in pressure would suggest that the capacity of the proximal connected drainage pathway had expanded. The source of melt water to this area of the bed may have also decreased or changed route in response to these developing pathways, potentially accelerating this decline. Subglacial drainage routes expand in the summer as melt water inputs increase, and enhance the amount of frictional melting within channels. This allows drainage routes to be sustained and augments the rate of channel expansion. As the summer progresses, it is also likely that more numerous small-scale drainage routes will develop. These factors will act to increase drainage efficiency and thus, reduce pressures in unconnected regions of the bed.

The rate of decline in water pressure increased from day 218, suggesting that the glacier drainage system had become fully developed and was responding to the elevated external temperatures that had been sustained since day 174 (Figure 8.3).

Resistance began to show oscillations from day 170 and then decreased from day 214, in conjunction with water pressure (Figure 8.2a). However, resistance displayed an out of phase relationship with water pressure. This decline in values indicated wetter conditions, as water pressure decreased. The resistance sensor had not changed in unison with water pressure since the start of the winter record (days 252-264). Resistance had remained elevated and relatively unresponsive to changes in water pressure for the majority of the winter and spring records. The previous decline in resistance occurred during the spring record in good agreement with an increase in water pressures above overburden. Summer resistance values had not changed prior to this, reflecting dry conditions, despite water pressures in excess of overburden.

The impassive nature of the resistance record was thought to reflect the probe's location within the deforming bed. As resistance had indicated dry conditions despite pressures above overburden, it was even more unusual that resistance should decrease with pressure from day 214. The reduction in resistance in combination with water pressure may reflect a change in the location of the probe, or the processes operating within the deforming bed during the summer. Alternatively, this change might suggest that the resistance sensor was responding to changes in the mineral content of the water, as opposed to the actual volume of water in the till. The mineral concentration of water will decrease as the amount of melt water rises. The decrease in resistance at the end of the summer may reflect an increase in mineral concentration, as water pressures fell. Ultimately, it is difficult to ascertain the cause for this activity and the relationship with water pressure without further calibration and testing. The readings of average weekly probe temperature did show a good agreement with changes in water pressure (Figure 8.2a). Values showed a two step change on days 175 and 213 in association with the staggered decline in water pressure (Figure 8.2a). However, temperatures did not increase to those observed at the start of the sensor record, reflecting different conditions within the till, as opposed to at the ice-bed interface after deployment.

8.3.3 Drainage morphology

The Probe 8 water pressure record was highly elevated. However, only minor fluctuations were recorded. This suggests that, following the spring event, Probe 8 was located in an inactive unconnected region of the bed that was highly pressurised. Unfortunately, there are no corresponding probe records for the connected regions of the bed from the 2004/5. As such, it is difficult to draw any conclusions about the nature of the connected drainage network at this time. However, it is likely that the high magnitude pressures were sustained by a strong hydraulic gradient with a highly efficient connected drainage system. Efficient summer drainage systems would typically form a discrete drainage morphology. The decrease in water pressure from day 218, associated with prolonged elevated external temperatures, suggests that the connected drainage network had become highly developed by this point. The sudden reduction in Probe 8 water pressure may reflect an expansion (increase in capacity) of the connected system or a transfer of that system to another area.

8.3.4 Probe movement

The movement of Probe 8 within the till is displayed by the tilt record (Figure 8.2b). Consistent change along the x and y axes was recorded throughout the spring. Activity had begun to increase from day 101, but the greatest rates of change occurred during the summer months. At the start of the summer (day 121), the angle of tilt along the x and y axes increased (days 121-216), but not in the same direction. This signifies that the probe was not rotating but it was experiencing increased movement during this time, in both the rate and direction of motion. This reflects the probe changing orientation within the glacier bed. In this period (days 121-215), it tilted backwards, near to horizontal (23°) and moved in orientation.

The direction of rotation along the x-axis changed from day 216 and began to move in the same direction as the y-axis (Figure 8.2b). This caused the probe to rotate clockwise about its y-axis, whilst tilting backwards along its x-axis (Figure 8.4b). This pattern was sustained for the rest of the record (days 216-236). The rate of rotation (rate of change) increased throughout the summer. At the start of the summer the x and y axes showed rates of 0.4° day $^{-1}$ and 0.3° day $^{-1}$, respectively. At

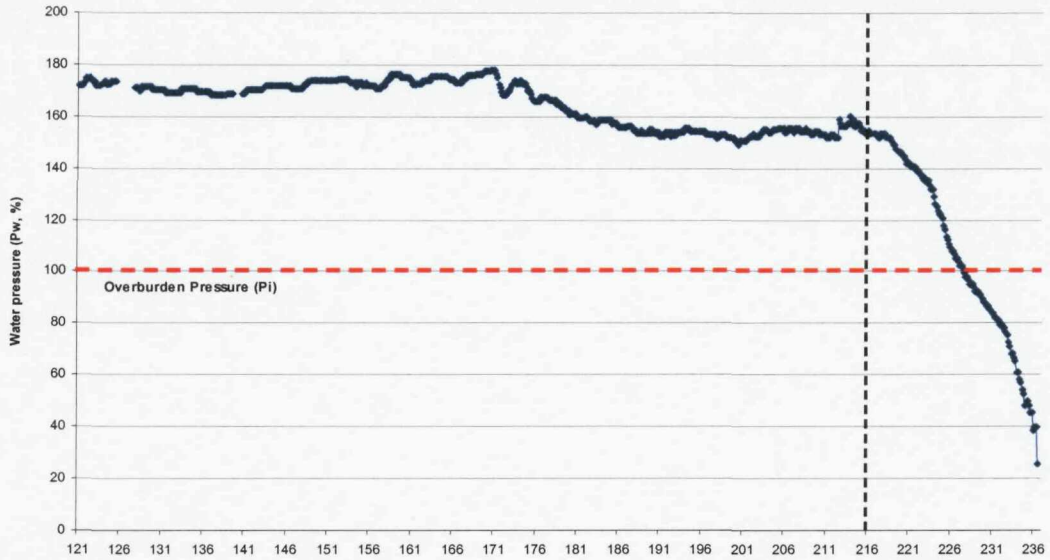
the end of the record values peaked at 0.6° day^{-1} on the x-axis, and 1° day^{-1} on the y-axis.

8.3.5 Basal motion

The Probe 8 water pressure and tilt records can be interpreted to determine the dominant mechanisms of basal motion. Water pressure recorded values in excess of overburden between days 121-223 (Figure 8.4a; Table 8.1). This magnitude of pressure would be sufficient to allow the overlying ice to float and become decoupled from its bed. This would reduce basal drag in this area of the bed and provide ideal conditions for enhanced sliding. It would be useful to have the strain records for this period, in order to determine if the probe was experiencing a reduction in case strain in response to decoupling. However, as section 7.10 (Chapter 7) highlighted, even with a record for case strain, there may not be a straightforward relationship between the two. The tilt record (Figure 8.2b) suggests that the probe was changing orientation quite quickly between days 121-215.

The activity in tilt changed between days 216-236 and the probe began to rotate, varying in tilt at a faster rate. This change suggests that the dominant mechanism of basal motion had switched. If sliding occurred previously, the rotation of the probe (days 216-236) indicated that deformation was now the dominant mechanism of basal motion (Table 8.1). This shows that the fastest rates of change in tilt occurred during the period of till deformation (days 216-236). Probe rotation began just prior to the rapid decline in water pressure from day 218, when values were still above overburden. Thus, deformation was not expected, given the magnitude of water pressures. The probe's rotation would also indicate that, although the process of decoupling requires pressures to be in excess of overburden, it may not always occur when these conditions are achieved. If the tilt record is accepted, this might suggest that pressures in excess of 154% were required for decoupling to occur. In addition, processes of sliding and deformation may occur in unison, to different degrees. In general, the overall decline in pressures implies that the glacier was becoming more strongly coupled with the bed. An increase in basal drag is associated with deformation and the enhanced rates of change in tilt at the end of the summer.

a)



b)

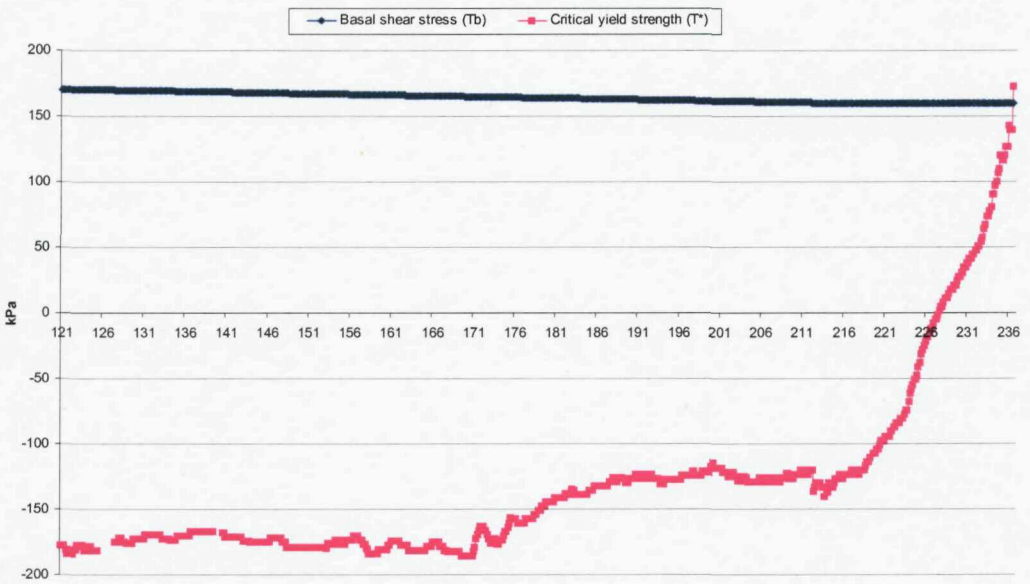


Figure 8.4: Summer record for Probe 8 showing: a) water pressure (Pw) in relation to overburden pressure (Pi), highlighting the most likely period of basal motion via enhanced sliding; and b) the critical yield strength (τ^*) of the till in relation to the basal shear stress (τ_b), showing the most likely period of till deformation when $\tau^* < \tau_b$. Note: the area to the right of the black dashed line marks the period of probe rotation.

Table 8.1: Variations in the timing (in days) of the dominant mechanism of basal motion (sliding or deformation) according to readings of water pressure, critical yield strength and basal shear stress, and probe rotation.

Probe	Sliding (Pw>Pi)	Deformation (T*<Tb)	Deformation (probe rotation)
8	121-223	121-236	216-236

In order to investigative the relationship between sliding and deformation further, the critical yield strength of the sediment associated with Probe 8 was calculated and plotted in relation to the applied basal shear stress (Figure 8.4b). In a Coulomb-plastic model of till rheology, deformation occurs when the critical yield strength of till is exceeded. Figure 8.4b demonstrates that basal shear stresses were in excess of sediment yield stress between days 121-236. This suggests that deformation was occurring throughout the summer (Table 8.1), even when pressures were in excess of overburden and the glacier was thought to be decoupled from its bed and sliding (days 121-223; Figure 8.4a). However, probe rotation was only recorded between days 216-236, limiting the time of deformation. Clearly, there is a conflict of results.

The rotation of the probe and the values of yield strength do coincide between days 216-236 suggesting that this would be the optimum time for deformation to occur. A decrease in sediment strength is associated with increases in the water pressures and thus water content, which would act to weaken the till by reducing frictional strength. However, water pressures in excess of overburden are thought to decouple the glacier from its bed, which would disable deformation. Thus, although basal shear stresses exceeded till strength, the lack of probe rotation and the magnitude of water pressure would suggest that deformation was not occurring until pressures fell below 154%. Alternatively, the overlap between decoupling and probe rotation may suggest that there was a period when both sliding and deformation were in operation. Deformation may only have led as the dominant mechanism of basal motion from day 224, when water pressures fell below overburden and the ice was much more strongly coupled to its bed. At this time, it does not seem possible to differentiate between these two eventualities with confidence.

8.4 2005/6

Probes 10, 12 and 15 were still operational during the summer period (days 121-the end of the sensor records). Probes 10 and 12 lasted over a year within the subglacial environment (days 213-221 and 217-221, respectively), whilst the Probe 15 record ended just short of a year (days 217-207). The relative positions of the probes are displayed in Figure 5.18 (section 5.5, Chapter 5) and the summer records are shown

in Figures 8.5 and 8.6. The record for Probe 15 is displayed from days 121-149. The remainder of the sensor record (days 150-207) is displayed and discussed independently in section 8.5.6, for simplification.

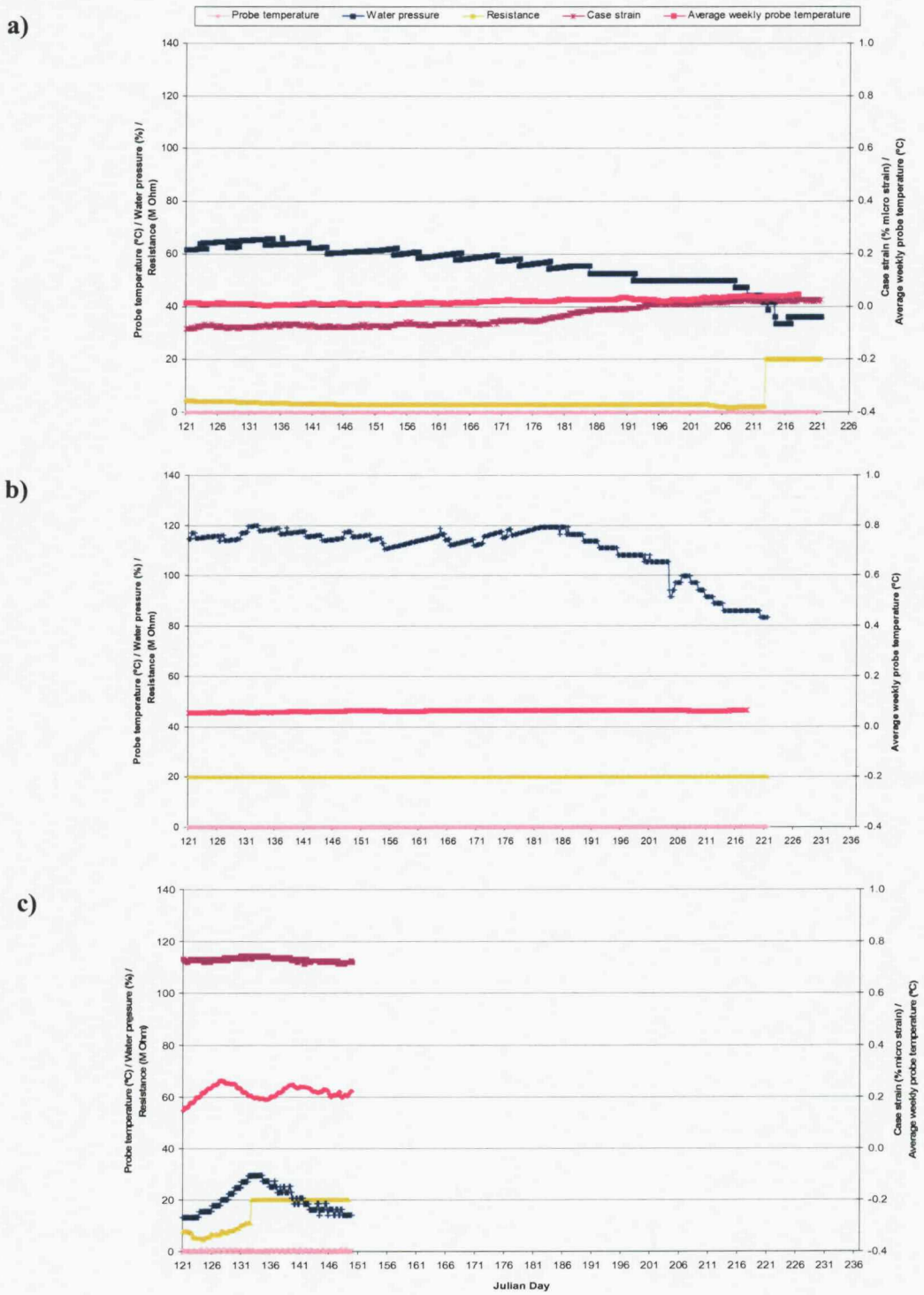


Figure 8.5: Summer sensor records showing probe temperature, water pressure, resistance, case strain and average weekly probe temperatures for: a) Probe 10; b) Probe 12; and c) Probe 15 (2005/6). Note: Probe 15 case strain is also plotted on the secondary y-axis.

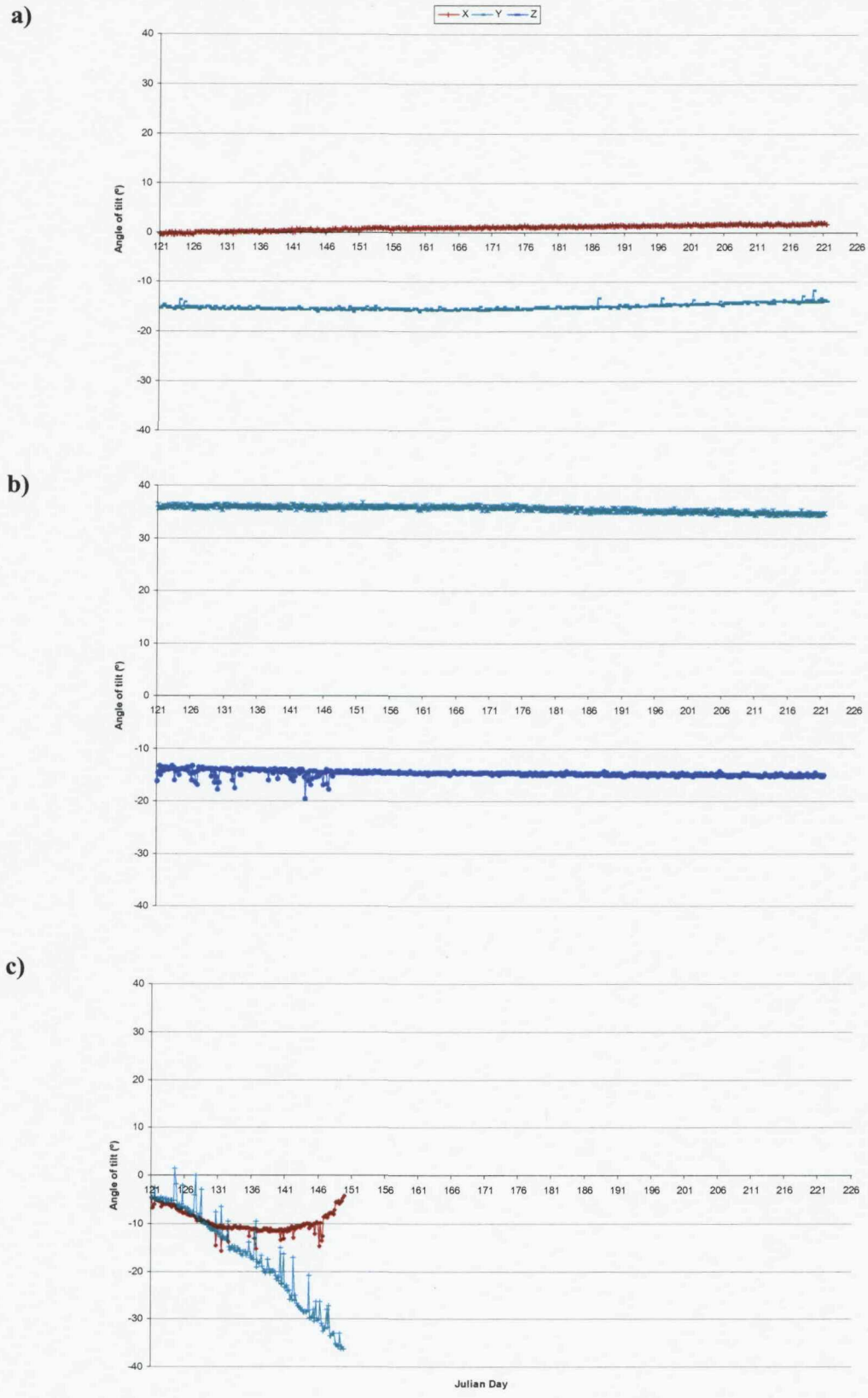


Figure 8.6: Summer tilt sensor records for: a) Probe 10; b) Probe 12; and c) Probe 15 (2005/6).

8.4.1 Probe 10

Probe 10 showed relatively little variation in the summer Figures 8.5a and 8.6a. Average probe temperatures continued to oscillate throughout the summer, showing a general increase in values throughout this time (Figure 8.5a). Values exceeded 0.02°C on day 168 and remained above 0.04°C (day 216) in the final days of the record. Water pressure fluctuated between 61.7-66.1% (days 121-139), before showing a gradual, 'terraced' decline in values from day 140. Pressure remained consistent at 49.9% (days 192-207), falling to 36.1% (days 217-221). Resistance decreased gradually during the start of the summer from values of 4.3 M Ohm (day 121). The rate of decline slowed throughout this period and values remained constant between days 206-212 (1.9 M Ohm). Resistance returned to 20.2 M Ohm on day 213, for the rest of the record. Case strain showed minor oscillations throughout the summer. Values were relatively stable between days 121-169, but began to increase steadily from day 170, showing minor fluctuations (days 209-221). Probe 10 showed relatively little change in tilt over the summer period (Figure 8.6a). Over the summer, frequent small-scale fluctuations (<1°) were recorded and a slight net increase in the angle of tilt.

8.4.2 Probe 12

Probe 12 displayed minimal activity during the summer record (Figure 8.5b). Average probe temperatures continued to increase, with minor oscillations between days 121-148. Values then stabilised at 0.06°C for the rest of the record. Water pressure displayed small-scale oscillations between 110.7-120.0% (days 121-184). This was followed by a general trend of decline from 119.3-83.2% (days 121-221). Pressure fell below overburden on day 204. Resistance remained constant at 20.2 M Ohm. There was little activity in the tilt record (Figure 8.6b). The z and y axes showed a net decline in values, with minor oscillations (days 121-147).

8.4.3 Probe 15

The Probe 15 record displayed the most activity during the summer (Figure 8.5c). Probe temperature ranged between 0.06-0.8°C (days 121-176) and fluctuations began to exceed 1°C from day 177. Average probe temperatures displayed a peak-trough

sequence of variations. Peak average temperatures of 0.3°C occurred on days 127 and 139, with a minimum of 0.2°C on day 134. Water pressure increased from 13.3-29.5% (days 121-132), before decreasing gradually to 14.1% (days 134-149). At the start of the record, resistance decreased from 7.9-4.6 M Ohm (days 121-124). Values then began to increase, accompanied by small oscillations, between days 124-132. Resistance abruptly rose to 20.2 M Ohm (days 132-149), before falling to 0.8 M Ohm. Case strain showed small-scale fluctuations throughout the record. The direction of applied strain (days 121-134) changed from days 135-149. The tilt record for Probe 15 is shown in Figure 8.6c. The x and y axes showed similar activity at the start of the summer, changing in the same direction quite rapidly. Tilt on the x-axis experienced a rapid change in the direction of tilt from day 142, accompanied by short term oscillations. Tilt on the y-axis continued to increase in the opposite direction, recording more frequent oscillations (days 165-149).

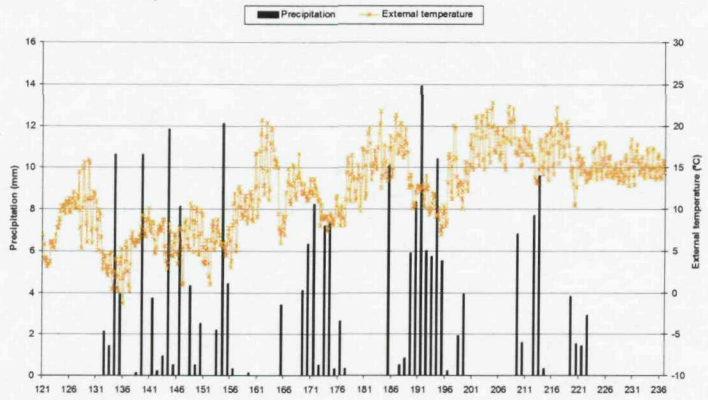
8.5 Interpretation: 2005/6

The 2005/6 summer period follows the end of Event 2c in the spring record. The end of the spring event marked the start of new processes, associated with summer conditions, within the subglacial environment. Similar to Probe 8, the probe sensor activity was analysed to determine any links with external weather conditions and mechanisms of basal motion. Sensor readings should indicate whether the sliding or deformation was occurring, over what time period, and in what areas.

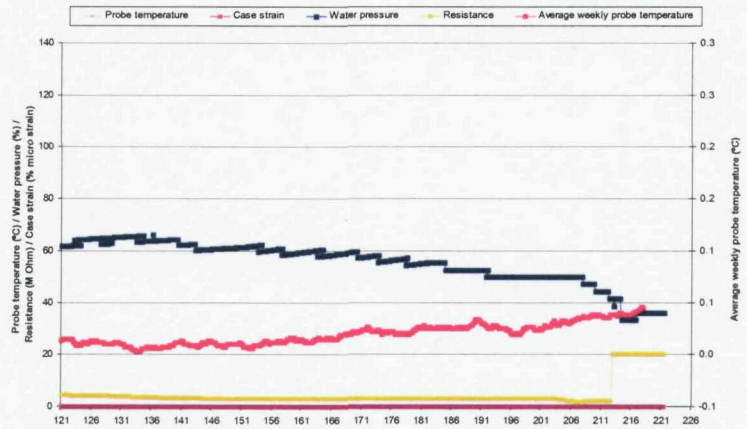
8.5.1 Correlations with external weather conditions

Probes 12 and 15did not show any direct correlation to oscillations in external weather conditions (Figure 8.7). However, Probe 10 displayed a tenuous link to external weather conditions. Water pressures began to decline four days after external temperatures increased, and remained, above 0°C (day 136). None of the probes responded to the numerous precipitation events recorded from day 132. On a larger scale, all the probes experienced a general decline in pressures during the summer as external temperatures increased. This reduction in pressure is likely to reflect the development of connected drainage systems across the glacier bed, removing water, or increasing the rate of transfer, from these unconnected regions.

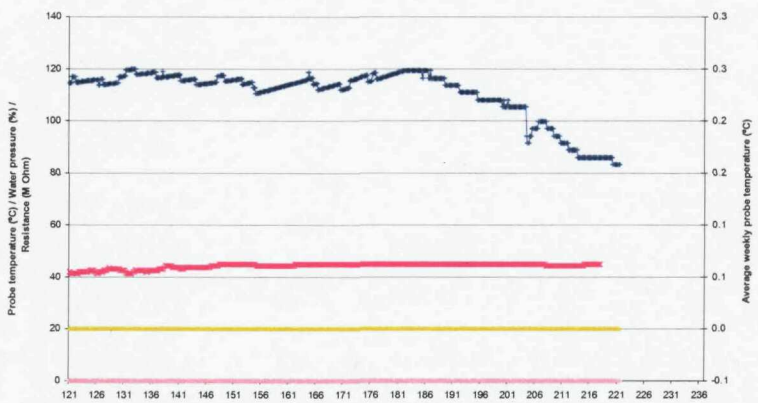
a)



b)



c)



d)

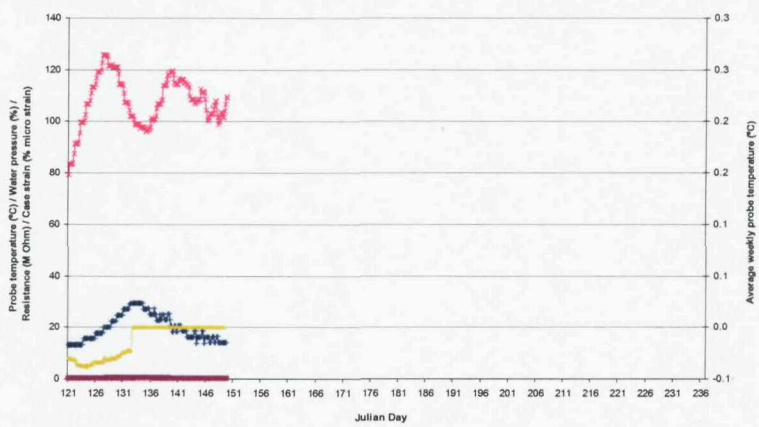


Figure 8.7: Comparison of summer sensor records for: a) external weather conditions; b) Probe 10; c) Probe 12; and d) Probe 15 (2005/6).

8.5.2 Subglacial processes

Probes 10 and 12 recorded few variations during the summer period. Probe 10 water pressures declined gradually and resistance remained low, reflecting the moderate water pressures (66.1-41.6%). Resistance rose at the end of the summer when pressures fell below 41.6% (Figure 8.7b). Average probe temperature increased during the summer reflecting the overall decrease in water pressure within the subglacial environment. Probe 12 saw a similar pattern but values declined from above overburden (119.2%) from day 185 (Figure 8.7c). Resistance did not vary and average probe temperatures showed fewer fluctuations.

The lack of diurnal oscillations in the pressure records confirms the location of the probes within a unconnected region of the bed (Chapter 7). The decline in values and lack of fluctuations in general suggests that water was being drawn away from these areas of the bed. This occurs in response to the development of high capacity connected drainage networks in the connected regions of the glacier bed during the summer months. This is in good agreement with the continued elevation in external temperatures, increasing melt water inputs and maintaining channels at the ice-bed interface. Probes 10 and 12 did not record heightened summer oscillations. However, Probe 12 did display pressure in excess of overburden, suggesting that large quantities of water in this area of the bed.

Probe 15 showed more fluctuations during the summer (Figure 8.7d). Water pressure increased to 29.5% between days 121-132. This may reflect continued activity in response to the spring event, as pressures showed an overall trend of decline from day 134, in keeping with Probes 10 and 12. Diurnal fluctuations were not recorded signifying that Probe 15 was no longer subject to pressure forcing from the connected region of the bed. The spring event drove the development of a high capacity summer drainage network that could now be sustained by external weather conditions. As a result, the water pressure within the area of the bed around Probe 15 was in decline, as water was drawn away into the more efficient drainage routes.

The responses in the other Probe 15 sensors were quite unusual throughout the summer period. This reflected a change in the processes operating around Probe 15, following the spring event. The increase in resistance reflecting drier conditions was

in poor agreement with the slight increase in water pressure at this time. However, this could reflect a larger-scale, or long term, response to the overall decline in water pressures after the spring event.

Average probe temperature also displayed an odd record of fluctuating values. Temperatures increased just prior to the pressure peak on day 134, in conflict with the relationship normally associated between the two. This had not occurred previously and may reflect a change in the probe's location, different subglacial processes, or sensor response, following the spring event. Probe temperatures also increased above 0.3°C (day 176), which had not previously been recorded within the subglacial environment. In light of the continued decline in water pressure, this increase strongly suggested that the probe had changed location. Temperatures in excess of 0.3°C have been associated with englacial conditions and would suggest that the probe was moving into an englacial cavity. This scenario is discussed in more detail in association with probe movement in the next section. Case strain continued to show oscillations in varied directions throughout the summer reflecting the movement of the probe with the subglacial environment.

8.5.3 Drainage morphology

The probes recorded relatively little activity in water pressure following the spring event. Probes 10 and 12, and from day 134 Probe 15, showed a gradual decline in pressures, without any indication of diurnal oscillations or other fluctuations. This suggests that they remained within unconnected regions of the bed, following the spring event. These sensor readings provide little indication as to the nature of the connected subglacial drainage network during the summer. However, Probe 12 displayed pressure in excess of overburden, indicating a strong hydraulic gradient with a well developed connected area, likely to be characterised by a discrete drainage network. The minimal pressures and the lack of fluctuations recorded by Probe 15 also suggests that the proximal connected area had become sufficiently developed to accommodate an increasing influx of melt water in the summer months. In fact, the gradual decline in pressures recorded by all three probes might suggest a general expansion of the connected regions, with an increasing drainage efficiency resulting in a gradual reduction in pressure in these regions. The formation of

discrete, high capacity (low pressure) drainage networks would be required in order to draw water away from other low capacity (high pressure) regions of the bed. Again this implies that a high capacity summer drainage network had formed following the spring event.

8.5.4 Probe movement

Probes 10 and 12 showed relatively little movement during the summer record (Figure 8.6a, b). Probe 10 saw a gradual change in tilt in the same direction along the x and y axes, indicating that it was rotating slowly. Probe 12 recorded similar activity with one degree of change along the z and y axes, signifying a small amount of rotation. The rates of change in tilt recorded by Probes 10 and 12 were generally low. However, Probe 10 experienced a small increase in the rate of rotation towards the end of the summer, whilst Probe 12 recorded a slight decrease.

In contrast, Probe 15 was subject to numerous changes in activity and orientation (Figure 8.6c). The movement of Probe 15 had actually begun to change from day 113, increasing in the same direction along the x and y axes (days 113-141). This implied that the probe had begun to rotate within the till. This ceased from day 142 when the direction of tilt on the x-axis and increased rapidly in the opposite direction. The probe had stopped rotating and had begun to show a general change in orientation, towards a more upright position. In the period when Probe 15 was rotating (days 113-141), the rates of change were high, at 0.8° day^{-1} on the x-axis, and 0.6° day^{-1} on the y-axis. These rates slowed from day 130, to 0.2° day^{-1} and 0.3° day^{-1}, respectively, before rotation ceased on day 142 (i.e. tilt on the x and y axes began to change in opposite directions, section 8.5.6).

8.5.5 Basal motion

The tilt records indicate if deformation is occurring through probe rotation, whereas the other sensor readings can indicate if sliding is operating. The slow changes in tilt (rotation) recorded by Probes 10 and 12 suggest that these areas of the bed were not subject to significant till deformation. However, the case strain record for Probe 10 (Figure 8.8a) displayed a change in the direction of applied strain. This would

suggest that rotation, and thus deformation, was occurring, despite the seemingly small changes in tilt (Table 8.2).

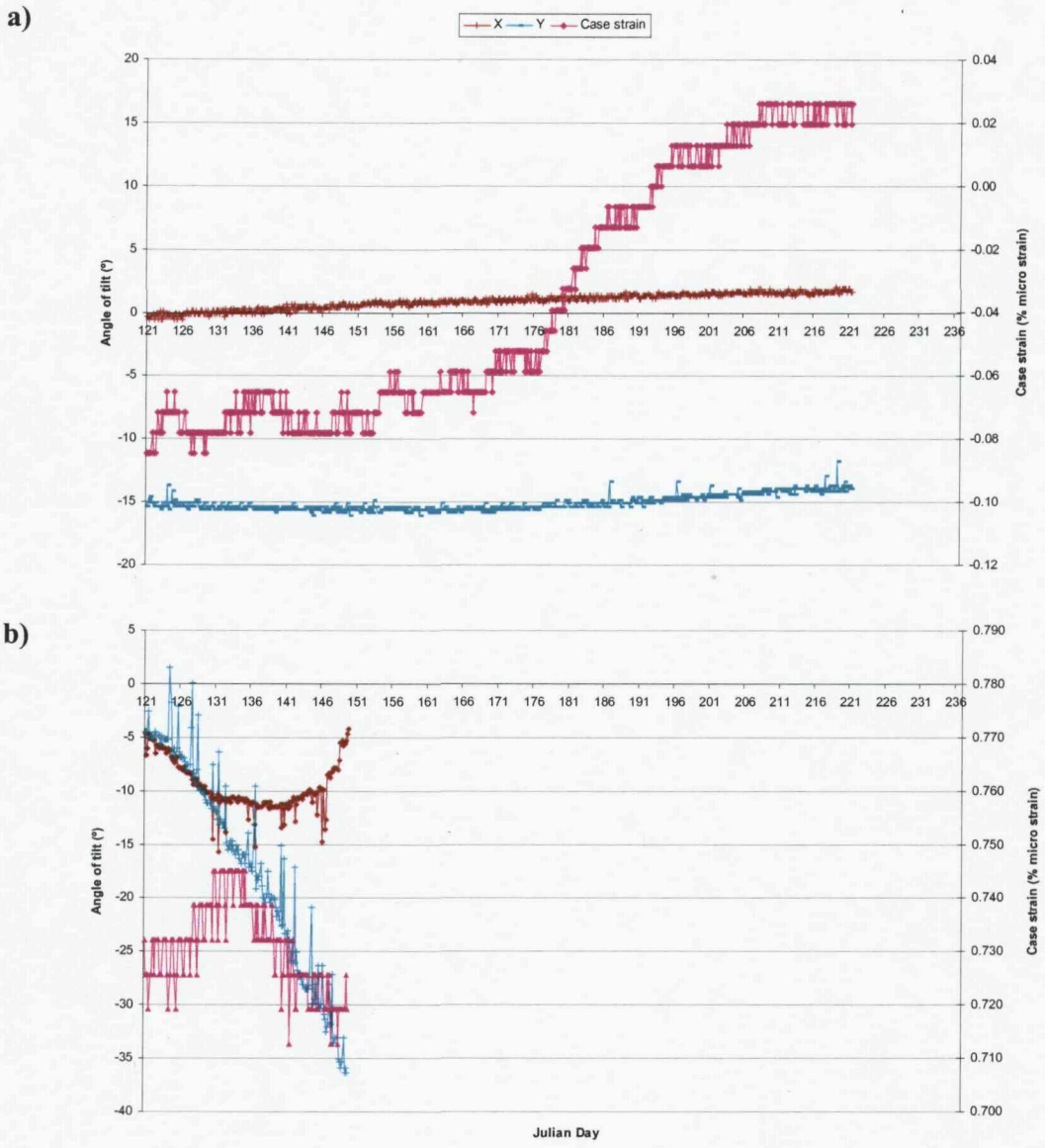


Figure 8.8: Comparison between tilt and case strain sensor records for: a) Probe 10; and b) Probe 15. Note: different scales on the y-axes.

Table 8.2: Variations in the timing (in days) of the dominant mechanism of basal motion (sliding or deformation) according to readings of water pressure, critical yield strength and basal shear stress, and probe rotation.

Probe	Sliding (Pw>Pi)	Deformation (T*<Tb)	Deformation (probe rotation)
10	-	214-221	121-221
12	121-203	-	121-221
15	-	121-149	121-142

The critical yield strength calculated for the till associated with Probe 10 supports this idea (Figure 8.9a). Sediment strengths were less than the applied shear stress throughout the summer, indicating that the till was likely to deform, in agreement with the rotation of the probe (Table 8.2). Probe 10 water pressures declined and readings were not in excess of overburden, making it unlikely that the glacier became decoupled in this area (Figure 8.10). Although, water pressures may have sustained some sliding, the tilt record suggests that deformation was the dominant form of basal motion. Yield strength began to increase as water pressure decreased during the summer. Overall, these sensor readings implied that the rates of glacier motion were low in this area of the bed throughout the summer. This might be expected in an unconnected region of the bed.

In contrast, whilst Probe 12 showed only a slight indication of rotation, pressures were in excess of overburden between days 121-203 (Figure 8.10). This suggests that the glacier was decoupled in this area of the bed and that sliding was occurring as the dominant mechanism of basal motion during this time (Table 8.2). This is supported by the calculated yield strength, which remained in excess of basal shear stresses throughout the summer (Figure 8.9b). This signifies that the strength of till was greater than the applied stresses and thus unlikely to deform. Consequently, although the probe rotated to a small degree, it is unlikely that significant deformation was occurring (Table 8.2). A record for case strain would help to constrain this further. As water pressures decreased, so too did the rate of rotation, which was already very low. Water pressures fell below overburden (day 204) and yield strengths remained high, implying that velocities of basal motion (sliding and/or deformation) were very low in this area of the bed. This corresponds well with the minimal activity recorded by the other sensors during this time.

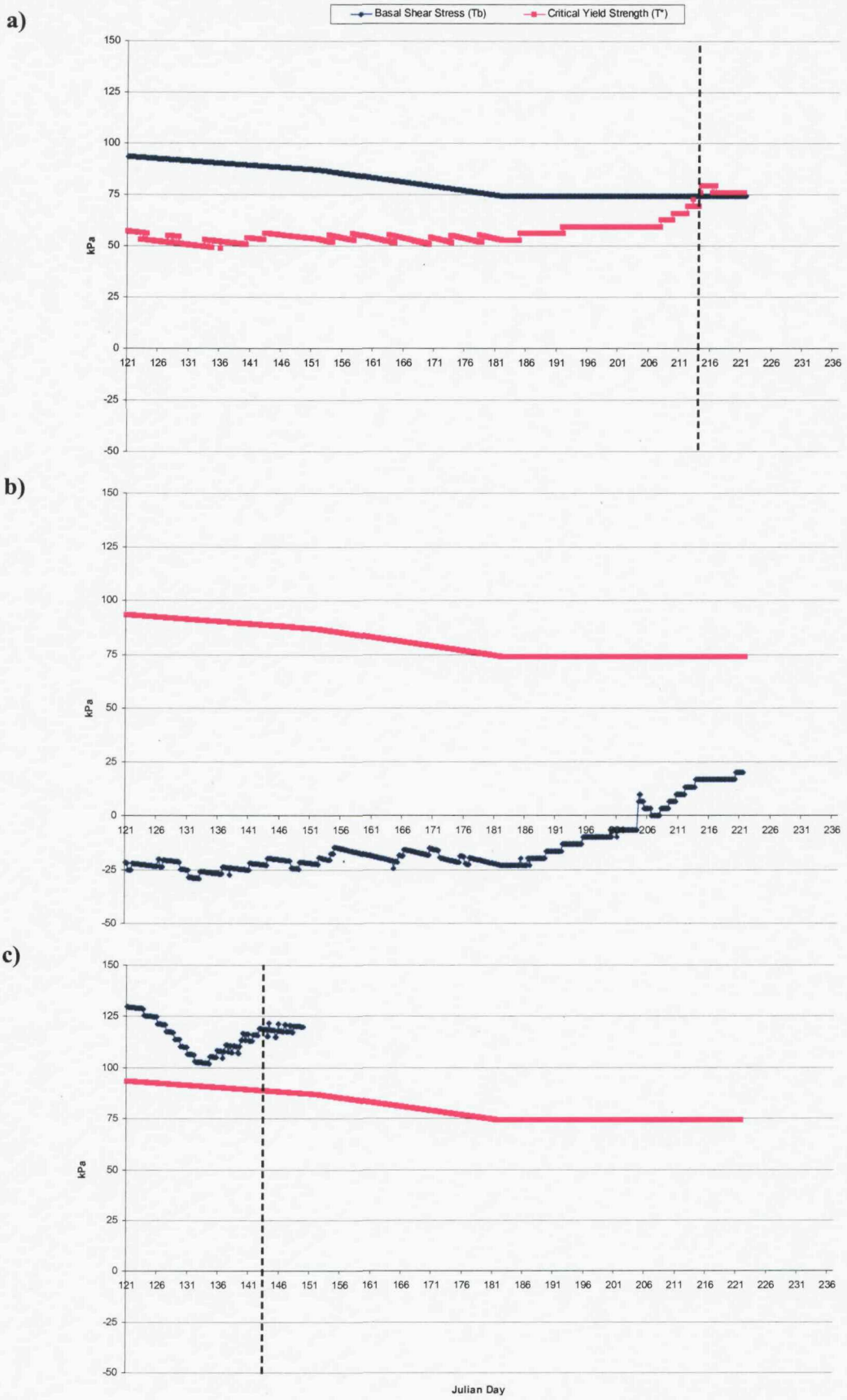


Figure 8.9: Summer records for basal shear stress (τ_b) and sediment yield strength (τ^*), highlighting the most likely periods of till deformation (when $\tau^* < \tau_b$) for: a) Probe 10; b) Probe 12; and c) Probe 15. Note: the area to the left of the black dashed line marks the periods of probe rotation.

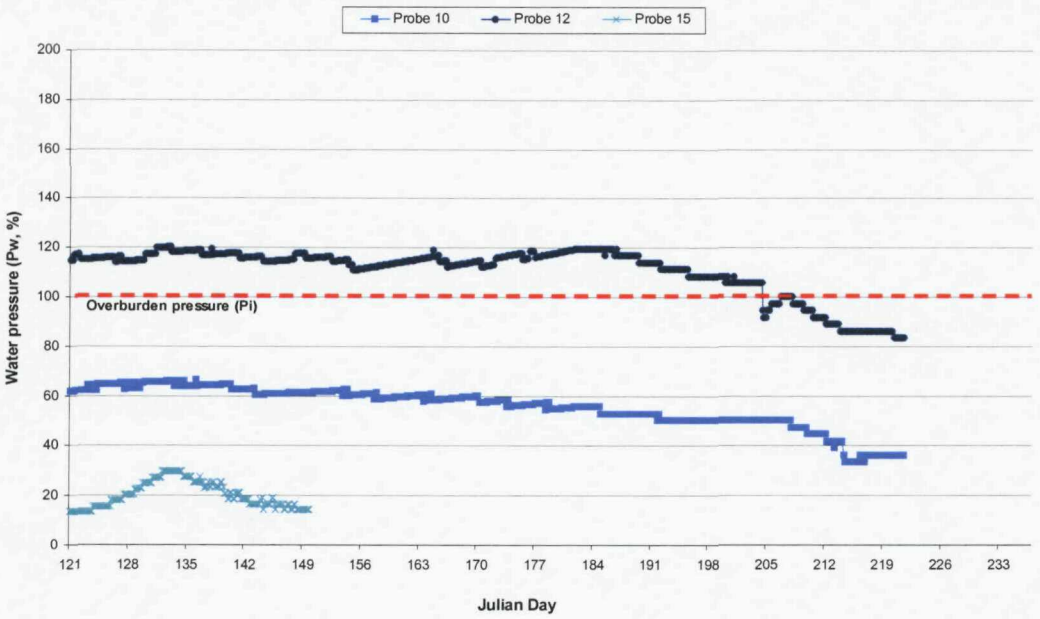


Figure 8.10: Summer water pressure (P_w) records in relation to overburden pressure (P_i) for Probes 10, 12 and 15.

Probe 15 was subject to different activity during the summer. The tilt record displayed relatively rapid rotation between days 113-141, indicating that this area of the bed was subject to deformation (Table 8.2). The record for case strain showed a change in the direction of the applied strain during this initial period, reflecting the probe's interaction with the till (Figure 8.8b). Sediment strengths were also less than applied shear stress indicating that deformation was occurring (Figure 8.9c). Water pressures, during this time, were insufficient to result in glacier decoupling and enhanced basal motion via sliding (Figure 8.10). Thus, deformation appears to provide the dominant contribution to basal motion in the initial stages of the summer months (Table 8.2). Probe rotation ceased from day 142 and water pressures remained low (section 8.5.6). Yield strengths were still low, indicating that deformation could still occur. However, the change in tilt activity reflects a change in the location of the probe. This idea is discussed further in section 8.5.6.

8.5.6 Probe 15: days 150-207

The Probe 15 summer sensor record has been discussed between days 121-149. Activity during this time was generally in keeping with that of the other probes. However, changes in the sensor readings from day 150 suggested that the location of

the probe was changing (Figure 8.11). As a result, the unusual activity observed between days 150-207 is discussed separately in this section.

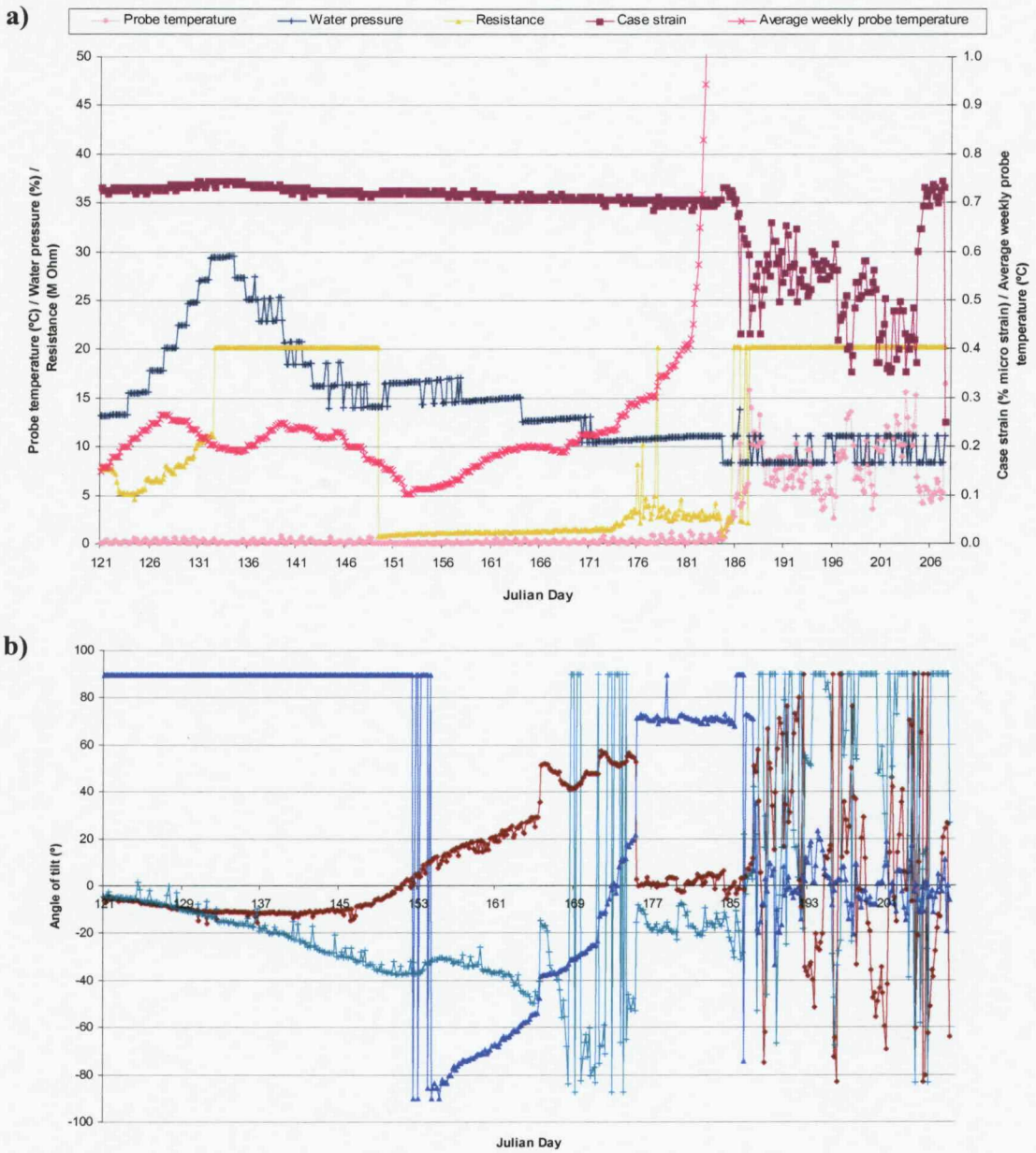


Figure 8.11: Total summer sensor record for Probe 15 (days 121-207), showing: a) probe temperature, water pressure, resistance, case strain and average weekly probe temperature; and b) tilt.

The change in sensor trends began from day 150 when resistance fell despite a continued reduction in water pressures (Figure 8.11a). As resistance fell, probe temperatures began to show greater fluctuations, and average values increased

steadily from day 153. The rate of change in probe tilt was relatively rapid at this time and fluctuations along the z-axis began from day 152 (Figure 8.11b). On day 165, Probe 15 recorded an abrupt step change in the angle of tilt along both the x and y axes (Figure 8.11b). Tilt along the y-axis showed large-scale rapid fluctuations from this point, with net change in the same direction. Variations along all these axes indicated that the probe was oscillating greatly.

Average weekly probe temperature began to increase more rapidly from day 168 and exceeded previous maximum values of 0.3°C on day 176 (Figure 8.11a). Water pressures continued to decline between days 150-181, and then oscillate between 8.3-11.1% (days 182-207). The resistance sensor showed an increase in fluctuations and values from day 173, whilst case strain saw an increase in the amplitude of fluctuations from day 177. This rapid motion in combination with the change in sensor readings implies that the probe's location at the glacier bed was changing. In particular, the increase in probe temperatures would suggest that the probe had moved into a subglacial or englacial cavity, or certainly, an area linked to or exposed to surface conditions.

Probe activity stabilised between days 175-186, as the x and y axes showed small-scale oscillations with an overall decline in the angle of tilt in the same direction. This step change in values suggests that the probe had suddenly reorientated itself and had begun to oscillate to a lesser degree from this new position. Although net tilt on the x and y axes changed in the same direction, the continual accompanying fluctuations would act to disrupt this process. These changes in sensor trends reflect the transition of the probe into a different area of the bed (e.g. a subglacial or englacial cavity).

A final change in conditions was recorded within the Probe 15 record just prior to failure (Figure 8.11). An abrupt and rapid change in sensor readings was observed from day 185. At this point, probe temperature exceeded 2°C and began to show greater fluctuations. Average probe temperature exceeded 0.5°C on day 182 and actual values reached 10.4°C on day 186. Resistance rose back to 20.2 M Ohm (day 185) and the direction of applied case strain changed and began to show large-scale oscillations from day 186. A sudden change in the type and rate of tilt activity was

also evident from day 186, displaying numerous rapid oscillations. The degree of variations recorded indicated that the probe was no longer constrained within the subglacial environment.

These variations mark the start of a different trend in probe activity. The trends recorded between days 186-207 suggested that the probe had experienced a significant change in external conditions. The probe temperatures (reaching up to 16.5°C), in combination with the tilt record implied that the probe had worked its way out of the subglacial environment and had become exposed at the glacier surface. Presumably this occurred via a crevasse or englacial pathway, repositioning the probe at the glacier surface. The probe was actually found at the glacier surface, away from the original site of deployment, by a glacier guide at Briksdalsbreen.

8.6 Probe Failure

The summer records displayed by the probes (2004/5 and 2005/6), except for Probe 15, showed relatively little activity. The sensor readings did not display any untoward oscillations that might have caused the probes to break. The probe power supply was sufficient to last in excess of a year and the probe volt readings indicated that the batteries were almost fully charged throughout the probes' operation. It seems most probable that the loss of the probes was due to communication failures.

The base station was positioned on the surface of the glacier, which moves more rapidly than the till beneath (Harper *et al.*, 1998, 2002). As such, it is likely that the base station moved out of communication distance with the remaining probes. The records suggest that it took roughly one year for this to occur. The absolute distance between the probes and the base station may not have been significant. However, as the probes became more fully incorporated into the deforming bed the transfer of radio waves through a greater thickness of till and then ice may have disrupted communications. The use of a more diverse spatial array of transceivers from the base station may help to alleviate this problem. Probe 15 provided an exception to this trend, where the sensor readings provided a definite indication that the location

of the probe had changed. Communications with the probe ceased once it had been moved at the glacier surface.

In general, it has been difficult to establish a convincing cause or mechanism for the failure of the probes throughout the investigation. Sustaining communications with the probes appears to be the dominant cause of disruption to the records. However, the communication system for the sensor network can be developed further. The design of the probes is such that the integrity of the probe case is unlikely to be damaged. Thus, with the use of enhanced communication links in the future, the duration of the sensor records should only be limited by battery life and possibly removal or transport of the probe from the subglacial environment via a channel.

8.7 Theoretical Background to Deformation

This chapter has focused on the movement of the probes, contributing to the debate on the transport of clasts within the deforming bed. Analysis of the orientation of clasts within tills (i.e. fabric analysis) has suggested that clasts can move and become orientated within subglacial sediments in response to the application of shear stresses (e.g. Benn, 1994). Two hypotheses have been put forward dictating how clasts move and orientate themselves in response to different stress fields. One theory supports the idea of grain rotation through mechanisms of Jeffrey and/or Taylor rotation; whilst the other suggests that grains remain immobile, as passive markers within the till (March rotation). The mechanisms outlined by Jeffrey (1922) and March (1932) both describe the orientation of clasts as a result of shear. The Jeffrey model dictates that this rotation is active, whilst the March model states that rotation is passive. A variety of field evidence has been found in support of each mechanism, for example: Jeffrey rotation - Hart, 1994; Taylor rotation - Carr and Rose, 2003; and March rotation - Benn, 1995; Benn and Evans, 1996.

Jeffery (1922) presented an empirical analysis of the motion of ellipsoidal particles within a viscous fluid, subjected to uniform simple shear. This revealed that ellipsoidal particles would rotate as rigid elements in response to the motion of the viscous fluid. As a result of this movement, particles would align themselves

perpendicular to the direction and gradient of velocity (Figure 8.12a). A prolate spheroidal particle, to which the shape of the probe is best approximated, would rotate in a steady motion with constant angular velocity (Jeffrey, 1922). In a steady state of motion the axes of the particles set themselves in a particular direction (i.e. align). If the clasts are not within a steady state, but experience periodic rotation within the viscous fluid, they will align their axes in random directions (Jeffrey, 1922).

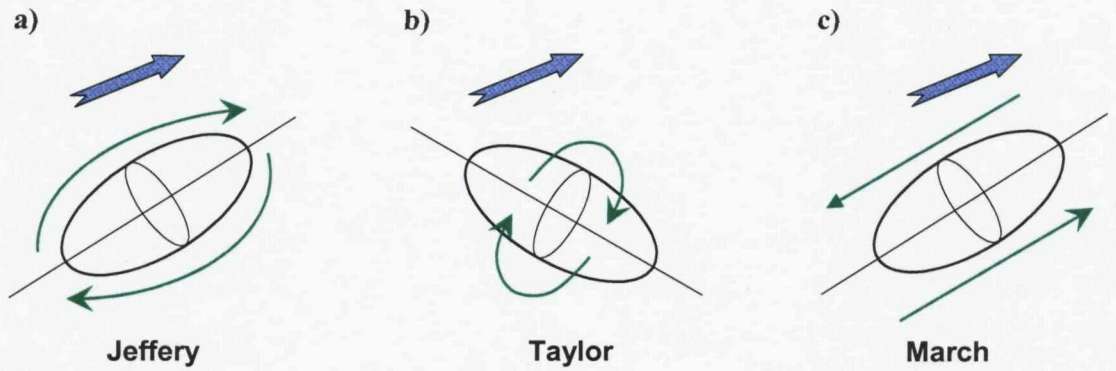


Figure 8.12: Conceptual diagram depicting mechanisms of: a) Jeffery; b) Taylor; and c) March rotation (adapted from Carr and Rose 2003, p.1421).

At very high strains, it is predicted that the clasts will roll on the axis transverse to direction of shear to dissipate the least energy (Jeffery, 1922). This would result in a shift to Taylor rotation (Taylor, 1923). Taylor (1923) furthered the work on prolate and oblate clasts and found that there was a tendency for particles to re-orientate themselves transverse to the shear plane (Figure 8.12b), given an extended time within the till (Taylor, 1923). Glen *et al.* (1957) subsequently determined that rotation around the a-axis occurred because it allowed the particle to achieve minimum energy dispersion. An increase in the viscosity of a fluid is most likely to promote Taylor rotation and such changes have been associated with subglacial sediments (Glen *et al.*, 1957; Taylor, 1923). Again, these orientations occur through periodic rotations within a viscous fluid.

The second model predicts the opposite effect on clast motion. Hooyer and Iverson (2000), based on the work of March (1932), proposed that grains remain immobile

within the bed, behaving like passive markers (Figure 8.12c). A ring shear device was used to analyse the activity of clasts at high shear strains within both till, and a putty, which equated to Jeffrey's (1922) viscous fluid. The till displayed a strong fabric, as clasts rotated into and then remained parallel within the shear plane (Hooyer and Iverson, 2000). This alignment occurred through a process of slip between the clast and the surrounding matrix, corresponding with the March (1932) model of clast rotation. In contrast, the viscous putty behaved in good agreement with trends outline by Jeffrey (1922). The difference in outcomes resulted from variations in the rheology of the materials used. This suggested that the viscous fluid used by Jeffrey (1922) did not provide a good approximation to the rheology of till. Instead, the behaviour of till as a plastic granular material (Iverson *et al.*, 1998) enabled the action of slip, causing the clasts to act as passive markers.

At Briksdalsbreen the probe tilt records were assessed to determine the nature of probe movement within the deforming bed; and whether or not that motion could be associated with Jeffrey, Taylor, or March models of clast activity under shear (Figure 8.12). The first trend of note was that the probes did record movement within the till. The tilt of the probes also indicated that the subglacial sediments were deforming, causing the probes to rotate, as a result of the application of shear stress from the ice above (section 8.4.5 and 8.6.4). This activity suggests that the probes provided a good approximation to clasts within a deforming bed and that other clasts associated with the deforming bed at Briksdalsbreen could also move in a similar manner.

In light of the theoretical basis to clast movement outlined above and the dimensions of the probes, it would appear that they were rotating around their b-axis during deformation in line with the Taylor mechanism of rotation. The probes also showed periods where they stopped rotating and simply changed orientation. It is difficult to determine if this represented periods of March rotation, where the probes were actually acting as passive markers and aligning with other clasts and the shear plane. Generally the activity in water pressure that accompanied these periods of probe oscillation supported the idea that sliding rather than deformation would be occurring at these times. As a result, these changes in orientation may be associated with water flows through the till.

8.8 Summary

The summer probe records were characterised by minimal sensor activity. The dominant trends observed are summarised below.

- Water pressures showed few fluctuations. Pressures were often elevated at the start of the summer, but declined towards the winter (Figures 8.2a and 8.5).
- The decline in water pressures was associated with weather conditions. Probe 8 and 12 water pressures began to decrease as external temperatures increased above 20°C during the summer (Figures 8.3 and 8.7c).
- The lack of diurnal pressure oscillations and general fluctuations suggested that the probes were located within unconnected regions of the subglacial drainage system. This included Probe 15, which was no longer experiencing pressure forcing (Figure 8.5). This implies that a highly efficient connected drainage network had become established elsewhere at the glacier bed.
- The probes displayed an increase in tilt in the same direction along both the x and y axes during the summer, indicating that they were rotating within the deforming bed (Figures 8.2b and 8.6).
- The change in tilt reflected rotation around the probes' b-axis, corresponding to movement via the Taylor (1923) mechanism of rotation (section 8.8; Figure 8.12).
- The other sensor readings showed relatively little activity, remaining generally consistent and displaying few fluctuations (e.g. Figure 8.5).
- The significant increase in sensor activity recorded by Probe 15 at the end of the summer (Figure 8.11) reflected its transition from within the subglacial environment to the glacier surface (section 8.6.6).
- Sensor readings did not show any increase in activity prior to the end of the probe records, suggesting that the loss of probe data was the result of communications failure rather than probe damage.

The records for tilt and water pressure, in combination with calculated values of sediment critical yield strength, provided an indication of the dominant mechanisms of basal motion employed during the summer. Pressures in excess of overburden were associated with processes of decoupling and thus sliding (e.g. Fischer and

Clarke, 1997). In contrast, deformation was associated with a reduction in water pressure, basal shear strengths in excess of critical yield strength and probe rotation. The mechanisms of basal motion recorded by each probe are summarised below.

- Probe 8 displayed a transition from sliding at the start of the summer, to a dominance of deformation at the end of the summer (Figure 8.4; Table 8.1). Probe 8 recorded deformation (an increase in the rate of probe rotation) as water pressures fell, and the glacier became more strongly coupled to its bed (Figure 8.2).
- Deformation remained the dominant form of basal motion for Probes 10 and 15 throughout the summer (Figures 8.8 and 8.9a,c; Table 8.2).
- Probe 12 recorded sliding as the dominant mechanism of basal motion (Figure 8.9b; Table 8.2).

In the summer, basal motion was considered to be low in these unconnected areas of the bed, in accordance with the minimal activity recorded in the probe sensor records (Figures 8.2 and 8.5). However, the rotation of the probes, particularly Probes 8 and 15 (Figures 8.2b and 8.6c), did suggest that sediment deformation was contributing to glacier motion during the summer months. The absence of general summer velocity data and drag-spool measurements of sliding was highly unfortunate. In practice, records of surface, englacial and basal velocities are required to determine the relative spatial distribution of motion that contributes to net glacier velocities (e.g. Willis *et al.*, 2003). As such, no definitive figures can be given for the relative contribution of sliding versus deformation to basal motion in the period 2004-6. However, preliminary results do suggest a transition in the dominant mechanism of basal motion from sliding in the spring, to deformation in the summer.

To summarise, the probes displayed minimal sensor activity during the summer. They were located in unconnected regions of the subglacial hydrological system. The dominant mechanism of basal motion was deformation, characterised by the rotation of the probes according to the Taylor (1923) mechanism of clast motion. Four of the probes recorded over a year of data readings. The probes ceased data transfer during August as a result of communications failure.

Chapter 9

Sedimentology

9.1 Introduction

It is important that the physical properties and characteristics of till are examined so that we can determine how till deforms and responds to changing conditions within a subglacial environment. The numerous variables associated with both conditions at the glacier bed, and the mechanical properties of a granular material, such as till, make this difficult to achieve. Initial studies of till rheology (e.g. Alley *et al.*, 1986; Clarke, 1987; Kamb, 1991) would suggest that the mechanisms of deformation in many ways relate to till sedimentology, through aspects such as: void ratio, porosity, frictional strength, and relative proportions of sand to fine grained material.

Improvements in field techniques means that disturbed samples can now be collected *in situ* from beneath glaciers, complimenting those from the proglacial environment (section 4.3.6, Chapter 4). In addition, new ways of approaching the analysis of till sedimentology (e.g. micromorphology) have highlighted several areas of uncertainty within this field. These areas may relate to the erosional history, and capabilities of grains within the deforming bed, and how this may affect the deformation process. Processes of erosion may be equally as important to till deformation as more documented processes, such as dilation and overconsolidation. This has implications for erosion rates, as well as the transport and deposition of sediments within the glacier system (Boulton, 1996; Boulton and Dent; 1974; Boulton *et al.*, 1974). Information gathered from sites at contemporary glaciers can also provide a modern

analogue to the sedimentological analysis and interpretation of sequences from the Quaternary.

This chapter will examine the sedimentology and erosional history of grains at Briksdalsbreen. Sediment samples were taken from proglacial and subglacial sites during this investigation (2004-6). The samples were analysed through techniques of grain size classification and under the SEM (section 4.5, Chapter 4). These techniques were carried out in order to compare subglacial and proglacial samples and sampling techniques; and determine the erosional history of grains within the deforming bed via the SEM. The data and conclusions drawn from grain size classification techniques will be discussed first, followed by interpretations of SEM analysis. The work outlined here is also presented as a publication in Appendix B (Rose and Hart, 2008).

9.2 Grain Size Analysis

The proglacial and subglacial samples collected at Briksdalsbreen (2004-6) were analysed for grain size distribution (section 4.5.2, Chapter 4). The collection and subsequent results from the samples obtained will be outlined in this section.

9.2.1 Proglacial samples

A summary of the till samples collected is provided in Table 9.1. The grain size cumulative frequency and ternary diagram for the samples are displayed in Figures 9.1 and 9.2, respectively. The amount of till collected within the proglacial environment ranged between 74-614 g. The mean grain size collected ranged between 655-11917 μm and the samples were generally poorly sorted and finely skewed. The ternary diagram indicates that the majority of proglacial samples were gravels or muddy sandy-gravels.

Table 9.1: Summary of the sediment samples collected from the proglacial environment at Briksdalsbreen (2004-6) and their average grain size. Samples were taken from two grid tests and a flute in 2004, whereas only one bulk sample was obtained in 2006.

Year	Sample Point	Sample Number	Texture	Weight of Till Sample (g)	Average Grain Size (µm)	Sorting
2004 Grid 1	G1 P1	-	boulder	-	-	-
	G1 P2	Br04_PG1	coarse till	210.7	11917	4.751
	G1 P3	Br04_PG2	coarse till	277.8	3968	6.159
	G1 P4	Br04_PG3	till	248.6	1466	13.16
	G1 P5	Br04_PG4	till	181.8	2704	11.26
	G1 P6	Br04_PG5	till	243.2	5480	3.638
	G1 P7	-	boulder	-	-	-
	G1 P8	Br04_PG6	till	184.4	4197	5.379
	G1 P9	Br04_PG7	coarse till	129.6	2330	12.27
Grid 2	G2 P1	Br04_PG8	boulder	209.1	3525	4.083
	G2 P2	Br04_PG9	till (flute)	73.9	665	7.477
	G2 P3	Br04_PG10	coarse till	225.1	2733	4.680
	G2 P4	Br04_PG11	till	169.8	1180	12.81
	G2 P5	Br04_PG12	till	216.4	4241	7.267
	G2 P6	Br04_PG13	till	315.4	7842	3.110
	G2 P7	-	boulder	-	-	-
	G2 P8	Br04_PG14	till	220.2	11786	2.634
	G2 P9	-	boulder	-	-	-
Average Grid 1		Br04_PG1a	22% boulder 33% coarse till 44% till	210.9	4580.11	8.09
Average Grid 2		Br04_PG2a	33% boulder 11% coarse till 55% till	204.3	4567.25	6.01
	Flute	Br04_PG15	-	614.4	1765	9.692
2006		Br06_PG1	-	394.2	7436.1	4.076

[1]Average grain size according to the Folk and Ward (1957) method (Gradistat v5, Blott and Pye, 2001).

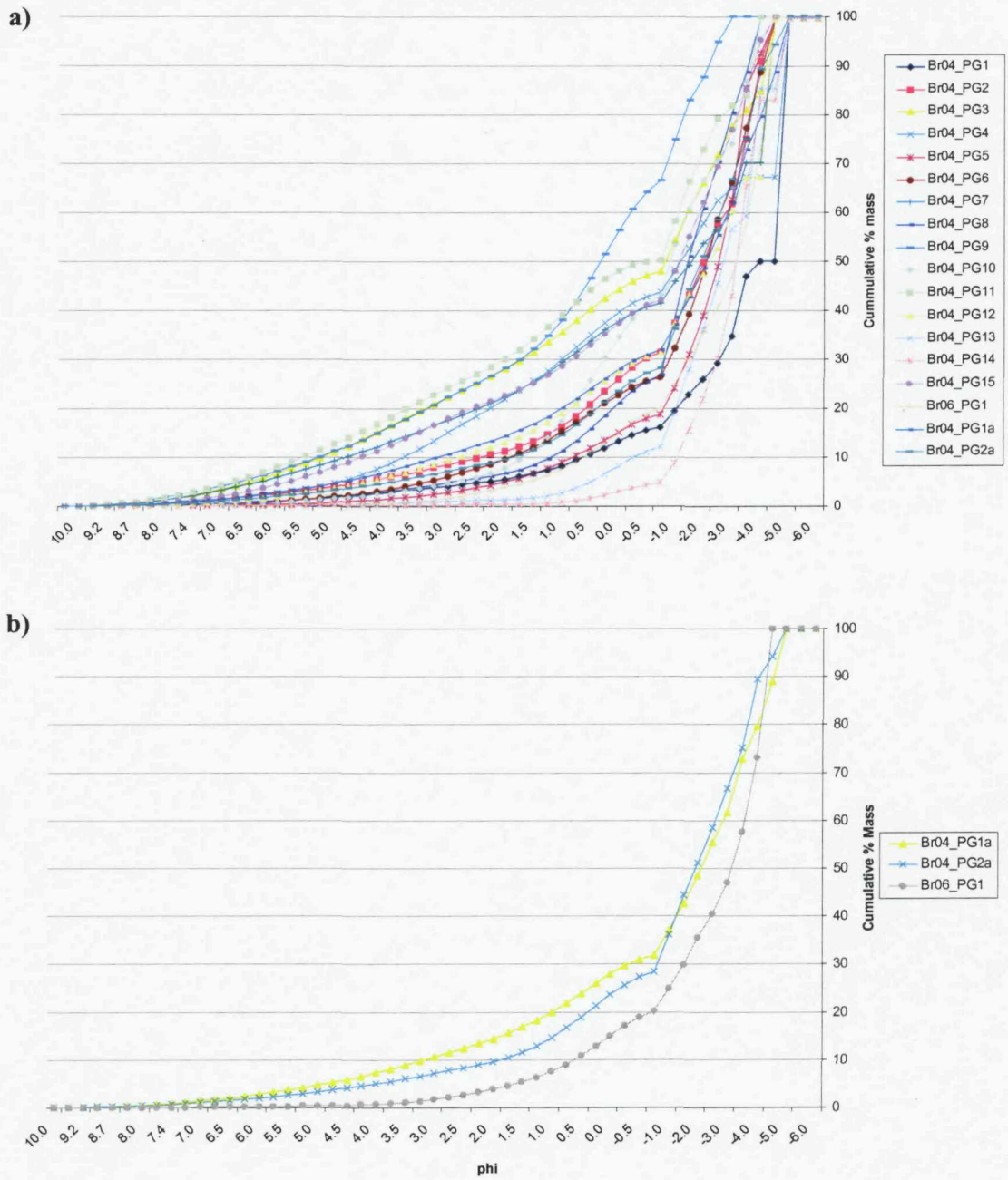


Figure 9.1: Grain size cumulative frequency for proglacial samples from 2004 and 2006 showing: a) frequency curves for each sample; and b) average frequency curves for grids 1 and 2 (2004), accompanied by the single 2006 bulk sample.

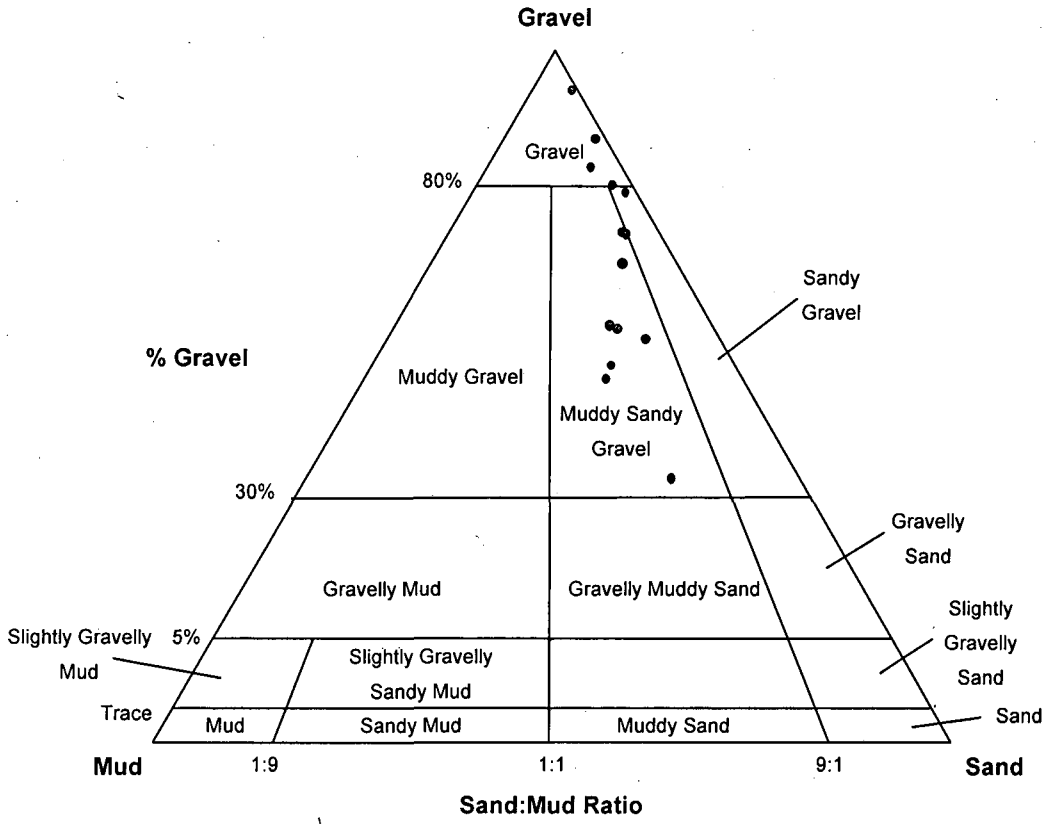


Figure 9.2: Ternary diagram to show the texture of proglacial sediment samples from 2004 and 2006 (Gradistat v5, Blott and Pye, 2001).

9.2.2 Subglacial samples

The details of the subglacial samples collected are outlined in Table 9.2 and 9.3. The results of subsequent grain size analysis are displayed in Figures 9.3 and 9.4. The amount of till collected within the subglacial environment ranged from 8-217 g. The mean grain size varied between 311-8584 μm and the samples were generally poorly sorted and finely skewed. The mean grain size of the <-2 φ fraction was 1679 μm, with 7% silt and clay. The ternary diagram indicates that the majority of subglacial samples were muddy-sandy gravels.

Table 9.2: Summary of *in situ* subglacial sediment samples. Note: values do not add up to 100 % because the BoreCam was not used in every borehole.

Year	Number of boreholes to the bed	Average depth and range (m)		% showing till at base	% of till sites showing a boulder
2004	15	69	60.5-85	60	22
2005	12	52	41-55	92	-
2006	12	30	25-35	83	-
Average	13	50.3	-	78.3	22

Table 9.3: Summary of the *in situ* subglacial samples collected from Briksdalsbreen (2004-6).

Year	Borehole	Sample No.	Borehole Depth (m)	Weight of Till Sample (g)	Average Grain Size[1] (μm)	Sorting
2004	1	Br04_1	70.0	41.3	342.1	6.50
	4	Br04_2	69.0	55.7	3828.4	3.90
	6	Br04_3	68.0	21.0	3321.5	2.50
	12	Br04_4	66.0	9.6	1224.5	5.30
Average 2004			68.3	31.9	2179.1	4.58
2005	A	Br05_1	50.0	105.0	942.4	4.652
	C	Br05_2	54.0	23.6	1284.7	3.194
	D	Br05_3	55.0	7.8	189.0	3.444
	E	Br05_4	41.0	56.5	629.1	4.544
	F	Br05_5	50.0	59.4	990.7	3.834
	H	Br05_6	54.0	27.0	724.1	6.768
	I	Br05_7	54.0	55.5	902.5	2.858
	J	Br05_8	54.0	116.2	310.8	2.709
	L	Br05_9	54.0	90.4	802.6	8.632
Average 2005			51.8	60.2	752.9	4.63
2006	1	Br06_1	34.0	13.8	8583.7	1.835
	7	Br06_2	27.0	217.4	5627.1	3.797
	11	Br06_3	33.0	48.6	2409.6	4.785
Average 2006			31.3	169.1	6014.1	3.47

[1]Average grain size according to the Folk and Ward (1957) method (Gradistat v5, Blott and Pye, 2001).

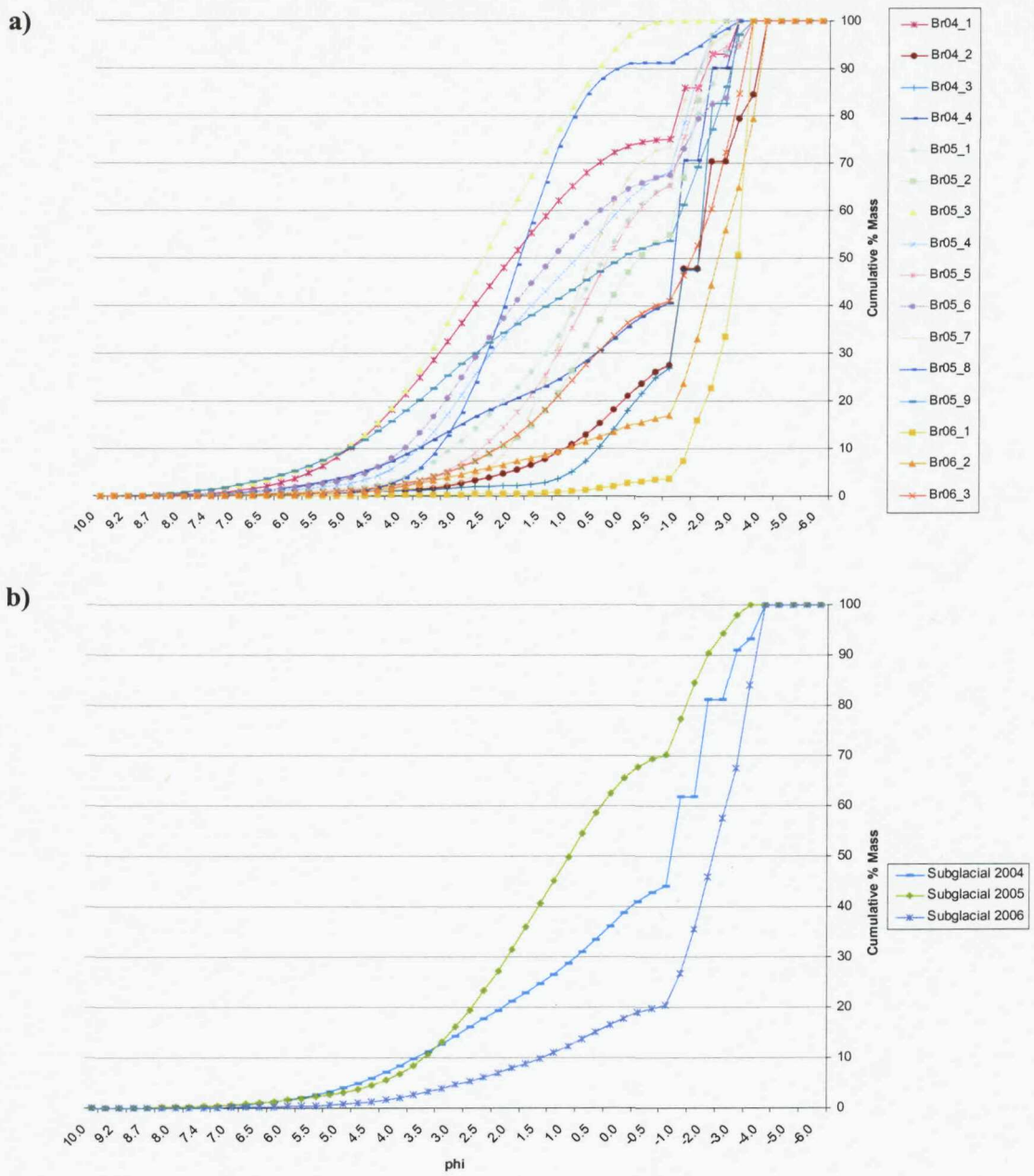


Figure 9.3: Grain size cumulative frequency for *in situ* subglacial sediment samples (2004-6) for: a) all samples; and b) average yearly sample values.

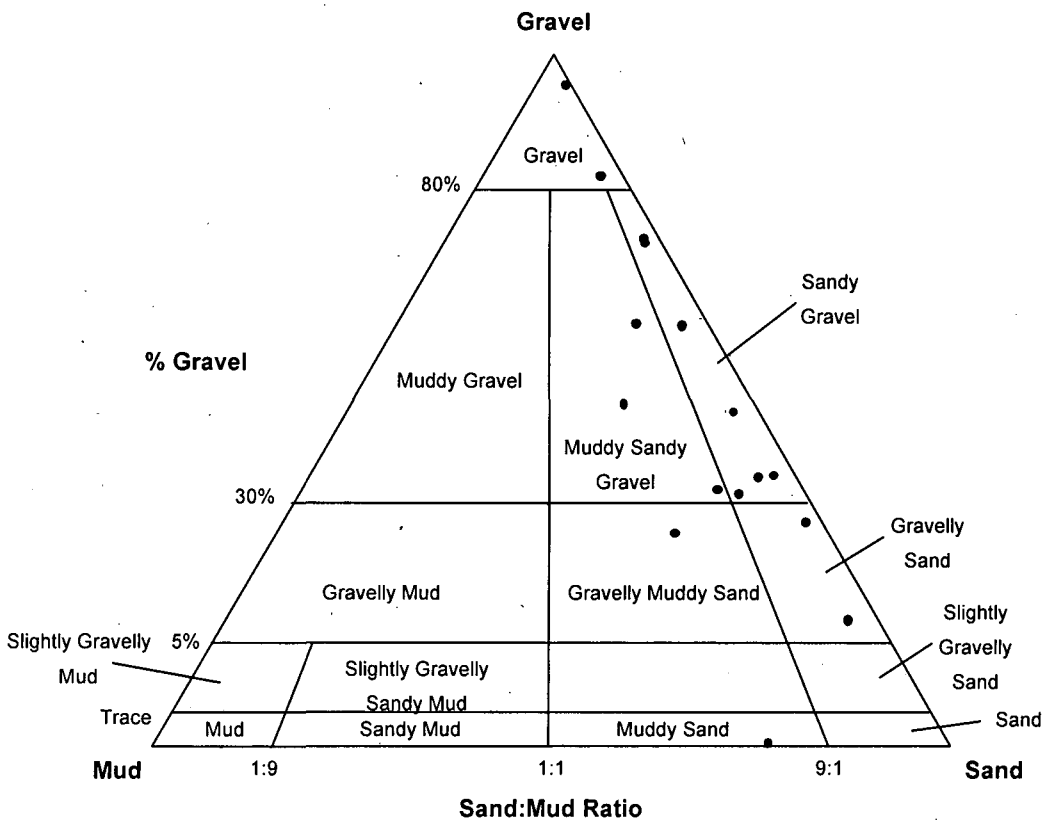


Figure 9.4: Ternary diagram to show the texture of *in situ* subglacial sediment samples (2004-6) (Gradistat v5, Blott and Pye, 2001).

9.3 Interpretation

Grain size analysis was performed on sediment samples in order to determine the average grain size associated with the deforming bed at Briksdalsbreen (Tables 9.1 and 9.3). At Briksdalsbreen, the flutes located within the glacier foreland, coupled with the net retreat of the glacier since 2001, suggested that the proglacial area reflected an exposed subglacial surface. Thus, the comparison of proglacial and subglacial samples also provided the opportunity to determine any spatial variations in sedimentology (texture and grain size distribution); and to test whether the method of borehole sampling, as well as the sampling instrument used, generated a representative sample of till.

9.3.1 Texture

The grid tests were performed within the proglacial environment, in order to reconstruct the random acquisition of *in situ* subglacial sediments, according to the location of boreholes and the variability of sampling success (section 4.5.1, Chapter 4). This was based on the assumption that the proglacial environment represented an exposed subglacial surface. The grid tests found that 'boulders' were the dominant texture in 22-33% of the samples (Table 9.1). A further 11-33% of the samples comprised 'coarse till', but the majority of the samples were 'till' (44-55%). In terms of the *in situ* samples, 22% of the boreholes intercepted a boulder (Table 9.2). Till was observed in an average of 78% of the boreholes, in keeping with an average of 67-77% (total till) observed in the grid tests. These findings suggest that the till texture observed from the grid point tests corresponds with the texture observed with the BoreCam at the base of the borehole array (Tables 9.1 and 9.2). Figure 9.5 displays the sediment textures for both the proglacial and subglacial samples. The subglacial samples show a slightly greater spread of readings and have a slightly more sandy texture. However, there is generally good agreement between the two.

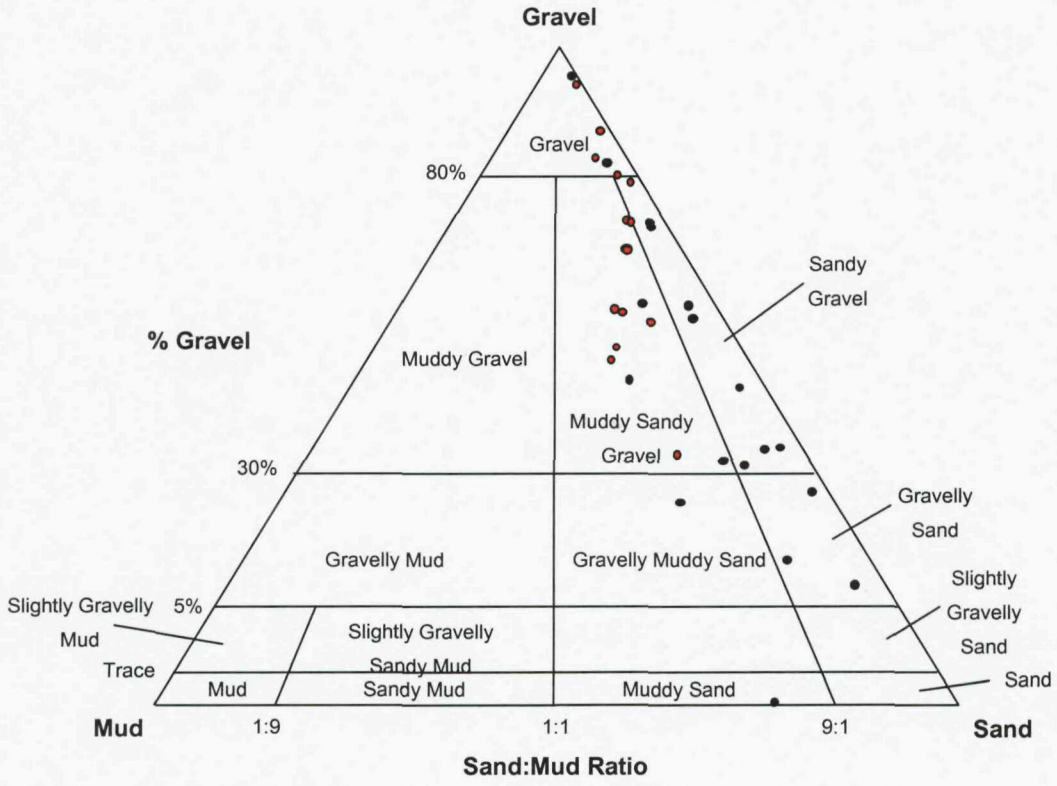


Figure 9.5: Ternary diagram to show the texture of both proglacial (red) and *in situ* subglacial (black) sediment samples (Gradistat v5, Blott and Pye, 2001).

9.3.2 Grain size distribution

It has been suggested that grain size is a key factor in determining subglacial processes. Consequently, the reliability of the sediment sampler was questioned, particularly as two different instrument sizes were used (section 4.3.6, Chapter 4). This method of collecting subglacial samples *in situ* was problematic, as sampling was almost impossible if boulders were present on the till surface. In addition, although till was viewed in the majority of boreholes accessed by the BoreCam (Table 9.2), samples could not always be extracted. The size of the chamber meant that there was a tendency for only fine-grained samples to be extracted, as boulders cannot fit through the window of the chamber (Figure 4.23, Chapter 4). It is also likely that some of the finest fraction was removed as water drains out of the chamber during retrieval.

In 2004, one sample (Br04_1) was retrieved with the large sediment sampler, whilst three (Br04_2/3/4) were retrieved with the small one. The improved rate of success with the small sampler meant that it was solely used in subsequent years (2005-6), with continued sampling success. Figure 9.6 compares the grain size cumulative frequencies between the small and large sediment sampler and the proglacial and subglacial sample sets as a whole. There was a wide distribution of grain sizes collected from the subglacial samplers (Figure 9.6a). However, in general, the large sampler collected a greater proportion of the fine sand and silt fraction; whereas the small sampler included more medium sand and less very fine sand and silt. This was also illustrated by the average grain size values (Table 9.2). Overall, the small sampler collects samples that are more representative of the less than 0 φ fraction of till. Thus, although there was some preferential removal of fines during sample retrieval, this had a minimal effect on final grain size distributions.

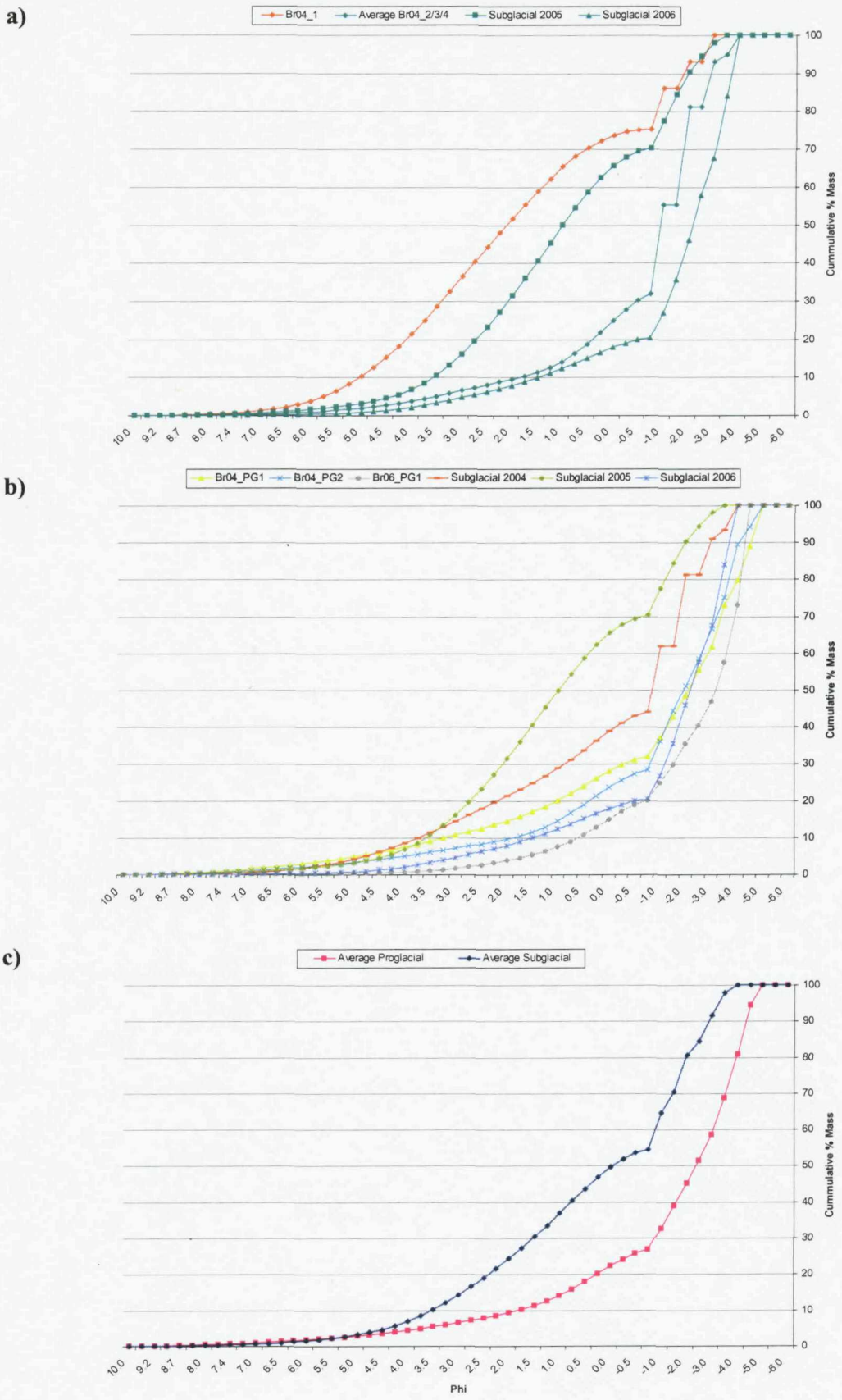


Figure 9.6: Grain size cummulative frequency curves comparing proglacial and *in situ* subglacial samples (2004-6) for: a) the large (orange) and small (green) sediment sampler; b) average proglacial and yearly subglacial samples; and c) total average values for the proglacial and subglacial sample sets.

In contrast, the bulk sampling of the exposed subglacial surface (2004 and 2006) showed less grain size variation (Figure 9.6b). The 2004 grid test samples had very similar cumulative frequency curves to the 2006 *in situ* samples and the 2004 small sampler set (Figure 9.6a, b). The *in situ* samples from 2005 showed the greatest difference with the proglacial samples and were closer in approximation to the large sediment sampler samples (Figure 9.6a, b). However, Figure 9.6c demonstrates that, in general, there was a strong similarity in grain size distribution between the exposed subglacial surface samples and those collected from the subglacial environment. The samples also displayed similar textures (Figure 9.5).

These results indicate that sampling from an array of boreholes did provide a representative picture of subglacial grain size distribution at Briksdalsbreen. In addition, the use of the small sediment sampler generated grain size distributions in good agreement with those from the proglacial zone. Thus, although the sampling technique did result in the removal of some fines (Figure 9.5), this did not significantly affect the sample distributions. Additional discussion of the foreland sedimentology at Briksdalsbreen is also presented by Hart (2006b).

9.4 SEM Analysis

SEM analysis was used to examine the surface texture of grains from the subglacial environment (section 4.5.3, Chapter 4). This technique is based on the observation of form and morphology of a random and representative number of sample grains. Any interpretation is the result of observation of a *combination* of grain features and not just one. Inferences can be made about the erosional history of grains based on their form and surface textures (Krinsley and Doornkamp, 1973). This may include information on the processes to which grains have been exposed, the relative amount of time that they have been within the deforming bed, and the amount of shear strain to which they have been subjected. Additional categories of classification (section 4.5.3.4, Chapter 4), were developed in order to aid in this interpretation. The samples were analysed under the SEM according to surface texture, shape (RA value), and erosional form. The a-axis of grains was also measured (Table 9.4).

Table 9.4: Summary of SEM analysis for non-glacial (2004) and subglacial (2004-6) samples.

Sample	Average a-axis (μm)	% with angular outline	RA value	% low relief	% small conchoidal fracture	% with low relief jointed surface	% of grain face with low relief jointing	Average a-axis with low relief jointed surface (μm)	Dominant Genetic Shape	Dominant Erosional Form
Br04_1	235	40	32	44	72	52	16	682	Ellipse	Intermediate
Br04_2	323	48	33	52	76	40	12	846	Ellipse	Intermediate
Br04_3	681	44	28	52	52	88	36	683	Diamond	Abraded
Br04_4	463	44	36	56	72	56	36	652	Ellipse	Intermediate
Average 2004	426	44	32	51	18	59	25	716	Ellipse	Intermediate
Br05_1	807	56	20	64	56	40	13	807	Ellipse	Intermediate
Br05_2	883	36	24	64	56	32	16	883	Triangle	Intermediate
Br05_3	624	54	25	50	56	12	32	624	Rectangle	Intermediate
Br05_4	754	52	24	60	28	16	12	754	Ellipse	Intermediate
Br05_5	843	20	12	84	56	44	14	843	Ellipse	Intermediate
Br05_6	504	56	28	84	28	16	5	504	Ellipse	Intermediate
Br05_7	799	44	0	68	44	40	10	799	Ellipse	Intermediate
Br05_8	557	68	12	64	44	12	12	557	Rectangle	Intermediate
Br05_9	170	64	24	68	40	24	16	170	Ellipse	Intermediate
Average 2005	660	50	19	67	45	26	14	660	Ellipse	Intermediate
Br06_1	398	56	48	96	80	48	24	210	Ellipse	Intermediate
Br06_2	141	64	52	88	60	8	15	27	Ellipse	Conchoidal
Br06_3	505	40	20	84	76	44	8	142	Ellipse	Intermediate
Average 2006	348	53	40	89	72	33	16	126	Ellipse	Intermediate
Average All Subglacial	537	31	26	67	56	36	17	574	Ellipse	Intermediate

The subglacial samples will be discussed as a whole, averaged between 2004, 2005 and 2006 (Figure 9.7). Adhering particles and edge abrasion are not included in the list of features because they were recorded on each grain in the subglacial samples. In terms of the adhering particles, this was also done because it was not possible to differentiate between those occurring naturally and those which remained following sample preparation (section 4.5.3, Chapter 4). The results are outlined in the following section. The surface textures that are indicative of glacial environments will be highlighted, before the erosional history of the grains is discussed.

9.4.1 Subglacial samples

Grain morphology is recorded in Figure 9.7a. Grains were generally intermediate in shape, accounting for 62% of the total sample. This is reflected by the RA value (Benn and Ballantyne, 1993) for the subglacial samples, which was relatively low, at 26%. This dominant grain form was ellipse (38%), although a range of other less rounded genetic forms was also present. In terms of surface morphology (Figure 9.7b), the majority of subglacial grains showed low relief (67%). Only 2% of the subglacial samples, over three years, had high relief. Grains showed a range of mechanical surface textures. There was a high frequency of conchoidal fractures, steps, blocks and fracture plates; as well as less frequent, but notable, troughs, meandering ridges, and grooves. The chemical surface textures of the subglacial grains were dominated by three features: pre-weathered surfaces, cracks and joints (Figure 9.7b). There was also a direct correlation between pre-weathered surfaces and the occurrence of low relief joints or scales in the subglacial samples. The most common erosional form was new impacts-low relief (Figure 9.7a). However, a number of conchoidal, abraded and new impact-high relief grains were also present. The jagged erosional form was the least common.

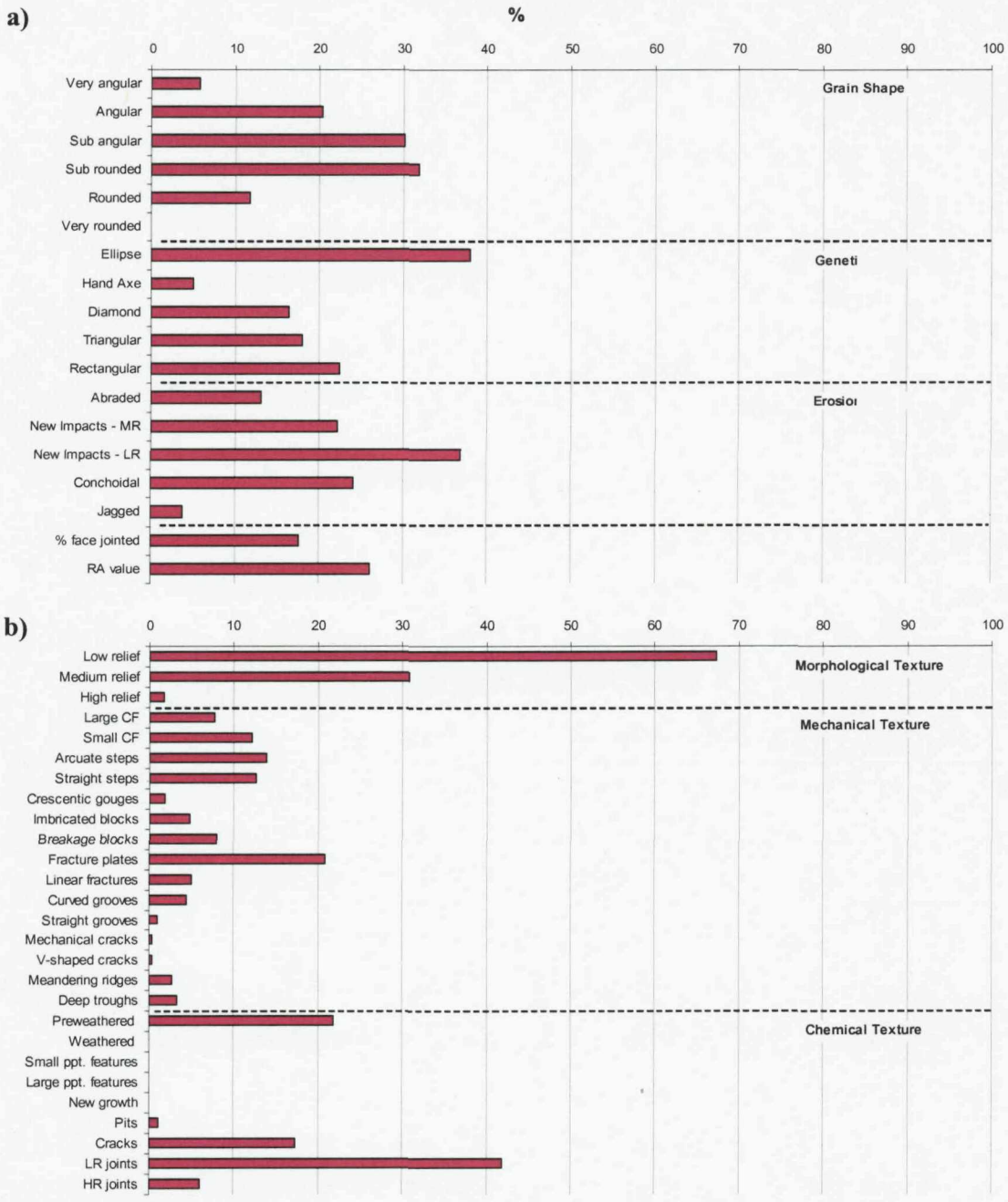


Figure 9.7: Results of SEM analysis averaged for all the subglacial samples (2004-6), showing: a) grain shape, genetic shape and erosional form; and b) morphological, mechanical and chemical textures. Note: the different categories of grain texture and form are delineated by the dashed lines; HR – high relief; LR – low relief; CF – conchoidal fracture.

9.5 Interpretation: Grain Provenance

The origin of the *in situ* subglacial samples was known. This means that the characteristics of the grains can be assessed to determine if they are in keeping with those used to diagnose glacial environments. This can help to validate grain provenance, according to the surface textures recorded in the literature (Sharp and Gomez, 1986).

9.5.1 Grain shape and surface texture

The subglacial samples had an average RA value of 26%, reflecting more rounded and intermediate grain forms (Table 9.4). The dominant mechanical textures recorded by the subglacial samples (Figure 9.7b), have been identified throughout the literature as characteristic of glacial environments (e.g. Krinsley and Doornkamp, 1973; Margolis and Kennet, 1971; Mahaney *et al.*, 1996; Helland and Holmes, 1997; Strand *et al.*, 2003). The subglacial grains also recorded a greater range of other mechanical surface textures, including deep troughs, meandering ridges, and grooves. Large conchoidal fractures, linear fractures and curved grooves were also frequent. It was also noted throughout analysis, that the surface textures of the subglacial grains were chaotic. The arrangement, size and style of features were variable, in keeping with findings from glacial environments (Krinsley and Doornkamp, 1973).

A high frequency of large conchoidal fractures, in combination with fracture plates, suggests that the grains have been subject to grinding, a process that tends to be associated with subglacial environments (Krinsley and Doornkamp, 1973). These features were found frequently in the subglacial samples. In addition, signs of abrasion, such as grain rounding, low relief and edge abrasion, were common. This reflects conditions beneath a glacier, where the forward motion of ice over sediment is likely to result in processes of both abrasion and grinding (Krinsley and Doornkamp, 1973; Boulton and Dent, 1974). The fracture faces and breakage blocks of the subglacial grains were chaotic and variable in nature. Fracturing is indicative of inter-granular percussion, whilst breakage blocks suggest crushing also occurred. This is indicative of the variable conditions and grain interactions associated with erosion in subglacial environments (Krinsley and Doornkamp, 1973).

The signal of chemical textures displayed by the subglacial grains was dominated by intermediate grain shapes, low relief joints and cracks (Figure 9.7b). This suggests that other processes, such as abrasion, which reduces surface relief, influenced the formation of grain surface textures. The occurrence of precipitation features was rare in the subglacial grains. In a glacial environment, precipitation features tend only to be noted on grains from Pleistocene deposits (Krinsley and Doornkamp, 1973; Mahaney, 1995), which have been removed from direct glacial action for some time and are thus exposed to other processes.

A number of features indicative of weathering were noted on the subglacial grains. However, direct weathering was not expected due to the relatively closed nature of the subglacial environment, from which the samples were taken. Traditionally, mechanical processes of erosion are thought to dominate the formation of surface textures on subglacial grains (Mahaney *et al.*, 1996). As a result, any features of weathering found on glaciated grains must represent weathering prior to grain incorporation into the subglacial environment. Consequently, any signs of 'weathering' were noted as 'pre-weathered' surface textures (Mahaney and Kalm, 1995, 2000). The generation and preservation of pre-weathered surfaces at Briksdalsbreen may be increased as a result of the oscillations in glacier mass balance (Winkler, 1996; Nesje, 2005). Intermittent periods of glacier retreat expose subglacial sediments and may cause them to undergo further weathering. As a result, it is unlikely that the pre-weathered surfaces recorded were solely the result of weathering prior to or during initial erosion from the underlying bedrock.

9.5.2 Grain formation

The dominant erosional form given to the subglacial samples was new impacts-low relief (Figure 9.7a; Table 9.4). The presence of rounded and abraded grains suggests that the fracturing observed was caused via grain interactions during transport. Grains become abraded as they are rubbed against one another. The process of smoothing is common to modern glaciated grains (Krinsley and Doornkamp, 1973; Whalley and Krinsley, 1974); whilst fracturing results from percussion with neighbouring grains in transport (Krinsley and Donahue, 1968).

9.5.3 Summary

The aim of this comparison was not to determine the environment of sample provenance, as this was already known. Instead, it was to establish that, under SEM analysis, the dominant surface textures of the subglacial grains were in keeping with those recorded within the literature. This was found to be the case. The subglacial grains exhibited surface textures representative of erosion and transport in a subglacial environment. The nature of these processes and mechanisms will be discussed further in the next section.

9.6 Interpretation: Subglacial Grain Erosion

Extensive work has been carried out since the late 1960s to determine the surface textures associated with grains from different source environments (Bull, 1981). Grains were tested with good success to determine if the textures observed were diagnostic and could be reproduced under controlled environmental conditions within the laboratory (Krinsley and Doornkamp, 1973). The observation and identification of surface features have been published extensively in order to standardise interpretations. Initial analysis has determined that the *in situ* samples displayed surface textures associated with those from glacial environments. As the provenance of samples was known, further clarification of the erosional history of grains (on the micro-scale) within the deforming bed is sought.

The form and surface textures of sediment grains from subglacial environments have been investigated to determine the processes (erosion and transport) to which they are subjected (e.g. Gjessing, 1965; Hart, 2006a, b). Elson (1988) suggested that deformation tills lack evidence of comminution. Tulaczyk *et al.* (1998) also found a scarcity of features indicative of comminution in the fine grained tills beneath Ice Stream B. However, other studies have demonstrated that till erosion does occur. This has been observed at the field scale, from the study of stoss-and-lee clasts (mini roche moutonnées) (Benn and Evans, 1996; Hart, 2006a), and at the microscale, from micromorphology and SEM studies (Boulton *et al.*, 1974; Hooke and Iverson, 1995; Iverson *et al.*, 1996; van der Meer *et al.*, 2003; Hart, 2006b). In the subglacial

environment, erosion can operate within the till, at the ice-bed interface, and at the base of the deforming layer.

Numerous researchers (Dreimanis and Vagners, 1971; Halderson 1981, 1983; Sharp and Gomez, 1986) have argued that crushing, associated with glacial erosion, allows till to reach a terminal grade. This process has also been observed in association with deformable beds at Breiðamerkurjökull. Boulton *et al.* (1974) concluded that *in situ* grain crushing had occurred because of the decrease in grain size that they found between the debris rich basal ice layer and upper layer of the deformation till. In agreement with this, Iverson *et al.* (1996) showed from experimental shearing on coarse grained mudstone particles (2.0-3.3 mm), that as deformation increased, first sand and then silt sized grains were produced. Tulaczyk *et al.* (1998) have argued that comminution is dependent on the geological setting and that the glacial erosion of strong brittle rocks is very different from that of weak sediments. The findings of Boulton *et al.* (1974) and Tulaczyk *et al.* (1998) can be compared in Figure 9.8. This provides a useful foundation from which to investigate the erosional history of grains from Briksdalsbreen, obtained *in situ* from a deforming bed resting on gneiss bedrock; in contrast to the *in situ* study of till from beneath Ice Stream B (Tulaczyk *et al.*, 1998).

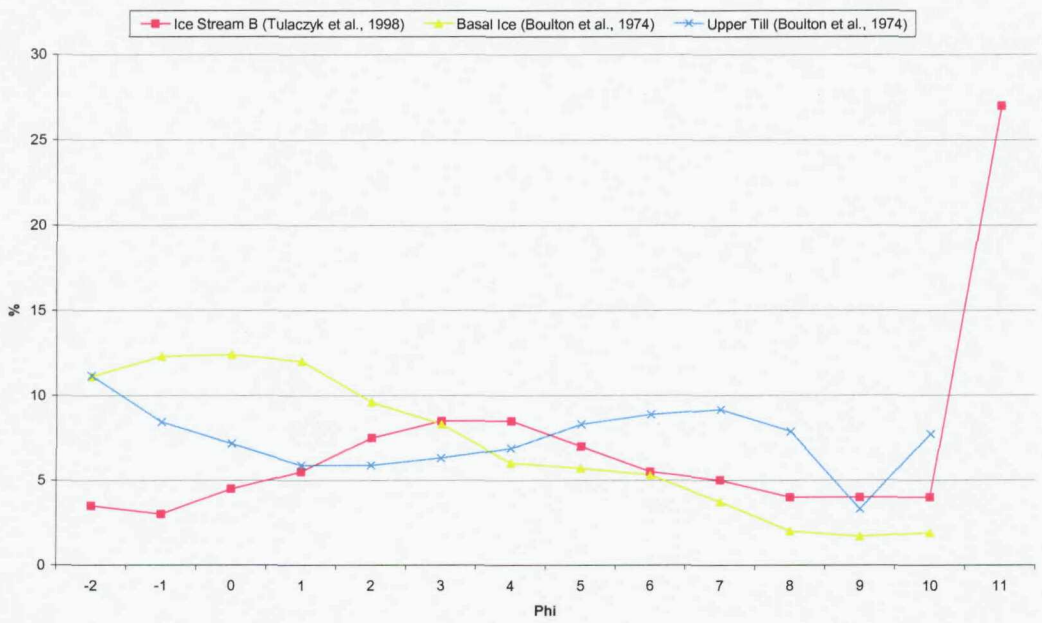


Figure 9.8: Grain size (< -2ϕ fraction) from two different basal tills: Ice Stream B, after Tulaczyk *et al.* (1998); and Breidamerkurjøkull, after Boulton *et al.* (1974).

9.6.1 Grain shape and surface textures

The dominant grain shape, surface textures and erosional forms associated with the subglacial samples were outlined in the previous section (Figure 9.7; Table 9.4). However, further details about the grain surface textures should be highlighted, as numerous features, diagnostic of glacial processes, were noted. Edge abrasion was extremely common to all of the grains, reflecting grinding of the grain surface, which is thought to signify glacial transport (Helland and Holmes, 1997; Figure 9.9a, c). Glacial grinding can act to abrade and round grains, but also to increase cleaving, so that flat angular surfaces are also retained (Krinsley and Doornkamp, 1973). As a result, this process tends to create very chaotic surface textures. Fractures on individual grains, for example, often vary in size, form, shape, direction and distribution as a result of such processes (Krinsley and Doornkamp, 1973). Adhering particles were also regularly noted and are again associated with processes of glacial grinding (Krinsley and Doornkamp, 1973; Mahaney *et al.*, 1996; Figure 9.9b). However, the presence of adhering particles may have been the result of the preparation technique, which did not involve grain washing.

Glacial grains are generally considered to be angular in nature, due to fracturing. However, mechanical action, such as abrasion, can act to round grains (Krinsley and Doornkamp, 1973). Helland and Holmes (1997) note the occurrence of subrounded grains in conjunction with more angular grains within their analysis of glacial deposits (Figure 9.9c, e). Low relief, edge and surface abrasion is often associated with grains that have experienced glacial transport (Mahaney *et al.*, 1996). Strand *et al.* (2003) suggest that high frequencies of steps, grooves and conchoidal fractures are indicative of glacial crushing. All of these textures were present at high frequencies in each sample year. Similarly, breakage blocks and arcuate steps indicate grain to grain impacts or the process of percussion (Krinsley and Donahue, 1968; Strand *et al.*, 2003). The formation of breakage blocks is also closely associated with fracture plates on grains of glacial origin. Again, these features were very common to the samples taken.

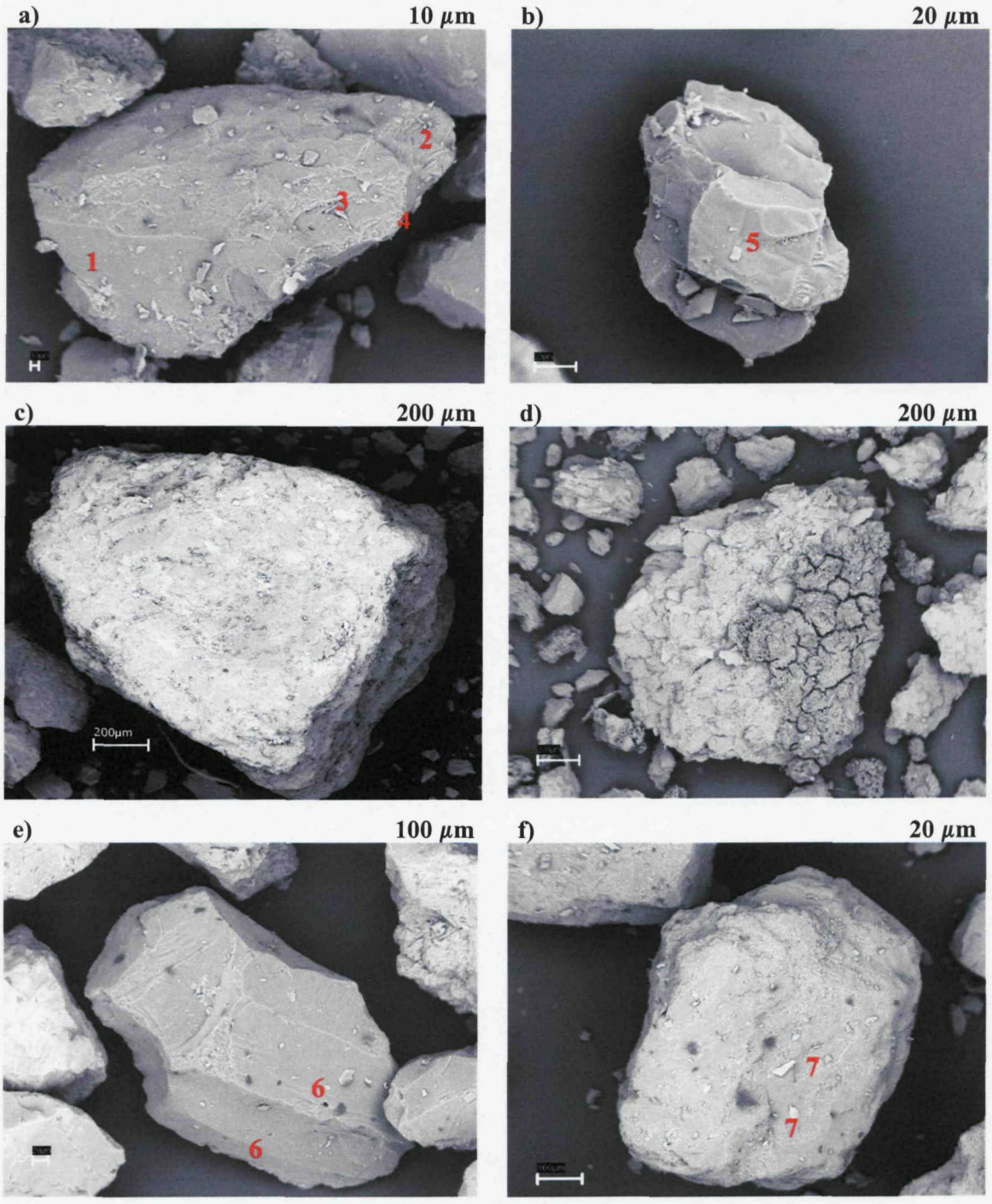


Figure 9.9: Photographs of grain surface textures according to SEM analysis, showing: a) an example of a typical subglacial grain, displaying features characteristic of glacial environments, namely fracture plates (1), arcuate steps (2), grooves (3), and conchoidal fractures (4); b) grain with adhering particles (5); c) grain showing a pre-weathered ('scaled') surface with low relief joints, rounding and edge and surface abrasion; d) grain showing a pre-weathered surface of high relief joints; e) grain with solution pits (6); and f) grain with two v-shaped percussion cracks (7) and some rounding.

The variety of chemical textures observed on the subglacial grains was generally limited to pre-weathered surfaces and cracks. However, solution pits were recorded on three grains (Figure 9.9e). V-shaped percussion cracks (Figure 9.9f) were also noted very occasionally (6 grains). Percussion cracks and solution pits are linked to subaqueous environments and transportation by water (Strand *et al.*, 2003). Low frequencies can indicate a relatively low energy fluvial environment with limited transport (and thus impact) capabilities (Helland and Holmes, 1997). This emphasises that the frequency of occurrence helps to determine the diagnostic nature of a feature. Consequently, if the origins of these samples were unknown, the presence of v-shaped percussion cracks and pits on less than 10 grains would be insufficient to attribute these samples to a fluvial source environment.

When linked to a glacial environment, Mahaney *et al.* (1996) suggest that v-shaped percussion cracks can result from fluvial action either prior, during, or post glaciation. The very low frequency of these features, may reflect fluvial transport prior to glaciation, with a subsequent glacial signature overlaid (Krinsley and Doornkamp. 1973). However, interaction with subglacial melt water during glaciation is also possible. Alternatively, after glaciation, they may result from a phase of proglacial exposure. As these samples were taken from the subglacial environment this could only apply if that fluvial action occurred during a temporary phase of retreat (e.g. in the 1950s; Hart, 2006b). It is perhaps most likely that these marks reflect a combination of these three processes.

One of the features of greatest interest identified during this analysis was the occurrence of pre-weathered surfaces. Two forms became evident within samples: low relief joints and high relief joints. The low relief joints gave the impression of a 'scaled' surface with low relief (Figure 9.9c). The high relief joints took on the form of breakage blocks, created *in situ* due to weathering (Figure 9.9d). The low relief pre-weathered surface was more common and was often associated with the rounding or abrasion of grains (Figure 9.9c), which enabled these surfaces to be preserved. The smoothing of grains via abrasion is associated with both modern and palaeo deposits (Krinsley and Doornkamp, 1973).

Other authors (Mahaney, 1990, 1995; Mahaney and Kalm, 1995, 2000; Mahaney *et al.*, 1996) have also supported the idea that pre-weathered surfaces may be visible on glaciated grains. Mahaney *et al.* (1996) frequently observed pre-weathered surfaces on grains that were later subjected to glacial transport and abraded. Such a scenario is hypothesised for Figure 9.9c. Mahaney *et al.* (1996) emphasise that the production of weathered surfaces is not consistent with processes of glacial transport. As a result, such weathering must predate glacial transport and thus, may accurately be classified as a 'pre-weathered' surface (Mahaney and Kalm, 1995, 2000).

The occurrence of pre-weathered surfaces was also associated with grain shape, whereby more angular grains generally recorded a lower number of pre-weathered surfaces. Angular grains are more likely to have pre-weathered surfaces removed as processes of percussion cause grain fracture, producing fresh grain surfaces, and increasing the rate at which grain size is reduced (Strand *et al.*, 2003). In contrast, abrasion acts to round, as opposed to fracture, allowing grain faces to remain intact for longer. As a result, the preservation of pre-weathered surfaces is more common. Given the evidence of erosion produced by these grains it is likely that the pre-weathered surfaces observed were the result of weathering on exposure during glacier retreat (Winkler, 1996; Hart, 2006b).

Krinsley and Doornkamp (1973) highlight that SEM analysis is a record of the form and morphology of grains. As a result, the allocation of erosional form, developed by Hart (2006b), was also very important to the analysis of the subglacial samples. This involved taking into account every feature of grain morphology, viewing each grain as a whole in order to infer the most appropriate form for that grain. This newly developed classification acts as an aid to the interpretation of the processes to which grains are exposed and the environment from which grains are derived. In light of these findings, a model for the erosional history of the grains has been proposed, with comparison to Ice Stream B (Tulaczyk *et al.*, 1998).

9.6.2 Erosional history

As stated above, previous *in situ* and sedimentological studies at Briksdalsbreen suggest that the subglacial till undergoes deformation (Hart, 2006b). It has been

argued that subglacial deformation is the result of simple shear (Hart and Boulton, 1991), which produces rotation and attenuation. Numerous researchers have demonstrated these processes on the thin section scale (e.g van der Meer, 1997; Khatwa and Tulaczyk, 2001; Roberts and Hart, 2005).

Hooke and Iverson (1995), based on the work of Drescher and de Josselin de Jong (1972), suggested that shearing grains will form alignments of clasts called bridges (Mandl *et al.*, 1977). These bridges can fail by fracture, sliding or rolling of grains. However, they have rarely been observed in till thin section studies (Khatwa and Tulaczyk, 2001). Khatwa *et al.* (1999) and Fischer and Hubbard (1999) questioned grain bridges as a diagnostic property of deforming till. However, Iverson *et al.* (1996) acknowledge that in reality the bridges combine with others to form complex geometrical networks. Hart *et al.* (2006) suggest that till within the deforming layer represents a multi-layered patchwork of different grain sizes, competence and pore-water pressures. Although overall deformation occurs via simple shear, this may result in grain bridges, zones of rotation, and brittle shears in localised areas, due to the heterogeneity of the till.

Iverson *et al.* (1996) demonstrated from laboratory experiments that at low shear strains the particle distribution was self–similar. However, after further deformation, the ratio of fine to coarse particles increased to produce a poorly sorted material, with large grains separated from each other by a finer matrix. They argued that increased shearing leads to sliding (abrasion) rather than crushing (fracture) (Figure 9.10a). Hart (2006b) argues that this process is more complex, as grains have many pathways into the deforming layer (e.g. from bedrock, ice, till advection), and undergo different styles of deformation (rotation, shearing and clast interaction) within the till (Figure 9.10b). In this model, abrasion dominates when grains experience continuous rotation and shear against smaller grains; and percussion processes result from grain impacts during rotation and shear (Hart, 2006b).

Grains will either be dominated by rotation to yield a smoothed and rounded form, or fracture to yield an angular conchoidal form (Figure 9.10b). However, because most grains are dominated by both processes they will yield a complex form. This is illustrated in Figure 9.11. A grain entering the subglacial environment (with some

preserved pre-weathered surfaces may suffer initial (low relief) erosional impacts (Figure 9.11a), before undergoing rotation (Figure 9.11b), or fracture followed by rotation (Figure 9.11c). The grain in Figure 9.11d has a medium relief, associated with both abrasion and fracture. After continued fracture this may develop a conchoidal form (Figure 9.11e), and then after rotation progress to a handaxe form (Figure 9.11f). Thus, although the overall erosional history of most grains will be complex, generally, continued fracture will act to increase the relief of the grains, whilst continued rotation (and thus abrasion) will smooth the grains, decreasing relief. Preservation of these features (angular and conchoidal fracture) can be indicative of short transportation distances (Higgs, 1979). The lack of preserved faces indicates a prolonged residence time within the deforming bed as all pre-weathered surfaces have been removed through erosion. Diamond forms, and the angular and fractured nature of the surface textures, reflect the process of cleaving from the bedrock (Higgs, 1979), and perhaps a preference of impact (percussion) based erosion processes.

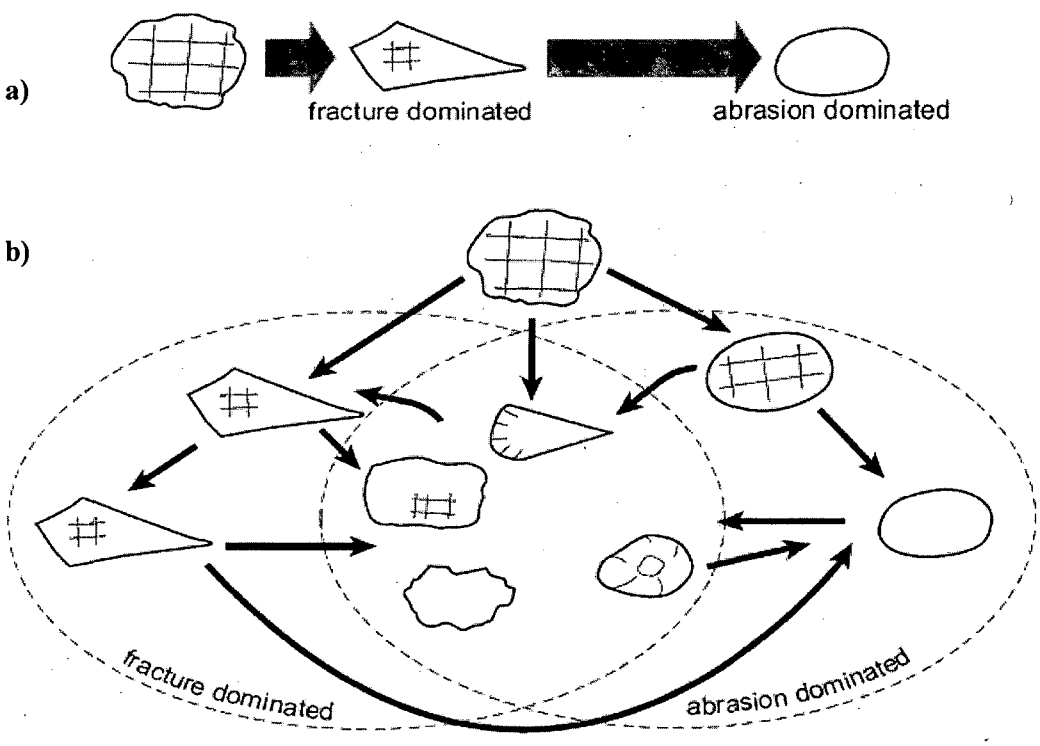


Figure 9.10: Erosional continuum (Rose and Hart, 2008), after: a) Iverson *et al.* (1996); and b) Hart (2006b).

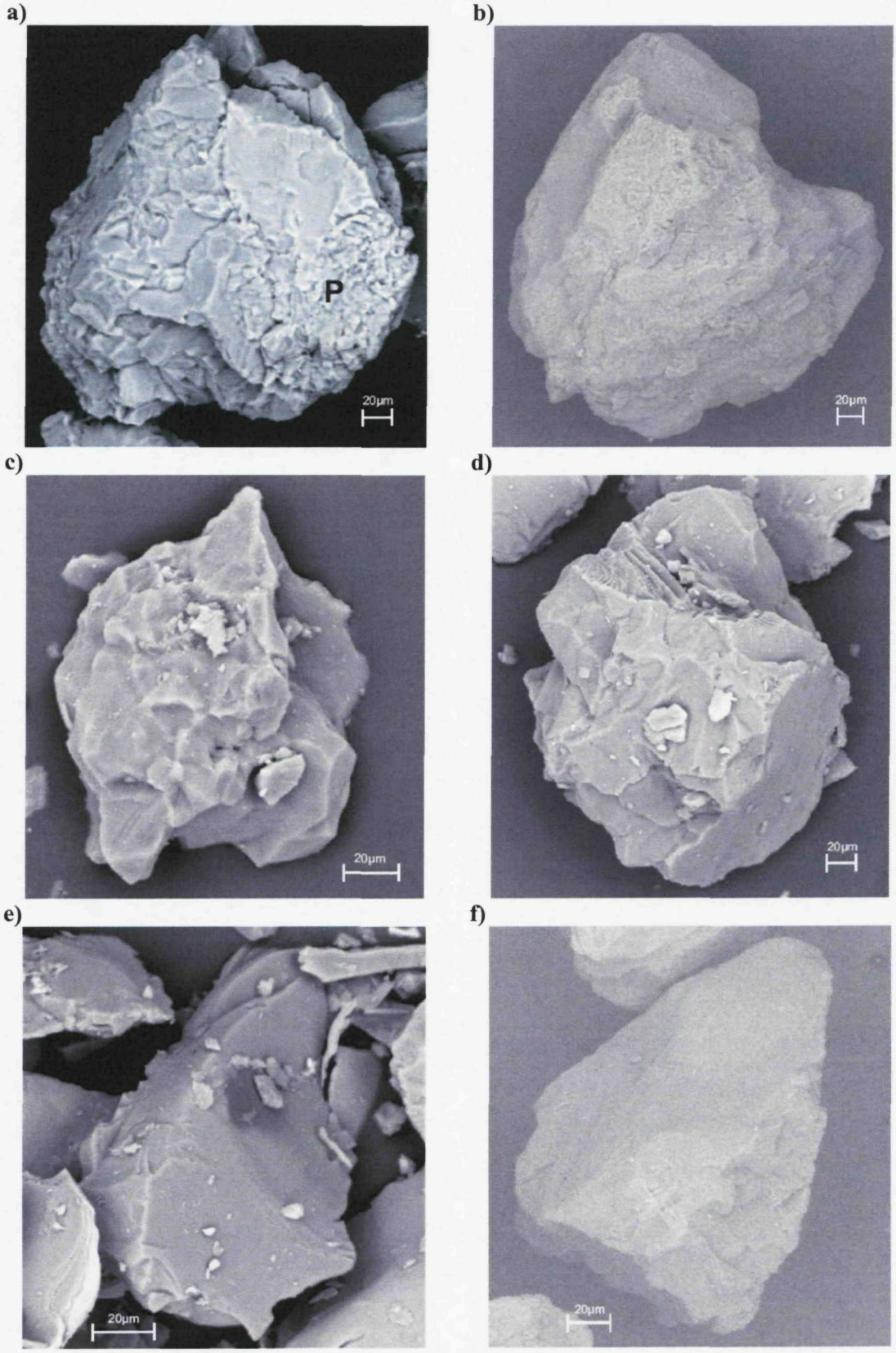


Figure 9.11: Photographs of grain surface textures, showing: a) grain showing low relief impacts with a pre-weathered surface (p) preserved; b) grain showing smoothing and rounding; c) grain showing a jagged form with initial conchoidal fracture and subsequent abrasion of the edges; d) grain with medium relief impacts; e) grain showing a conchoidal form; and f) grain showing a 'hand axe' form (from Rose and Hart, 2008).

The subglacial grains were typically rounded (generally elliptical in shape) with 59% of the samples showing an intermediate erosional form (Figure 9.12; Table 9.4). In addition, 36% of grains showed preservation of a pre-weathered surface and *in situ* jointed blocks. The preservation of pre-weathered surfaces has been viewed by Mahaney and Kalm (2000) on both highly abraded grains, and overprinted grains with new fracture textures. The rounded shapes show perhaps a dominance of abrasive erosion processes in this area of the glacier bed. However, the combination of abrasion textures, crushing and fracture textures (e.g. *in situ* jointed blocks) and pre-weathered surfaces is reflected by the dominance of intermediate grain forms. This indicates that no one process of erosion had dominated the surface texture of the grains. Abrasion alone was insufficient to cause breakage patterns (Krinsley and Donahue, 1968). As such, the nature of the grains reflects a mélange or continuum of both abrasive and percussive processes of erosion (Figure 9.10b).

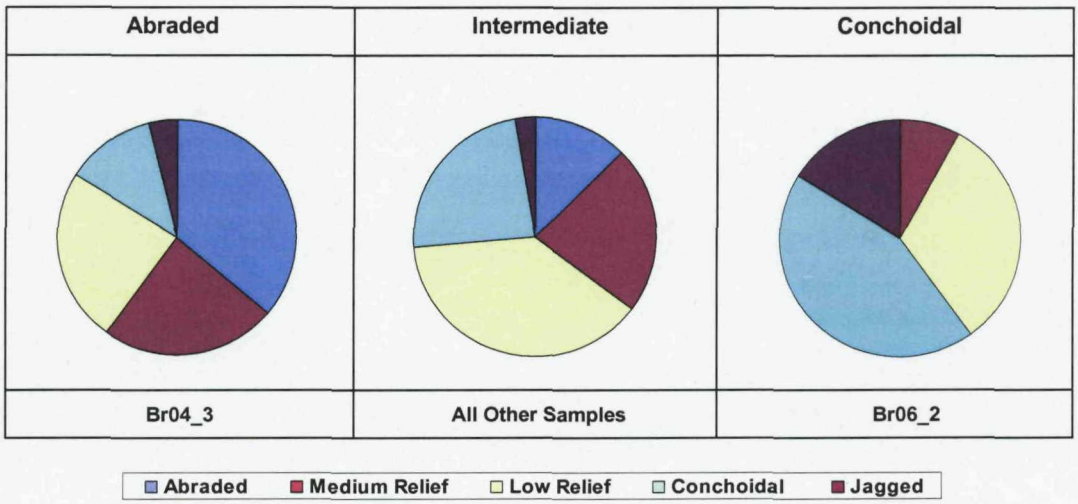


Figure 9.12: Pie charts to show the relative occurrence of the different erosional forms for subglacial samples (2004-6). Pie charts are generated from the results for each sediment sample, as displayed in Table 9.4, final column 'dominant erosional form'.

The style of erosion recorded must reflect either the initial grain-size and/or the total strain experienced within the deforming bed. The sample locations were close to the valley wall. In this area, the till plain (prior to the re-advance) would have been dominated by coarser, more angular material, generated from the valley sides via

processes of physical weathering. However, the samples contained a good proportion of silt-sized particles. This would suggest that the initial grain-size of the material had little impact on the resultant grain size produced by subglacial erosion. In light of this, it would appear that the poorly sorted, smoothed and rounded nature of the subglacial grains, with the preservation of pre-weathered surfaces, reflects an overall low strain experienced by the till. The till in this area of the bed reveals a relatively simple deformation history, reflecting the breakdown of the coarse bedrock, initially by fracture and then abrasion, as suggested by Iverson *et al.* (1996) and Hart (2006b).

9.6.2.1 Comparison with Ice Stream B

In order to investigate the relationship between grain size and erosional processes the grain size data (-2 φ and less) from Briksdalsbreen was plotted against the examples from Ice Stream B and Breidamerkurjøkull (Figure 9.13). The till at Briksdalsbreen was the coarsest, containing only 7% silt and 0% clay; compared with 35% silt and 32% clay at Ice stream B (Tulaczyk *et al.* 1998), and 24-45% silt and 2-9% clay at Breiðamerkurjökull (Boulton *et al.*, 1974). Till derived from a fine grained bedrock or source material, such as the marine sediments at Ice Stream B, are unlikely to suffer a reduction in grain size. This is because the clay-rich tills support high water pressures and prevent inter-particle stress concentrations (Tulaczyk *et al.*, 1998). However, coarser grained tills will undergo inter-particle stress, which results in the crushing of the fine fraction and the production of a silt-rich till (Boulton *et al.*, 1974). In contrast, Briksdalsbreen supported the coarsest and most competent initial bedrock. Thus, although there was evidence of subglacial erosion, a significant silt fraction had not been produced (Figure 9.13).

This data highlights the effect of grain size on the resultant erosional form of grains. The clay rich tills of Ice Stream B showed little comminution (Tulaczyk *et al.*, 1998). In contrast, fine sand-rich tills (e.g. Breidamerkurjøkull) will generate a significant silt component (Boulton *et al.*, 1974), whilst the coarse sand rich tills at Briksdalsbreen showed complex erosional styles, but no significant silt component.

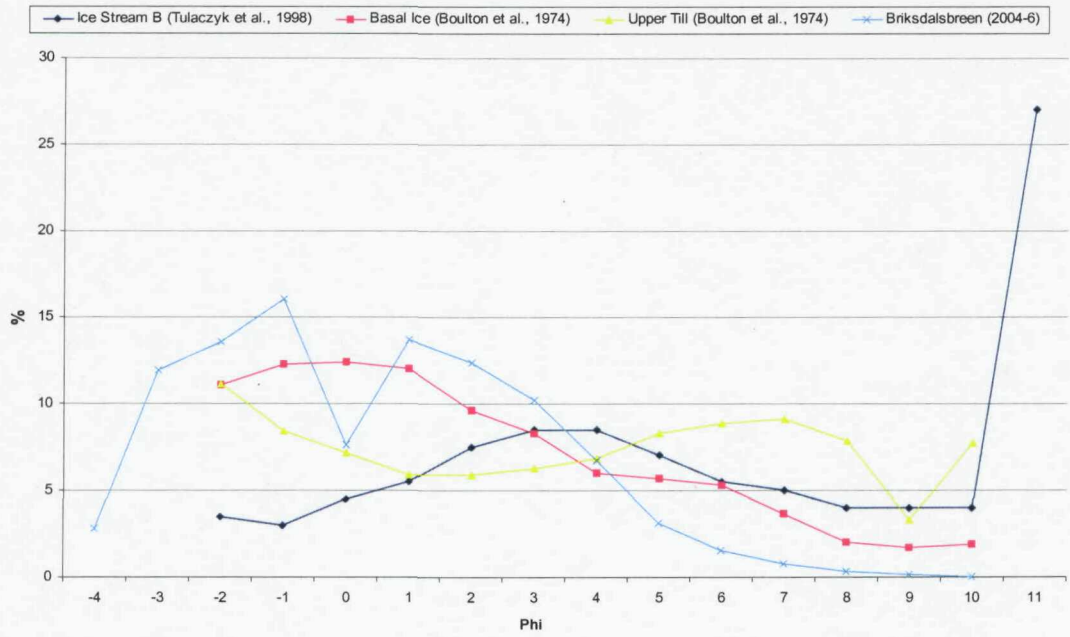


Figure 9.13: Grain size (<-2ϕ) from different deformation tills: Ice Stream B, after Tulaczyk *et al.* (1998); Breidamerkurjøkull, after Boulton *et al.* (1974); and subglacial samples from Briksdalsbreen, averaged from 2004-6.

9.6.2.2 Comparison with the probes

SEM analysis was employed to determine the erosional history of grains on the micro-scale. However, the movement and interaction of grains within the till matrix has implications for the movement of larger scale clasts within the deforming bed. The relationship between grains on a variety of scales has been highlighted to some extent within micromorphological studies. Small grains, for example, are often seen to rotate around larger grains (e.g. van der Meer, 1997). The records of probe movement outlined in Chapter 8 were also indicative of clast rotation. This pattern appears to be in keeping with the occurrence of rotational (abrasion) processes observed on the micro-scale.

9.7 Summary

A series of sedimentological investigations were carried out at Briksdalsbreen through means of grain size classification and SEM analysis. Firstly, comparisons between proglacial and subglacial sampling were made to test if the *in situ* subglacial

sampling technique was representative of the subglacial environment. This comparative study showed a close similarity between the bulk samples taken in 2004 and 2006, and all the subglacial *in situ* samples. In addition, the reliability or bias of the sediment sampler was tested. The small sampler was in good agreement with the proglacial samples, whereas the large sampler preferentially collected the sand and silt fraction.

The process of SEM analysis was also verified through comparison of the subglacial sample surface textures with those documented in the literature. The main purpose of the SEM analysis was to investigate the nature of subglacial erosion associated with the coarse grained deformation till collected *in situ* from the subglacial environment. This demonstrated the presence and nature of the intra-granular erosion within the till, by crushing (fracture) and rotational (abrasion) processes. The erosion of grains reflected a relatively simple pattern of first fracture and then abrasion, associated with the model proposed by Iverson *et al.* (1996) and Hart (2006b). It would appear that the resultant style of glacial erosion associated with deformation tills is controlled by the nature of the bedrock and overall strain imposed on the till (Rose and Hart, 2008).

Chapter 10

Conclusions

10.1 Introduction

The research presented in this thesis was primarily concerned with the data that could be obtained about the deforming glacier bed from an autonomous, wireless, multi-sensor subglacial probe, set within an ESN. To achieve this, Briksdalsbreen, a glacier with a deforming bed, was chosen for *in situ* instrumentation and sedimentological analyses. The field site was surveyed, an ESN was established, the glacier was instrumented and sedimentological analyses were performed. This was done to characterise the subglacial processes and sediments operating at Briksdalsbreen. In this chapter an overview of the main findings of this research is presented and some suggestions for future research are proposed.

10.2 Theoretical Background

There has been continued research into the factors that govern glacier dynamics. In recent years this has been driven by increasing concerns on the stability of ice masses in response to changes in global climate. Initial investigations suggested that glaciers moved solely via sliding, advancing on a thin film of water over rigid bedrock bases (Nye, 1952; Weertman, 1972). However, the work of Boulton and co-workers in the 1970s and 80s revealed a saturated layer of sediment, typically weaker than glacier ice, which could deform and contribute to glacier motion (Boulton and Hindmarsh, 1987). This prompted a paradigm shift in research to determine the properties of this layer and its influence on glacier dynamics.

The acknowledgement that some glaciers are underlain by unlithified sediments affected a number of research areas within the field of glaciology. The influence of till deformation on the dynamics of glaciers is of key importance to glacier flow laws, and thus models of both palaeo and contemporary glacier motion. The impact that this layer has on ice sheet stability, and thus potential scenarios of sea level rise, has become of increasing concern given recent changes in global climate. The deforming bed has implications for the reinterpretation of glacial geomorphology, the production of bed forms, and the deposition of sedimentary sequences. These examples highlight the importance of the deforming bed to glaciological research.

The paradigm shift prompted extensive new research. Investigations included: the sedimentological analysis of stratigraphic sequences and bedforms; laboratory experiments and geotechnical testing; direct observation and instrumentation; and more recently, the use of geophysical techniques and remotely sensed data. These methodological approaches can provide much information about the deforming bed. However, the most detailed descriptions of the properties of the deforming bed and its role within the glacial system, are obtained from *in situ* experimentation. This has been achieved through the use of custom-designed borehole instrumentation, combined with surface data (e.g. ice velocities, weather conditions and river discharge data). These investigations have generated a wealth of information concerning the nature of the deforming bed and its interaction with the glacier above.

Several questions still remain unanswered despite the number and variety of investigations undertaken. A generally accepted rheological model for till and an accompanying flow law for ice masses on soft beds are still lacking. Conflicting data sets detailing the mechanical response of the deforming bed to changes in physical conditions, most notably water pressures, has meant that these processes are not yet fully constrained. The spatial and temporal contribution of the deforming bed to the glacial system is also relatively unknown, both in site specific locations and globally. Indeed, it would appear that as more information is gathered concerning the deforming bed the heterogeneity of the system has become more pronounced. In light of these difficulties, it is evident that further investigation is still required. However, in order to improve on previous investigations, and learn more about the

subglacial environment and the deforming bed, improvements are required in the instrumentation used and the methodological approach employed.

A new instrument was designed in collaboration with the Electronics and Computer Science department at the University of Southampton. The new instrument houses a variety of micro sensors, including: temperature, pressure, case strain, resistance, and tilt. Wireless capabilities were employed so that the instrument could behave more naturally within the subglacial environment; in comparison to the tethered instruments traditionally used to study the bed of glaciers. The inclusion of numerous sensors within one instrument also enabled a greater array of data to be collected, increasing spatial and temporal comparisons of subglacial conditions.

The new methodological approach employed involved the use of an Environmental Sensor Network (ESN). This system supported wireless communications and a greater spatial array of instruments. It also allowed the data obtained from the instruments to be relayed to a sensor network server, where it could be accessed remotely by the end user via the internet. The application of an ESN to a glacial environment was an experiment in both sensor network capabilities and instrument design. It was hoped that the new instrument would provide the improvements in monitoring capabilities required to generate new data concerning the deforming bed and the processes operating within the subglacial environment, further contributing to the questions that remain unanswered in this field of study.

10.3 Key Research Findings

This section will outline the main findings of this research project. The probe results will be summarised according to season, as outlined in Chapters 6, 7 and 8, followed by the sedimentological findings (Chapter 9). The success of the methodological approach employed in this project is also assessed.

10.3.1 Winter

The incorporation of the probes into the subglacial environment was critical to monitoring the processes operating within the deforming bed. A conceptual model to

account for the variety of potential probe locations was developed for comparison with sensor readings. The location of the probes was determined using the tilt record, with supporting information from the temperature sensor. The majority of the probes were located upright within the base of the boreholes and rapidly became incorporated into the subglacial environment, in accordance with rates of glacier movement. Incorporation was marked by a sudden change in tilt sensor readings and a reduction in probe temperatures to around 0°C. The transition of the probes into the deforming bed was demonstrated, where possible, by combined readings of case strain and tilt. As the probes became encompassed by the till, readings of case strain increased and began to oscillate in agreement with variations in the tilt record. This reflected the probes' interaction with the till as they began to rotate within the deforming bed. The normal time for incorporation ranged between 21-57 days.

The probes showed stochastic associations with external weather conditions. The lack of direct correlations with melt water events indicated that direct inputs via boreholes were minimal. This may have been the result of rapid movement of the borehole over the probe and away from the initial location of deployment. The probes showed a wide range of sensor readings during the winter months. This indicated that activity continued within the subglacial environment (to varying degrees) throughout the winter. The 2004/5 probes saw a step change in readings that was not evident in the 2005/6 sensor readings. This marked a change in the activity of water flows within the subglacial environment. In contrast, less activity was recorded by the 2005/6 probes.

A relationship between water pressure and probe temperature was determined, whereby increases in pressure resulted in a decrease in probe temperature. The resistance records were variable and correlations with water pressures were often intermittent. In comparison to water pressure, resistance generally demonstrated a greater sensitivity to the presence of water within the subglacial environment. An absence of diurnal oscillations suggested that the probes were located in unconnected regions of the bed. However, the range and often magnitude of pressure oscillations revealed that water flow through these regions was often more significant than previously thought. In mid-October, changes in sensor patterns reflected a reduction in activity and change in conditions within the subglacial environment. This was

thought to represent the start of a transition from a summer to a winter drainage regime. However, due to the lack of supporting data this is only a tentative observation.

Probe 4 provided a good record of activity from within the ice column. The activity in probe temperature and case strain, and the variety of oscillations in tilt were in strong contrast with those from the subglacial environment. As such, Probe 4 acted as a bench mark, against which other probes could be compared and interpreted. Probe 4 also showed poor correlations with external weather conditions, confirming that direct borehole inputs were minimal. A range of sensor activity also continued throughout the winter period suggesting that the englacial environment was not completely dormant during this time.

10.3.2 Spring

The spring marked the period of greatest activity within the sensor records. The pressure activity displayed by the probes confirmed that they were located in unconnected, but often active, regions of the bed. Probe 15 showed diurnal fluctuations that were out of phase with the expected timing of daily pressure peaks and troughs. This indicated that it was experiencing forcing from a connected region of the bed and thus, acted as a proxy for activity in that area. Probe fluctuations in water pressure began as early as the end of December, marking the start of spring activity within the subglacial environment. Patterns of water pressure were associated with external weather conditions and their nature corresponded with a spring event. An emergent spring event was recorded at the start of the year, displaying some of the characteristics of a spring event. The main spring event occurred later, and was characterised by a sudden and rapid high magnitude increase in water pressure. Diurnal fluctuations were also observed in the connected region. The spring event resulted in lasting changes in the processes operating within the subglacial environment. This was shown by a sustained change in sensor patterns into the summer months. The timing of the spring event was in keeping with changes in the external weather conditions and removal of the snow pack.

The transition in sensor activity following the spring event also implied that the subglacial drainage system had undergone modification. The forcing signal from the connected region did not reappear, suggesting that the connected drainage system had developed from a low capacity distributed system, into a more efficient discrete drainage network capable of discharging high summer flows. The analysis of records of tilt, case strain, and calculated yield strength, implied that sliding was the dominant mechanism of basal motion during the spring. This occurred through a process of decoupling, associated with the high magnitude spring pressure events in excess of overburden. Periods of decoupling have often been associated with enhanced sliding (velocities) and glacier uplift during the spring event. However, this could not be confirmed by direct measurement at Briksdalsbreen.

Hydro-mechanical interactions between the till and water pressures were investigated briefly. The direct correlation between readings of water pressure and case strain (sediment strength) were contrary to those normally associated with the subglacial environment. Although, this has been observed before, explanations for this trend were lacking. This highlighted an area of uncertainty within this field of research, and the need for further investigation and a new model to explain this inconsistency. This was beyond the scope of this thesis.

Probe 4 showed an increase in activity within the ice column during the spring. Water pressures increased as melt water inputs reached the borehole through the snow pack with changing external weather conditions. The activity in the tilt and case strain records suggested that the ice column was experiencing an increase in ice deformation as the spring progressed. In the ice column, Probe 4 appeared to be dominantly affected by changes in tilt and case strain, rather than variations in water pressure.

10.3.3 Summer

The summer was characterised by relatively little activity in accordance with the location of the probes within unconnected regions of the bed. Sensor readings showed few fluctuations and water pressures of varying magnitudes declined generally throughout this period. This activity suggested that an efficient discrete

drainage system had become established, increasing the efficiency of water transport at the glacier bed and reducing flows in the unconnected regions. The movement of the probes was determined according to their tilt records. The probes were active and displayed mechanisms of Taylor (1923) rotation, moving about their b-axis. This has implications for fabric analysis and models of clast movement. Mechanisms of basal motion were interpreted from the tilt and water pressure records. Overall, those probes with high water pressures were characterised by decoupling and enhanced sliding. However, as water pressures decreased they showed a transition from sliding to deformation. Those probes which recorded low water pressures and sediment yield strengths recorded deformation as the dominant mechanism of basal motion during the summer. Deformation appeared to dominate in the summer, but in general it appeared that basal motion was relatively limited in unconnected regions.

10.3.4 Sedimentology

The presence of flutes and push moraines within the glacier foreland suggested that Briksdalsbreen was underlain by unlithified sediments. Thus, it was assumed that the glacier foreland represented an exposed subglacial surface. This was tested through comparisons between sediment samples from the foreland and those collected *in situ* via boreholes. This enabled any bias in the *in situ* sampling technique to be assessed. The texture and grain size distribution of bulk samples showed a close correlation with those from the subglacial environment. The large sediment sampler collected a greater proportion of fines. However, the small sediment sampler also showed a good agreement with the proglacial samples, indicating that the removal of fines in the sampling process was not significant. The sediments were generally poorly sorted gravels or muddy-sandy-gravels.

The erosional history of grains from the *in situ* subglacial samples was determined through analysis with the SEM. The surface textures observed were in keeping with those traditionally associated with glacial environments. The dominant erosional form of grains was new impacts-low relief. This intermediate form resulted from exposure to a combination of both impact (fracture) and rotation (abrasion) processes within the deforming bed. This erosional continuum was demonstrated through

surface textures, grain forms and the observation of preserved pre-weathered surfaces. The rotation described within this continuum was in keeping with micro-scale observations of rotational structures and, at the clast scale, was comparable with the rotational movement recorded by the probes.

The initial grain-size of the material appeared to have little effect on the style of erosion recorded, revealing a relatively simple deformation history. The relationship between grain size and erosional history was demonstrated through comparison with examples from Ice Stream B (Tulaczyk *et al.*, 1998) and Breidamerkurjøkull (Boulton *et al.*, 1974). This revealed that: clay rich tills showed little comminution; fine sand-rich tills generated a significant silt component; and the coarse sand-rich tills at Briksdalsbreen showed no significant silt component, but a more complex erosional style.

10.3.5 ESN project overview

The primary aim of this investigation was based on the development of a new instrument and the establishment of an ESN from which it would function. This was achieved successfully in conjunction with the ECS department. The probe represented a good approximation to a clast that might be found within the subglacial environment. It was comprised of a variety of micro-sensors that enabled the relevant physical and mechanical properties of the deforming bed to be monitored. It was also equipped with wireless capabilities. All of these features enabled the probe to become incorporated into the deforming bed and monitor conditions more realistically, with minimal disturbance to the subglacial environment.

The instrument design and methodological approach was a great success in that it enabled the objectives outlined within the introduction to be achieved. The data collected allowed conclusions to be drawn about the processes operating within the subglacial environment over time and space. The movement of the probes was assessed with respect to current models of clast rotation within the deforming bed. The probe was also cost efficient, combining numerous sensors within one unit. This provides the potential to increase the spatial coverage of instrument observations and the number of parameters assessed.

In order for the probes to function, an ESN was established successfully. This was the first time that an ESN had been developed in a glacial environment. Creating a base station that could remain on the ice was relatively straight forward and easy to maintain. The main challenge to this system was radio communications through the ice. This was improved upon annually through in-field testing. As a result, the quantity of data collected, and accordingly the duration of probe survival, increased between years. This system was also designed so that data could be saved and stored at each transfer point within the system to minimise data loss. This meant that the quantity and range of data produced by this system exceeded the majority of previous *in situ* investigations, and was in keeping with the few that had achieved long term data collection (e.g. Murray and Porter, 2001). This system has demonstrated a widespread applicability to all glacial environments that can only help to increase monitoring capabilities within remote localities. As improvements in communications continue, the use of ESNs is set to show only further potential for future use in glacial environments and environmental monitoring as a whole.

10.3.6 Summary of key findings

The research conducted for this thesis culminates in the following key findings:

1. Wireless instrument sensing capabilities within the framework of an ESN can be achieved within glacial environments.
2. Wireless capabilities enabled the probes to become fully incorporated into the deforming bed. This enabled the conditions within the deforming bed to be monitored more realistically with minimal environmental disturbance.
3. Long term records from unconnected regions of the bed were produced, revealing greater activity in these areas of the bed than perhaps previously thought. The first long term records of pore-water pressure were also generated.
4. A two stage spring event was recorded. An emergent spring event marked a warm up to the spring event, showing some of the same characteristics. The actual spring event occurred later in the year and was followed by a change in the processes operating within the subglacial environment. Activity so early in the year has implications for the stability of ice masses and enhanced glacier velocities during the spring.

5. Sensor readings were used to infer the transition of the subglacial hydrological system from an inefficient distributed drainage system to a discrete drainage network. Sensor patterns also suggested that sliding was the dominant form of glacier motion in the spring.
6. The movement of the probes increased during the summer and was associated with mechanisms of Taylor rotation. This has implications for fabric analysis of deforming beds and models of clast rotation. The other sensor readings showed little variation in keeping with probe locations within unconnected regions.
7. Deformation appeared to dominate in the summer, although motion was thought to be relatively minimal in unconnected regions of the bed.
8. The sensor readings displayed by the englacial probe showed continued activity within the ice column to varying degrees throughout the winter. Activity increased during the spring and the record for case strain suggested that ice deformation had become more active.
9. The erosional history of grains was relatively simple and unaffected by initial grain-size. The coarse sand-rich tills at Briksdalsbreen showed no significant silt component but displayed a complex erosional style. The resultant grain forms were generated through a combination of fracture and abrasion processes within an erosional continuum.
10. The use of an ESN and wireless sensing capabilities was successful and has great potential within hostile environments.

10.4 Future Research

This research has developed a new instrument for monitoring conditions within glacial environments, in particular the deforming bed. This study provides a basis for future research with respect to both the methodological approach used, and the observations made on the deforming bed.

10.4.1 Instrument design

The combination of numerous micro-sensors within one instrument has shown the potential of monitoring a range of criteria at each location at the glacier bed. The incorporation of further sensors will provide added benefits to this system. The tilt

sensors used during the investigation produced readings that were problematic to interpret. As a result, a new tilt sensor that monitors pitch, dip and roll has been developed. This will be used in the next probe version, in combination with a compass, which remains unaffected by the probe's electronics. This will allow the precise orientation and heading of the probe to be determined. A light sensor has also been included within the probe design. An LED will send out a pulse of light, and the reflection strength of that light will be assessed by a neighbouring detector. This will function under the assumption that the reflection strength will be greater within the ice than within the till. In combination with records of temperature, resistance, tilt and case strain, this will provide further evidence for the incorporation of the probes within the till.

The micro-sensors employed within the probes also need to undergo continued rigorous calibration and testing. This applies to both new and old probe sensors. Further testing of case strain, for example, may help to constrain its relationship with the pressure records further. Similarly, the data sets highlighted that resistance readings need to be assessed further in relation to till wetness, conductivity and turbidity. Calibration is essential to determine what the sensors are *actually* showing, so that the records can be interpreted correctly and errors reduced.

The area of probe advancement that has perhaps the greatest potential is the development of a positioning system that would enable the precise location and rate of probe movement to be assessed. A positioning system could be achieved using a greater array of transceivers within the ice column to create an ad-hoc network that allows communication between sensor nodes. The location of the probes could then be determined as a function of signal strengths between neighbouring nodes. This could also increase communications success by allowing data to be transferred between probes to the glacier surface. The best data transfer route can then be used as the location of instruments change within the subglacial environment. An array of probes could also be placed at a variety of depths within a borehole to monitor changing rates of ice deformation and activity at different depths within the ice column. Linked to this, a greater number of englacial probes would enable further comparison with those in the subglacial environment.

10.4.2 Glaciological research

The probe records have revealed much information concerning the nature of the subglacial environment that can drive future investigations. The probes generated the first long-term pore-water pressure records and demonstrated activity within the till much earlier in the spring than previously observed. This was associated with the emergent spring event. This activity may have implications for the movement of the glacier during the winter and its stability in response to changing conditions in the spring. The emergent spring event should be looked for in glaciers elsewhere, in combination with more detailed records on glacier velocities and surface elevation.

Readings of water pressure and case strain also demonstrated a complicated interplay between mechanisms of deformation and sliding at the glacier bed; and calculations of sediment yield strength and basal shear stress. This demonstrates that there is still much to be learnt about the hydro-mechanical interactions between the till and the ice above. A satisfactory model that explains the unusual result observed is required. This can be resolved through further calibration of the probe sensor readings and continued *in situ* investigations. The probe sensor readings can also be used to make further estimates of the rheological parameters associated with the till. Greater understanding should be achieved from readings taken directly within the deforming bed. The results generated may have implications for modelling the rheology of till and generating a flow law for glaciers with deforming beds.

The activity recorded during the winter suggest that the focus of *in situ* investigations should also be extended to include more observations of the summer/winter transition in glacier activity (Harper *et al.*, 2002). The timing and nature of this transition might provide further explanation as to the early season activity recorded at Briksdalsbreen and perhaps even help to predict the processes that will dominate in the following spring. This could be achieved with continuous sensor records, persisting for longer than a year. This was almost accomplished with the probes at Briksdalsbreen. Attempts to increase the spatial coverage of instrumentation on glaciers may also help to solve some of these problems. This could help to constrain the spatial and temporal contribution of deforming beds to the glacier system, for example, as simultaneous measurements are required to determine processes of coupling and load transfer. Hopefully the nature of the probes, as self contained

multi-sensor instruments, and the ease with which they can be deployed, will enable greater spatial coverage in future investigations. Continued observation of subglacial interactions can only help to develop our understanding of glacier dynamics and the response of ice masses to changes in external conditions.

The sedimentological investigations performed at Briksdalsbreen demonstrated the application of a new series of criteria (based on SEM analysis) for the classification of grain forms on the micro-scale (Hart 2006b; Rose and Hart, 2008). The continuum of erosion presented can be applied to further study sites and with continued development may enable more robust identification of subglacially deformed materials within quaternary sedimentary sequences. A greater knowledge of grain interactions within the deforming bed may also enhance current understanding of processes of glacier erosion, transport, till dilation and rheological parameters such as porosity and hydraulic conductivity. If further tilt records can be produced from the probes this will also help to determine the movement of clasts within the deforming bed and their interaction with the till matrix. This might help to constrain the conditions, or preferred till properties, under which each model of clast rotation occurs.

10.5 Summary

This chapter has presented an overview of the debates surrounding the deforming bed, the research carried out, and the key findings made. The aim of this project was:

> *"To investigate the deforming glacier bed with the use of an autonomous, wireless, multi-sensor subglacial probe."*

This research was driven by a desire to challenge current monitoring capabilities, in order to improve our understanding of the deforming bed. The use of an ESN has pushed the boundaries of wireless capabilities within hostile environments. The data obtained from the wireless multi-sensor probes has contributed new information to current understanding of the properties and processes associated with the deforming

bed. The sedimentological investigations that complimented the probe records have added to the debate on grain interactions and erosion within the deforming bed, and the classification of sediments through SEM analysis. It is hoped that the findings of this research will fuel continued investigation into the importance and implications of the processes operating within the subglacial environment.

APPENDIX A

Journal of Glaciology, Vol. 52, No. 178, 2006

Instruments and Methods

A wireless multi-sensor subglacial probe: design and preliminary results

Jane K. HART,[1] Kirk MARTINEZ,[2] Royan ONG,[3] Alistair RIDDOCH,[2] Kathryn C. ROSE,[1] Paritosh PADHY[2]

[1]School of Geography, University of Southampton, Southampton SO17 1BJ, UK
E-mail: jhart@soton.ac.uk
[2]School of Electronics and Computer Science, University of Southampton Southampton SO17 1BJ, UK
[3]Department of Engineering, University of Leicester, Leicester LE1 7RH, UK

ABSTRACT. This paper introduces a new way to investigate in situ processes, the wireless multi-sensor probe, as part of an environmental sensor network. Instruments are housed within a 'probe' which can move freely and so behave like a clast. These were deployed in the ice and till at Briksdalsbreen, Norway. The sensors measure temperature, resistivity, case stress, tilt angle and water pressure and send their data to a base station on the glacier surface via radio links. These data are then forwarded by radio to a reference station with mains power 2.5 km away, from where they are sent to a web server in the UK. The system deployed during 2004/05 was very successful and a total of 859 probe days worth of data from the ice and till were collected, along with GPS, weather and diagnostic data about the system.

INTRODUCTION

An understanding of subglacial processes is vital to understanding glacier dynamics, as it has been suggested that both modern and ancient glaciers are controlled by the nature of the bed (Boulton and Jones, 1979; Alley and others, 1986) and subglacial deformation has been recorded at many modern glaciers by in situ process studies (Murray, 1997; Fischer and Clarke, 2001) and proglacial foreland studies (Hart and Rose, 2001).

One of the major developments over the past 20 years in glaciology has been the use of subglacial instrumentation to study subglacial processes (for a summary see Boulton and others, 2001). Most studies use tiltmeters to investigate whether the till is actively shearing (Iverson and others, 1995), ploughmeters to measure sediment strength (Fischer and Clarke, 1994) and drag spools to measure sliding velocity (Blake and others, 1994). These studies have demonstrated that both till deformation and basal sliding occur beneath the glacier, and that changes in pore-water pressure and sediment strength fluctuate rapidly on very short timescales.

However, all these studies have an intrinsic problem, in that the instruments are connected by wires to a data logger at the glacier surface, and although spare cable is often left to reduce movement disturbance, the instruments cannot move freely. The use of loggers also makes data and maintenance access intermittent.

The aim of the GlacsWeb project was to construct a wire-free autonomous probe which was part of a wireless sensor network (Martinez and others, 2004). The sensors were encased in a probe that was designed to be able to replicate natural clast behaviour. These were inserted into the ice and the till and were able to send information back to the surface via radio communications, which could then be accessed in near-real time via the internet.

Harrison and others (2004) also developed probes with a wireless system using very low-frequency (500 Hz) radio, which they inserted into the subglacial sediment at Black Rapids Glacier, Alaska, USA, via a hole drilled in the till with a very heavy slide hammer. Their system comprised three large (61 cm long) probes at one location, with data collected a few metres away by a wired receiver and accessed by manual logger downloads. The system demonstrated that subglacial wireless sensing was possible, though not without difficulties.

The GlacsWeb system was installed at Briksdalsbreen in southern Norway (Fig. 1a) because the foreland showed potential evidence for the presence of a deforming bed (push moraines and flutes in fine-grained till; Hart, 2006), as well as good access and communications systems. The latter included GSM (global system for mobile) telephone coverage on the glacier and a local (2.5 km away) ISDN (integrated services digital network) telephone connection, which allows the transmission of data to the UK.

In this paper, we outline the three elements of the system (probes, base station and reference station), discuss some of the challenges in developing such a system and provide a summary of the preliminary results.

FIELD SITE

The study sites on the glacier were chosen where the glacier was flat and crevasse-free with safe access (Fig. 1b). The glacier and foreland were mapped with a Topcon differential GPS (global positioning system) (DGPS) and the thickness of the glacier was determined from measured borehole depths, drilled with a Kärcher HD100DE car wash, and from a ground-penetrating radar (GPR) survey. For the latter, an EKKO 100 GPR with a 1000 V transmitter was used, with a common-offset survey using 50 MHz antennas on a grid pattern with a 2 m antenna spacing and a 0.5 m sampling interval. In addition, the velocity of radar in ice was found to be 0.16 m ns^{-1} taken from a common-midpoint (CMP) survey. The boreholes and till were examined with a

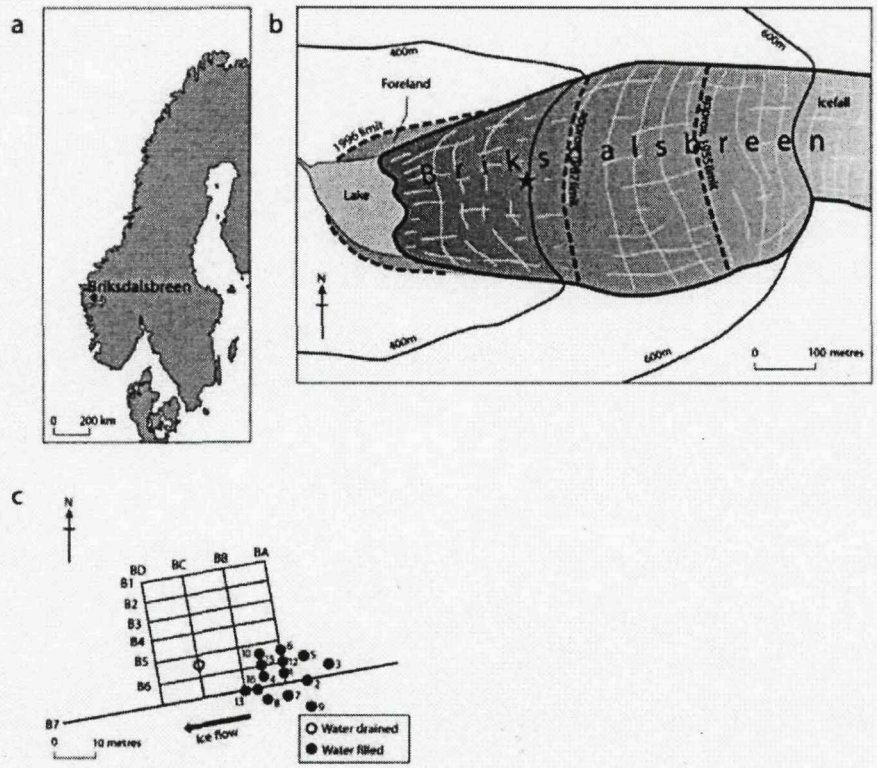


Fig. 1. (a) The location of Briksdalsbreen in southern Norway. (b) Map of the glacier and foreland with site locations marked (site A = 2003; site B = 2004). (c) GPR transects and boreholes shown.

custom-made infrared (900 nm) camera. In addition, a till sampler was attached to a subglacial hammer (Blake and others, 1992) to verify the presence or absence of till.

Although the borehole deviation from the vertical was unconstrained, the measured depths of the boreholes (measured with a marked drill pipe and the camera cable) were very close to the calculated depths from the radar taken in the same area. This similarity of results allows us to interpret the glacier depth in the survey area to range from 62 to 71 m. The details of the boreholes are summarized in Table 1.

SYSTEM OVERVIEW

A general system overview is shown in Figure 2. Sensor probes are inserted into the ice or till, and send their information to a base station on the ice surface; this then sends its information to a fixed reference station. The reference station is the gateway for transferring data and allows remote control or monitoring of the entire system if necessary.

There were a number of factors that influenced the design of the system:

Radio frequency. Radio-wave propagation in pure ice depends on relative permittivity and dielectric loss factor. The dielectric constant of ice at 0°C is approximately 3.17 (Glen and Paren, 1975) and the absorption of radio over 100 m of ice at –1°C at 100–1000 MHz is less than 10 dB (Evans and Smith, 1969). Budd and others (1970) and Dowdeswell and Evans (2004) argue there is no significant loss by absorption up to frequencies of 800 MHz. However, glaciers contain sediment, water and air bubbles which significantly affect radio transmission.

Probe size. The probes needed to be small and inexpensive to allow as many as possible to be constructed and inserted into the ice and subglacial till. A hot-water drill was used to drill the holes, so the hole diameter sets a maximum size for the probes. The probes were also designed to be elliptical in shape, so their movement could be compared with theoretical studies of clast behaviour in a viscous medium (e.g. Jeffery, 1922; Glen and others, 1957).

Power management. The probes need sufficient power to function for a year or more. Unlike the majority of environmental monitoring situations, there is no alternative (e.g. solar) power source under the ice.

In order to satisfy both miniaturization and frequency requirements, the radio frequency has to be a compromise between antenna size and transmission loss. Higher-frequency systems allow shorter antennas but at the expense of greater propagation losses (shorter communication range and/or higher transmission power), and conversely. In addition, the greatest radio loss occurs in the upper part of

Table 1. Borehole characteristics

Borehole	Borehole depth	Till present*	Probe No.	Probe depth	Initial transmission distance	Estimated maximum working transmission distance	Probe in till or ice
	m			m	m	m	
1	70	v	7	70	36	36.26	till
2	70	n	4	19	19	19	ice
3	~71	n	–	–	–	–	–
4	69	s, v	2	69	34	–	till
			Transceiver	35			
5	70	c, v	–	–	–	–	–
6	68	c, v, s	–	–	–	–	–
7	75	v	6	72	37	–	ice
8	68	c, v	3	68	33	–	clast
9	~70	v	–	–	–	–	–
10	68	n	1	–	37	–	ice
11	30	n	–	–	–	–	–
12	66	s, v	–	–	–	–	–
13	69	v	8	69	33	33.6	till
14	63	v	–	–	–	–	–
15	62	v	–	–	–	–	–
16	68	c, v	5	68	33	33.4	till

*s: till sample taken; v: till seen on video; c: clast seen at base.

the glacier where there is more liquid water. To avoid this, a transceiver was hung beneath the ice surface with a long serial/power cable (the method to determine the optimal depth for the transceiver is discussed below). To facilitate power requirements, the probes would remain 'asleep' for most of the time, only 'wake up' and record their data six times a day, and transmit these data once a day to the base station on the glacier surface.

The system described here was able to measure probes' tilt angle, water pressure, resistivity, temperature, case stress and battery voltage, as well as the base station's tilt angle, temperature and battery voltage, plus a GPS recording of the location of the base station, the weather at the base station and data from a 'traditional wired' tiltmeter and ploughmeter inserted into the till.

Probes

The probes are custom-made and comprise a microcontroller, storage, sensors, radio communications system and power controller and supply held within a bespoke case (Fig. 3; Table 2). The probe's circuitry remains largely unpowered until they are 'woken' by their real-time clock.

The probes contained a PIC (peripheral interface controller) 8-bit microcontroller, responsible for reading and storing sensor data, configuring the real-time clock and interpreting commands. Each probe had one 1.7 MPa pressure sensor, two dual-axis 180° micro-electromechanical system (MEMS) tilt angle sensors and a temperature sensor. There were two additional bolts through the case to measure external resistivity, and strain gauges to measure the stress on the case. The probes could not contain a compass because of the metals within the probes. The x and y tilt sensors measure the angle of tilt from the vertical (0° x tilt, 0° y tilt represents the probe standing vertically). The analogue values of the pressure and tilt angle sensors were converted on board by the microcontroller; the temperature sensor was accessed via the inter-integrated communication (I^2C) protocol (connector bus). This protocol also accesses the real-time clock and 64 KB FlashROM, where a back-up of about 2 years of data can be stored.

The radio communications system included conventional helical antennas with a power amplifier to boost the 10 mW output to around 100 mW. A custom packet-based protocol (a basic unit of information carriage) with error detection was devised for communication with the base station.

The probes were powered by lithium thionyl chloride cells chosen for their high capacity-to-volume ratio and good characteristics at low temperatures. This consisted of six half AA sized cells providing 6 A h (ampere-hours).

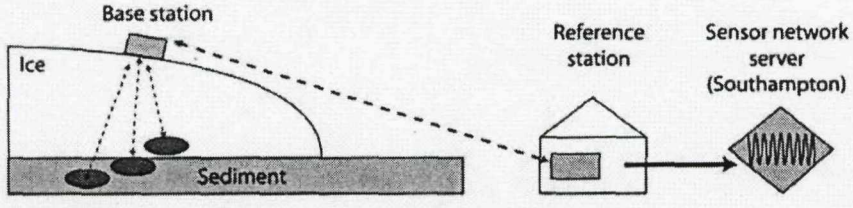


Fig. 2. Overall system diagram.

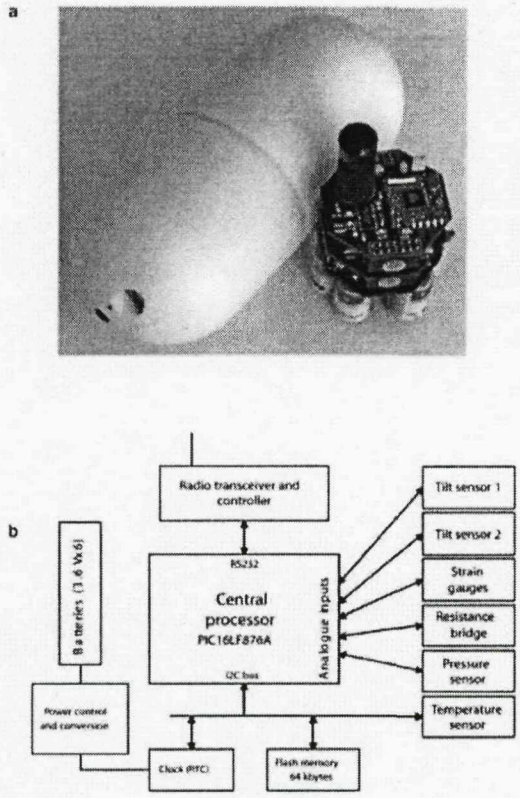


Fig. 3. Probes: (a) photograph of 16 cm long probe (showing the resistivity bolts and pressure sensors at the end); (b) schematic.

The electronics and sensors were enclosed in a polyester cylindrical capsule composed of two halves and sealed with epoxy resin (Fig. 3a). This probe was 16 cm long, with an axial ratio of 2.9 : 1. The probes were tested in a pressurized tank at the National Oceanography Centre, Southampton, up to 100 m of water pressure.

In sleep mode, the probes only consume 9 μA and when powered 4.2 mA (with the transceiver off) at 3.6 V. Battery voltage is also measured each day as a vital diagnostic. Once collected, the data are stored in a ring buffer fashion (64 KB) in the FlashROM until they are accessed. The oldest data are overwritten by the newest only when the entire memory is full. This allows the data to be preserved even if communications fail for many months.

Base station

The base station is responsible for fetching data from the probes, recording local data, a GPS file and weather station data. It also transmits data either via radio down the valley or by mobile-phone text messages. As size is not critically important, it has two large 12 V lead acid batteries with 96 A h capacity in total, as well as a 15 W solar panel and a 60 W wind generator (Rutland 503). A pyramidal tripod was designed to hold the antennas and sensors; this was tethered to the ice with an anchor (15 m down a borehole) and rocks on the base (Fig. 4a). The customized base station comprised

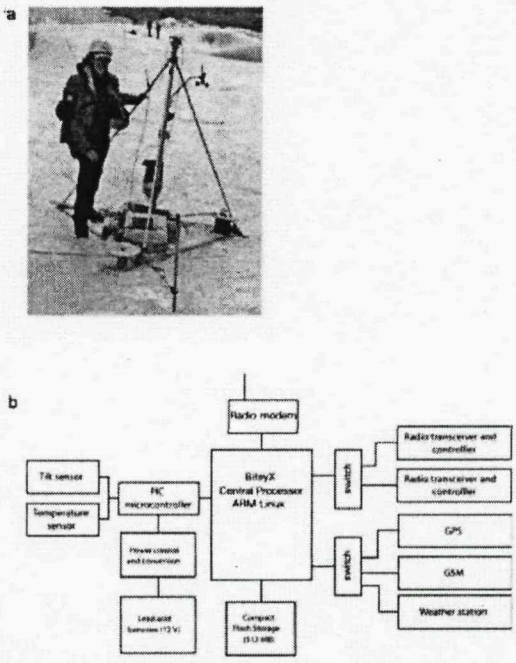


Fig. 4. Base station: (a) photograph; (b) schematic.

a central processing unit (CPU), storage, sensors, radio communications system and power controller (Fig. 4b; Table 2).

The base station is controlled by a StrongARM-based board (BitsyX) running Linux, allowing remote access and standard software to be used. There are a series of peripherals attached to the processor board through a custom interface board. Sensors measure the local conditions of the base station (tilt angle, temperature and battery voltage), and wired tiltmeters and ploughmeters were inserted into the till. These were connected via a PIC. The GPS, weather and GSM systems were connected via serial connections. The storage system is a CompactFlash card.

A 500 mW radio modem provided a 9600 baud (signals per second) link 2.5 km down-valley to the reference station personal computer (PC). Robust communications are essential to prevent radio noise from interfering with system operations and to maintain data integrity. A GSM modem allowed probe data to be sent directly to the UK server via text messages (SMS) if the long-range link was not functioning.

Reference station

The reference station is a mains-powered mini-ITX PC running Linux, located in a building in the valley (Melkevoll Campsite Office, approximately 2.5 km from the glacier). It was connected to the base station via the radio modem, and periodically to the internet via ISDN. It is the position reference point and records a GPS file daily. This PC relays the data from the probes and base station to a data server in Southampton on a daily basis and archives the data on disk as a back-up.

Table 2. Details of the system

	Probes	Base station
Microcontroller/ CPU	PIC16LF876A	StrongARM BitsyX
Storage	64 KB FlashROM	CompactFlash card
Sensors	Tilt angle Strain gauge Pressure sensor Temperature Resistivity	Tilt angle Temperature Tilt angle cells Ploughmeter GPS Weather station
Communication	433 MHz helical antenna	433 MHz helical antenna 468 MHz radio modem GSM phone
Power controller and supply	6 × 0.5 AA lithium thionyl chloride cells	Lead acid batteries 10 W solar panel 60 W wind generator Switch mode regulators
Case	Polyester – push closed	Pelican case

Table 3. Communication sequence

Time	Probe	Base station	Reference station
0000 h	Data log		
0300 h		GPS log	GPS log
0400 h	Data log		
0800 h	Data log		
	Data log		
1200 h	Communications	Communications	Communications
1600 h	Data log		
1900 h			Transfer
2000 h	Data log		

System

The real-time clocks in the base station and probes control the timing of data collection and transmission according to a time schedule (Table 3). At the end of each period, the probe and base station configure their clocks to the next 'wake-up' time before 'sleeping'. Probes only record data from their sensors during data log periods. During the communication period, they enable their radio transceivers for a fixed duration after recording their sensors. The base station powers up during this period and reads its own sensors, broadcasts the system time and requests undelivered sensor readings from the probes. A communication window opens for a short time once the systems are idle and it is possible to log in from the UK. The base station and reference station also 'wake up' during the GPS log period to read GPS data. All the data that have been recorded over the day are transferred to the data server in Southampton during the transfer period.

It became increasingly clear that diagnostic information should be built into the system and data because of the system complexity and the need to understand failures. A daily log file was sent to the UK with extra status information including a log of all probe communications, battery voltage (probe and base station) and base station sensors (tilt angle). This provided valuable information, and problems in the reference station could be solved by remote reprogramming. However, it was necessary to travel to the site in the spring and autumn in order to install replacement parts and upgrades as well as to check the system for weather damage.

SUMMARY OF THE RESULTS

Prior to inserting the probes, the subglacial environment was surveyed by GPR, borehole drilling, till sampling and borehole video in order to find the best locations for probe deployment. Areas with subglacial channels needed to be avoided, and areas with thick till preferentially chosen.

Data from the GPR survey from 2003 and 2004 were used to determine the appropriate depth for the transceiver. The surface zone is characterized by high-amplitude reflectors which suggest high water content at the glacier surface (Fig. 5a). In order to locate the depth of this highly reflective zone, a threshold was determined by manual

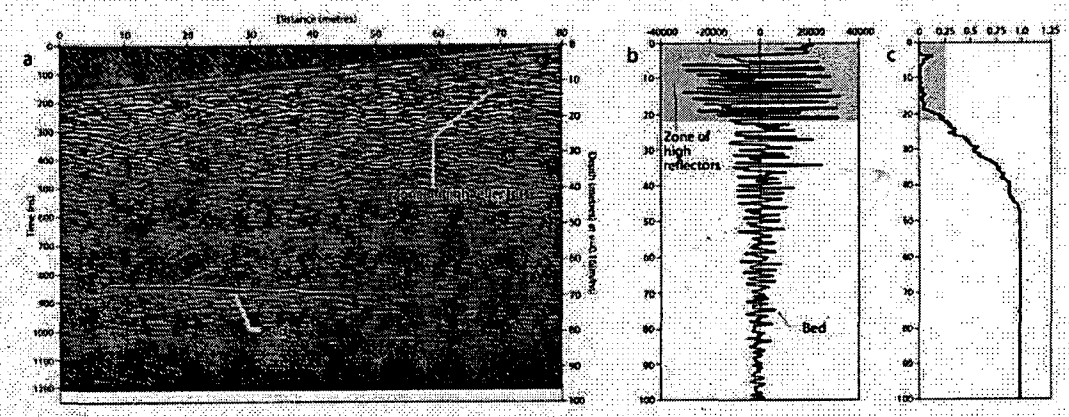


Fig. 5. GPR results: (a) 50 MHz antennae radar transect (these data have been topographically corrected, filtered using a low-frequency cut-off (de-wow), had a spreading and exponential compensation (SEC) gain applied and migrated using the Kirchhoff function). (b) A typical radar trace. (c) Average conditional values to demonstrate the location of the base high-amplitude reflections.

Table 4. Depth of surface high reflectors

Year	Transect	Depth of surface disturbance m
2003	A1	19.6
	A2	19.68
	A3	17.76
	AA	12.0
	AB	2.8
	AC	21.04
2004	B1	13.12
	B2	29.92
	B3	30.24
	B4	30.64
	B5	30.8
	B6	29.29
	B7	8.96
	BA	29.04
	BB	34.64
	BC	31.6
	BD	37.44

inspection and used to detect the boundary using the following method (Fig. 5b):

1. For each individual trace the amplitude was tested to see whether it was above a given threshold; taking A_x as the running 16 ns mean amplitude (as this was the mean length of a cycle) and T_1 as a threshold value of 10^8, $A_x^2 \geq T_1$ was evaluated (0 if true, 1 if false).

2. For each transect, the means of the conditional values were calculated, and the first time they passed a threshold value, this was taken as the depth of the surface radar disturbance if $X \leq T_2$ (where X is the conditional value mean over the transect, $T_2 = 0.25$).

Figure 5c shows X plotted against the radar signal strength to demonstrate how this method can automatically detect the base of the zone of high reflectors.

Table 4 shows that the results from 2003 range from 3 to 21 m with an average of 15 m and in 2004 the zone ranged from 9 to 37 m in depth with an average of 28 m, so the transceivers at 35 m were at sufficient depth to collect radio data from the bed.

Probe insertion

During summer 2004, three probes were inserted into the ice and five into the till (including one resting on a clast). The probe insertion technique depended on the nature of the borehole. After drilling, the boreholes either drained or remained water-filled. In those that remained water-filled, the probes were installed by gently dropping them into the holes and relying on gravity for them to sink to the base. In the boreholes that drained, the probes were lowered on fishing line, which was detached afterwards.

Towards the end of the hot-water drilling, till was 'blasted' away at the base by maintaining the jet at the bottom for a further 15 min. We then lowered the probes into this space, and assumed that the till would subsequently close in around them. Although we attempted to remove till from the base of the borehole with a special attachment to the subglacial sampler, this failed to convincingly remove any more till than the hot-water drilling technique.

In 2004 there were large clasts exposed at the base of some of the boreholes. In this situation, the probes rested on top of these large clasts, and this simulated the imbrication commonly seen in tills. In all cases, the borehole camera was used to check that the probes were placed correctly.

Probe data

The base station functioned from 10 to 15 August, 18 October to 8 November, 23 November–6 December and 18 February to 24 May, and 7 August onwards. A total of 859 days of probe data (36 078 sensor readings) were received. Table 5 shows the details of each probe: 66% of the englacial probes responded (total of 269 days, ranging from 1 to 268 days) and 100% of the subglacial probes communicated (total of 574 days, ranging from 1 to 377 days). There was no correlation between communication distance and survival rate (Table 1). Table 5 also shows how the sensors in the different probes functioned. Case stress failed to function in three of the probes, probably due to damage when sealing the probes.

Figure 6 shows how the success rate (calculated as the percentage of probe days received) declined over the year. Loss was greatest in the autumn, but stabilized during the winter. The reason for probe loss is not known. Probes 2 and 6 failed after the first day, and probes 3–5 failed whilst the base station was not working, so their 'death' was not monitored. Only probes 7 and 8 were monitored during their final days, but since there were no sudden changes in

Table 5. Probe data collected August 2004–August 2005

Probe	Days data sent	Working sensors					Date lost
		Water pressure	Tilt	Temperature	Case stress	Resistivity	
1	0	–	–	–	–	–	–
2	1	✓	✓	✓	✓	✓	7 August 2004
3	9	✓	✓	✓	✓	✓	15 August 2004
4	268	✓	✓	✓	✓	✓	24 May 2005
5	117	✓	✓	✓	✓	✓	6 December 2004
6	1	✓	✓	✓	✓	✓	7 August 2004
7	70	✓	✓	✓	×	✓	20 October 2004
8	377	✓	✓	✓	×	✓	24 August 2005

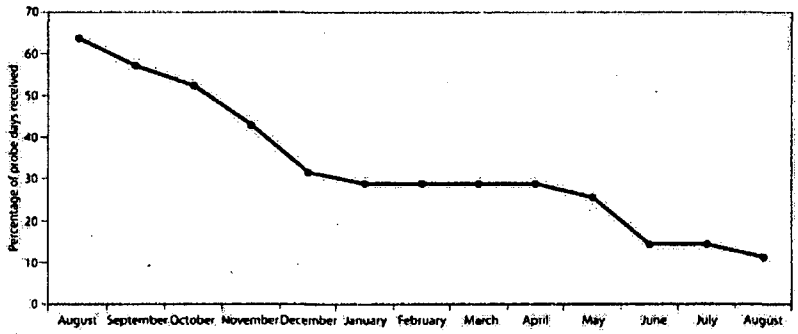


Fig. 6. Success rate (measured as a percentage of probe days per month from the initial eight probes that responded) from August 2004 to August 2005.

any of the readings (nor an increase in data errors), we assume they were removed by subglacial processes (e.g. glacial or fluvial erosion).

In Table 1 an initial communication distance is shown, which is the distance from the transceiver to the probe when it was deployed. However, as the upper part of the glacier moves faster than the base, the communication distance increases over time. Glacier surface velocity at the site was measured to be approximately 20 m a^{-1} between August 2004 and August 2005. It is assumed that the transceiver (which was positioned at 50% of the ice depth) moved 72% of the englacial ice movement (Harper and others, 1998) and that the till moved 25–85% of the surface ice movement (Boulton and others, 2001). This could increase the potential communication distance by approximately 1–4 m in 1 year. The maximum transmission distance for each probe that worked longer than 10 days was calculated, taking into consideration the geometry of the probes relative to the transceiver, the length of survival and the relative movement in ice and till described above. The results are shown in Table 1 and it could be seen that the maximum communication distance attained over the 2004/05 period was 36.26 m.

Results from probes in the ice and till

Figure 7 shows the resistivity and *x* tilt angle data from the two probes with the longest records. Although the *x* and *y* directions are relative, an estimate of their position can be determined by reference to the borehole video taken after deployment. Probe 4 was inserted into a borehole that did not reach the bed, so the results must reflect an ice probe. Probe 8 was deployed in a till-based borehole, and video images show it resting on the till surface. Table 6 summarizes the mean and standard deviation (SD) of the data from the englacial (probe 4) and subglacial (probe 8) probes over the same time period (August 2004–May 2005).

There are distinct differences between the englacial and the subglacial probes, in both their overall values and seasonal pattern. The resistivity of the ice probe (probe 4) was generally low, until March when it rose to a maximum level, at the same time as the *x* tilt angle became constant (after fluctuating for the previous 7 months) and the temperature remained at a constant low value (0.03°C, SD = 0.03). We suggest this reflects the ice probe becoming frozen into the ice in March after spending the winter in an englacial water-filled cavity (which explains the overall high temperatures, low water pressures and variable tilt angles).

In contrast, the resistivity of the subglacial probe (probe 8) was generally high, apart from oscillations in the autumn and a low-resistivity event in April. We suggest that in autumn the boreholes are still open to the atmosphere and the resistivity responds to precipitation events, the generally high resistivity during the winter reflects the probe's contact with dry and/or moist till, and the April event reflects water in the subglacial environment supplied from the 'spring event' (Iken and others, 1983). The temperature was constantly low (but higher than the ice probe once it was frozen in) and the tilt angles in the subglacial probe had low variability, but slowly increased throughout the year (January–August) reflecting increasing ice velocity. We suggest that the subglacial probe became incorporated into the till on the basis of resistivity, temperature and tilt angle readings although the depth of incorporation is not known.

CONCLUSIONS AND FUTURE RESEARCH

Designing a sensor network for glaciers was a challenging task because of the problems in predicting the behaviour of radio systems and power sources and because of difficulties in building electronic devices that are sufficiently strong and waterproofed to survive such a hostile environment.

The probes transmitted their data from 1–366 days over at least 36 m through ice and till, and provided data on temperature, water pressure, case stress, resistivity and tilt angle. Weather, GPS, other glaciological data and diagnostic data were also collected.

The next steps for the research are:

1. To increase reliability of the probes – future probes will be designed to operate at 173 MHz and have an improved sealing technique.
2. To design a probe location system.
3. To develop 'smarter' probes, which are networked together to allow inter-probe communication and modify their own data sampling strategies.
4. To design the system to be more 'user-friendly' for glaciologists to install and operate.

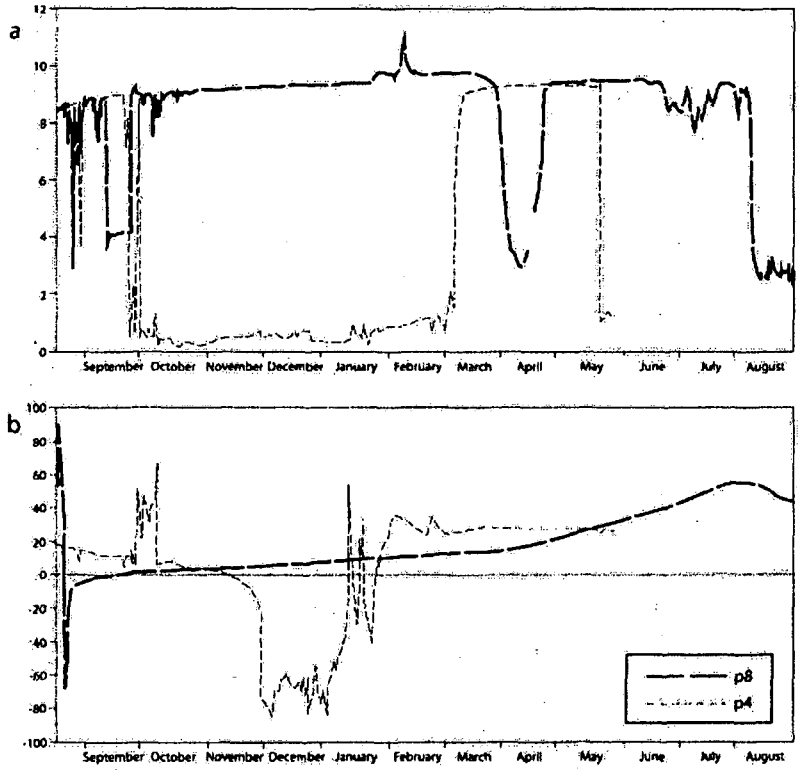


Fig. 7. Probe data from August 2004 to August 2005 from probes 4 (in the ice; short dashes) and 8 (in the till; long dashes): (a) resistivity; (b) x tilt angle.

The use of 'smart' devices to monitor the environment is a logical next step in Earth system science. The glacial environment is a particularly difficult one in which to make such a system function because of the logistical problems associated with ice, water, sediment and the hazards of a continually changing glacier surface (crevassing, etc.), all situated in a remote location. However, if such a system can be made to work in glaciers then the technology may be transferable to other remote and hostile locations. We have reported on the design and success of the GlacsWeb system which will be an important tool in the monitoring and understanding of subglacial processes and glacier dynamics.

Table 6. Summary of mean sensor values in the ice and till (August 2004–May 2005)

	Ice (probe 4)		Till (probe 8)	
	Mean	SD	Mean	SD
Temperature (°C)	0.8	0.80	0.15	0.03
Water pressure (m)	9.64	19.83	24.88	31.67
Resistivity (MΩ)	3.84	4.09	8.69	1.68
Tilt angle (x) (°)	4.33	33.95	9.63	11.72
Tilt angle (y) (°)	−39.3	29.82	−16.42	6.28

ACKNOWLEDGEMENTS

We thank Intelisys, BTExact and Topcon for support and the UK Natural Environment Research Council (NERC) Geophysical Equipment Pool for hire of the GPR and training and advice. We also thank I. and G. Melkevoll for help with logistics, and S. Way, D. Robertson, D. Miles, H. Brown, S. Ward and K. Dowsett for field support. Thanks also to T. Aspen and his colleagues in the Cartographic Unit, School of Geography, University of Southampton. This research is funded by the Royal Society Paul Instrument Fund, the Royal Society, the UK Department of Trade and Industry (DTI) NextWave programme and the UK Engineering and Physical Sciences Research Council.

REFERENCES

Alley, R.B., D.D. Blankenship, C.R. Bentley and S.T. Rooney. 1986. Deformation of till beneath Ice Stream B, West Antarctica. *Nature*, **322**(6074), 57–59.

Blake, E., G.K.C. Clarke and M.C. Gérin. 1992. Tools for examining subglacial bed deformation. *J. Glaciol.*, **38**(130), 388–396.

Blake, E.W., U.H. Fischer and G.K.C. Clarke. 1994. Direct measurement of sliding at the glacier bed. *J. Glaciol.*, **40**(136), 595–599.

Boulton, G.S. and A.S. Jones. 1979. Stability of temperate ice caps and ice sheets resting on beds of deformable sediment. *J. Glaciol.*, **24**(90), 29–43.

Boulton, G.S., K.E. Dobbie and S. Zatsepin. 2001. Sediment deformation beneath glaciers and its coupling to the subglacial hydraulic system. *Quat. Int.*, **86**(1), 3–28.

Budd, W.F., D. Jenssen and U. Radock. 1970. Calculated dielectric absorptions for Antarctica and Greenland. *In* Gudmandsen, P., *ed. Proc. Int. Meeting on Glaciology.* Lyngby, Technical University of Denmark, 71–80.

Dowdeswell, J.A. and S. Evans. 2004. Investigations of the form and flow of ice sheets and glaciers using radio-echo sounding. *Rep. Prog. Phys.*, **67**, 1821–1861.

Evans, S. and B.M.E. Smith. 1969. A radio echo equipment for depth sounding in polar ice sheets. *J. Phys. E*, **2**(2), 131–136.

Fischer, U.H. and G.K.C. Clarke. 1994. Ploughing of subglacial sediment. *J. Glaciol.*, **40**(134), 97–106.

Fischer, U.H. and G.K.C. Clarke. 2001. Review of subglacial hydro-mechanical coupling: Trapridge Glacier, Yukon Territory, Canada. *Quat. Int.*, **86**, 29–43.

Glen, J.W. and J.G. Paren. 1975. The electrical properties of snow and ice. *J. Glaciol.*, **15**(73), 15–38.

Glen, J.W., J.J. Donner and R.G. West. 1957. On the mechanism by which stones in till become oriented. *Am. J. Sci.*, **255**(3), 194–205.

Harper, J.T., N.F. Humphrey and W.T. Pfeffer. 1998. Three-dimensional deformation measured in an Alaskan glacier. *Science*, **281**(5381), 1340–1342.

Harrison, W.D., M. Truffer, K.A. Echelmeyer, D.A. Pomraning, K.A. Abnett and R.H. Ruhkick. 2004. Probing the till beneath Black Rapids Glacier, Alaska. *J. Glaciol.*, **50**(171), 608–614.

Hart, J.K. 2006. An investigation of subglacial processes at the microscale from Briksdalsbreen, Norway. *Sedimentology*, **51**, 125–146.

Hart, J.K. and J. Rose. 2001. Approaches to the study of glacier bed deformation. *Quat. Int.*, **86**(1), 45–58.

Iken, A., H. Röthlisberger, A. Flotron and W. Haeberli. 1983. The uplift of Unteraargletscher at the beginning of the melt season – a consequence of water storage at the bed? *J. Glaciol.*, **29**(101), 28–47.

Iverson, N.R., B. Hanson, R.LeB. Hooke and P. Jansson. 1995. Flow mechanism of glaciers on soft beds. *Science*, **267**(5194), 80–81.

Jeffery, G.B. 1922. The motion of ellipsoidal particles immersed in a viscous fluid. *Proc. R. Soc. London, Ser. A*, **102**(715), 161–179.

Martinez, K., J.K. Hart and R. Ong. 2004. Environmental sensor networks. *IEEE Computer*, **37**(8), 50–56.

Murray, T. 1997. Assessing the paradigm shift: deformable glacier beds. *Quat. Sci. Rev.*, **16**(9), 995–1016.

MS received 18 May 2004 and accepted in revised form 6 April 2006

APPENDIX B

Available online at www.sciencedirect.com
ScienceDirect
Sedimentary Geology 203 (2008) 87–97
Sedimentary Geology
www.elsevier.com/locate/sedgeo

Subglacial comminution in the deforming bed: Inferences from SEM analysis

Kathryn C. Rose, Jane K. Hart *

School of Geography, University of Southampton, Highfield, Southampton, SO17 1BJ, UK

Received 11 May 2007; received in revised form 4 October 2007; accepted 13 November 2007

Abstract

This study investigates the variations in erosional processes beneath Briksdalsbreen; a Norwegian valley glacier, with a thin coarse grained deforming bed. The subglacial zone was investigated *in situ*, close to the central glacial flow line (Site A) and close to the valley wall (Site B), via boreholes. The till was collected using two different sediment samplers and the bed was examined using a borehole video camera. In order to evaluate how representative borehole sampling was of the subglacial environment, the results from *in situ* subglacial samples were compared with random samples taken from an exposed subglacial surface in the glacier foreland, as well as a sample taken from the site after glacier retreat. The results indicated that the texture of the exposed subglacial surface was similar to *in situ* samples from subglacial Site B (close to the valley wall), and that the samples collected with the 'small' sediment sampler had the closest fit. SEM analysis revealed eroded quartz grains at both sites as a result of rotation (abrasion) and fracture. The samples from close to the valley wall were very poorly sorted, with evidence for rounding and preservation of pre-weathered surfaces, which suggest that a relatively simple pattern of erosion from crushing to rotation dominated. However, the till from the centre of the glacier was better sorted, more angular, and with few pre-weathered surfaces. We suggest that this results from a more complex glacial erosional history associated with greater strain and longer residence time within the deforming layer. When compared with other deformation tills, it was confirmed that there is a relationship between grain size and erosional style. Clay-rich tills show little comminution, fine sand-rich tills generate a significant silt component, whilst the coarse sand-rich tills at Briksdalsbreen showed complex deformational styles but no significant silt component.
© 2007 Elsevier B.V. All rights reserved.

Keywords: Till sedimentology; Borehole studies; SEM; Subglacial erosion

1. Introduction

The subglacial environment is an area that has continued to challenge glaciologists for decades, not least due to the inaccessibility of this zone. Since the late 1980s the identification of a saturated layer of sediment, typically weaker than glacier ice, which can deform and contribute to glacial movement (Boulton and Hindmarsh, 1987) has prompted widespread investigations into the sedimentology of till within the subglacial environment.

It is important that the physical properties and characteristics of till are examined so that we can determine how till deforms and responds to changing conditions within a subglacial environment. The numerous variables associated with both, conditions at the glacier bed, and the mechanical properties of a granular material, such as till, make this difficult to achieve. However, initial studies of till rheology (e.g. Alley et al., 1986; Clarke, 1987; Kamb, 1991) would suggest that the mechanisms of deformation in many ways relate to till sedimentology (e.g. through void ratio, porosity, frictional strength, relative proportions of sand to fine-grained material). New ways of approaching the analysis of till sedimentology have highlighted several areas of uncertainty within this field, particularly in relation to the erosional history and capabilities of grains within the deforming bed, and how this may affect the deformation process. Processes of erosion may be equally as important to till deformation as more documented processes, such as dilation and overconsolidation.

* Corresponding author. Tel.: +44 2380 594615; fax: +44 2380 593295.
E-mail address: jhart@soton.ac.uk (J.K. Hart).

0037-0738/$ - see front matter © 2007 Elsevier B.V. All rights reserved.
doi:10.1016/j.sedgeo.2007.11.003

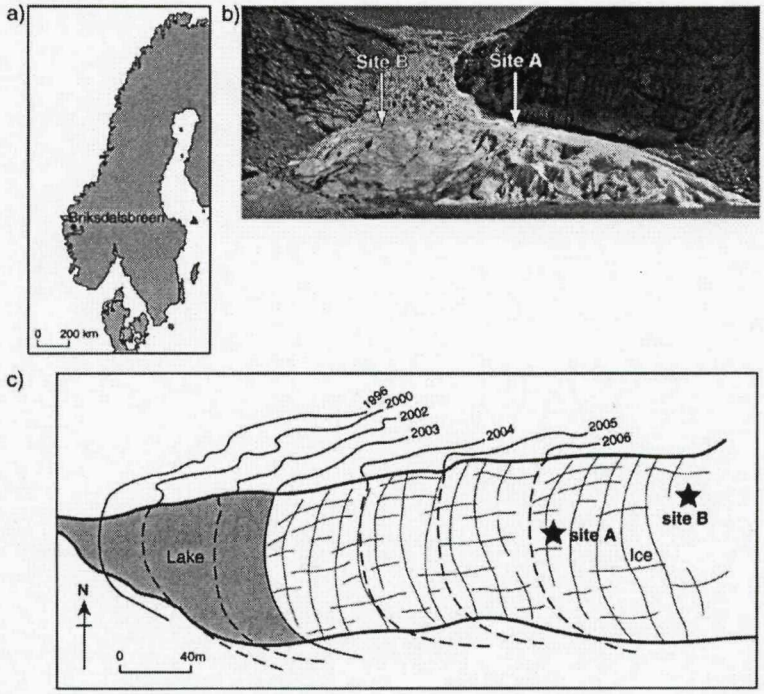


Fig. 1. a) Location of Briksdalsbreen; b) Photograph of the glacier in 2003 with the two subglacial sites shown; c) Map of Briksdalsbreen (2003) with the site locations and annual glacier limits shown (note Site A, sampled 2003 and Site B, sampled 2004).

Although the majority of glacial erosional studies have been carried out in rigid bedrock environments, there have been a number of studies investigating till erosion associated with deformable beds. Gjessing (1965) and Hart (2006a) have investigated the sedimentology of this process, while Cuffey and Alley (1996) and Hindmarsh (1996) have carried out modelling studies.

Elson (1988) suggested that deformation tills lack evidence of comminution, and Tulaczyk et al. (1998) found a scarcity of features indicative of comminution in the fine-grained tills beneath Ice Stream B. However, other studies have demonstrated both at the field scale, from the study of stoss-and-lee clasts (mini roche moutonnées) (Benn and Evans, 1996; Hart, 2006a), and at the microscale, from micromorphology and SEM studies (Boulton et al., 1974; Hooke and Iverson, 1995; Iverson et al., 1996; van der Meer et al., 2003; Hart, 2006b) that till erosion does occur. Erosion can operate within the till, at the till/ice interface, and at the base of the deforming layer.

Numerous researchers (Dreimanis and Vagners, 1971; Haldersen, 1981, 1983; Sharp and Gomez, 1986) have argued that crushing, associated with glacial erosion, allows till to reach a terminal grade. This process has also been observed in association with deformable beds, at Breiðamerkurjökull. Boulton et al. (1974) concluded that *in situ* grain crushing had occurred because of the decrease in grain size that they found between the debris rich basal ice layer and the upper layer of the deformation till. In agreement with this, Iverson et al. (1996) showed from experimental shearing on coarse grained mudstone particles (2.0–3.3 mm), that as deformation increased, first sand and then silt-sized grains were produced.

Tulaczyk et al. (1998) have argued that comminution is dependent on the geological setting and that the glacial erosion of strong brittle rocks is very different from that of weak sediments. Our study uses a scanning electron microscope (SEM) to investigate *in situ* till erosion from a deforming bed glacier resting on gneiss bedrock, as a contrast to the *in situ* study of till from beneath Ice Stream B. Since it has

been suggested that grain size is a key factor in determining subglacial processes, a study was carried out to determine the effectiveness of the *in situ* sampling method. Once the sampling method was proved satisfactory, SEM analysis was used to determine the erosional history of grains within the deforming bed from two sites, one towards the central flow line (Site A) and the other towards the side wall of the glacier (Site B).

2. Study site and methodology

This study was performed at Briksdalsbreen, a temperate valley glacier calving into a proglacial lake, located in southern Norway (Fig. 1a and b). Between 1986 and 1996 Briksdalsbreen advanced 400 m. This has been attributed to increased precipitation due to a positive phase of the North Atlantic Oscillation (NAO) (Nesje et al., 2000). Subsequently, the glacier has retreated approximately 500 m between 1997 and 2007, in association with a negative phase of the NAO, combined with 'global warming'.

The recent retreat of the ice has resulted in the formation of annual push moraines and the exposure of a fluted subglacial surface. A detailed examination of the flutes at Briksdalsbreen is explored by Hart (2006b). The glacier and proglacial area (Fig. 1c) was mapped in detail with a TOPCOM dGPS and the subglacial environment was studied via boreholes in two areas during the summers of 2003 (Site A) and 2004 (Site B). These areas were chosen because they were relatively flat and crevasse free.

In situ subglacial experiments using a wireless multi-sensor probe (Hart et al., 2006) and a study of the proglacial and subglacial sedimentology (Hart, 2006b), have indicated the presence of a thin deforming layer beneath Briksdalsbreen. The deforming layer is associated with clast rotation, which provides the background for this present study.

2.1. *In situ subglacial sampling*

A Kärcher HDS1000DE hot water drill was used to drill a series of holes to the ice base (Table 1). Eleven holes were drilled to the bed in 2003 at Site A, where the ice thickness ranged from 55 m to 75 m. An additional 15 holes were drilled to the glacier bed in 2004 at Site B, with depths ranging between 60.5 m and 85 m.

A custom-made CCD borehole video camera was used to view the glacier bed. At Site A till was observed in 8 of the 11 boreholes (73%; Table 1). At Site B the camera showed till in only 9 out of 15 boreholes (60%; Table 1), and of these 9, 2 had a boulder at the base (Table 1).

Table 1
Borehole details

	No. of boreholes (to bed)	Average depth and range (m)	% till	% of till sites showing a boulder
Site A	11	69 (55–75)	73	0
Site B	15	69 (60.5–85)	60	22

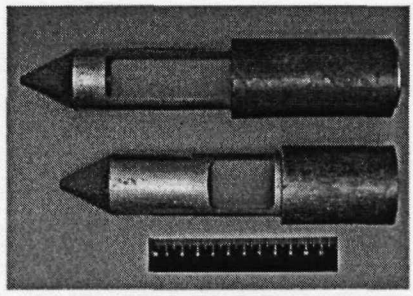


Fig. 2. *In situ* subglacial till samplers (large sampler shown at top, small sampler shown at the bottom).

The till was collected with a subglacial sediment sampler attached to a subglacial percussion hammer (Blake et al., 1992). The sampler comprises a chamber with a moveable sheath (Fig. 2). When hammered into the subglacial sediment this sheath is forced upwards exposing a window to the hollow interior of the chamber, into which the sediment is forced. Two sizes of sampler were used; a 'large' sampler with a sediment collection volume of 106.8 cm^3 and a window size of 22.8 cm^2, and a 'small' sampler with a sediment collection volume of 125.7 cm^3 and a window size of 12.0 cm^2. All 7 samples were retrieved from Site A using the large sampler, while only 4 samples were successfully extracted from Site B, one with the large sampler (Br1/04), and three with the small sampler (Br2/04, Br3/04 and Br4/04).

This method of collecting subglacial samples *in situ* is problematic, as sampling is almost impossible if boulders are present on the till surface. In some holes till could not be extracted even though it was observed on the borehole video. In addition, the size of the chamber means that there is a tendency for only fine-grained samples to be extracted, as boulders cannot fit through the window of the chamber. It is also likely that some of the finest fraction is removed as water drains out of the chamber during retrieval.

Table 2
Details of the *in situ* subglacial till samples

Site A (2003)				Site B (2003)			
Sample	Amount of till collected (g)	Mean grain size (μm)	Sorting	Sample	Amount of till collected (g)	Mean grain size (μm)	Sorting
Br1/03	7.00	192	1.87	Br1/04	41.32	342	6.50
Br2/03	16.04	514	2.74	Br2/04	55.72	3828	3.90
Br3/03	9.88	790	4.80	Br3/04	21.01	3321	2.50
Br4/03	23.48	160	2.03	Br4/04	9.63	1225	5.30
Br5/03	10.69	131	3.11				
Br6/03	11.75	204	2.54				
Mean	13.14	332	2.86	Mean	31.92	2179	4.58
SD	5.86	264	1.02	SD	20.58	1664	1.71

The grain size composition of these samples was determined through a combination of dry sieving and laser granulometry, and then examined using the GRADISTATv5 programme (Blott and Pye, 2001, 2006). Mean grain sizes were calculated using the Folk and Ward (1957) method. These are shown in Table 2 and Fig. 3.

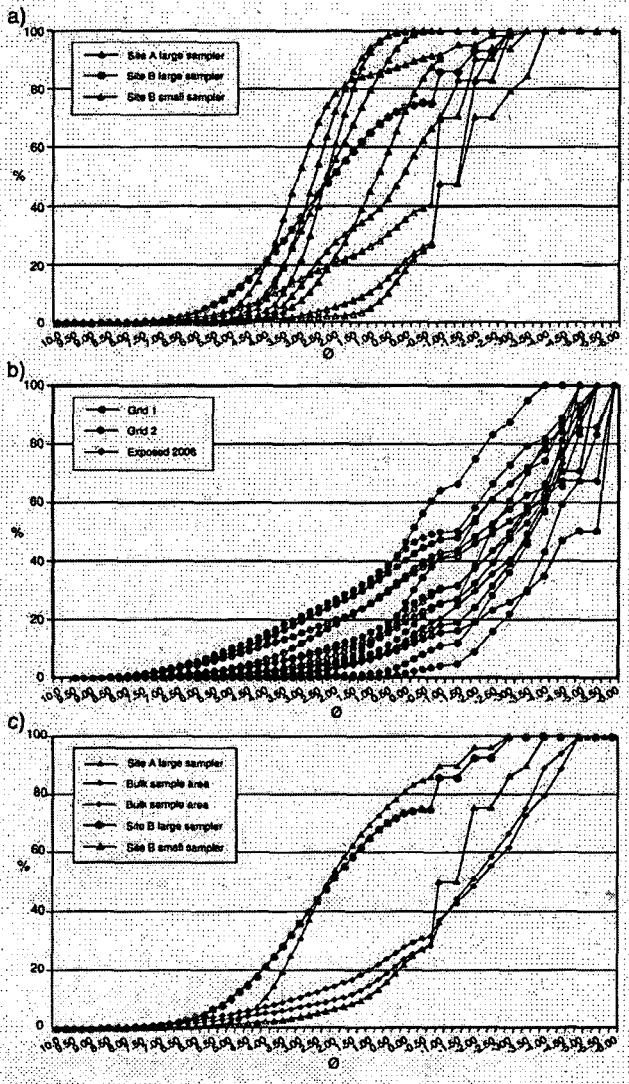


Fig. 3. Grain size cumulative frequency: a) *in situ* subglacial till samples, b) bulk till samples from the exposed subglacial surface; c) summary of *in situ* and bulk till samples.

Table 3
Details of the exposed subglacial surface areas

Area 1 (2004)			Area 2 (2004)		
Sample	Texture	Mean grain size (μm)	Sample	Texture	Mean grain size (μm)
1	Coarse till	1049	1	Boulder	–
2	Boulder	–	2	Boulder	–
3	Coarse till	1881	3	Coarse till	2740
4	Till	1026	4	Coarse	2813
5	Till	1238	5	Till	883
6	Till	1960	6	Till	1817
7	Till	1422	7	Till	1954
8	Boulder	–	8	Till (flute)	610
9	Coarse till	2077	9	Till	1304
Mean	–	1522	Mean	–	1731
SD	–	445	SD	–	856

2.2. Bulk sampling from the exposed subglacial surface

In order the test how representative the sampling method for the *in situ* subglacial samples were, studies were made on the exposed subglacial surface. Two 10 m × 10 m areas were chosen at random, to represent the variety of basal conditions that would be encountered if the area were overlain with ice and accessed by hot water drilling. Each area was divided into 9 sample points, 5 m apart.

The texture of the material at each sample point was noted as either 'till', 'coarse till' (contained clasts which were too coarse to be collected by the subglacial sampler) or 'boulder'. Samples (~200 g each) were obtained from all grid points except those that were just 'boulders'. The grain size of each sample was analysed as outlined above and the results are shown in Table 3 and Fig. 3.

By November 2006, the glacier had retreated so much that the subglacial surface at Site B had become exposed. As a result, a bulk sample was taken from this area, and the grain size was analysed (Fig. 3). The mean grain size was 7436 μm with a sorting value of 4.07.

2.3. Scanning electron microscope methodology

The subglacial samples collected *in situ* from beneath the glacier were analysed with a LEO1450VP scanning electron microscope. Samples from each of the boreholes were mounted on stubs and coated with gold. They were analysed with X-ray elemental mapping (at ×100 or ×150 scale) to measure the intensity levels of silicon and aluminium. This technique means that quartz grains can be easily identified through their signal of elements. Other element signals, for example a high Al or K signal which might reflect a feldspar grain, were removed. Eliminating these other signals ensures that only the quartz grains are chosen for analysis. An IMIX Image processing package was used on a UNIX Workstation to analyse each pixel of the image to isolate the quartz grains. These grains were then examined at a higher magnification by a number of techniques described below.

The surface textures of the grains were analysed based on the techniques proposed by Mahaney et al. (1996). This involves selecting 25 quartz grains per sample and identifying the various different textures (morphological and mechanical) of each grain, according to a standardised table of features (Fig. 4 and Table 4). The features listed in Table 4 are in accord (both in number and type) with standard lists of surface features noted from numerous examples within the literature (e.g. Mahaney et al., 1996; Helland and Holmes, 1997; Strand et al., 2003). Example features photographed within the literature (e.g. Krinsley and Donahue, 1968; Krinsley and Doornkamp, 1973; Mahaney and Kalm, 1995) enable comparisons between data sets to ensure standardisation of analysis and prevent subjective interpretation.

In addition, the *a*-axis of the grains was measured, the overall shape of each grain noted (ellipse, triangle, diamond, rectangle, pentagonal or irregular) and the 'erosional form' recorded (Hart, 2006b; Fig. 5). The latter technique categorises the grains into one of six classes; smoothed and rounded forms (Fig. 5b); irregular jagged forms (Fig. 5c); conchoidal forms (Fig. 5e); 'hand axe' forms with one rounded end and one sharp, angular end (Fig. 5f); and two grain forms that are both rounded and conchoidal. These latter two are distinguished by the topography of the grain surface. 'Low relief impacts' comprise small irregularities on a relatively planar surface (Fig. 5a), whilst 'medium relief impacts' comprise larger irregularities and few planar surfaces (Fig. 5d).

3. Results

We will first discuss the results of the textural analysis and evaluate the sampling method, before reviewing the SEM results.

The exposed subglacial surface grid test (Table 3) found that 'boulders' were the dominant texture in 11–22% of the samples. 33% of the samples (at both sites) comprised 'coarse till', but the majority (44–55%) of the samples were till. These findings give an indication of till texture that corresponds with the grain size distribution results obtained for samples collected from subglacial Site B (Fig. 3; Table 2). In this area, 22% of the boreholes intercepted a boulder, and till was recovered from 26% of the boreholes. In contrast, at Site A, no boulders were intercepted but till was extracted from 55% of the boreholes. However, our ability to extract till may be as much a result of the sampling technique, as it was of the subglacial conditions (note the limitations mentioned in Section 2.1).

The average cumulative frequencies of grain size distribution for the samples are compared in Fig. 3. Results from the *in situ* sampling (Fig. 3a) show that, although there is a wide distribution of grain sizes collected from the subglacial samplers, in general, the large sampler collects a greater proportion of the fine sand and silt fraction. This is also illustrated by the average grain size shown in Table 2. However, the till from Site B, irrespective of the size of the sampler, is more poorly sorted than Site A. In contrast, the bulk sampling of the exposed subglacial surface (from 2004 and 2006) shows less grain size variation (Fig. 3b). These results are summarised and compared in Fig. 3c. The samples from the subglacial surface test sites have very similar cumulative frequency curves to the *in situ* small sampler from

Site B. The main differences include more medium sand and less very fine sand and silt in the small sampler.

The strong similarity in grain size distribution between the exposed subglacial surface samples and those collected from the *in situ* subglacial environment with the small sediment sampler suggests that, compared with the large sampler, the small sampler collects samples that are more representative of the less than 0φ fraction of till. Although there is some preferential removal of fines during sample retrieval, this has a minimal effect.

3.1. Erosional form

The SEM results showed that samples from both sites are dominated by small conchoidal fractures. However, the grains from Site B are more rounded, and with a lower relief, than those from Site A. Samples from both sites also show low relief, jointed surfaces (Fig. 5a), though this feature is more common from Site B (where it is preferentially found on the larger and more rounded grains; see Table 4). In addition, more grains have *in situ* jointed blocks at Site B. A study of the overall shape of the grains shows that the diamond form is most common at Site A and the ellipse form at Site B (Table 4). It can be seen from Fig. 6 that the samples from Site A have a mostly conchoidal or intermediate erosional form, while those from Site B have an intermediate or smoothed and rounded erosional form. Although it is shown above that the nature of the sampler had an effect on the grain size collected, the average *a*-axis length of the grains investigated in the study (irrespective of the sampler size) was greater at Site B.

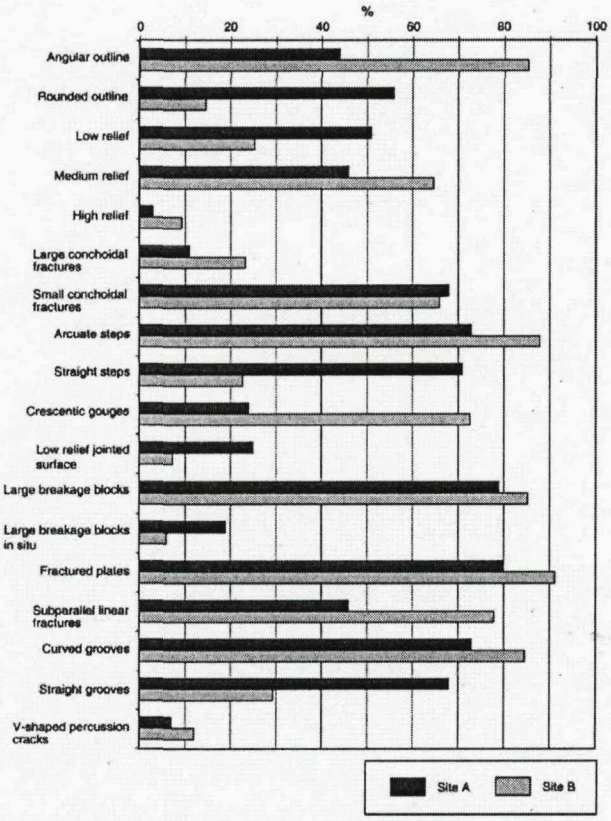


Fig. 4. Surface textures from the scanning electron microscope (SEM), adapted from Mahaney et al. (1996).

Table 4
Details of the SEM results

Sample	Average *a*-axis (μm)	% with angular outline	% low relief	% small conchoidal fracture	% with low relief jointed surface (μm)	Average *a*-axis with low relief jointed surface	Most frequent shape	Erosional Form
Br1/03	216	80	24	28	24	223	Triangle	Smoothed and rounded
Br2/03	263	88	12	76	0	–	Diamond	Intermediate
Br3/03	207	84	20	64	8	219	Diamond	Conchoidal
Br4/03	287	80	16	80	0	–	Diamond	Conchoidal
Br5/03	197	88	40	80	8	125	Rectangle	Conchoidal
Br6/03	140	92	40	68	2	125	Diamond	Intermediate
Average 2003	218	85	25	66	7	175	Diamond	Intermediate
Br1/04	335	40	44	72	16	682	Ellipse	Intermediate
Br2/04	323	48	52	76	12	846	Ellipse	Intermediate
Br3/04	618	44	52	52	36	683	Diamond	Smoothed and rounded
Br4/04	463	44	56	72	36	652	Ellipse	Intermediate
Average 2004	401	44	51	68	25	715	Ellipse	Intermediate

Features typical of subglacial erosion are common in all samples, including arcuate steps, crescentic gouges, large breakage blocks, fractures plates and subparallel linear fractures (Margolis and Kennet, 1971; Krinsley and Doornkamp, 1973; Krinsley, 1980; Mahaney et al., 1996). The low relief recorded by grains at both sample sites can be characteristic of glacial environments and crystalline source rocks (Higgs, 1979). In addition, Mahaney (1990), Mahaney et al. (1996) and Mahaney and Kalm (2000) have suggested that pre-weathered surfaces can be identified using SEM. We suggest that this is reflected by our observation of low relief jointed surfaces, which are similar to the dimpled surfaces highlighted by Mahaney and Kalm (1995, 2000).

4. Discussion

As stated above, previous *in situ* and sedimentological studies at Briksdalsbreen (Hart, 2006b) suggest that the subglacial till undergoes deformation. It has been argued that

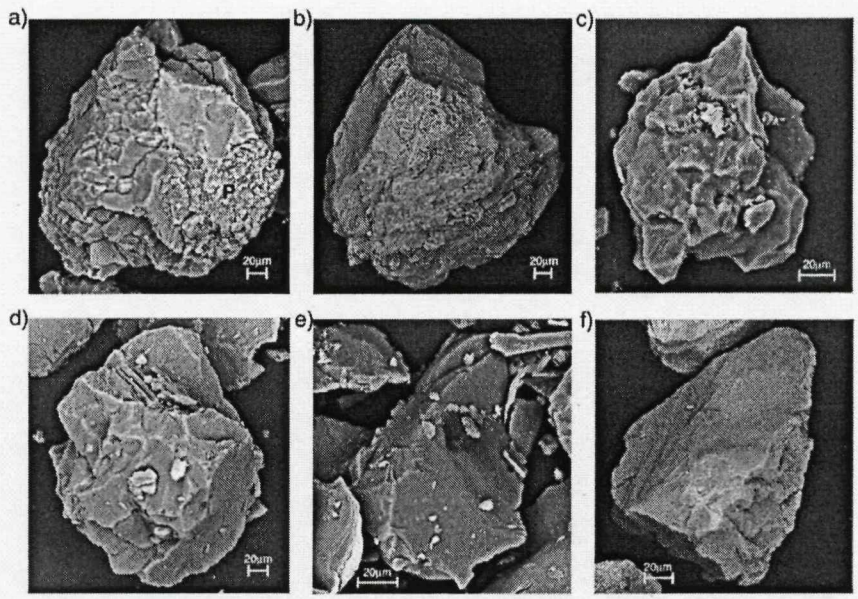


Fig. 5. Photographs of grain surface textures: a) grain showing low relief impacts that with a pre-weathered surface (p) preserved; b) grain showing smoothing and rounding; c) grain showing a jagged form with initial conchoidal fracture and subsequent abrasion of the edges; d) grain with medium relief impacts; e) grain showing a conchoidal form; f) grain showing a 'hand axe' form.

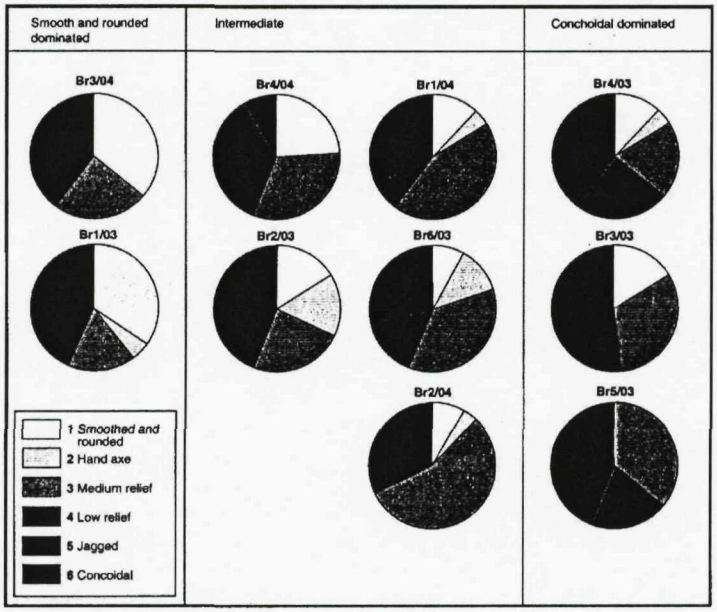


Fig. 6. Pie diagrams showing the relative occurrence of the different erosional forms from each sample.

subglacial deformation is the result of simple shear (Hart and Boulton, 1991), which produces rotation and attenuation. Numerous researchers have demonstrated these processes on the thin section scale (van der Meer, 1997; Khatwa and Tulaczyk, 2001; Roberts and Hart, 2005).

Hooke and Iverson (1995), based on the work of Drescher and de Josselin de Jong (1972), suggested that shearing grains will form alignments of clasts called bridges (Mandl et al., 1977), which fail by fracture, sliding, or rolling of grains. These features have rarely been observed in till thin section studies (Khatwa and Tulaczyk, 2001). Khatwa et al. (1999) and Fischer and Hubbard (1999) questioned grain bridges as a diagnostic property of deforming till. However, Iverson et al. (1996) acknowledge that in reality the bridges combine with others to form complex geometrical networks. Hart et al. (2006) suggest that till within the deforming layer represents a multi-layered patchwork of different grain sizes, competence and pore-water pressures. Although overall deformation is by simple shear, this may result in grain bridges, zones of rotation, and brittle shears in localised areas due to the heterogeneity of the till.

Iverson et al. (1996) demonstrated from laboratory experiments that at low shear strains the particle distribution was self-similar. However, after further deformation the ratio of fine to coarse particles increased to produce a poorly sorted material, with large grains separated from each other by a finer matrix. They argued that increased shearing leads to sliding (abrasion) rather than crushing (fracture) (Fig. 7a).

Hart (2006b) argues that this process is more complex, as grains have many pathways into the deforming layer (e.g. from bedrock, ice, till advection), and undergo different styles of deformation (rotation and clast interaction) within the till (Fig. 7b). Grains will either be dominated by rotation to yield a smoothed and rounded form, or fracture to yield a conchoidal form. However, most grades are dominated by both processes to yield a complex form, as illustrated in Fig. 5. A grain entering the subglacial environment (with some preserved pre-weathered surfaces may suffer initial (low relief) erosional impacts (Fig. 5a), before undergoing abrasion (Fig. 5b), or fracture following by abrasion (Fig. 5c). The grain in Fig. 5d has a medium relief associated with both abrasion and fracture, after continued fracture this may develop a conchoidal form (Fig. 5e), and then after rotation develop a hand axe form (Fig. 5f). So, although the overall erosional history of most grains will be complex, generally, continued fracture will act to increase the relief of the grains, whilst continued abrasion through rotation will smooth the grains, decreasing relief.

On average, the sediments from Site A are very angular (general diamond shape), with ~50% of the samples being dominated by conchoidal fracture (Fig. 6). Preservation of these features can be indicative of short transportation distances (Higgs,

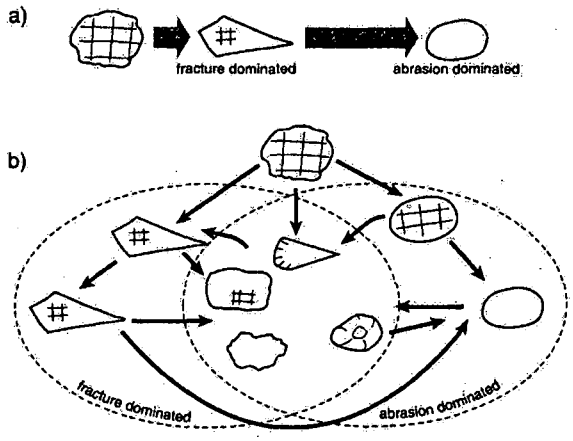


Fig. 7. Erosional continuum: a) after Iverson et al. (1996); b) after Hart (2006b).

1979), which is feasible given the sample location. Few grains have any original surface preserved, and none were observed to have any *in situ* jointed blocks. The lack of preserved faces indicates a prolonged residence time within the deforming bed as all pre-weathered surfaces have been removed through erosion. The dominance of diamond forms, and the angular and fractured nature of the surface textures, reflects the process of cleaving from the bedrock (Higgs, 1979) and a dominance of impact (percussion) based erosion processes. The angular nature of grains, conchoidal fractures, and jointed surfaces are generally indicative of a glacial environment of origin (see Section 3.1).

In contrast, the grains from Site B are more typically rounded (generally elliptical in shape), with ~75% of the samples showing an intermediate erosional form (Fig. 6). In addition, more grains show preservation of a pre-weathered surface and a higher percentage of grains have *in situ* jointed blocks intact. The rounded shapes show a dominance of abrasive erosion processes in this area of the glacier bed. The preservation of pre-weathered surfaces has been viewed by Mahaney and Kalm (1995, 2000) in combination with both highly abraded grains, and overprinted grains showing new fracture textures. The combination of abrasion textures, crushing and fracture textures (e.g. *in situ* jointed blocks) and pre-weathered surfaces reflects the dominance of intermediate grain forms at Site B. No one process of erosion has dominated the surface texture of the grains. Abrasion alone is insufficient to cause breakage patterns (Krinsley and Donahue, 1968). As such, grain textures indicate a mélange or continuum of both abrasive and percussive processes of erosion.

These different styles of erosion must also reflect either the initial grain size and/or the total strain experienced within the deforming bed. The till at Site A had a slightly finer grain size than Site B, and was better sorted. Site B was located closer to the valley wall, where the till plain (prior to the readvance) would have been dominated by coarser, more angular material generated via processes of physical weathering. The till at Site A may have incorporated silt-sized sediments from the glacial lake, which would have been in this area prior to the advance. However, Site B contains a higher percentage of silt-sized particles. So we conclude that initial grain size appears to have had little impact on the resultant grain size.

Instead we suggest that the poorly sorted, smoothed and rounded nature of Site B, with the preservation of pre-weathered surfaces, reflects an overall low strain. In contrast the well sorted, angular nature, combined with the lack of preserved pre-weathered surfaces at Site A, must reflect a greater total strain experienced by the till. We propose that the till from Site B reveals a relatively simple deformation history, reflecting the breakdown of the coarse bedrock, initially by fracture and then abrasion, as suggested by Iverson et al. (1996). Meanwhile, the tills at Site A reflect a far more complex deformational history, due to the heterogeneous sediment inputs (i.e. bedrock and lake material) combined with a longer time within the deforming layer.

In order to investigate the relationship between grain size and erosional processes, the grain size data (-2φ and less) from Briksdalsbreen was plotted against two other examples (Fig. 8). The till at Briksdalsbreen was the coarsest containing only 7% silt and 0% clay. In comparison, Ice Stream B measured 35% silt and 32% clay (Tulaczyk et al., 1998), and Breiðamerkurjökull recorded 24–45% silt and 2–9% clay at (Boulton et al., 1974).

Till derived from a fine-grained bedrock, such as Ice Stream B, are unlikely to suffer a reduction in grain size because the clay-rich tills allow high water pressures and prevent inter-particle stress concentrations (Tulaczyk et al., 1998). However, coarser grained tills will undergo inter-particle stress, which results in the crushing of the fine fraction and the production of a silt-rich till (Boulton et al., 1974; Fig. 8). However, Briksdalsbreen represented the coarsest and most competent initial bedrock and,

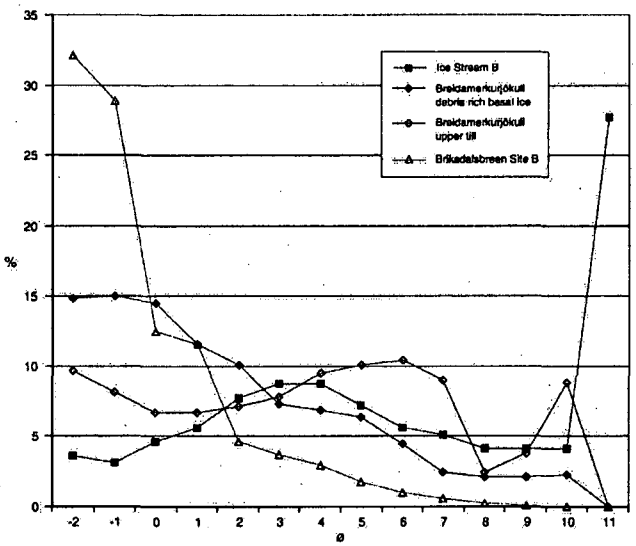


Fig. 8. Grain size (less than -2φ) from different deformation tills: Ice Stream B, after Tulaczyk et al. (1998); Breidamerkurjökull, after Boulton et al. (1974).

although there was evidence of subglacial erosion, a significant silt fraction had not been produced.

5. Conclusions

The aim of this study was to investigate the nature of subglacial erosion associated with coarse grained deformation till collected *in situ* from the subglacial environment. Firstly, to test if the *in situ* subglacial sampling technique was representative of the subglacial environment, the results were compared with a random sample of till from an exposed subglacial surface in the foreland. This comparative study showed a close similarity between the bulk samples taken in 2004 and 2006, and the subglacial *in situ* samples from Site B taken with the small sampler. In contrast, the large sampler preferentially collected the sand and silt fraction.

SEM analysis demonstrated the presence and nature of the intra-granular erosion within the till by crushing (fracture) and rotational (abrasion) processes. The study also demonstrated the variation in erosional processes and strain histories beneath the glacier. It was argued that at the site close to the valley wall, the erosion reflected a relatively simple pattern of first fracture and then abrasion, associated with the model proposed by Iverson et al. (1996). However, towards the centre of the glacier, the erosion of more heterogeneous source material (proglacial lake sediments, till, gneiss bedrock) must have produced complex erosional pathways, whose erosional style reflect greater overall strain and possibly time within the deforming layer.

From this study it is clear, that subglacial processes do vary across the glacier bed, and so care is needed when taking sedimentary or *in situ* process data from one point. The resultant style of glacial erosion associated with deformation tills is controlled by the nature of the bedrock and overall strain imposed on the till. Clay-rich tills show little comminution compared with fine sand grained till, whilst the coarse-sand tills at Briksdalsbreen show good evidence for erosion but little evidence for a significant silt component. Glacial erosion within till associated with coarse grained deformation till is a very active process and reflects the dynamic nature of the subglacial environment.

Acknowledgements

The authors would thank Intellisys, BTExact and TOPCOM for their support, Inge and Gro Melkevoll for their help with logistics, and Kirk Martinez, Royan Ong, Sue Way, David Robertson, Daniel Miles, Paritosh Padhy, Richard Waller, Hannah Brown and Sarita Ward for field support. Also, thanks to Richard Pearce at the Southampton National Oceanography Centre for his help with the SEM; Adrian Palmer, Department of Geography, Royal Holloway for the grain size analysis; and Tim Aspen and his colleagues in the Cartographic Unit, School of Geography, for cartography. This research is funded by the Royal Society Paul Instrument Fund, the Royal Society and the DTI NextWave programme.

References

Alley, R.B., Blankenship, D.D., Bentley, C.R., Rooney, S.T., 1986. Deformation of till beneath ice stream B, West Antarctica. Nature 322, 57–59.

Benn, D.I., Evans, D.J.A., 1996. The interpretation and classification of subglacially-deformed materials. Quaternary Science Reviews 15 (1), 23–52.
Boulton, G.S., Hindmarsh, R.C.A., 1987. Sediment deformation beneath glaciers: rheology and geological consequences. Journal of Geophysical Research 92 (B9), 9059–9082.
Boulton, G.S., Dent, D.L., Morris, E.M., 1974. Subglacial shearing and crushing, and the role of water pressure in tills from south-east Iceland. Geografiska Annaler. Series A 56, 135–145.
Blake, E.W., Clarke, G.K.C., Gerin, M.C., 1992. Tools for examining subglacial bed deformation. Journal of Glaciology 38 (130), 388–396.
Blott, S.J., Pye, K., 2001. GRADISTAT: a grain size distribution and statistics package for the analysis of unconsolidated sediments. Earth Surface Processes and Landforms 26, 1237–1248.
Blott, S.J., Pye, K., 2006. Particle size distribution analysis of sand-sized particles by laser diffraction: an experimental investigation of instrument sensitivity and the effects of particle shape. Sedimentology 53 (3), 671–685.
Clarke, G.K.C., 1987. Subglacial till: a physical framework for its properties and processes. Journal of Geophysical Research 92 (B9), 8942–8984.
Cuffey, K., Alley, R.B., 1996. Is erosion by deforming subglacial sediments significant? (Towards till continuity). Annals of Glaciology 22, 17–24.
Dreimanis, A., Vagners, U.J., 1971. Bimodal distribution of rock and mineral fragments in basal tills. In: Goldthwaite, R.P. (Ed.), Till: A Symposium. Ohio State University Press, Columbus, OH, pp. 237–250. Ohio.
Drescher, A., de Josselin de Jong, G., 1972. Photoelastic verification of a mechanical model for flow of a granular material. Journal of the Mechanics and Physics of Solids 20, 337–351.
Elson, J.A., 1988. Comment on glacitectonite, deformation till, and comminution till. In: Goldthwaite, R.P., Matsch, C.L. (Eds.), Genetic Classification of Glacigenic Deposits. A.A. Balkema, pp. 85–88.
Fischer, U.H., Hubbard, B., 1999. Subglacial sediment textures: character and evolution at Haut Glacier d'Arolla, Switzerland. Annals of Glaciology 28, 241–246.
Folk, R.L., Ward, W.C., 1957. Brazos River bar: a study in the significance of grain size parameters. Journal of Sedimentay Petrology 27, 3–26.
Gjessing, J., 1965. On 'plastic scouring' and 'subglacial erosion'. Norsk Geologisk Tidsskr 20, 1–37.
Haldersen, S., 1981. The enrichment of quartz in tills. In: Evenson, E.B., Schluchter, C., Rabassa, J. (Eds.), Tills and Related Deposits. A.A. Balkema, Rotterdam, pp. 141–150.
Haldersen, S., 1983. Mineralogy and geochemistry of basal till and their relationship to till forming processes. Norsk Geologisk Tidsskrift 63, 15–25.
Hart, J.K., 2006a. Deforming layer erosion over rigid bed rock at Athabasca Glacier, Canada. Earth Surface Processes and Landforms 31, 65–80.
Hart, J.K., 2006b. An investigation of subglacial processes at the microscale from Briksdalsbreen, Norway. Sedimentology, 53 (1), 125–146.
Hart, J.K., Boulton, G.S., 1991. The interrelationship between glaciotectonic deformation and glaciodeposition. Quaternary Science Reviews 10, 335–350.
Hart, J.K., Martinez, K., Ong, R., Riddoch, A., Rose, K.C., Padhy, P., 2006. An autonomous multi-sensor subglacial probe: design and preliminary results from Briksdalsbreen, Norway. Journal of Glaciology 52 (178), 89–397.
Helland, P.E., Holmes, M.A., 1997. Surface textural analysis of quartz sand grains from ODP Site 918 off the southeast coast of Greenland suggests glaciation of southern Greenland at 11 Ma. Palaeogeography, Palaeoclimatology, Palaeoecology 135, 109–121.
Higgs, R., 1979. Quartz-grain surface features of Mesozoic–Cenozoic sands from the Labrador and western Greenland continental margins. Journal of Sedimentary Petrology 49 (2), 599–610.
Hindmarsh, R.C.A., 1996. Sliding of till over bedrock: scratching, polishing, comminution and kinematic wave theory. Annals of Glaciology 22, 41–47.
Hooke, R. LeB., Iverson, N.R., 1995. Grain-size distribution in deforming subglacial tills: role of grain fracture. Geology 23 (1), 57–60.
Iverson, N.R., Hooyer, T.S., Hooke, R. LeB., 1996. A laboratory study of sediment deformation: stress heterogeneity and grain-size evolution. Annals of Glaciology 22, 167–175.
Kamb, B., 1991. Rheological nonlinearity and flow instability in the deforming-bed mechanism of ice stream motion. Journal of Geophysical Research 96, 16585–16595.
Khatwa, A., Tulaczyk, S., 2001. Microstructural interpretations of modern and Pleistocene subglacially deformed sediments: the relative role of parent material and subglacial processes. Journal of Quaternary Science 16, 507–517.
Khatwa, A., Hart, J.K., Payne, A.J., 1999. Grain textural analysis across a range of glacial facies. Annals of Glaciology 28, 111–117.
Krinsley, D.H., 1980. Scanning electron microscope examination of quartz sand grain micro textures. Kwartalnik Geologiczny 24, 217–232.
Krinsley, D.H., Donahue, J., 1968. Environmental interpretation of sand grain surface textures by electron microscopy. Geological Society of America Bulletin 79, 743–748.
Krinsley, D.H., Doornkamp, J.C., 1973. Atlas of Quartz Sand Surface Textures. Cambridge University Press, Cambridge, p. 91.
Mahaney, W.C., 1990. Glacially-crushed quartz grains in late Quaternary deposits in the Virunga Mountains, Rwanda — indicators of wind transport from the north. Boreas 19, 81–84.
Mahaney, W.C., Kalm, V., 1995. Scanning electron microscopy of Pleistocene tills in Estonia. Boreas 24, 13–29.
Mahaney, W.C., Kalm, V., 2000. Comparative scanning electron microscopy study of orientated till blocks, glacial grains and Devonian sands in Estonia and Latvia. Boreas 29, 35–51.
Mahaney, W.C., Claridge, G., Campbell, I., 1996. Microtextures on quartz grains in tills from Antarctica. Palaeogeography, Palaeoclimatology, Palaeoecology 121, 89–103.
Mandl, G., de Jong, L.N.J., Maltha, A., 1977. Shear zones in granular material — an experimental study of their structure and mechanical genesis. Rock Mechanics 9, 95–144.
Margolis, S.V., Kennet, J.P., 1971. Cenozoic paleoglacial history of Antarctica recorded in subantarctic deep-sea cores. American Journal of Science 271, 1–36.
Nesje, A., Lie, Ø., Dahl, S.O., 2000. Is the North Atlantic Oscillation reflected in Scandinavian glacier mass balance records? Journal of Quaternary Science 15, 587–601.
Roberts, D.A., Hart, J.K., 2005. The deforming bed characteristics of a stratified till assemblage in north East Anglia, UK: investigating controls on sediment rheology and strain signatures. Quaternary Science Reviews 24 (1–2), 123–140.
Sharp, M., Gomez, B., 1986. Process of debris comminution in the glacial environment and implications for quartz sand-grain micromorphology. Sedimentary Geology 46, 33–47.
Strand, K., Passchier, S., Näsi, J., 2003. Implications of quartz grain micro-textures for onset Eocene/Oligocene glaciation in Prydz Bay, ODP Site 1166, Antarctica. Palaeogeography, Palaeoclimatology, Palaeoecology 198, 101–111.
Tulaczyk, S.M., Kamb, B., Scherer, R.P., Engelhardt, H.F., 1998. Sedimentary processes at the base of a west Antarctic ice stream: constraints from textural and compositional properties of subglacial debris. Journal of Sedimentary Research 68 (3), 487–496.
van der Meer, J.J.M., 1997. Particle and aggregate mobility in till: microscopic evidence of subglacial processes. Quaternary Science Reviews 16, 827–831.
van der Meer, J.J.M., Menzies, J., Rose, J., 2003. Subglacial till: the deforming glacier bed. Quaternary Science Reviews 22, 1659–1685.

References

Akyildiz, I.F., Su, W.L., Sankarasubramaniam, Y., and Cayirci, E. A survey on sensor networks. Communications Magazine, IEEE 40(8), 102-114. 2002.

Alley, R.B., Blankenship, D.D., Bently, C.R., and Rooney, S.T., (1986). Deformation of till beneath ice stream B, West Antarctica. *Nature*, 322: 57-59.

Alley, R.B., Blankenship, D.D., Bently, C.R., and Rooney, S.T., (1987a). Till beneath ice stream B. 3. Till deformation: evidence and implications. *Journal of Geophysical Research*, 92(B9): 8921-8929.

Alley, R.B., Blankenship, D.D., Rooney, S.T., and Bently, C.R., (1987b). Till beneath ice stream B. 4. A coupled ice-till flow model. *Journal of Geophysical Research*, 92(B9): 8931-8940.

Alley, R.B., (1989a). Water-pressure coupling of sliding and bed deformation: I. Water System. *Journal of Glaciology*, 35(119): 108-118.

Alley, R.B., (1989b). Water-pressure coupling of sliding and bed deformation: II. Velocity-depth profiles. *Journal of Glaciology*, 35(119): 119-129.

Alley, R.B., (1991). Deforming-bed origin for southern Laurentide till sheets? *Journal of Glaciology*, 37(125): 67-76.

Alley, R.B., (1993). In search of ice-stream sticky spots. *Journal of Glaciology*, 39(133): 447-454.

Anderson, R.S., Anderson, S.P., MacGregor, K.R., Waddington, E.D., O'Neel, S., Riihimaki, C.A., and Loso, M.G., (2004). Strong feedbacks between hydrology and sliding of a small alpine glacier. *Journal of Geophysical Research*, 109(F3): 10.1029/2004JF000120.

Arnold, N. and Sharp, M., (2002). Flow variability in the Scandinavian ice sheet: modelling the coupling between ice sheet flow and hydrology. *Quaternary Science Reviews*, 21: 485-502.

Benn, D.I. and Ballantyne, C.K., (1993). The description and representation of particle shape. *Earth Surface Processes and Landforms*, 18: 665-672.

Benn, D.I., (1994). Fabric shape and the interpretation of sedimentary fabric data. *Journal of Sedimentary Research*, 64: 910-915.

Benn, D.I., (1995). Fabric signature of subglacial till deformation, Breidamerkurjøkull, Iceland. *Sedimentology*, 42: 735-747.

Benn, D.I. and Evans, D.J.A., (1996). The interpretation and classification of subglacially deformed materials. *Quaternary Science Reviews*, 15: 23-52.

Bingham, R.G., Nienow, P.W., Sharp, M.J., and Boon, S., (2005). Subglacial drainage processes at a High Arctic polythermal valley glacier. *Journal of Glaciology*, 51(172): 15-24.

Blake, E.W., Clarke, G.K.C., and Gerin, M.C., (1992). Tools for examining subglacial bed deformation. *Journal of Glaciology*, 38(130): 388-396.

Blake, E.W. and Clarke, G.K.C., (1992). Interpretation of borehole-inclinometer data: a general theory applied to a new instrument. *Journal of Glaciology*, 38(128): 113-124.

Blake, E.W., Fischer, U.H., and Clarke, G.K.C., (1994). Direct measurement of sliding at the glacier bed. *Journal of Glaciology*, 40(135): 595-599.

Blankenship, D.D., Bently, C.R., Rooney, S.T., and Alley, R.B., (1986). Seismic measurements reveal a saturated porous layer beneath an active Antarctic ice stream. *Nature*, 322: 54-57.

Blankenship, D.D., Bently, C.R., Rooney, S.T., and Alley, R.B., (1987). Till beneath ice stream B. 1. Properties derived from seismic travel times. *Journal of Geophysical Research*, 92(B9): 8903-8911.

Blott, S.J. and Pye, K., (2001). GRADISTAT: a grain size distribution and statistics package for the analysis of unconsolidated sediments. *Earth Surface Processes and Landforms*, 26: 1237-1248.

Blott, S.J. and Pye, K., (2006). Particle size distribution and analysis of sand-sized particles by laser diffraction: an experimental investigation of instrument sensitivity and the effects of particle shape. *Sedimentology*, 53(3): 671-685.

Bonaccorso, A., Falzone, G., and Gambino, S., (1999). An investigation into shallow borehole tiltmeters. *Geophysical Research Letters*, 26(11): 1637-1640.

Boulton, G.S. and Dent, D.L., (1974). The nature and rates of post-depositional changes in recently deposited till from south-east Iceland. *Geografiska Annaler Series A, Physical Geography*, 56(3/4): 121-134.

Boulton, G.S., Dent, D.L., and Morris, E.M., (1974). Subglacial shearing and crushing and the role of water pressures in tills from south-east Iceland. *Geografiska Annaler Series A, Physical Geography*, 56(3/4): 135-145.

Boulton, G.S. and Paul, M.A., (1976). The influence of genetic processes on some geotechnical properties of glacial tills. *Quarterly Journal of Engineering Geology*, 9(3): 159-194.

Boulton, G.S. and Jones, A.S., (1979). Stability of temperate ice caps and ice sheets resting on beds of deformable sediment. *Journal of Glaciology*, 24(90): 29-42.

Boulton, G.S., (1979). Processes of glacier erosion on different substrata. *Journal of Glaciology*, 23: 15-38.

Boulton, G.S., Smith, G.D., Jones, A.S., and Newsome, J., (1985). Glacial geology and glaciology of the last mid-latitude ice sheets. *Journal of the Geological Society of London*, 142: 447-474.

Boulton, G.S., (1986). A paradigm shift in glaciology? *Nature*, 322: 18.

Boulton, G.S. and Hindmarsh, R.C.A., (1987). Sediment deformation beneath glaciers: rheology and geological consequences. *Journal of Geophysical Research*, 92(B9): 9059-9082.

Boulton, G.S. and Clark, C.D., (1990). A highly mobile ice sheet revealed by satellite images of glacial lineations. *Nature*, 346: 813-817.

Boulton, G.S., (1996). Theory of glacial erosion, transport and deposition as a consequence of subglacial sediment deformation. *Journal of Glaciology*, 42(140): 43-62.

Boulton, G.S., Dobbie, K.E., and Zatsepin, S., (2001). Sediment deformation beneath glaciers and its coupling to the subglacial hydraulic system. *Quaternary International*, 86: 3-28.

Boyce, J. and Eyles, N., (1991). Drumlin carved by deforming till streams below the Laurentide ice sheet. *Geology*, 19: 787-790.

Bull, P.A., (1981). Environmental reconstruction by electron microscopy. *Progress in Physical Geography*, 5: 368-397.

Carol, H., (1947). The formation of roche moutonnees. *Journal of Glaciology*, 1(2): 57-59.

Carr, S.J. and Rose, J., (2003). Till fabric patterns and significance: particle response to subglacial stress. *Quaternary Science Reviews*, 22: 1415-1426.

Chong, C.-Y. and Kumar, S.P., (2003). Sensor Networks: Evolution, Opportunities and Challenges. *Proceedings of the IEEE*, 91(8): 1247-1256.

Clark, C.D., (1993). Mega-scale glacial lineations and cross-cutting ice-flow landforms. *Earth Surface Processes and Landforms*, 18: 1-29.

Clark, C.D., (1997). Reconstructing the evolutionary dynamics of former ice sheets using multi-temporal evidence, remote sensing and GIS. *Quaternary Science Reviews*, 16: 1067-1092.

Clark, C.D., (1999). Glaciodynamic context of subglacial bedform generation and preservation. *Annals of Glaciology*, 28: 23-32.

Clark, C.D., Evans, D.J.A., Khatwa, A., Bradwell, T., Jordan, C.J., Marsh, S.H., Mitchell, W.A., and Bateman, M.D., (2004). Map and GIS database of landforms and features related to the last British Ice Sheet. *Boreas*, 33(4): 359-375.

Clark, P.U., (1992). Surface form of the southern Laurentide Ice Sheet and its implications to ice-sheet dynamics. *Geological Society of America Bulletin*, 104(5): 595-605.

Clark, P.U. and Walder, J.S., (1994). Subglacial drainage, eskers, and deforming beds beneath the Laurentide and Eurasian ice sheets. *Geological Society of America Bulletin*, 106(2): 304-314.

Clarke, G.K.C., (1987). Subglacial till: A physical framework for its properties and processes. *Journal of Geophysical Research*, 92(B9): 9023-9036.

Clarke, G.K.C., (1987b). A short history of scientific investigations on glaciers. *Journal of Glaciology*, Special Issue: 4-24.

Clarke, G.K.C., (1996). Lumped-element analysis of subglacial hydraulic circuits. *Journal of Geophysical Research*, 101(B8): 17547-17559.

Clarke, G.K.C., (2005). Subglacial processes. *Annual Review of Earth and Planetary Sciences*, 33: 247-276.

Clayton, L., Teller, J.T., and Attig, Jr.J.W., (1985). Surging of the southwestern part of the Laurentide ice sheet. *Boreas*, 14(3): 235-241.

Clayton, L., Mickelson, D.M., and Attig, J.W., (1989). Evidence against pervasively deformed bed material beneath rapidly moving lobes of the southern Laurentide ice sheet. *Sedimentary Geology*, 62(3-4): 203-208.

Cuffey, K. and Alley, R.B., (1996). Is erosion by deforming subglacial sediments significant? (Towards till continuity). *Annals of Glaciology*, 22: 17-24.

De Roure, D., (2005). Floodnet: A new flood warning system. *Royal Academy of Engineering Quarterly*, 23: 48-51.

Delin, K.A., Harvey, R.P., Chabot, N.A., Jackson, S.P., Adams, M., Johnson, D.W., and Britton, J.T. (2003) Sensor web in Antarctica: developing an intelligent, autonomous platform for locating biological flourishes in cryogenic environments. Proceedings of the 34th Lunar and Planetary Science Conference.

Delin, K.A., Jackson, S.P., Johnson, D.W., Burleigh, S.C., Woodrow, R.R., McAuley, M., Britton, J.T., Dohm, J.M., Ferré, T.P.A., Felipe, I.P., Rucker, D.F., and Baker, V.R. (2004). Sensor web for spatio-temporal monitoring of a hydrological environment. Proceedings of the 35th Lunar and Planetary Science Conference.

Dowdeswell, J.A. and Evans, S., (2004). Investigations on the form and flow of ice sheets and glaciers using radio-echo sounding. *Reports on Progress in Physics*, 67: 1821-1861.

Dreimanis, A. and Vagners, U.J., (1971). Bimodal distribution of rock and mineral fragments in basal tills. In: R.P.Goldthwaite (Editor), *Till: A Symposium.* Ohio State University Press, Columbus, Ohio, pp. 237-250.

Drescher, A. and de Josselin de Jong, G., (1972). Photoelastic verification of a mechanical model for flow of a granular material. *Journal of the Mechanics and Physics of Solids*, 20: 337-351.

Echelmeyer, K. and Zhongxiang, W., (1987). Direct observation of basal sliding and deformation of basal drift at sub-freezing temperatures. *Journal of Glaciology*, 33(113): 83-98.

Eklund, A. and Hart, J.K., (1996). Glaciotectonic deformation within a flute from the glacier Isfallsglaciaren, Sweden. *Journal of Quaternary Science*, 11: 299-310.

Elson, J.A., (1988). Comment on glacitectonite, deformation till and communition till. In: R.P.Goldthwaite and C.L.Matsch (Editors), *Genetic Classification of Glacigenic Deposits*. A.A. Balkema, Rotterdam, pp. 85-88.

Elvehøy, H., (2001). Briksdalsbreen. In: B.Kjøllmoen (Editor), *Glaciological investigations in Norway in 2000. Norwegian Water Resources and Energy Directorate, Report* 2. pp. 26-30.

Engelhardt, H., Harrison, W.D., and Kamb, B., (1978). Basal sliding and conditions at the glacier bed as revealed by bore-hole photography. *Journal of Glaciology*, 20(84): 469-508.

Engelhardt, H., Humphrey, N., Kamb, B., and Fahnestock, M., (1990). Physical conditions at the base of a fast moving Antarctic ice stream. *Science*, 248: 57-59.

Engelhardt, H. and Kamb, B., (1997). Basal hydraulic system of a West Antarctic ice stream constraints from borehole observations. *Journal of Glaciology*, 43(144): 207-230.

Engelhardt, H. and Kamb, B., (1998). Basal sliding of ice stream B, West Antarctica. *Journal of Glaciology*, 44(147): 223-230.

Evans, D.J.A., Clark, C.D., and Mitchell, W.A., (2005). The last British Ice Sheet: a review of the evidence utilised in the compilation of the Glacial Map of Britain. *Earth Science Reviews*, 70: 253-312.

Evans, D.J.A., Phillips, E.R., Hiemstra, J.F., and Auton, C.A., (2006). Subglacial till: formation, sedimentary characteristics and classification. *Earth Science Reviews*, 78: 115-176.

Evans, S. and Smith, B.M.E., (1969). A radio echo equipment for depth sounding in polar ice sheets. *Journal of the Physics E* , 2(2): 131-136.

Fischer, U.H. and Clarke, G.K.C., (1994). Ploughing of subglacial sediment. *Journal of Glaciology*, 40(134): 97-106.

Fischer, U.H. and Clarke, G.K.C., (1997). Stick-slip sliding behaviour at the base of a glacier. *Annals of Glaciology*, 24: 390-396.

Fischer, U.H. and Clarke, G.K.C., (1997b). Clast collision frequency as an indicator of glacier sliding rate. *Journal of Glaciology*, 43(145): 460-466.

Fischer, U.H., Iverson, N.R., Hanson, B., Hooke, R.L., and Jansson, P., (1998). Estimation of hydraulic properties of subglacial till from ploughmeter measurements. *Journal of Glaciology*, 44(148): 517-522.

Fischer, U.H., Clarke, G.K.C., and Blatter, H., (1999). Evidence for temporally varying "sticky spots" at the base of Trapridge Glacier, Yukon Territory, Canada. *Journal of Glaciology*, 45(150): 352-360.

Fischer, U.H. and Hubbard, B., (1999). Subglacial sediment textures: character and evolution at Haut Glacier d'Arolla, Switzerland. *Annals of Glaciology*, 28: 241-246.

Fischer, U.H. and Clarke, G.K.C., (2001). Review of subglacial hydro-mechanical coupling: Trapridge Glacier, Yukon Territory, Canada. *Quaternary International*, 86: 29-43.

Fitzsimons, S.J., Lorrain, R.D., and Vandergoes, M.J., (2000). Behaviour of subglacial sediment and basal ice in a cold glacier. In: A.J.Maltman, B.Hubbard, and M.J.Hambrey (Editors), *Deformation of Glacial Materials.* pp. 181-190.

Flowers, G.E. and Clarke, G.K.C., (2000). An integrated modelling approach to understanding subglacial hydraulic release events. *Annals of Glaciology*, 31: 222-228.

Folk, R.L. and Ward, W.C., (1957). Brazos River bar: a study in the significance of grain size parameters. *Journal of Sedimentary Petrology*, 27(1): 3-26.

Fountain, A.G. and Walder, J.S., (1998). Water flow through temperate glaciers. *Reviews of Geophysics*, 36(3): 299-328.

Fowler, A.C., (2003). On the rheology of till. *Annals of Glaciology*, 37: 55-59.

Freeze, R.A. and Cherry, J.A., (1979). *Groundwater.* Prentice-Hall, Engelwood Cliffs, NJ.

Fudge, TJ., Harper, J.T., Humphrey, N.F., and Pfeffer, W.T., (2005). Diurnal water-pressure fluctuations: timing and pattern of termination below Bench Glacier, Alaska, USA. *Annals of Glaciology*, 40: 102-106.

Gades, A.M., Raymond, C.F., Conway, H., and Jacobel, R.W., (2000). Bed properties of Siple Dome and adjacent ice streams, West Antarctica, inferred from radio-echo sounding measurements. *Journal of Glaciology*, 46(152): 88-94.

Gharavi, H. and Kumar, S.P., (2003). Special issue on sensor networks and applications. *Proceedings of the IEEE*, 91(8): 1151-1153.

Gjessing, J., (1965). On 'plastic scouring' and 'subglacial erosion'. *Norsk Geologisk Tidsskr*, 20: 1-37.

Glen, J.W., Donner, J.J., and West, R.G., (1957). On the mechanism by which stones in till become oriented. *American Journal of Science*, 255(3): 194-205.

Glen, J.W. and Paren, J.G., (1975). The electrical properties of snow and ice. *Journal of Glaciology*, 15(73): 15-38.

Gordon, S., Sharp, M., Hubbard, B., Smart, C., Ketterling, B., and Willis, I., (1998). Seasonal reorganization of subglacial drainage inferred from measurements in boreholes. *Hydrological Processes*, 12: 105-133.

Gordon, S., Sharp, M., Hubbard, B., Willis, I., Smart, C., Copland, L., Harbor, J., and Ketterling, B., (2001). Borehole drainage and its implications for the investigation of glacier hydrology: experiences from Haut Glacier d'Arolla, Switzerland. *Hydrological Processes*, 15: 797-813.

Grove, J.M., (1988). *The Little Ice Age.* Methuen, London.

Haeberli, W., Frauenfelder, R., Hoelzle, M., and Maisch, M., (1999). On rates and acceleration trends of global glacier mass changes. *Geografiska Annaler Series A, Physical Geography*, 81(4): 585-591.

Haefeli, R., (1951). Some observations on glacier flow. *Journal of Glaciology*, 1(9): 496-500.

Haldersen, S., (1981). The enrichment of quartz in tills. In: E.B.Evenson, C.Schluchter, and J.Rabassa (Editors), *Tills and Related Deposits.* A.A. Balkema, Rotterdam, pp. 141-150.

Haldersen, S., (1983). Mineralogy and geochemistry of basal till and their relationship to till forming processes. *Norsk Geologisk Tidsskrift*, 63: 15-25.

Harbor, J., Sharp, M., Copland, L., Hubbard, B., Nienow, P., and Mair, D., (1997). Influence of subglacial drainage conditions on the velocity distribution within a glacier cross section. *Geology*, 25(8): 739-742.

Harper, J.T., Humphrey, N.F., and Pfeffer, W.T., (1998). Three-dimensional deformation measured in an Alaskan glacier. *Science*, 281(5381): 1340-1342.

Harper, J.T., Humphrey, N.F., and Greenwood, M.C., (2002). Basal conditions and glacier motion during the winter/spring transition, Worthington Glacier, Alaska, USA. *Journal of Glaciology*, 48(160): 42-50.

Harper, J.T., Humphrey, N.F., Pfeffer, W.T., Fudge, T., and O'Neel, S., (2005). Evolution of subglacial water pressure along a glacier's length. *Annals of Glaciology*, 40: 31-36.

Harrison, W.D., Echelmeyer, K.A., and Engelhardt, H., (1993). Short-period observations of speed, train and seismicity on ice stream B, Antarctica. *Journal of Glaciology*, 39(133): 463-470.

Harrison, W.D., Truffer, M., Echelmeyer, K.A., Pomraning, D.A., Abnett, K.A., and Ruhkick, R.H., (2004). Probing the till beneath Black Rapids Glacier, Alaska, USA. *Journal of Glaciology*, 50(171): 608-614.

Hart, J.K. and Boulton, G.S., (1991). The glacial geology of north east Norfolk. In: J.Rose, P.L.Gibbard, and J.Elhers (Editors), *The Glacial Deposits of Britain.* Balkema, Rotterdam, pp. 233-244.

Hart, J.K. and Boulton, G.S., (1991b). The interrelationship between glaciotectonic deformation and glaciodeposition. *Quaternary Science Reviews*, 10: 335-350.

Hart, J.K., (1994). Till fabric associated with deformable beds. *Earth Surface Processes and Landforms*, 19: 15-32.

Hart, J.K., (1995). An investigation of the deforming layer/debris-rich ice continuum, illustrated from three Alaskan glaciers. *Journal of Glaciology*, 41: 619-633.

Hart, J.K., (1999). Identifying fast ice flow from landform assemblages in the geological record: a discussion. *Annals of Glaciology*, 28: 59-66.

Hart, J.K. and Rose, J., (2001). Approaches to the study of glacier bed deformation. *Quaternary International*, 86: 45-58.

Hart, J.K., (2006a). Deforming layer erosion over rigid bedrock at Athabasca Glacier, Canada. *Earth Surface Processes and Landforms*, 31: 65-80.

Hart, J.K., (2006b). An investigation of subglacial processes at the microscale from Briksdalsbreen, Norway. *Sedimentology*, 53 (1): 125-146.

Hart, J.K. and Martinez, K., (2006). Environmental sensor networks: a revolution in the earth system science? *Earth Science Reviews*, 78: 177-191.

Hart, J.K., Martinez, K., Ong, H.L.R., Riddoch, A., Rose, K.C., and Padhy, P., (2006). A wireless multi-sensor subglacial probe: design and preliminary results. *Journal of Glaciology*, 52(178): 389-397.

Helland, P.E. and Holmes, M.A., (1997). Surface textural analysis of quartz sand grains from ODP Site 918 off the southeast coast of Greenland suggests glaciation of southern Greenland at 11 Ma. *Palaeogeography, Palaeoclimatology, Palaeoecology*, 135: 109-121.

Hiemstra, J.F. and van der Meer, J., (1997). Pore-water controlled grain fracturing as an indicator for subglacial shearing in tills. *Journal of Glaciology*, 43(145): 446-454.

Higgs, R., (1979). Quartz-grain surface features of mesozoic-cenozoic sands from the Labrador and western Greenland continental margins. *Journal of Sedimentary Petrology*, 49(2): 599-610.

Hindmarsh, R.C.A., (1997). Deforming beds: viscous and plastic scales of deformation. *Quaternary Science Reviews*, 16: 1039-1056.

Hodge, S.M., (1976). Direct measurements of basal water pressures: a pilot study. *Journal of Glaciology*, 16(74): 205-218.

Hooke, R.L., Holmlund, P., and Iverson, N.R., (1987). Extrusion flow demonstrated by bore-hole deformation measurements over a riegel, Storglaciaren, Sweden. *Journal of Glaciology*, 33(113): 72-78.

Hooke, R.L., Pohjola, V.A., Jansson, P., and Kohler, J., (1992). Intra-seasonal changes in deformation profiles revealed by borehole studies, Storglaciären, Sweden. *Journal of Glaciology*, 38(130): 348-358.

Hooke, R.L. and Iverson, N.R., (1995). Grain-size distribution in deforming subglacial tills: role of grain fracture. *Geology*, 23(1): 57-60.

Hooke, R.L., Hanson, B., Iverson, N.R., Jansson, P., and Fischer, U.H., (1997). Rheology of till beneath Storglaciären, Sweden. *Journal of Glaciology*, 43(143): 172-179.

Hooyer, T.S. and Iverson, N.R., (2000). Clast-fabric development in a shearing granular material: implications for subglacial till and fault gouge. *Geological Society of America Bulletin*, 112(5): 683-692.

Hubbard, B.P., Sharp, M.J., Willis, I.C., Nielsen, M.K., and Smart, C.C. (1995). Borehole water-level variations and the structure of the subglacial hydrological system of Haut Glacier d'Arolla, Valais, Switzerland. *Journal of Glaciology*, 41(139): 572-583.

Hubbard, B. and Nienow, P., (1997). Alpine subglacial hydrology. *Quaternary Science Reviews*, 16: 939-955.

Hubbard, B. and Glasser, N., (2005). *Field Techniques in Glaciology and Glacial Geomorphology.* John Wiley and Sons, Ltd., Chichester.

Hulbe, C.L. and Payne, A.J., (2001). Numerical modelling of the West Antarctic Ice Sheet. *Antarctic Research Series*, 77: 201-220.

Humphrey, N., Kamb, B., Fahnestock, M., and Engelhardt, H., (1993). Characteristics of the bed of the Lower Columbia Glacier, Alaska. *Journal of Geophysical Research*, 98(B1): 837-846.

Iverson, N.R., Jansson, P., and Hooke, R.L., (1994). In-situ measurement of the strength of deforming subglacial till. *Journal of Glaciology*, 40(136): 497-503.

Iverson, N.R., Hanson, B., LeB.Hooke, R., and Jansson, P., (1995). Flow mechanism of glaciers on soft beds. *Science*, 267: 80-81.

Iverson, N.R., Hooyer, T.S., and Hooke, R.L., (1996). A laboratory study of sediment deformation: stress heterogeneity and grain-size evolution. *Annals of Glaciology*, 22: 167-175.

Iverson, N.R., Baker, R.W., and Hooyer, T.S., (1997). A ring-shear device for the study of till deformation: tests on tills with contrasting clay contents. *Quaternary Science Reviews*, 16: 1057-1066.

Iverson, N.R., Hooyer, T.S., and Baker, R.W., (1998). Ring-shear studies of till deformation: Coulomb-plastic behaviour and distributed strain in glacier beds. *Journal of Glaciology*, 44(148): 634-642.

Iverson, N.R., Cohen, D., Hooyer, T.S., Fischer, U.H., Jackson, M., Moore, P.L., Lappegard, G., and Kohler, J., (2003). Effects of basal debris on glacier flow. *Science*, 301: 81-83.

Iverson, N.R., Hooyer, T.S., Fischer, U.H., Cohen, D., Moore, P.L., Jackson, M., Lappegard, G., and Kohler, J., (2007). Soft-bed experiments beneath Engabreen, Norway: regelation infiltration, basal slip and bed deformation. *Journal of Glaciology*, 53(182): 323-340.

Jeffery, G.B., (1922). The motion of ellipsoidal particles immersed in a viscous fluid. *Proceedings of the Royal Society of London, Series A.*, 102(715): 161-179.

Jenson, J.W., MacAyeal, D.R., Clarke, P.U., Ho, C.L., and Vela, J.C., (1996). Numerical modelling of subglacial sediment deformation: implications for the behaviour of the Lake Michigan Lobe, Laurentide Ice Sheet. *Journal of Geophysical Research, Series B*, 101(B4): 8717-8728.

Jones, P.D., Jonsson, T., and Wheeler, D., (1997). Extension to the North Atlantic Oscillation using early instrumental pressure observations from Gibraltar and south-west Iceland. *International Journal of Climatology*, 17: 1433-1450.

Kamb, B., Raymond, C.F., Harrison, W.D., Engelhardt, H., Echelmeyer, K.A., Humphrey, N., Brugman, M.M., and Pfeffer, T., (1985). Glacier surge mechanism: 1982-1983 surge of Variegated Glacier, Alaska. *Science*, 227: 469-479.

Kamb, B. and Echelmeyer, K., (1986). Stress-gradient coupling in glacier flow: I. Longitudinal averaging of the influence of ice thickness and surface slope. *Journal of Glaciology*, 32(111): 267-284.

Kamb, B., (1987). Glacier surge mechanism based on linked cavity configuration of the basal water conduit system. *Journal of Geophysical Research*, 92(B9): 9083-9100.

Kamb, B., (1991). Rheological non-linearity and flow instability in the deforming bed mechanism of ice stream motion. *Journal of Geophysical Research*, 96(B10): 16585-16595.

Kamb, W.B. and LaChapelle, E.R., (1964). Direct observation of the mechanism of glacier sliding over bedrock. *Journal of Glaciology*, 5(38): 159-172.

Kavanaugh, J.L. and Clarke, G.K.C., (2000). Evidence for extreme pressure pulses in the subglacial water system. *Journal of Glaciology*, 46(153): 206-212.

Kavanaugh, J.L. and Clarke, G.K.C., (2001). Abrupt glacier motion and reorganization of basal shear stress following the establishment of a connected drainage system. *Journal of Glaciology*, 47(158): 472-480.

Khatwa, A., Hart, J.K., and Payne, A.J., (1999). Grain textural analysis across a range of glacial facies. *Annals of Glaciology*, 28: 111-117.

Khatwa, A. and Tulaczyk, S., (2001). Microstructural interpretations of modern and Pleistocene subglacially deformed sediments: the relative role of parent material and subglacial processes. *Journal of Quaternary Science*, 16: 507-517.

Krinsley, D.H. and Donahue, J., (1968). Environmental interpretation of sand grain surface textures by electron microscopy. *Geological Society of America Bulletin*, 79: 743-748.

Krinsley, D.H. and Doornkamp, J.C., (1973). *Atlas of quartz sand surface textures.* Cambridge University Press, Cambridge.

Lappegard, G., Kohler, J., Jackson, M., and Hagen, J.O., (2006). Characteristics of subglacial drainage systems deduced from load-cell measurements. *Journal of Glaciology*, 52(176): 137-148.

Lee, J.R., (2001). Genesis and palaeogeographical significance of the Corton Diamicton (basal member of the North Sea Drift Formation), East Anglia, UK. *Proceedings of the Geologists Association*, 112(1): 29-43.

Lilboutry, L., (1979). Local friction laws for glaciers: a critical review and new openings. *Journal of Glaciology*, 23(89): 67-95.

Lorinez, K., Malan, D., Fulford-Jones, T.R.F., Nawoj, A., Clavel, A., Shnayder, V., Mainland, G., Moulton, S., and Welsh, M., (2004). Sensor networks for emergency response: challenges and opportunities. *IEEE Special Issue on Pervasive Computing for First Response*, 3(4): 16-23.

MacKenzie, W.S. and Adams, A.E., (2000). *A colour atlas of rocks and minerals in thin section.* Grafos SA, Barcelona, Spain.

Mahaney, W.C., (1990). Glacially-crushed quartz grains in late Quaternary deposits in the Virunga Mountains, Rwanda - indicators of wind transport from the north. *Boreas*, 19: 81-84.

Mahaney, W.C. and Kalm, V., (1995). Scanning electron microscopy of Pleistocene tills in Estonia. *Boreas*, 24: 13-29.

Mahaney, W.C., (1995). Pleistocene and Holocene glacier thicknesses, transport histories and dynamics inferred from SEM microtextures on quartz particles. *Boreas*, 24: 293-304.

Mahaney, W.C., Claridge, G., and Campbell, I., (1996). Microtextures on quartz grains in tills from Antarctica. *Palaeogeography, Palaeoclimatology, Palaeoecology*,(121): 89-103.

Mahaney, W.C. and Kalm, V., (2000). Comparative scanning electron microscopy study of orientated till blocks, glacial grains and Devonian sands in Estonia and Latvia. *Boreas*, 29: 35-51.

Mair, D., Nienow, P., Willis, I., and Sharp, M., (2001). Spatial patterns of glacier motion during a high-velocity event: Haut Glacier d'Arolla, Switzerland. *Journal of Glaciology*, 47(156): 9-20.

Mair, D., Nienow, P., Sharp, M.J., Wohlleben, T., and Willis, I., (2002a). Influence of subglacial drainage system evolution on glacier surface motion: Haut Glacier d'Arolla, Switzerland. *Journal of Geophysical Research*, 107(B8): 10.1029/-2001JB000514.

Mair, D.W.F., Sharp, M.J., and Willis, I.C., (2002b). Evidence for basal cavity opening from analysis of surface uplift during a high-velocity event: Haut Glacier d'Arolla, Switzerland. *Journal of Glaciology*, 48(161): 208-216.

Mair, D., Willis, I., Fischer, U.H., Hubbard, B., Nienow, P., and Hubbard, A., (2003). Hydrological controls on patterns of surface, internal and basal

motion during three "spring events": Haut Glacier d'Arolla, Switzerland. *Journal of Glaciology*, 49(167): 555-567.

Mandl, G., de Jong, L.N.J., and Maltha, A., (1977). Shear zones in granular material - an experimental study of their structure and mechanical genesis. *Rock Mechanics*, 9: 95-144.

March, A., (1932). Mathematische theorie der regelung nach der korngestalt bei affiner deformation. *Zeitschrift für Kristallographie*, 81: 285-297.

Margolis, S.V. and Kennet, J.P., (1971). Cenozoic paleoglacial history of Antarctica recorded in subantarctic deep-sea cores. *American Journal of Science*, 217: 1-36.

Martinez, K., Hart, J.K., and Ong, H.L.R., (2004a). Environmental Sensor Networks. *IEEE Computer*, 37(8): 50-56.

Martinez, K., Ong, H.L.R., and Hart, J.K., (2004b). Glacsweb: a sensor network for hostile environments. *Proceedings of The First IEEE Communications Society Conference on Sensor and Ad Hoc Communications and Networks*.

Martinez, K., Padhy, P., Elsaify, A., Zou, G., Riddoch, A., and Hart, J.K., (2006). Deploying a sensor network in an extreme environment. *Proceedings of Sensor Networks*, Ubiquitous and Trustworthy Computing: 186-193.

Mcmanus, J. and Duck, R.W., (1988). Localised enhanced sedimentation from icebergs in a proglacial lake in Briksdal, Norway. *Geografiska Annaler Series A, Physical Geography*, 70(3): 215-223.

Murray, T. and Dowdeswell, J.A., (1992). Water throughflow and the physical effects of deformation on sedimentary glacier beds. *Journal of Geophysical Research*, 97(B6): 8993-9002.

Murray, T. and Clarke, G.K.C., (1995). Black-box modelling of the subglacial water system. *Journal of Geophysical Research, Series B*, 100(B6): 10231-10245.

Murray, T., (1997). Assessing the paradigm shift: deformable glacier beds. *Quaternary Science Reviews*, 16: 995-1016.

Murray, T., Stuart, G.W., Miller, P.J., Woodward, J., Smith, A.M., Porter, P.R., and Jiskoot, H., (2000). Glacier surge propagation by thermal evolution at the bed. *Journal of Geophysical Research, Series B*, 105(B6): 13,491-13,507.

Murray, T. and Porter, P.R., (2001). Basal conditions beneath a soft-bedded polythermal surge-type glacier: Bakaninbreen, Svalbard. *Quaternary International*, 86: 103-116.

Nesje, A., Kvamme, M., Rye, N., and Lovlie, R., (1991). Holocene glacial and climate history of the Jostedalsbreen region, western Norway; evidence from lake sediments and terrestrial deposits. *Quaternary Science Reviews*, 10: 87-114.

Nesje, A. and Kvamme, M., (1991). Holocene glacier and climate variations in western Norway: evidence for early Holocene glacier demise and multiple Neoglacial events. *Geology*, 19: 610-612.

Nesje, A., Johannessen, T., and Birks, H.J.B., (1995). Briksdalsbreen, western Norway: climatic effects on the terminal response of a temperate glacier between AD 1901 and 1994. *The Holocene*, 5(3): 343-347.

Nesje, A., Lie, O., and Dahl, S.O., (2000). Is the North Atlantic Oscillation reflected in Scandinavian glacier mass balance records? *Journal of Quaternary Science*, 15(6): 587-601.

Nesje, A. and Dahl, S.O., (2003). The 'Little Ice Age' - only temperature? *The Holocene*, 13(1): 139-145.

Nesje, A., (2005). Briksdalsbreen in western Norway: AD 1900-2004 frontal fluctuations as a combined effect of variations in winter precipitation and summer temperature. *The Holocene*, 15(8): 1245-1252.

Nienow, P., Sharp, M., and Willis, I., (1996). Velocity-discharge relationships derived from dye tracer experiments in glacial meltwaters: implications for subglacial flow conditions. *Hydrological Processes*, 10: 1411-1426.

Nienow, P., Sharp, M., and Willis, I., (1998). Seasonal changes in the morphology of the subglacial drainage system, Haut Glacier d'Arolla, Switzerland. *Earth Surface Processes and Landforms*, 23(9): 825-843.

Nye, J.F., (1952). The mechanics of glacier flow. *Journal of Glaciology*, 2: 82-93.

Nye, J.F., (1973). Water at the bed of a glacier. *International Association of Hydrology Publication*, 95: 189-194.

Oerlemans, J., (2000). Holocene glacier fluctuations: is the current rate of retreat exceptional? *Annals of Glaciology*, 31: 39-44.

Padhy, P., Martinez, K., Riddoch, A., Ong, H.L.R., and Hart, J.K., (2005). Glacial environment monitoring using sensor networks. *Proceedings of Real-World Wireless Sensor Networks.*

Paterson, W.S.B., (1977). Secondary and tertiary creep of glacier ice as measured by borehole closure rates. *Reviews of Geophysics and Space Physics*, 15: 47-55.

Paterson, W.S.B., (1994). *The Physics of Glaciers*. Elsevier Science Ltd., Oxford.

Pawley, S.M., Rose, J., Lee, J.R., Moorlock, B.S.P., and Hamblin, R.J., (2004). Mid Pleistocene sedimentology and lithostratigraphy of Weybourne, northeast Norfolk, England. *Proceedings of the Geologists Association*, 115(1): 25-42.

Payne, A.J., (1999). A thermomechanical model of ice flow in West Antarctica. *Climate Dynamics*, 15(2): 115-125.

Payne, A.J. and Baldwin, D.J., (1999). Thermomechanical modelling of the Scandinavian ice sheet: implications for ice-stream formation. *Annals of Glaciology*, 28: 83-89.

Payne, A.J., Hunt, J.C.R., and Wingham, D.J., (2006). Evolution of the Antarctic ice sheet: new understanding and challenges. *Philosophical Transactions of the Royal Society A: Mathematical, Physical and Engineering Sciences*, 364(1844): 1867-1872.

Piotrowski, J.A., Mickelson, D.M., Tulaczyk, S., Krzyszkowski, D., and Junge, F.W., (2001). Were deforming subglacial beds beneath past ice sheets really widespread? *Quaternary International*, 86: 139-150.

Porter, P.R., Murray, T., and Dowdeswell, J.A., (1997). Sediment deformation and basal dynamics beneath a glacier surge front: Bakaninbreen, Svalbard. *Annals of Glaciology*, 24: 21-26.

Porter, P.R. and Murray, T., (2001). Mechanical and hydraulic properties of till beneath Bakaninbreen, Svalbard. *Journal of Glaciology*, 47(157): 167-175.

Powers, M.C., (1953). A new roundness scale for sedimentary particles. *Journal of Sedimentary Petrology*, 23: 117-119.

Roberts, D.A. and Hart, J.K., (2005). The deforming bed characteristics of a stratified till assemblage in north East Anglia, UK: investigating controls on sediment rheology and strain signatures. *Quaternary Science Reviews*, 24(1-2): 123-140.

Rooney, S.T., Blankenship, D.D., Alley, R.B., and Bently, C.R., (1987). Till beneath ice stream B. 2. Structure and continuity. *Journal of Geophysical Research*, 92(B9): 8913-8920.

Rose, K.C. and Hart, J.K., (2008). Subglacial comminution in the deforming bed: inferences from SEM analysis. *Sedimentary Geology*, 203(1-2): 87-97.

Röthlisberger, H., (1972). Water pressure in intra- and subglacial channels. *Journal of Glaciology*, 11: 177-203.

Schwerzmann, A., Funk, M., and Blatter, H., (2006). Borehole logging with an eight-arm caliper-inclinometer probe. *Journal of Glaciology*, 52(178): 381-388.

Sharp, M. and Gomez, B., (1986). Processes of debris comminution in the glacial environment and implications for quartz sand-grain morphology. *Sedimentary Geology*, 46: 33-47.

Sharp, M., Richards, K., Willis, I., Arnold, N., and Nienow, P., (1993). Geometry, bed topography and drainage system structure of the Haut Glacier d'Arolla, Switzerland. *Earth Surface Processes and Landforms*, 18: 557-571.

Shoemaker, E.M., (1992). Subglacial floods and the origin of low-relief ice-sheet lobes. *Journal of Glaciology*, 38(128): 105-112.

Siegert, M.J., Taylor, J., Payne, A.J., and Hubbard, B., (2004). Macro-scale bed roughness of the Siple Coast ice streams in West Antarctica. *Earth Surface Processes and Landforms*, 29: 1591-1596.

Smith, A.M., (1997). Variations in basal condition on Rutford Ice Stream, West Antarctica. *Journal of Glaciology*, 43(146): 245-255.

Steere, D.C., Baptista, A., McNamee, D., Pu, C., and Walpole, J. (2000). Research challenges in environmental observations and forecasting systems. Proceedings of the ACM/IEEE International Conference on Mobile Computing and Networking (MOBICOMM), 292-299.

Stone, D.B., Clarke, G.K.C., and Blake, E.W., (1993). Subglacial measurement of turbidity and electrical conductivity. *Journal of Glaciology*, 39(132): 415-420.

Stone, D.B. and Clarke, G.K.C., (1996). In-situ measurements of basal water quality and pressure as an indicator of the character of subglacial drainage systems. *Hydrological Processes*, 10: 615-628.

Strahler, A.H. and Strahler, A., (2002). *Physical Geography*. John Wiley & Sons, Inc., New York.

Strand, K., Passchier, S., and Nasi, J., (2003). Implications of quartz grain microtextures for onset Eocene/Oligocene glaciation in Prydz Bay, ODP Site 1166, Antarctica. *Palaeogeography, Palaeoclimatology, Palaeoecology*, 198: 101-111.

Szewczyk, R., Polastre, J., Mainwaring, A., and Culler, D. Lessons from a sensor network expedition. 1st European Workshop on Wireless Sensor Networks (EWSN'04). 2004. 19-1-2004.
Ref Type: Conference Proceeding

Taylor, G.I., (1923). The motion of ellipsoidal particles in a viscous fluid. *Proceeding of the Royal Society of London, Series A.*, 103: 58-61.

Truffer, M., Harrison, W.D., and Echelmeyer, K.A., (2000). Glacier motion dominated by processes deep in underlying till. *Journal of Glaciology*, 46(153): 213-221.

Truffer, M., Echelmeyer, K.A., and Harrison, W.D., (2001). Implications of till deformation on glacier dynamics. *Journal of Glaciology*, 47(156): 123-134.

Truffer, M. and Harrison, W.D., (2006). In situ measurements of till deformation and water pressure. *Journal of Glaciology*, 52(177): 175-182.

Tulaczyk, S., Kamb, B., Scherer, R.P., and Engelhardt, H.F., (1998). Sedimentary processes at the base of a West Antarctic ice stream: constraints from textural and compositional properties of subglacial debris. *Journal of Sedimentary Research*, 68(3): 487-496.

Tulaczyk, S.M., Kamb, B., and Engelhardt, H., (2000). Basal mechanics of ice stream B, West Antarctica. 1. Till mechanics. *Journal of Geophysical Research*, 105(B1): 463-481.

van der Meer, J., (1997). Particle and aggregate mobility in till: microscopic evidence of subglacial processes. *Quaternary Science Reviews*, 16: 827-831.

van der Meer, J., Menzies, J., and Rose, J., (2003). Subglacial till: the deforming glacier bed. *Quaternary Science Reviews*, 22: 1659-1685.

Vieli, A., Payne, A.J., Du, Z.J., and Shepherd, A., (2006). Numerical modelling and data assimilation of the Larsen B ice shelf, Antarctic Peninsula. *Philosophical Transactions of the Royal Society A: Mathematical, Physical and Engineering Sciences*, 364(1844): 1815-1839.

Walder, J.S., (1986). Hydraulics of subglacial cavities. *Journal of Glaciology*, 32(112): 439-445.

Walder, J.S. and Fowler, A., (1994). Channelized subglacial drainage over a deformable bed. *Journal of Glaciology*, 40(134): 3-15.

Weertman, J., (1964). The theory of glacier sliding. *Journal of Glaciology*, 5(39): 287-303.

Weertman, J., (1972). General theory of water flow at the base of a glacier or ice sheet. *Reviews of Geophysics and Space Physics*, 10(1): 287-333.

Weertman, J., (1983). Creep deformation of ice. *Annual Review of Earth and Planetary Sciences*, 11: 215-240.

Whalley, W.B. and Krinsley, D.H., (1974). A scanning electron microscope study of surface textures of quartz grains from glacial environments. *Sedimentology*, 21: 87-105.

Willis, I.C., Sharp, M.J., and Richards, K.S., (1990). Configuration of the drainage system of Midtdalsbreen, Norway, as indicated by dye-tracing experiments. *Journal of Glaciology*, 36(122): 89-101.

Willis, I., (1995). Intra-annual variations in glacier motion: a review. *Progress in Physical Geography*, 19(1): 61-106.

Willis, I., Mair, D., Hubbard, B., Nienow, P., Fischer, U.H., and Hubbard, A., (2003). Seasonal variations in ice deformation and basal motion across the tongue of Haut Glacier d'Arolla, Switzerland. *Annals of Glaciology*, 36: 157-167.

Winkler, S., (1996). Front variations of outlet glaciers from Jostedalsbreen, western Norway, during the twentieth century. *Norges Geologiske Undersokelse Bulletin*, 431: 33-47.

Winkler, S. and Nesje, A., (1999). Moraine formation at an advancing temperate glacier: Brigsdalsbreen, Western Norway. *Geografiska Annaler Series A, Physical Geography*, 81(1): 17-30.

Woodward, J., Murray, T., Clark R.A., and Stuart, G.W., (2003). Glacier surge mechanisms inferred from ground-penetrating radar: Kongsvegen, Svalbard. *Journal of Glaciology*, 49(167): 473-480.

Woodward, J. and Burke, M., (2007). Applications of ground-penetrating radar to the investigation of glacial and frozen materials. *Journal of Environmental and Engineering Geophysics*, 12(1): 69-85.

Zwally, H.J., (1987). Technology in the advancement of glaciology. *Journal of Glaciology*, Special Issue: 66-77.

Zwally, H.J., Abdalati, W., Herring, T., Larson, K., Saba, J., and Steffen, K., (2002). Surface melt-induced acceleration of Greenland ice-sheet flow. *Science*, 297(5579): 218-222.